frontiers | Research Topics

Prognostic gene signatures in skin cancer

Edited by
Colette Pameijer, Wen-Qing Li and Gagan Chhabra

Published in
Frontiers in Oncology

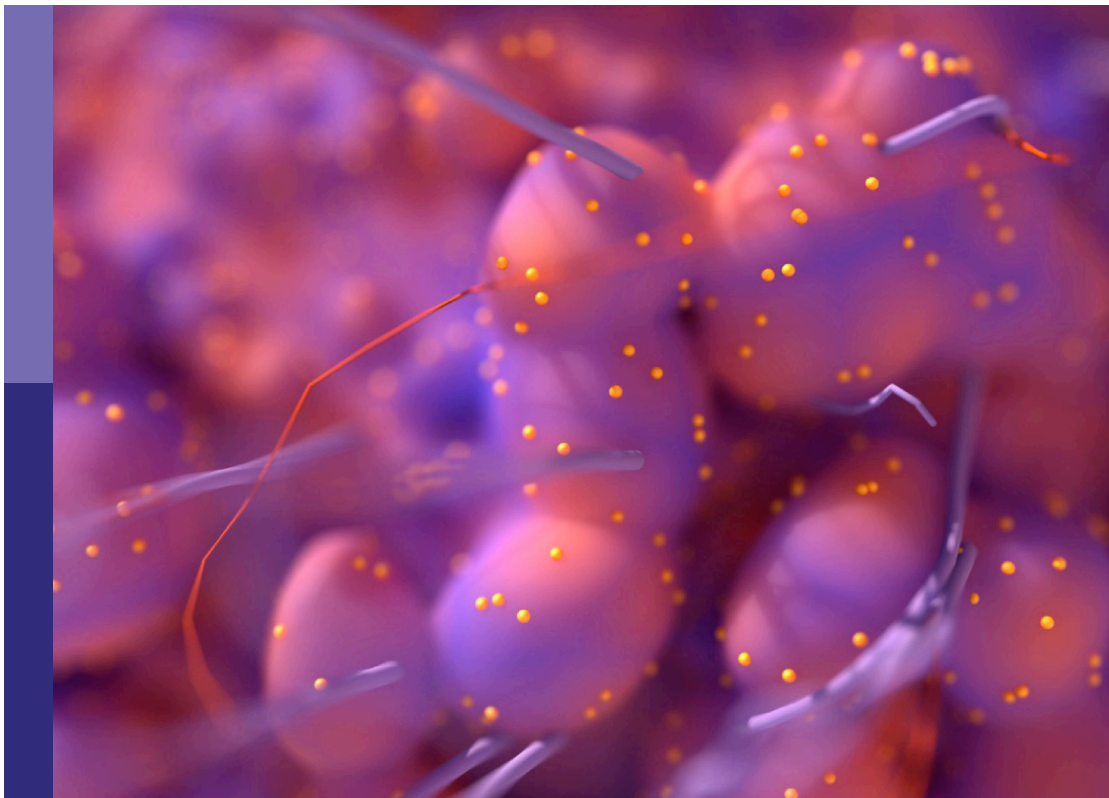

ISSN 1664-8714
ISBN 978-2-8325-2496-1
DOI 10.3389/978-2-8325-2496-1

About Frontiers

Frontiers is more than just an open access publisher of scholarly articles: it is a pioneering approach to the world of academia, radically improving the way scholarly research is managed. The grand vision of Frontiers is a world where all people have an equal opportunity to seek, share and generate knowledge. Frontiers provides immediate and permanent online open access to all its publications, but this alone is not enough to realize our grand goals.

Frontiers journal series

The Frontiers journal series is a multi-tier and interdisciplinary set of open-access, online journals, promising a paradigm shift from the current review, selection and dissemination processes in academic publishing. All Frontiers journals are driven by researchers for researchers; therefore, they constitute a service to the scholarly community. At the same time, the *Frontiers journal series* operates on a revolutionary invention, the tiered publishing system, initially addressing specific communities of scholars, and gradually climbing up to broader public understanding, thus serving the interests of the lay society, too.

Dedication to quality

Each Frontiers article is a landmark of the highest quality, thanks to genuinely collaborative interactions between authors and review editors, who include some of the world's best academicians. Research must be certified by peers before entering a stream of knowledge that may eventually reach the public - and shape society; therefore, Frontiers only applies the most rigorous and unbiased reviews. Frontiers revolutionizes research publishing by freely delivering the most outstanding research, evaluated with no bias from both the academic and social point of view. By applying the most advanced information technologies, Frontiers is catapulting scholarly publishing into a new generation.

What are Frontiers Research Topics?

Frontiers Research Topics are very popular trademarks of the *Frontiers journals series*: they are collections of at least ten articles, all centered on a particular subject. With their unique mix of varied contributions from Original Research to Review Articles, Frontiers Research Topics unify the most influential researchers, the latest key findings and historical advances in a hot research area.

Find out more on how to host your own Frontiers Research Topic or contribute to one as an author by contacting the Frontiers editorial office: frontiersin.org/about/contact

Prognostic gene signatures in skin cancer

Topic editors

Colette Pameijer — The Pennsylvania State University, United States
Wen-Qing Li — Peking University, China
Gagan Chhabra — University of Wisconsin-Madison, United States

Citation

Pameijer, C., Li, W.-Q., Chhabra, G., eds. (2023). *Prognostic gene signatures in skin cancer*. Lausanne: Frontiers Media SA. doi: 10.3389/978-2-8325-2496-1

Table of contents

frontiers | Frontiers in Oncology

TYPE Editorial
PUBLISHED 03 May 2023
DOI 10.3389/fonc.2023.1163642

OPEN ACCESS

EDITED AND REVIEWED BY
Ari VanderWalde,
Caris Life Sciences Inc., United States

*CORRESPONDENCE
Gagan Chhabra
gchhabra@dermatology.wisc.edu

RECEIVED 11 February 2023
ACCEPTED 19 April 2023
PUBLISHED 03 May 2023

CITATION
Chhabra G, Li W-Q and Pameijer C (2023) Editorial: Prognostic gene signatures in skin cancer. *Front. Oncol.* 13:1163642. doi: 10.3389/fonc.2023.1163642

Editorial: Prognostic gene signatures in skin cancer

Gagan Chhabra[1]*, Wen-Qing Li[2] and Colette Pameijer[3]

[1]Department of Dermatology, University of Wisconsin-Madison, Madison, WI, United States, [2]Key Laboratory of Carcinogenesis and Translational Research (Ministry of Education/Beijing), Department of Cancer Epidemiology, Peking University Cancer Hospital & Institute, Beijing, China, [3]College of Medicine, The Pennsylvania State University, Hershey, PA, United States

KEYWORDS

skin cancer, prognosis, gene signature, melanoma, editorial

Editorial on the Research Topic
Prognostic gene signatures in skin cancer

Skin cancer is the most commonly occurring cancer worldwide with two major subcategories of melanoma and non-melanoma (1). Conventionally, skin cancers are treated with surgery and/or radiotherapy, however, if not diagnosed and treated early these malignancies can progress to locally advanced or metastatic stages. Over the past decade, a mechanistic understanding of immune regulation in skin cancer fueled the development of novel immunotherapy, including immune checkpoint inhibitors (ICIs), which has transformed the prognosis for many patients (2). Despite tremendous progress, currently, available therapeutics are still associated with sub-optimal responses due to drug resistance, especially against metastatic melanoma (3, 4). Hence, the identification of novel diagnostic, prognostic, and therapeutic targets is required for the management of skin cancers.

Bioinformatics analyses through several web servers and online tools (5) based on publicly available databases such as Genotype-Tissue Expression (GTEx) (6) and the Cancer Genome Atlas (TCGA) (7) have been used to identify potential prognostic markers in various cancers, leading to the establishment of predictive models to assess survival of individual patients (8). Importantly, prognostic gene signatures could help design novel strategies for the management of skin cancer. These studies are also important in guiding treatment selection and predicting patient outcomes. Moreover, the identification of potential biomarkers of skin cancers may also provide crucial information for the early detection of tumor relapse.

In this Research Topic, a total of 14 manuscripts were published focusing on prognostic genes in various skin cancer types including cutaneous melanoma (CM), uveal melanoma (UM), and cutaneous squamous cell carcinoma (cSCC). Overall, each team of investigators identified and validated either an individual gene or a multi-gene signature using several bioinformatics tools and/or *in vitro* experimental analyses. Below, we first discuss the studies focused on CM highlighting individual genes, and then a multi-gene signature, followed by the studies analyzing prognostic genes in UM and cSCC.

Zhang F et al. determined that eukaryotic translation initiation factor 6 (eIF6) may serve as a diagnostic and prognostic biomarker for predicting the survival of patients with cutaneous melanoma. Using immunohistochemistry (IHC) analysis of clinical specimens, the authors found that eIF6 was overexpressed in melanoma tumors compared to normal

skin. eIF6 was also found to be significantly associated with decreased survival rates of patients with melanoma. Further, using *in vitro* experiments, this study showed that overexpression of eIF6 increased the proliferation and migration of melanoma cells. In addition, this study provided insights into the potential role of eIF6 in pan-cancer epigenetic regulation.

Zhong et al. described the oncogenic role of MYB proto-oncogene like 2 (MYBL2), a transcription factor that regulates the cell cycle. The authors showed overexpression of MYBL2 in malignant and metastatic melanoma patient samples, which was significantly associated with poor prognosis. The authors performed a loss-of-function study and demonstrated that MYBL2 depletion significantly decreased melanoma cell proliferation and migration as well as prevented cell cycle progression. They also showed that MYBL2 promoted the formation of melanoma stem-like cell populations, indicating its potential as a therapeutic target for treating resistant melanoma. Additionally, they constructed an MYBL2 regulatory network in melanoma by integrating RNA-seq and ChIP-seq data and identified three core target genes of MYBL2 that were EPPK1, PDE3A, and FCGR2A. Overall, this study concluded that MYBL2 may be a potential target for melanoma diagnosis and treatment.

Zhang J et al. showed decreased protocadherin 9 (PCDH9) expression in melanoma tissues compared to normal skin and pigmented nevus tissues using IHC analyses. The authors performed cell viability, cell cycle, apoptosis, and wound healing assay to determine the role of PCDH9 in melanoma. This study showed that an increase in PCDH9 could suppress melanoma cells and inhibit migration without exerting significant effects on the cell cycle. At a mechanistic level, the authors found that PCDH9 was negatively correlated with MMP2 and RAC1, while positively correlated with Cyclin D1. The authors concluded that PCDH9 could be useful as an independent prognostic marker for melanoma, and strategies to increase the expression of PCDH9 can be developed for the treatment of melanoma.

The study by Tong et al. aimed to identify new biomarkers for cutaneous melanoma and established a novel risk score system in melanoma prognosis. This study used univariate and multivariate Cox regression analyses to determine a model with four genes (ADAMDEC1, GNLY, HSPA13, and TRIM29). This four-gene risk score model was shown to be useful to predict the prognosis and treatment response in cutaneous melanoma. This model could be helpful to develop efficient therapeutic approaches against melanoma, however, additional studies are required to validate these findings.

Despite the success of immunotherapy that has transformed the prognosis for many cancer patients, no combined immune biomarkers are formally validated and recommended as a clinical tool for melanoma prognosis. In this regard, Zhang JA et al. described an immune-related prognostic gene signature in melanoma and correlated it with the immune infiltrating cells as well as the molecular subtypes of melanoma. The authors determined several differentially expressed genes such as IGHV1-18, CXCL11, LTF, and HLA-DQB1, which were associated with immune cell infiltration in patients with melanoma. In addition, the authors established a prognostic risk score for several types of immune infiltrating cells. These findings could be useful for future studies focusing on developing additional therapeutic strategies against melanoma.

Zhang H et al. constructed a 14-gene prognostic risk model based on cytolytic activity (CYT) level, an index of cancer immunity, in cutaneous melanoma using RNA sequencing data and clinical information from TCGA and GEO databases. The authors found that patients with high CYT levels had better prognoses. They also verified the expression of CYT-related genes in this prognostic risk model at the transcriptional as well as protein levels. In addition, the authors showed the utility of this model to predict and compare the response of patients to chemotherapy and immunotherapy. Altogether, this model could be helpful in the clinical management of melanoma.

Cutaneous melanoma is characterized by high immune cell infiltration in the tumor microenvironment (TME). However, an excess release of lactate, a major metabolic product, into the TME causes immunosuppression. Xie et al. determined the predictive value of lactate-related genes (LRGs) for prognosis and response to immunotherapy in patients with melanoma. This study found an inverse relation between the immune cells infiltration levels and clinical prognosis with patients' risk scores based on the lactate-related prognostic signature and suggested that the low-risk cases could benefit better from immunotherapy. Overall, this lactate-related prognostic risk model may be explored in future clinical studies to predict survival and immunotherapy outcomes in patients with melanoma.

Interestingly, genes involved in DNA damage response could serve as promising candidates to predict response against ICIs. In this regard, Fischer et al. studied nine genes associated with xeroderma pigmentosum (XP), a genetic disorder caused by mutations in the genes of the nucleotide excision repair [7] pathway, which is primarily involved in the repair of ultraviolet radiation-induced DNA damage. As treatment with ICIs has been shown effective in XP patients with melanoma, the authors concluded that expression of XP-related genes could be used to predict melanoma prognosis as a well response to ICI treatment.

Zeng et al. established a prognostic nomogram based on metabolism-related genes (MRGs) and clinicopathological factors to predict melanoma prognosis. The authors identified several prognostic MRGs by comparing melanoma tumors with normal skin samples and suggested that two MRGs, tryptophanyl-tRNA Synthetase (WARS) and microsomal glutathione S-transferase 1 (MGST1) could be used as independent prognostic genes in melanoma.

Receptor tyrosine kinases (RTKs) are known to be overexpressed in tumors. In this regard, Lei et al. evaluated the association between overexpression of RTKs and survival in patients with melanoma based on several databases, which utilized IHC analyses. This study showed that overexpression of vascular endothelial growth factor receptor 2 (VEGFR2) was associated with worse patient survival in melanoma. Further, several other RTKs including epidermal growth factor receptor (EGFR), vascular endothelial growth factor receptor 1 (VEGFR1), insulin-like growth factor 1 receptor (IGF-1R), and mesenchymal-epithelial transition factor (MET) were also found to be associated

with overall survival of patients with melanoma. This study concluded that overexpression of RTKs might be useful in accurate prognostic evaluation.

In another interesting study, Cheung et al. utilized next-generation sequencing (NGS) and performed hotspot mutation profiling on early-stage melanoma tumors obtained from patients at the Iowa City Veterans Affairs Medical Center. The authors found the highest prevalence of alterations in BRAF, TP53, NRAS, CDKN2A, KIT, and BAP1. In addition, they found significantly higher TP53 mutation in Veterans with prior history of melanoma. Overall, this study concluded that TP53 may be a useful marker to predict recurrent melanoma in the military population.

Luo et al. aimed to identify prognostic genes in uveal melanoma, the most common adult ocular tumor. The authors described prognostic implications of a ten-gene signature showing interactions with the immunodominant TME, which might be helpful to predict individual patient prognosis and develop new therapeutic strategies for patients with uveal melanoma.

Johnson et al. determined the role of complement factor H (CFH), a regulatory factor of the complement cascade, in the development of cSCC, the 2nd most common type of cancer in the US, following basal cell carcinoma. CFH has been shown to be associated with poor outcomes in different cancer types by affecting cell-mediated immunity. For this study, the authors utilized skin samples from sun-exposed normal individuals as well as cSCC patients. The results of this study showed that increased CFH levels in cSCC patients were independent of sun exposure and potentially linked to reduced effectiveness of the immune response leading to cSCC progression. The authors suggest that CFH levels might serve as a prognostic factor in cSCC.

Thind et al. performed whole-genome sequencing on lymph node metastases and blood DNA from cSCC patients with regional metastases of the head and neck. They designed a multifaceted computational analysis at the whole genome level to provide a deeper understanding of the genomic landscape of metastatic cSCC. The information provided in this study could be helpful to identify predictive biomarkers in primary as well as metastatic cSCC.

Taken together, the published studies in this Research Topic range from research articles to meta-analyses identifying various novel genes important in skin cancer prognosis and are appropriately collected under the title "Prognostic Gene Signatures in Skin Cancer".

Author contributions

GC wrote the draft, W-QL and CP edited and finalized it with substantial intellectual inputs. All the authors approve this editorial for publication.

Conflict of interest

The authors declare that the research was conducted in the absence of any commercial or financial relationships that could be construed as a potential conflict of interest.

Publisher's note

References

1. American Cancer Society. *Key statistics for melanoma skin cancer* (2023). Available at: https://www.cancer.org/cancer/melanoma-skin-cancer/about/key-statistics.html.

2. Zaidi N, Jaffee EM. Immunotherapy transforms cancer treatment. *J Clin Invest.* (2019) 129:46–7. doi: 10.1172/JCI126046

3. Huang AC, Zappasodi R. A decade of checkpoint blockade immunotherapy in melanoma: understanding the molecular basis for immune sensitivity and resistance. *Nat Immunol* (2022) 23:660–70. doi: 10.1038/s41590-022-01141-1

4. Thornton J, Chhabra G, Singh CK, Guzmán-Pérez G, Shirley CA, Ahmad N. Mechanisms of immunotherapy resistance in cutaneous melanoma: recognizing a shapeshifter. *Front Oncol* (2022) 19:880876(12). doi: 10.3389/fonc.2022.880876

5. Zheng H, Zhang G, Zhang L, Wang Q, Li H, Han Y, et al. Comprehensive review of web servers and bioinformatics tools for cancer prognosis analysis. *Front Oncol* (2020) 5:68(10). doi: 10.3389/fonc.2020.00068

6. Barrett T, Wilhite SE, Ledoux P, Evangelista C, Kim IF, Tomashevsky M, et al. NCBI GEO: archive for functional genomics data sets–update. *Nucleic Acids Res* (2013) 41(Database issue):D991–5. doi: 10.1093/nar/gks1193

7. Tomczak K, Czerwińska P, Wiznerowicz M. The cancer genome atlas (TCGA): an immeasurable source of knowledge. *Contemp Oncol (Pozn)* (2015) 19(1A):A68–77. doi: 10.5114/wo.2014.47136

8. Smith JC, Sheltzer JM. Genome-wide identification and analysis of prognostic features in human cancers. *Cell Rep* (2022) 38(13):110569. doi: 10.1016/j.celrep.2022.110569

frontiers in Oncology

ORIGINAL RESEARCH
published: 09 September 2020
doi: 10.3389/fonc.2020.01710

Prognostic Implications of Metabolism Related Gene Signature in Cutaneous Melanoma

Furong Zeng [1,2], Juan Su [1,2], Cong Peng [1,2], Mengting Liao [1,2], Shuang Zhao [1,2], Ying Guo [1,2], Xiang Chen [1,2] and Guangtong Deng [1,2]**

[1] Hunan Key Laboratory of Skin Cancer and Psoriasis, Department of Dermatology, Hunan Engineering Research Center of Skin Health and Disease, Xiangya Hospital, Central South University, Changsha, China, [2] National Clinical Research Center for Geriatric Disorders, Xiangya Hospital, Central South University, Changsha, China

Metabolic reprogramming is closely related to melanoma. However, the prognostic role of metabolism-related genes (MRGs) remains to be elucidated. We aimed to establish a nomogram by combining MRGs signature and clinicopathological factors to predict melanoma prognosis. Eighteen prognostic MRGs between melanoma and normal samples were identified using The Cancer Genome Atlas (TCGA) and GSE15605. *WARS* (HR = 0.881, 95% CI = 0.788–0.984, $P = 0.025$) and *MGST1* (HR = 1.124, 95% CI = 1.007–1.255, $P = 0.037$) were ultimately identified as independent prognostic MRGs with LASSO regression and multivariate Cox regression. The MRGs signature was established according to these two genes and externally validated in the Gene Expression Omnibus (GEO) dataset. Kaplan-Meier survival analysis indicated that patients in the high-risk group had significantly poorer overall survival (OS) than those in the low-risk group. Furthermore, the MRGs signature was identified as an independent prognostic factor for melanoma survival. An MRGs nomogram based on the MRGs signature and clinicopathological factors was developed in TCGA cohort and validated in the GEO dataset. Calibration plots showed good consistency between the prediction of nomogram and actual observation. The receiver operating characteristic curve and decision curve analysis indicated that MRGs nomogram had better OS prediction and clinical net benefit than the stage system. To our knowledge, we are the first to develop a prognostic nomogram based on MRGs signature with better predictive power than the current staging system, which could assist individualized prognosis prediction and improve treatment.

Keywords: melanoma, metabolism related genes, overall survival, prognosis, nomogram

OPEN ACCESS

Edited by:
Colette Pameijer, Pennsylvania State University, United States

Reviewed by:
Gagan Chhabra, University of Wisconsin-Madison, United States
Aurobind Vidyarthi, Yale University, United States

***Correspondence:**
Xiang Chen
chenxiangck@126.com
Guangtong Deng
dengguangtong@outlook.com

Specialty section:
This article was submitted to Skin Cancer, a section of the journal Frontiers in Oncology

Received: *13 March 2020*
Accepted: *31 July 2020*
Published: *09 September 2020*

Citation:
Zeng F, Su J, Peng C, Liao M, Zhao S, Guo Y, Chen X and Deng G (2020) Prognostic Implications of Metabolism Related Gene Signature in Cutaneous Melanoma. Front. Oncol. 10:1710. doi: 10.3389/fonc.2020.01710

INTRODUCTION

Cutaneous melanoma (hereafter "melanoma"), a tumor most commonly observed in fair-skin populations, is the most lethal form of skin malignancy with great heterogeneity. Its incidence has been increasing worldwide over recent decades (1), and the prognosis of melanoma patients is poor due to its invasiveness and metastasis (2). Numerous efforts have been made to develop useful tools for melanoma prognosis predictions. The most frequently

used tool is the American Joint Committee on Cancer's staging system for tumor-node-metastasis, but it is not satisfactory in current clinical practice. Increasing studies show that patients differed considerably in prognosis even at the same tumor-node-metastasis stage due to the discrepant genetic backgrounds (3). Therefore, it is still necessary to explore novel melanoma prognostic biomarkers for optimal therapeutic strategies.

Metabolic reprogramming, an emerging hallmark of cancer, allows cancer cells to survive, proliferate, and disseminate (4, 5). In the 1920s, Otto Warburg observed that proliferating ascites tumor cells preferentially performed glycolysis, even in oxygen-rich circumstances (6). This seminal finding has been observed in a wide variety of cancers and currently has been exploited clinically using 18F-deoxyglucose positron emission tomography (7). Mechanically, in proliferating tumor cells, glycolysis, instead of pure mitochondrial metabolism, could provide essential intermediates for biosynthetic pathways, such as lipid or nucleotide synthesis (8). Emerging studies highlight the close association between melanoma and metabolic reprogramming. For example, 18F-deoxyglucose positron emission tomography was applied for the detection of the early response to the B-Raf proto-oncogene, serine/threonine kinase (*BRAF*) inhibitor, vemurafenib, in *BRAF*-mutant melanoma patients (9). Also, some potential drugs navigating metabolic pathways have been exploited for melanoma in preclinical or clinical scenarios (10). Therefore, metabolism-related genes (MRGs) are promising therapeutic targets and prognostic predictors in melanoma.

Nomogram has become a reliable and convenient tool in cancer prognosis predictions (11, 12). Several prognostic nomograms have been established for predicting the prognosis of melanoma in recent years (13–15), while global expression pattern based on MRGs has not previously been recognized in melanoma. In this study, we aimed to develop and validate a novel prognostic nomogram based on MRGs signature and clinicopathological factors for ideally predicting the prognosis of melanoma patients.

MATERIALS AND METHODS

Acquisition of MRGs

MRGs were extracted from all 41 metabolic pathways in the Kyoto Encyclopedia of Gene and Genomes (KEGG) pathway (c2.cp.kegg.v7.0.symbols.gmt) from the Gene Set Enrichment Analysis (GSEA) website (https://www.gsea-msigdb.org/gsea/downloads.jsp#msigdb). Finally, a total of 948 MRGs were identified for our study.

Data Retrieval and Processing

The training cohort dataset with 460 melanoma RNA-sequencing data and clinical information was obtained from The Cancer Genome Atlas (TCGA) (https://portal.gdc.cancer.gov/). GSE15605 and GSE54467 were derived from the Gene Expression Omnibus (GEO) database (https://www.ncbi.nlm.nih.gov/geo/). GSE15605, which included 46 primary melanoma samples and 16 normal skin samples, was used to identify differentially expressed genes (DEGs) using GEO2R. An adjusted $P < 0.01$ and a $|\log_2 (FC)| > 2$ were considered the cutoffs for identifying DEGs. GSE54467, which included 79 melanoma patients, was used as the GEO validation dataset. The intersected genes in TCGA cohort and GSE54467 dataset were extracted, and their expressions were normalized using the "limma" and "sva" packages using R software version 3.6.0. MRGs in these intersected genes were used for the following univariate Cox regression analysis. Patient clinical and pathological characteristics in TCGA and GEO cohorts are summarized in **Supplementary Table 1**.

Construction and Validation of the Prognostic MRGs Signature

A univariate Cox regression analysis was performed to screen out the prognosis related MRGs. Then the prognosis related MRGs were overlapped with the DEGs to obtain the prognostic MRGs. The least absolute shrinkage and selection operator (LASSO) regression analysis with tenfold cross-validation was subsequently applied by using "glmnet" and "survival" packages (16). The independent prognostic MRGs were generated through a multivariate Cox regression analysis and used to construct the prognostic MRGs signature with the following formula: Risk score $= (\beta 1 \times \text{expression of MRG1}) + (\beta 2 \times \text{expression of MRG2}) + \cdots + (\beta n \times \text{expression MRGn})$. Patients were divided into high-risk and low-risk groups according to the median risk score. Kaplan-Meier survival analysis was performed to evaluate the association between the prognostic MRGs signature and overall survival (OS) in melanoma patients. Moreover, univariate and multivariate Cox regression was used to identify the independent prognostic factors, including age, stage, and MRGs signature. The prognostic MRGs signature was externally validated in the GEO dataset and calculated with the same formula and cutoff. $P < 0.05$ was regarded as statistically significant.

Functional Enrichment Analysis

Gene ontology and KEGG pathway analyses were performed for the differentially expressed MRGs using "org.Hs.eg.db," "clusterProfiler," "enrichplot," "ggplot2," and "GOplot" packages in R. The adjusted $P < 0.05$ was considered statistically significant.

Validation of the Independent Prognostic MRGs

Gene Expression Profiling Interactive Analysis (GEPIA) is a web-based tool to analyze gene expression and function based on the RNA-seq data from TCGA (one normal sample and 460 melanoma samples) and Genotype-Tissue Expression (GETx) (557 normal samples). The differential expression of these independent prognostic MRGs was verified using GEPIA. Their expression of *WARS* and *MGST1* were validated using clinical specimens from the Human Protein Atlas (HPA) database (http://www.proteinatlas.org). A Kaplan-Meier survival analysis was conducted to validate the prognostic value of the independent prognostic MRGs using GEPIA.

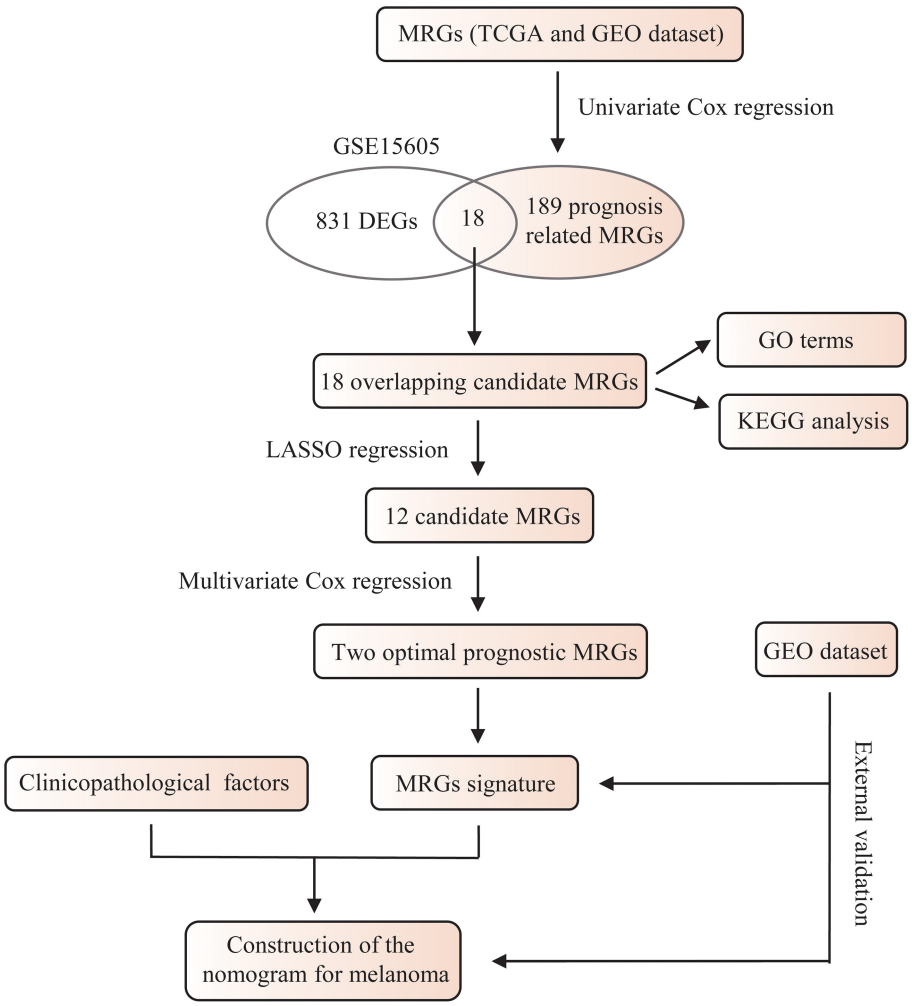

FIGURE 1 | A flowchart of the study procedure.

GSEA

GSEA was performed in java GSEA (version 4.0.3) based on the Molecular Signatures Database version 6.2. Through comparing the high- and low- risk groups in 460 melanoma patients from TCGA dataset. C2 (curated gene sets), C5 (GO gene sets), and C6 (Oncogenic signature) were searched to identify enriched KEGG pathways, biological processes, cellular components, molecular functions, and oncogenic signatures. FDR $q < 0.05$, $|NES| > 1$ were considered statistically significant.

Construction and Validation of the Nomogram

All the independent prognostic factors were enrolled to establish a nomogram in TCGA training cohort. A calibration curve was plotted to evaluate the consistency between the nomogram and actual observation. The concordance index (C index) and the area under the curve (AUC) in receiver operating characteristic (ROC) curves were applied to assess the predictive accuracy. Decision curve analysis, an approach to assess the clinical value of models by integrating the preferences of the patients into the analysis, was used to evaluate the clinical benefits of stages and our nomogram to facilitate decisions about test selection and use (17).

RESULTS

WARS and *MGST1* Were the Independent Prognostic MRGs

The whole flowchart for the study procedure is presented in **Figure 1**. A total of 849 DEGs were found in GSE15605 by volcano plot ($P \leq 0.01$, $|\log_2 FC| \geq 2$; **Figure 2A**). Using univariate Cox regression, 207 MRGs associated with OS were identified in TCGA training cohort (**Supplementary Table 2**). Differentially expressed MRGs were the intersection of the above two gene sets, and finally, 18 overlapping prognostic MRGs were obtained (**Figure 2B**). Gene ontology functional

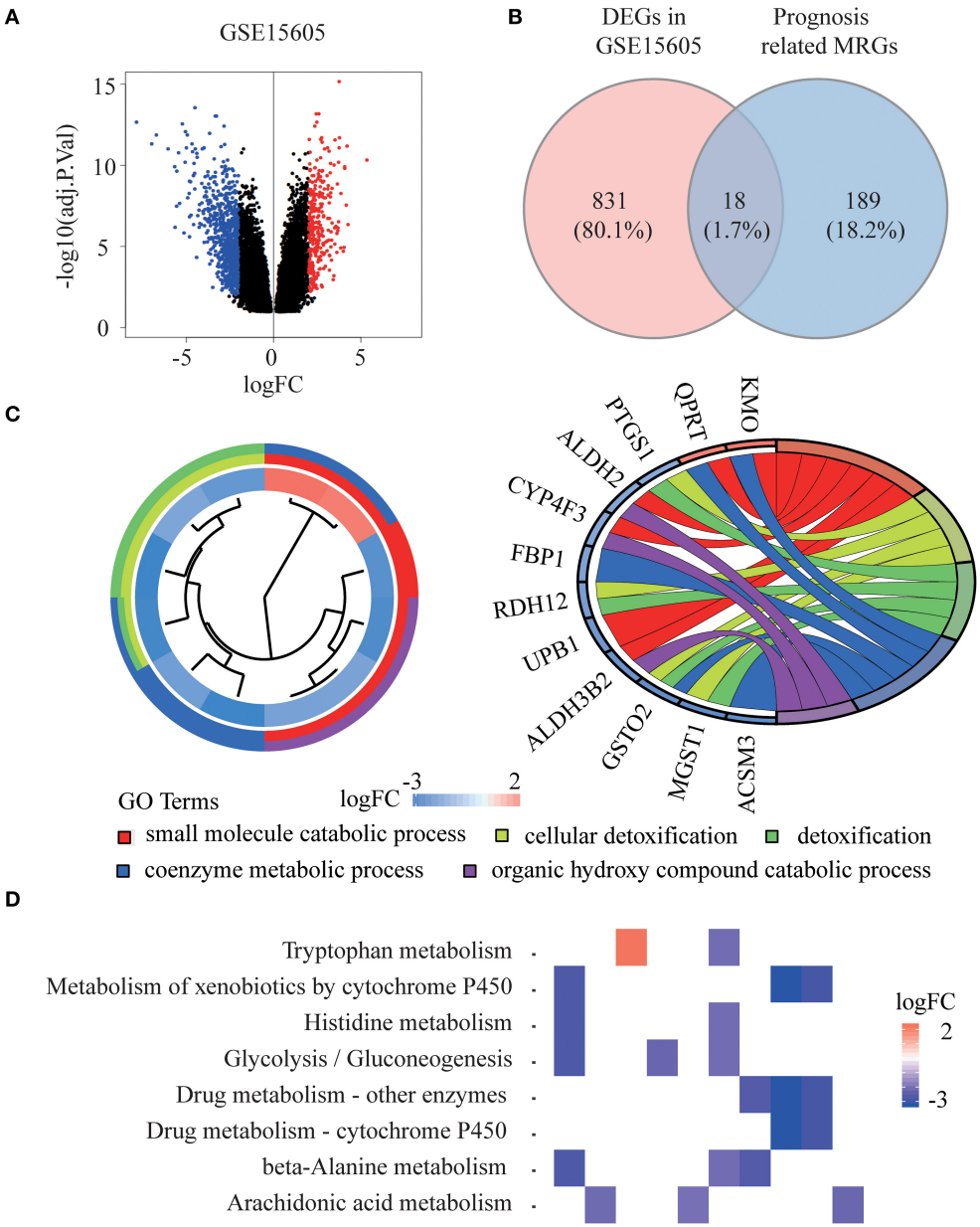

FIGURE 2 | Identification of prognostic metabolism related genes (MRGs) and functional enrichment analysis. **(A)** Volcano plot of differentially expressed genes (DEGs) between melanoma and normal samples of GSE15605 dataset. The red dots represent up-regulated genes, and the green dots represent down-regulated genes (adj. $P < 0.01$ and $|\log_2 (FC)| > 2$). **(B)** Venn diagram showing the intersection of the DEGs in GSE15605 and prognosis related MRGs. **(C,D)** Gene ontology (GO) terms **(C)** and Kyoto Encyclopedia of Gene and Genomes (KEGG) pathways **(D)** of 18 prognostic MRGs.

enrichment and KEGG analyses were performed on the prognostic MRGs (**Figures 2C,D**). Gene ontology enrichment analysis showed that these DEGs were mainly enriched in small molecule catabolic processes, cellular detoxification, and detoxification. KEGG analysis revealed that the DEGs were mainly enriched in tryptophan metabolism, metabolism of xenobiotics by cytochrome P450, and histidine metabolism. To avoid collinearity, the differentially expressed MRGs were entered into a LASSO regression with ten-fold cross-validation, and 12 candidate MRGs were ultimately selected (**Figures 3A,B**). Then, multivariate Cox regression was applied and results showed that tryptophanyl-tRNA synthetase 1 (*WARS*) (HR = 0.881, 95% CI = 0.788–0.984, $P = 0.025$) and microsomal glutathione S-transferase 1 (*MGST1*) (HR = 1.124, 95% CI = 1.007–1.255, $P = 0.037$) were the independent prognostic MRGs (**Figure 3C**).

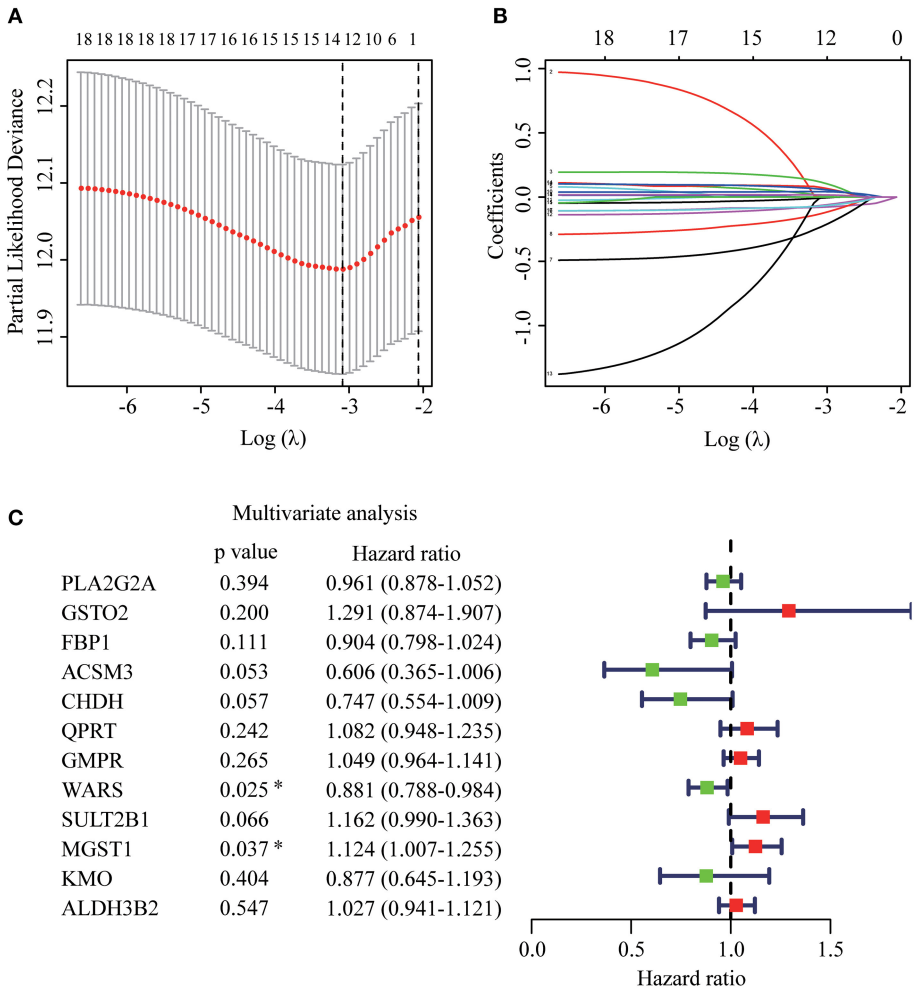

FIGURE 3 | Establishment of prognostic MRGs signature. **(A)** Selection of the optimal parameter in the least absolute shrinkage and selection operator (LASSO) regression with tenfold cross-validation. **(B)** LASSO coefficient profiles of the candidate prognosis related MRGs. **(C)** Multivariate Cox regression analysis of 12 candidate prognosis related MRGs.

Verification of *WARS* and *MGST1* Expression and Prognosis

WARS and *MGST1* were highly expressed and downregulated in GSE15605 melanoma datasets, separately (**Figure 4A**). The differential expression of these two genes was further validated in the GEPIA database (**Figure 4B**). Interestingly, their expressions were independent of the status of key melanoma mutations, including *BRAF*, neurofibromin 1 (*NF1*), and *RAS* mutations and triple wild type in melanoma (**Figure 4C**). Moreover, the protein level encoded by these two genes was consistent with their gene expression using the HPA website. *WARS* was strongly positive in melanoma tissue, while *MGST1* was weakly positive in normal skin tissue (**Figure 4D**). Kaplan-Meier survival curves were further conducted to evaluate the prognostic value of each gene. Though *WARS* and *MGST1* were not associated with disease free survival (**Figure S1**), we arrived at the same conclusion that *WARS* was a protective gene (HR = 0.59, $P < 0.001$), while *MGST1* was a risk gene (HR = 1.3, $P = 0.031$) for OS in melanoma (**Figures 4E,F**).

MRGs Signature Acts as an Independent Prognostic Predictor

Based on *WARS* and *MGST1*, MRGs signature was established to predict melanoma prognosis according to the formula: MRGs signature = (−0.139 × expression of WARS) + (0.122 × expression of MGST1). The prognostic signature for each patient in TCGA training cohort was calculated. All patients were divided into high-risk or the low-risk groups using the median signature as the cutoff (−0.804). The result demonstrated that patients with higher risk scores had worse OS than those in the low-risk group (**Figure 5A**). The distributions of risk score, survival status, and a heatmap of the gene expression profile are presented in **Figure 5B**. Interestingly, in our MRGs signature, disease free survival was also much shorter in the high-risk

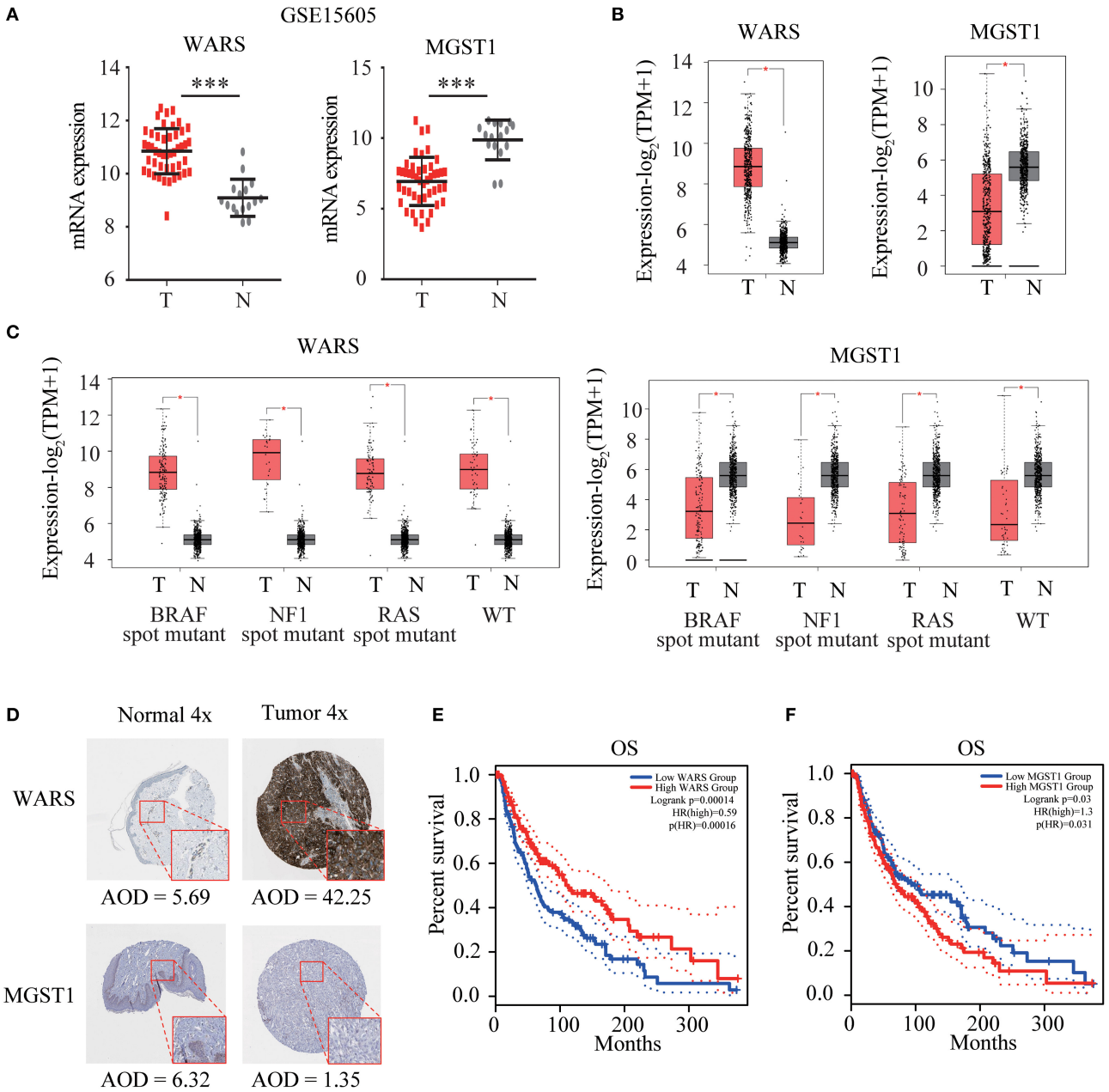

FIGURE 4 | Verification of *WARS* and *MGST1*. **(A)** The expression of *WARS* and *MGST1* between melanoma and normal skin in GSE15605. *N* (T) = 46 and *N* (N) = 16. ***$P < 0.001$. **(B)** The expression of *WARS* and *MGST1* between melanoma and normal skin using Gene Expression Profiling Interactive Analysis (GEPIA) database. The number of sorts: *N* (T) = 460 and *N* (N) = 558. **(C)** The expression of *WARS* and *MGST1* in three mutational signatures (BRAF, NF1 and RAS) and wild types (WT) of melanoma. The number of sorts: N (T) = 147 and N (N) = 558 in BRAF mutation; N (T) = 27 and N (N) = 558 in NF1 mutation; N (T) = 91 and N (N) = 558 in RAS mutation; N (T) = 47 and N (N) = 558 in WT. **(D)** The representative protein expressions of *WARS* and *MGST1* between normal and melanoma tissues in the Human Protein Atlas database (http://www.proteinatlas.org). AOD, average optical density, calculated by integrated optical density/area. The expressions were quantified by Image J (version 1.52a). **(E,F)** Kaplan-Meier curves for overall survival (OS) of *WARS* **(E)** and *MGST1* **(F)** in melanoma patients using GEPIA. N (high) = 229, N (low) = 229. T, tumor; N, normal skin. *$P < 0.05$.

group (**Figure S2**), suggesting that the MRGs signature is a better predictor than individual gene. To examine the robustness of the MRGs signature, we used a GEO dataset to externally validate the prognostic value of the model. The same signature formula and the cutoff were applied to classify the melanoma patients into the high-risk group ($n = 38$) and low-risk group ($n = 41$) in the GEO validation dataset. Consistently, the results showed that patients in the high-risk group generally had increased *MGST1*, decreased

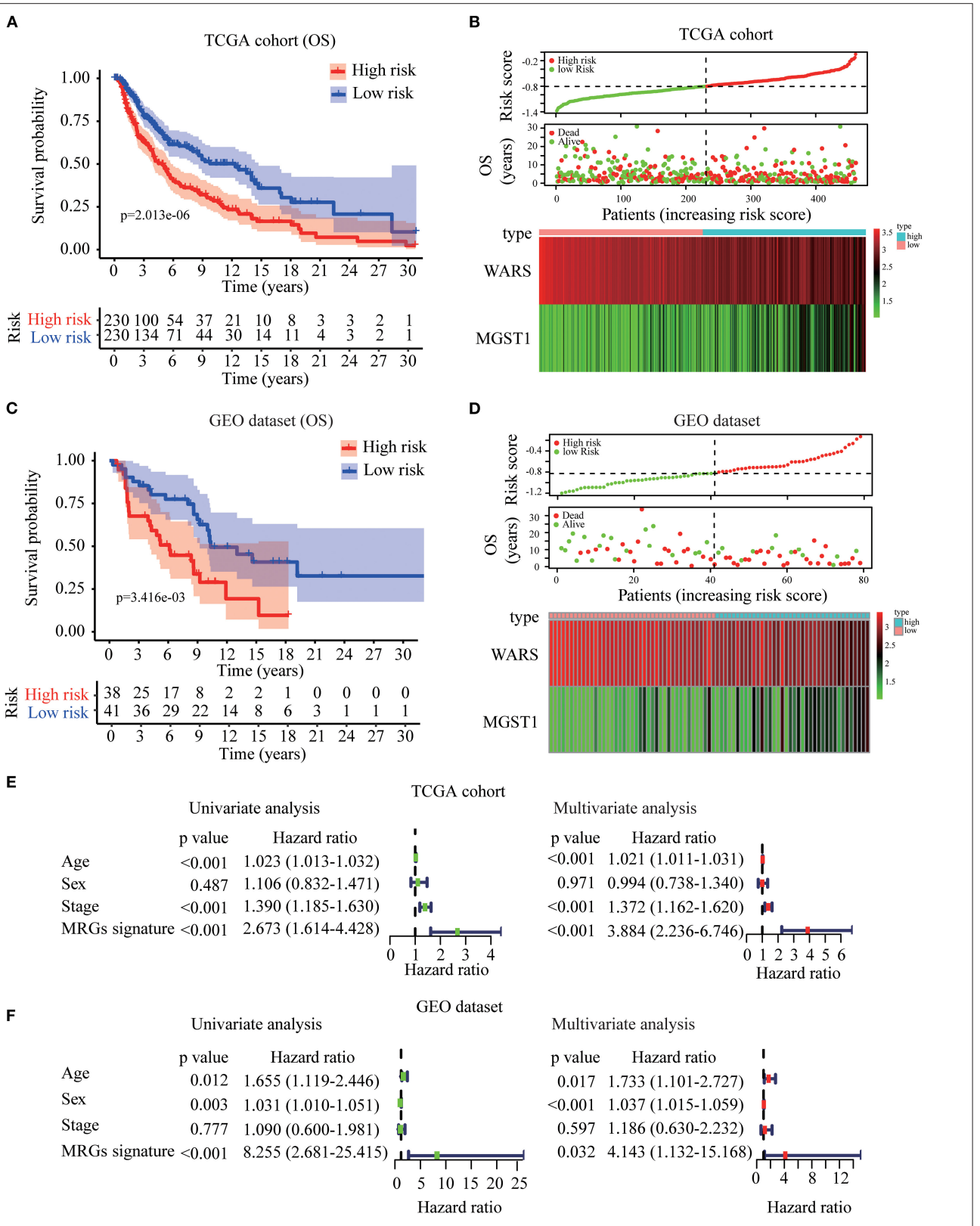

FIGURE 5 | Construction and validation of MRGs signature in melanoma. **(A–D)** Kaplan-Meier analysis for OS based on the MRGs signature of melanoma patients in TCGA training cohort **(A)** and GEO validation dataset **(C)**. The distribution of risk score, survival status and expression heatmap of the two MRGs in TCGA training cohort **(B)** and GEO validation dataset **(D)**. **(E,F)** Cox regression analysis of MRGs signature and clinicopathological risk factors in TCGA training cohort **(E)** and GEO validation dataset **(F)**.

WARS, and worse overall survival than those in the low-risk group (**Figures 5C,D**). To determine whether MRGs signature could act as an independent prognostic factor, MRGs signature and clinicopathological factors including age, sex, and stage were entered into a univariate Cox regression analysis, indicating that the MRGs signature was significantly associated with OS (HR = 2.673, 95% CI = 1.614–4.428, $P < 0.001$; **Figure 5E**). A multivariate Cox regression analysis revealed that the MRGs signature was an independent prognostic factor (HR = 3.884, 95% CI = 2.236–6.746, $P < 0.001$; **Figure 5E**). These results were consistent in the GEO dataset (univariate Cox regression analysis: HR = 8.255, 95% CI = 2.681–25.415, $P < 0.001$; multivariate Cox regression analysis: HR = 4.143, 95% CI = 1.132–15.168, $P < 0.001$; **Figure 5F**).

GSEA for MRGs Signature

To identify the underlying molecular mechanism of the MRGs signature, we conducted GSEA to compare the high- and low-risk groups in 460 melanoma patients from TCGA dataset. In the high-risk group, no GO terms, KEGG pathways or oncologic signatures were significantly enriched. However, in the low-risk group, 574 GO terms were significantly enriched especially in regulation of type I interferon production, NF-κB pathway and regulation of autophagy **Figure S3A**. 20 KEGG pathways highlighted that antigen processing and presentation, apoptosis, and JAK/STAT signaling pathways were enriched in the low-risk group **Figure S3B**. Moreover, 14 oncogenic signatures were significantly enriched in low-risk group including the CAMP, MEK, P53, and other pathways **Figure S3C**. These significant terms in each module were summarized in **Table S3**.

Construction and Validation of MRGs Nomogram

To construct a clinically applicable method for predicting the prognosis of melanoma patients, independent prognostic predictors including age, stage, and MRGs signature were enrolled to establish a nomogram to predict the survival probability at 3 and 5 years based on TCGA training cohort (**Figure 6A**). The calibration plots (**Figures 6B,C**) showed an excellent match with the ideal curve at 3- and 5-years survival rates in TCGA training cohort. In the validation dataset, the calibration plots also showed good agreement between the predicted and actual outcome of 5-years OS rates (**Figure 6D**). The C index of the nomogram was 0.707 in TCGA training cohort. Moreover, the ROC curve showed a more favorable predictive ability for the 3-years OS rates (AUC = 0.746) as compared to MRGs signature (AUC = 0.640), age (AUC = 0.607), and stage (AUC = 0.672; **Figure 6E**), as well as for the 5-years OS rates (AUC = 0.697) as compared to MRGs signature (AUC = 0.635), age (AUC = 0.613), and stage (AUC = 0.592; **Figure 6F**). In the validation dataset, the C index of the nomogram for predicting OS was 0.730. The nomogram also has the largest discrimination ability (AUC = 0.813) as compared to MRGs signature (AUC = 0.723), age (AUC = 0.637), and stage (AUC = 0.680) for 5-years OS rates (**Figure 6G**). Decision curve analysis results in both TCGA training cohort and the GEO validation dataset suggested that our nomogram could be more beneficial than traditional stages in predicting the survival for melanoma patients (**Figures 6H–J**).

DISCUSSION

Altered metabolism is considered to be related to cancer cell survival and growth (4, 18). Various metabolisms, such as the glucose and glutamine metabolism of cancer cells, can be significantly changed by tumor microenvironment across an individual tumor (19, 20). However, the tumor can also acclimatize itself to metabolic reprogramming, suggesting the specificity of metabolic targets to each cancer (20). Metabolic gene signatures have been shown to have a prognostic role in cancers (21, 22). Melanoma is a type of tumor highly related to metabolic reprogramming, including glycolysis, protein/amino acid metabolism, and lipid metabolism (23). The melanoma cells need to increase oxidative stress and undergo metabolic changes during metastasis (24). A recent study showed that metabolic differences among melanoma cells conferred differences in metastatic potential, which was due to the differences in the function of the *MCT1* transporter (25). All these studies highlight the potential value of generating a metabolism-related model for the prognosis prediction of melanoma.

In the present study, we first identified 207 metabolism-related genes, based on TCGA, significantly correlated with prognosis in the univariate Cox regression analysis. In GSE15605, which contains the largest normal samples in the GEO database, 849 DEGs were identified by a volcano plot. Then the intersected genes between DEGs and prognostic MRGs were entered into a LASSO regression and multivariate Cox regression. Ultimately, MRGs signature, including *WARS* and *MGST1*, were obtained. According to the median risk score of MRGs signature, 460 melanoma patients in TCGA were divided into the high- or low-risk group. GSEA results showed a series of signaling pathway changes in the low-risk group including NF-κB pathway, regulation of autophagy, apoptosis, and JAK/STAT signaling pathways.

The role of *WARS* and *MGST1* in melanoma has not been reported. The *WARS* gene encodes tryptophanyl-tRNA synthetase, an aminoacyl-tRNA synthetase involved in protein synthesis and the regulation of RNA transcription and translation (26). *WARS* has been reported to be an IFN-γ-inducible enzyme, which protects indoleamine-2,3-dioxygenase expressing cells from tryptophan catabolism and mediates high-affinity tryptophan uptake into human cells (26, 27). Considering that tryptophan represents a powerful immunosuppressive mechanism hijacked by tumors for protection against immune destruction, *WARS* mediated tryptophan metabolism plays an essential role in immuno-oncology (28). *WARS* is dysregulated in different cancers with paradoxical roles on tumor invasiveness (29–34). In colorectal cancer, *WARS* was negatively correlated with lymph node metastasis and tumor stage, which could be

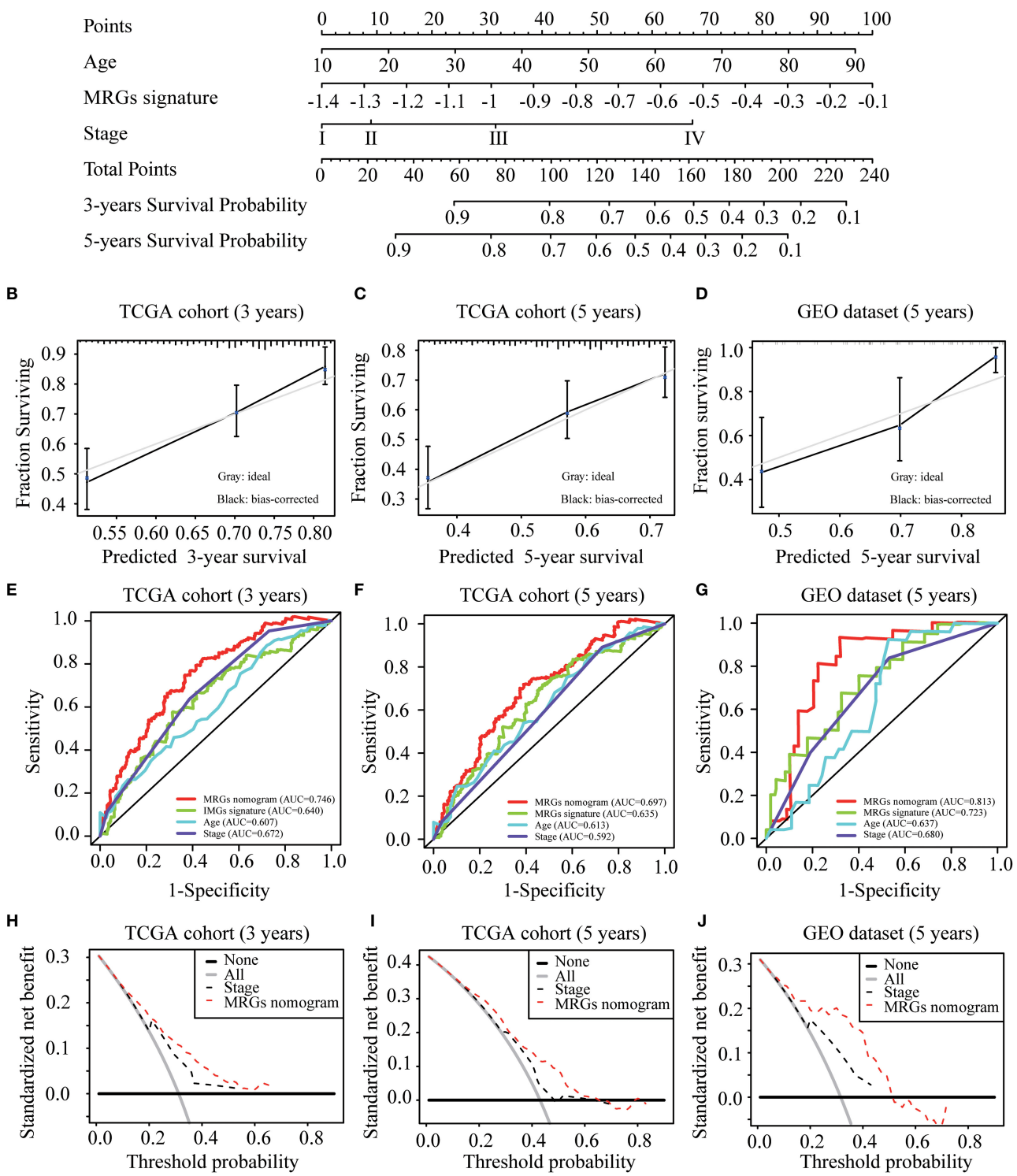

FIGURE 6 | Development and validation of MRGs nomogram. **(A)** Development of MRGs nomogram. **(B–D)** Calibration plots for predicting 3-years **(B)**, 5-years **(C)** OS in the TCGA training cohort and 5-years OS in the GEO validation dataset **(D)**. **(E–G)** Receiver operating characteristic (ROC) curves of the MRGs nomogram, MRGs signature, age and stage at 3-years **(E)** and 5-years **(F)** OS in the TCGA training cohort and 5-years OS in the GEO validation dataset **(G)**. **(H–J)** Decision curve analysis of the MRGs nomogram and stage at 3-years **(H)** and 5-years **(I)** prediction in the TCGA training cohort and 5-years prediction in the GEO validation dataset **(J)**.

explained by its antiangiogenic properties (31). Moreover, down-regulation of *WARS* by hypoxia could be a factor responsible for pancreatic cancer with high metastatic ability (35). However, in oral cancer, *WARS* is overexpressed and positively correlates with cancer invasiveness (32). Through bioinformatics analysis, we identified that *WARS* was a protective gene in melanoma. *WARS* prevents tumor cell progression, probably by inhibiting the neoangiogenic potential of the tumor (36). Further mechanism studies are needed to elucidate the paradoxical roles of *WARS* in tumors.

The *MGST1* gene encodes Microsomal Glutathione Transferase 1, a member of the *MAPEG* family (membrane associated proteins in eicosanoid and glutathione metabolism), which plays a well-established role in the conjugation of electrophiles and oxidative stress protection (37). The enzyme exhibits glutathione transferase and peroxidase activity, and shows activity against a variety of active substrates, from lipid peroxidation to cytostatic drugs (38). *MGST1* is overexpressed in various cancers (38, 39) and associated with drug resistance (37). Linnerth et al. suggested that overexpression of *MGST1* has been identified as an early marker in lung cancer (40). Further, Zeng and his colleagues demonstrated *MGST1* knockdown could inhibit lung adenocarcinoma cell proliferation by inactivating the AKT/GSK-3β pathway signaling and promote cell apoptosis by regulating the mitochondrial apoptosis pathway related proteins (39). Moreover, *MGST1* overexpression was correlated to higher metastatic potential in human prostate cancer (41). Surprisingly *MGST1* mRNA or protein cannot be detected in neuroblastoma cells or tissues (42). Here we reported that *MGST1* is a risk factor of melanoma and the detailed mechanism deserved further investigations. Our study provided not only a clinical tool for prognosis predictions but also the theoretical basis for future research studies.

After identifying the two metabolic prognostic genes, an MRGs signature was developed to predict the prognosis of melanoma patients. The MRGs signature was able to stratify OS in both training and validation cohorts and was a risk factor independent of clinicopathologic factors. We next established a nomogram for predicting 3- and 5-years OS based on MRGs signature, age, and stage. The ROC analysis and calibration plots were then applied to verify the prognostic accuracy, showing a good predictive performance of our model. Finally, the decision curve analyses in both training and validation datasets indicated that our model provided more clinical net benefits. Nomograms have been widely used in cancer management and prediction (43, 44). Several nomograms have been established for melanoma in recent years. Clinical and pathological features were applied to construct a nomogram to predict sentinel lymph node metastases in melanoma (45, 46). Nomograms were also developed to identify the risk, recurrence, and mortality in patients with negative sentinel lymph nodes (47, 48). There are two studies establishing models based on long non-coding RNA signatures to predict prognosis in melanoma patients (15, 49). To our knowledge, we conducted the first study to develop a nomogram to predict melanoma prognosis based on MRGs signature and clinicopathologic factors, exhibiting higher prognostic accuracy compared with the tumor-node-metastasis staging system.

Despite the potential clinical benefits of our results, our study has some limitations. We mainly focused on the effect of MRGs on melanoma prognosis; other genes, such as autophagy-related genes and immune-related genes, also contribute to the development and progression of melanoma. Additionally, our study was based on the whole population of melanoma patients, and the application to sub-populations still need investigated. Lastly, multicenter, large-scale prospective clinical trials are needed for further external validation of our nomogram.

In conclusion, a prognostic nomogram incorporating both MRGs signature and clinicopathological features for individual survival prediction was developed and validated, which is superior to the tumor-node-metastasis staging system.

DATA AVAILABILITY STATEMENT

The raw data supporting the conclusions of this article will be made available by the authors, without undue reservation, to any qualified researcher.

AUTHOR CONTRIBUTIONS

GD, XC, and FZ conceived and designed the study. JS and CP contributed to the outline development. FZ and GD analyzed the data and wrote the manuscript. ML, SZ, and YG revised the manuscript. All authors read and approved the final manuscript.

FUNDING

This study was supported by the grants from the National Natural Science Foundation of China (No. 81620108024).

ACKNOWLEDGMENTS

We would like to thank TCGA and GEO projects for data sharing, and thank Editage (www.editage.cn) for English language editing.

SUPPLEMENTARY MATERIAL

The Supplementary Material for this article can be found online at: https://www.frontiersin.org/articles/10.3389/fonc.2020.01710/full#supplementary-material

Figure S1 | Kaplan-Meier curves for disease free survival (DFS) of *WARS* **(A)** and *MGST1* **(B)** in melanoma patients using GEPIA. *N* (high) = 229, *N* (low) = 229. T, tumor; N, normal skin.

Figure S2 | TCGA melanoma patients between high-risk and low-risk group based on the MRGs signature. Kaplan-Meier curves for DFS **(A)**, and the distribution of risk score, survival status and expression heatmap **(B)**.

Figure S3 | Gene set enrichment and pathway analysis (GSEA). GO terms **(A)**, KEGG pathways **(B)**, and oncogenic signatures **(C)**.

REFERENCES

1. Che G, Huang B, Xie Z, Zhao J, Yan Y, Wu J, et al. Trends in incidence survival in patients with melanoma, 1974-2013. *Am J Cancer Res.* (2019) 9:1396–414.
2. Weiss SA, Hanniford D, Hernando E, Osman I. Revisiting determinants of prognosis in cutaneous melanoma. *Cancer.* (2015) 121:4108–23. doi: 10.1002/cncr.29634
3. Tian J, Yang Y, Li MY, Zhang Y. A novel RNA sequencing-based prognostic nomogram to predict survival for patients with cutaneous melanoma: clinical trial/experimental study. *Medicine (Baltimore).* (2020) 99:e18868. doi: 10.1097/MD.0000000000018868
4. Hanahan D, Weinberg RA. Hallmarks of cancer: the next generation. *Cell.* (2011) 144:646–74. doi: 10.1016/j.cell.2011.02.013
5. Ward PS, Thompson CB. Metabolic reprogramming: a cancer hallmark even warburg did not anticipate. *Cancer Cell.* (2012) 21:297–308. doi: 10.1016/j.ccr.2012.02.014
6. Lunt SY, Vander Heiden MG. Aerobic glycolysis: meeting the metabolic requirements of cell proliferation. *Annu Rev Cell Dev Biol.* (2011) 27:441–64. doi: 10.1146/annurev-cellbio-092910-154237
7. Leray H, Gabiache E, Courbon F, Brenot-Rossi I, Colineaux H, Lepage B, et al. FDG-PET/CT identifies predictors of survival in patients with locally advanced cervical carcinoma para-aortic lymph node involvement to increase treatment. *J Nucl Med.* (2020). doi: 10.2967/jnumed.119.238824
8. DeBerardinis RJ, Lum JJ, Hatzivassiliou G, Thompson CB. The biology of cancer: metabolic reprogramming fuels cell growth and proliferation. *Cell Metab.* (2008) 7:11–20. doi: 10.1016/j.cmet.2007.10.002
9. McArthur GA, Puzanov I, Amaravadi R, Ribas A, Chapman P, Kim KB, et al. Marked, homogeneous, and early [18F]fluorodeoxyglucose-positron emission tomography responses to vemurafenib in BRAF-mutant advanced melanoma. *J Clin Oncol.* (2012) 30:1628–34. doi: 10.1200/JCO.2011.39.1938
10. Li X, Wenes M, Romero P, Huang SC, Fendt SM, Ho PC. Navigating metabolic pathways to enhance antitumour immunity and immunotherapy. *Nat Rev Clin Oncol.* (2019) 16:425–41. doi: 10.1038/s41571-019-0203-7
11. Sun W, Jiang YZ, Liu YR, Ma D, Shao ZM. Nomograms to estimate long-term overall survival and breast cancer-specific survival of patients with luminal breast cancer. *Oncotarget.* (2016) 7:20496–506. doi: 10.18632/oncotarget.7975
12. Liu Y, Wu L, Ao H, Zhao M, Leng X, Liu M, et al. Prognostic implications of autophagy-associated gene signature s in non-small cell lung cancer. *Aging (Albany NY).* (2019) 11:11440–62. doi: 10.18632/aging.102544
13. Zhang Z, Cortese G, Combescure C, Marshall R, Lee M, Lim HJ, et al. Overview of model validation for survival regression model with competing risks using melanoma study data. *Ann Transl Med.* (2018) 6:325. doi: 10.21037/atm.2018.07.38
14. Yang J, Pan Z, Zhou Q, Liu Q, Zhao F, Feng X, et al. Nomogram for predicting the survival of patients with malignant melanoma: a population analysis. *Oncol Lett.* (2019) 18:3591–8. doi: 10.3892/ol.2019.10720
15. Yang L, Liu J, Zhang R, Li M, Li Z, Zhou X, et al. Epidemiological and clinical features of 200 hospitalized patients with corona virus disease 2019 outside Wuhan, China: a descriptive study. *J Clin Virol.* (2020) 129:104475. doi: 10.1016/j.jcv.2020.104475
16. Tibshirani R. The lasso method for variable selection in the Cox model. *Stat Med.* (1997) 16:385–95. doi: 10.1002/(sici)1097-0258(19970228)16:4<385::aid-sim380>3.0.co;2-3
17. Fitzgerald M, Saville BR, Lewis RJ. Decision curve analysis. *JAMA.* (2015) 313:409–10. doi: 10.1001/jama.2015.37
18. Boroughs LK, DeBerardinis RJ. Metabolic pathways promoting cancer cell survival and growth. *Nat Cell Biol.* (2015) 17:351–9. doi: 10.1038/ncb3124
19. Hiller K, Metallo CM. Profiling metabolic networks to study cancer metabolism. *Curr Opin Biotechnol.* (2013) 24:60–8. doi: 10.1016/j.copbio.2012.11.001
20. Montrose DC, Galluzzi L. Drugging cancer metabolism: expectations vs. reality. *Int Rev Cell Mol Biol.* (2019) 347:1–26. doi: 10.1016/bs.ircmb.2019.07.007
21. Prusinkiewicz MA, Gameiro SF, Ghasemi F, Dodge MJ, Zeng PYF, Maekebay H, et al. Survival-associated metabolic genes in human papillomavirus-positive head and neck cancers. *Cancers (Basel).* (2020) 12:253. doi: 10.3390/cancers12010253
22. Wang D, Hu B, Hu C, Zhu F, Liu X, Zhang J, et al. Clinical characteristics of 138 hospitalized patients with 2019 novel coronavirus-infected pneumonia in Wuhan, China. *JAMA.* (2020) 323:1061–9. doi: 10.1001/jama.2020.1585
23. Fischer GM, Vashisht Gopal YN, McQuade JL, Peng W, DeBerardinis RJ, Davies MA. Metabolic strategies of melanoma cells: mechanisms, interactions with the tumor microenvironment, and therapeutic implications. *Pigment Cell Melanoma Res.* (2018) 31:11–30. doi: 10.1111/pcmr.12661
24. Piskounova E, Agathocleous M, Murphy MM, Hu Z, Huddlestun SE, Zhao Z, et al. Oxidative stress inhibits distant metastasis by human melanoma cells. *Nature.* (2015) 527:186–91. doi: 10.1038/nature15726
25. Tasdogan A, Faubert B, Ramesh V, Ubellacker JM, Shen B, Solmonson A, et al. Metabolic heterogeneity confers differences in melanoma metastatic potential. *Nature.* (2020) 577:115–20. doi: 10.1038/s41586-019-1847-2
26. Boasso A, Herbeuval JP, Hardy AW, Winkler C, Shearer GM. Regulation of indoleamine 2,3-dioxygenase and tryptophanyl-tRNA-synthetase by CTLA-4-Fc in human CD4+ T cells. *Blood.* (2005) 105:1574–81. doi: 10.1182/blood-2004-06-2089
27. Miyanokoshi M, Yokosawa T, Wakasugi K. Tryptophanyl-tRNA synthetase mediates high-affinity tryptophan uptake into human cells. *J Biol Chem.* (2018) 293:8428–38. doi: 10.1074/jbc.RA117.001247
28. Adam I, Dewi DL, Mooiweer J, Sadik A, Mohapatra SR, Berdel B, et al. Upregulation of tryptophanyl-tRNA synthethase adapts human cancer cells to nutritional stress caused by tryptophan degradation. *Oncoimmunology.* (2018) 7:e1486353. doi: 10.1080/2162402X.2018.1486353
29. Morita A, Miyagi E, Yasumitsu H, Kawasaki H, Hirano H, Hirahara F. Proteomic search for potential diagnostic markers and therapeutic targets for ovarian clear cell adenocarcinoma. *Proteomics.* (2006) 6:5880–90. doi: 10.1002/pmic.200500708
30. Arnouk H, Merkley MA, Podolsky RH, Stoppler H, Santos C, Alvarez M, et al. Characterization of molecular markers indicative of cervical cancer progression. *Proteomics Clin Appl.* (2009) 3:516–27. doi: 10.1002/prca.200800068
31. Ghanipour A, Jirstrom K, Ponten F, Glimelius B, Pahlman L, Birgisson H. The prognostic significance of tryptophanyl-tRNA synthetase in colorectal cancer. *Cancer Epidemiol Biomarkers Prev.* (2009) 18:2949–56. doi: 10.1158/1055-9965.EPI-09-0456
32. Lee CW, Chang KP, Chen YY, Liang Y, Hsueh C, Yu JS, et al. Overexpressed tryptophanyl-tRNA synthetase, an angiostatic protein, enhances oral cancer cell invasiveness. *Oncotarget.* (2015) 6:21979–92. doi: 10.18632/oncotarget.4273
33. Lu S, Wang LJ, Lombardo K, Kwak Y, Kim WH, Resnick MB. Expression of Indoleamine 2, 3-dioxygenase 1 (IDO1) and Tryptophanyl-tRNA Synthetase (WARS) in Gastric Cancer Molecular Subtypes. *Appl Immunohistochem Mol Morphol.* (2019) 28:360–8. doi: 10.1097/PAI.0000000000000761
34. Yang PP, Yu XH, Zhou J. Tryptophanyl-tRNA synthetase (WARS) expression in uveal melanoma - possible contributor during uveal melanoma progression. *Biosci Biotechnol Biochem.* (2020) 84:471–80. doi: 10.1080/09168451.2019.1686967
35. Paley EL, Paley DE, Merkulova-Rainon T, Subbarayan PR. Hypoxia signature of splice forms of tryptophanyl-tRNA synthetase marks pancreatic cancer cells with distinct metastatic abilities. *Pancreas.* (2011) 40:1043–56. doi: 10.1097/MPA.0b013e318222e635
36. Wakasugi K, Slike BM, Hood J, Otani A, Ewalt KL, Friedlander M, et al. A human aminoacyl-tRNA synthetase as a regulator of angiogenesis. *Proc Natl Acad Sci USA.* (2002) 99:173–7. doi: 10.1073/pnas.012602099
37. Morgenstern R, Zhang J, Johansson K. Microsomal glutathione transferase 1: mechanism and functional roles. *Drug Metab Rev.* (2011) 43:300–6. doi: 10.3109/03602532.2011.558511
38. Hetland TE, Nymoen DA, Emilsen E, Kaern J, Trope CG, Florenes VA, et al. MGST1 expression in serous ovarian carcinoma differs at various anatomic sites, but is unrelated to chemoresistance or survival. *Gynecol Oncol.* (2012) 126:460–5. doi: 10.1016/j.ygyno.2012.05.029
39. Zeng B, Ge C, Li R, Zhang Z, Fu Q, Li Z, et al. Knockdown of microsomal glutathione S-transferase 1 inhibits lung adenocarcinoma cell proliferation and induces apoptosis. *Biomed Pharmacother.* (2020) 121:109562. doi: 10.1016/j.biopha.2019.109562
40. Linnerth NM, Sirbovan K, Moorehead RA. Use of a transgenic mouse model to identify markers of human

lung tumors. *Int J Cancer.* (2005) 114:977–82. doi: 10.1002/ijc.20814
41. Chaib H, Cockrell EK, Rubin MA, Macoska JA. Profiling and verification of gene expression patterns in normal and malignant human prostate tissues by cDNA microarray analysis. *Neoplasia.* (2001) 3:43–52. doi: 10.1038/sj.neo.7900126
42. Kelner MJ, Diccianni MB, Yu AL, Rutherford MR, Estes LA, Morgenstern R. Absence of MGST1 mRNA and protein expression in human neuroblastoma cell lines and primary tissue. *Free Radic Biol Med.* (2014) 69:167–71. doi: 10.1016/j.freeradbiomed.2014.01.021
43. Deng G, Yao L, Zeng F, Xiao L, Wang Z. Nomogram for preoperative prediction of microvascular invasion risk in hepatocellular carcinoma. *Cancer Manag Res.* (2019) 11:9037–45. doi: 10.2147/CMAR.S216178
44. Chen L, Zeng F, Yao L, Fang T, Liao M, Long J, et al. Nomogram based on inflammatory indices for differentiating intrahepatic cholangiocarcinoma from hepatocellular carcinoma. *Cancer Med.* (2020) 9:1451–61. doi: 10.1002/cam4.2823
45. Pinero A, Canteras M, Ortiz E, Martinez-Barba E, Parrilla P. Validation of a nomogram to predict the presence of sentinel lymph node metastases in melanoma. *Ann Surg Oncol.* (2008) 15:2874–7. doi: 10.1245/s10434-008-0077-x
46. Naffouje SA, Naffouje R, Chen J, Salti GI. Validation and enhancement of the clinicopathological melanoma nomogram via incorporation of a molecular marker in the primary tumor. *Anticancer Res.* (2016) 36:6603–10. doi: 10.21873/anticanres.11266
47. Bertolli E, de Macedo MP, Calsavara VF, Pinto CAL, Duprat Neto JP. A nomogram to identify high-risk melanoma patients with a negative sentinel lymph node biopsy. *J Am Acad Dermatol.* (2019) 80:722–6. doi: 10.1016/j.jaad.2018.10.060
48. Verver D, van Klaveren D, Franke V, van Akkooi ACJ, Rutkowski P, Keilholz U, et al. Development and validation of a nomogram to predict recurrence and melanoma-specific mortality in patients with negative sentinel lymph nodes. *Br J Surg.* (2019) 106:217–25. doi: 10.1002/bjs.10995
49. Yang S, Xu J, Zeng X. A six-long non-coding RNA signature predicts prognosis in melanoma patients. *Int J Oncol.* (2018) 52:1178–88. doi: 10.3892/ijo.2018.4268

Conflict of Interest: The authors declare that the research was conducted in the absence of any commercial or financial relationships that could be construed as a potential conflict of interest.

frontiers in Oncology

ORIGINAL RESEARCH
published: 30 October 2020
doi: 10.3389/fonc.2020.567512

Prognostic Implications of Novel Ten-Gene Signature in Uveal Melanoma

Huan Luo[1,2,3], *Chao Ma*[2,4†], *Jinping Shao*[1*] and *Jing Cao*[1*]

[1] Department of Anatomy, College of Basic Medicine, Zhengzhou University, Zhengzhou, China, [2] Charité—Universitätsmedizin Berlin, Corporate Member of Freie Universität Berlin, Humboldt-Universität zu Berlin, and Berlin Institute of Health, Berlin, Germany, [3] Klinik für Augenheilkunde, Charité—Universitätsmedizin Berlin, Corporate Member of Freie Universität Berlin, Humboldt-Universität zu Berlin, and Berlin Institute of Health, Berlin, Germany, [4] Charité—Universitätsmedizin Berlin, BCRT—Berlin Institute of Health Center for Regenerative Therapies, Berlin, Germany

Background: Uveal melanoma (UM) is the most common primary intraocular cancer in adults. Genomic studies have provided insights into molecular subgroups and oncogenic drivers of UM that may lead to novel therapeutic strategies.

Methods: Dataset TCGA-UVM, download from TCGA portal, were taken as the training cohort, and dataset GSE22138, obtained from GEO database, was set as the validation cohort. In training cohort, Kaplan–Meier analysis and univariate Cox regression model were applied to preliminary screen prognostic genes. Besides, the Cox regression model with LASSO was implemented to build a multi-gene signature, which was then validated in the validation cohorts through Kaplan–Meier, Cox, and ROC analyses. In addition, the correlation between copy number aberrations and risk score was evaluated by Spearman test. GSEA and immune infiltrating analyses were conducted for understanding function annotation and the role of the signature in the tumor microenvironment.

Results: A ten-gene signature was built, and it was examined by Kaplan–Meier analysis revealing that significantly overall survival, progression-free survival, and metastasis-free survival difference was seen. The ten-gene signature was further proven to be an independent risk factor compared to other clinic-pathological parameters via the Cox regression analysis. Moreover, the receiver operating characteristic curve (ROC) analysis results demonstrated a better predictive power of the UM prognosis that our signature owned. The ten-gene signature was significantly correlated with copy numbers of chromosome 3, 8q, 6q, and 6p. Furthermore, GSEA and immune infiltrating analyses showed that the signature had close interactions with immune-related pathways and the tumor environment.

Conclusions: Identifying the ten-gene signature (SIRT3, HMCES, SLC44A3, TCTN1, STPG1, POMGNT2, RNF208, ANXA2P2, ULBP1, and CA12) could accurately identify patients' prognosis and had close interactions with the immunodominant tumor environment, which may provide UM patients with personalized prognosis prediction and new treatment insights.

Keywords: uveal melanoma, gene signature, risk score, prognosis, biomarkers

OPEN ACCESS

Edited by:
Nihal Ahmad,
University of Wisconsin-Madison,
United States

Reviewed by:
Takami Sato,
Thomas Jefferson University,
United States
Gagan Chhabra,
University of Wisconsin-Madison,
United States

***Correspondence:**
Jinping Shao
shaojinping@zzu.edu.cn
Jing Cao
caojing73@126.com

†ORCID:
Chao Ma
orcid.org/0000-0003-1444-4668

Specialty section:
This article was submitted to Skin Cancer, a section of the journal Frontiers in Oncology

Received: *23 June 2020*
Accepted: *15 September 2020*
Published: *30 October 2020*

Citation:
Luo H, Ma C, Shao J and Cao J (2020) Prognostic Implications of Novel Ten-Gene Signature in Uveal Melanoma. Front. Oncol. 10:567512. doi: 10.3389/fonc.2020.567512

INTRODUCTION

Uveal melanoma (UM) is the most common primary intraocular cancer in adults, and the second most common melanoma subtype after cutaneous melanoma, accounting for 5% of all melanomas (1–3). Treatment approaches for primary UM include surgery and radiotherapy, which can often achieve excellent local tumor control (4). Nevertheless, nearly half of UM patients still develop tumor metastasis, mainly in the liver (3). Metastases have a predilection for the liver and once they have developed, median survival is about 1 year (5). Existing treatments for UM are not effective against tumor metastases (6), therefore, most research shifted their efforts on the development of targeted therapies or immunotherapy methods, such as immune checkpoint inhibitors, vaccination, or adoptive T cell therapy (7–11). Identifying potential biomarkers of UM may provide critical information for early detection of relapse or treatment (12). At present, although some studies have clarified some important genes and pathways of UM, the prognosis of it remains poor (12–14). Therefore, there is an urgent need to reveal new markers to assess UM prognosis.

During the past few decades, genetic or epigenetic alterations have been confirmed to be associated with the tumorigenesis and progression of UM (14). Gene mutations and chromosomal copy number variations are closely related to UM prognosis. According to reports, GNAQ and GNA11 mutations can promote cell proliferation and metastasis (15). The loss of one copy of chromosome 3 (monosomy 3) in UM is associated with an increased risk of metastasis and poor prognosis (16). In addition, other chromosomal abnormalities have been shown to correlate with poor prognosis and these include 6q loss, lack of 6p gain, 1p loss, and 16q loss (16–20). Therefore, further exploration of gene mutation and copy number variation in UM can provide incisive information for prognosis.

Here, we conduct comprehensive mining of the TCGA and GEO database to determine the minimum number of potentially robust genes that can be used to predict the prognosis of UM patients. Importantly, we used the LASSO algorithm, which can effectively analyze high-dimensional sequencing data (21). Besides, we assessed the accuracy of this ten-gene signature and validated it by compared to variants of chromosomes 3 and 8q, and testing in a validation cohort. Moreover, GSEA and immune infiltrating analyses were conducted to explore the role of the signature in the tumor microenvironment.

MATERIALS AND METHODS

Data Mining From the Cancer Genome Atlas (TCGA) and Gene Expression Omnibus (GEO) Databases

The gene expression profiles of UM from 80 patients, along with their clinical and curated survival data were downloaded from TCGA Xena Hub (https://tcga.xenahubs.net) with cohort name: TCGA-UVM. Besides, we researched the GEO database by setting a filter: (1) more than 60 cases; (2) with expression profiling data; (3) with survival data. Finally, GSE22138 with 63 cases was chosen for this study. In our research, TCGA-UVM was used as the training cohort, while GSE22138 was taken as the validation cohort. The research was conducted in accordance with the Declaration of Helsinki, and was approved by the Ethics Committee of Zhengzhou University.

Identification and Validation of Prognostic Gene Signature

To begin with, in the training cohort, Kaplan-Meier analysis was applied to screen the potential prognostic genes based on overall survival, disease-specific survival, and progression-free survival, respectively. Only genes that showed significant in all overall, disease-specific, and progression-free survival analyses were considered to pass Kaplan–Meier analysis screening. $P < 0.0001$ in the log-rank test was considered as significant. Also, univariate Cox regression analysis was performed on the training cohort to find potential prognostic genes ($p < 0.0001$). Same as before, only genes that showed significant in all overall, disease-specific, and progression-free survival analyses were considered to pass univariate Cox regression analysis screening. The intersected genes of identified in Kaplan–Meier and univariate Cox analyses were then entered into the LASSO Cox regression model analysis, which was implemented in the training cohort utilizing R software and the "glmnet" package. 10-fold cross-validation was applied to detect the best penalty parameter lambda (21–24). Based on the detected optimal lambda, we could obtain a list of prognostic genes with correlation coefficients from gene expression and patient survival data.

The risk score of each patient was calculated by a linear combination of the expression level of each gene weighted by its multivariate LASSO regression coefficient. Using the median risk score as the cut-off point, the patients in the training cohort were distributed to high-risk or low-risk groups, and Kaplan–Meier analysis was applied to evaluate the survival difference between the two groups. Besides, Cox and ROC analyses were conducted to further assess the prognostic value of the gene signature in training cohort. Subsequently, we validated the prognostic value of the gene signature in the validation cohort. The same formula was conducted to compute risk scores like that in the training cohort. Kaplan–Meier, Cox, and ROC analyses were implemented as described earlier.

In UM, chromosomal aberrations and gene mutations have been shown to be closely related to treatment options and prognosis. In Robertson's research, the status of chromosome 3, 8q, 6q, 6p, and 1p of each patient in the TCGA-UVM cohort has been studied and specifically described (16). The Spearman rank correlation coefficient was applied to assess the correlation between copy number aberrations and risk score, further evaluating the prognostic value of the gene signature identified in this study. $P < 0.05$ was considered statistically significant.

Gene Set Enrichment Analysis

The Hallmark (v7.1) and KEGG (v7.1) gene set collections were obtained from the Molecular Signatures Database v7.1 download page (https://www.gsea-msigdb.org/gsea/downloads.jsp). GSEA was performed based on the downloaded gene set collections using GSEA software (v4.0.3, https://www.gsea-msigdb.org/).

The training cohort was taken for GSEA to reveal the functions and pathways in the differentially expressed genes between high-risk and low-risk groups. According to the GSEA User Guide, gene sets with | NES |> 1, NOM $p < 0.05$, and FDR $q < 0.25$ were considered significant.

Correlation of Risk Score With the Proportion of 20 Kinds of Tumor-Infiltrating Immune Cells (TICs)

The CIBERSORT calculation method was used to estimate the 20 kinds of TICs abundance distribution of all tumor samples in the training cohort. After quality filtering ($p < 0.05$) was performed on all the samples of TCGA-UVM, 36 samples were selected for the next analyses.

Statistical Analysis

All statistical calculations in this study were performed in R software. Kaplan–Meier analysis was performed to examine the prognostic differences between the groups, and the p-value was checked in the log-rank test. Univariate and multivariate Cox analyses were conducted to illustrate the relationship between the gene signature risk score and UM prognosis. The ROC curves were plotted with the "pROC" R package, to assess the sensitivity and specificity of the risk score for prognosis prediction. The area under the ROC curve (AUC) was used as an indicator of prognostic accuracy. The correlation between 20 kinds of TICs were examined by Pearson coefficient test. Spearman coefficient test was used for the correlation test between the TICs proportion and risk score. The Wilcoxon rank-sum test verified the differentiation of 20 kinds of immune cells between low and high-risk groups. In addition to noted before, all analyses $p < 0.05$ was a statistically significant threshold.

RESULTS

Clinical Characteristics

The flowchart of the present research is shown in **Figure 1**. Eighty UM cases that came from TCGA-UVM were taken as the training cohort. The dataset GSE22138 with 63 UM patients was used as the validation cohort. The detailed clinical characteristics of both cohorts were summarized in **Table 1**.

Construction of Prognostic Signature From Training Cohort

Kaplan–Meier and univariate Cox regression analysis were performed on 80 patients in the training cohort to assess the prognostic relationship between gene expression profiles and overall survival, disease-specific survival, and progression-free survival. Four hundred and twenty-three genes were extracted from the Kaplan–Meier analysis (**Supplementary Table 1**), while, 283 genes were identified significant in the Cox regression analysis (**Supplementary Table 2**). Taking together, 110 genes in the intersection of the two results are defined as potential prognostic genes for next analyses (**Supplementary Table 3**). These genes were then subjected to LASSO Cox regression analysis, and regression coefficients were calculated. The coefficient of each gene was plotted in **Figure 2A**. The model achieved the best performance when it included 10 genes (**Figure 2B**). These genes, their corresponding coefficients, and genomic location were shown in **Table 2**.

Prognostic Value of the Ten-Gene Signature in the Training and Validation Cohorts

According to the gene expression level, and the risk coefficient of each gene, the risk score of each patient was calculated. The median risk score was the cut-off value for assigning patients to high-risk or low-risk groups. The prognostic value of the risk score was evaluated by comparing the survival differences between the high-risk group and the low-risk group.

The distribution of risk scores and overall survival status and the expression profiles of the ten-gene signature of the patients in the training cohort were plotted in **Figure 3A**. As shown in the figure, there are more deceased in high-risk patients, and the survival time is shorter than that of low-risk patients. The heat map shows that SIRT3, HMCES, SLC44A3, TCTN1, STPG1, POMGNT2, and RNF208 were under expressed in high-risk patients, while, ANXA2P2, ULBP1, and CA12 were highly expressed in high-risk patients. In addition, we examined the performance of these ten-gene signature in predicting progression-free survival in the training cohort. As shown in **Figure 3B**, in the high-risk group, more events happened, and shorter survival time gained. The pattern did consistent with that in predicting overall survival. Furthermore, we checked the predictive power of this ten-gene signature for metastasis-free survival in the validation cohort. It could be seen that there were more metastasis events occurred in the high-risk group than in the low-risk group, and the survival time of the high-risk group was also shorter (**Figure 3C**).

As plotted in **Figure 4A**, Kaplan–Meier survival analysis in the training cohort showed that the overall survival of patients in the high-risk group was poorer than that in the low-risk group ($p < 0.0001$, **Figure 4A**). Also, an unfavorable progression-free survival was seen in the training cohort ($p < 0.0001$, **Figure 4B**). To further explore the efficacy of the ten-gene signature in predicting prognosis (metastasis-free survival) in UM patients, we tested the ten-gene signature in the validation cohort. Adopting the same classification method, patients were divided into high-risk and low-risk groups based on the median risk score. Consistent with previous results, patients in the high-risk group showed significantly worse metastasis-free survival than patients in the low-risk group ($p < 0.0001$, **Figure 4C**).

Univariate and multivariate Cox analyses were conducted in the training cohort based overall survival and progression-free survival, and validation cohort based on metastasis-free survival, using the available co-variables including risk score, age, gender, T classification, tumor stage, tumor thickness, tumor diameter, tumor side, tumor location, extrascleral extension, or retinal detachment to detect whether our ten-gene signature had the prognostic capacity that was independent from the clinic-pathologic characteristics. In the training cohort, both univariate and multivariate Cox regression analyses indicated that the ten-gene signature was a powerful variable associated with overall

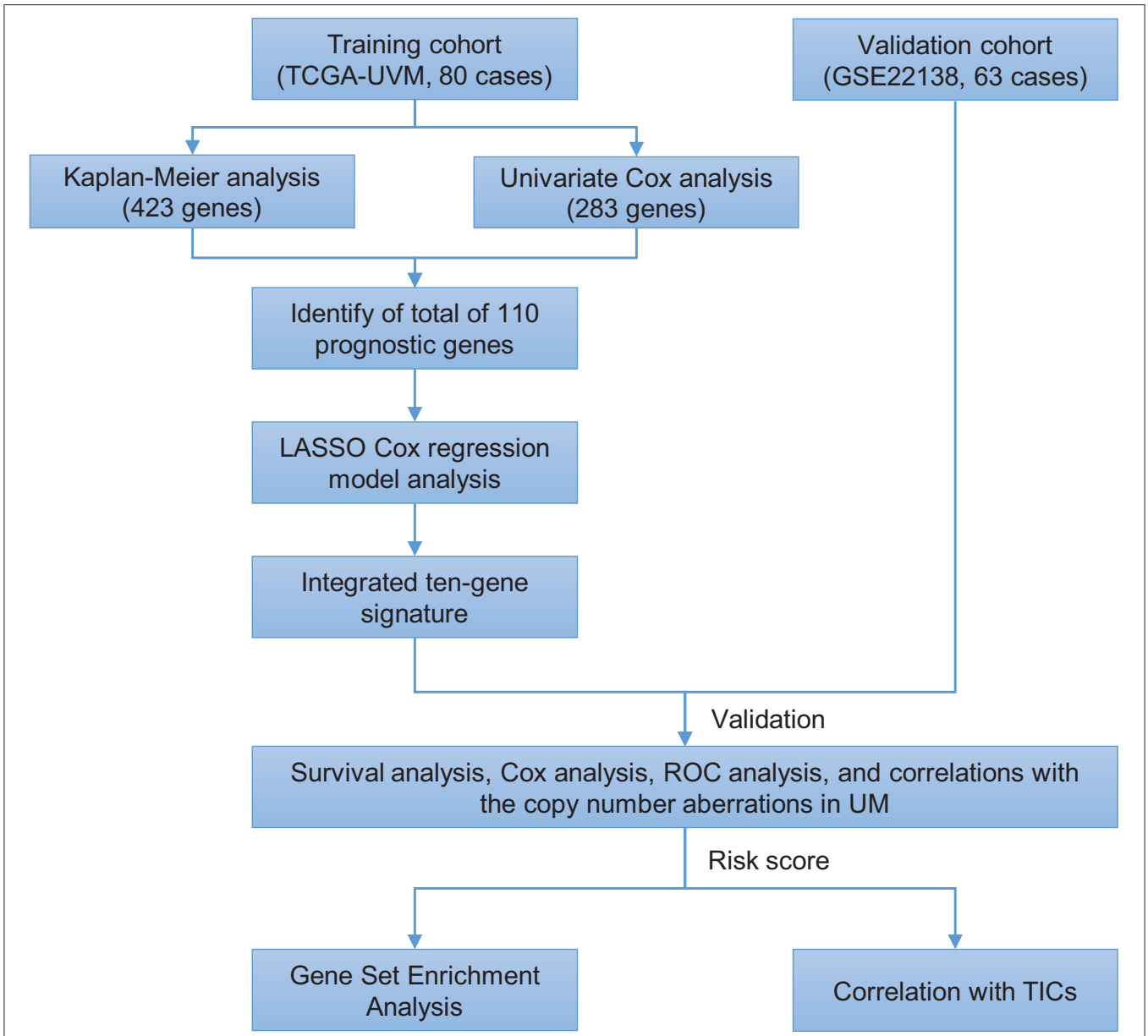

FIGURE 1 | Brief flow chart of this study. The study was performed using TCGA-UVM and GSE22138 cohorts. The training cohort was applied to detect prognostic genes. LASSO regression model was for establishing a prognostic signature based on the prognostic genes. Then we validated the prognostic signature we established in the validation cohort. Finally, GSEA and TIC analysis were implemented to explore potential mechanisms further on the prognosis signature we found. LASSO, the least absolute shrinkage and selection operator Cox regression model; ROC, receiver operating characteristic; TICs, tumor-infiltrating immune cells; UM, uveal melanoma; GSEA, Gene Set Enrichment Analysis.

survival (HR = 4.893, 95% CI = 2.749–8.710, $p < 0.001$, and HR = 5.623, 95% CI = 2.687–11.764, $p < 0.001$, respectively; **Figure 5A**), and progression-free survival (HR = 2.432, 95% CI = 1.766–3.349, $p < 0.001$, and HR = 2.558, 95% CI = 1.658–3.946, $p < 0.001$, respectively; **Figure 5B**). Consistent with that in the training cohort, the ten-gene signature displayed pronounced capability in the validation cohort in predicting metastasis-free survival (**Figure 5C**). These results proved that the ten-gene signature was to be a strong and independent variable.

Subsequently, we conducted ROC analyses to assess how the ten-gene signature could behave in predicting prognosis. As shown in **Figure 6A**, the area under the ROC curve (AUC) of the ten-gene risk score model performed on overall survival in the training cohort was 0.916, which was superior to those of age, gender, stage, T classification, tumor thickness, tumor diameter, and extrascleral extension (0.609, 0.611, 0.591, 0.603, 0.579, 0.611, and 0.556, respectively). Consistently, in the prediction model of progression-free survival predicted in the training cohort,

TABLE 1 | Clinical characteristics of patients involved in the study.

Characteristics	Training cohort (TCGA-UVM, $n = 80$)	Validation cohort (GSE22138, $n = 63$)
Age at diagnosis, years		
<60	36 (45.00%)	28 (44.44%)
≥60	44 (55.00%)	35 (55.56%)
Unknown	0 (0.00%)	0 (0.00%)
Gender		
Female	35 (43.75%)	24 (38.10%)
Male	45 (56.25%)	39 (61.90%)
Unknown	0 (0.00%)	0 (0.00%)
Stage		
I	0 (0.00%)	NA
II	36 (45.00%)	NA
III	40 (50.00%)	NA
IV	4 (5.00%)	NA
Unknown	0 (0.00%)	NA
T classification		
T1	0 (0.00%)	NA
T2	4 (5.00%)	NA
T3	36 (45.00%)	NA
T4	38 (47.50%)	NA
Unknown	2 (2.50%)	NA
N classification		
N0	76 (95.00%)	NA
N1	0 (0.00%)	NA
Unknown	4 (5.00%)	NA
M classification		
M0	73 (91.25%)	28 (44.44%)
M1	3 (3.75%)	35 (55.56%)
Unknown	4 (5.00%)	0 (0.00%)
Extrascleral extension		
No	68 (85.00%)	48 (76.19%)
Yes	7 (8.75%)	5 (7.94%)
Unknown	5 (6.25%)	10 (15.87%)
Tumor basal diameter, mm		
<12	6 (7.50%)	11 (17.46%)
≥12	73 (91.25%)	42 (66.67%)
Unknown	1 (1.25%)	10 (15.87%)
Tumor thickness		
<8	15 (18.75%)	3 (4.76%)
≥8	65 (81.25%)	60 (95.24%)
Unknown	0 (0.00%)	0 (0.00%)
Tumor side		
Right	NA	30 (47.62%)
Left	NA	33 (52.38%)
Unknown	NA	0 (0.00%)
Tumor location		
On equator	NA	42 (66.67%)
Anterior to equator	NA	3 (4.76%)
Posterior to equator	NA	9 (14.29%)
Other	NA	4 (6.35%)
Unknown	NA	5 (7.94%)
Retinal detachment		
No	NA	22 (34.92%)
Yes	NA	36 (57.14%)
Unknown	NA	5 (7.94%)

the ten-gene signature risk score also showed a powerful ability with AUC = 0.739, which was far better than other variates (**Figure 6B**). This finding was also confirmed in validation cohort for metastasis-free survival predication (AUC = 0.785, **Figure 6C**).

Furthermore, we performed correlation analyses to assess the relationship between the ten-gene signature and status of chromosome copy number aberrations. The status of chromosome copy number aberrations of each patient in the TCGA-UVM cohort was downloaded from Robertson's publication (**Supplementary Table 4**) (16). Spearman test was used to assess the correlation between copy chromosome numbers and the risk score. The results showed that the ten-gene signature was significantly correlated with copy numbers of chromosome 3, 8q, 6q, and 6p (**Figure 7**). Specifically, the gene signature displayed negative correlations with the copy number of chromosome 3 ($R = -0.69$, $p = 1e{-}12$), 6q ($R = -0.24$, $p = 0.031$), and 6p ($R = -0.51$, $p = 1.2e{-}06$) (**Figures 7A,C,D**), while, showed positive correlation with chromosome 8q copy number ($R = 0.51$, $p = 1.3e{-}06$) (**Figure 7B**).

Gene Set Enrichment Analysis With the Ten-Gene Signature

In view of the negative correlation between the level of the ten-gene signature risk score and the prognosis of UM patients, the GSEA was conducted between the high and the low-risk groups. As displayed in **Figure 8A** and **Supplementary Table 5**, all significantly enriched gene sets of HALLMARK collection were seen in the high-risk group in pathways relate to immune response, inflammatory response, reactive oxygen species, notch signaling, glycolysis, IL-6/JAK/STAT3 signaling, and allograft rejection. For HALLMARK collection defined by the Molecular Signatures Database, all gene sets were also enriched in the high-risk score group. These pathways were mostly associated with p53 signaling, autoimmune disease, proteasome, natural killer cell, cytosolic DNA-sensing, allograft rejection, leishmania infection, and glycolipid metabolism (**Figure 8B** and **Supplementary Table 6**). These findings indicated that the risk score was potentially closely related to the status of tumor microenvironment.

Correlation of Risk Score With the Proportion of Tumor-Infiltrating Immune Cells (TICs)

To further check the correlation between the risk score and the immune microenvironment, as shown in **Figure 9**, we used the CIBERSORT algorithm to analyze the proportion of tumor-infiltrating immune subpopulations and constructed 20 immune cell profiles in UM samples. Combining the results of correlation analysis (**Figure 10A**, **Supplementary Table 7**) and difference analysis (**Figure 10B**), a total of three TICs were associated with ten-gene signature risk score (**Figure 10C**). Among them, T cells CD4 memory activated was positively correlated with risk score, while, Monocytes and Mast cells resting were negatively correlated with risk score.

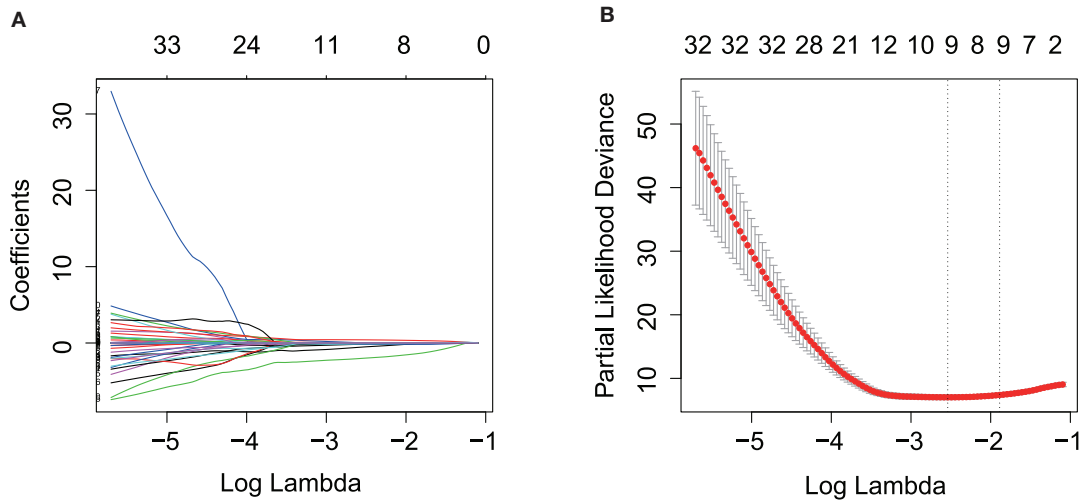

FIGURE 2 | Prognostic gene signature was established by LASSO regression analysis. **(A)** LASSO coefficient profiles of the 110 genes in training cohort. **(B)** A coefficient profile plot was generated against the log (lambda) sequence. Selection of the optimal parameter (lambda) in the LASSO model for training cohort. LASSO, the least absolute shrinkage and selection operator Cox regression model.

TABLE 2 | Genes in the prognostic gene signatures.

Gene symbol	Full name	Risk coefficient	Genomic location (GRCh38/hg38)
STPG1	Sperm Tail PG-Rich Repeat Containing 1	−0.150605911	chr1:24,356,999–24,416,934
HMCES	5-Hydroxymethylcytosine Binding, ES Cell Specific	−0.526265796	chr3:129,278,816–129,306,186
ANXA2P2	Annexin A2 Pseudogene 2	0.017480411	chr9:33,624,225–33,625,534
CA12	Carbonic Anhydrase 12	0.414736428	chr15:63,321,378–63,382,110
RNF208	Ring Finger Protein 208	−0.098017226	chr9:137,220,247–137,221,581
SLC44A3	Solute Carrier Family 44 Member 3	−0.175213008	chr1:94,820,342–94,895,247
TCTN1	Tectonic Family Member 1	−0.171507956	chr12:110,614,027–110,649,430
POMGNT2	Protein O-Linked Mannose N-Acetylglucosaminyltransferase 2 (Beta 1,4–)	−0.106148114	chr3:43,079,229–43,106,083
ULBP1	UL16 Binding Protein 1	0.037591702	chr6:149,963,943–149,973,715
SIRT3	Sirtuin 3	−2.002826257	chr11:215,030–236,931

DISCUSSION

In the present study, we built an UM prognostic signature by comprehensively analyzing the TCGA and GEO. By investigating the relationship using Kaplan–Meier, univariate Cox analyses, and LASSO Cox regression model between the patients' prognosis and gene expression in the training cohort, we obtained a ten-gene signature that was pronounced related to outcome. By applying this signature in the training cohort, statistical significance was observed in univariate and multivariate Cox analysis, ROC analysis, and Kaplan–Meier curve between high-risk and low-risk groups. The prognostic ability of the ten-gene signature was also validated in the validation cohort, showing the broadness and effectiveness of the ten-gene signature in predicting UM prognosis. In addition, we found that the risk score was correlated with the copy number of chromosome 3 negatively, and chromosome 8q positively, which further indicates the significance of the signature we found. Then the GSEA and immune infiltration analyses showed that the ten-gene signature risk score might be immune-related and involved in the tumor microenvironment in UM patients. For research in gene-signature of UM, we are the first to apply chromosomal variation to perform validation of gene-signature reliability. Such work we have done aimed to guide future research in UM.

After we constructed the ten-gene signature, we firstly confirmed its capacity to distinguish the prognosis of patients effectively. As shown in **Figure 3A**, the high-risk zone not only counted more deaths, but also the patients in it presented a shorter survival time than that in the low-risk zone. Moreover, the heatmap indicated that each of these ten genes had a

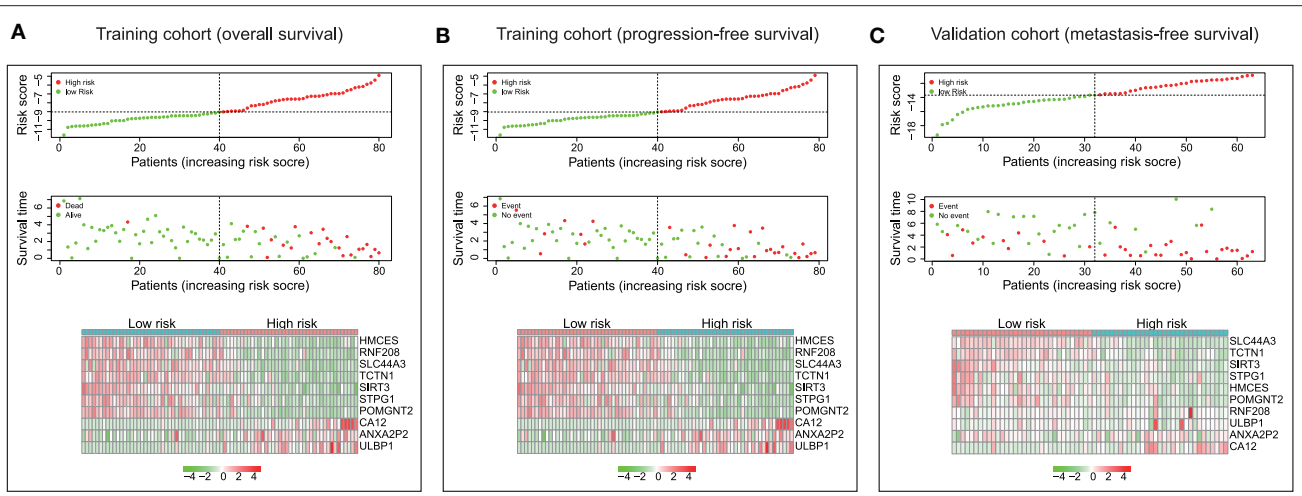

FIGURE 3 | Characteristics of the ten-gene signature. (Upper and middle) The distribution of ten-gene risk score and patients' survival time, and events for training cohort based on overall survival **(A)**, training cohort based on progression-free survival **(B)**, and validation cohort based on metastasis-free survival **(C)**. According to the median risk score, patients were divided into low-risk and high-risk groups. The left side of the black dotted line is the low-risk group, and the right side is the high-risk group. (Bottom) Heatmaps were plotted to illustrate the ten-gene expression profiles in the training cohort based on overall survival **(A)**, training cohort based on progression-free survival **(B)**, and validation cohort based on metastasis-free survival **(C)**.

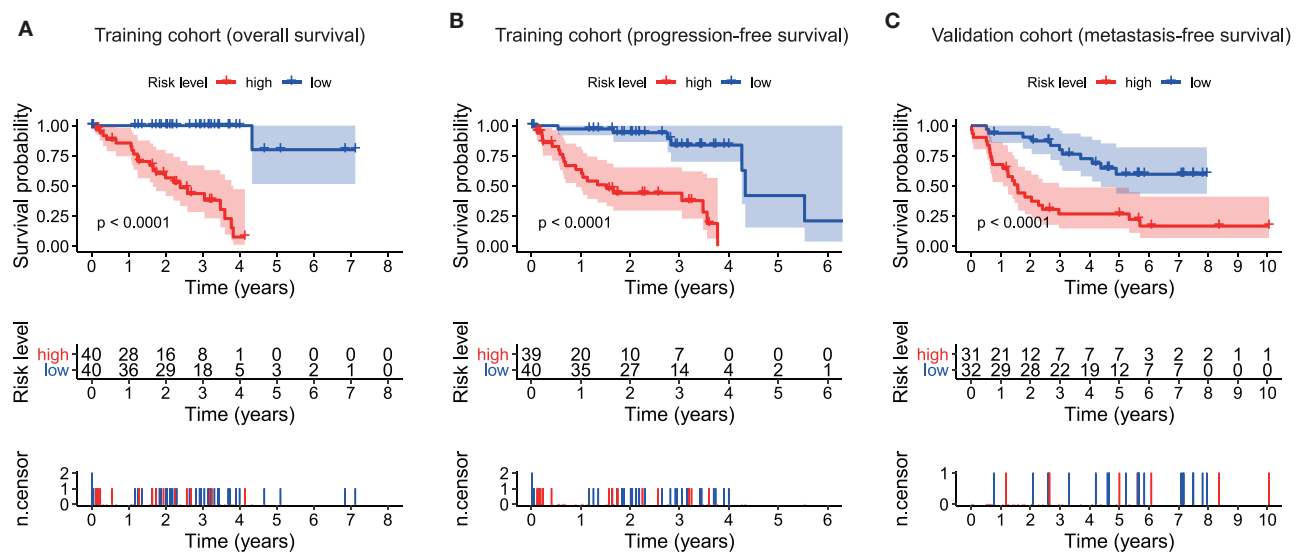

FIGURE 4 | Kaplan–Meier survival analyses based on the ten-gene signature. **(A)** Training cohort based on overall survival. **(B)** Training cohort based on progression-free survival. **(C)** Validation cohort based on metastasis-free survival. Differences between curves were detected by two-side log-rank test.

differential expression pattern between the low-risk and high-risk groups. Importantly, this ten-gene signature also owned pronounced performance in the training cohort for predicting progression-free survival (**Figure 3B**), and in the validation cohort for metastasis-free survival (**Figure 3C**).

In addition, we examined the prognostic value of the ten-gene signature by Kaplan–Meier analysis in the training cohort based on overall survival and progression-free survival, and in the validation cohort based on metastasis-free survival, finding its significantly predicting ability in UM patients (**Figure 4**). Furthermore, univariate and multivariate analyses were performed in the three cohorts to confirm that whether our ten-gene signature can be an independent from other variables in predicting UM outcome. As plotted in **Figure 5**, no matter in training cohort or validation cohort, no matter based on overall survival, progression-free survival, or metastasis-free survival, whether it is univariate or multivariate Cox regression analysis, the variable of risk score was always statistically significant. The

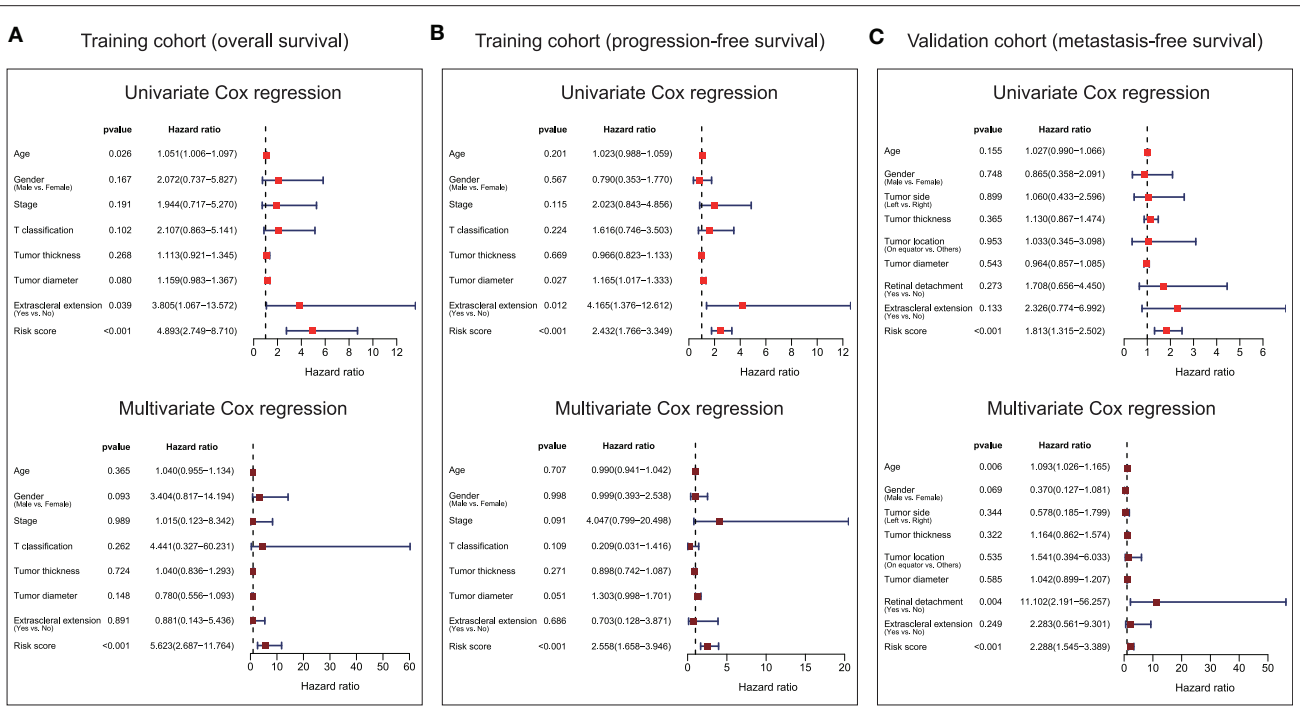

FIGURE 5 | Forest plot summary of univariate and multivariate Cox analyses of prognosis. Univariate (upper) and multivariate (bottom) analyses were carried out using the ten-gene signature and clinical covariates in the training cohort based on overall survival **(A)**, training cohort based on progression-free survival **(B)**, and validation cohort based on metastasis-free survival **(C)**. Colored solid squares represent HR, and the horizontal line across the HR represents the 95% CI. All *p*-values were calculated using the Cox regression hazards analysis. HR, hazard ratio; 95% CI, 95% confidence interval.

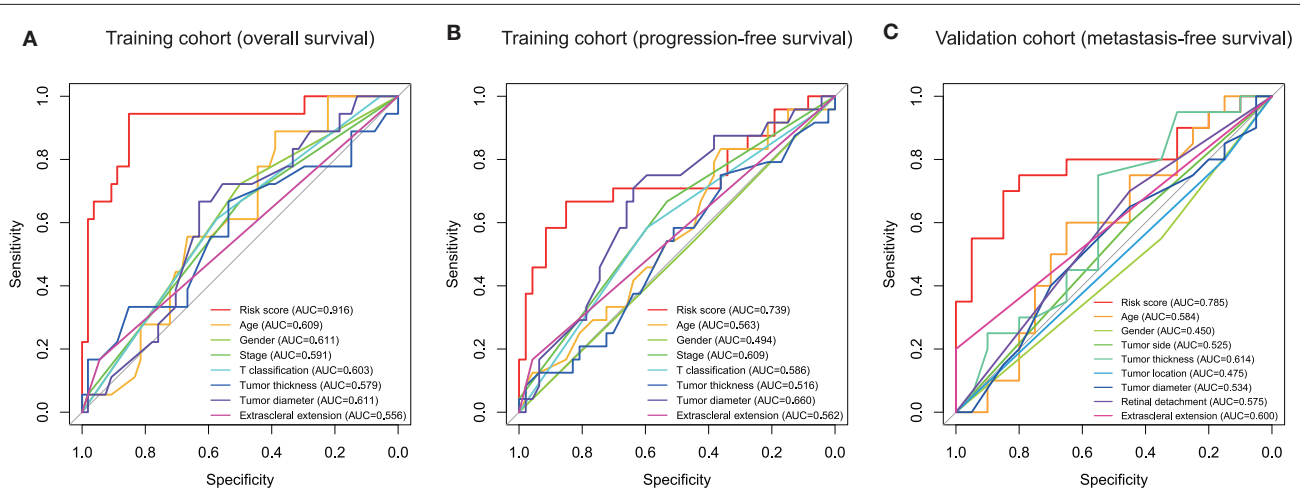

FIGURE 6 | Receiver operating characteristic (ROC) analysis of the ten-gene signature risk score. ROC analysis of the sensitivity and specificity of the prognosis prediction by the ten-gene risk score, age, gender, T classification, tumor stage, tumor thickness, tumor diameter, tumor side, tumor location, extrascleral extension, or retinal detachment in training cohort based on overall survival **(A)**, training cohort based on progression-free survival **(B)**, and validation cohort based on metastasis-free survival **(C)**. AUC, area under the ROC curve.

results, here, verified the predictive ability of the risk score, and its independence.

To further assess the predictive power of this ten-gene signature, we performed ROC analysis. AUC can be used to check the accuracy and predictive ability of biomarkers in diagnostic tests (25). ROC analysis indicated that the AUC of the ten-gene signature stayed above 0.7 in these two cohorts, and superior to other variates (**Figure 6**). These ROC results again suggested

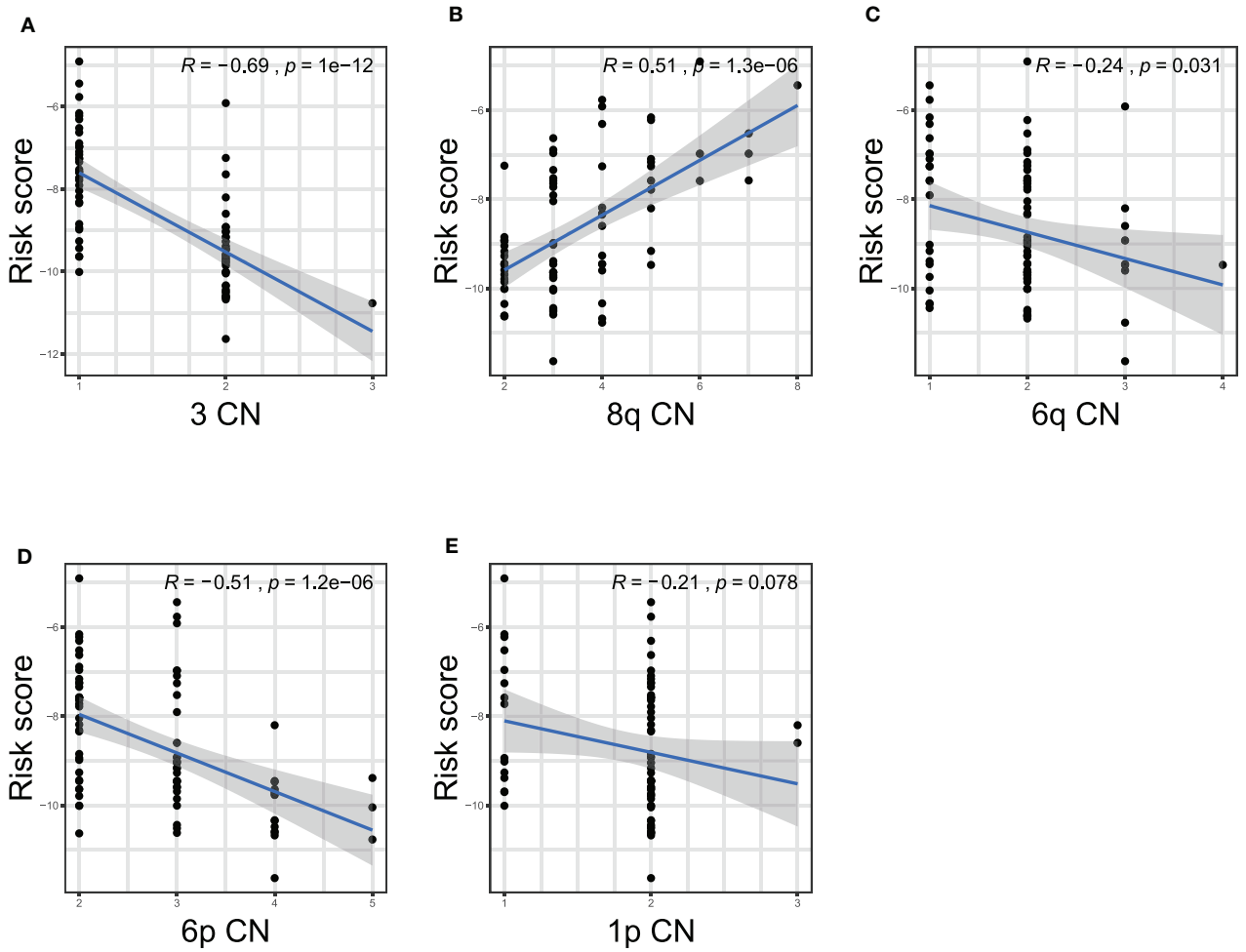

FIGURE 7 | The correlations between the ten-gene signature and the copy number aberrations in TCGA-UVM. The correlations between risk score and chromosome 3 **(A)**, 8q **(B)**, 6q **(C)**, 6p **(D)**, and 1p **(E)** mutations were plotted. The blue line in each plot was fitted linear model indicating the proportion tropism of the copy number along with risk score. The shade around the blue line represents the 95% confidence interval. The Spearman test was applied for the correlation examination. CN, copy number.

that our signature might strengthen the predictive accuracy of prognosis in UM.

Our signature was composed of ten genes, which were SIRT3, HMCES, SLC44A3, TCTN1, STPG1, POMGNT2, RNF208, ANXA2P2, ULBP1, and CA12, respectively. In the signature model, ANXA2P2, ULBP1, CA12 were unfavorably genes for the outcome, whereas other genes presented protective function on the prognosis of UM patients. Pseudogenes are nonfunctional segments of DNA that resemble functional genes (26, 27). Previous studies have suggested that pseudogenes will only participate in regulatory roles (28). Recent studies have shown that most pseudogene breaks follow a certain pattern, and it is likely that the pseudogenes of this pattern can be repaired under certain conditions to restore function (27). ANXA2P2 is one of three pseudogenes of annexin A2 that have recently been shown to be aberrantly transcribed in hepatocellular carcinoma (HCC) cells (29). A recent report revealed that the expression of ANXA2P2 was up-regulated in HCC and promoted HCC to be an aggressive phenotype (29). ULBP1 is related to MHC class I molecules, but its gene maps outside the MHC locus (30, 31). It functions as a stress-induced ligand for NKG2D receptor (31). In UM, NKG2D expression was detected in primary tumor lesions, in which a large amount of NKG2D lymphocyte infiltration was also observed (32). Metastatic UM lesions lost MIC expression and are absent of NKG2D+ lymphocytes (33). A recent study demonstrated that soluble NKG2D ligand is a biomarker related to the clinical outcome of immune checkpoint blockade therapy in patients with metastatic melanoma (34). CA12 is a membrane-associated enzyme. CA12 is highly expressed in many human cancers and often indicates a poor prognosis, so it is a promising target for cancer treatment (35). Among the genes that we found to have prognostic protection, SIRT3, the major deacetylase in mitochondria, plays a crucial role in modulating oxygen reactive species (ROS) and limiting the oxidative damage in cellular

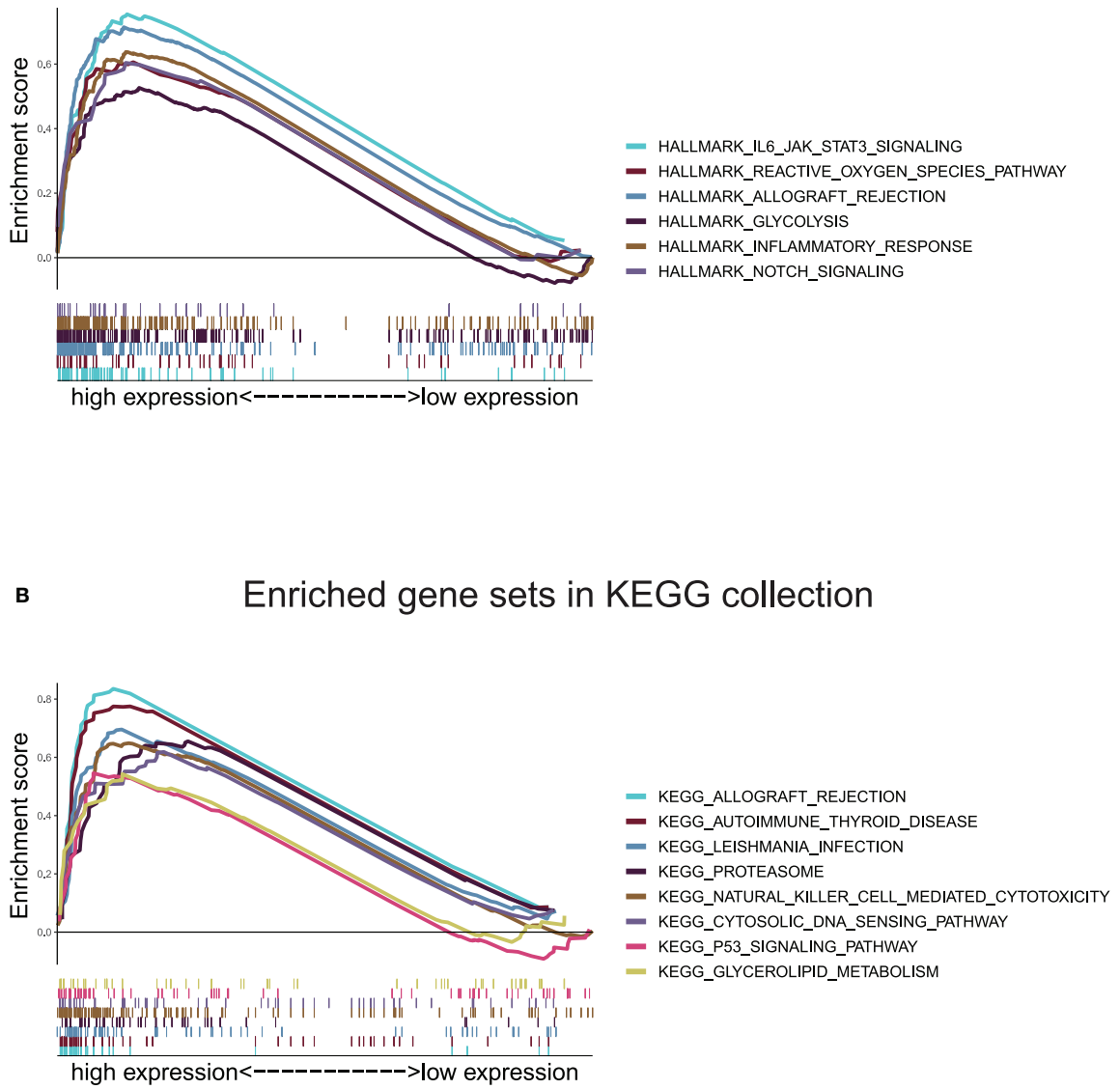

FIGURE 8 | Gene set enrichment analysis based on the ten-gene signature. **(A)** Enriched gene sets annotated by the HALLMARK collection between the high and low-risk groups in the training cohort. **(B)** Enriched gene sets annotated by the KEGG collection between the high and low-risk groups in the training cohort. Gene sets with |NES |> 1, NOM $p < 0.05$, and FDR $q < 0.25$ were considered significant.

components (36). In some types of cancer, SIRT3 functions as a tumoral promoter, since it keeps ROS levels under a certain threshold compatible with cell viability and proliferation. On the contrary, other studies describe SIRT3 as a tumoral suppressor, as SIRT3 could trigger cell death under stress conditions (36). HMCES is a critical component of the replication stress response, mainly upon base misincorporation (37). Deregulated APOBEC activity is the source of a variety of cancer mutagenesis (38). HMCES can respond to APOBEC-induced abasic sites, maintain genome stability, and promote replication extension; otherwise, replication will be slowed down by the participation of TLS polymerase (38). Therefore, HMCES plays a vital role in this tumorigenesis process (38). A lately study showed that SLC44A3 is different expressed between normal and UM (39), in addition, Li et al. (40) found it was found SLC44A3 were associated with better survival in UM and indicated their protective roles. Recent studies revealed that TCTN1 is widely up-regulated in various types of human cancer (41–44), and acts as an oncogene

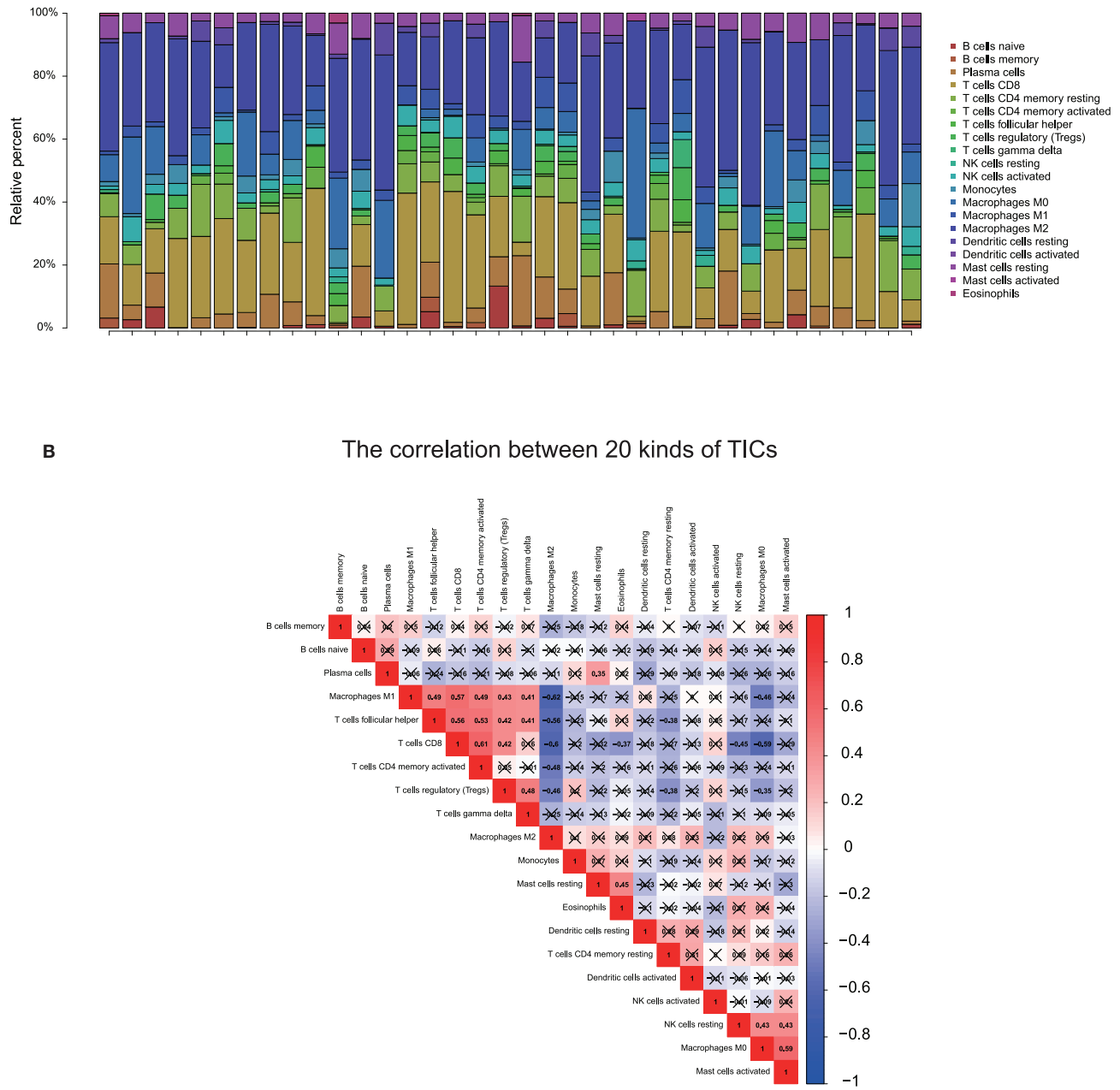

FIGURE 9 | TIC profile and correlation analysis. **(A)** The bar graph showed the proportion of 20 TICs in UM tumor samples in the training cohort. Each column indicates one sample. **(B)** Heatmap showing the correlation between 20 kinds of TICs. The numeric and shade of each small color box indicate the coefficient between two kinds of cells. X shape covered coefficient is no statistically significant. The Pearson coefficient was used for the significance tests. $P < 0.05$ is the cutoff. TIC, tumor-infiltrating immune cell; UM, uveal melanoma.

via promoting proliferation, migration, or inhibiting apoptosis. However, in a study conducted by Xue et al. (12), TCTN1 was found to be low expressed in high-risk patients with UM and has a protective effect on the prognosis of UM, which has been consistent with our study. STPG1 is found with few traces from existing studies, but shows to be a prognostic marker in endometrial cancer (favorable) and renal cancer (favorable) from The Human Protein Atlas portal (45). The high expression levels of human POMGNT2 in the brain, muscle, heart, and kidney in fetal as well as adult tissues suggest the importance of this

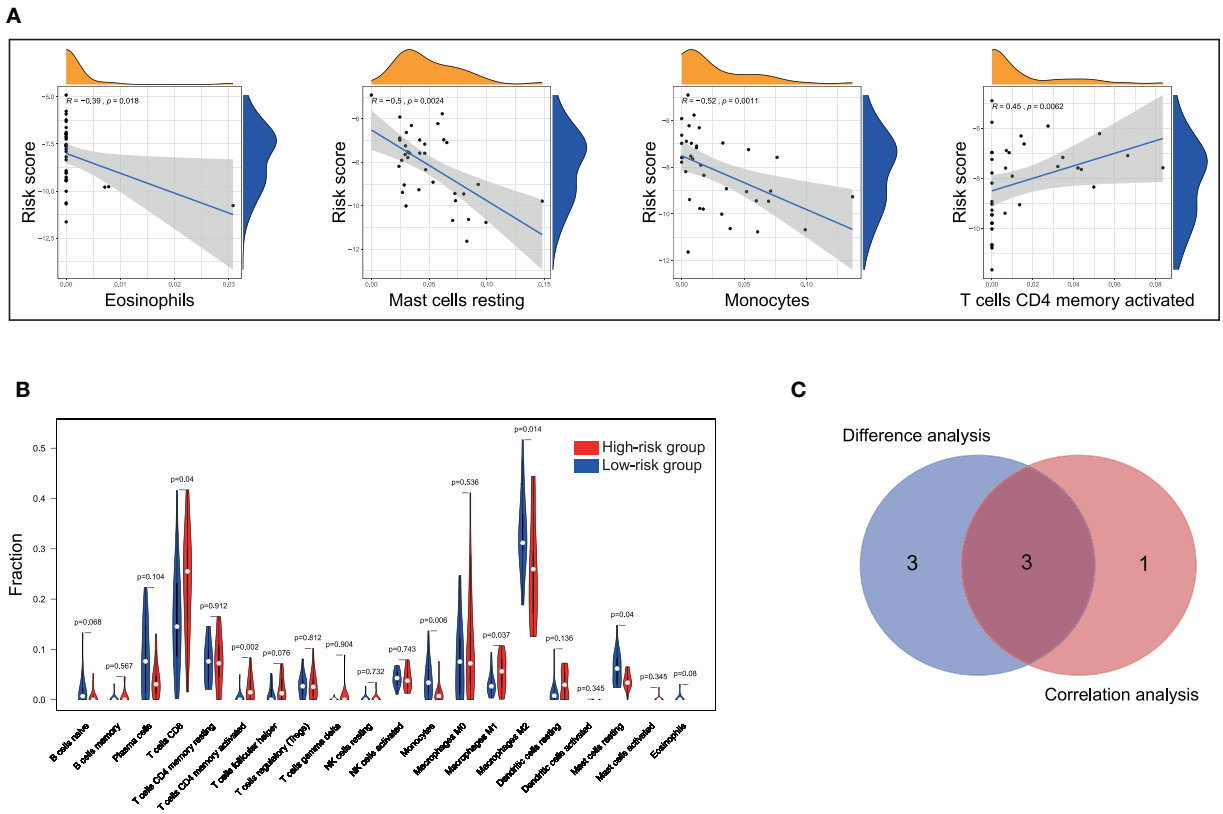

FIGURE 10 | Correlation of TICs proportion with ten-gene signature risk score in the training cohort. **(A)** Only significantly correlated TICs was plotted. The blue line in each plot was fitted linear model indicating the proportion tropism of the immune cell along with risk score. The shade around the blue line represents the 95% confidence interval. The Spearman coefficient was used for the correlation test. **(B)** The violin plot showed the ratio differentiation of 20 kinds of immune cells between UM tumor samples with low and high-risk groups and was tested by Wilcoxon rank-sum. **(C)** The Venn plot displayed three kinds of TICs correlated with risk score co-determined by difference and correlation tests shown in violin and scatter plots, respectively. $P < 0.05$ is the cutoff. TIC, tumor-infiltrating immune cell; UM, uveal melanoma.

gene during development (46). However, whether POMGNT2 plays a vital role in tumor progress remained unclear and needs more efforts in further research. RNF208 decreases the stability of soluble Vimentin protein through a polyubiquitin-mediated proteasomal degradation pathway, thereby suppressing metastasis of triple-negative breast cancer (TNBC) cells (47). In a comprehensive bioinformatics study, RNF208 was found to have decreased expression in UM and was associated with a better prognosis (12). There are relatively fewer studies related to these genes and UM. However, the ten-genes signature has a significant role in predicting and diagnosing UM in our research. The ten-gene signature or each of them may be the potential specific directions for future research on UM.

Studies showed that chromosome aberrations and gene mutations in UM are closely related to clinical results. The loss of a chromosome 3 in UM is associated with an increased risk of metastasis and poor prognosis (16). Recently, researchers also found that Monosomy 3 is associated with poor survival after UM treatment (19). Previous studies have shown that besides chromosome 3, the increase in chromosome 8q is also related to poor survival prognosis (48–51). In addition, other chromosomal abnormalities have been shown to correlate with poor prognosis and these include 6q loss, lack of 6p gain, 1p loss, and 16q loss (16–20). Among the ten gene signatures found in this study, five were located in the above-mentioned chromosomes (**Table 2**). Further on, we performed Spearman test to assess the correlation between the copy numbers of chromosome 3, 8q, 6q, 6p, and 1p and risk score, finding that the ten-gene signature risk score was significantly correlated with copy numbers of chromosome 3, 6q, and 6p negatively, and 8q positively (**Figure 7**), which further confirmed the crucial of the ten-gene signature in predicting prognosis of UM.

The GSEA found that gene sets enriched in pathways concerned with immune response, inflammatory response, p53 signaling, reactive oxygen species, Notch signaling, proteasome, natural killer cell, cytosolic DNA-sensing, and glycolipid metabolism. These findings demonstrated that ten-gene signature might potentially participate in the immune-dominant

tumor microenvironment. The proportion of TICs analysis based on CIBERSORT algorithm found that activated T cells CD4 memory were positively correlated with risk score, while, Monocytes and Mast cells resting were negatively correlated with risk score, further supporting that the signature interacted closely with the tumor environment. Strategies targeting the tumor microenvironment of UM have the potential to improve the efficacy of standard and genome-based molecular therapeutics, and, as well, to help resolve many of the challenges associated with developing new drugs and running clinical trials (52). In our GSEA, KEGG collection indicated that NK cells were associated with the ten-gene risk score. This finding is consistent with previous research (53). Durante et al. (53) recent work identified LAG3 as a potential candidate for immune checkpoint blockade in patients with high risk UM, and demonstrated that LAG3 was expressed on NK cells, CD8+ T cells, and regulatory T cells, highlighting the vital of NK cells in UM. However, through immune cell and V(D)J immune repertoire analysis, Durante et al. (53) group found NK cells were few present, and they were distributed equally across tumor samples. This finding explains why NK cells stood out in GSEA but were not prominent in our CIBERSORT result. We thought the main reason was that the small amount of NK cells was "ignored" by the CIBERSORT algorithm, which led to the discrepancy of data analysis results. In Durante et al.'s (53) research, T cells were found present in all tumor samples and collaborated with LAG3 operating UM development. This conclusion was similar to our finding that the infiltration of CD4 T cells was correlated with the ten-gene risk score. Moreover, NK cells can recognize and directly kill early activated T cells, which can determine the quality and intensity of T cell responses, thereby affecting the immune process (54). As described above, although NK cells were "ignored" by the CIBERSORT algorithm, their ability in UM progress were not hidden, but be potentially "stolen" by T cells that are strictly related to it, further explained why NK cells appeared in our GSEA results but disappeared in the CIBERSORT conclusions.

The immune system uses multiple antigens to distinguish tumor cells from healthy cells (55). In many cancers, immune infiltration within the tumor is usually associated with a better prognosis and a favorable immunotherapy response (56). However, in primary UM, market-specific immunohistochemistry has demonstrated that dense infiltrate of leukocytes or macrophages is associated with monosomy 3 and a poor prognosis (57–59). UM cells express tumor-specific antigens, including the Melanoma Antigen Gene (MAGE) family proteins, premelanosome protein gp100, and tyrosinase (60, 61). But, both the innate and adaptive effector immune responses can be circumvented by UM cells (55), and previous studies have shown that UM cells have established a specific immune escape mechanism, leading to its progressive process and poor prognosis (55, 60–63). Contrary to other cancers, the increase in HLA class I expression is related to the poor prognosis of UM and is considered to be a mechanism by which natural killer cell-mediated cytotoxicity in the blood escapes tumors (64, 65). A recent study demonstrated that immune infiltration in UM is highly correlated with the upregulation of stimuli and targets (such as HLA and IFNG) that are fundamental for T cell-mediated immunotherapy (16). More recent reports suggest that disseminated conjunctival melanoma may be responsive to targeted molecular therapies, such as BRAF and MEK inhibitors in BRAF-mutant tumors (66), and checkpoint inhibitor immunotherapeutic agents, such as pembrolizumab (67). A better understanding of UM immunology can help select patients who may benefit from immunotherapy. However, the current knowledge of UM immunology is still in its infancy, and further research is needed to clarify the mechanism of UM inhibition and identify new targets to enhance anti-tumor immune reactivity.

DecisionDx-UM is a prognostic test that determines the metastatic risk associated with UM (68). Specifically, the assay determines the activity or "expression" of 15 genes which indicate a patient's individual risk, or class. The test classifies tumors as: Class 1 (low metastatic risk); Class 2 (high metastatic risk) (68). According to the report of the Collaborative Eye Oncology Group (COOG), the DecisionDx-UM GEP test is an accurate prospectively validated molecular classifier whose results are highly correlated with metastatic potential (69, 70). In a prospective multicenter study, Plasseraud et al. (71) demonstrated that the DecisionDecxD-UM could accurately predict the risk of metastasis in patients with UM. Compared with the seminal work of DecisionDx-UM, the present study obtained robust ten-gene signature by applying various statistical methods and validation in an independent cohort. Fewer gene numbers can save costs and improve efficiency in clinical practice. However, the results of the predecessors have been applied in commerce and have been widely reported and verified. In this regard, our research has great potential while still a long way to go.

Our research also has some limitations. Although TCGA-UVM is a cohort that is currently recognized by most scholars, the data in it are from large uveal melanoma treated with enucleation. Similarly, the GSE22138 cohort, which was published online on the GEO database platform, and its academic recognition is also undoubted. Still, most of the data in it came from large eye tumors. Such sample distribution in these two cohorts may not be consistent with the clinical population. Therefore, our research may have a selection bias for database selection. Our ten-gene signature came from retrospective data, and more prospective data were needed for proving the clinical utility of it. In addition, due to the limited clinical characteristics of patients included in TCGA cohort, we could not perform certain clinical subgroup analyses. Besides, there is currently no wet experimental data explaining the relationship between these ten-genes and their mechanism in UM samples. Therefore, between the ten-gene signature and the prognosis of UM, more effort is needed to clarify the potential relationship.

CONCLUSION

In conclusion, our research defined a robust ten-gene signature in UM. It is a comprehensive analysis of the TCGA and the GEO database. This signature was related to the prognosis of UM and can accurately identify the prognostic risk of patients. Notably, we evaluated the reliability and accuracy of the signature by compared to variants of chromosomes 3 and

8q, and examining in a validation cohort. What is more, the functions and immune infiltrating analyses revealed that the signature had close interactions with the immunodominant tumor environment, which may advance the development of new therapies for UM treatment.

DATA AVAILABILITY STATEMENT

Publicly available datasets were analyzed in this study. These data can be found here: TCGA: https://portal.gdc.cancer.gov/; GEO: https://www.ncbi.nlm.nih.gov/geo/.

AUTHOR CONTRIBUTIONS

HL organized and wrote the manuscript. CM and JC contributed to the literature search for the manuscript. CM designed and produced the figures. JS made contributed to the statistical analysis of this manuscript. JC revised the manuscript. All authors reviewed the manuscript and approved the manuscript for publication.

FUNDING

This work was supported by the National Natural Science Foundation of China (grant numbers 81671091 and 81971061).

ACKNOWLEDGMENTS

HL and CM thank Zhengzhou University Overseas Virtual Research Institute. CM thanks China Scholarship Council (No. 201708410121).

SUPPLEMENTARY MATERIAL

The Supplementary Material for this article can be found online at: https://www.frontiersin.org/articles/10.3389/fonc.2020.567512/full#supplementary-material

REFERENCES

1. Singh AD, Turell ME, Topham AK. Uveal melanoma: trends in incidence, treatment, and survival. *Ophthalmology.* (2011) 118:1881–5. doi: 10.1016/j.ophtha.2011.01.040
2. Virgili G, Gatta G, Ciccolallo L, Capocaccia R, Biggeri A, Crocetti E, et al. Incidence of uveal melanoma in Europe. *Ophthalmology.* (2007) 114:2309–15. doi: 10.1016/j.ophtha.2007.01.032
3. Singh AD, Bergman L, Seregard S. Uveal melanoma: epidemiologic aspects. *Ophthalmol Clin North Am.* (2005) 18:75–84, viii. doi: 10.1016/j.ohc.2004.07.002
4. Kaliki S, Shields CL. Uveal melanoma: relatively rare but deadly cancer. *Eye (Lond).* (2017) 31:241–57. doi: 10.1038/eye.2016.275
5. Rietschel P, Panageas KS, Hanlon C, Patel A, Abramson DH, Chapman PB. Variates of survival in metastatic uveal melanoma. *J Clin Oncol.* (2005) 23:8076–80. doi: 10.1200/JCO.2005.02.6534
6. Augsburger JJ, Correa ZM, Shaikh AH. Effectiveness of treatments for metastatic uveal melanoma. *Am J Ophthalmol.* (2009) 148:119–27. doi: 10.1016/j.ajo.2009.01.023
7. Bol KF, van den Bosch T, Schreibelt G, Mensink HW, Keunen JE, Kiliç E, et al. Adjuvant dendritic cell vaccination in high-risk uveal melanoma. *Ophthalmology.* (2016) 123:2265–7. doi: 10.1016/j.ophtha.2016.06.027
8. Verdegaal EM. Adoptive cell therapy: a highly successful individualized therapy for melanoma with great potential for other malignancies. *Curr Opin Immunol.* (2016) 39:90–5. doi: 10.1016/j.coi.2016.01.004
9. Larkin J, Chiarion-Sileni V, Gonzalez R, Grob JJ, Cowey CL, Lao CD, et al. Combined nivolumab and ipilimumab or monotherapy in untreated melanoma. *N Engl J Med.* (2015) 373:23–34. doi: 10.1056/NEJMc1509660
10. Weber JS, D'Angelo SP, Minor D, Hodi FS, Gutzmer R, Neyns B, et al. Nivolumab versus chemotherapy in patients with advanced melanoma who progressed after anti-CTLA-4 treatment (CheckMate 037): a randomised, controlled, open-label, phase 3 trial. *Lancet Oncol.* (2015) 16:375–84. doi: 10.1016/S1470-2045(15)70076-8
11. Hodi FS, O'Day SJ, McDermott DF, Weber RW, Sosman JA, Haanen JB, et al. Improved survival with ipilimumab in patients with metastatic melanoma. *N Engl J Med.* (2010) 363:711–23. doi: 10.1056/NEJMx100063
12. Xue M, Shang J, Chen B, Yang Z, Song Q, Sun X, et al. Identification of prognostic signatures for predicting the overall survival of uveal melanoma patients. *J Cancer.* (2019) 10:4921–31. doi: 10.7150/jca.30618
13. Wan Q, Tang J, Lu J, Jin L, Su Y, Wang S, et al. Six-gene-based prognostic model predicts overall survival in patients with uveal melanoma. *Cancer Biomark.* (2020) 27:343–56. doi: 10.3233/CBM-190825
14. Li Y, Yang X, Yang J, Wang H, Wei W. An 11-gene-based prognostic signature for uveal melanoma metastasis based on gene expression and DNA methylation profile. *J Cell Biochem.* (2018) 120. doi: 10.1002/jcb.28151
15. Huang JL, Urtatiz O, Van Raamsdonk CD. Oncogenic G protein GNAQ induces uveal melanoma and intravasation in mice. *Cancer Res.* (2015) 75:3384–97. doi: 10.1158/0008-5472.CAN-14-3229
16. Robertson AG, Shih J, Yau C, Gibb EA, Oba J, Mungall KL, et al. Integrative analysis identifies four molecular and clinical subsets in uveal melanoma. *Cancer Cell.* (2017) 32:204–20.e215. doi: 10.1016/j.ccell.2017.07.003
17. Damato B, Dopierala JA, Coupland SE. Genotypic profiling of 452 choroidal melanomas with multiplex ligation-dependent probe amplification. *Clin Cancer Res.* (2010) 16:6083–92. doi: 10.1158/1078-0432.CCR-10-2076
18. Onken MD, Worley LA, Harbour JW. A metastasis modifier locus on human chromosome 8p in uveal melanoma identified by integrative genomic analysis. *Clin Cancer Res.* (2008) 14:3737–45. doi: 10.1158/1078-0432.CCR-07-5144
19. Scholes AG, Damato BE, Nunn J, Hiscott P, Grierson I, Field JK. Monosomy 3 in uveal melanoma: correlation with clinical and histologic predictors of survival. *Invest Ophthalmol Vis Sci.* (2003) 44:1008–11. doi: 10.1167/iovs.02-0159
20. White VA, Chambers JD, Courtright PD, Chang WY, Horsman DE. Correlation of cytogenetic abnormalities with the outcome of patients with uveal melanoma. *Cancer.* (1998) 83:354–9. doi: 10.1002/(SICI)1097-0142(19980715)83:2<354::AID-CNCR20>3.0.CO;2-R
21. Tibshirani R. The lasso method for variable selection in the Cox model. *Stat Med.* (1997) 16:385–95. doi: 10.1002/(SICI)1097-0258(19970228)16:4<385::AID-SIM380>3.0.CO;2-3
22. Friedman J, Hastie T, Tibshirani R. Regularization paths for generalized linear models via coordinate descent. *J Stat Softw.* (2010) 33:1–22. doi: 10.18637/jss.v033.i01
23. Goeman JJ. L1 penalized estimation in the Cox proportional hazards model. *Biom J.* (2010) 52:70–84. doi: 10.1002/bimj.200900028
24. Sauerbrei W, Royston P, Binder H. Selection of important variables and determination of functional form for continuous predictors in multivariable model building. *Stat Med.* (2007) 26:5512–28. doi: 10.1002/sim.3148
25. Hanley JA, McNeil BJ. The meaning and use of the area under a receiver operating characteristic (ROC) curve. *Radiology.* (1982) 143:29–36. doi: 10.1148/radiology.143.1.7063747
26. Lou W, Ding B, Fu P. Pseudogene-derived lncRNAs and their miRNA sponging mechanism in human cancer. *Front Cell Dev Biol.* (2020) 8:85. doi: 10.3389/fcell.2020.00085
27. Anand A, Olson CA, Yang L, Sastry AV, Catoiu E, Choudhary KS, et al. Pseudogene repair driven by selection pressure applied in experimental

evolution. *Nat Microbiol.* (2019) 4:386–9. doi: 10.1038/s41564-018-0340-2
28. Xiao-Jie L, Ai-Mei G, Li-Juan J, Jiang X. Pseudogene in cancer: real functions and promising signature. *J Med Genet.* (2015) 52:17–24. doi: 10.1136/jmedgenet-2014-102785
29. Wang QS, Shi LL, Sun F, Zhang YF, Chen RW, Yang SL, et al. High expression of ANXA2 pseudogene ANXA2P2 promotes an aggressive phenotype in hepatocellular carcinoma. *Dis Markers.* (2019) 2019:9267046. doi: 10.1155/2019/9267046
30. Radosavljevic M, Cuillerier B, Wilson MJ, Clement O, Wicker S, Gilfillan S, et al. A cluster of ten novel MHC class I related genes on human chromosome 6q24.2–q25.3. *Genomics.* (2002) 79:114–23. doi: 10.1006/geno.2001.6673
31. Cosman D, Mullberg J, Sutherland CL, Chin W, Armitage R, Fanslow W, et al. ULBPs, novel MHC class I-related molecules, bind to CMV glycoprotein UL16 and stimulate NK cytotoxicity through the NKG2D receptor. *Immunity.* (2001) 14:123–33. doi: 10.1016/S1074-7613(01)00095-4
32. Vetter CS, Lieb W, Brocker EB, Becker JC. Loss of nonclassical MHC molecules MIC-A/B expression during progression of uveal melanoma. *Br J Cancer.* (2004) 91:1495–9. doi: 10.1038/sj.bjc.6602123
33. Wu J. NKG2D ligands in cancer immunotherapy: target or not? *Austin J Clin Immunol.* (2014) 1:2.
34. Maccalli C, Giannarelli D, Chiarucci C, Cutaia O, Giacobini G, Hendrickx W, et al. Soluble NKG2D ligands are biomarkers associated with the clinical outcome to immune checkpoint blockade therapy of metastatic melanoma patients. *Oncoimmunology.* (2017) 6:e1323618. doi: 10.1080/2162402X.2017.1323618
35. Uda NR, Stenner F, Seibert V, Herzig P, Markuly N, Vand M, et al. Humanized monoclonal antibody blocking carbonic anhydrase 12 enzymatic activity leads to reduced tumor growth *in vitro*. *Anticancer Res.* (2019) 39:4117–28. doi: 10.21873/anticanres.13570
36. Torrens-Mas M, Oliver J, Roca P, Sastre-Serra J. SIRT3: oncogene and tumor suppressor in cancer. *Cancers (Basel).* (2017) 9:90. doi: 10.3390/cancers9070090
37. Srivastava M, Su D, Zhang H, Chen Z, Tang M, Nie L, et al. HMCES safeguards replication from oxidative stress and ensures error-free repair. *EMBO Rep.* (2020) 21:e49123. doi: 10.15252/embr.201949123
38. Mehta KPM, Lovejoy CA, Zhao R, Heintzman DR, Cortez D. HMCES maintains replication fork progression and prevents double-strand breaks in response to APOBEC deamination and abasic site formation. *Cell Rep.* (2020) 31:107705. doi: 10.1016/j.celrep.2020.107705
39. Xu B, Ma R, Ren H, Qian J. Genome-wide analysis of uveal melanoma metastasis-associated LncRNAs and their functional network. *DNA Cell Biol.* (2018) 37:99–108. doi: 10.1089/dna.2017.4015
40. Li YZ, Huang Y, Deng XY, Tu CS. Identification of an immune-related signature for the prognosis of uveal melanoma. *Int J Ophthalmol.* (2020) 13:458–65. doi: 10.18240/ijo.2020.03.14
41. Dai X, Dong M, Yu H, Xie Y, Yu Y, Cao Y, et al. Knockdown of TCTN1 strongly decreases growth of human colon cancer cells. *Med Sci Monit.* (2017) 23:452–61. doi: 10.12659/MSM.899595
42. Wang Z, Gao Y, Liu Y, Xie Y, Yu Y, Cao Y, et al. Tectonic1 contributes to the growth and migration of prostate cancer cells *in vitro*. *Int J Mol Med.* (2015) 36:931–8. doi: 10.3892/ijmm.2015.2313
43. Wang X, Yu Q, Zhang Y, Ling Z, Yu P. Tectonic 1 accelerates gastric cancer cell proliferation and cell cycle progression in vitro. *Mol Med Rep.* (2015) 12:5897–902. doi: 10.3892/mmr.2015.4177
44. Li J, Wang H, Hang C, Fan Y, Ma C, Pan Y. Lentivirus-mediated knockdown of TCTN1 inhibits glioma cell proliferation. *Appl Biochem Biotechnol.* (2015) 176:13–21. doi: 10.1007/s12010-015-1498-1
45. Uhlen M, Zhang C, Lee S, Sjostedt E, Fagerberg L, Bidkhori G, et al. A pathology atlas of the human cancer transcriptome. *Science.* (2017) 357:eaan2507. doi: 10.1126/science.aan2507
46. Endo Y, Dong M, Noguchi S, Ogawa M, Hayashi YK, Kuru S, et al. Milder forms of muscular dystrophy associated with POMGNT2 mutations. *Neurol Genet.* (2015) 1:e33. doi: 10.1212/NXG.0000000000000033
47. Pang K, Park J, Ahn SG, Lee J, Park Y, Ooshima A, et al. RNF208, an estrogen-inducible E3 ligase, targets soluble Vimentin to suppress metastasis in triple-negative breast cancers. *Nat Commun.* (2019) 10:5805. doi: 10.1038/s41467-019-13852-5
48. Sisley K, Rennie IG, Parsons MA, Jacques R, Hammond DW, Bell SM, et al. Abnormalities of chromosomes 3 and 8 in posterior uveal melanoma correlate with prognosis. *Genes Chromosomes Cancer.* (1997) 19:22–28. doi: 10.1002/(SICI)1098-2264(199705)19:1<22::AID-GCC4>3.0.CO;2-2
49. Versluis M, de Lange MJ, van Pelt SI, Ruivenkamp CA, Kroes WG, Cao J, et al. Digital PCR validates 8q dosage as prognostic tool in uveal melanoma. *PLoS One.* (2015) 10:e0116371. doi: 10.1371/journal.pone.0116371
50. Caines R, Eleuteri A, Kalirai H, Fisher AC, Heimann H, Damato BE, et al. Cluster analysis of multiplex ligation-dependent probe amplification data in choroidal melanoma. *Mol Vis.* (2015) 21:1–11.
51. Cassoux N, Rodrigues MJ, Plancher C, Asselain B, Levy-Gabriel C, Lumbroso-Le Rouic L, et al. Genome-wide profiling is a clinically relevant and affordable prognostic test in posterior uveal melanoma. *Br J Ophthalmol.* (2014) 98:769–74. doi: 10.1136/bjophthalmol-2013-303867
52. Rossi E, Schinzari G, Zizzari IG, Maiorano BA, Pagliara MM, Sammarco MG, et al. Immunological backbone of uveal melanoma: is there a rationale for immunotherapy? *Cancers (Basel).* (2019) 11:1055. doi: 10.3390/cancers11081055
53. Durante MA, Rodriguez DA, Kurtenbach S, Kuznetsov JN, Sanchez MI, Decatur CL, et al. Single-cell analysis reveals new evolutionary complexity in uveal melanoma. *Nat Commun.* (2020) 11:496. doi: 10.1038/s41467-019-14256-1
54. Pallmer K, Oxenius A. Recognition and regulation of T cells by Nk Cells. *Front Immunol.* (2016) 7:251. doi: 10.3389/fimmu.2016.00251
55. Basile MS, Mazzon E, Fagone P, Longo A, Russo A, Fallico M, et al. Immunobiology of uveal melanoma: state of the art and therapeutic targets. *Front Oncol.* (2019) 9:1145. doi: 10.3389/fonc.2019.01145
56. Lee N, Zakka LR, Mihm MC Jr, Schatton T. Tumour-infiltrating lymphocytes in melanoma prognosis and cancer immunotherapy. *Pathology.* (2016) 48:177–87. doi: 10.1016/j.pathol.2015.12.006
57. Bronkhorst IH, Ly LV, Jordanova ES, Vrolijk J, Versluis M, Luyten GP, et al. Detection of M2-macrophages in uveal melanoma and relation with survival. *Invest Ophthalmol Vis Sci.* (2011) 52:643–50. doi: 10.1167/iovs.10-5979
58. Maat W, Ly LV, Jordanova ES, de Wolff-Rouendaal D, Schalij-Delfos NE, Jager MJ. Monosomy of chromosome 3 and an inflammatory phenotype occur together in uveal melanoma. *Invest Ophthalmol Vis Sci.* (2008) 49:505–10. doi: 10.1167/iovs.07-0786
59. Ksander BR, Geer DC, Chen PW, Salgaller ML, Rubsamen P, Murray TG. Uveal melanomas contain antigenically specific and non-specific infiltrating lymphocytes. *Curr Eye Res.* (1998) 17:165–73. doi: 10.1076/ceyr.17.2.165.5607
60. Chen PW, Murray TG, Salgaller ML, Ksander BR. Expression of MAGE genes in ocular melanoma cell lines. *J Immunother.* (1997) 20:265–75. doi: 10.1097/00002371-199707000-00003
61. Mulcahy KA, Rimoldi D, Brasseur F, Rodgers S, Lienard D, Marchand M, et al. Infrequent expression of the MAGE gene family in uveal melanomas. *Int J Cancer.* (1996) 66:738–42. doi: 10.1002/(SICI)1097-0215(19960611)66:6<738::AID-IJC5>3.0.CO;2-0
62. Apte RS, Mayhew E, Niederkorn JY. Local inhibition of natural killer cell activity promotes the progressive growth of intraocular tumors. *Invest Ophthalmol Vis Sci.* (1997) 38:1277–82.
63. Knisely TL, Niederkorn JY. Emergence of a dominant cytotoxic T lymphocyte antitumor effector from tumor-infiltrating cells in the anterior chamber of the eye. *Cancer Immunol Immunother.* (1990) 30:323–30. doi: 10.1007/BF01786881
64. de Lange MJ, van Pelt SI, Versluis M, ordanova ES, Kroes WG, Ruivenkamp C, et al. Heterogeneity revealed by integrated genomic analysis uncovers a molecular switch in malignant uveal melanoma. *Oncotarget.* (2015) 6:37824–35. doi: 10.18632/oncotarget.5637
65. Jager MJ, Hurks HM, Levitskaya J, Kiessling R. HLA expression in uveal melanoma: there is no rule without some exception. *Hum Immunol.* (2002) 63:444–51. doi: 10.1016/S0198-8859(02)00389-0
66. Dagi Glass LR, Lawrence DP, Jakobiec FA, Freitag SK. Conjunctival melanoma responsive to combined systemic BRAF/MEK inhibitors. *Ophthalmic Plast Reconstr Surg.* (2017) 33:e114–e6. doi: 10.1097/IOP.0000000000000833
67. Kini A, Fu R, Compton C, Miller DM, Ramasubramanian A. Pembrolizumab for recurrent conjunctival melanoma. *JAMA Ophthalmol.* (2017) 135:891–2. doi: 10.1001/jamaophthalmol.2017.2279

68. Harbour JW, Chen R. The DecisionDx-UM gene expression profile test provides risk stratification and individualized patient care in uveal melanoma. *PLoS Curr.* (2013) 5:ecurrents.eogt.af8ba80fc776c8f1ce8f5dc485d4a618. doi: 10.1371/currents.eogt.af8ba80fc776c8f1ce8f5dc485d4a618
69. Onken MD, Worley LA, Char DH, Augsburger JJ, Correa ZM, Nudleman E, et al. Collaborative Ocular Oncology Group report number 1: prospective validation of a multi-gene prognostic assay in uveal melanoma. *Ophthalmology.* (2012) 119:1596–603. doi: 10.1016/j.ophtha.2012.02.017
70. Onken MD, Worley LA, Tuscan MD, Harbour JW. An accurate, clinically feasible multi-gene expression assay for predicting metastasis in uveal melanoma. *J Mol Diagn.* (2010) 12:461–8. doi: 10.2353/jmoldx.2010.090220
71. Plasseraud KM, Cook RW, Tsai T, Shildkrot Y, Middlebrook B, Maetzold D, et al. Clinical performance and management outcomes with the DecisionDx-UM gene expression profile test in a prospective multicenter study. *J Oncol.* (2016) 2016:5325762. doi: 10.1155/2016/5325762

Conflict of Interest: The authors declare that the research was conducted in the absence of any commercial or financial relationships that could be construed as a potential conflict of interest.

frontiers in Oncology

ORIGINAL RESEARCH
published: 21 January 2021
doi: 10.3389/fonc.2020.602555

Development of an Immune-Related Gene Signature for Prognosis in Melanoma

Jia-An Zhang†, *Xu-Yue Zhou*†, *Dan Huang*, *Chao Luan*, *Heng Gu*, *Mei Ju** *and Kun Chen**

Institute of Dermatology, Jiangsu Key Laboratory of Molecular Biology for Skin Diseases and STIs, Chinese Academy of Medical Science and Peking Union Medical College, Nanjing, China

Melanoma remains a potentially deadly malignant tumor. The incidence of melanoma continues to rise. Immunotherapy has become a new treatment method and is widely used in a variety of tumors. Original melanoma data were downloaded from TCGA. ssGSEA was performed to classify them. GSVA software and the "hclust" package were used to analyze the data. The ESTIMATE algorithm screened DEGs. The edgeR package and Venn diagram identified valid immune-related genes. Univariate, LASSO and multivariate analyses were used to explore the hub genes. The "rms" package established the nomogram and calibrated the curve. Immune infiltration data were obtained from the TIMER database. Compared with that of samples in the high immune cell infiltration cluster, we found that the tumor purity of samples in the low immune cell infiltration cluster was higher. The immune score, ESTIMATE score and stromal score in the low immune cell infiltration cluster were lower. In the high immune cell infiltration cluster, the immune components were more abundant, while the tumor purity was lower. The expression levels of TIGIT, PDCD1, LAG3, HAVCR2, CTLA4 and the HLA family were also higher in the high immune cell infiltration cluster. Survival analysis showed that patients in the high immune cell infiltration cluster had shorter OS than patients in the low immune cell infiltration cluster. IGHV1-18, CXCL11, LTF, and HLA-DQB1 were identified as immune cell infiltration-related DEGs. The prognosis of melanoma was significantly negatively correlated with the infiltration of CD4+ T cells, CD8+ T cells, dendritic cells, neutrophils and macrophages. In this study, we identified immune-related melanoma core genes and relevant immune cell subtypes, which may be used in targeted therapy and immunotherapy of melanoma.

Keywords: melanoma, immune gene, tumor environment, prognostic, ssGSEA

OPEN ACCESS

Edited by:
Suzie Chen,
The State University of New Jersey, United States

Reviewed by:
Gagan Chhabra,
University of Wisconsin-Madison, United States
Lixin Wan,
Moffitt Cancer Center, United States

****Correspondence:***
Mei Ju
jumeiweng@163.com
Kun Chen
kunchen181@aliyun.com

†These authors have contributed equally to this work

Specialty section:
This article was submitted to Skin Cancer, a section of the journal Frontiers in Oncology

Received: *04 September 2020*
Accepted: *14 December 2020*
Published: *21 January 2021*

Citation:
Zhang JA, Zhou XY, Huang D, Luan C, Gu H, Ju M and Chen K (2021) Development of an Immune-Related Gene Signature for Prognosis in Melanoma. Front. Oncol. 10:602555. doi: 10.3389/fonc.2020.602555

INTRODUCTION

Melanoma still remains a potentially deadly malignant tumor at the beginning of the 21st century. The incidence of melanoma unfortunately continues to rise, while the incidence of many tumor types is declining (1). Melanoma is mainly seen in young and middle-aged people, and the median age at diagnosis is 57 years old. It has been observed that the incidence increases

linearly from 25 to 50 years old and then slows down, especially in women (2). Although most patients have localized disease at the time of diagnosis and are treated by surgically removing the primary tumor, many patients develop metastasis (3). It is generally understood that the normal function of a healthy immune system can protect and prevent the development of malignant tumors, and people with a genetically compromised immune system may have increased susceptibility to tumors (4). Immunotherapy has become a new treatment method and is widely used in a variety of tumors, such as gastric and esophageal cancer, pancreatic cancer and ovarian cancer (5–7). Experiments have shown that immune stimulation can participate in the treatment of melanoma (8). Targeted therapy for specific genes is also a research hotspot (9). Combining targeted therapy and immunotherapy is an important strategy to treat melanoma (10–12). Therefore, screening immune-related biological targets has become particularly important.

MATERIALS AND METHOD

Data Collection

RNA sequence and clinical data of melanoma were collected from TCGA (13). We downloaded the expression profiles of mRNAs (level 3) in cases including tumor tissues and normal tissues from TCGA database (http://cancergenome.nih.gov/) on april 15, 2019. The sequenced data were obtained from Illumina HiSeqRNASeq. The corresponding clinical information of patients was also downloaded from TCGA database. ssGSEA groups TCGA melanoma transcriptome data. From the results of Bindea et al (14), we used a set of marker genes for immune cell types. We utilized 29 immune data sets (including immune-related pathways, immune cell types and immune-related functions) and the ssGSEA method with the R software gene set variation analysis (GSVA) package to operate the related expression pathways, penetration levels of different immune cells and Activity of immune-related functions. The melanoma

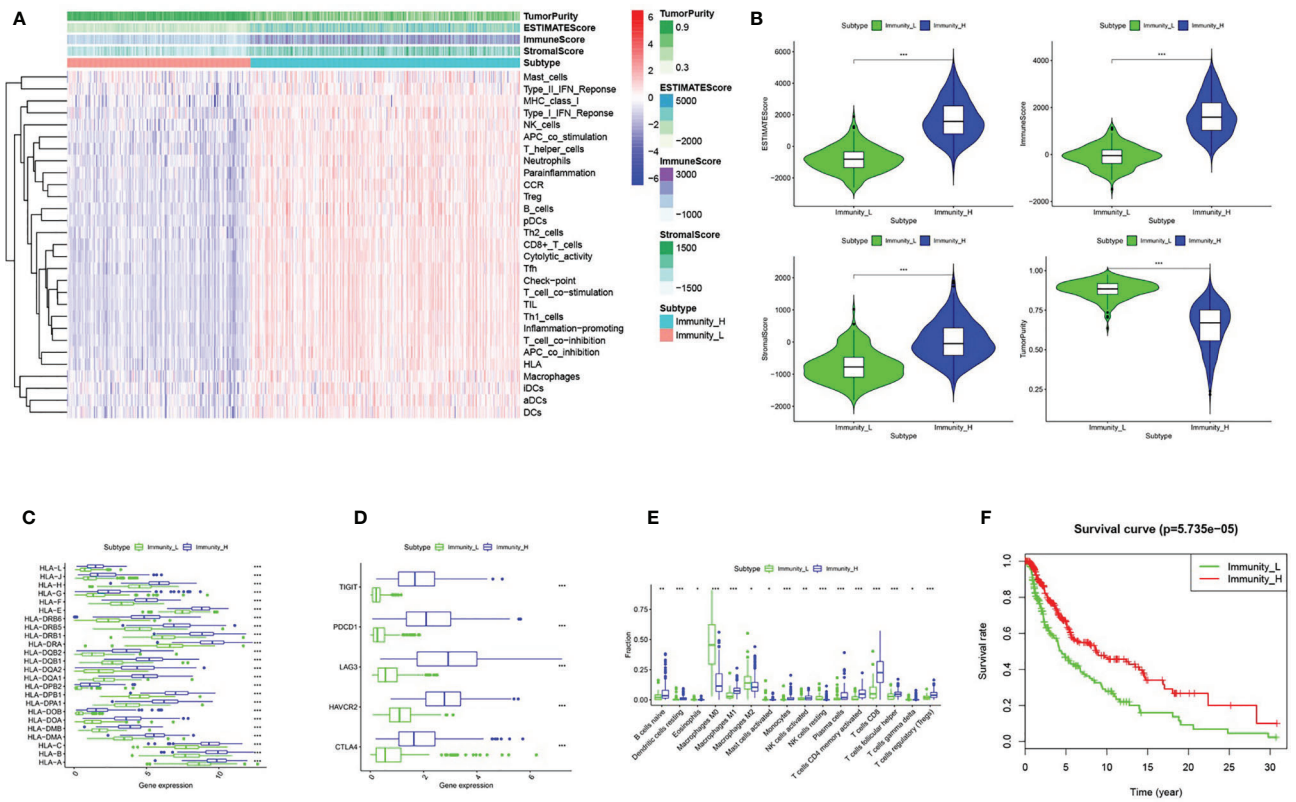

FIGURE 1 | Grouping and verification of melanoma. **(A)** The immune cells were highly expressed in the high immune cell infiltration group (Immunity_H), and the low expression in the low immune cell infiltration group (Immunity_L). The Tumor Purity, ESTIMATE Score, Immune Score and Stromal Score were illustrated along with the grouping information. **(B)** There is a statistical difference of the Tumor Purity, ESTIMATE Score, Immune Score and Stromal Score between the high immune cell infiltration cluster and the low immune cell infiltration cluster **(C, D)** The expression of HLA family genes, TIGIT, PDCD1, LAG3, HAVCR2, and CTLA4 in the high immune cell infiltration cluster (red) were significantly higher than that of the low immune cell infiltration cluster (green) **(E)** The statistical graph shows the difference in the proportion of each immune cell between the high immune cell infiltration cluster (red) and the low immune cell infiltration cluster (green). **(F)** Survival difference between high immune cell infiltration cluster and low immune cell infiltration cluster. $^{*}P < 0.05$, $^{**}P < 0.01$, $^{***}P < 0.001$.

samples from TCGA were divided into low- and high- immune cell infiltration cluster by "hclust" package (15). GSE15605 from the GEO database including 58 melanoma samples was recruited for external validation.

Verification of Effective Immune Grouping

The ESTIMATE algorithm was for identification of the differentially expressed genes (DEGs) in the melanoma expression profile data. The ESTIMATE algorithm was used to analyze the Immune Score, Stromal Score, Tumor Purity and ESTIMATE Score, and cluster heat maps and statistics were drawn for effective grouping.

Selection of Immune-Related Genes in Melanoma

TCGA data was divided into high- and low- immune cell infiltration cluster. According to the standards of $p < 0.05$ and $|\log2FC| > 2$, we used the edgeR package to analyze DEGs. We used the same criteria to perform differential analysis on cancer groups and para-cancer groups to screen immune-related cancerous genes. The Venn diagram identified real immune-related genes from the above two analyses.

Screen Prognostic Genes and Tap Their Characteristics

We utilized Univariate, lasso and multivariate analysis to dig out the correlation between the OS of patients and the expression level of immune-related genes. We calculated the regression coefficient and hazard ratio (HRs) of each gene, and finally the satisfactory mRNAs was identifed.

Construct a Prognostic Model of Immune-Related Genes

The prognostic risk scoring model of melanoma patients in training cohort is a collection of each optimal prognosis mRNA expression level and relative regression coefficient weights calculated from the multivariate model as the following method:

$$Risk\ Score(patient) = \sum_i \text{Coefficient}(\text{mRNA}_i) \times \text{Expression}(\text{mRNA}_i)$$

Relying on the median risk score, all patients in the cohort were classified into high- and low-risk groups. Kaplan–Meier survival curves of the two groups were completed. We proposed ROC curves (16) to evaluate the specificity and sensitivity of the model. We also conducted a multivariate analysis of several clinical characteristics of melanoma patients to check the independence of the prognostic models without their clinical characteristics.

Verify the Effect of Prognostic Models

With the cut-off values calculated from the training cohort, we compared the risk scores from the testing and entire cohort and then patient can be classified into high- or low-risk groups. Kaplan-Meier curve, Time-dependent ROC and Cox multivariate analysis were all conducted. Based on the clinicopathological characteristics, we conducted a stratification analysis of the entire cohort samples.

Confirmation of Hub Immune Related Genes

The "rms" package established the nomogram and calibrate curve, checking the accuracy and the consistency index

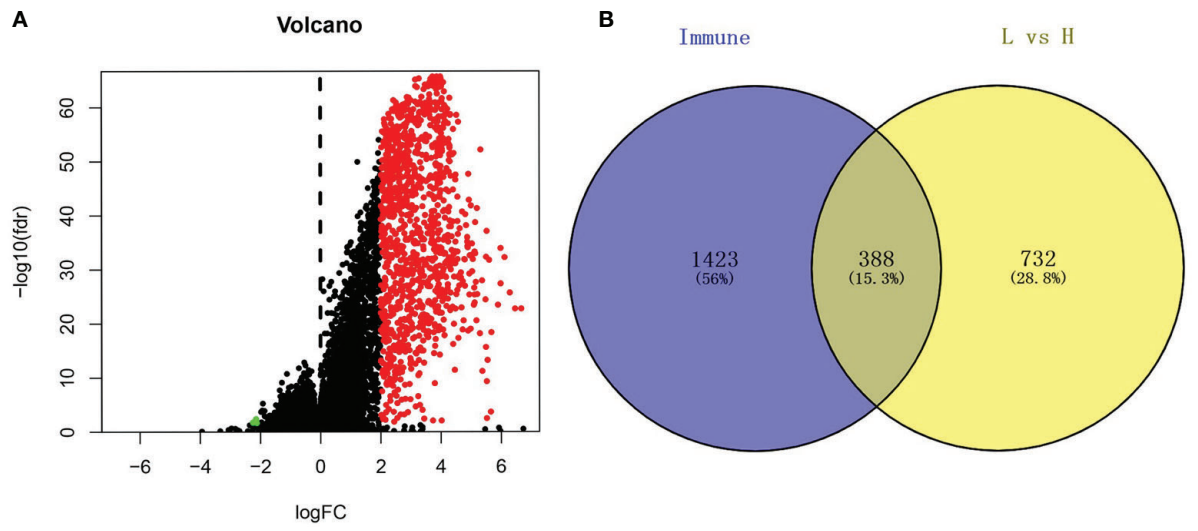

FIGURE 2 | Analysis of differentially expressed genes. **(A)** The volcano graph shows the distribution of differential genes between high immune cell infiltration cluster and low immune cell infiltration cluster, red dots represent up-regulated genes, green dots represent down-regulated genes. **(B)** Using the Venn diagram to extract intersection points, we obtained a total of 388 differentially expressed genes.

between the predicted probability and the actual observation frequency. We next displayed the results in the calibration curve, in order to represent the performance of nomogram.

Analysis of Correlation With Immune Cell Infiltration

Immune infiltration data can be obtained from the tumor obtained from immune estimation resource (TIMER) database (17). We rely on the Pearson correlation coefficient to calculate the degree of correlation between immune infiltration and risk score. Meanwhile, we used the tumor-immune system interactions and drugbank (TISIDB) database to investigate the expression of these core immune-related genes in different molecular subtypes of cutaneous melanoma (18).

RNA Extraction, cDNA Synthesis, and qRT-PCR

Total RNA was extracted respectively from melanoma cell line A375, A815, SK-MEL-28 and normal human epidermal melanocytes (NHEM) using TRIzol® reagent (Invitrogen, Carlsbad, CA) according to the manufacturer's protocol. cDNA was synthesized using reverse transcription kit (TaKaRa Biotechnology, Shiga, Japan). RNA expression levels were detected using the SYBR Green Mix (TaKaRa Biotechnology, Shiga, Japan). Target gene expression values were normalized to human GAPDH. The primer sequences were as follows: GAPDH (forward: 5′-ACTTTGGTATCGTGGAAGGACTA-3′, reverse: 5′-GTCTCTCTCTTCCTCTTGTGCTC-3′); IGHV1-18((forward: 5′-AACCAGGCCAGTCATGTGAG-3′, reverse: 5′-TGTAAGCGCTGATCCATCCC-3′); CXCL11 (forward: 5′-GACGCTGTCTTTGCATAGGC-3′, reverse: 5′-GGATTTAGGCATCGTTGTCCTTT-3′); LTF(forward: 5′-AGTCTACGGGACCGAAAGACA-3′, reverse: 5′-CAGACCTTGCAGTTCGTTCAG-3′); and HLA-DQB1(forward: 5′-GCGGGATCTTGCAGAGGAG-3′, reverse: 5′-ACTTTGATCTGGCCTGGATAGAA-3′).

RESULTS

Differentiated Grouping of Melanoma Tissue

We obtained melanoma samples and normal skin tissue samples from the TCGA database. We used ssGSEA to analyze the transcriptome data of melanoma tissue samples to assess the immune cell infiltration state. After controlling for the enrichment of multiple immune cell types, melanoma samples were divided into high and low immune cell infiltration clusters according to the degree of immune infiltration (**Figure 1A**). To test the authenticity of the above grouping scheme, we used the ESTIMATE algorithm to analyze the expression profile of melanoma and calculated the immune score, ESTIMATE score, stromal score, and tumor purity. The results suggested that the tumor purity of the high immune cell infiltration group was lower than that of the low immune cell infiltration cluster. In contrast, the values of the ESTIMATE score, immune score and stromal score were higher in the high immune cell infiltration cluster than in the low immune cell infiltration cluster (**Figure 1A**). The box chart shows that the high immune cell infiltration cluster had significantly higher immune score, ESTIMATE score and stromal score and lower tumor purity than the low immune cell infiltration cluster (**Figure 1B**). There were more immune components in the high immune cell infiltration cluster than in the low immune cell infiltration cluster, but the tumor purity of the high immune cell infiltration cluster was lower, and the expression levels of TIGIT, PDCD1, LAG3, HAVCR2, CTLA4 and the HLA family were also higher in the high immune cell infiltration cluster (**Figures 1C, D**). The CIBERSORT method was used to analyze the above two clusters and showed that there were more types of immune cells in the high immune cell infiltration cluster (**Figure 1E**). Survival analysis demonstrated that patients from the low immune cell infiltration cluster had worse prognosis than patients in the high immune cell infiltration cluster (**Figure 1F**).

Analysis of DEGs With High and Low Immune Cell Infiltration

Based on the cutoff, which was $|\log2FC| > 2$ and FDR < 0.05, we identified 1120 DEGs between the low and high immune cell infiltration clusters, which included 1116 upregulated DEGs and 4 downregulated DEGs (**Figure 2A**). We conducted a Venn analysis based on the immune genes from the import database and the DEGs from the high and low immune cell infiltration clusters. Then, we found 388 overlapping genes (**Figure 2B**), which were considered to be real DEGs.

Prognosis Models of Immune Cell Infiltration-Related DEGs

After integrating clinical information into gene expression profiles, we obtained 453 samples. We randomly selected 228 samples as the training cohort and the remaining 225 samples comprised the test cohort. All the samples together are referred to as the entire cohort. Then, we built a prognostic model with each cohort. In the training cohort, based on $p < 0.05$, univariate Cox regression analysis identified 171 genes (**Table 1**). The LASSO Cox regression algorithm was performed next (**Figures 3A, B**). Finally, multivariate Cox proportional hazards regression analysis was conducted, and the risk scores were calculated (**Figure 3C**). IGHV1-18, CXCL11, LTF and HLA-DQB1 were identified as immune cell infiltration-related DEGs. The risk score was calculated using the following formula: -0.000600085×IGHV1-18-0.032242183×CXCL11+0.003776394×LTF-0.007893899×HLA-DQB1. The survival status and risk score calculated by the prognostic model are illustrated in **Figure 4A**. Samples were classified into low- and high-risk clusters according to the median risk score. Survival analysis indicated

TABLE 1 | Univariate Cox proportional hazards regression analysis.

id	HR	HR.95L	HR.95H	pvalue
CXCL13	0.984348	0.973053	0.995773	0.007377
IGLC3	0.999731	0.999385	1.000076	0.126396
LTA	0.718796	0.561118	0.920782	0.008971
IL21R	0.800788	0.691007	0.92801	0.003146
LYZ	0.999125	0.997604	1.000648	0.259777
TRAV17	0.826178	0.681196	1.002016	0.052439
CD79A	0.99371	0.985742	1.001743	0.124528
CD8A	0.983734	0.969986	0.997677	0.02238
TRAV24	0.821879	0.652012	1.036	0.0968
IGHD3-9	0.972616	0.929259	1.017996	0.232728
IGLV5-48	0.91922	0.788898	1.071071	0.280237
TRAV1-1	0.649291	0.420767	1.00193	0.051027
IGKV5-2	0.997661	0.98566	1.009809	0.704548
IRF1	0.963002	0.942933	0.983497	0.00045
TRAV9-2	0.924825	0.794167	1.076979	0.314579
TNFSF10	0.962967	0.935795	0.990928	0.009766
IGKV1D-42	1.035907	0.9516	1.127684	0.415348
IGLV7-43	0.995479	0.988942	1.002059	0.177635
CD72	0.900216	0.837435	0.967703	0.004371
IGKV1D-13	0.998284	0.992279	1.004325	0.576791
IGKV3D-20	0.985753	0.97008	1.001679	0.079284
IGLV3-22	0.289776	0.094598	0.887653	0.030112
TRBJ2-2	0.830183	0.688906	1.000433	0.050534
IGKV1-6	1.000115	0.999664	1.000567	0.616898
TRBV20-1	0.971925	0.941046	1.003817	0.083868
CHIT1	1.005764	0.980735	1.031431	0.654887
CCL19	0.997498	0.99449	1.000516	0.104117
TRBV5-6	0.812817	0.679419	0.972406	0.023458
TRAV20	0.661623	0.456921	0.958033	0.028746
HCST	0.970771	0.952567	0.989323	0.002131
IL21	0.170536	0.026202	1.10993	0.064194
TRAV12-3	0.888752	0.777468	1.015966	0.084007
IGHV3-23	0.99981	0.999441	1.000179	0.313097
CXCR5	0.467469	0.162574	1.344173	0.158217
GNLY	0.969729	0.931052	1.010013	0.138824
TRAV4	0.850566	0.739477	0.978344	0.023417
SH2D1A	0.919189	0.857848	0.984917	0.01679
TRBJ2-7	0.936429	0.882962	0.993132	0.028545
TRAV12-2	0.934148	0.847216	1.03	0.17167
TRBC2	0.987932	0.979453	0.996485	0.00577
IGHA2	1.000057	0.997625	1.002495	0.963297
TRAV2	0.84817	0.710529	1.012474	0.068342
IGHV1-18	0.998585	0.997382	0.999791	0.021452
CTSS	0.988036	0.980716	0.995411	0.001512
PRF1	0.988879	0.977689	1.000196	0.054079
CXCL11	0.932669	0.898252	0.968404	0.00028
SECTM1	0.958286	0.928803	0.988705	0.007531
PTPN6	0.963732	0.939021	0.989093	0.005312
TRDV3	0.241489	0.022423	2.600813	0.241296
IDO1	0.983781	0.969629	0.998139	0.026967
PTPRC	0.976049	0.955428	0.997116	0.026074
IGLV4-69	0.99909	0.997747	1.000434	0.184465
TRAV26-2	0.700281	0.510627	0.960374	0.027045
IGKV3D-11	0.944423	0.88656	1.006062	0.076294
TRAV14DV4	0.89659	0.747191	1.07586	0.240504
IGLV3-16	0.955149	0.892531	1.022159	0.184697
IGLV1-40	0.999581	0.999035	1.000127	0.132357
GZMB	0.976692	0.959624	0.994064	0.008746
IGKV3D-7	0.78275	0.484053	1.265766	0.317857
IGHD	0.991429	0.974885	1.008254	0.316063
IL34	0.999049	0.994983	1.003132	0.647628
IGHA1	0.999931	0.999704	1.000158	0.549881
TRAJ5	0.687367	0.427064	1.10633	0.122629
IGLV3-10	0.999536	0.998487	1.000586	0.385935
IGHV3-64	0.984209	0.957531	1.011629	0.256252
KIR2DL3	0.019139	0.000305	1.1992	0.060942
IGHV4-34	0.996772	0.99374	0.999813	0.037507
IGHV3-38	0.968389	0.866286	1.082527	0.572049
IGHV4-31	0.995077	0.988644	1.001551	0.135798
IGKV1D-12	0.992894	0.93578	1.053494	0.813484
IGKV1-12	0.994344	0.978067	1.010892	0.500597
IGHV3-7	0.982059	0.946401	1.01906	0.337349
CD48	0.961365	0.934992	0.988482	0.005499
IGHD2-2	0.992012	0.967391	1.017258	0.531639
KIR3DL1	0.002304	1.80E-05	0.295324	0.014187
BLNK	0.834012	0.717151	0.969915	0.018445
IGHV1-24	0.99813	0.995787	1.000479	0.118614
TRBV11-3	0.411952	0.183004	0.927328	0.032177
IGHV3-11	0.999077	0.996708	1.001452	0.445862
RARRES3	0.989528	0.983129	0.995968	0.00147
TRAV35	0.798858	0.563439	1.132643	0.207406
IGKV2D-28	0.974061	0.91315	1.039035	0.425044
XCL1	0.712237	0.555962	0.91244	0.007253
TRAV25	0.656972	0.425497	1.014373	0.058016
IGKV1-5	0.999478	0.998807	1.00015	0.127654
CD19	0.944771	0.876754	1.018063	0.136132
TRBV11-1	0.549395	0.274752	1.098574	0.090255
SOCS1	0.892873	0.830715	0.959683	0.002086
CYBB	0.980011	0.966519	0.993692	0.004308
IGHV7-81	1.005581	0.977871	1.034076	0.69627
TRBV19	0.899731	0.82719	0.978633	0.013757
IFNG	0.860939	0.76748	0.965778	0.010653
IGHV2-5	0.986947	0.971414	1.002729	0.104539
CCR3	2.76E-05	1.00E-08	0.075664	0.009351
CCL25	0.322467	0.109665	0.948202	0.039723
PTAFR	0.915076	0.861884	0.971552	0.003678
IGKV2-28	0.970064	0.91002	1.034069	0.351177
IL27	0.245756	0.10748	0.561927	0.000881
IGHV3-49	0.994136	0.987745	1.000569	0.073918
IGHD3-22	0.982886	0.93641	1.031669	0.48489
IGHV2-70	1.000499	0.999137	1.001863	0.472696
IGHG1	0.999821	0.999656	0.999985	0.032441
TRAV36DV7	0.587123	0.377844	0.912319	0.017883
IGKV1-13	1.001958	0.972058	1.032776	0.899314
IGKV1-27	0.996958	0.992173	1.001767	0.21461
IGKV3-7	1.002734	0.982339	1.023553	0.794533
IGHG2	1.000014	0.999913	1.000115	0.784598
TRAV3	0.827716	0.690175	0.992667	0.041416
TRAV26-1	0.851723	0.645984	1.122988	0.255242
RAC2	0.991108	0.983664	0.998608	0.020225
IGLV2-33	0.902229	0.647986	1.256227	0.542373
TRGV9	0.004802	4.81E-05	0.479311	0.023021
PNOC	0.81392	0.63008	1.0514	0.11497
NCR3	0.766893	0.609303	0.965241	0.023735
CCL4	0.96172	0.935473	0.988702	0.005696
TRGC2	0.864399	0.760495	0.9825	0.025737
CD28	0.956191	0.852977	1.071895	0.442093
TNFSF8	0.783604	0.616645	0.995767	0.04608
TRBC1	0.78364	0.629949	0.974826	0.028607
CR2	0.954569	0.896751	1.016114	0.144698
TRAV39	0.770688	0.539998	1.099931	0.15124
IGKV2-24	0.998599	0.996005	1.001199	0.290712
TRBV6-6	0.842065	0.70615	1.00414	0.055625
IGLV7-46	1.000504	0.989546	1.011583	0.928594
ITK	0.847464	0.736534	0.975101	0.020766
CXCR3	0.963645	0.931746	0.996635	0.031067

(Continued)

TABLE 1 | Continued

id	HR	HR.95L	HR.95H	pvalue
TRAV29DV5	0.786441	0.644109	0.960225	0.018353
TRAV41	0.830592	0.646538	1.067042	0.146428
TRBV3-1	0.835045	0.720849	0.967332	0.016277
GPR33	0.007939	6.37E-06	9.8891	0.18357
IGLV3-1	0.99919	0.997691	1.000691	0.290134
TRBV7-3	0.719028	0.559452	0.92412	0.009986
CCR8	0.556926	0.297076	1.044065	0.067929
LTF	1.003849	1.000802	1.006904	0.013244
HLA-DQA2	0.993171	0.987225	0.999154	0.025332
TRBV7-7	0.853551	0.529137	1.376863	0.51629
INPP5D	0.931525	0.879298	0.986853	0.015974
CCL4L2	0.96138	0.918554	1.006202	0.090259
IGHV3-73	1.000297	0.9991	1.001496	0.626649
TRAC	0.990849	0.98393	0.997816	0.010127
CD1C	0.903242	0.800211	1.019537	0.09959
CYSLTR1	0.479634	0.261508	0.879701	0.01759
CCL8	0.913252	0.867414	0.961512	0.000553
IL2	0.046599	0.000773	2.809707	0.142642
ICOS	0.848494	0.733654	0.981311	0.026813
HLA-DOB	0.857442	0.776066	0.947351	0.002502
IGLV3-21	0.999785	0.999371	1.000199	0.309226
TNFRSF13C	0.951518	0.877325	1.031985	0.230204
FASLG	0.857629	0.762338	0.96483	0.010596
TRBV5-4	0.792528	0.644195	0.975017	0.02786
CD4	0.983991	0.972281	0.995842	0.008239
LTB	0.980002	0.962611	0.997708	0.027026
DES	1.000368	0.999574	1.001162	0.364319
CD3D	0.980379	0.966894	0.994051	0.005043
IGKV1-33	0.995864	0.954131	1.039422	0.849491
IGLV1-36	0.991292	0.979571	1.003153	0.149511
TRAV13-2	0.670833	0.493213	0.912419	0.010959
IGLV4-60	0.996695	0.990285	1.003146	0.314602
TRAV19	0.891057	0.808903	0.981555	0.019429
PTGDR	0.105933	0.021996	0.510174	0.005125
TRAV16	0.750522	0.573039	0.982975	0.037097
TRAV38-1	0.763484	0.528509	1.102929	0.150451
PDCD1	0.951432	0.914032	0.990362	0.014962
IGLV3-25	0.998951	0.997816	1.000087	0.070359
CD3E	0.983987	0.971234	0.996906	0.015286
IGHV5-51	0.998909	0.997801	1.000019	0.054012
IGLV1-44	0.999146	0.997812	1.000482	0.210314
KIR2DS4	0.395255	0.123802	1.261908	0.117067
TRAV10	0.731238	0.483965	1.10485	0.137157
CXCR6	0.93358	0.875641	0.995354	0.035516
PRKCB	0.968932	0.897984	1.045486	0.415955
TRAJ1	0.687138	0.478207	0.987354	0.042481
HLA-DQB1	0.987582	0.981567	0.993635	6.11E-05
IGLV1-47	1.000034	0.999873	1.000194	0.68076
IGKV1D-33	1.012493	0.97154	1.055172	0.555619
PTGER2	0.736064	0.549563	0.985856	0.039829
IGKV1-9	1.000002	0.999348	1.000657	0.995328
CCR7	0.972217	0.941698	1.003724	0.083358
IL2RG	0.985634	0.974714	0.996675	0.010901
TRGC1	0.444086	0.210248	0.937998	0.033359
CD3G	0.90894	0.834923	0.98952	0.02759
TRBV10-1	1.013973	0.762105	1.349081	0.92412
IGHV3-13	0.978668	0.953074	1.00495	0.11077
TRAV30	0.598581	0.358763	0.998706	0.049423
IGHV3-15	1.000011	0.999379	1.000643	0.972605
TRAV8-1	0.748404	0.534113	1.048671	0.092211
IGLV9-49	0.99951	0.997646	1.001378	0.607
HLA-DPA1	0.994536	0.991677	0.997403	0.000191
TRBJ2-1	0.9131	0.84178	0.990463	0.028459
TRAV8-4	0.770147	0.606726	0.977585	0.031852
TRBV6-1	0.854175	0.742895	0.982124	0.026881
CD1B	0.558271	0.298965	1.042485	0.067342
TNFSF14	0.409643	0.212892	0.788226	0.007527
TRAJ3	0.871951	0.662436	1.147732	0.328445
IGHV3-35	0.93667	0.819885	1.07009	0.335587
HLA-DRB5	0.997537	0.995973	0.999103	0.002066
IL32	0.981307	0.966859	0.995971	0.012652
TNFRSF18	0.80822	0.705821	0.925475	0.002067
CXCL9	0.995984	0.993101	0.998876	0.006531
IGLV1-50	0.901099	0.774313	1.048646	0.178295
IGKV2D-30	0.975436	0.906451	1.04967	0.506311
TRAV22	0.638368	0.423484	0.96229	0.03207
IL7R	0.968323	0.928411	1.009952	0.133912
FCGR3A	0.98762	0.979817	0.995486	0.002085
IGKV1D-16	0.978818	0.94709	1.011609	0.202856
TRAV23DV6	0.653167	0.440552	0.968392	0.034021
CLEC4M	0.608771	0.252406	1.468279	0.269204
IGHV4-4	0.983161	0.960424	1.006436	0.154864
TRBV7-6	0.757145	0.604004	0.949112	0.015823
IGHJ3	0.997271	0.992332	1.002236	0.28083
TRBV10-3	0.840569	0.734592	0.961835	0.01154
IGHG4	0.99985	0.999522	1.000178	0.369527
IGHV6-1	0.99903	0.976513	1.022067	0.933511
TRAV1-2	0.891762	0.747441	1.06395	0.203453
TRAV8-3	0.886507	0.780229	1.007262	0.064471
IGKV1D-39	1.001275	0.995844	1.006735	0.646172
IGHV4-28	0.998921	0.99413	1.003735	0.659886
TRDV1	0.736006	0.544399	0.995052	0.046349
CCR5	0.937949	0.896262	0.981574	0.00575
HLA-DMA	0.989833	0.984344	0.995353	0.000316
IGLV3-27	0.994248	0.981759	1.006897	0.371138
IGHV1-45	1.002258	0.996857	1.007688	0.41334
HLA-DOA	0.972465	0.956169	0.989039	0.001203
IL2RA	0.88327	0.801561	0.973308	0.012202
CD1E	0.622906	0.404843	0.958428	0.031311
XCL2	0.843041	0.757858	0.937797	0.00168
HLA-DRA	0.999395	0.999083	0.999706	0.000141
IGLV8-61	0.99894	0.994593	1.003307	0.633755
VAV1	0.919914	0.865543	0.977701	0.007243
IGHV1-2	0.999971	0.999682	1.000259	0.842042
IGLV5-45	0.997252	0.990007	1.00455	0.459541
IGLV2-8	0.996932	0.99271	1.001171	0.155837
FLT3	0.436393	0.207338	0.918495	0.028971
PRKCQ	0.842273	0.716929	0.989531	0.0368
IGKV2D-24	1.004247	0.92161	1.094294	0.922937
IGHG3	0.999201	0.99834	1.000063	0.069351
IGHV4-59	0.99918	0.997748	1.000615	0.262682
IGLC6	0.79439	0.665276	0.948563	0.010975
IGKV1D-8	1.001325	0.996262	1.006415	0.608671
CCL5	0.996567	0.993823	0.99932	0.014543
IGLV6-57	0.997351	0.994576	1.000134	0.06212
IGHV1-58	0.998696	0.995351	1.002052	0.44587
ITGAL	0.970307	0.946315	0.994907	0.018291
IGKV6D-21	0.998215	0.991737	1.004736	0.590799
IGLC2	0.999607	0.999248	0.999967	0.032221
IGKJ5	0.993873	0.977175	1.010857	0.477168
ITGB2	0.987468	0.977836	0.997195	0.011681
CMKLR1	0.999697	0.980758	1.019001	0.975215
FGR	0.911703	0.851101	0.97662	0.008437
TRBJ2-3	0.891422	0.810397	0.980547	0.018078
IGLV2-18	1.001432	0.993677	1.009247	0.718248
TRBV4-2	0.93851	0.865915	1.017193	0.122354

(Continued)

TABLE 1 | Continued

id	HR	HR.95L	HR.95H	pvalue
IGLV3-12	0.928852	0.842442	1.024124	0.138479
CD247	0.898749	0.831399	0.971555	0.00723
IGLJ1	0.829772	0.628275	1.095891	0.18858
HLA-DPB1	0.996537	0.99467	0.998407	0.000288
IL12RB1	0.870102	0.799937	0.946422	0.00118
HLA-DRB1	0.998863	0.998319	0.999407	4.27E-05
IGHJ2	0.994165	0.983602	1.004841	0.28289
TLR8	0.853271	0.739648	0.984349	0.029531
TNFRSF13B	0.807552	0.572644	1.138823	0.222938
IGHE	0.938187	0.841135	1.046437	0.25211
TRAV8-6	0.782565	0.642955	0.95249	0.014467
IGHV3-21	0.999647	0.998987	1.000308	0.295134
TRBV10-2	1.032769	0.92244	1.156293	0.575909
IGHV4-61	0.973169	0.948904	0.998055	0.034766
IGKV1D-17	1.000348	0.998996	1.001703	0.61404
IGLV3-19	0.999794	0.999433	1.000155	0.263626
IL12B	0.00779	0.000143	0.423188	0.017226
HLA-DQA1	0.983727	0.975499	0.992025	0.000129
TRBV15	0.629736	0.436528	0.908458	0.013381
TRBV28	0.979161	0.96181	0.996825	0.020967
IGHV3-43	0.994268	0.98251	1.006166	0.343573
IGLV1-51	1.000029	0.999947	1.000111	0.486773
XCR1	0.763403	0.537731	1.083784	0.131056
IGKV1-39	0.98647	0.943986	1.030866	0.54418
TYROBP	0.995021	0.991542	0.998513	0.005232
TRBV7-4	0.745151	0.441872	1.256585	0.269886
LCK	0.962643	0.934168	0.991985	0.012946
TRBV9	0.899328	0.825984	0.979185	0.014502
IGHV2-26	0.99669	0.990276	1.003145	0.314161
CCR9	1.498761	0.376537	5.965639	0.565886
IGKV3-20	0.999422	0.998877	0.999967	0.037554
CD8B	0.963847	0.9336	0.995074	0.023604
TRBV30	0.822089	0.665262	1.015886	0.069674
SCGB3A1	1.009583	1.000513	1.018735	0.03833
CD40LG	0.844627	0.693676	1.028427	0.092776
IGHD3-3	1.000226	0.991038	1.0095	0.961674
MARCO	0.990272	0.977431	1.003283	0.142145
TNF	0.744613	0.575395	0.963596	0.024968
TRAV13-1	0.924656	0.835519	1.023303	0.129882
IGLV2-23	0.999573	0.998905	1.000241	0.209806
CD74	0.999549	0.999305	0.999792	0.000283
IGHV1-69	0.998389	0.995399	1.001388	0.292067
CSF2RB	0.914809	0.857012	0.976503	0.007495
IGHV3-20	0.994732	0.982661	1.006951	0.39648
IL18	0.908756	0.851412	0.969962	0.004014
CCRL2	0.749188	0.591398	0.949077	0.016707
TRBV2	0.862911	0.728245	1.022478	0.088533
IGLV10-54	0.966349	0.927966	1.006318	0.097848
TNFRSF1B	0.981432	0.967345	0.995723	0.011051
KIR2DL4	0.667522	0.51547	0.864427	0.00218
C3	0.993528	0.987138	0.99996	0.048595
KLRD1	0.476615	0.281335	0.807443	0.005866
IGLJ3	0.573863	0.331941	0.9921	0.046772
EBI3	0.925119	0.871703	0.981808	0.010317
TRBV18	0.791619	0.658424	0.951758	0.012919
IGHV3-53	0.999341	0.994257	1.004451	0.800085
IGKV2-30	0.992261	0.977885	1.006848	0.296785
IGLJ2	0.923443	0.83405	1.022417	0.125228
PIK3CG	0.97465	0.884587	1.073884	0.603738
IGHV1-46	0.998067	0.995325	1.000817	0.168072
IGHV3-74	0.999289	0.996461	1.002125	0.622735
IGHV1-3	0.99012	0.976618	1.003809	0.156401
TRBJ2-4	0.676673	0.471436	0.97126	0.034166
IGKV1D-43	1.004241	0.973598	1.035849	0.788953
TRBV29-1	0.946347	0.892433	1.003518	0.065384
IGKV3-11	0.999853	0.999454	1.000251	0.46783
IGKC	0.999876	0.999728	1.000023	0.098663
TRDC	0.769485	0.650771	0.909856	0.002177
IGKV1-16	0.999835	0.998703	1.000968	0.774937
TRBV12-4	1.007399	0.985876	1.029392	0.50349
IGKV4-1	0.999419	0.998872	0.999966	0.03751
ZAP70	0.922358	0.865082	0.983428	0.013479
IGKV2D-29	0.999748	0.996581	1.002925	0.876288
IGLV3-9	0.997901	0.993281	1.002543	0.374931
KIR3DL2	0.026264	0.001736	0.39737	0.008645
CCL22	0.91853	0.803383	1.050181	0.21368
CXCL10	0.993961	0.990185	0.997752	0.001816
IL10RA	0.956127	0.923944	0.98943	0.010222
TRBV6-5	0.932299	0.856419	1.014903	0.105567
HLA-DMB	0.964458	0.945515	0.98378	0.000349
TRAV6	0.652322	0.42155	1.009429	0.055132
TRBV12-5	0.62701	0.334467	1.175427	0.145431
IGKV3-15	0.99935	0.99849	1.000211	0.139011
TRBV27	0.669834	0.50164	0.894422	0.006602
PMCH	0.587635	0.151747	2.2756	0.441512
IGLV2-11	0.999238	0.998003	1.000475	0.22729
INSL3	0.264349	0.11061	0.631775	0.002762
IL2RB	0.973233	0.950341	0.996677	0.025479
IGLV2-14	0.999765	0.999344	1.000186	0.273154
IGHV4-39	0.999588	0.998904	1.000273	0.238744
CIITA	0.880804	0.819196	0.947045	0.000602
IGHV3-66	0.993763	0.979889	1.007833	0.383061
TRBV13	0.733836	0.58598	0.918999	0.007023
CELA1	0.017899	0.00026	1.233778	0.062505
IGHV3-48	0.997463	0.99359	1.00135	0.200473
TRBV4-1	0.945288	0.853279	1.047218	0.281522
CD79B	0.990187	0.971681	1.009046	0.305611
IL15RA	0.876656	0.792057	0.970291	0.011008
TRAV21	0.870157	0.783858	0.965956	0.009056
TRAV8-2	0.799841	0.65272	0.980122	0.031274
TRGV2	0.659298	0.429353	1.012392	0.056952
TRAV27	0.597365	0.382695	0.932453	0.023342
TRAV5	0.83798	0.67931	1.033712	0.098863
IGHJ1	0.981717	0.947547	1.01712	0.307336
CCR4	0.847081	0.667148	1.075544	0.173135
IL18RAP	0.449836	0.251667	0.80405	0.007018
TRBV7-9	0.9426	0.896452	0.991122	0.020991
TRBV12-3	0.738332	0.518661	1.051043	0.092246
TNFRSF17	0.928495	0.857256	1.005655	0.068529
IL9R	0.152866	0.018961	1.232431	0.07778
IGLC7	0.98671	0.966924	1.0069	0.19546
CD86	0.894026	0.840241	0.951254	0.000402
IGKV1-17	0.999297	0.997911	1.000685	0.320906
IL22RA2	0.035078	0.000723	1.702522	0.090774
TRAV12-1	0.900541	0.800563	1.013006	0.081028
CCL21	0.999681	0.999065	1.000298	0.311412
TRBV5-1	0.871976	0.775543	0.980399	0.021963
CARD11	0.90201	0.832149	0.977735	0.012162
TRBV14	0.694339	0.494855	0.974238	0.034772
KLRC1	0.390563	0.187834	0.8121	0.011828
IGLV5-52	0.811665	0.345463	1.907003	0.632089
HCK	0.955146	0.924763	0.986527	0.005397
IGHM	0.999505	0.998903	1.000108	0.107537
IGHV3-30	0.998836	0.997389	1.000285	0.115289
TLR7	0.806583	0.669315	0.972002	0.023926
IGKV2D-40	0.996216	0.988696	1.003792	0.326674

(Continued)

TABLE 1 | Continued

id	HR	HR.95L	HR.95H	pvalue
TRBV11-2	0.834541	0.694854	1.002309	0.052956
TRAV34	0.418904	0.159133	1.102731	0.078079
TRBV5-5	0.655048	0.453642	0.945874	0.02402
KIR2DL1	0.038509	0.001678	0.883633	0.041615
IGHV3-33	0.999745	0.998291	1.0012	0.730882
IGHV3-72	0.997166	0.992445	1.001909	0.241071
IGKV1-8	0.990277	0.973341	1.007508	0.266967
CCR6	0.151986	0.008686	2.65949	0.197003
IGKV6-21	0.999792	0.998969	1.000616	0.620933
TNFRSF9	0.848128	0.734197	0.979739	0.025216

that low-risk patients had significantly longer overall survival times than high-risk patients (**Figure 4B**). ROC curve analysis showed that the specificity and sensitivity were highest when the risk score was 0.72, 0.72, and 0.696 according to the 1-, 3-, and 5-year survival of the area under the receiver operating characteristic curve (AUC) value, respectively (**Figure 4C**). For the testing cohort, the risk score and survival status indicated by the prognostic model are displayed in **Figure 4D**. Samples were divided into low- and high-risk clusters according to the median risk score. Survival analysis indicated that low-risk patients had significantly longer overall survival times than high-risk patients (**Figure 4E**). ROC curve analysis showed that the specificity and sensitivity were highest when the risk score was 0.669, 0.622, and 0.599 according to the 1-, 3-, and 5-year survival of the area under the AUC value, respectively (**Figure 4F**). For the entire cohort, the risk score and survival status are illustrated in **Figure 4G**. Samples were classified into low- and high-risk clusters according to the median risk score. Survival analysis indicated that low-risk patients had significantly longer overall survival times than high-risk patients (**Figure 4H**). ROC curve analysis showed that the specificity and sensitivity were highest when the risk score was 0.694, 0.67, and 0.647 according to the 1-, 3-, and 5-year survival of the area under the AUC value, respectively (**Figure 4I**). The univariate model of the training, testing and entire cohorts is shown in **Figures 5A–C**, while the multivariate model of the training, testing and entire cohorts is shown in **Figures 5D–F**. The results all demonstrated that the prognostic model has independent and moderate prognostic power for immune cell infiltration. Taking the median risk score as the standard, we divided the sample of the entire cohort into a high-risk cluster and a low-risk cluster. Based on different clinical factors, we conducted a survival analysis of the two groups of samples. In the subgroup analysis stage II, stage III, stage IV, age ≤ 60, age > 60, female, male, with tumor and free of tumor, patients in the high-risk group had shorter overall survival times than those in the low-risk group (**Figure 6**).

Construction of the Predictive Nomogram

To predict the survival rate of melanoma patients from a clinical point of view, we constructed a nomogram using TCGA data to estimate the likelihood that the OS will last for 1, 3, and 5 years. We used the following six independent prognostic factors to predict the nomogram: age, AJCC stage, grade, histological type, risk score and tumor status (**Figure 7A**). The calibration chart shows that the effectiveness of the nomogram was very good, and the 45° line represents the best predicted case. (**Figure 7B**). ROC curve analysis illustrated that the 1-, 3-, and 5-year risk score AUC values were 0.719, 0.675 and 0.688, respectively. The AUC values for the 1-, 3- and 5-year clinical factors were 0.622, 0.731 and 0.753, respectively (**Figures 8D–F**). The 1-, 3-, and 5-year AUC values for age, gender, AJCC stage, and tumor status are shown in **Figures 8A–C**.

Validation of the Screened Genes by qRT-PCR and External Melanoma Database

Compared with the normal melanocytes, IGHV1-18, CXCL11 and HLA-DQB1 were highly expressed in melanoma cell line A375,

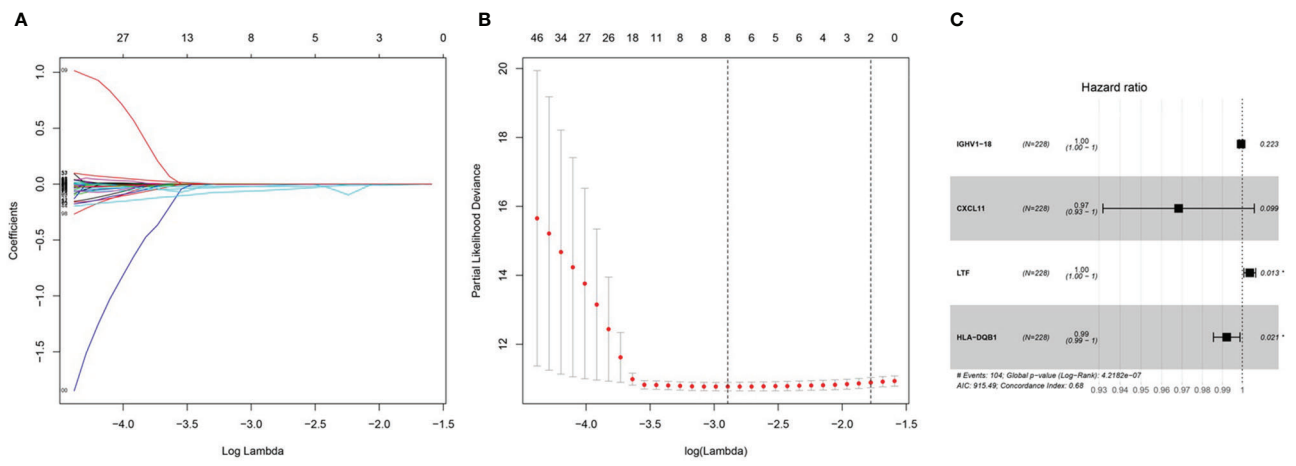

FIGURE 3 | Prognosis model of training cohort. **(A, B)** LASSO Cox regression analysis of training cohort. **(C)** multivariate Cox proportional hazards regression analysis of training cohort.

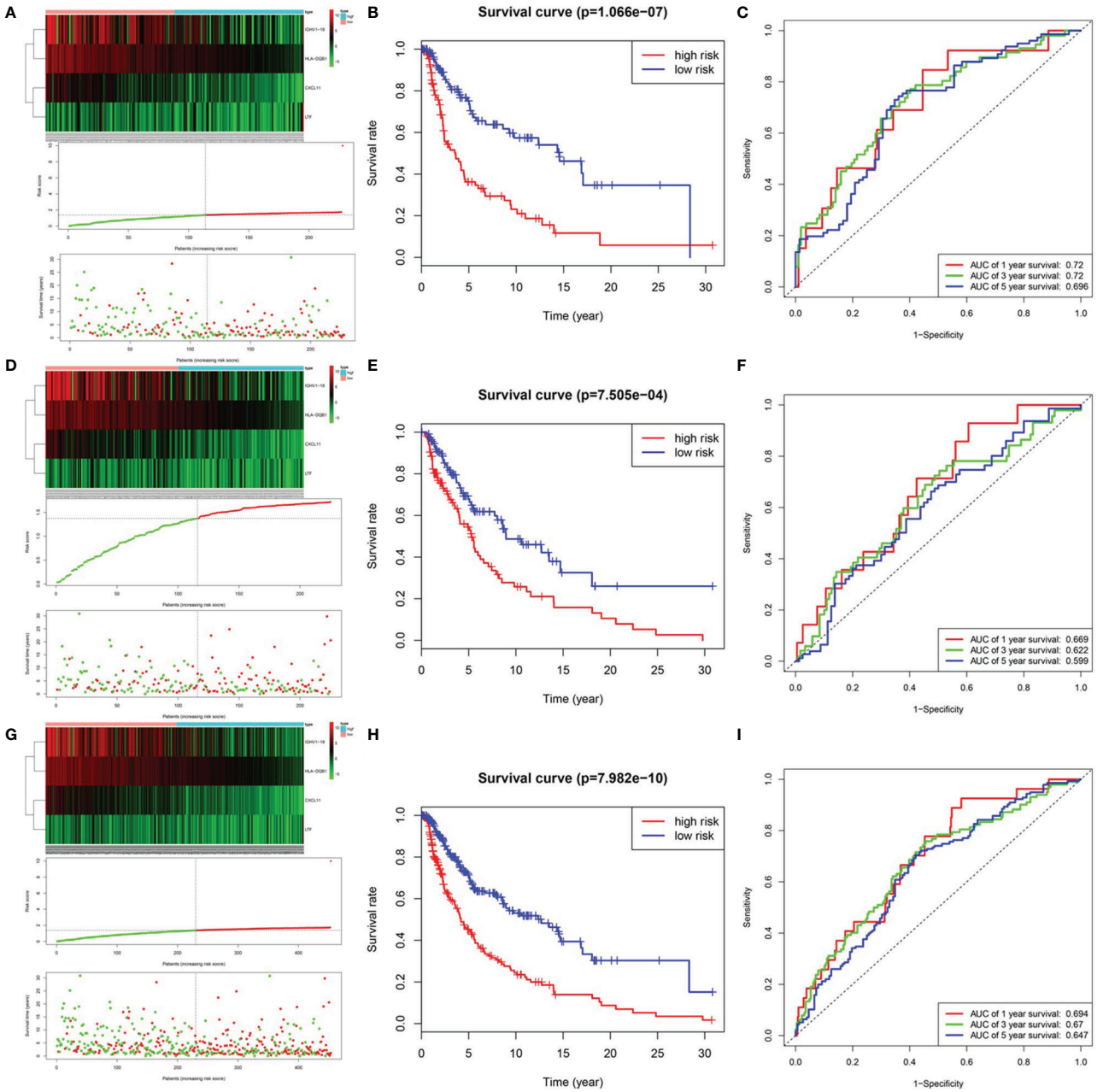

FIGURE 4 | Prognosis model of training, testing and entire cohort. **(A)** The risk score and survival status of training cohort. **(B)** Survival analysis between low-risk patients and high-risk patients of training cohort. **(C)** ROC curve analysis of training cohort. **(D)** The risk score and survival status of testing cohort. **(E)** Survival analysis between low-risk patients and high-risk patients of testing cohort **(F)** ROC curve analysis of testing cohort. **(G)** The risk score and survival status of entire cohort. **(B)** Survival analysis between low-risk patients and high-risk patients of entire cohort **(H)** Survival analysis between low-risk patients and high-risk patients of training cohort **(I)** ROC curve analysis of entire cohort.

A815 and SK-MEL-28, and LTF was downregulated in melanoma cell line A375, A815 and SK-MEL-28 (**Figure 9**), and both had statistical significance ($P < 0.05$). And the stability of the identified prognostic immune-related genes were substantiated by the external validation dataset GSE15605 containing 58 melanoma samples. Consistent with previous results, the expression of CXCL11 was higher while LTF was lower in the melanoma samples compared with normal samples. (**Figure S1**).

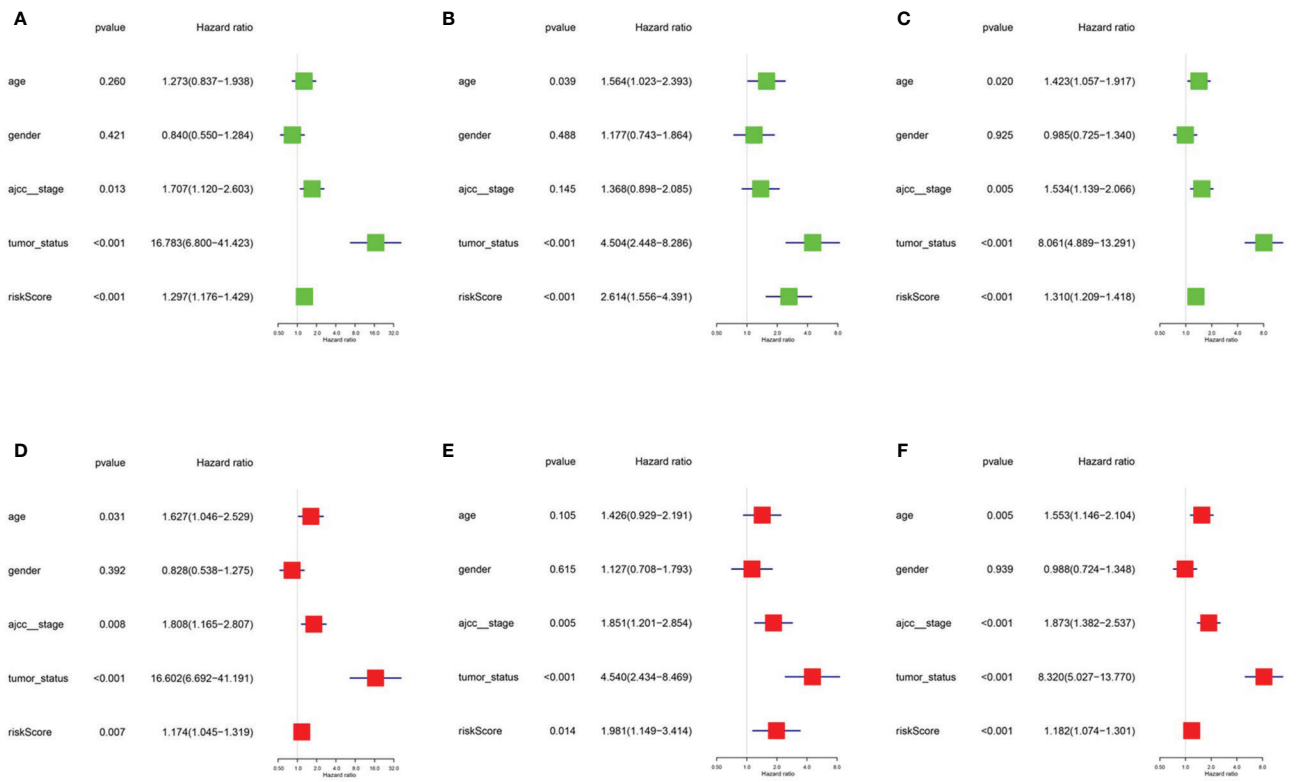

FIGURE 5 | Univariate model and multivariate model of the training, testing and entire cohort. **(A)** Univariate model of training cohort. **(B)** Univariate model of testing cohort **(C)** Univariate model of entire cohort **(D)** multivariate model of training cohort **(E)** multivariate model of testing cohort **(F)** multivariate model of entire cohort.

Correlation of the Identified Prognostic Immune-Related Genes With the Immune Cell Subtypes That Infiltrate Melanoma and the Molecular Subtypes of Cutaneous Melanoma

Because the 4 genes IGHV1-18, CXCL11, LTF and HLA-DQB1 are associated with tumor immunity, we used the TIMER database to analyze the correlation between the prognosis of these 4 genes and the infiltration of immune cell subtypes in melanoma (**Figure 10**). The correlation value of B cells with the risk score was −0.241, and the correlation value of CD4+ T cells with the risk score was −0.235. The correlation value of CD8+ T cells with the risk score was -0.422. The correlation values of dendritic cells with the risk score was −0.511. The correlation value of macrophages with the risk score was −0.255, and the correlation value of neutrophils with the risk score was −0.442. The above results suggest that the prognosis of melanoma is significantly negatively correlated with infiltration by these immune cell subtypes. In addition, compared with the normal control, the expression of IGHV1-18, CXCL11 and HLA-DQB1 were higher in the patients with cutaneous melanoma, while the expression of LTF was lower (**Figure S2**). We divide cutaneous melanoma into four subtypes (BRAF-mutant, NF1-deficient, NRAS-mutant and triple wild-type). We found that the expression of CXCL11 (P = 0.1), LTF (P = 0.28), and HLA-DQB1 (P = 0.67) had no significant relation to the subtypes of cutaneous melanoma through TISIDB database (**Figure S3**).

DISCUSSION

Melanoma is the most invasive form of skin cancer, and the incidence continues to rise worldwide. Although intense intermittent sun exposure is the main risk factor for melanoma, family history of melanoma, genetic susceptibility, environmental factors, and immunosuppression are other factors that affect the incidence (19). In recent years, immunotherapy and targeted therapy of specific factors have been increasingly used to treat melanoma. Liao et al. developed a predictive model based on two gene signatures including CCL8 and DEFB1 but lacked an exploration of its relationship with immune cells (20). Meng et al. established a signature consisted of 33 immune-related gene (IRG) pairs which associated with OS in malignant melanoma and analyzed the variations of the abundance of immune cells (21). Liu et al. identified 10 DE IRGs between primary and metastatic melanoma, and

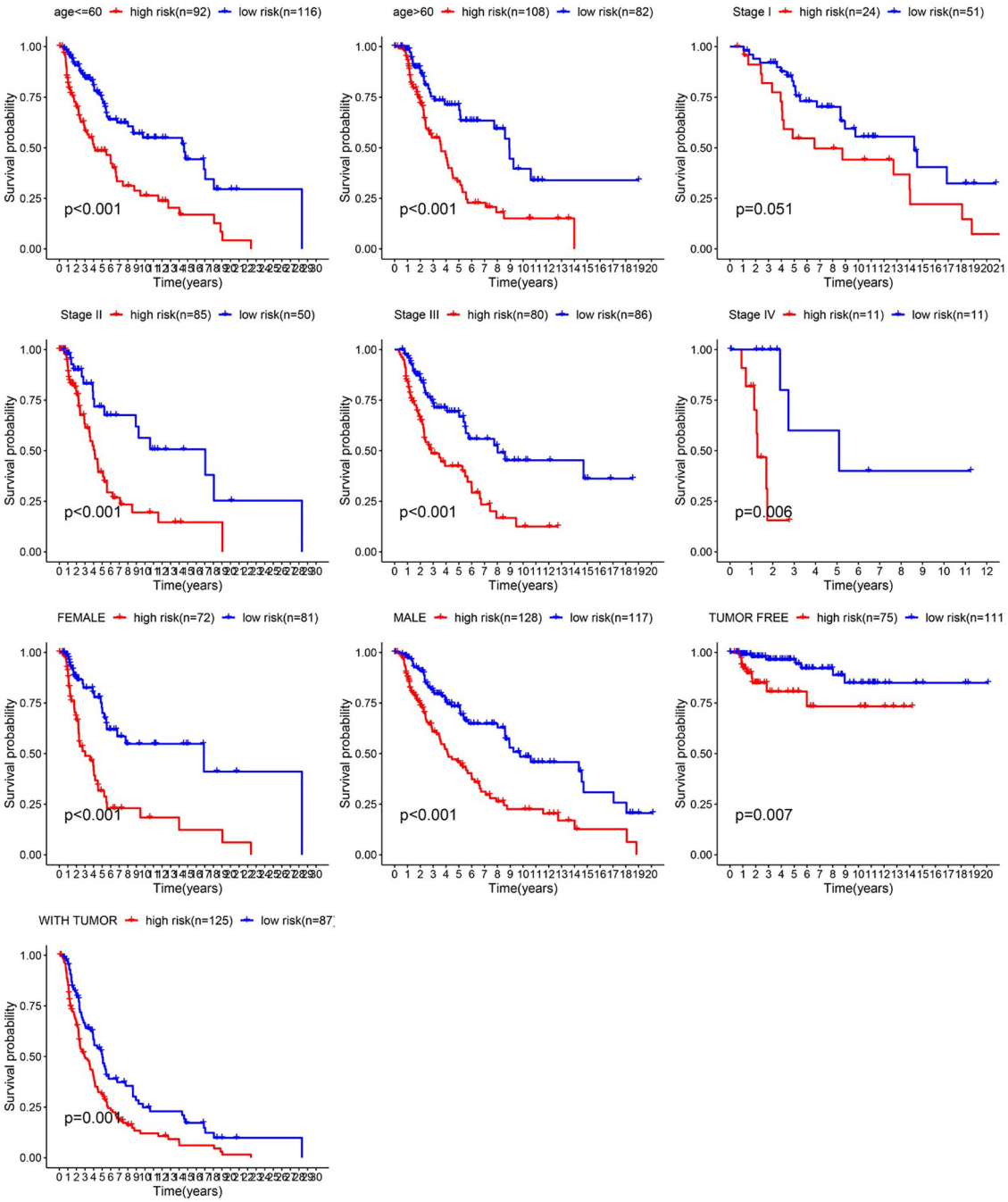

FIGURE 6 | Survival time of patients in high-risk and low-risk cluster of different subgroups.

investigated the immune infiltration and tumor mutation burden in different risk groups (22).

In this study, we focused on the immune infiltrating status in melanoma and selected IGHV1-18, CXCL11, LTF and HLA-DQB1 from immune cell infiltration cluster as immune cell infiltration-related DEGs through the analysis of differences in melanoma samples and the construction of prognostic models. In addition, we further explored the correlation of the immune cell infiltration-related DEGs with the specific immune cell subtypes, which may provide more details for the exploration of the mechanisms by which DEGs regulate the development and prognosis of melanoma.

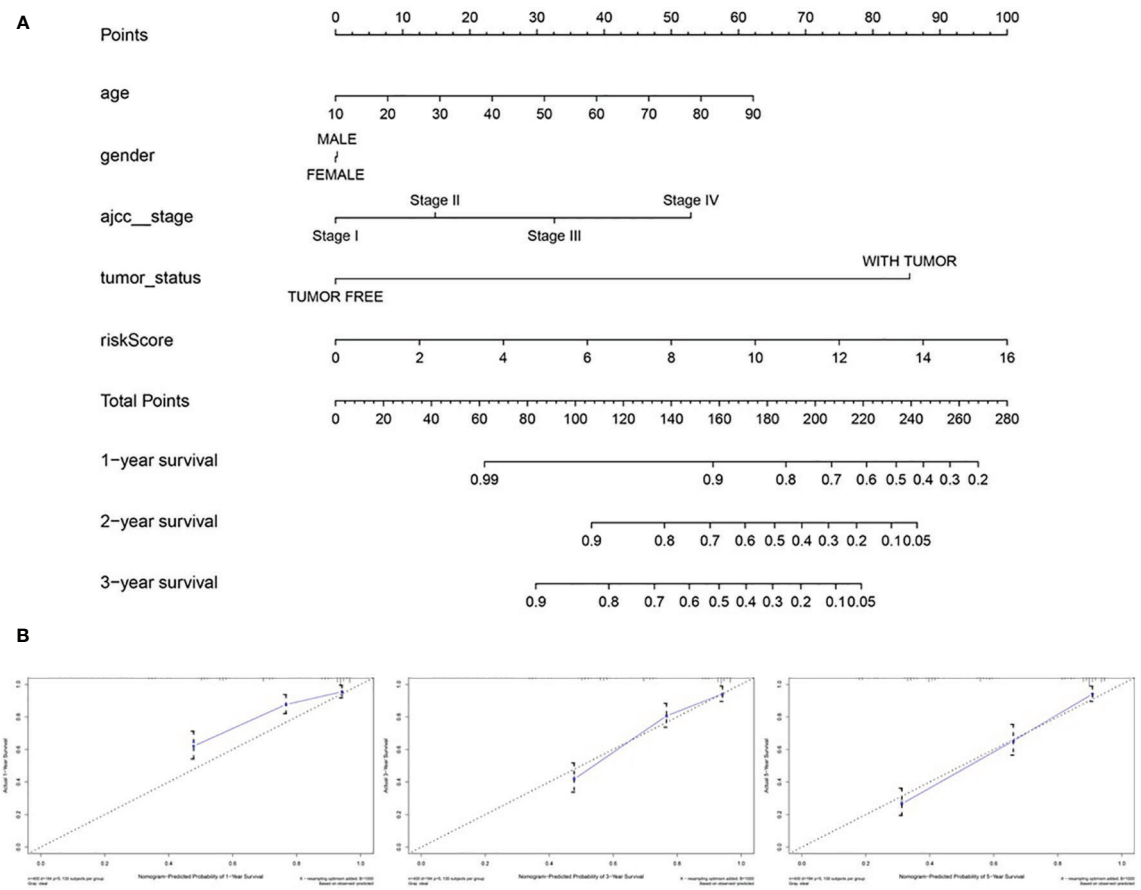

FIGURE 7 | The nomogram of predicting 1-, 3-, or 5-year OS and prognostic value of 4 genes in the entire set. **(A)** The nomogram for predicting 1-, 3-, or 5-year OS. **(B)** The calibration plots for predicting 1-, 3- or 5- year OS. Nomogram-predicted probability of survival is plotted on the x-axis; actual survival is plotted on the y-axis.

The CXCL9, -10, -11/CXCR3 axis is involved in inflammatory responses, leukocyte trafficking, adaptive resistance, hematopoiesis, cancer cell transfer and angiogenesis. Tokunaga et al. found that the CXCL9, CXCL10, and CXCL11/CXCR3 axis can be used as novel tumor treatment targets (23). C-X-C motif chemokine 11 (CXCL11) is regarded as the dominant CXCR3 agonist and can be induced by IFN-γ and type I interferons (24). CXCL11 has been found uniquely expressed in the melanoma with rich lymphocyte, and may play a potential role in the construction of tumor microenvironment by recruiting activated T-cells (25). Kremenovic et al. revealed that CXCL11, as a myeloid activation (MA) signature gene, had a positive correlation with the presence of M1 macrophages, mature dendritic cells (DC) and $CD8^+$ T cells in cutaneous melanoma patients (26).

The lactoferrin (LTF) gene, located at 3p21.3, acts as a tumor suppressor gene in diverse tumors. Zhang et al. demonstrated that LTF is dysregulated in nasopharyngeal carcinoma cell lines (27). Yi HM and others discovered expression, genetic and epigenetic alterations of the LTF gene in nasopharyngeal carcinoma cell lines (28). Wei et al. found that in B16-F10 melanoma metastasis model, the metastatic rate was higher in the LTF knockout mice (29). LTF may play a protective role in melanoma metastasis by inducing differentiation and apoptosis of myeloid-derived suppressor cells (MDSCs) and up-regulating TLR9 expression.

Polymorphisms of human leukocyte antigen (HLA) genes are thought to be associated with the susceptibility to a variety of malignancies and involved in the progress of carcinogenesis, tumor proliferation and immune escape (30). HLA-DQB1 is more extensively studied in gastric cancer and cervical cancer (31, 32). HLA-DQB1 * 0301 has been reported to be closely associated with the risk of melanoma development and progression (33). As far as we know there are indeed few reports on IGHV1-18 in melanoma. IGHV1-18 is commonly expressed in normal B cells, and the tumor or inflammatory conditions can affect B cells, which may result in mutations in the heavy chain clone gene and influence the antibody gene family usage preference (34, 35). Although IGHV1-18 has not been reported in melanoma, current studies suggest that the dynamic balance of B cells and antibodies may be related to the occurrence, development and prognosis of melanoma. In

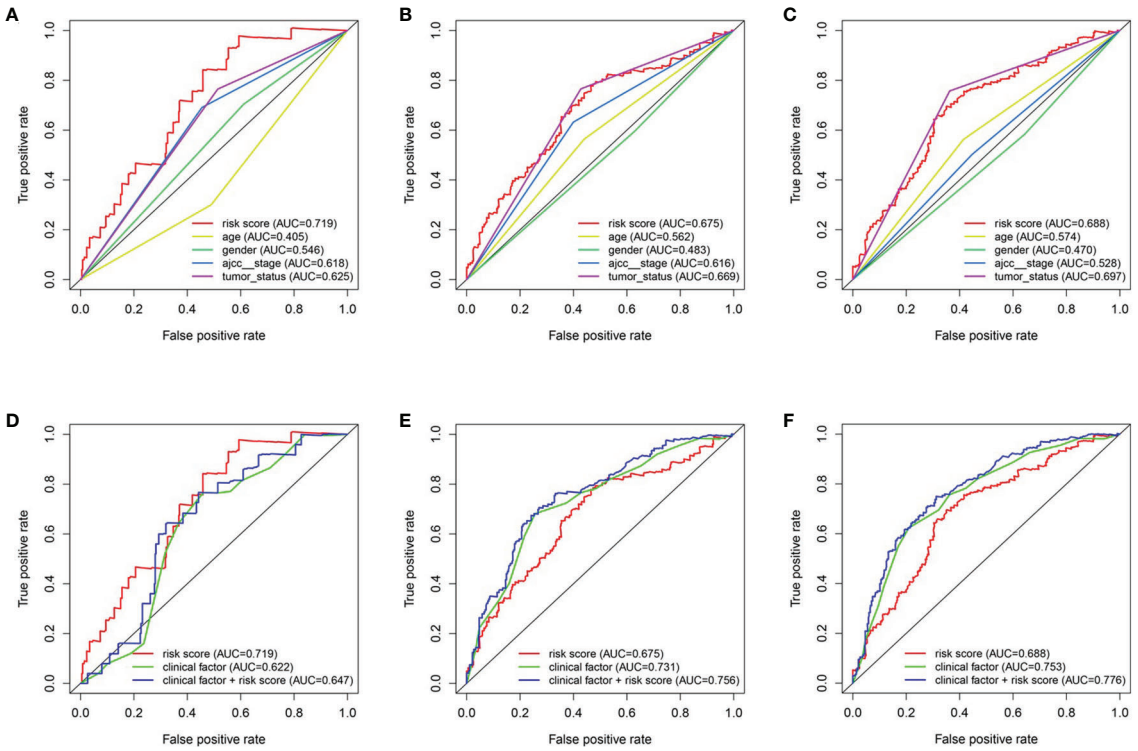

FIGURE 8 | The relationship between four genes mRNA signature and different clinical features. **(A, D)** training cohort. **(B, E)** testing cohort. **(C, F)** entire cohort.

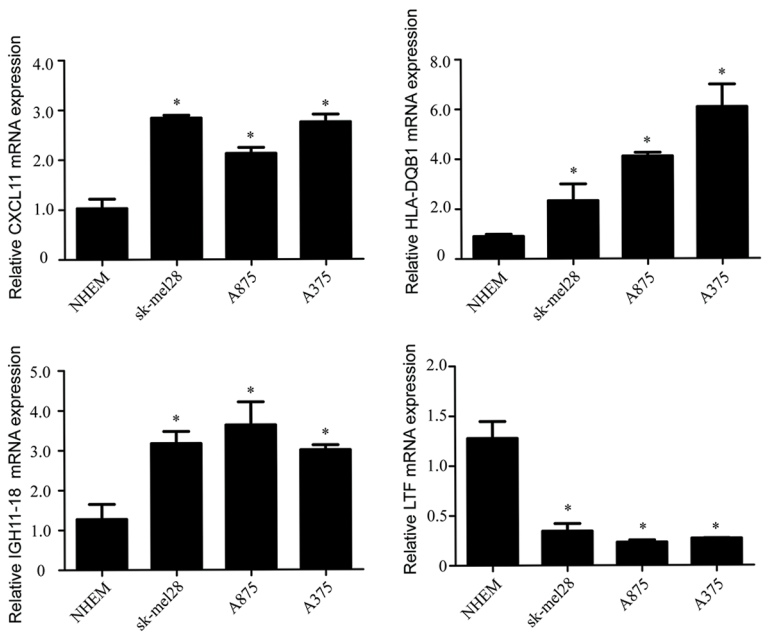

FIGURE 9 | The mRNA levels of IGHV1-18, CXCL11, LTF and HLA-DQB1 in melanoma cell line A375, A815, SK-MEL-28 and NHEM. Data are expressed as mean ± SEM. *P < 0.05. NHEM, normal human epidermal melanocytes.

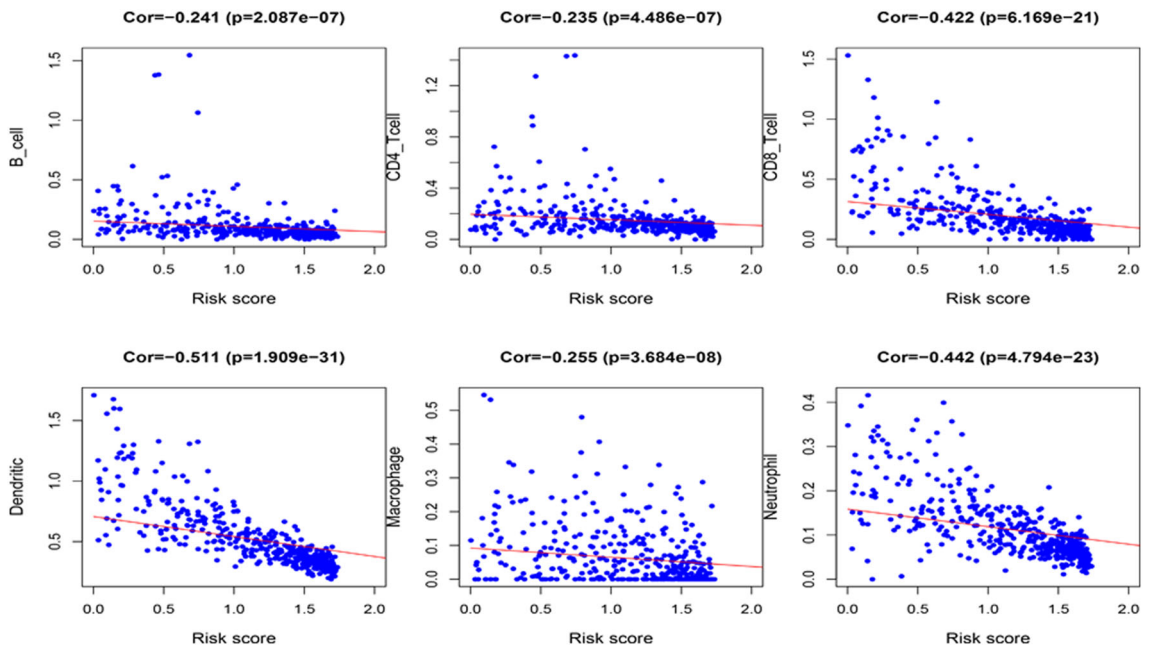

FIGURE 10 | Correlation between the 4 immune-related genes prognostic signature for melanoma and the infiltration of immune cell subtypes. The six most relevant infiltration of immune cell subtypes are shown in the figure.

melanoma, B-cells can be polarized to produce IgG4, which has low anti-tumor efficacy and may represent a possible mechanism of tumor escape (36). In addition, although it is generally believed that Ig is produced only by B lymphocytes, recent studies have reported that IgG can also be produced by non-B cells, such as epithelial cancer cells. For example, compared with normal epithelial cells, IgG from cancer cells often show unique V(D)J rearrangement or mutation hotspots (37). Therefore, further research on IGHV1-18 changes in melanoma patients may be helpful for the diagnosis and prognosis of melanoma. We have included this part of discussion in our revised manuscript accordingly.

Immunotherapy, along with surgery, radiation therapy and chemotherapy, is rapidly becoming the standard treatment for cancer. In recent years, it has been demonstrated in a variety of tumor types that the level of immune cell infiltration is inversely related to tumor purity but positively correlated with responsiveness to immune checkpoint inhibitors, which results in better prognosis and immune response (38, 39). Our results showed that the status of overall increased infiltrating immune cells in melanoma has the potential to predict clinical prognosis. Melanoma could be divided into ”hot” and “cold” status (enrich in or lack of immune cells infiltration), and the hot status is likely to correlate with antigen processing and higher expression of interferons, TNF and chemokines pathways (40). We further analyzed the infiltrating immune cell subtypes which correlated with the prognosis of melanoma. CD8+ cytotoxic T lymphocytes (CTLs) are the preferred tool for targeting tumors, and effective antitumor immunity also requires CD4+ T cells (41). Experiments have shown that CD8+ T cells and CD4+ T cells play a role in the treatment of breast cancer, colon cancer, etc. (42, 43), especially in melanoma (44, 45). Enhanced dendritic actin network formation is clearly proven to have an effect on melanoma (46). Samaniego R and others found that macrophage expression can predict human primary cutaneous melanoma progression (47). Protumor activities of macrophages have also been detected in the progression of melanoma (48). Forsthuber A and others found that CXCL5 played a role as a regulator of neutrophil function in cutaneous melanoma (49). Soler-Cardona A and others also confirmed that this mechanism is related to lymph node metastasis (50). The above results indicate that our screening and prediction about immune cell subtypes are reliable, which is beneficial to further research on melanoma immunotherapy.

Nevertheless, our study remains certain limitations. First, the data on which the prediction model was established were obtained from available public databases, though we validated it in melanoma cell lines through qRT-PCR and other external datasets, the immunohistochemistry staining of the protein level associated with DEGs and infiltrating immune cell in tumor tissues also deserves further validation. In addition, the immune cell types were identified by marker genes, but the expression level of them may not constant per cell, and hence, the cell number may be incompletely relevant to the expression level of marker genes (51). Further, a more comprehensive analysis of more types of immune cells and the stromal cells should be a focus of future research.

CONCLUSION

In this study, by analyzing the differences between melanoma samples and immune cell infiltration data, we constructed a prognostic model and identified immune-related melanoma core genes. Relevant immune cell subtypes were also identified. In the future, the identified genes and subtypes may be used in targeted therapy and immunotherapy to provide new clinical treatment ideas.

DATA AVAILABILITY STATEMENT

The original contributions presented in the study are included in the article/**Supplementary Material**. Further inquiries can be directed to the corresponding authors.

AUTHOR CONTRIBUTIONS

J-AZ and X-YZ contributed equally to this work. J-AZ and MJ together with KC designed the experiment. DH, CL, and HG provided conceptual advice and critically reviewed the article. J-AZ, X-YZ and MJ together with KC conceptually designed the study and prepared the article. All authors contributed to the article and approved the submitted version.

FUNDING

This study was supported by CAMS Innovation Fund for Medical Sciences (CIFMS-2017-I2M-1-017), the National Natural Science Foundation of China (grant nos. 81703152, 81872545 and 82073445), and the Jiangsu Province Natural Science Foundation (No. BK20170161).

SUPPLEMENTARY MATERIAL

The Supplementary Material for this article can be found online at: https://www.frontiersin.org/articles/10.3389/fonc.2020.602555/full#supplementary-material

SUPPLEMENTARY FIGURE 1 | The expression of CXCL11and LTF in melanoma patients from the GEO cohort (GSE15605), $P < 0.001$.

SUPPLEMENTARY FIGURE 2 | The expression of CXCL11, LTF, and HLA-DQB1 in the group of cutaneous melanoma and normal control.

SUPPLEMENTARY FIGURE 3 | Analysis of the expression of IGHV1-18, CXCL11, LTF, and HLA-DQB1 in different molecular subtypes of cutaneous melanoma.

REFERENCES

1. Rastrelli M, Tropea S, Rossi CR, Alaibac M. Melanoma: epidemiology, risk factors, pathogenesis, diagnosis and classification. *In Vivo* (2014) 28(6):1005–11.
2. Ribero S, Glass D, Bataille V. Genetic epidemiology of melanoma. *Eur J Dermatol* (2016) 26(4):335–9. doi: 10.1684/ejd.2016.2787
3. Duncan LM. The classification of cutaneous melanoma. *Hematol Oncol Clin North Am* (2009) 23(3):501–13, ix. doi: 10.1016/j.hoc.2009.03.013
4. Haas OA. Primary Immunodeficiency and Cancer Predisposition Revisited: Embedding Two Closely Related Concepts Into an Integrative Conceptual Framework. *Front Immunol* (2018) 9:3136. doi: 10.3389/fimmu.2018.03136
5. Odunsi K. Immunotherapy in ovarian cancer. *Ann Oncol* (2017) 28(suppl_8): viii1–7. doi: 10.1093/annonc/mdx444
6. Morrison AH, Byrne KT, Vonderheide RH. Immunotherapy and Prevention of Pancreatic Cancer. *Trends Cancer* (2018) 4(6):418–28. doi: 10.1016/j.trecan.2018.04.001
7. Park R, Williamson S, Kasi A, Saeed A. Immune Therapeutics in the Treatment of Advanced Gastric and Esophageal Cancer. *Anticancer Res* (2018) 38(10):5569–80. doi: 10.21873/anticanres.12891
8. Pampena MB, Cartar HC, Cueto GR, Levy EM, Blanco PA, Barrio MM, et al. Dissecting the Immune Stimulation Promoted by CSF-470 Vaccine Plus Adjuvants in Cutaneous Melanoma Patients: Long Term Antitumor Immunity and Short Term Release of Acute Inflammatory Reactants. *Front Immunol* (2018) 9:2531. doi: 10.3389/fimmu.2018.02531
9. Lee YT, Tan YJ, Oon CE. Molecular targeted therapy: Treating cancer with specificity. *Eur J Pharmacol* (2018) 834:188–96. doi: 10.1016/j.ejphar.2018.07.034
10. Atherton MJ, Morris JS, McDermott MR, Lichty BD. Cancer immunology and canine malignant melanoma: A comparative review. *Vet Immunol Immunopathol* (2016) 169:15–26. doi: 10.1016/j.vetimm.2015.11.003
11. da Silveira Nogueira Lima JP, Georgieva M, Haaland B, de Lima Lopes G. A systematic review and network meta-analysis of immunotherapy and targeted therapy for advanced melanoma. *Cancer Med* (2017) 6(6):1143–53. doi: 10.1002/cam4.1001
12. Sullivan RJ. The role of targeted therapy for melanoma in the immunotherapy era. *Semin Cutan Med Surg* (2018) 37(2):112–9. doi: 10.12788/j.sder.2018.021
13. Tomczak K, Czerwińska P, Wiznerowicz M. The Cancer Genome Atlas (TCGA): an immeasurable source of knowledge. *Contemp Oncol (Pozn)* (2015) 19(1a):A68–77. doi: 10.5114/wo.2014.47136
14. Bindea G, Mlecnik B, Tosolini M, Kirilovsky A, Waldner M, Obenauf AC, et al. Spatiotemporal dynamics of intratumoral immune cells reveal the immune landscape in human cancer. *Immunity* (2013) 39(4):782–95. doi: 10.1016/j.immuni.2013.10.003
15. Gonnord P, Costa M, Abreu A, Peres M, Ysebaert L, Gadat S, et al. Multiparametric analysis of CD8(+) T cell compartment phenotype in chronic lymphocytic leukemia reveals a signature associated with progression toward therapy. *Oncoimmunology* (2019) 8(4):e1570774. doi: 10.1080/2162402x.2019.1570774
16. Heagerty PJ, Zheng Y. Survival model predictive accuracy and ROC curves. *Biometrics* (2005) 61(1):92–105. doi: 10.1111/j.0006-341X.2005.030814.x
17. Li T, Fan J, Wang B, Traugh N, Chen Q, Liu JS, et al. TIMER: A Web Server for Comprehensive Analysis of Tumor-Infiltrating Immune Cells. *Cancer Res* (2017) 77(21):e108–e10. doi: 10.1158/0008-5472.Can-17-0307
18. Ru B, Wong CN, Tong Y, Zhong JY, Zhong SSW, Wu WC, et al. TISIDB: an integrated repository portal for tumor-immune system interactions. *Bioinformatics* (2019) 35(20):4200–2. doi: 10.1093/bioinformatics/btz210
19. Schadendorf D, Fisher DE, Garbe C, Gershenwald JE, Grob JJ, Halpern A, et al. Melanoma. *Nat Rev Dis Primers* (2015) 1:15003. doi: 10.1038/nrdp.2015.3
20. Liao M, Zeng F, Li Y, Gao Q, Yin M, Deng G, et al. A novel predictive model incorporating immune-related gene signatures for overall survival in melanoma patients. *Sci Rep* (2020) 10(1):12462. doi: 10.1038/s41598-020-69330-2
21. Meng L, He X, Zhang X, Zhang X, Wei Y, Wu B, et al. Predicting the clinical outcome of melanoma using an immune-related gene pairs signature. *PloS One* (2020) 15(10):e0240331. doi: 10.1371/journal.pone.0240331
22. Liu N, Liu Z, Liu X, Duan X, Huang Y, Jin Z, et al. Identification of an Immune-Related Prognostic Signature Associated With Immune Infiltration in Melanoma. *Front Genet* (2020) 11:1002. doi: 10.3389/fgene.2020.01002
23. Tokunaga R, Zhang W, Naseem M, Puccini A, Berger MD, Soni S, et al. CXCL9, CXCL10, CXCL11/CXCR3 axis for immune activation - A target for novel cancer therapy. *Cancer Treat Rev* (2018) 63:40–7. doi: 10.1016/j.ctrv.2017.11.007

24. Kuo PT, Zeng Z, Salim N, Mattarollo S, Wells JW, Leggatt GR. The Role of CXCR3 and Its Chemokine Ligands in Skin Disease and Cancer. *Front Med (Lausanne)* (2018) 5:271. doi: 10.3389/fmed.2018.00271
25. Harlin H, Meng Y, Peterson AC, Zha Y, Tretiakova M, Slingluff C, et al. Chemokine expression in melanoma metastases associated with CD8+ T-cell recruitment. *Cancer Res* (2009) 69(7):3077–85. doi: 10.1158/0008-5472.Can-08-2281
26. Kremenovic M, Rombini N, Chan AA, Gruber T, Bäriswyl L, Lee DJ, et al. Characterization of a Myeloid Activation Signature that Correlates with Survival in Melanoma Patients. *Cancers (Basel)* (2020) 12(6):1431. doi: 10.3390/cancers12061431
27. Zhang H, Feng X, Liu W, Jiang X, Shan W, Huang C, et al. Underlying mechanisms for LTF inactivation and its functional analysis in nasopharyngeal carcinoma cell lines. *J Cell Biochem* (2011) 112(7):1832–43. doi: 10.1002/jcb.23101
28. Yi HM, Li YC, Zhong RH. [Expression, genetic and epigenetic alterations of LTF gene in nasopharyngeal carcinoma cell lines]. *Zhonghua Zhong Liu Za Zhi* (2010) 32(10):729–33. doi: 10.3760/cma.j.issn.0253-3766.2010.10.003
29. Wei L, Zhang X, Wang J, Ye Q, Zheng X, Peng Q, et al. Lactoferrin deficiency induces a pro-metastatic tumor microenvironment through recruiting myeloid-derived suppressor cells in mice. *Oncogene* (2020) 39(1):122–35. doi: 10.1038/s41388-019-0970-8
30. Sabbatino F, Liguori L, Polcaro G, Salvato I, Caramori G, Salzano FA, et al. Role of Human Leukocyte Antigen System as A Predictive Biomarker for Checkpoint-Based Immunotherapy in Cancer Patients. *Int J Mol Sci* (2020) 21 (19):7295. doi: 10.3390/ijms21197295
31. Zhou SK, Yang LL, Chen R, Lu Y, Zheng YH. HLA-DQB1*03 genotype and perioperative blood transfusion are not conducive to the prognosis of patients with gastric cancer. *J Clin Lab Anal* (2018) 32(7):e22443. doi: 10.1002/jcla.22443
32. Shim H, Park B, Shin HJ, Joo J, Yoon KA, Kim YM, et al. Protective association of HLA-DRB1*13:02, HLA-DRB1*04:06, and HLA-DQB1*06:04 alleles with cervical cancer in a Korean population. *Hum Immunol* (2019) 80 (2):107–11. doi: 10.1016/j.humimm.2018.10.013
33. Lee JE, Reveille JD, Ross MI, Platsoucas CD. HLA-DQB1*0301 association with increased cutaneous melanoma risk. *Int J Cancer* (1994) 59(4):510–3. doi: 10.1002/ijc.2910590413
34. Ghia P, Stamatopoulos K, Belessi C, Moreno C, Stella S, Guida G, et al. Geographic patterns and pathogenetic implications of IGHV gene usage in chronic lymphocytic leukemia: the lesson of the IGHV3-21 gene. *Blood* (2005) 105(4):1678–85. doi: 10.1182/blood-2004-07-2606
35. Feng J, Fan S, Sun Y, Zhang Z, Ren H, Li W, et al. Study of B Cell Repertoire in Patients With Anti-N-Methyl-D-Aspartate Receptor Encephalitis. *Front Immunol* (2020) 11:1539. doi: 10.3389/fimmu.2020.01539
36. Karagiannis P, Gilbert AE, Josephs DH, Ali N, Dodev T, Saul L, et al. IgG4 subclass antibodies impair antitumor immunity in melanoma. *J Clin Invest* (2013) 123(4):1457–74. doi: 10.1172/jci65579
37. Geng ZH, Ye CX, Huang Y, Jiang HP, Ye YJ, Wang S, et al. Human colorectal cancer cells frequently express IgG and display unique Ig repertoire. *World J Gastrointest Oncol* (2019) 11(3):195–207. doi: 10.4251/wjgo.v11.i3.195
38. Sharma P, Allison JP. The future of immune checkpoint therapy. *Science* (2015) 348(6230):56–61. doi: 10.1126/science.aaa8172
39. Zhou X, Qiu S, Nie L, Jin D, Jin K, Zheng X, et al. Classification of Muscle-Invasive Bladder Cancer Based on Immunogenomic Profiling. *Front Oncol* (2020) 10:1429. doi: 10.3389/fonc.2020.01429
40. Olbryt M, Rajczykowski M, Widłak W. Biological Factors behind Melanoma Response to Immune Checkpoint Inhibitors. *Int J Mol Sci* (2020) 21(11):4071. doi: 10.3390/ijms21114071
41. Borst J, Ahrends T, Bąbała N, Melief CJM, Kastenmüller W. CD4(+) T cell help in cancer immunology and immunotherapy. *Nat Rev Immunol* (2018) 18 (10):635–47. doi: 10.1038/s41577-018-0044-0
42. Jagtap SV. Evaluation of CD4+ T-cells and CD8+ T-cells in triple-negative invasive breast cancer. *Indian J Pathol Microbiol* (2018) 61(4):477–8. doi: 10.4103/ijpm.Ijpm_201_18
43. Zhang L, Yu X, Zheng L, Zhang Y, Li Y, Fang Q, et al. Lineage tracking reveals dynamic relationships of T cells in colorectal cancer. *Nature* (2018) 564 (7735):268–72. doi: 10.1038/s41586-018-0694-x
44. Veatch JR, Lee SM, Fitzgibbon M, Chow IT, Jesernig B, Schmitt T, et al. Tumor-infiltrating BRAFV600E-specific CD4+ T cells correlated with complete clinical response in melanoma. *J Clin Invest* (2018) 128(4):1563–8. doi: 10.1172/jci98689
45. Li H, van der Leun AM, Yofe I, Lubling Y, Gelbard-Solodkin D, van Akkooi ACJ, et al. Dysfunctional CD8 T Cells Form a Proliferative, Dynamically Regulated Compartment within Human Melanoma. *Cell* (2019) 176(4):775–89.e18. doi: 10.1016/j.cell.2018.11.043
46. Mohan AS, Dean KM, Isogai T, Kasitinon SY, Murali VS, Roudot P, et al. Enhanced Dendritic Actin Network Formation in Extended Lamellipodia Drives Proliferation in Growth-Challenged Rac1(P29S) Melanoma Cells. *Dev Cell* (2019) 49(3):444–60.e9. doi: 10.1016/j.devcel.2019.04.007
47. Samaniego R, Gutiérrez-González A, Gutiérrez-Seijo A, Sánchez-Gregorio S, García-Giménez J, Mercader E, et al. CCL20 Expression by Tumor-Associated Macrophages Predicts Progression of Human Primary Cutaneous Melanoma. *Cancer Immunol Res* (2018) 6(3):267–75. doi: 10.1158/2326-6066.Cir-17-0198
48. Wang H, Yang L, Wang D, Zhang Q, Zhang L. Pro-tumor activities of macrophages in the progression of melanoma. *Hum Vaccin Immunother* (2017) 13(7):1556–62. doi: 10.1080/21645515.2017.1312043
49. Forsthuber A, Lipp K, Andersen L, Ebersberger S, Graña C, Ellmeier W, et al. CXCL5 as Regulator of Neutrophil Function in Cutaneous Melanoma. *J Invest Dermatol* (2019) 139(1):186–94. doi: 10.1016/j.jid.2018.07.006
50. Soler-Cardona A, Forsthuber A, Lipp K, Ebersberger S, Heinz M, Schossleitner K, et al. CXCL5 Facilitates Melanoma Cell-Neutrophil Interaction and Lymph Node Metastasis. *J Invest Dermatol* (2018) 138 (7):1627–35. doi: 10.1016/j.jid.2018.01.035
51. Kwak M, Erdag G, Slingluff CL Jr. Gene expression analysis in formalin fixed paraffin embedded melanomas is associated with density of corresponding immune cells in those tissues. *Sci Rep* (2020) 10(1):18336. doi: 10.1038/s41598-020-74996-9

Conflict of Interest: The authors declare that the research was conducted in the absence of any commercial or financial relationships that could be construed as a potential conflict of interest.

frontiers in Oncology

ORIGINAL RESEARCH
published: 24 March 2021
doi: 10.3389/fonc.2021.639874

A Four-Gene-Based Prognostic Model Predicts Overall Survival in Patients With Cutaneous Melanoma

Xiaoxia Tong[1,2†], *Xiaofei Qu*[1,2†] *and Mengyun Wang*[1,2*]

[1] Cancer Institute, Fudan University Shanghai Cancer Center, Shanghai, China, [2] Department of Oncology, Shanghai Medical College, Fudan University, Shanghai, China

OPEN ACCESS

Edited by:
Wen-Qing Li,
Peking University Cancer Hospital, China

Reviewed by:
Yun Hak Kim,
Pusan National University, South Korea
Ioana Cosgarea,
Newcastle University, United Kingdom

***Correspondence:**
Mengyun Wang
wangmengyun@fudan.edu.cn

†These authors have contributed equally to this work

Specialty section:
This article was submitted to Skin Cancer, a section of the journal Frontiers in Oncology

Received: 24 December 2020
Accepted: 29 January 2021
Published: 24 March 2021

Citation:
Tong X, Qu X and Wang M (2021) A Four-Gene-Based Prognostic Model Predicts Overall Survival in Patients With Cutaneous Melanoma. Front. Oncol. 11:639874. doi: 10.3389/fonc.2021.639874

Background: Cutaneous melanoma (CM) is one of the most aggressive cancers with highly metastatic ability. To make things worse, there are limited effective therapies to treat advanced CM. Our study aimed to investigate new biomarkers for CM prognosis and establish a novel risk score system in CM.

Methods: Gene expression data of CM from Gene Expression Omnibus (GEO) datasets were downloaded and analyzed to identify differentially expressed genes (DEGs). The overlapped DEGs were then verified for prognosis analysis by univariate and multivariate COX regression in The Cancer Genome Atlas (TCGA) datasets. Based on the gene signature of multiple survival associated DEGs, a risk score model was established, and its prognostic and predictive role was estimated through Kaplan-Meier (K-M) analysis and log-rank test. Furthermore, the correlations between prognosis related genes expression and immune infiltrates were analyzed *via* Tumor Immune Estimation Resource (TIMER) site.

Results: A total of 103 DEGs were obtained based on GEO cohorts, and four genes were verified in TCGA datasets. Subsequently, four genes (*ADAMDEC1, GNLY, HSPA13*, and *TRIM29*) model was developed by univariate and multivariate Cox regression analyses. The K-M plots showed that the high-risk group was associated with shortened survival than that in the low-risk group ($P < 0.0001$). Multivariate analysis suggested that the model was an independent prognostic factor (high-risk vs. low-risk, HR= 2.06, $P < 0.001$). Meanwhile, the high-risk group was prone to have larger breslow depth ($P< 0.001$) and ulceration ($P< 0.001$).

Conclusions: The four-gene risk score model functions well in predicting the prognosis and treatment response in CM and will be useful for guiding therapeutic strategies for CM patients. Additional clinical trials are needed to verify our findings.

Keywords: prognosis, cutaneous melanoma, risk score, gene signature, survival

INTRODUCTION

Cutaneous melanoma (CM) accounts for over 74% of skin cancer related death each year (1), which makes it one of the most malignant cancers, with tremendously poor prognosis (2, 3). The incidence of CM has continued to increase annually. Although tremendous efforts toward early detection and therapeutics were made, advanced stage melanoma patients still exhibit disappointing prognosis with 5-year overall survival rate ranging from 45% for stage III to 18% for stage IV (4, 5).

Cutaneous melanoma is a highly heterogeneous tumor, in terms of clinical and complicated molecular (5). Several clinical features, such as age, gender, stage, ulceration and breslow thickness have been shown to be the important clinicopathological characteristics for predicting the outcome of CM patient (6). However, due to the high potentiality for CM metastasis, the prognosis remains poor. Molecular biomarkers are important in guiding treatment selection and predicting outcome in tumor patients (7–9). For example, the 21-gene recurrence score assay is prognostic for women with node-negative, estrogen-receptor-positive breast cancer treated with tamoxifen (10). Although hundreds of studies have explored the prognostic value of molecular markers, there is still no recommended molecular marker to predict CM prognosis.

In the current study, we were devoted to exploring new biomarkers and establishing a risk score model to predict prognosis, aiming to provide appropriate therapeutic methods for CM patients.

MATERIALS AND METHODS

Gene Expression Omnibus (GEO) Datasets Collection and Enrichment Analysis

Gene expression raw microarray cell intensity (CEL) profiles of CM were evaluated in three independent datasets from the GEO database (accession number: GSE7553, GSE46517, and GSE15605), which included 57 tumor tissue samples and three normal skin samples; 85 tumor tissue samples and eight normal skin samples; 60 tumor tissue samples and six normal skin samples, respectively. The microarray data GSE65904 containing 214 patients was downloaded to verify our risk model. Four patients were deleted due to lack of follow-up information. When more than one probe matched the same gene ID, the mean expression value of the gene was used for our study.

The Cancer Genome Atlas (TCGA) Dataset

The TCGA CM dataset, containing 459 tumor samples which included raw counts of RNAseq expression data and clinicopathological characteristics were obtained from cBioPortal website. The TCGA dataset was randomly divided into two parts: the training cohort and the validation cohort.

Identification of Common Differential Expression Genes (DEG)

The GSE7553, GSE46517, and GSE15605 expression profiles were normalized and the DEG were calculated using the LIMMA package. In this study, Gene sets with False Discovery Rate (FDR) < 0.05 and with the threshold of |logFC|>1 were defined as DEGs. All the data processing and normalization were performed using the R software.

Identification and Selection of Prognosis-Related Genes

Univariate and multivariate Cox regression analyses model were commonly employed in survival analysis. Genes were considered significant when the *P* value were <0.05 in the univariate and multivariate Cox regression analysis based on training and validation cohorts. These genes were used to construct the risk model. The fitness of the models was compared based on Akaike information criterion (AIC) and the lowest value of AIC provided the sensitivity and specificity. Subsequently, four genes (*ADAMDEC1, GNLY, HSPA13*, and *TRIM29*) were selected.

Construction and Assessment of Risk Score System

Based on the prognosis associated genes, a risk score model was constructed for the CM patients. Each gene was added one at a time in the risk score system and the risk score for each patient was calculated as the sum of each gene's score as follows:

$$\text{Risk score} = \beta\text{gene1}^{*}\text{Exp gene1} + \beta\text{gene2}^{*}\text{Exp gene2} + \cdots + \beta\text{gene}(n)^{*}\text{Exp gene(n)}$$

In this formula, βgene(n) represents the coefficient of each gene from univariate Cox regression analysis, and Exp gene(n) displays the expression of each gene.

Then all TCGA patients were separated into high and low-risk subgroups according to the optimal cut-off value of risk score. The optimal cut-off value of risk score was determined by the time-dependent receiver operating characteristic (ROC) curve using "survivalROC" package. To compare the survival time difference between the low- and high-risk group, K-M curve was produced by the "Survminer" package using the log-rank test. The predictive accuracy of this risk score model was determined by time-dependent ROC curve analysis. The area under the curve (AUC) was calculated to measure the predictive ability of the gene signature for clinical outcomes.

Immune Infiltration Analysis

The abundance of tumor infiltrating immune cells in CM was predicted using the Tumor Immune Estimation Resource (TIMER) algorithm. The correlation between prognostic gene expression and the abundance of different immune cells, including CD8+ T cells, CD4+ T cells, macrophages, B cells, neutrophils, and dendritic cells was measured using the

Spearman's test. All hypothetical tests were two-sided and *P* values < 0.05 were considered statistically significant.

RESULTS

Screening of DEG

To describe our study more clearly, a flow chart of the analysis procedure was developed (**Figure 1**). After the analyses of GSE7553, GSE46517, and GSE15605 data sets, DEGs were identified and selected. The overlap among three data sets included 103 DEGs was shown in the Venn diagram (**Figure 2A**). The volcano plots and heatmap of each data set are shown in **Figures 2B–G**.

Construction of Risk Score System

We conducted univariate and multivariate Cox regression to investigate the correlation of the DEGs with the overall survival of TCGA CM patients in training, validation and total cohort. Basic characteristics of the patients are shown in **Table 1**. The result revealed that *GNLY, DFNA28, ADAMDEC1, ALOXE3, EFNA3, EPN3, EVPL, FERMT1, HSPA13, JAG2, RAPGEFL1, SULT2B1, TGM3*, and *TRIM29* were significant prognostic factors. Furthermore, in order to select the best performance efficacy predictive model with the lowest AIC value, we performed the stepwise multivariate Cox regression analysis to identify independent predictors for overall survival of total TCGA CM patients. Finally, four prognosis–associated genes *(GNLY, ADAMDEC1, HSPA13*, and *TRIM29*) were selected for constructing the risk score system (**Table 2**). The formula was as follows:

$$Riskscore = (-0.101)^{*}ExpADAMDEC1 + (-0.091)^{*}ExpGNLY + (-0.284)^{*}ExpHSPA13 + 0.102^{*}ExpTRIM29$$

To evaluate the prognostic significance of the risk score, K-M plot of high and low risk CM patients were conducted. According to the optimal cut-off value of risk score, the patients in the total TCGA cohort were classified into high (312 patients) and low (147 patients) risk groups. Compared to the high-risk group with the median OS time of 27.76 months,

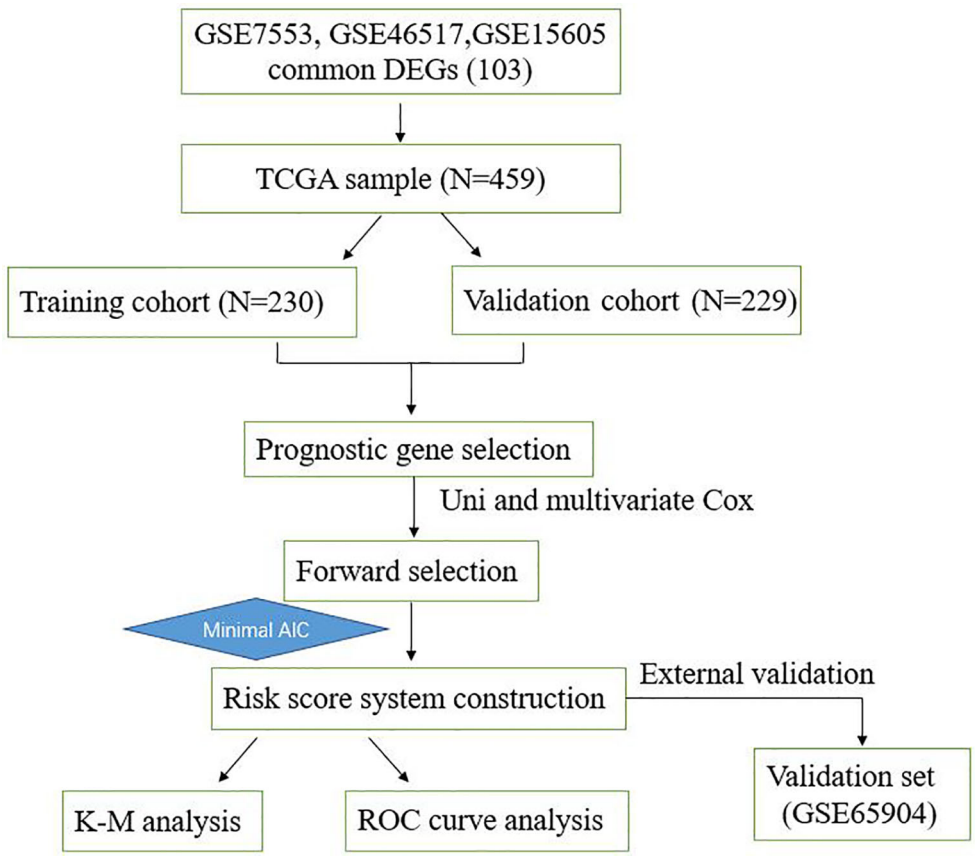

FIGURE 1 | Overall workflow describing the process used to develop and validate the prognostic model to predict prognostic outcomes.

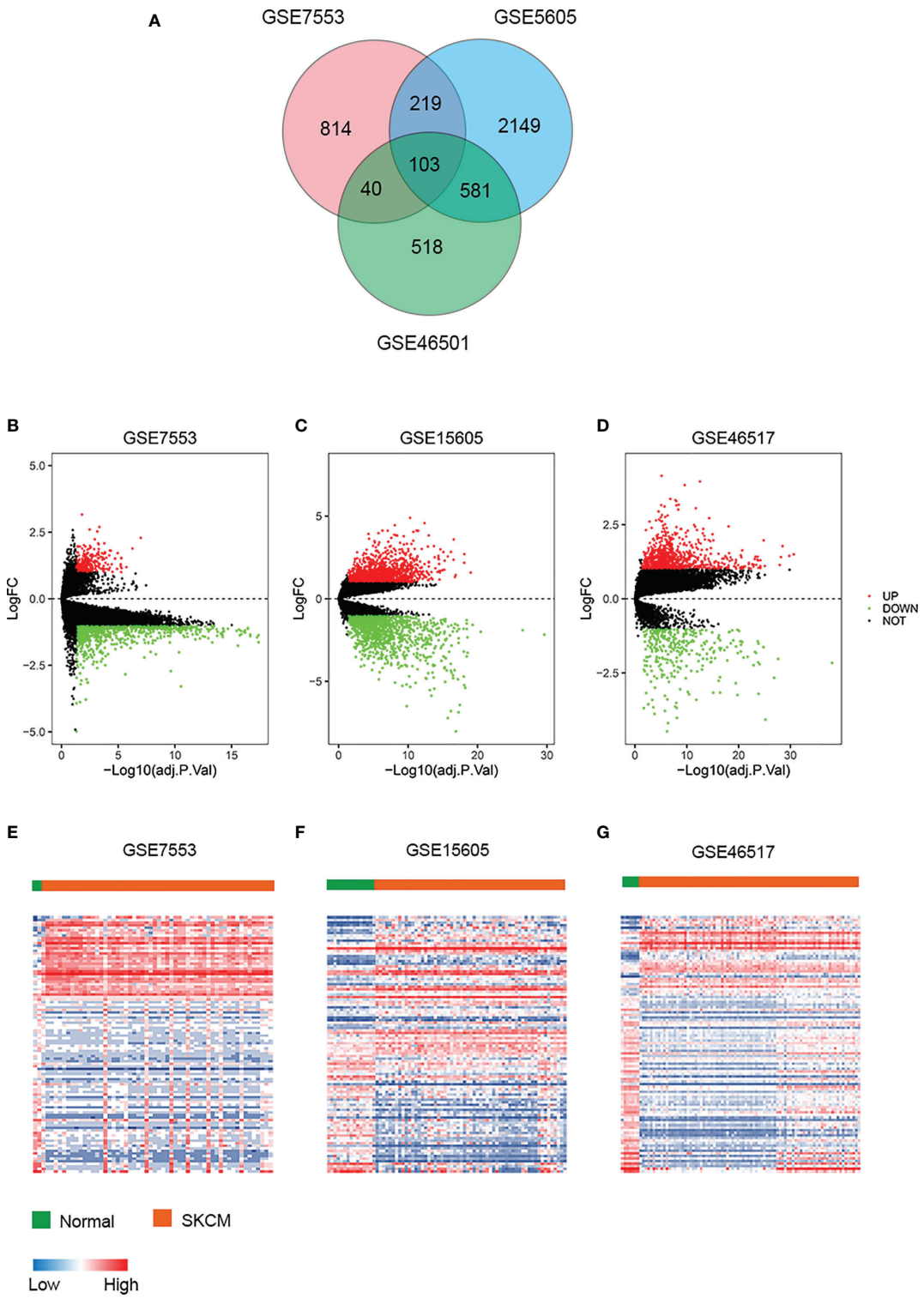

FIGURE 2 | DEGs in three data sets. **(A)** Venn diagram of DEGs. **(B–D)** The volcano plots visualize the DEGs in GSE7553, GSE15605, and GSE46517, respectively. The red nodes represent upregulated genes. The green nodes represent downregulated genes. **(E–G)** Heatmap of the top 103 DEGs according to the value of |logFC| > 1 and FDR < 0.05. The color in heat maps from blue to red shows the progression from low expression to high expression. logFC, log fold change.

TABLE 1 | Basic characteristics of TCGA CM patients.

Characteristics	Groups	Total (N=459)		Training cohort (N=229)		Validation cohort (N=230)	
		No	%	No	%	No	%
Age	≤58	233	50.7	116	50.7	117	50.9
	>58	226	49.3	113	49.3	113	49.1
Sex	Female	175	38.1	82	35.8	93	40.4
	Male	284	61.9	147	64.2	137	59.6
Metastasis	No	410	89.3	209	91.3	201	87.4
	Yes	23	5	9	3.9	14	6.1
	missing	26	5.7	11	4.8	15	6.5
Ulceration	No	145	31.6	70	30.6	75	32.6
	Yes	165	35.9	92	40.2	73	31.7
	Missing	149	32.5	67	29.2	82	35.7
Pathologic Stage	0	6	1.3	3	1.3	3	1.3
	I	77	16.8	40	17.5	37	16.1
	II	139	30.3	73	31.8	66	28.7
	III	169	36.8	81	35.4	88	38.3
	IV	22	4.8	9	4	13	5.6
	Missing	46	10	23	10	23	10
Tumor Site	Trunk	166	36.2	86	37.6	80	34.8
	Extremities	194	42.3	100	43.7	94	40.9
	Head and neck	35	7.6	15	6.5	20	8.7
	Missing	64	13.9	28	12.2	36	15.6
Breslow thickness (mm)	≤2	136	29.6	73	31.9	63	27.4
	2–5	113	24.6	52	22.7	61	26.5
	>5	105	22.9	59	25.8	46	20
	Missing	105	22.9	45	19.6	60	26.1
Chemotherapy	No	323	70.4	153	66.8	170	73.9
	Yes	88	19.2	49	21.4	39	17
	Missing	48	10.4	27	11.8	21	9.1
Radiotherapy	No	341	74.3	170	74.2	171	74.3
	Yes	73	15.9	34	14.9	39	17
	Missing	45	9.8	25	10.9	20	8.7

TABLE 2 | Univariate and multivariate analysis of prognosis genes for TCGA CM.

Training cohort		Univariate analysis			Multivariate analysis	
Genes	coef	HR (95%CI)	*P*	coef	HR (95%CI)	*P*
ADAMDEC1	–0.098	0.906 (0.848–0.969)	0.004	–0.099	0.906 (0.845–0.971)	0.005
D2S69E	–0.084	0.919 (0.847–0.998)	0.043	–0.089	0.915 (0.839–0.998)	0.045
HSPA13	–0.346	0.708 (0.594–0.844)	0.000	–0.251	0.778 (0.648–0.936)	0.007
TRIM29	0.088	1.092 (1.033–1.154)	0.002	0.074	1.077 (1.017–1.141)	0.011
Validation cohort		Univariate analysis			Multivariate analysis	
Genes	coef	HR (95%CI)	*P*	coef	HR (95%CI)	*P*
ADAMDEC1	–0.102	0.903 (0.852–0.958)	0.000	–0.113	0.893 (0.834–0.956)	0.001
D2S69E	–0.099	0.905 (0.843–0.971)	0.006	–0.092	0.090 (0.844–0.986)	0.021
HSPA13	–0.232	0.793 (0.637–0.987)	0.038	–0.227	0.797 (0.641–0.991)	0.042
TRIM29	0.112	1.119 (1.066–1.174)	0.000	0.101	1.106 (1.052–1.164)	0.000
Total		Univariate analysis			Multivariate analysis	
Genes	coef	HR (95%CI)	*P*	coef	HR (95%CI)	*P*
ADAMDEC1	–0.101	0.905 (0.866–0.945)	0.000	–0.108	0.898 (0.857–0.940)	0.000
D2S69E	–0.091	0.913 (0.865–0.963)	0.000	–0.093	0.911 (0.862–0.964)	0.000
HSPA13	–0.284	0.753 (0.657–0.864)	0.000	–0.264	0.768 (0.669–0.882)	0.000
TRIM29	0.102	1.108 (1.068–1.148)	0.000	0.091	1.095 (1.055–1.136)	0.000

the low-risk group with the median OS time of 56.8 months had a higher survival ratio (P<0.001; **Figure 3A**).

Furthermore, we analyzed the correlation between risk score and clinicopathological characteristics, which showed that high risk score was positively associated with elder age, ulceration, and breslow depth. Patients who received chemotherapy and radiotherapy prone to low-risk (**Figures 3B–J**).

Stratification Analysis

According to K-M analysis, CM patients with high risk score and larger breslow depth had the worst outcomes (**Figure 4A**), and CM patients with the ulceration and high- risk score had a shorter survival time than those with the non-ulceration group (**Figure 4B**). Furthermore, high risk score was also associated with poor prognosis in CM patients treated with chemotherapy

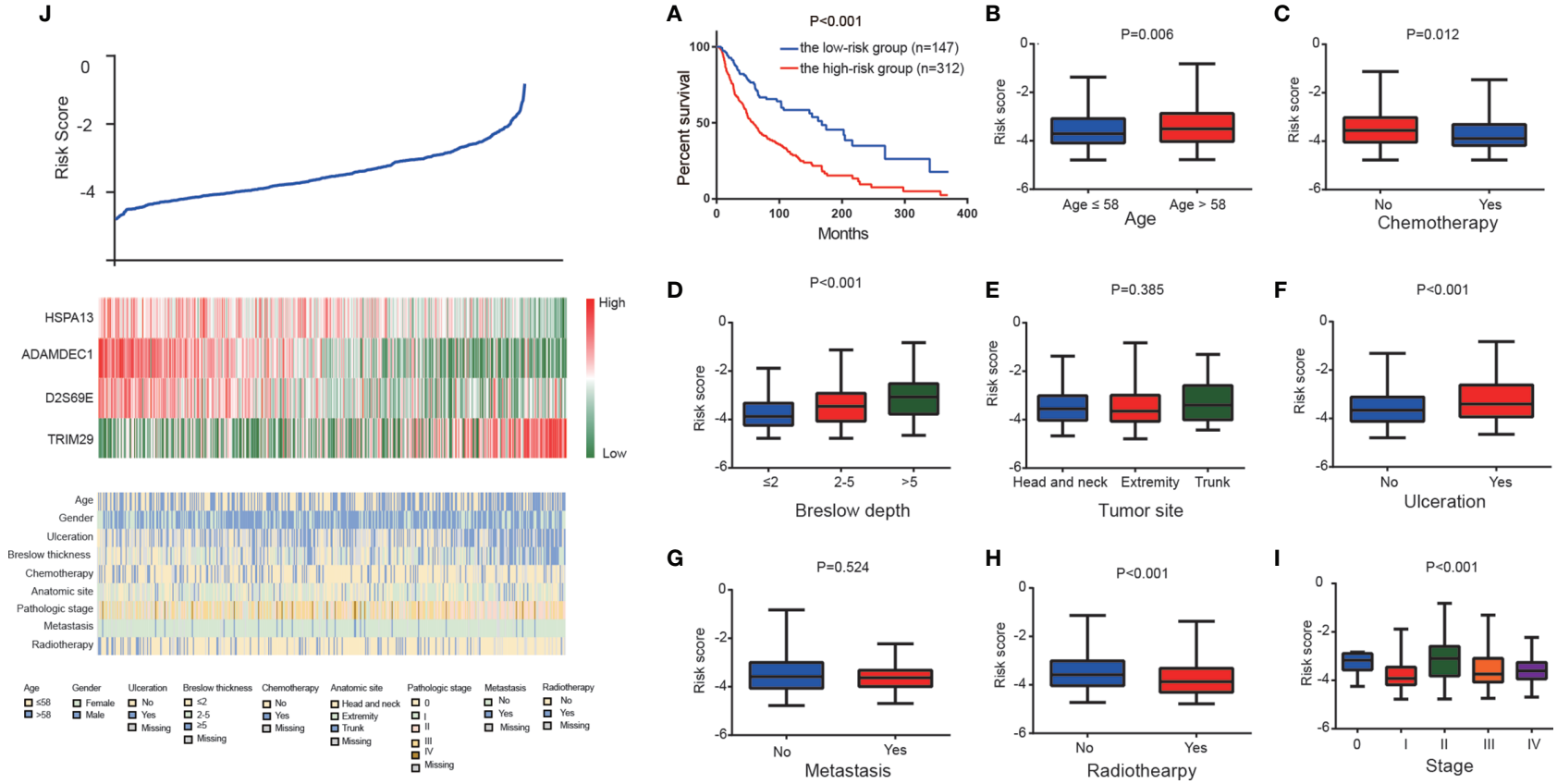

FIGURE 3 | The four-gene signature-derived risk score. **(A)** Kaplan–Meier overall survival analysis among TCGA CM patients stratified by risk score. Association between the risk model and different clinical characteristics. **(B)** Age. **(C)** Chemotherapy. **(D)** Breslow depth. **(E)** Tumor site. **(F)** Ulceration. **(G)** Metastasis. **(H)** Radiotherapy. **(I)** Stage. **(J)** The value of risk score (top), The corresponding expression of four genes (middle), and the associated clinicopathological parameters (bottom).

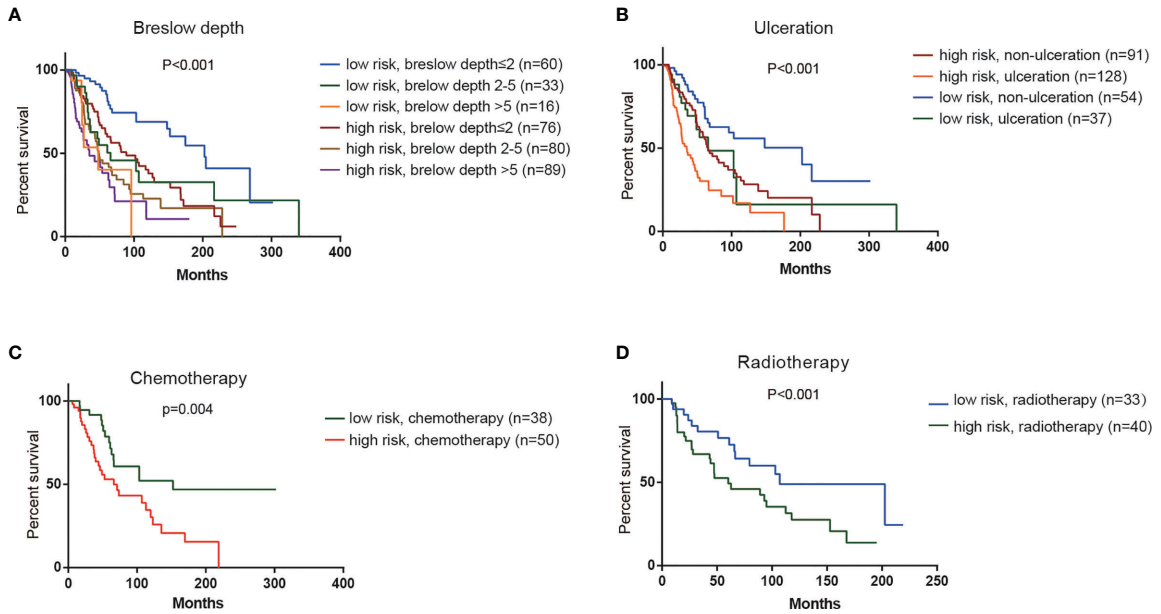

FIGURE 4 | Stratification analysis. Kaplan–Meier overall survival analysis of TCGA CM patients stratified by risk scores combined with **(A)** Breslow depth. **(B)**. Ulceration. **(C)** Chemotherapy. **(D)** Radiotherapy.

or radiotherapy (**Figures 4C, D**), indicating that the risk score could predict the therapeutic reaction.

Survival Predictive Model Based on Clinical Factors Alone or Their Combination With Risk Score

We constructed a survival prediction model to identify whether risk score in the presence of clinical factors to better discriminate survival of CM patients. Compared with the model with clinical factors alone, the model with addition of the risk score improved the sensitivity and specificity of discriminating 1-year (AUC, 0.57 to 0.66, **Figure 5A**), 3-year (AUC, 0.61 to 0.66, **Figure 5B**), and 5-year survival (AUC, 0.61 to 0.70, **Figure 5C**). When the model had both the risk score and clinical factors, its predictive ability for survival was greater [Concordance index (C-index) = 0.66] than that with clinical factors alone (C-index=0.59).

External Validation of the Model in GSE65904

GSE65904 dataset was used to validate the prediction performance of the model and each patient's risk score was calculated according to the formula of the model. All patients were divided into two groups: the high-risk group and the low-risk group by the optimal cut-off value of risk score. The K-M curve revealed significant difference in overall survival between groups in GSE65904. High-risk group had markedly poorer outcome than low-risk group with $P < 0.05$ in **Figure 6**.

The Association Between Prognosis Related Gene and Immune Markers

In order to detect the correlation between prognosis related gene and the immune infiltration level, we concentrated particularly on the relationship between prognosis related gene and immune

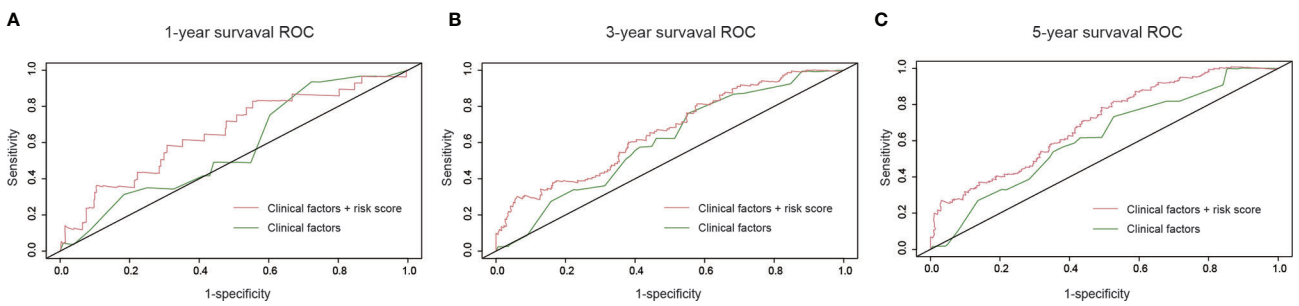

FIGURE 5 | Survival prediction model under the comparison of clinical factors versus the combination of risk score and clinical factors. **(A)** One-year survival receiver operating characteristic curves (ROC); **(B)** 3-year survival ROC; **(C)** 5-year survival ROC.

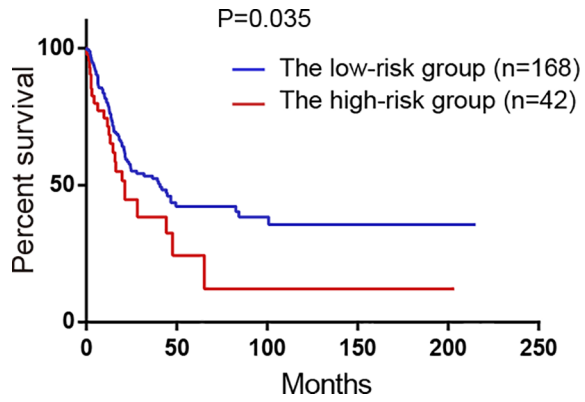

FIGURE 6 | Survival analysis of the high-risk group and the low-risk group divided by the model in GSE65904 validation set. All 214 patients were classified into two groups: the high-risk group and the low-risk group by the optimal cut-off value of risk scores.

markers of various immune cells in CM using the TIMER database. There was a positive correlation between ADAMDEC1 expression and the dendritic cell (Cor=0.67, p=4.72e−59), neutrophils (Cor=0.652, p=3.99e−56), CD8+

T cells (Cor=0.572, p=2.05e−39), macrophages (Cor=0.404, p=3.12e−19), CD4+ T cells (Cor=0.385, p=3.45e−17), B cells (Cor=0.371, p=4.51e−16). Similar results were obtained for GNLY and HSPA13 (**Figures 7A–C**). While, the correlation between TRIM29 and immune infiltration is not obvious (**Figure 7D**). According to K-M analysis, high *ADAMDEC1, HSPA13*, and *GNLY* expression was significantly correlated with better prognosis, while high TRIM29 expression was markedly correlated with poor prognosis (**Figures 7E–H**).

DISCUSSION

In present study, we selected and constructed a four-gene based risk score model for CM. We analyzed GSE7553, GSE46517, and GSE15605 data sets, 103 DEGs were identified and selected. Subsequently, univariate and multivariate COX regression were employed for the key genes. Fourteen genes (*GNLY, DFNA28, ADAMDEC1, ALOXE3, EFNA3, EPN3, EVPL, FERMT1, HSPA13, JAG2, RAPGEFL1, SULT2B1, TGM3*, and *TRIM29*) were finally identified to be the prognostic genes. Here we adopted stepwise multivariate Cox regression analysis to select the best performance efficacy predictive model with the lowest AIC value. Finally, a four-gene based model including *GNLY, ADAMDEC1*, *HSPA13*, and *TRIM29* was successfully developed.

Furthermore, in order to evaluate the prognostic significance of the new risk model, we performed log-rank test and the ROC curve analysis to investigate association between the model and clinical parameters. As we expected, the high-risk cohort was correlated with poor outcome and was tend to larger breslow depth and ulceration.

For our prognosis related genes, researchers have revealed that some of them may be crucial in cancer development, including CM. For instance, ALOXE3, which encodes arachidonate lipoxygenase3, can serve as a potential predictive biomarker for colon adenocarcinoma patients. Low expression of ALOXE3 had a favorable prognosis of COAD (11). Gómez-Maldonado et al. identified EFNA3, a member of the ephrin type A ligands, is induced by hypoxia-inducible factor in human tumors and this induction is predictive of poor prognosis and increased risk of metastasis in breast cancer patients (12). EPN3 expression is upregulated in wounded epithelial tissues and it can drive breast tumorigenesis by increasing E-cadherin endocytosis, EPN3 is overexpressed in 40% of breast cancers and its overexpression is an independent predictor of distant metastasis (13, 14).. Envoplakin (EVPL) is a protein component of desmosomes and the DNA variant in intron of EVPL (rs2071194) has been found associated with papillary and follicular thyroid cancer risk (15). FERMT1, as an oncogene, promotes the degradation of IκBα, thereby activating NF-κB signaling and promoting gastric cancer (16). JAG2 is one of Notch ligands, which recently appear to exert various carcinogenesis. JAG2 expression significantly correlates with angiogenic processes and vascular development in breast cancer, and is induced at the transcriptional level in hypoxic tumor cells. The oncogene c-myc can also modulate JAG2 expression under hypoxic conditions (17). In 2013, Takahashi et al. reported that RAPGEFL1 was highly methylated in some ESCC cell lines and RAPGEFL1 could regulate by most miRNAs. Therefore, RAPGEFL1 may be the potential pathogenic genes for ESCC (18). TGM3 could affect epithelial-mesenchymal transition, play an essential role in tumorigenesis and progression. It might serve as a useful biomarker and potential therapeutic target for hepatocellular carcinoma treatment (19).

Several genes in our risk model had been investigated in immune response. TRIM29, a member of the tripartite interaction motif (TRIM) family of proteins, functions as a negative regulator of innate immune response. Studies have shown that knockdown of TRIM29 in airway epithelial cells enhances type I interferon production (20). TRIM29 is also recognized as an oncogene, and elevated gene expression in multiple tumors such as colorectal cancer and bladder cancer and so on (21). But the function of TRIM29 in cutaneous melanoma remained still unknown. Elizabeth et al. discovered that ADAMDEC1, an orphan ADAM-like metalloprotease, is expressed in the immune system, by dendritic cells and macrophages. *In vitro*, the expression of ADAMDEC1 was significantly elevated in M1 but not M2 macrophages. More research is needed to determine the associations between ADAMDEC1 and immune response and associations with survival for cancers (22). Granulysin (GNLY) is a cytolytic apoptotic molecule highly expressed in activated immune cells, particularly human cytotoxic T lymphocytes (CTLs) and natural killer (NK) cells (23). GNLY functions as a lytic molecule to carry out lysis or apoptosis product in target cells, including tumor

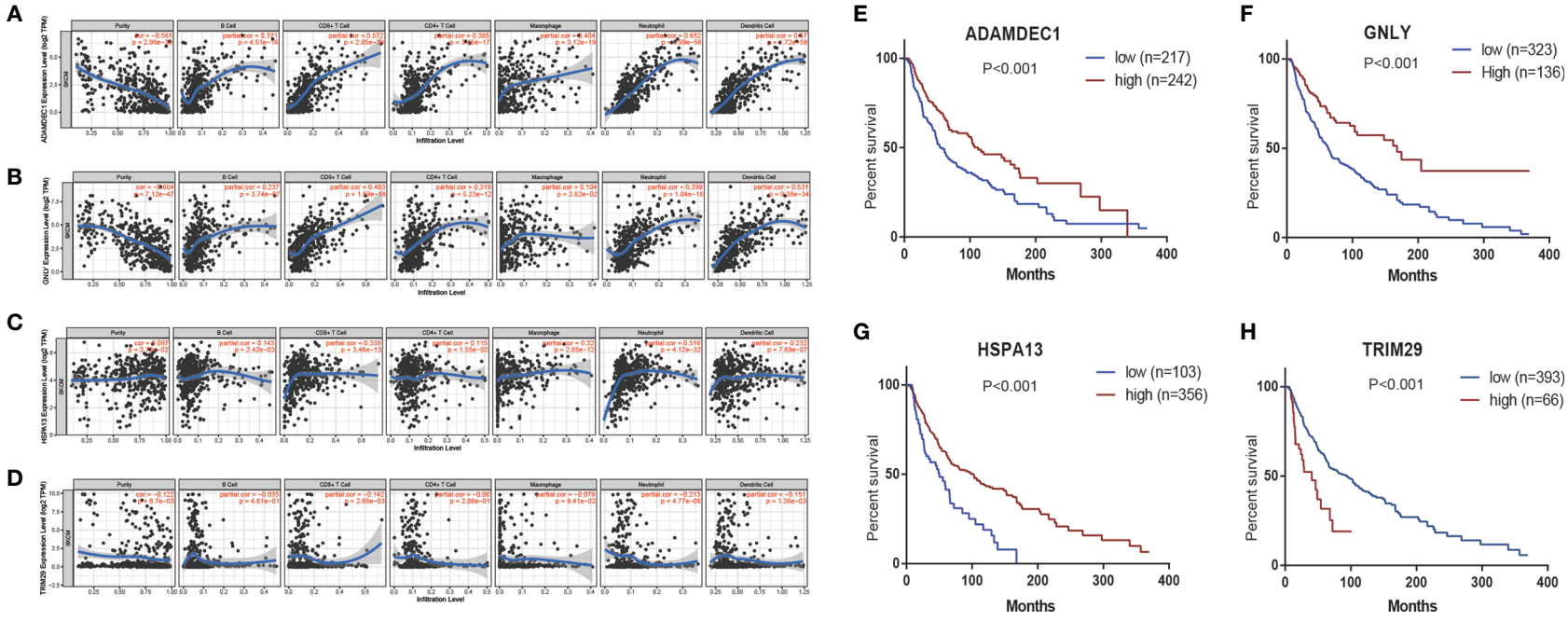

FIGURE 7 | The correlation between prognostic genes expression and immune cell infiltration in CM (TIMER database). The correlation between the abundance of immune cell and the expression of **(A)** ADAMDEC1; **(B)** GNLY; **(C)** HSPA13; **(D)** TRIM29. Prognostic values of **(E)** ADAMDEC1, **(F)** GNLY, **(G)** HSPA13, **(H)** TRIM29 in TCGA CM.

cells or cells infected by pathogens. GNLY can also activate antigen-presenting cells through TLR4 (24). Multiple publications have confirmed the anti-tumor activity of GNLY (25–29). Ya-Wen reported that the serum level of GNLY was negatively correlated with the proliferation of transplanted tumor cells in HIS mice (30). All gene in this risk model are firstly studied in cutaneous melanoma.

To sum up, our research results indicate that the four-gene prognostic model is a reliable tool for predicting the overall survival of CM, it may be useful for guiding therapeutic strategies to improve the clinical outcome of melanoma patients. The low-risk group should avoid some unnecessary treatment to reduced drug toxicities, and high-risk group can receive other intensive treatment. For clinical application, more clinical studies are needed to further verify the prognostic and predictive significance of the risk score model.

CONCLUSIONS

In conclusion, the new risk score system functions well in predicting the prognosis and treatment response in CM patients, with the potential to optimize treatment options. More studies are needed to explore the biological function of these four genes in CM progression and to further verify the prognostic value of the model for clinical practice.

DATA AVAILABILITY STATEMENT

The original contributions presented in the study are included in the article/supplementary material. Further inquiries can be directed to the corresponding author.

AUTHOR CONTRIBUTIONS

This work was carried out in collaboration with all authors. MW designed the theme of the article. XT wrote and XQ reviewed the article. All authors contributed to the article and approved the submitted version.

ACKNOWLEDGMENTS

We thank Yuhu Xin, Ping Zhang, and Na Wang for their support over the past years.

REFERENCES

1. Carr S, Smith C, Wernberg J. Epidemiology and Risk Factors of Melanoma. *Surg Clin North Am* (2020) 100:1–12.
2. Rebecca VW, Somasundaram R, Herlyn M. Pre-clinical modeling of cutaneous melanoma. *Nat Commun* (2020) 11(1):2858. doi: 10.1038/s41467-020-15546-9
3. de Assis LVM, Moraes MN, Castrucci AML. The molecular clock in the skin, its functionality, and how it is disrupted in cutaneous melanoma: a new pharmacological target? *Cell Mol Life Sci* (2019) 76(19):3801–26. doi: 10.1007/s00018-019-03183-5
4. Siegel RL, Miller KD, Jemal A. Cancer statistics, 2015. *CA Cancer J Clin* (2015) 65(1):5–29. doi: 10.3322/caac.21254
5. Hartman RI, Lin JY. Cutaneous Melanoma-A Review in Detection, Staging, and Management. *Hematol Oncol Clin North Am* (2019) 33(1):25–38. doi: 10.1016/j.hoc.2018.09.005
6. Balch CM, Gershenwald JE, Soong SJ, Thompson JF, Atkins MB, Byrd DR, et al. Final version of 2009 AJCC melanoma staging and classification. *J Clin Oncol* (2009) 27(36):6199–206. doi: 10.1200/JCO.2009.23.4799
7. Bertoli G, Cava C, Castiglioni I. MicroRNAs: New Biomarkers for Diagnosis, Prognosis, Therapy Prediction and Therapeutic Tools for Breast Cancer. *Theranostics* (2015) 5(10):1122–43. doi: 10.7150/thno.11543
8. Sparano JA, Gray RJ, Makower DF, Pritchard KI, Albain KS, Hayes DF, et al. Adjuvant Chemotherapy Guided by a 21-Gene Expression Assay in Breast Cancer. *N Engl J Med* (2018) 379(2):111–21. doi: 10.1056/NEJMoa1804710
9. Daoud AZ, Mulholland EJ, Cole G, McCarthy HO. MicroRNAs in Pancreatic Cancer: biomarkers, prognostic, and therapeutic modulators. *BMC Cancer* (2019) 19(1):1130. doi: 10.1186/s12885-019-6284-y
10. Albain KS, Barlow WE, Shak S, Hortobagyi GN, Livingston RB, Yeh IT, et al. Prognostic and predictive value of the 21-gene recurrence score assay in postmenopausal women with node-positive, oestrogen-receptor-positive breast cancer on chemotherapy: a retrospective analysis of a randomised trial. *Lancet Oncol* (2010) 11(1):55–65. doi: 10.1016/S1470-2045(09)70314-6
11. Ruan GT, Gong YZ, Zhu LC, Gao F, Liao XW, Wang XK, et al. The Perspective of Diagnostic and Prognostic Values of Lipoxygenases mRNA Expression in Colon Adenocarcinoma. *Onco Targets Ther* (2020) 13:9389–405. doi: 10.2147/OTT.S251965
12. Gomez-Maldonado L, Tiana M, Roche O, Prado-Cabrero A, Jensen L, Fernandez-Barral A, et al. EFNA3 long noncoding RNAs induced by hypoxia promote metastatic dissemination. *Oncogene* (2015) 34(20):2609–20. doi: 10.1038/onc.2014.200
13. Spradling KD, McDaniel AE, Lohi J, Pilcher BK. Epsin 3 is a novel extracellular matrix-induced transcript specific to wounded epithelia. *J Biol Chem* (2001) 276(31):29257–67. doi: 10.1074/jbc.M101663200
14. Schiano Lomoriello I, Giangreco G, Iavarone C, Tordonato C, Caldieri G, Serio G, et al. A self-sustaining endocytic-based loop promotes breast cancer plasticity leading to aggressiveness and pro-metastatic behavior. *Nat Commun* (2020) 11(1):3020. doi: 10.1038/s41467-020-16836-y
15. Sigurdson AJ, Brenner AV, Roach JA, Goudeva L, Muller JA, Nerlich K, et al. Selected single-nucleotide polymorphisms in FOXE1, SERPINA5, FTO, EVPL, TICAM1 and SCARB1 are associated with papillary and follicular thyroid cancer risk: replication study in a German population. *Carcinogenesis* (2016) 37(7):677–84. doi: 10.1093/carcin/bgw047
16. Fan H, Zhang S, Zhang Y, Liang W, Cao B. FERMT1 promotes gastric cancer progression by activating the NF-kappaB pathway and predicts poor prognosis. *Cancer Biol Ther* (2020) 21(9):815–25. doi: 10.1080/15384047.2020.1792218
17. Pietras A, von Stedingk K, Lindgren D, Pahlman S, Axelson H. JAG2 induction in hypoxic tumor cells alters Notch signaling and enhances endothelial cell tube formation. *Mol Cancer Res* (2011) 9(5):626–36. doi: 10.1158/1541-7786.MCR-10-0508
18. Takahashi T, Matsuda Y, Yamashita S, Hattori N, Kushima R, Lee YC, et al. Estimation of the fraction of cancer cells in a tumor DNA sample using DNA methylation. *PloS One* (2013) 8(12):e82302. doi: 10.1371/journal.pone.0082302
19. Hu JW, Yang ZF, Li J, Hu B, Luo CB, Zhu K, et al. TGM3 promotes epithelial-mesenchymal transition and hepatocellular carcinogenesis and predicts poor prognosis for patients after curative resection. *Dig Liver Dis* (2020) 52(6):668–76. doi: 10.1016/j.dld.2019.10.010
20. Xing J, Weng L, Yuan B, Wang Z, Jia L, Jin R, et al. Identification of a role for TRIM29 in the control of innate immunity in the respiratory tract. *Nat Immunol* (2016) 17(12):1373–80. doi: 10.1038/ni.3580

21. Sun J, Zhang T, Cheng M, Hong L, Zhang C, Xie M, et al. TRIM29 facilitates the epithelial-to-mesenchymal transition and the progression of colorectal cancer via the activation of the Wnt/beta-catenin signaling pathway. *J Exp Clin Cancer Res* (2019) 38(1):104. doi: 10.1186/s13046-019-1098-y
22. Bates EE, Fridman WH, Mueller CG. The ADAMDEC1 (decysin) gene structure: evolution by duplication in a metalloprotease gene cluster on chromosome 8p12. *Immunogenetics* (2002) 54(2):96–105. doi: 10.1007/s00251-002-0430-3
23. Vujaklija DV, Gulic T, Sucic S, Nagata K, Ogawa K, Laskarin G, et al. First trimester pregnancy decidual natural killer cells contain and spontaneously release high quantities of granulysin. *Am J Reprod Immunol* (2011) 66(5):363–72. doi: 10.1111/j.1600-0897.2011.01015.x
24. Tewary P, Yang D, de la Rosa G, Li Y, Finn MW, Krensky AM, et al. Granulysin activates antigen-presenting cells through TLR4 and acts as an immune alarmin. *Blood* (2010) 116(18):3465–74. doi: 10.1182/blood-2010-03-273953
25. Clayberger C, Krensky AM. Granulysin. *Curr Opin Immunol* (2003) 15 (5):560–5. doi: 10.1016/S0952-7915(03)00097-9
26. Lin J, Huang Y, Zhang L, Tang W, Li X, Wang X, et al. Evaluation of serum granulysin as a potential biomarker for nasopharyngeal carcinoma. *Clin Chim Acta* (2016) 454:72–6. doi: 10.1016/j.cca.2015.12.035
27. Aporta A, Catalan E, Galan-Malo P, Ramirez-Labrada A, Perez M, Azaceta G, et al. Granulysin induces apoptotic cell death and cleavage of the autophagy regulator Atg5 in human hematological tumors. *Biochem Pharmacol* (2014) 87(3):410–23. doi: 10.1016/j.bcp.2013.11.004
28. Jiang W, Zhu D, Wang C, Zhu Y. An immune relevant signature for predicting prognoses and immunotherapeutic responses in patients with muscle-invasive bladder cancer (MIBC). *Cancer Med* (2020) 9(8):2774–90. doi: 10.1002/cam4.2942
29. Saini RV, Wilson C, Finn MW, Wang T, Krensky AM, Clayberger C. Granulysin delivered by cytotoxic cells damages endoplasmic reticulum and activates caspase-7 in target cells. *J Immunol* (2011) 186(6):3497–504. doi: 10.4049/jimmunol.1003409
30. Hsiao YW, Lai TC, Lin YH, Su CY, Lee JJ, Liao AT, et al. Granulysin expressed in a humanized mouse model induces apoptotic cell death and suppresses tumorigenicity. *Oncotarget* (2017) 8(48):83495–508. doi: 10.18632/oncotarget.11473

Conflict of Interest: The authors declare that the research was conducted in the absence of any commercial or financial relationships that could be construed as a potential conflict of interest.

frontiers in Oncology

ORIGINAL RESEARCH
published: 31 January 2022
doi: 10.3389/fonc.2022.810058

The Prognostic and Predictive Role of Xeroderma Pigmentosum Gene Expression in Melanoma

Sarah Fischer[1,2], *Mohamed Hamed*[1], *Steffen Emmert*[3], *Olaf Wolkenhauer*[2,4], *Georg Fuellen*[1] *and Alexander Thiem*[3*]

[1] Institute for Biostatistics and Informatics in Medicine and Ageing Research, Rostock University Medical Center, Rostock, Germany, [2] Department of Systems Biology and Bioinformatics, University of Rostock, Rostock, Germany, [3] Clinic and Policlinic for Dermatology and Venereology, Rostock University Medical Center, Rostock, Germany, [4] Leibniz-Institute for Food Systems Biology, Technical University of Munich, Freising, Germany

OPEN ACCESS

Edited by:
Gagan Chhabra,
University of Wisconsin-Madison,
United States

Reviewed by:
Mithalesh Singh,
University of Wisconsin-Madison,
United States
Shengqin Su,
Shanghai Hengrui Pharmaceutical Co., Ltd., China
Elizabeth Thompson,
University of Minnesota Twin Cities,
United States
Laura Niedernhofer,
University of Minnesota Twin Cities,
United States, in collaboration with reviewer ET

***Correspondence:**
Alexander Thiem
alexander.thiem@med.uni-rostock.de

Specialty section:
This article was submitted to Skin Cancer, a section of the journal Frontiers in Oncology

Received: 05 November 2021
Accepted: 07 January 2022
Published: 31 January 2022

Citation:
Fischer S, Hamed M, Emmert S, Wolkenhauer O, Fuellen G and Thiem A (2022) The Prognostic and Predictive Role of Xeroderma Pigmentosum Gene Expression in Melanoma. Front. Oncol. 12:810058. doi: 10.3389/fonc.2022.810058

Background: Assessment of immune-specific markers is a well-established approach for predicting the response to immune checkpoint inhibitors (ICIs). Promising candidates as ICI predictive biomarkers are the DNA damage response pathway genes. One of those pathways, which are mainly responsible for the repair of DNA damage caused by ultraviolet radiation, is the nucleotide excision repair (NER) pathway. Xeroderma pigmentosum (XP) is a hereditary disease caused by mutations of eight different genes of the NER pathway, or POLH, here together named the nine XP genes. Anecdotal evidence indicated that XP patients with melanoma or other skin tumors responded impressively well to anti-PD-1 ICIs. Hence, we analyzed the expression of the nine XP genes as prognostic and anti-PD-1 ICI predictive biomarkers in melanoma.

Methods: We assessed mRNA gene expression in the TCGA-SKCM dataset (n = 445) and two pooled clinical melanoma cohorts of anti-PD-1 ICI (n = 75). In TCGA-SKCM, we applied hierarchical clustering on XP genes to reveal clusters, further utilized as XP cluster scores. In addition, out of 18 predefined genes representative of a T cell inflamed tumor microenvironment, the TIS score was calculated. Besides these scores, the XP genes, immune-specific single genes (CD8A, CXCL9, CD274, and CXCL13) and tumor mutational burden (TMB) were cross-correlated. Survival analysis in TCGA-SKCM was conducted for the selected parameters. Lastly, the XP response prediction value was calculated for the two pooled anti-PD-1 cohorts by classification models.

Results: In TCGA-SKCM, expression of the XP genes was divided into two clusters, inversely correlated with immune-specific markers. A higher ERCC3 expression was associated with improved survival, particularly in younger patients. The constructed models utilizing XP genes, and the XP cluster scores outperformed the immune-specific gene-based models in predicting response to anti-PD-1 ICI in the pooled

clinical cohorts. However, the best prediction was achieved by combining the immune-specific gene CD274 with three XP genes from both clusters.

Conclusion: Our results suggest pre-therapeutic XP gene expression as a potential marker to improve the prediction of anti-PD-1 response in melanoma.

Keywords: melanoma, anti-PD-1, biomarker, DNA damage response, nucleotide excision repair, xeroderma pigmentosum, RNA-seq, gene expression

INTRODUCTION

Immune checkpoint inhibitors (ICIs) are a standard treatment for advanced melanoma and other immunogenic tumors. For the therapy of melanoma, they include ipilimumab, a monoclonal antibody directed against the cytotoxic T-lymphocyte-associated antigen 4 (CTLA-4) receptor, and nivolumab or pembrolizumab, antibodies targeting programmed cell death-1 (PD-1) receptor (1–3). Despite the impressive and long-lasting clinical activity of ICIs in some patients, many do not respond. Furthermore, severe side effects are frequent, especially in the combined application of ipilimumab and nivolumab (4). These typically include immune-related adverse events of multiple organs and tissues, leading to inflammations such as thyreoiditis, pneumonitis, colitis or hypophysitis (1, 3, 4). Thus, predictive biomarkers of ICI response are urgently needed in order to identify those patients who achieve the greatest ICI benefit (1–3).

For the efficacy of anti-PD-1 ICIs, different predictive biomarkers have been proposed (5, 6). These can be classified as follows: *tumor-intrinsic* biomarkers (e.g., tumor mutational burden (TMB) or neoantigen load), which are indirect measures of tumor antigenicity generated by somatic tumor mutations, and *immune-specific* biomarkers (e.g., T cell-inflamed gene expression profiles (GEPs) or programmed-death-ligand 1 (PD-L1) expression), which are indicative of a T cell-inflamed tumor microenvironment (TME) (6, 7).

Particularly, many studies on immune-specific biomarkers have been conducted recently (8). For instance, Ayers et al. (9) analyzed GEPs using RNA from baseline tumor samples of patients treated with pembrolizumab and eventually defined an 18-gene GEP, hereafter referred to as the *Tumor Inflammation Signature* (TIS). This signature was predictive in 220 patients with nine different cancers and contained IFN-gamma–responsive genes related to antigen presentation, chemokine expression, cytotoxic activity, and adaptive immune resistance (9). In a current large-scale metanalysis of 1,008 ICI treated cases (n = 353 with melanoma), different predictive biomarkers of ICI response were compared with each other (10). In the markers of immune infiltration category, the TIS single genes *CXCL9*, *CD8A*, and TIS itself were the predictors with the strongest effect size. The gene *CXCL13* was also a highly predictive gene marker in the whole tumor cohort. Intriguingly, in the three melanoma anti-PD-1 cohorts (7, 11, 12) included in this meta-analysis, *CD274* (coding for PD-L1) was a further predictive marker. However, looking at each cohort individually, only in the cohort published by Cristescu et al. (7) TIS, *CXCL9*, and *CD274* were significantly positively associated with ICI response. Finally, the authors concluded that 34 predefined biomarkers (among them the markers of immune infiltration) could only explain about 60% of the total proportion of variance in ICI response, indicating that the remaining factors determining ICI response still need to be discovered (10).

Recent studies revealed that mutational processes directly altering the DNA damage response (DDR) could influence response to ICI (13–16). As one mechanism, DDR defects can lead to a higher TMB, which implicates a greater abundance of immunogenic neoantigens; this is impressively illustrated by the strong clinical activity of anti-PD-1 ICI in mismatch-mediated repair (MMR) deficient tumors (17–21). Notably, besides MMR, two other pathways are responsible for the repair of DNA single-strand breaks (SSB): base excision repair (BER) and nucleotide excision repair (NER). In contrast, DNA double-strand breaks (DSB) are repaired by homologous recombination and further by more error-prone nonhomologous end joining and microhomology-mediated end joining (22–25) Another DNA repair pathway is the Fanconi Anemia/BRCA pathway that restores DNA interstrand crosslinks.

In addition to an increased TMB, other more specific mechanisms leading to altered immunogenicity have been attributed to modified DDR pathways and signaling (6, 15, 25). These mechanisms include upregulation of PD-L1 expression by enhanced DDR signaling through SSB or DSB. Expression of PD-L1 is additionally increased by depletion of BRCA2, which is involved in homologous recombination, or by depletion of Ku70/80, a critical factor of nonhomologous end joining, and by BER reduction (26, 27). Importantly, increased PD-L1 expression after DSB and SSB was associated with the activation of STAT1, STAT3 and IRF-1, which are all part of the canonical interferon (IFN)-gamma-pathway (28). Additionally, for loss of interstrand crosslink repair function in breast cancer, an increased IFN-related gene expression, namely, the two critical mediators of $CD4^+$ and $CD8^+$ T-cell chemotaxis, *CXCL10* and *CCL5*, was discovered (29). Those and other cytokines are involved in T-cell inflammation, which is often a prerequisite for anti-PD-1 ICI response (30). Mechanistically, the crosstalk between immune and cancer cells within the TME, leading to PD-L1 upregulation on cancer cells, is the basis for the mode of action of anti-PD-1 ICI (31). These observations support the joint analysis of DDR pathway and immune-specific gene expression in the TME (32).

Although several case reports stated impressive anti-PD-1 ICI responses of patients with NER germline defects, and while some of them have identified a higher TMB, the further immunogenic impact by alterations of this DDR pathway is far less explored

(13, 25, 33–37). Biallelic pathogenic variants in one of the seven NER genes coding for the so-called complementation groups, *XPA*, *ERCC3*, *XPC*, *ERCC2*, *DDB2*, *ERCC4*, *ERCC5*, the NER gene *ERCC1*, and the gene coding for XP variant, *POLH*, are the causes of the rare hereditary disease Xeroderma pigmentosum (XP) (38). They lead to an absent or inactivated protein and are hereafter referred to as the nine *XP genes*. The NER is mainly responsible for the repair of UV-induced DNA lesions and is divided into a global genome (GG) and transcription-coupled (TC) repair subpathway, which shares a common end section (39). XP patients under age 20 years have a 10,000-fold increased risk for non-melanoma skin cancer and a 2,000-fold increased risk for melanoma, making skin cancer the most common cause of death in this population (40). Hence, XP patients with skin tumors could benefit greatly from successful ICI treatment, requesting investigation of the role of these nine XP genes for ICI response.

A recent study correlated DDR pathway mutations irrespective of XP disease with overall survival of 1,661 ICI-treated patients and revealed that the NER pathway was predictive of ICI benefit—independent of TMB and tumor type. However, in 40,181 unique cancers, only 3.4% of melanomas possessed NER gene mutations (41). Moreover, Litchfield et al. found no predictive role of DDR pathway mutations for ICI response in seven different tumor types (10). An aspect, presumably limiting further the predictive role of DDR mutations, is that different genes in the same DDR pathway can unevenly affect the TME and the ICI response, as shown for BRCA1 and BRCA2 mutations (11, 42).

Based on the discussion above, we focused on analyzing the nine XP genes away from mutation data to gene expression data to investigate the predictive role of XP gene expression as an anti-PD-1 response marker in melanoma. Accordingly, *The Cancer Genome Atlas Skin Cutaneous Melanoma project* (TCGA-SKCM) (43) dataset, consisting of systemic treatment-naïve primary and metastatic melanoma samples, was used to identify two primary clusters of XP gene expression. We discovered that these were inversely correlated with the expression of TIS and single immune infiltration genes. In TCGA-SKCM, no significant negative correlations between XP genes and TMB were observed. Importantly, besides being predictive for the response to a specific treatment, biomarkers can also be prognostic by providing information about the patients overall cancer outcome, regardless of therapy (44). Because this can potentially interfere with their predictive value, we used TCGA-SKCM to analyze the prognostic role of different factors, and from the XP genes found only the expression of *ERCC3* to be prognostic. In contrast, expression of XP genes and clusters thereof could better predict response to anti-PD-1 ICs than well-established *immune-specific* biomarkers in two pooled clinical cohorts.

MATERIAL AND METHODS

Study Design

In **Figure 1**, we outline our analysis workflow beginning with the pre-processing of our three input datasets from TCGA-SKCM (43),

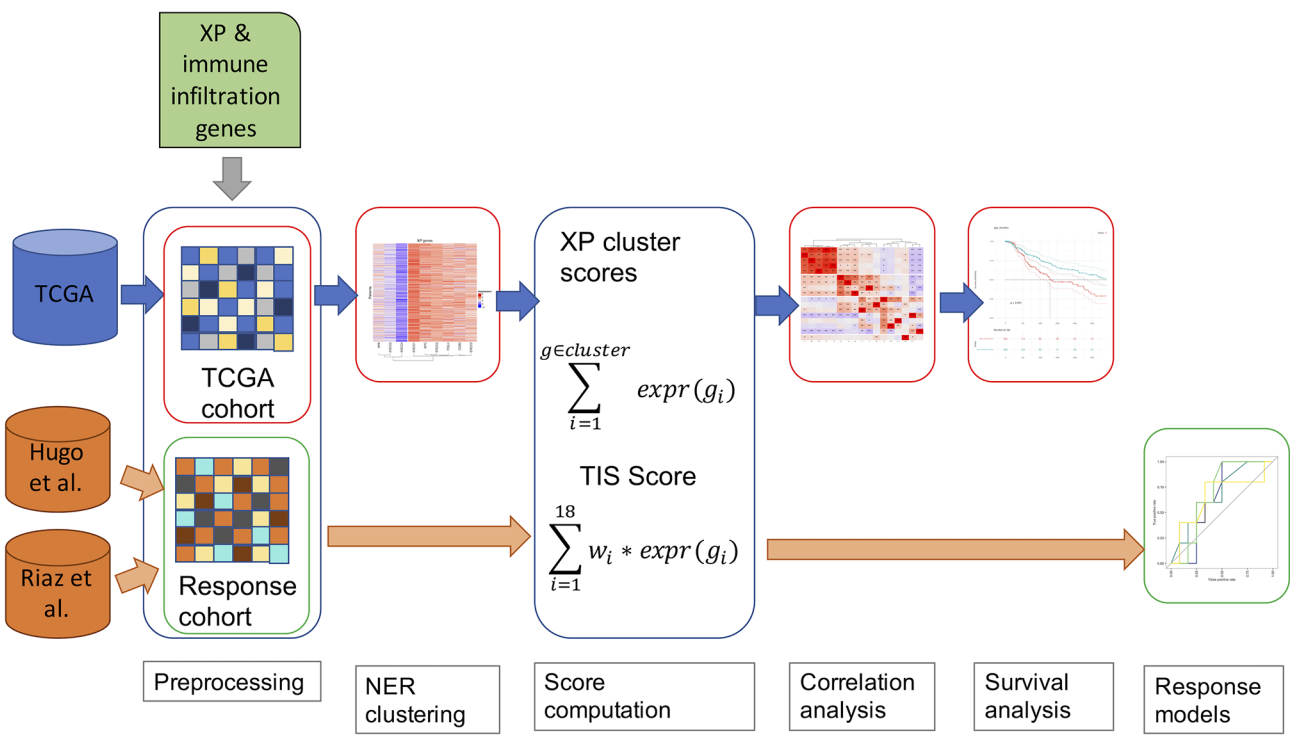

FIGURE 1 | A schematic diagram of our workflow, including TCGA-SKCM and two anti-PD-1 cohorts of melanoma patients.

Hugo et al. (11), and Riaz et al. (12). In parallel, we parsed the genes to be analyzed, the nine XP genes (*XPA*, *ERCC3*, *XPC*, *ERCC2*, *ERCC4*, *ERCC5*, *DDB2*, *POLH*, *ERCC1*), the 18 genes of the T- cell inflamed signature (9) (here named *Tumor Inflammation signature*, TIS) and the predictive biomarker, *CXCL13*, were retrieved through literature research (6, 10). The further utilized TIS score was calculated as the weighted sum of the 18 gene expression values according to Ayers et al. and Cristescu et al. (7, 45).

Accordingly, the XP gene expression in TCGA-SKCM was clustered hierarchically to define two XP clusters consisting of the mean expression of the corresponding genes. As an additional parameter, we included the TMB for the TCGA-SKCM data in our workflow. An underlying association was investigated *via* Spearman correlation between the computed scores, the particular gene expressions of XP genes, and predictive biomarkers and TMB. Afterwards, we assessed in TCGA-SCKM whether XP or TIS score, single XP or immune infiltration gene expression, or TMB could be prognostic for survival. Except for the pre-processing, the specified workflow was repeated for multiple sample subgroups split by clinical parameters such as age, sample type or gender.

To evaluate the potential of the XP genes as a predictive biomarker for the ICI response, we utilized the two anti-PD-1 datasets and developed simple prediction models using Youden's index and Xtreme gradient boosting.

All data analyses were performed using R version 3.6.3 (46). A p-value <0.05 was considered statistically significant in all analyses, and a p-value <0.005 was highly statistically significant.

Data Collection and Preprocessing

>Gene expression data used in this manuscript were obtained from TCGA-SKCM (http://cancergenome.nih.gov/, n = 464) (43) and two datasets of anti-PD-1 ICI cohort studies in melanoma patients, Hugo et al. (n = 28, GEO: GSE78220) (11) and Riaz et al. (n = 110, GEO: GSE91061) (12). The TCGA-SKCM dataset was reduced to n = 445 samples, which are fully annotated with clinical information, such as age, gender, and survival time. Likewise, we included samples of the other datasets after filtering for the mentioned clinical data availability and exclusion of on-treatment samples from the ICI cohorts, resulting in n = 26 (11) and n = 49 (12). All analyzed RNA-seq data were formatted as FPKM and $\log_2$ transformed. For TCGA-SKCM, somatic mutations were obtained from the TCGA data portal, and the TMB was calculated as $\log_{10}$ of the number of non-synonymous mutations per 50 Mb (package "*maftools*" v.2.2.10) (47). Responder (complete response [CR] or partial response [PR]) and non-responder (stable disease [SD] or progressive disease [PD]) were defined by RECIST criteria-based radiological response (7, 10). The clinical characteristics plus the scope of the computed scores of the utilized cohorts are listed in **Table S1**.

Clustering

In the process of clustering method selection, multiple clustering methods and distance metrics of hierarchical clustering were tested (**Table S2**). Clusters containing only one single gene were excluded because singe genes analysis of XP genes was performed apart. Hence, as the final XP clusters we selected the best performing partition with at least two genes per cluster, which was supported by the majority of all tested clustering methods and distance metrics.

Calculation of Scores

To identify a T cell-inflamed TME, we followed Ayers et al., based on the $\log_2$ transformed FPKM values; the TIS score was calculated as the weighted sum of the expression values of the 18 genes, enumerated in **Table S3**, applying the predefined weights derived by Ayers et al. (7, 9, 45). Considering the generation of scores based on the sum of signature related genes, we accordingly defined two XP gene cluster scores by summing up the expression values of genes in the same cluster.

Correlation Analysis

To assess the co-expression relationship between the considered genes, we cross-correlated the specified parameters. The Spearman rank correlation with p-value adjustment using Benjamini–Hochberg was performed by R package "*psych*" (v.2.1.3) (48) and visualized with package "ComplexHeatmap" (v.2.2.0) (49) using complete clustering with Euclidean distance for the dendrogram displayed at the columns.

Survival Analysis

For the survival analysis of the TCGA-SKCM data, we defined the overall survival (OS) as the time between melanoma diagnosis and the death or the last follow-up of the patient. The median follow-up was 669.50 days, while the survival status was decoded by 0 (alive) and 1 (dead). The constructed univariant Cox regression model predicted the overall survival from the continuous scores and gene expression values obtained from R packages "*survival*" (v.3.2-11) (50, 51) and "*survminer*" (v.0.4.9) (52). Kaplan–Meier analysis was used to calculate the survival probability of stratified patients, and the log-rank p-values for each analysis were given.

Response Prediction Model Construction

For anti-PD-1 response analysis, expression data of the two clinical cohorts (11, 12) were downloaded and reanalyzed using the Wilcoxon test and comparing expression levels of scores and single genes between responder and non-responder samples. The Youden index with associated ROC was determined for each parameter with R package "*cutpointr*" (v.1.1.0) (53, 54). The analysis was extended by multivariable predictive models for classification with the machine learning algorithm XGBoost (v.1.4.1.) (55) by partitioning the samples 75%/25% to training and testing data, respectively. The performed classification into responder and non-responder used "*caret*" (v. 6.0-86) (56) with the "xgbTree" method (55) and 10-fold cross-validation for combinations of multiple parameters.

RESULTS

Heterogeneity of XP Gene Expression in TCGA-SKCM

First, we explored the nine XP genes *XPA*, *ERCC3*, *XPC*, *ERCC2*, *ERCC4*, *ERCC5*, *DDB2*, *POLH*, and *ERCC1* in

TCGA-SKCM and observed heterogeneous expression patterns. By unsupervised clustering, we could identify two XP gene expression clusters, referred to as XP gene clusters 1 and 2 (**Figure 2**). Cluster 1 comprised the genes *XPA*, *ERCC4*, and *ERCC5*, while cluster 2 included *ERCC3*, *XPC*, *ERCC2*, *DDB2*, *POLH*, and *ERCC1*. Remarkably, the same clustering appeared if the cohort had been priorly divided by sample type (primary or metastatic, **Figures S1A, B**), age (younger or older than median age of 58, **Figures S1C, D**), or gender (male or female, **Figures S1E, F**). Genes of both XP clusters and their function in the NER pathway and of *POLH* are summed up in **Table 1**.

Altogether, median XP gene expression did not vary significantly in the analysis of subgroups. However, *ERCC4*, *XPC*, and *POLH* were expressed substantially greater in metastatic samples, whereas *DDB2* was expressed considerably higher in primary tumors. Subdividing the whole TCGA-SKCM cohort by median age, we found that in melanoma tissue from younger patients, XP cluster 1 genes and also *XPC* and *DDB2*, belonging to XP cluster 2, were expressed to a relatively higher extent (**Table S4**). In samples from female patients, all XP genes, except *ERCC1* and *ERCC2*, were expressed to a greater extent than in males.

Correlation Analysis Between XP & Immune Infiltration Genes, TMB and Computed Scores

Next, we investigated the correlation of XP genes and associated XP expression clusters to well-established predictive biomarkers of anti-PD-1 ICI response (**Figure 3**).

The expression of XP cluster 1 score with the 18-gene immune infiltration TIS score (p = 0.00034; R = 0.1793) as well with its single genes *CD274* (p = 6.858 e−07; R = 0.244), *CXCL9* (p = 1.640 e−06; R = 0.237), *CXCL13* (p = 2.666 e−06; R = 0.232), and *CD8A* (p = 0.0107; R = 0.131) showed weak but significant positive correlations. Likewise, the XP cluster 1 genes

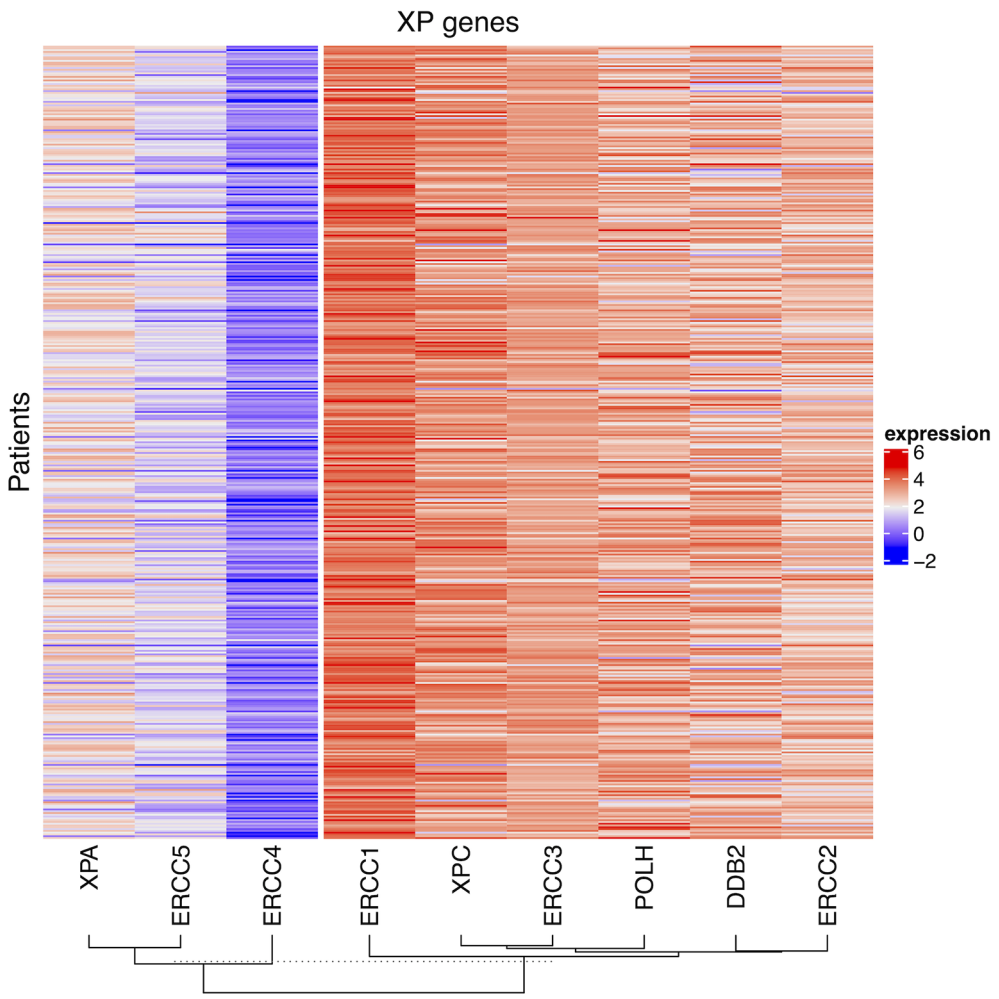

FIGURE 2 | The heatmap of $\log_2$ transformed FPKM values of the nine XP genes for all patient samples in TCGA-SKCM. The columns are clustered by hierarchical clustering with Manhattan distance and complete linkage.

TABLE 1 | XP genes with corresponding clusters, their encoding proteins and their functionality in the NER pathway and translesion synthesis, respectively.

Genes	Cluster Membership	Corresponding Proteins	Main Function
XPA	1	XPA	Involved in multiple NER steps, e.g., DNA damage verification; interacts with almost all other NER proteins
ERCC4	1	XPF	DNA lesion excision in a complex with ERCC1 at 5′ end from the lesion
ERCC5	1	XPG	DNA lesion excision at 3′ end from the lesion
ERCC3	2	XPB	DNA damage verification as TFIIH basal transcription factor complex DNA helicase subunit
XPC	2	XPC	DNA-damage recognition in GG-NER
ERCC2	2	XPD	DNA damage verification as TFIIH basal transcription factor complex DNA helicase subunit
DDB2	2	XPE	Auxiliary DNA-damage-recognition factor in GG-NER
POLH	2	XPV	DNA polymerase η, which is an enzyme of translesion synthesis, that bypasses unrepaired DNA damage
ERCC1	2	ERCC1	DNA lesion excision in a complex with XPF at 5′ end from the lesion

GG, global genome; NER, nucleotide excision repair; TFIIH, transcription initiation factor IIH.

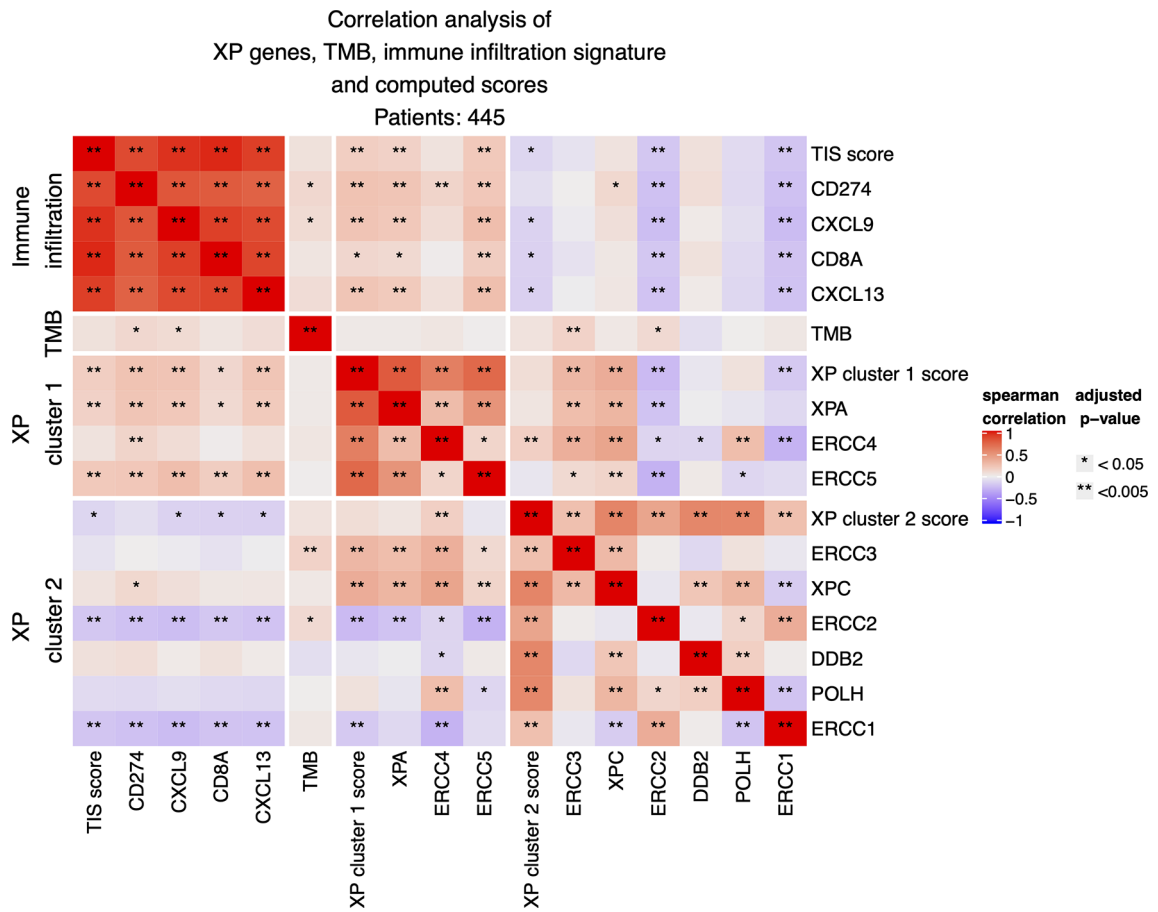

FIGURE 3 | Correlation analysis between expression of the nine XP genes, of computed XP and TIS scores and of single immune infiltration genes.

XPA and *ERCC5* were significantly positively correlated with TIS score and the above-mentioned immune infiltration genes. However, expression of *ERCC4* was only significantly correlated with *CD274* (p = 0.004; R= 0,146). Expression of XP cluster 2 score, on the other hand, was negatively correlated with the expression of TIS score (p = 0.037; R = −0.108), *CXCL9* (p = 0.013; R = −0.127), *CD8A* (p = 0.012; R = −0.129), and *CXCL13* (p = 0.01; R = −0.133). Importantly, the XP cluster 2 score genes *ERCC1* and *ERCC2* were individually highly significantly negatively correlated with TIS score (p = 0.0002, R = −0.186 and p = 0.0004, R = −0.176), immune infiltration genes and the XP cluster 1 score (**Figure 3**).

Tumor mutation burden (TMB) had weak positive correlations only with *CD274* (p = 0.01342; R = 0.127), *CXCL9* (p = 0.038; R = 0.1078), and also with the XP cluster 2 genes *ERCC3* (p = 0.00196; R = 0.157) and *ERCC2* (p = 0.027; R = 0.114). Importantly, no significant negative correlations between XP genes and TMB were observed.

When considering primary and metastatic samples separately, some differences were evident (**Figures S2A, B**): in primary samples only (n = 96), XP cluster 1 and cluster 2 scores had a positive correlation (p = 0.017; R = 0.279). Furthermore, the expression of the genes *ERCC3* and *XPC* was closely correlated with the expression of the XP cluster 1 score and its genes *XPA*, *ERCC4*, and *ERCC5*. Now, with a few exceptions, there were no significant correlations between XP genes and TIS score or immune infiltration genes but a positive correlation of TMB with TIS score (p = 0.00993; R = 0.3), *CD274* (p = 0.0048; R = 0.323), *CXCL9* (p = 0.0046; R = 0.327), *CD8A* (p = 0.004; R = 0.325), and *CXCL13* (p = 8.56 e−05; R = 0.422). Correlation of the by far larger group of metastatic samples (n = 349) revealed almost the same picture as for the whole group.

Further splitting by age and gender led to identical correlation patterns of XP gene clusters 1 and 2 with TIS score and immune infiltration genes, as we had observed for the whole TCGA-SKCM cohort (**Figures S2C–F**). Of note, the significant positive correlation of TMB with *CD274* was only detected if considering just males or the younger subgroup of patients.

XP & Immune Infiltration Genes, TMB, and Computed Scores as Prognostic Biomarkers for Survival

The great majority of TCGA-SKCM samples were obtained in the pre-ICI era. Only two patients received anti-PD-1 ICI after acquiring their tumor, but the removal of these two patients did not lead to significantly different results (**Table S5**) (43). Hence, we sought to analyze if there is a linear association between the expressions of the XP genes or cluster scores with survival of patients in TCGA-SKCM, and independent of ICI. Additionally, we analyzed the prognostic value of parameters predictive of anti-PD-1 ICI response: The TIS score, selected single score genes (*CD274*, *CXCL9*, *CD8A*), *CXCL13* TMB, and age.

Figures S3C, D demonstrated that neither single XP cluster 1 nor cluster 2 score were associated with survival in TCGA-SKCM. Considering the univariate Cox regression, out of the single XP genes, only *ERCC3* expression (hazard ratio, HR = 0.66, p = 0.043) revealed a significant association with survival (**Figure 4A**). In contrast, TIS score (HR: 0.87), *CXCL13* (HR = 0.93), TMB (HR = 0.74), and age (HR = 1.03) were all prognostic. TIS score and age also remained significant after segregation by the median. **Figures S3A, B** illustrate the corresponding Kaplan–Meier survival curves (log ranked p-values for age, p = 0.0014; TIS score, p = 0.0077).

The same analysis was repeated independently for age-divided sub-cohorts to decrease the influence of age as a dominant factor. Through this fractioning, the median overall survival dropped from 3,424 days to 1,927 days in the older patient group, while it increased to 4,634 days for the younger patients.

In those subgroups, we noted some differences (**Figures 4B, C** and **Figures S4–S7**). Although age and TIS score remained significant prognostic parameters, *ERCC3* (HR = 0.48, p = 0.0084) was the best predictor for survival and the only prognostic factor in the younger cohort. In the subgroup of older patients, *CXCL13* (HR = 0.93) and, newly, XP gene cluster 1 (HR = 0.87) were additional prognostic parameters.

XP & Immune Infiltration Genes and Computed Scores as Predictive Biomarkers for Response to Anti-PD-1 ICI

Because of the remarkable anecdotal benefit of XP patients to anti-PD-1 ICI, we analyzed XP gene expression as a predictive biomarker for response to anti-PD-1 ICI in two pooled publicly available melanoma cohorts (n = 75) (11, 12).

The distribution of the responding (complete or partial response) patients differed significantly from the non-responders based on the XP cluster 1 score (p = 0.015), with a higher score indicating a greater response (**Figure 5A**). A similar significant difference between these two groups was also applied for the single XP cluster 1 gene *ERCC5* (p = 0.026) (**Figure 5B**). Importantly, XP cluster 2 score, TIS score, and single genes indicative of immune infiltration, except *CD27* and *PSMB10*, were not significantly associated with response in the pooled anti-PD-1 melanoma cohorts (**Figure S8**).

To assess the predictive performance of these single genes for ICI response, we computed the Youden index for each parameter (a XP gene or signature) and compared the areas under the receiver operating characteristic curves (AUC) (**Table S6**) (7). In this analysis, *ERCC5* (AUC = 0.660), XP cluster 1 score (AUC = 0.654), XP cluster 2 score (AUC = 0.632), and *CD8A* (AUC = 0.627) were the best performing variables. Except *XPA* (AUC = 0.532), *POLH* (AUC = 0.545), and *CD274* (AUC = 0.533), all other parameters outperformed TIS score (AUC = 0.586).

Expansion of these restricted single parameter analyses by combining multiple variables from two to five possible parameters led to many response classification models. Due to infinitive values for two samples, this analysis was limited to 73 patients. The combination of two parameters had the best results if one immune infiltration gene (like *CD274* or *CXCL13*) was combined with one XP gene (CD274_*ERCC4*, AUC = 0.7; CXCL13_ERCC5, AUC = 0.68), or if XP gene cluster 2 gene *ERCC2* was combined with *ERCC5* (AUC 0.69). All these combinations outperformed any combination involving the TIS score (**Table S7** and **Figure 6A**). The three-parameter-based analysis performed better than the combination of two parameters and revealed that combining XP genes provided the best classification triplet for response (*ERCC3_XPC_ERCC4*, AUC = 0.8; *XPC_ERCC4_ERCC1*, 0.75). (**Table S8** and **Figure 6B**). The prediction of the combination of four variables had the best AUC value of 0.85, and even outperformed the combination of five parameters (**Tables S9**, **S10** and **Figure 6C**). Of note, it included the combination of one immune infiltration gene (*CD274*), two XP cluster 1 genes (*XPA*, *ERCC4*) and one XP cluster 2 gene (*ERCC2*).

DISCUSSION

Clustering by using mRNA gene expression levels can identify higher-level structures and relationships and establish a new molecular classification of tumors (57, 58). Furthermore,

A

Variable	N	Hazard ratio	p
XPA	443	0.81 (0.62, 1.05)	0.114
ERCC3	443	0.66 (0.44, 0.99)	0.043
XPC	443	0.88 (0.67, 1.14)	0.328
ERCC2	443	1.30 (0.98, 1.74)	0.071
DDB2	443	0.97 (0.80, 1.18)	0.782
ERCC4	443	0.90 (0.69, 1.16)	0.402
ERCC5	443	0.83 (0.64, 1.09)	0.183
POLH	443	1.16 (0.93, 1.44)	0.196
ERCC1	443	0.80 (0.59, 1.08)	0.144
CXCL13	443	0.93 (0.89, 0.98)	0.005
TP53	443	0.93 (0.78, 1.11)	0.432
TMB	443	0.74 (0.54, 1.00)	0.050
TIS score	443	0.87 (0.81, 0.94)	<0.001
cluster 1 XP score	443	0.91 (0.81, 1.01)	0.087
cluster 2 XP score	443	0.99 (0.90, 1.08)	0.786
Age	443	1.03 (1.02, 1.04)	<0.001

B

Variable	N	Hazard ratio	p
XPA	232	0.77 (0.54, 1.11)	0.164
ERCC3	232	0.73 (0.43, 1.24)	0.244
XPC	232	0.76 (0.52, 1.11)	0.158
ERCC2	232	1.40 (0.90, 2.17)	0.137
DDB2	232	0.79 (0.61, 1.03)	0.080
ERCC4	232	0.79 (0.58, 1.06)	0.113
ERCC5	232	0.78 (0.54, 1.12)	0.178
POLH	232	0.94 (0.68, 1.29)	0.687
ERCC1	232	0.86 (0.57, 1.30)	0.476
CXCL13	232	0.93 (0.87, 0.99)	0.031
TP53	232	0.85 (0.68, 1.07)	0.164
TMB	232	0.77 (0.55, 1.08)	0.126
TIS score	232	0.85 (0.76, 0.96)	0.007
cluster 1 XP score	232	0.87 (0.75, 1.00)	0.046
cluster 2 XP score	232	0.89 (0.77, 1.02)	0.090
Age	232	1.06 (1.03, 1.10)	<0.001

C

Variable	N	Hazard ratio	p
XPA	211	0.88 (0.59, 1.31)	0.54
ERCC3	211	0.48 (0.27, 0.85)	0.01
XPC	211	0.93 (0.63, 1.37)	0.71
ERCC2	211	1.16 (0.78, 1.71)	0.46
DDB2	211	1.24 (0.92, 1.66)	0.16
ERCC4	211	1.22 (0.78, 1.90)	0.38
ERCC5	211	0.99 (0.66, 1.47)	0.95
POLH	211	1.32 (0.97, 1.79)	0.08
ERCC1	211	0.72 (0.46, 1.13)	0.15
CXCL13	211	0.94 (0.88, 1.00)	0.07
TP53	211	1.12 (0.83, 1.51)	0.46
TMB	211	0.66 (0.39, 1.13)	0.13
TIS score	211	0.89 (0.80, 0.99)	0.03
cluster 1 XP score	211	1.01 (0.83, 1.22)	0.94
cluster 2 XP score	211	1.04 (0.91, 1.18)	0.60
Age	211	1.03 (1.01, 1.06)	0.02

FIGURE 4 | Overview of the univariate cox regression analysis for all TCGA-SKCM patients **(A)**. The bar indicates the reference Hazard ratio of 1. The patients split by median age into older patients **(B)** and younger patients **(C)** show different Hazard ratios for the same parameters.

hierarchical clustering based on gene expression profiles (GEPs) can be used to, e.g., reveal immune competency or sensitivity to ICI treatment (9, 59).

Because melanoma has been the "model tumor" for the development of ICI and was also the first tumor entity in which ICI was approved, we focused our exploratory analysis on melanoma. Our study analyzed XP gene expression and deduced two different expression clusters (XP gene clusters 1 and 2, see **Figure 2** and **Table 1**) with heterogeneous functions in the NER pathway and translesion synthesis. The proteins encoded by the XP cluster 1 genes *ERCC4*, i.e., XPF, and *ERCC5*, i.e., XPG, are responsible for the dual incision of DNA damage. Cluster 1 further includes XPA, the central NER coordinator, because of its interaction with almost all other NER factors (39, 60). Accordingly, it also interacts with ERCC1, an endonuclease and fulfills its function as a heterodimer with XPF (61, 62). Surprisingly, *ERCC1* is part of XP cluster 2 instead of cluster 1, and there was a strong negative correlation between *ERCC1* and *ERCC4* expression in the TCGA-SKCM samples (**Figure 3**). Besides, in NER, the ERCC1–XPF complex is involved in interstrand crosslink and DSB repair, and mutations in one of the two genes result in a very

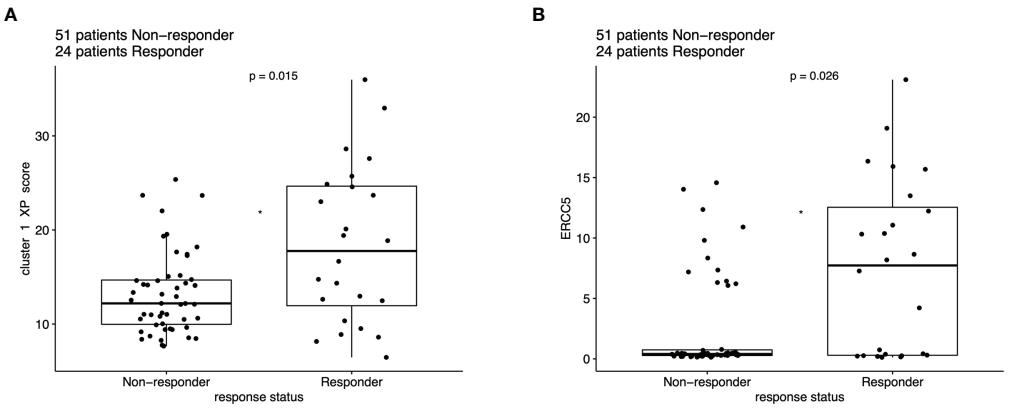

FIGURE 5 | Boxplot of ICI response data (n = 75), compared with Wilcoxon test based on the expression of **(A)** XP cluster 1 score and **(B)** *ERCC5*.

complex constellation of clinical symptoms (39, 63). In epithelial ovarian cancer, ERCC1 and ERCC4 expression correlated on mRNA and protein level with one another, however, *ERCC1* mRNA was negatively correlated, and *ERCC4* mRNA was unrelated with its protein expression, suggesting a posttranscriptional mode of regulation (64). Because protein expression data was unavailable for most of our nine XP genes, we could not expand our analysis to protein correlations, which might have revealed substantially different clusters due to extensive posttranslational modifications in NER (39). In global genome-NER, damage recognition is performed by XPC and involves XPE (encoded by *DDB2*), which are both parts of XP cluster 2. Different genes of cluster 2 include *ERCC2* (codes for XPD) and *ERCC3* (codes for XPB), which are DNA helicases and part of transcription initiation factor IIH complex verifying DNA damage lesions. *POLH*, whose defect leads to XP variant, codes for the DNA error-prone polymerase eta involved in translesion synthesis (39, 65).

Subsequently, we investigated the correlation of the XP genes and clusters with well-known, ICI predictive biomarkers of a T cell-inflamed TME: The TIS score, namely, its single genes *CD8A*, *CXCL9*, *CD274*, and the recently postulated biomarker *CXCL13*, that could be characteristic of clonal neoantigen-reactive CD8 T infiltrating lymphocytes (6, 7, 9, 10). Of note, we revealed that XP cluster 1 and its genes *XPA* and *ERCC5* had a highly significant positive correlation with the TIS score and all other immune infiltration associated genes (**Figure 3**). In line with this, Boonstra et al. (66) compared UVB suppression of ConA-induced IFN-γ production in XPA, XPC, and CSB deficient mice and demonstrated that only XPA mice showed a substantial reduction of IFN-γ production by UVB. Regarding gene correlations in TCGA-SKCM, our results are different from those of BER/SSB repair genes, which more homogeneously and almost exclusively present a negative correlation with *CD274* expression (26).

A negative correlation with *CD274*, TIS score, or the other genes representative of immune infiltration was identified for the XP cluster 2 genes *ERCC1* and *ERCC2*, which was true especially for samples of younger patients. However, neither the expression of *ERCC1*, *ERCC2*, nor of other XP genes was negatively correlated with TMB. Likewise, the frequency of XP gene mutations with median TMB values was not correlated in different cancers (41). Noteworthy, from the XP genes, *ERCC3* expression even had a highly significant positive correlation with TMB in samples of the whole cohort and the younger subcohort (**Figure 3** and **Figure S2C**). Taken together, the results from Hsiehchen et al. (41) and ourselves illustrate that the implications for tumor immunogenicity through XP gene mutations and diverse expression are presumably more complex than being based solely on the more abundant generation of neoantigens caused by somatic tumor mutations. Admittedly, we cannot precisely determine if the XP gene expression we assessed is preferentially constituted by tumor or other, e.g., immune cells in the TME (67). Circadian XP gene expression particularly affects *XPA* and could potentially impact the results of our analysis; however, it seems not to be relevant in actively proliferating tissues as tumors (68, 69).

Just recently, survival prognosis in melanoma was correlated with immune-related gene signatures (70–72). Of note, Danaher et al. (73) found that TIS was also highly statistically significantly prognostic in TCGA-SKCM, limiting its predictive value in melanoma patients. Accordingly, we analyzed the predictive role of all markers and found out that besides TIS, *CXCL13*, TMB, age, and *ERCC3* were prognostic. Age and TMB have been revealed as prognostic biomarkers in different studies and cancer entities before, though results for TMB are not homogeneous and depend on the used thresholds (74–77). Correspondingly, in our univariate analysis with segregated parameters for high and low values based on medians, we found no difference between TMB groups (**Table S11**). *CXCL13* was suggested as a prognostic biomarker in melanoma before, but the correlation of *ERCC3* with survival needs further validation (78, 79).

Notably, after dividing the cohort by age, in younger patients, *ERCC3* (HR 0.48) and TMB (0.66) revealed the lowest HR values; however, for TMB, it was not significant. This observation,

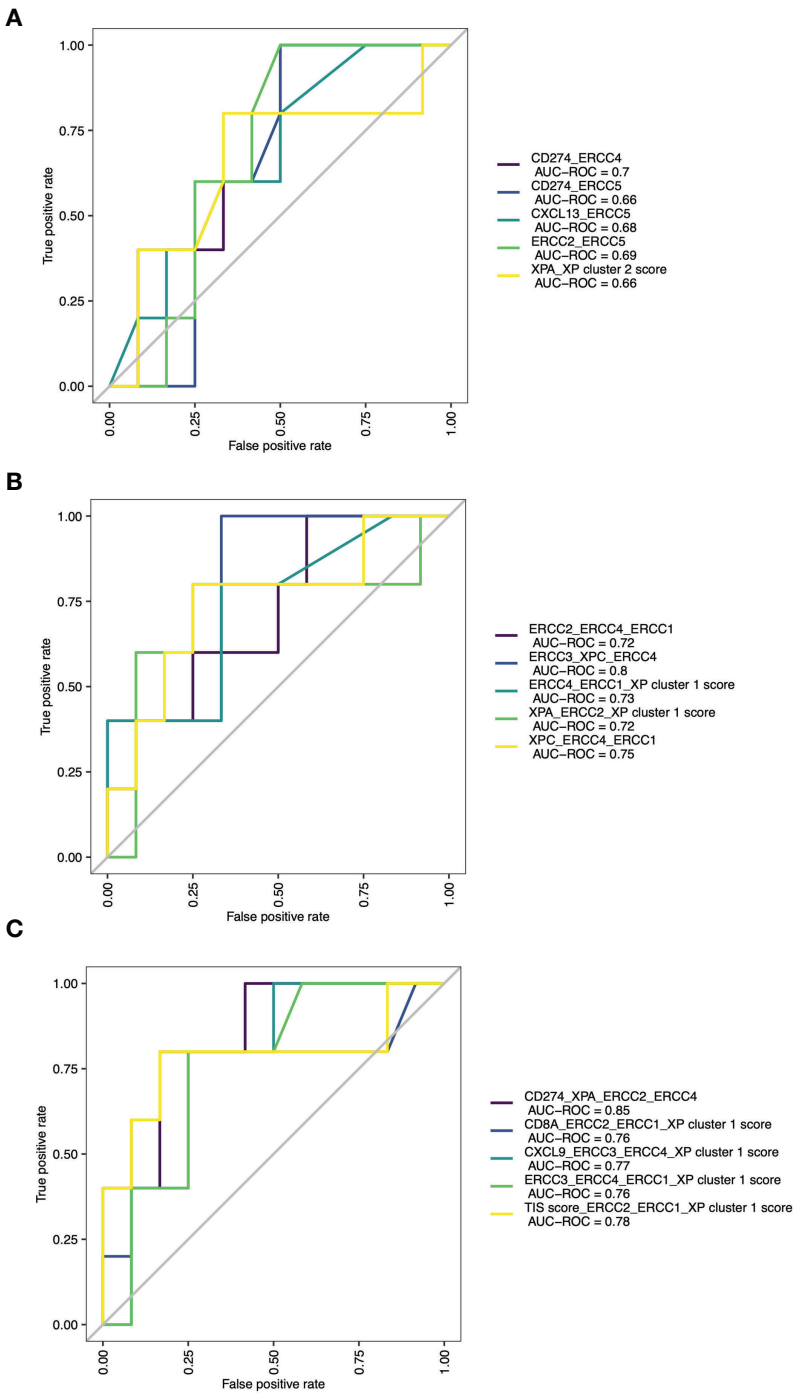

FIGURE 6 | ROC curves with AUCs of top 5 combinations of **(A)** 2 parameters, **(B)** 3 parameters and **(C)** 4 parameters for prediction of ICI response.

together with the positive correlation between *ERCC3* and TMB in younger patients, suggests that *ERCC3* might have specific relevance for disease progression, especially in the young. In contrast, earlier reports have suggested that the presence of an intense immune infiltrate in older persons could have more prognostic weight (75). This assumption might explain that in our analysis, *CXCL13* expression, as a specific marker of exhausted T cells, was only prognostic in melanoma tissue of older when subdividing by patient age. The same accounted for XP cluster 1, which in samples of older was highly correlated with TIS score and other immune infiltration genes (**Figure 4** and **Figure S2D**).

An ongoing challenge is the identification of reliable biomarkers predictive of ICI response. Recent efforts leave single parameters and evolve into combinatorial biomarkers (6, 7, 10). Especially, the combination of tumor intrinsic factors, like TMB, and genes representative of immune infiltration in the TME, like TIS or *CXCL13*, show promise in exploratory studies (7, 9, 10, 80). Hence, we tested the single and combinational predictive performance of our parameters in two pooled anti-PD-1 cohorts. The existing *immune-specific* biomarkers were only of limited value and constructed prediction models (10). Importantly, we observed that the combination of either an immune-infiltrating gene (*CD274*) with three XP genes, or the combination of only three XP genes from both clusters provided the best ROC and AUC values (**Table 2**). Of note, the prediction was not improved by extension to five parameters; hence, we did not test further combinations of even more variables. Because of our small, pooled cohort and to avoid overfitting, we did conduct only a split of our data in training and testing set for our prediction models. We, therefore, admit that our constructed models lacked robustness to establish new ICI predictive biomarkers.

Our study has several limitations. First, we restricted our analysis to melanoma, and the samples sizes of the two clinical cohorts that we analyzed were small, limiting our results' comparability. For example, TIS score and genes indicative of immune infiltration, which, except for *CD8A*, performed poor as singular splitting parameters in our pooled data of two anti-PD-1 cohorts (11, 12), were significantly predictive in the study of Cristescu et al. (AUC of TIS score = 0.638) (7, 10). Second, due to the standardized pre-processing, the sample size of the two cohorts had to be further reduced. For the anti-PD-1 cohorts, we did not analyze survival data restricting our analysis to ICI response, which is not an appropriate measure of long-term treatment benefit. Third, 11 of 26 patients included from the cohort of Hugo et al. (11) and 26 of 49 patients in the cohort of Riaz et al. (12) were not treatment-naïve and had received prior MAPK inhibitor treatment or anti-CTLA-4 ICI, respectively, before sample acquisition, potentially influencing gene expression. Nevertheless, primary and acquired resistance constitutes a major problem in the systemic therapy of melanoma, suggesting the analysis of the XP gene clusters in additional patients with therapy failure (2, 3, 6, 81). Fourth, in the two clinical cohorts that we considered, mainly metastatic tissue was analyzed, and our analysis was made regardless of gender and age, which could have had an influence, especially on XP GEPs. Fifth, due to limited data, TMB and clonal TMB, which were the best performing predictive markers in the meta-analysis of Litchfield et al. (10), could not be assessed in our study. Likewise, we did also not assess the expression of genes in other DDR pathways.

Despite all these limitations, our analysis provides significant new findings that deserve attention: Firstly, XP genes are expressed in two heterogeneous clusters in melanoma. Secondly, these clusters correlate differentially with markers of a T cell-inflamed TME, and correlations depend to a certain degree on melanoma tissue origin (primary vs metastatic), age, and gender. Thirdly, a higher *ERCC3* expression could be associated with a better prognosis in melanoma, especially in younger patients. Lastly, the differentiated consideration of XP gene expression in the TME and its combination with established ICI predictive biomarkers could be useful in predicting anti-PD-1 ICI response in melanoma and should be explored by further studies.

TABLE 2 | Combination of the best 25 performing models, based on the AUC values, across the different number of used parameters.

Parameter for predictive model	AUC	# parameters
CD274_XPA_ERCC2_ERCC4	0.85	4
ERCC3_XPC_ERCC4	0.80	3
TIS score_*ERCC2_ERCC1*_cluster 1 XP score	0.78	4
TIS score_*CXCL13_CXCL9_CD274*_cluster 1 XP score	0.78	5
*CXCL9_CD8A_CD274_ERCC2*_cluster 1 XP score	0.78	5
*CXCL9_CD8A_XPC_ERCC1*_cluster 1 XP score	0.78	5
*CD8A_CD274_ERCC3_ERCC4*_cluster 1 XP score	0.78	5
*XPA_ERCC2_ERCC1*_cluster 1 XP score_cluster 2 XP score	0.78	5
*CXCL9_ERCC3_ERCC4*_cluster 1 XP score	0.77	4
CXCL9_CD8A_XPA_ERCC2_ERCC5	0.77	5
CXCL9_CD274_XPA_ERCC4_ERCC1	0.77	5
*CD8A_CD274_DDB2_ERCC1*_cluster 1 XP score	0.77	5
CD274_XPA_XPC_ERCC4_ERCC1	0.77	5
*CD274_DDB2_ERCC4_ERCC1*_cluster 1 XP score	0.77	5
*CD8A_ERCC2_ERCC1*_cluster 1 XP score	0.76	4
*ERCC3_ERCC4_ERCC1*_cluster 1 XP score	0.76	4
XPC_ERCC4_ERCC1	0.75	3
TIS score_*XPA_ERCC2*_cluster 1 XP score	0.75	4
*CXCL9_CD8A_XPC*_cluster 1 XP score	0.75	4
*CXCL9_CD274_ERCC1*_cluster 2 XP score	0.75	4
TIS score_*CXCL13_CD8A_ERCC4_ERCC1*	0.75	5
TIS score_*CD8A_CD274_ERCC1*_cluster 1 XP score	0.75	5
TIS score_*CD8A_CD274*_cluster 1 XP score_cluster 2 XP score	0.75	5
TIS score_*CD8A_ERCC3_ERCC4*_cluster 1 XP score	0.75	5
TIS score_*CD274_ERCC2_ERCC4*_cluster 1 XP score	0.75	5

DATA AVAILABILITY STATEMENT

The original contributions presented in the study are included in the article/**Supplementary Material**. Further inquiries can be directed to the corresponding author.

AUTHOR CONTRIBUTIONS

SF and AT designed this study, conducted the analysis, and wrote the article. MH, SE, OW and GF provided conceptual advice and critically reviewed the article. All authors contributed to the article and approved the submitted version.

FUNDING

AT is supported by the "Hiege Foundation—the German Skin Cancer Foundation" and the "Forschungsförderung der Universitätsmedizin Rostock (FORUN)". Support for computing equipment was provided by the European Union

(EFRE, "Europäischer Fonds für regionale Entwicklung"). The funders had no role in the study design, collection, analysis, interpretation of the data, writing of the manuscript, or the decision to submit the paper for publication.

ACKNOWLEDGMENTS

The results published in this article are based upon data generated by the TCGA Research Network (https://www.cancer.gov/tcga) and publicly available data from clinical studies. We thank all the patients, who participated, and investigators who provided their research and shared their data openly.

SUPPLEMENTARY MATERIAL

The Supplementary Material for this article can be found online at: https://www.frontiersin.org/articles/10.3389/fonc.2022.810058/full#supplementary-material

REFERENCES

1. Robert C. A Decade of Immune-Checkpoint Inhibitors in Cancer Therapy. *Nat Commun* (2020) 11(1):3801. doi: 10.1038/s41467-020-17670-y
2. Moreira A, Heinzerling L, Bhardwaj N, Friedlander P. Current Melanoma Treatments: Where Do We Stand? *Cancers (Basel)* (2021) 13(2):221. doi: 10.3390/cancers13020221
3. Schadendorf D, van Akkooi ACJ, Berking C, Griewank KG, Gutzmer R, Hauschild A, et al. Melanoma. *Lancet* (2018) 392(10151):971–84. doi: 10.1016/S0140-6736(18)31559-9
4. Larkin J, Chiarion-Sileni V, Gonzalez R, Grob JJ, Rutkowski P, Lao CD, et al. Five-Year Survival With Combined Nivolumab and Ipilimumab in Advanced Melanoma. *N Engl J Med* (2019) 381(16):1535–46. doi: 10.1056/NEJMoa1910836
5. Havel JJ, Chowell D, Chan TA. The Evolving Landscape of Biomarkers for Checkpoint Inhibitor Immunotherapy. *Nat Rev Cancer* (2019) 19(3):133–50. doi: 10.1038/s41568-019-0116-x
6. Sharma P, Siddiqui BA, Anandhan S, Yadav SS, Subudhi SK, Gao J, et al. The Next Decade of Immune Checkpoint Therapy. *Cancer Discov* (2021) 11(4):838–57. doi: 10.1158/2159-8290.CD-20-1680
7. Cristescu R, Mogg R, Ayers M, Albright A, Murphy E, Yearley J, et al. Pan-Tumor Genomic Biomarkers for PD-1 Checkpoint Blockade-Based Immunotherapy. *Science* (2018) 362(6411):eaar3593. doi: 10.1126/science.aar3593
8. Gnjatic S, Bronte V, Brunet LR, Butler MO, Disis ML, Galon J, et al. Identifying Baseline Immune-Related Biomarkers to Predict Clinical Outcome of Immunotherapy. *J Immunother Cancer* (2017) 5(1):44. doi: 10.1186/s40425-017-0243-4
9. Ayers M, Lunceford J, Nebozhyn M, Murphy E, Loboda A, Kaufman DR, et al. IFN-Gamma-Related mRNA Profile Predicts Clinical Response to PD-1 Blockade. *J Clin Invest* (2017) 127(8):2930–40. doi: 10.1172/JCI91190
10. Litchfield K, Reading JL, Puttick C, Thakkar K, Abbosh C, Bentham R, et al. Meta-Analysis of Tumor- and T Cell-Intrinsic Mechanisms of Sensitization to Checkpoint Inhibition. *Cell* (2021) 184(3):596–614.e14. doi: 10.1016/j.cell.2021.01.002
11. Hugo W, Zaretsky JM, Sun L, Song C, Moreno BH, Hu-Lieskovan S, et al. Genomic and Transcriptomic Features of Response to Anti-PD-1 Therapy in Metastatic Melanoma. *Cell* (2016) 165(1):35–44. doi: 10.1016/j.cell.2016.02.065
12. Riaz N, Havel JJ, Makarov V, Desrichard A, Urba WJ, Sims JS, et al. Tumor and Microenvironment Evolution During Immunotherapy With Nivolumab. *Cell* (2017) 171(4):934–49.e16. doi: 10.1016/j.cell.2017.09.028
13. Bever KM, Le DT. DNA Repair Defects and Implications for Immunotherapy. *J Clin Invest* (2018) 128(10):4236–42. doi: 10.1172/JCI122010
14. Keenan TE, Burke KP, Van Allen EM. Genomic Correlates of Response to Immune Checkpoint Blockade. *Nat Med* (2019) 25(3):389–402. doi: 10.1038/s41591-019-0382-x
15. Mouw KW, D'Andrea AD. DNA Repair Deficiency and Immunotherapy Response. *J Clin Oncol* (2018) 36(17):1710–3. doi: 10.1200/JCO.2018.78.2425
16. Teo MY, Seier K, Ostrovnaya I, Regazzi AM, Kania BE, Moran MM, et al. Alterations in DNA Damage Response and Repair Genes as Potential Marker of Clinical Benefit From PD-1/PD-L1 Blockade in Advanced Urothelial Cancers. *J Clin Onc ol* (2018) 36(17):1685–94. doi: 10.1200/JCO.2017.75.7740
17. Germano G, Lamba S, Rospo G, Barault L, Magri A, Maione F, et al. Inactivation of DNA Repair Triggers Neoantigen Generation and Impairs Tumour Growth. *Nature* (2017) 552(7683):116–20. doi: 10.1038/nature24673
18. Le DT, Durham JN, Smith KN, Wang H, Bartlett BR, Aulakh LK, et al. Mismatch Repair Deficiency Predicts Response of Solid Tumors to PD-1 Blockade. *Science* (2017) 357(6349):409–13. doi: 10.1126/science.aan6733
19. Le DT, Uram JN, Wang H, Bartlett BR, Kemberling H, Eyring AD, et al. PD-1 Blockade in Tumors With Mismatch-Repair Deficiency. *N Engl J Med* (2015) 372(26):2509–20. doi: 10.1056/NEJMoa1500596
20. Schumacher TN, Schreiber RD. Neoantigens in Cancer Immunotherapy. *Science* (2015) 348(6230):69–74. doi: 10.1126/science.aaa4971
21. Gladbach YS, Wiegele L, Hamed M, Merkenschlager AM, Fuellen G, Junghanss C, et al. Unraveling the Heterogeneous Mutational Signature of Spontaneously Developing Tumors in MLH1(-/-) Mice. *Cancers (Basel)* (2019) 11(10):1485. doi: 10.3390/cancers11101485
22. Jeggo PA, Pearl LH, Carr AM. DNA Repair, Genome Stability and Cancer: A Historical Perspective. *Nat Rev Cancer* (2016) 16(1):35–42. doi: 10.1038/nrc.2015.4
23. Patterson-Fortin J, D'Andrea AD. Exploiting the Microhomology-Mediated End-Joining Pathway in Cancer Therapy. *Cancer Res* (2020) 80(21):4593–600. doi: 10.1158/0008-5472.Can-20-1672
24. Sfeir A, Symington LS. Microhomology-Mediated End Joining: A Back-Up Survival Mechanism or Dedicated Pathway? *Trends Biochem Sci* (2015) 40(11):701–14. doi: 10.1016/j.tibs.2015.08.006
25. Stewart RA, Pilie PG, Yap TA. Development of PARP and Immune-Checkpoint Inhibitor Combinations. *Cancer Res* (2018) 78(24):6717–25. doi: 10.1158/0008-5472.CAN-18-2652
26. Permata TBM, Hagiwara Y, Sato H, Yasuhara T, Oike T, Gondhowiardjo S, et al. Base Excision Repair Regulates PD-L1 Expression in Cancer Cells. *Oncogene* (2019) 38(23):4452–66. doi: 10.1038/s41388-019-0733-6
27. Sato H, Niimi A, Yasuhara T, Permata TBM, Hagiwara Y, Isono M, et al. DNA Double-Strand Break Repair Pathway Regulates PD-L1 Expression in Cancer Cells. *Nat Commun* (2017) 8(1):1751. doi: 10.1038/s41467-017-01883-9
28. Garcia-Diaz A, Shin DS, Moreno BH, Saco J, Escuin-Ordinas H, Rodriguez GA, et al. Interferon Receptor Signaling Pathways Regulating PD-L1 and PD-L2 Expression. *Cell Rep* (2017) 19(6):1189–201. doi: 10.1016/j.celrep.2017.04.031
29. Parkes EE, Walker SM, Taggart LE, McCabe N, Knight LA, Wilkinson R, et al. Activation of STING-Dependent Innate Immune Signaling By S-Phase-Specific DNA Damage in Breast Cancer. *J Natl Cancer Inst* (2016) 109(1):djw199. doi: 10.1093/jnci/djw199
30. Trujillo JA, Sweis RF, Bao R, Luke JJ. T Cell-Inflamed Versus Non-T Cell-Inflamed Tumors: A Conceptual Framework for Cancer Immunotherapy Drug Development and Combination Therapy Selection. *Cancer Immunol Res* (2018) 6(9):990–1000. doi: 10.1158/2326-6066.CIR-18-0277
31. Ribas A. Adaptive Immune Resistance: How Cancer Protects From Immune Attack. *Cancer Discov* (2015) 5(9):915–9. doi: 10.1158/2159-8290.CD-15-0563
32. Mouw KW, Goldberg MS, Konstantinopoulos PA, D'Andrea AD. DNA Damage and Repair Biomarkers of Immunotherapy Response. *Cancer Discov* (2017) 7(7):675–93. doi: 10.1158/2159-8290.Cd-17-0226
33. Chambon F, Osdoit S, Bagny K, Moro A, Nguyen J, Reguerre Y. Dramatic Response to Nivolumab in Xeroderma Pigmentosum Skin Tumor. *Pediatr Blood Cancer* (2018) 65(2):e26837. doi: 10.1002/pbc.26837

34. Deinlein T, Lax SF, Schwarz T, Giuffrida R, Schmid-Zalaudek K, Zalaudek I. Rapid Response of Metastatic Cutaneous Squamous Cell Carcinoma to Pembrolizumab in a Patient With Xeroderma Pigmentosum: Case Report and Review of the Literature. *Eur J Cancer* (2017) 83:99–102. doi: 10.1016/j.ejca.2017.06.022
35. Hauschild A, Eichstaedt J, Mobus L, Kahler K, Weichenthal M, Schwarz T, et al. Regression of Melanoma Metastases and Multiple Non-Melanoma Skin Cancers in Xeroderma Pigmentosum by the PD1-Antibody Pembrolizumab. *Eur J Cancer* (2017) 77:84–7. doi: 10.1016/j.ejca.2017.02.026
36. Salomon G, Maza A, Boulinguez S, Paul C, Lamant L, Tournier E, et al. Efficacy of Anti-Programmed Cell Death-1 Immunotherapy for Skin Carcinomas and Melanoma Metastases in a Patient With Xeroderma Pigmentosum. *Br J Dermatol* (2018) 178(5):1199–203. doi: 10.1111/bjd.16270
37. Steineck A, Krumm N, Sarthy JF, Pritchard CC, Chapman T, Stacey AW, et al. Response to Pembrolizumab in a Patient With Xeroderma Pigmentosum and Advanced Squamous Cell Carcinoma. *JCO Precis Oncol* (2019) 3:PO.19.00028. doi: 10.1200/PO.19.00028
38. Kraemer KH, DiGiovanna JJ. Xeroderma Pigmentosum. In: Adam MP, Ardinger HH, Pagon RA, et al, editors. *GeneReviews®* [Internet]. Seattle (WA): University of Washington, Seattle 1993–2021 (2003). Available at: https://www.ncbi.nlm.nih.gov/books/NBK1397/
39. Marteijn JA, Lans H, Vermeulen W, Hoeijmakers JH. Understanding Nucleotide Excision Repair and Its Roles in Cancer and Ageing. *Nat Rev Mol Cell Biol* (2014) 15(7):465–81. doi: 10.1038/nrm3822
40. Bradford PT, Goldstein AM, Tamura D, Khan SG, Ueda T, Boyle J, et al. Cancer and Neurologic Degeneration in Xeroderma Pigmentosum: Long Term Follow-Up Characterises the Role of DNA Repair. *J Med Genet* (2011) 48(3):168–76. doi: 10.1136/jmg.2010.083022
41. Hsiehchen D, Hsieh A, Samstein RM, Lu T, Beg MS, Gerber DE, et al. DNA Repair Gene Mutations as Predictors of Immune Checkpoint Inhibitor Response Beyond Tumor Mutation Burden. *Cell Rep Med* (2020) 1 (3):100034. doi: 10.1016/j.xcrm.2020.100034
42. Samstein RM, Krishna C, Ma X, Pei X, Lee KW, Makarov V, et al. Mutations in BRCA1 and BRCA2 Differentially Affect the Tumor Microenvironment and Response to Checkpoint Blockade Immunotherapy. *Nat Cancer* (2021) 1 (12):1188–203. doi: 10.1038/s43018-020-00139-8
43. Genomic Classification of Cutaneous Melanoma. *Cell* (2015) 161(7):1681–96. doi: 10.1016/j.cell.2015.05.044
44. Oldenhuis CN, Oosting SF, Gietema JA, de Vries EG. Prognostic Versus Predictive Value of Biomarkers in Oncology. *Eur J Cancer* (2008) 44(7):946–53. doi: 10.1016/j.ejca.2008.03.006
45. Ayers M, Loboda A, Lunceford J, Mcclanahan T, Murphy E, Nebozhyn M, et al. WO2016094377 (2016). 2016-06-16. Available at: https://p ubchem.n cbi.nlm.nih.gov/patent/WO-2016094377- A1
46. Team RC. *R: A Language and Environment for Statistical Computing Vienna, Austria*. Vienna, Austria: R Foundation for Statistical Computing (2019). Available at: https://www.R-project.org/.
47. Mayakonda A, Lin DC, Assenov Y, Plass C, Koeffler HP. Maftools: Efficient and Comprehensive Analysis of Somatic Variants in Cancer. *Genome Res* (2018) 28(11):1747–56. doi: 10.1101/gr.239244.118
48. Revelle W. *Psych: Procedures for Psychological, Psychometric, and Personality Research* (2021). Available at: https://CRAN.R-project.org/package=psych.
49. Gu Z, Eils R, Schlesner M. Complex Heatmaps Reveal Patterns and Correlations in Multidimensional Genomic Data. *Bioinformatics* (2016) 32 (18):2847–9. doi: 10.1093/bioinformatics/btw313
50. Therneau TM, Grambsch PM. *Modeling Survival Data: Extending the Cox Model*. New York: Springer Nature (2000).
51. Therneau TM. *A Package for Survival Analysis in R* (2021). Available at: https://CRAN.R-project.org/package=survival.
52. Kassambara A, Kosinski M, Biecek P. *Survminer: Drawing Survival Curves Using 'Ggplot2'* (2021). Available at: https://cran.r-project.org/web/packages/survminer.
53. Thiele C. *Cutpointr: Determine and Evaluate Optimal Cutpoints in Binary Classification Tasks* (2021). Available at: https://cran.r-project.org/web/packages/cutpointr.
54. Thiele C, Hirschfeld G. Cutpointr: Improved Estimation and Validation of Optimal Cutpoints in R. *J Stat Softw* (2021) 98(11):1 – 27. doi: 10.18637/jss.v098.i11
55. Chen T, He T, Benesty M, Khotilovich V, Tang Y, Cho H, et al. *Xgboost: Extreme Gradient Boosting* (2021). Available at: https://CRAN.R-project.org/package=xgboost.
56. Kuhn M. *Caret: Classification and Regression Training* (2020). Available at: https://CRAN.R-project.org/package=caret.
57. Hoadley KA, Yau C, Hinoue T, Wolf DM, Lazar AJ, Drill E, et al. Cell-Of-Origin Patterns Dominate the Molecular Classification of 10,000 Tumors From 33 Types of Cancer. *Cell* (2018) 173(2):291–304.e6. doi: 10.1016/j.cell.2018.03.022
58. Vidman L, Kallberg D, Ryden P. Cluster Analysis on High Dimensional RNA-Seq Data With Applications to Cancer Research - An Evaluation Study. *PloS One* (2019) 14(12):e0219102. doi: 10.1371/journal.pone.0219102
59. Vitale I, Shema E, Loi S, Galluzzi L. Intratumoral Heterogeneity in Cancer Progression and Response to Immunotherapy. *Nat Med* (2021) 27(2):212–24. doi: 10.1038/s41591-021-01233-9
60. Scharer OD. Nucleotide Excision Repair in Eukaryotes. *Cold Spring Harb Perspect Biol* (2013) 5(10):a012609. doi: 10.1101/cshperspect.a012609
61. Orelli B, McClendon TB, Tsodikov OV, Ellenberger T, Niedernhofer LJ, Scharer OD. The XPA-Binding Domain of ERCC1 Is Required for Nucleotide Excision Repair But Not Other DNA Repair Pathways. *J Biol Chem* (2010) 285 (6):3705–12. doi: 10.1074/jbc.M109.067538
62. Tsodikov OV, Ivanov D, Orelli B, Staresincic L, Shoshani I, Oberman R, et al. Structural Basis for the Recruitment of ERCC1-XPF to Nucleotide Excision Repair Complexes by XPA. *EMBO J* (2007) 26(22):4768–76. doi: 10.1038/sj.emboj.7601894
63. McNeil EM, Melton DW. DNA Repair Endonuclease ERCC1-XPF as a Novel Therapeutic Target to Overcome Chemoresistance in Cancer Therapy. *Nucleic Acids Res* (2012) 40(20):9990–10004. doi: 10.1093/nar/gks818
64. Deloia JA, Bhagwat NR, Darcy KM, Strange M, Tian C, Nuttall K, et al. Comparison of ERCC1/XPF Genetic Variation, mRNA and Protein Levels in Women With Advanced Stage Ovarian Cancer Treated With Intraperitoneal Platinum. *Gynecol Oncol* (2012) 126(3):448–54. doi: 10.1016/j.ygyno.2012.05.006
65. Biertumpfel C, Zhao Y, Kondo Y, Ramon-Maiques S, Gregory M, Lee JY, et al. Structure and Mechanism of Human DNA Polymerase Eta. *Nature* (2010) 465 (7301):1044–8. doi: 10.1038/nature09196
66. Boonstra A, van Oudenaren A, Baert M, van Steeg H, Leenen PJ, van der Horst GT, et al. Differential Ultraviolet-B-Induced Immunomodulation in XPA, XPC, and CSB DNA Repair-Deficient Mice. *J Invest Dermatol* (2001) 117(1):141–6. doi: 10.1046/j.0022-202x.2001.01390.x
67. Fontes FL, Pinheiro DM, Oliveira AH, Oliveira RK, Lajus TB, Agnez-Lima LF. Role of DNA Repair in Host Immune Response and Inflammation. *Mutat Res Rev Mutat Res* (2015) 763:246–57. doi: 10.1016/j.mrrev.2014.11.004
68. Altman BJ, Hsieh AL, Sengupta A, Krishnanaiah SY, Stine ZE, Walton ZE, et al. MYC Disrupts the Circadian Clock and Metabolism in Cancer Cells. *Cell Metab* (2015) 22(6):1009–19. doi: 10.1016/j.cmet.2015.09.003
69. Kang T-H. Circadian Rhythm of NER and ATR Pathways. *Biomolecules* (2021) 11(5):715. doi: 10.3390/biom11050715
70. Luo H, Ma C, Shao J, Cao J. Prognostic Implications of Novel Ten-Gene Signature in Uveal Melanoma. *Front Oncol* (2020) 10:567512(2154). doi: 10.3389/fonc.2020.567512
71. Tong X, Qu X, Wang M. A Four-Gene-Based Prognostic Model Predicts Overall Survival in Patients With Cutaneous Melanoma. *Front Oncol* (2021) 11:639874(400). doi: 10.3389/fonc.2021.639874
72. Zhang JA, Zhou XY, Huang D, Luan C, Gu H, Ju M, et al. Development of an Immune-Related Gene Signature for Prognosis in Melanoma. *Front Oncol* (2020) 10:602555(3280). doi: 10.3389/fonc.2020.602555
73. Danaher P, Warren S, Lu R, Samayoa J, Sullivan A, Pekker I, et al. Pan-Cancer Adaptive Immune Resistance as Defined by the Tumor Inflammation Signature (TIS): Results From The Cancer Genome Atlas (TCGA). *J Immunother Cancer* (2018) 6(1):63. doi: 10.1186/s40425-018-0367-1
74. McNamara MG, Jacobs T, Lamarca A, Hubner RA, Valle JW, Amir E. Impact of High Tumor Mutational Burden in Solid Tumors and Challenges for Biomarker Application. *Cancer Treat Rev* (2020) 89:102084. doi: 10.1016/j.ctrv.2020.102084
75. Weiss SA, Han J, Darvishian F, Tchack J, Han SW, Malecek K, et al. Impact of Aging on Host Immune Response and Survival in Melanoma: An Analysis of 3 Patient Cohorts. *J Transl Med* (2016) 14(1):299. doi: 10.1186/s12967-016-1026-2
76. Xiong J, Bing Z, Guo S. Observed Survival Interval: A Supplement to TCGA Pan-Cancer Clinical Data Resource. *Cancers (Basel)* (2019) 11(3):280. doi: 10.3390/cancers11030280

77. Wu HX, Wang ZX, Zhao Q, Chen DL, He MM, Yang LP, et al. Tumor Mutational and Indel Burden: A Systematic Pan-Cancer Evaluation as Prognostic Biomarkers. *Ann Transl Med* (2019) 7(22):640. doi: 10.21037/atm.2019.10.116
78. Si Z, Hu H. Identification of CXCL13 as an Immune-Related Biomarker Associated With Tumorigenesis and Prognosis in Cutaneous Melanoma Patients. *Med Sci Monit* (2021) 27:e932052. doi: 10.12659/msm.932052
79. Zhou X, Peng M, He Y, Peng J, Zhang X, Wang C, et al. CXC Chemokines as Therapeutic Targets and Prognostic Biomarkers in Skin Cutaneous Melanoma Microenvironment. *Front Oncol* (2021) 11:619003. doi: 10.3389/fonc.2021.619003
80. Spranger S, Luke JJ, Bao R, Zha Y, Hernandez KM, Li Y, et al. Density of Immunogenic Antigens Does Not Explain the Presence or Absence of the T-Cell-Inflamed Tumor Microenvironment in Melanoma. *Proc Natl Acad Sci USA* (2016) 113(48):E7759–68. doi: 10.1073/pnas.1609376113
81. Bai R, Chen N, Li L, Du N, Bai L, Lv Z, et al. Mechanisms of Cancer Resistance to Immunotherapy. *Front Oncol* (2020) 10:1290. doi: 10.3389/fonc.2020.01290

Conflict of Interest: The authors declare that the research was conducted in the absence of any commercial or financial relationships that could be construed as a potential conflict of interest.

frontiers in Oncology

ORIGINAL RESEARCH
published: 10 February 2022
doi: 10.3389/fonc.2022.819580

Complement Factor H in cSCC: Evidence of a Link Between Sun Exposure and Immunosuppression in Skin Cancer Progression

Ellise M. Johnson[1†], Chandana K. Uppalapati[2†], Agnes S. Pascual[1], Sarah I. Estrada[3], Richard L. Averitte[3], Kathryn J. Leyva[2] and Elizabeth E. Hull[1]*

[1] Biomedical Sciences Program, College of Graduate Studies, Midwestern University, Glendale, AZ, United States, [2] Department of Microbiology and Immunology, College of Graduate Studies, Midwestern University, Glendale, AZ, United States, [3] Affiliated Dermatology & Affiliated Laboratories, Scottsdale, AZ, United States

OPEN ACCESS

Edited by:
Gagan Chhabra,
University of Wisconsin-Madison,
United States

Reviewed by:
Lubka T. Roumenina,
U1138 Centre de Recherche des Cordeliers (CRC)(INSERM), France
Hongbin Wang,
California Northstate University,
United States

***Correspondence:**
Elizabeth E. Hull
ehull@midwestern.edu

[†]These authors share first authorship

Specialty section:
This article was submitted to Skin Cancer, a section of the journal Frontiers in Oncology

Received: 21 November 2021
Accepted: 12 January 2022
Published: 10 February 2022

Citation:
Johnson EM, Uppalapati CK, Pascual AS, Estrada SI, Averitte RL, Leyva KJ and Hull EE (2022) Complement Factor H in cSCC: Evidence of a Link Between Sun Exposure and Immunosuppression in Skin Cancer Progression. Front. Oncol. 12:819580. doi: 10.3389/fonc.2022.819580

Cutaneous squamous cell carcinoma (cSCC) is a common form of skin cancer with an estimated 750,000 cases diagnosed annually in the United States. Most cases are successfully treated with a simple excision procedure, but ~5% of cases metastasize and have a 5-year survival rate of 25-45%. Thus, identification of biomarkers correlated to cSCC progression may be useful in the early identification of high-risk cSCC and in the development of new therapeutic strategies. This work investigates the role of complement factor H (CFH) in the development of cSCC. CFH is a regulatory component of the complement cascade which affects cell mediated immune responses and increases in complement proteins are associated with poor outcomes in multiple cancer types. We provide evidence that sun exposure may increase levels of CFH, suggesting an immunomodulatory role for CFH early in the development of cSCC. We then document increased levels of CFH in cSCC samples, compared to adjacent normal tissue (ANT) routinely excised in a dermatology clinic which, in paired samples, received the same level of sun exposure. We also provide evidence that levels of CFH are even greater in more advanced cases of cSCC. To provide a potential link between CFH and immune modulation, we assessed immune system function by measuring interferon gamma (IFN-γ) and FOXP3 in patient samples. IFN-γ levels were unchanged in cSCC relative to ANT which is consistent with an ineffective cell-mediated immune response. FOXP3 was used to assess prevalence of regulatory T cells within the tissues, indicating either a derailed or inhibitory immune response. Our data suggest that FOXP3 levels are higher in cSCC than in ANT. Our current working model is that increased CFH downstream of sun exposure is an early event in the development of cSCC as it interferes with proper immune surveillance and decreases the effectiveness of the immune response, and creates a more immunosuppressive environment, thus promoting cSCC progression.

Keywords: cutaneous squamous cell carcinoma (cSCC), Complement Factor H, immunomodulation, FOXP3, interferon gamma (IFNγ), sun exposure, complement cascade, immunoevasion

INTRODUCTION

Cutaneous squamous cell carcinoma (cSCC) is typically treated by tumor excision with a success rate of >95%. As a minority of cSCC are known to metastasize and cause clinically serious disease, research on cSCC is sparse and therapies for the ~5% of cases that do metastasize are limited, resulting in a 5-year survival rate of only 25-45% (1, 2). However, as the incidence of cSCC is increasing (3), an understanding of the factors that may increase the ability of these tumors to metastasize is of particular importance.

Evidence is accumulating that the tumor microenvironment is a key factor in the progression of all tumor types. The immunomodulatory nature of the tumor microenvironment has been shown to be particularly relevant due to discovery of the clinical efficacy of treatments targeting immune checkpoints. In this work, we focus on the potential role of two complement regulatory proteins, complement factor H (CFH) and complement factor I (CFI), in the immune response to tumors.

As regulatory proteins, CFH and CFI modulate the complement cascade at multiple points, but their most impactful effect is through reducing levels of several potent anaphylatoxins (including C3a and C5a). Local anaphylatoxin production increases recruitment of both innate and adaptive immune cells to the tumor. In addition, recently characterized as immune checkpoints (4), C3aR and C5aR signaling modulates the T cell response by promoting T cell survival and favoring differentiation of pro-inflammatory Th1 effector cells over immunosuppressive FOXP3+ regulatory T cells. Thus, the complement system is an integral part of a coordinated immune (5) response to tumors. As CFH and CFI are known to decrease levels of C3a and C5a, these two complement regulatory proteins function to dampen cell-mediated immune responses in inflammation and, although many questions still remain, have been shown to decrease immune responses by non-canonical mechanisms (5, 6).

Complement regulatory proteins may also play a direct role in promoting cSCC development. Keratinocytes have been shown to synthesize both CFH and CFI, as well as other complement proteins (7–10). Suggestive of a functional role, these regulatory proteins were shown to increase migration and proliferation when added to cSCC cell cultures and CFI appears to be related to tumor growth *in vivo* (7, 8). Interestingly, synthesis of CFH and CFI by human keratinocytes is upregulated by the pro-inflammatory cytokine interferon gamma (IFN-γ) (5–7). This suggests that cSCC may have the ability to upregulate complement regulatory proteins to actively derail the immune response to tumors once an immune response to a tumor is established. Thus, elevated complement regulatory expression may directly promote tumor survival and metastasis in addition to derailing the immune response to tumors.

To underscore the clinical importance of these regulatory components, analysis of the TCGA dataset reveals that CFH and CFI expression are unfavorable prognostic markers in renal and urothelial cancers respectively (11), and several studies have identified CFH as a cancer biomarker (12–14). Furthermore, clinical therapies using anaphylatoxin receptor antagonists and anti-CFH antibodies are being investigated (4, 15). In addition, recent data suggests that the role of complement in tumorigenesis is unexpectedly complex. Several complement components increase ERK 1/2 and it is interesting that these components both promote and inhibit formation of membrane attack complex (MAC) (7, 8, 16, 17). In addition, CFH has recently been shown to have intracellular activities and to promote tumor progression independently of the canonical extracellular role of complement (6, 18–20).

In this work, we seek to extend the understanding of the role of these complement regulatory proteins in the development of cSCC. First, we ask if sun exposure alters CFH and CFI expression using existing datasets. Second, focusing on cSCC tissue samples removed from patients routinely seen in a dermatology clinic, we ask if a difference in CFH levels can be detected in cSCC tissue samples compared to adjacent normal tissue; these paired tissue samples received the same level of sun exposure. Third, we ask if there is a shift in the cell-mediated immune response between cSCC and adjacent normal tissues by assaying IFN-γ and FOXP3 levels.

METHODS

Patient Consent and Tissue Collection

All experimentation on human tissue samples was approved by Western IRB (WIRB Protocol #20142461) to Affiliated Laboratories BioRepository (ALBR). Additionally, the Midwestern Institutional Review Board approved the use of these clinic-based biorepository samples at Midwestern University (AZ#807). The single criterion for the collection of tissues for these procedures is a biopsy-proven diagnosis of cSCC. The initial diagnosis and classification of cSCC type was completed at the clinic as part of routine patient care prior to transfer of the sample to the research laboratory. No exclusion criteria were outlined in the original IRB protocol but samples from patients with a known blood-borne communicable disease were not used. All tissue specimens were obtained from patients who consented to donate excised tissue removed during Mohs surgery. For viable tissue used in explant cultures, cSCC tissue from the center of the apical side of the tumor was removed before processing the sample for histology. If needed for wound closure, the surgeon removed adjacent normal tissue (ANT) and these were matched with the tumor sample for paired analysis.

Explant Culture and Immunofluorescence of cSCC and ANT

Tissues were processed for culture and immunofluorescence as described in Belden et al. (21). Briefly, post-Mohs tissue was rinsed briefly in 70% ethanol to sterilize, covered with media, minced with a razor blade, and placed into 35 mm culture dishes. 20 µl of fetal bovine serum (FSB) was placed in each culture dish to cover tissue slices and left to dry in the culture hood for 20 minutes. 1 ml of culture media (1:1 mixture of DMEM : Ham's F-12 supplemented with 10% FBS, 25 mM Hepes, and 100 IU/ml of penicillin and 100 µg/ml streptomycin) was then added to each

dish/tissue slice and incubated at 37°C in a humidified CO_2 incubator. When approximately 80% confluent, cultures of mixed cultures were passaged onto glass coverslips for immunofluorescence.

For immunofluorescence, explant cells were grown on eight-well chamber slides, washed with 1x PBS, fixed for 15 minutes with 4% paraformaldehyde in 1x PBS, rinsed with 1x PBS, and incubated in 0.05% Triton X-100 in 1x PBS for 5 minutes to permeabilize the cells, and followed by blocking with 1% BSA in 1x PBS for one hour. Blocking reagent was aspirated and cells were rinsed with 1x PBS and incubated overnight with 1:200 mouse anti-CFH (Abnova, OX-24) at room temperature. Primary antibody was omitted as a negative control. After washing with 1x PBS, cells were incubated with Alexa Fluor 488 goat anti-mouse and Alexa Fluor 568 phalloidin (1:500) for one hour at room temperature, washed with 1x PBS, mounted in fluoromount with DAPI (Electron Microscopy Sciences) and imaged with a Zeiss Apotome microscope.

Immunoblotting

Total protein from patient derived frozen tissue samples (Affiliated Dermatology Laboratory) were isolated using RIPA buffer (50 mM Tris HCl, pH 8.0; 150 mM NaCl; 1% NP-40; 0.5% sodium deoxycholate; 0.1% SDS; HALT (Protease and Phosphatase Inhibitor), DNaseI and DTT following an established protocol (21). Forty micrograms of total protein from each sample were resolved on either a 10% (FOXP3) or 4-20% (all other proteins) Mini-PROTEAN® TGX™ Precast Protein gel (Bio-Rad), transferred to a low fluorescent PVDF membrane, and blocked using 5% NFDM (non-fat dry milk, 1X TBS, 0.1% Tween 20) for one hour at room temperature. Primary antibodies in 1% NFDM used were 1:200 rabbit monoclonal histone H3 antibody (D1H2) (Cell Signaling Technology), 1:1000 rabbit anti-GAPDH (Cell Signaling Technology), 1:200 mouse monoclonal CFH (OX-24) (Abnova, OX-24), 1:200 mouse monoclonal IFN-γ (Santa Cruz Biotechnology), and 1:200 mouse monoclonal antibody FOXP3 (F9) (Santa Cruz Biotechnology). 1:10,000 AlexaFluor® 790 (Abcam) or 1:5,000 HRP-conjugated (Santa Cruz Biotechnology) were used as secondary antibodies. All blots were performed in triplicate and relative protein expression was measured using either an Odyssey® CLx (LI-COR Biotechnology) or ChemiDoc XRS (BioRad) imaging system. Band intensities were normalized to either GAPDH or H3 using Image J software (NIH).

Immunohistochemistry

Slides of formalin-fixed, paraffin-embedded (FFPE) cSCC and ANT tissue sections were either purchased (US Biomax & Biochain) or obtained from ALBR. A standard immunohistochemistry protocol was performed by baking the sections at 60°C for 60 minutes, de-paraffinizing by placing in xylene followed by reducing concentrations of ethanol (100% to 70%). De-paraffined sections were permeabilized using 0.25% Trypsin with no EDTA. For heat induced epitope retrieval, FFPE tissue sections were incubated in either citrate buffer (CFH) or basic buffer (FOXP3) at 95°C for 25 minutes, followed by blocking and overnight incubations at 37°C, and 4°C with primary antibodies, mouse anti-CFH (OX-24) (Novus Biological) and rabbit monoclonal anti-FOXP3 (Cell Marque). CFH slides were incubated with AP-conjugated secondary and permanent red stain. FOXP3 slides were incubated with an HRP-conjugated secondary and DAB stain (for array slides) or an AP-conjugated secondary antibody and permanent red stain (for ALBR slides). Mayer's Hematoxylin was used as a counterstain (nuclei) followed by mounting with Flourmount G mounting medium. Slides were imaged using bright field Olympus (DP73 camera) microscope at 40X, 100X and 400X magnifications. An isotype control was performed for each tissue type and against each antibody species. Semi-quantitative analysis of IHC images was performed based on colorimetric intensity over a specified area of tissue sections using a 0-3+ scale, with 0 indicating no staining, 1+ indicating <10% staining, 2+ indicating 10-50% staining, and 3+ indicating >50% staining, and verified using ImageJ (NIH) (22).

Statistical Analysis

Analysis of GTEx (Genotype-Tissue Expression) data was performed using non-parametric tests in GraphPad Prism v9. A Mann-Whitney two-tailed T-test was used to analyse unpaired data and a two-tailed Wilcoxon matched-pair signed-rank test was used to analyse paired data. Statistical significance did not vary with or without removal of outliers using the ROUT method of identifying outliers. Correlation of paired data was performed using Spearman's rank-order correlation coefficient.

Band intensities from immunoblot data were normalized to histone H3 or GAPDH. A ROUT test with an alpha value of 0.05 was used to identify potential outliers within each dataset. D'Agostino and Shapiro-Wilk tests followed by a T-test (paired or unpaired depending on the comparison) were used for determining the significance of differences for normally distributed independent variables. D'Agostino and Shapiro-Wilk tests followed by a Mann–Whitney U-test was used for determining the significance of differences between two non-normally distributed independent variables. A *post-hoc* power analysis was applied to data that did not show significance. Data analysis was performed with GraphPad Prism. Alpha (α) was set at 0.05 for all statistical tests and data with a $p \leq 0.05$ were considered statistically significant.

RESULTS

Sun Exposure and CFH Expression in Normal Tissue

To assess the effect of sun exposure on CFH and CFI, we interrogated all available data in the GTEx portal. In the dataset of 473 exposed (lower leg) and 387 non-exposed (suprapubic) unpaired patient samples, CFH mRNA expression is higher in exposed skin than non-exposed skin ($p < 0.0001$) but no difference in CFI mRNA levels was seen.

To determine the effects of sun exposure using paired patient samples, we analysed the subset of 278 subjects with GTEx values

for both sun-exposed and non-exposed skin. Analysis of these paired data suggests that CFH mRNA in exposed skin increased significantly over non-exposed skin ($p < 0.0001$) (**Figure 1A**). CFH mRNA in non-exposed skin correlates with levels in exposed skin (coefficient = 0.35, $p < 0.0001$) (**Figure 1B**) which suggests that complement levels before sun exposure significantly contribute to CFH levels after sun exposure. Levels of CFI mRNA were much lower than CFH mRNA and no difference in CFI mRNA was seen between exposed and non-exposed levels (**Figure 1C**).

To investigate these findings further, we next analysed the data from the 278 subjects with paired data by initial value of CFH mRNA in unexposed skin. While most initial CFH mRNA values are relatively low, those subjects with the highest values show a marked elevation in CFH mRNA in unexposed skin (blue line, **Figure 1D**). The mean fold change in CFH mRNA after sun exposure ranged from 9.2 to 596-fold with an average fold increase of 114.7 ± 5.4 tpm (transcripts per million ± SEM). These fold increase values gradually decrease with increasing CFH levels in unexposed skin (orange points and linear fit (black line), **Figure 1D**). Interestingly, while levels of CFI were not different between sun-exposed vs non-exposed skin, the correlative pattern was also seen in the CFI data and, suggestive of a link between these complement factors in paired patient samples, CFH levels correlate with CFI levels (coefficient = 0.58, $p < 0.0001$ in non-exposed and coefficient = 0.37, $p < 0.0001$ for exposed, data not shown).

CFH in cSCC Samples

Biopsy proven cSCC and adjacent normal tissue (ANT) from sun exposed skin were collected during routine Mohs micrographic surgery as previously described and primary cultures were established for both cSCC and ANT samples (21). Patients in the population had diagnoses of cSCC in situ, cSCC, early invasive cSCC, and invasive cSCC. As excised cSCC samples were typically small and had clean margins, it is expected that the cSCC samples analysed in this work contain a significant amount of ANT. This was confirmed by the observation that 75% of sections from excised tumor samples showed no evidence of cSCC after H&E staining as they sampled ANT removed with the biopsy proven cSCC (data not shown). We verified that CFH is produced by cells cultured from these tumor and adjacent normal tissue samples using immunofluorescent staining for CFH (**Figure 2A**). Cells in the mixed explant culture appear to synthesize CFH (top panel) and this staining appears to be in intracellular secretory vesicles (bottom panels). The intense punctate staining suggests that the majority of CFH may be contained within intracellular vesicles. In contrast, CFI was detected in positive control serum samples by immunoblotting but not reproducibly detected in cultured cells by immunofluorescence or in tissues samples by immunoblotting suggestive of lower expression levels of CFI in these samples consistent (data not shown). CFH was detected in immunoblots of cSCC and ANT tissue samples with patient serum included on the immunoblot as a positive control (**Figure 2B**). The differential splice product of the CFH gene, known as Factor H-like (FH-L),

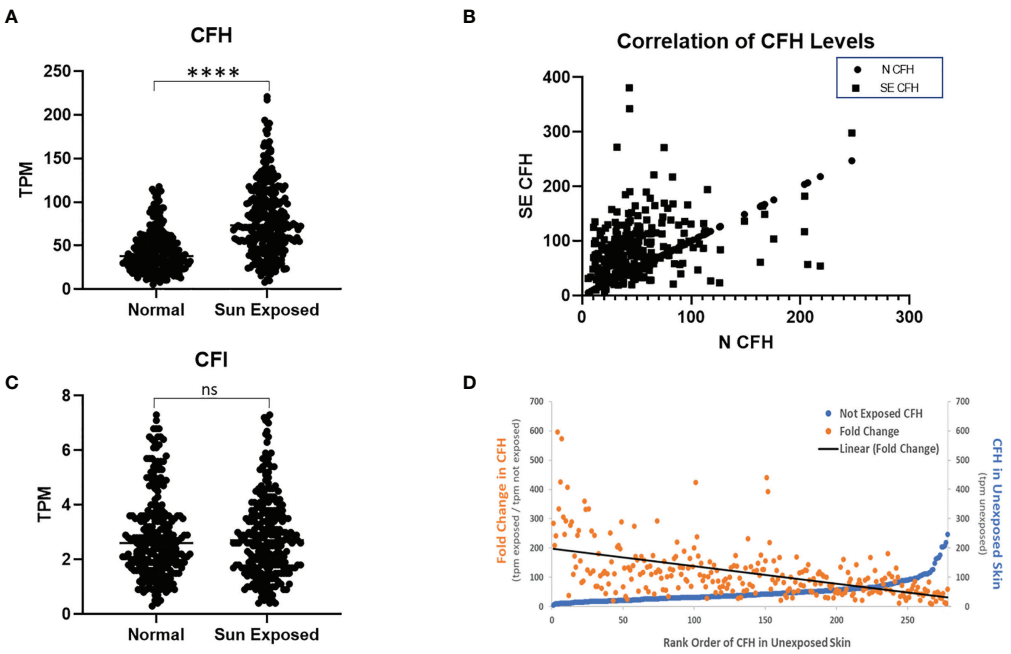

FIGURE 1 | CFH Transcript Number is Increased in Sun-Exposed Skin. GTEx data of 278 paired sun exposed (lower leg) and non-sun exposed (suprapubic) patient samples were analysed. CFH levels are increased in exposed skin ($p<0.0001$, two-tailed Wilcoxon matched-pairs signed rank test) but not CFI **(A, C)**. Levels of CFH mRNA (TPM) in exposed skin correlates with unexposed skin ($p<0.0001$, Spearman's rank-order correlation) **(B)**. When sorted by non-exposed CFH levels, the levels and fold increase in paired exposed samples decreases with the exception being at the highest values of CFH in non-exposed skin **(D)**. (****$p<0.0001$; ns, not significant).

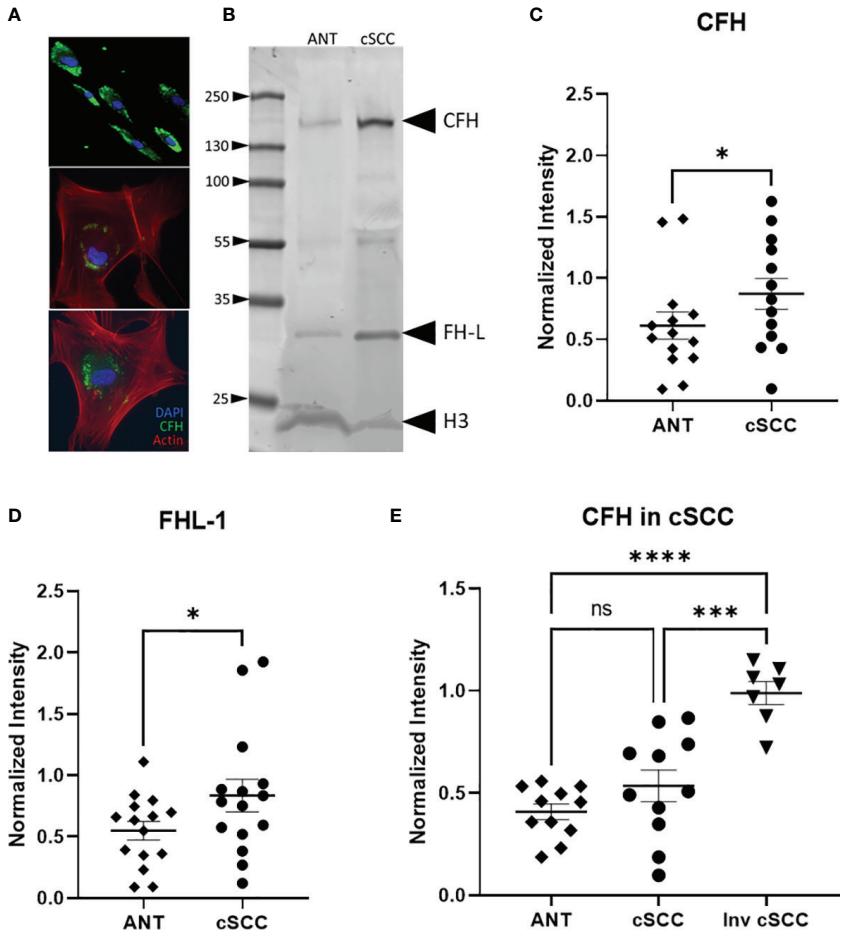

FIGURE 2 | CFH and FH-L Expression in cSCC is Increased. Immunofluorescent microscopy of cells cultured from cSCC tissue show CFH staining (green) in cytosolic vesicles **(A)**. Bands at the expected molecular weight for CFH and Factor H-like (FH-L) are detected in both adjacent normal tissue and cSCC samples **(B)**. The ratio of CFH and FH-L band intensities, normalized to histone H3 intensity, was higher in cSCC tissue compared to ANT [**(C)**, p=0.031 & **(D)**, p=0.034, respectively]. In paired samples for non-invasive cSCC, CFH levels normalized to GAPDH are not significant. When CFH levels in ANT are compared to invasive cSCC, the difference is highly significant [**(E)**, p<0.0001]. (*p<0.05; ***p=0.0001; ****p<0.0001; ns, not significant).

is also detected in our analysis. As FH-L retains key complement regulatory activities (7, 23), we included this product in the analysis.

Analysis of band intensities indicates a 1.76- and 1.53-fold increase in expression for CFH and FHL-1 respectively when compared to paired ANT (p = 0.031, n=13 and p = 0.034, n=15 respectively) (**Figures 2C, D**). Although the magnitude of the difference is small, as noted above, the analysed Mohs samples contained a significant amount of normal tissue which may act to decrease the magnitude of the change in CFH seen in the cSCC samples. Tissues included in these analyses were derived from 7 patients diagnosed with cSCC in situ, 4 invasive cSCC, and 2 early invasive cSCC samples. CFH expression in invasive cSCC tissues increases 1.17-fold over non-invasive cSCC (p = 0.0001, n=12 cSCC, n=7 invasive cSCC). When compared to unpaired ANT, levels of CFH are 2.10 fold higher in invasive cSCC despite the large amount of non-cSCC included in the Mohs samples (p < 0.0001, n=12 ANT, n=7 invasive cSCC) (**Figure 2E**).

Immunomodulation in cSCC Samples

Levels of interferon gamma (IFN-γ) in the patient-derived cSCC samples above was quantitated next. This pro-inflammatory cytokine may mark an effective immune response and synthesis of CFH in keratinocytes has been reported to be under the control of IFN-γ (5–7). Immunoblotting revealed bands associated with the monomer and the biologically active glycosylated dimer form (**Figure 3A**, **Supplementary Figure 1**) (24, 25). After quantitation of both IFN-γ bands, no significant change in the level of IFN-γ between paired cSCC and ANT when normalized to histone H3 was detected (p = 0.150, n=11) (**Figure 3B**). In addition, when normalized to GAPDH, neither non-invasive or invasive cSCC IFN-γ levels change (p = 0.8511 and p = 0.687 respectively, n=15 ANT and noninvasive, n=7 invasive) (**Figure 3C**).

The transcription factor FOXP3 is often used to detect the presence of regulatory T cells which are reflective of a dampened immune response. Immunoblotting revealed a band at the expected molecular weight for FOXP3 (**Figure 4A**, **Supplementary Figure 2**).

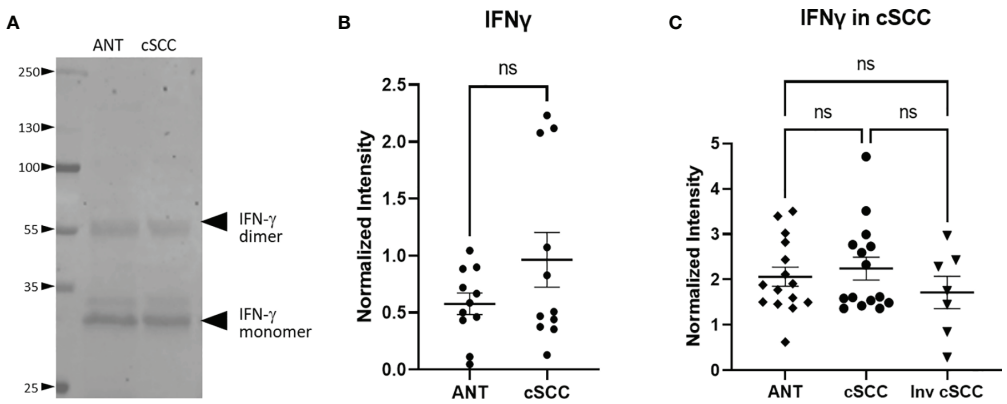

FIGURE 3 | IFN-γ Expression in cSCC is Unchanged. Bands at the expected molecular weight for glycosylated IFN-γ monomer and IFN-γ dimer are detected at in both adjacent normal tissue and cSCC samples **(A)**. The ratio of intensity for both IFN-γ bands in paired samples was normalized to histone H3 intensity and is not significant (ns) **(B)**. The ratio of intensity for both IFN-γ bands in unpaired non-invasive and invasive cSCC samples normalized to GAPDH compared to control was also not significant (ns) **(C)**.

Levels of FOXP3 were quantitated in both non-invasive and invasive cSCC and compared to levels in adjacent normal tissue in our clinic samples. As seen in **Figure 4B**, paired non-invasive cSCC shows a significant increase in this transcription factor ($p<0.001$). However, when FOXP3 levels in invasive cSCC are compared to non-invasive, there is no change (**Figure 4C**). These data are consistent with an increase in FOXP3 levels during the initial stages of tumor development but FOXP3 may not be playing a role in promoting tumor progression once cancer has developed.

Relative CFH and FOXP3 in cSCC Samples by IHC

We next compared levels of CFH and FOXP3 in our patient-derived ANT and cSCC samples to commercially available arrays of advanced cSCC by immunohistochemistry (IHC). This allows us to directly assess levels of these proteins in newly diagnosed cSCC excised in a dermatology clinic as part of routine practice (ALBR Samples), which may not be as progressed, with the more advanced cSCC samples utilized in most studies. In addition, as the samples in these analyses retain the tissue integrity, they allowed for determination of colocalization of these proteins within the tumor tissues.

As shown in **Figure 5**, levels of CFH seen in ANT were compared to cSCC in routine clinic (ALBR; **Figure 5A**) and advanced cSCC (Array; **Figure 5B**) samples by IHC. As CFH is a secreted protein which may be detected intracellularly as well as bound to the extracellular matrix, no specific localization was expected. Consistent with being secreted by keratinocytes, higher levels of CFH appear to be localized in epidermal than dermal layers (red color) in both the ANT and cSCC samples. Suggestive of a relationship to sun exposure, CFH appears higher (1+) in

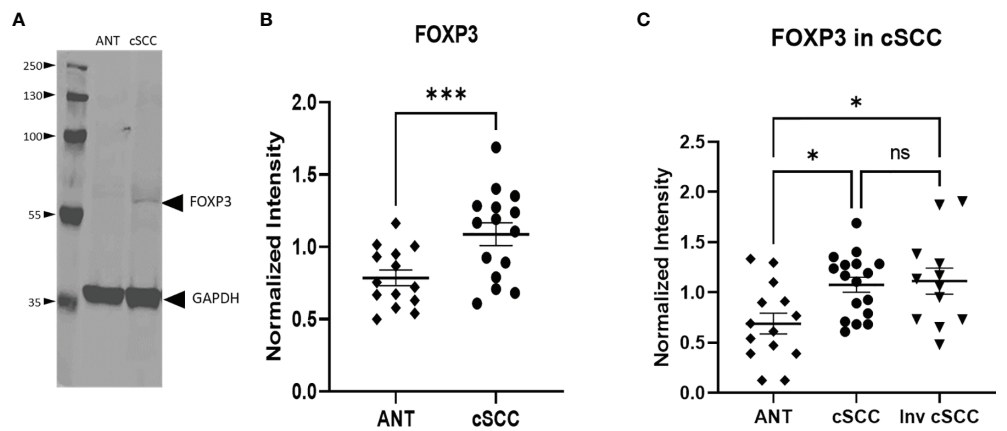

FIGURE 4 | Levels of FOXP3 are Increased in cSCC. Immunoblots detected a band at the expected molecular weight for FOXP3 in both adjacent normal tissue and cSCC samples **(A)**. The ratio of FOXP3 band intensity normalized to GAPDH intensity was higher in cSCC tissue compared to paired ANT [**(B)**, $p<0.001$] and non-invasive cSCC compared to unpaired ANT but there is no difference between non-invasive and invasive cSCC **(C)**. (*$p<0.05$; ***$p=0.0001$; ns, not significant).

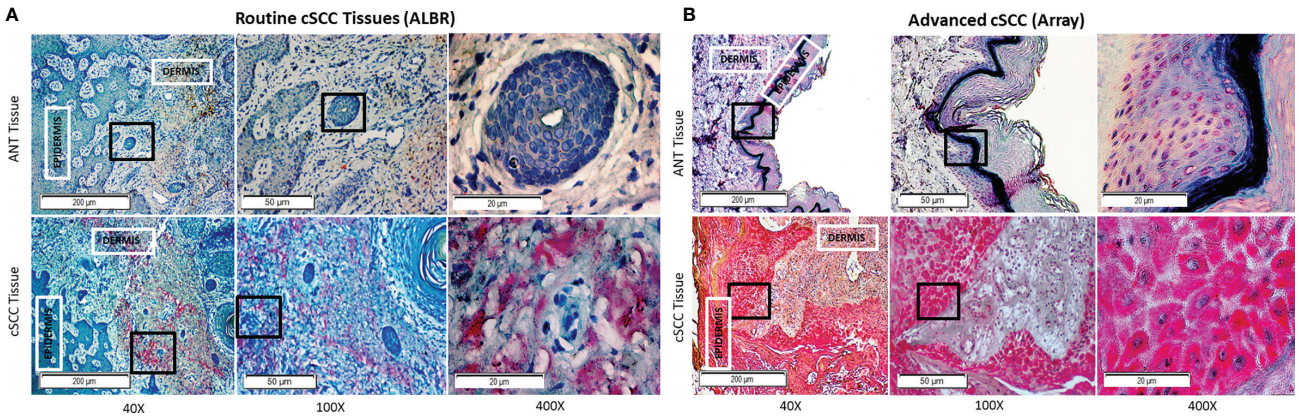

FIGURE 5 | CFH in Routine Mohs and Advanced cSCC Samples by IHC. cSCC removed from routine clinic patients by Mohs surgery [fixed after cryosectioning; **(A)**] and an array of advanced cSCC [formalin fixed; **(B)**] were labeled with mouse anti-CFH (OX-24) and an AP-conjugated secondary antibody with permanent red stain. Mayer's Hematoxylin was used as a counterstain (nuclei). The degree of CFH staining in the ANT and cSCC samples was semi-quantitatively determined by using a 0-3+ scale, with 0 indicating no staining, 1+ indicating <10% staining, 2+ indicating 10-50% staining, and 3+ indicating >50% staining. ANT samples [**(A, B)**, top panels] were scored as either 0 or 1+, the Mohs cSCC samples [**(A)**, bottom panel] were scored as 2+, and the advanced cSCC samples [**(B)**, bottom panel] were scored as 3+. The boxes within the 40x and 100x images delineate the tissue location shown in the 100x and 400x images, respectively.

sun damaged regions, as easily seen in the ALBR ANT sample but also in the Array ANT sample. Comparing cSCC tissues, CFH staining appears more intense than in ANT tissues, increasing to 2+ in routine clinic samples (ALBR cSCC) and to 3+ in advanced samples (Array cSCC). Additional IHC images at 400x magnification are provided in **Supplementary Figures 3**, **4**. Thus, despite the limitation of variations in color due to the different sources and initial preparation of slides, these data suggest that more advanced tumors have higher levels of CFH than our patient-derived samples used in this study.

Next, levels of FOXP3 in ANT and cSCC tissues from routine clinic (ALBR; **Figure 6A**) and advanced cSCC samples (Array; **Figure 6B**) were determined using IHC. As a transcription factor associated with development of regulatory T cells and, due to our results showing elevated CFH in these tumor samples, we expected FOXP3 staining to be more intense within the immune infiltrate surrounding tumor tissue (arrows). As shown in **Figure 6B**, moderate FOXP3 staining (2+) is seen in more advanced cSCC (Array samples). Additional IHC images at 400x magnification are provided in **Supplementary Figures 5**, **6**. Although there are similar limitations of color variation due to different initial slide preparation as in **Figure 5**, there appears to be substantially less FOXP3 staining in routine clinic samples (**Figure 6A**) although we do see more FOXP3 staining in our less advanced patient-derived cSCC tissues (1+) than in ANT tissue (0). Our patient-derived cSCC tissues may not be as advanced as the tissues used for the commercial Array slides, which may explain the lack of significance between the two patient-derived cSCC tissues (**Figure 4C**) while the more advanced cSCC images show abundant FOXP3 staining using IHC (**Figure 6B**). Results suggest the FOXP3 positive immune infiltrate is increased in the advanced cSCC samples when compared to those in routine clinic samples, again correlated to the increased CFH observed in these advanced cSCC samples.

DISCUSSION

Data presented here strengthen the link between cSCC and CFH. By focusing on cSCC tumors excised from patients seen in routine Mohs microsurgery patients in an Arizona-based dermatology practice (where the typical patient likely received significant sun exposure), the link between CFH is extended to newly diagnosed and non-invasive cSCC. Although the observed CFH elevation was small, this is perhaps due to the relatively small size of the tumor and the amount of normal tissue included in the patient samples excised in the Mohs procedure. Indeed, we suspect that this may be the reason that CFI was not reliably detected in our samples as others have found that CFI levels in tissues are lower than CFH and consistent with GTEx data (**Figure 1**). Our GTEx analysis showed a significant difference in CFH levels between sun-exposed vs non-exposed tissues, suggesting that sun exposure influences CFH levels. While we observed increases in CFH levels in our patient-derived tissues consistent with sun exposure, we showed that our cSCC tissues express higher levels of CFH than ANT tissues. However, as our samples were paired, with each pair receiving the same level of sun exposure, the elevation in CFH in cSCC compared to ANT cannot be explained by sun exposure alone. Consistent with a role in progression, more advanced cSCC show markedly more dramatic increases in CFH and FOXP3 by IHC than the routine patient-derived samples. Thus, these data suggest that elevation in CFH appears early in the development of cSCC and is significant despite these complicating factors. Comparison of these data to an invasive cSCC set suggests a link with cSCC progression and raises the possibility that CFH levels may be an important prognostic factor in assessing cSCC.

As our collective data sets provide support for sun exposure affecting overall levels of CFH, we suggest that immune modulation is an early event in the development of cSCC.

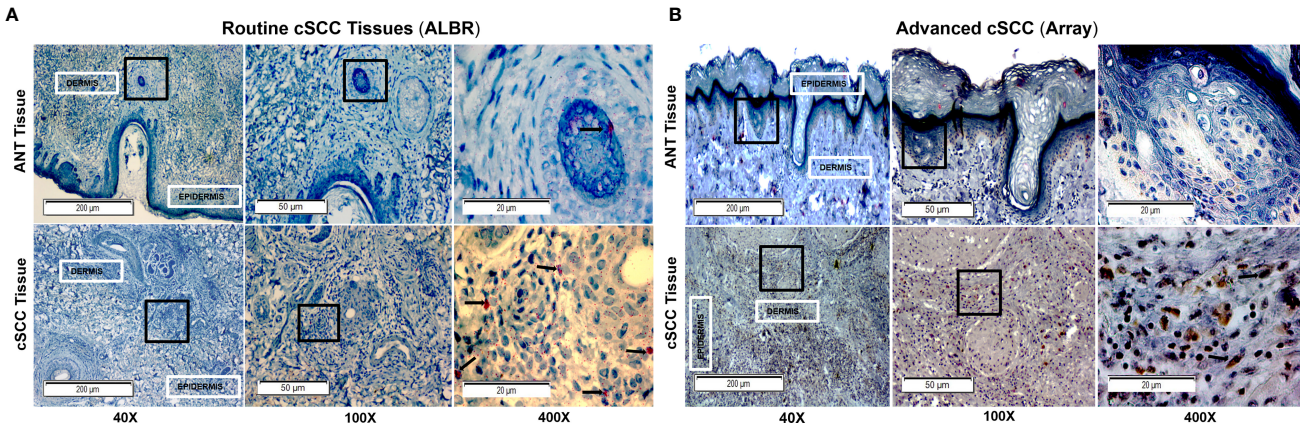

FIGURE 6 | FOXP3 in Routine Mohs and Advanced cSCC Samples by IHC. cSCC removed from routine clinic patients by Mohs surgery [fixed after cryosectioning; **(A)**] and an array of advanced cSCC [formalin fixed; **(B)**] were labeled with a rabbit monoclonal anti-FOXP3 (Cell Marque) and stained with an HRP-conjugated secondary antibody and DAB stain (for Array samples) and with an AP-conjugated secondary antibody and permanent red stain (for ALBR samples). Mayer's Hematoxylin was used as a counterstain (nuclei). The degree of FOXP3 staining in the ANT and cSCC samples was semi-quantitatively determined by using a 0-3+ scale, with 0 indicating no staining, 1+ indicating <10% staining, and 2+ indicating 10-50% staining, and 3+ indicating >50% staining. ANT samples [**(A, B)**, top panels] were scored as 0, the Mohs cSCC samples [**(A)**, bottom panel; arrows in the 400x image denote positive nuclear localization] were scored as 1+, and the advanced cSCC samples [**(B)**, bottom panel; arrows in the 400x image denote positive nuclear localization] were scored as 2+. The boxes within the 40x and 100x images delineate the tissue location shown in the 100x and 400x images, respectively.

This finding is not unexpected as an increase in CFH is expected to reduce both innate and adaptive immune responses to tumors, a necessary step in tumor progression. Furthermore, the fact that IFN-γ levels do not increase in our cSCC samples when compared to ANT may be consistent with an ineffective immune response. It is interesting that we do not see elevated levels of IFN-γ as this cytokine has been shown to increase CFH secretion (5, 7). It is possible that in the early stages of an immune response to developing tumors, IFN-γ secretion leads to increased CFH expression which ultimately derails the immune response and allows tumor progression. Alternatively, elevated CFH may be downstream of sun exposure rather than increased IFN-γ levels. That said, it is also plausible that our immunoblotting techniques were not sensitive enough to detect any increase in IFN-γ (particularly as our cSCC samples contain substantial amounts of ANT). However, we suggest that the putative increase in regulatory T cells is more consistent with insufficient IFN-γ levels for an effective immune response. Specifically, although the pro-inflammatory tumor infiltrate is not directly assessed, we do detect increased levels of FOXP3 within cSCC samples (**Figure 6**). These data are consistent with published results (26). Although FOXP3 is often a marker for regulatory T cells, other cell types have been reported to transiently express FOXP3, including regulatory B cells and M2 macrophages [as more recently reviewed in (27)], which have been shown to be elevated in various tumors and are associated with anti-inflammatory and immunosuppressive roles (28–31). While we cannot definitively confirm all the FOXP3+ cells are regulatory T cells, we can conclude that the environment within the cSCC tissues is immunosuppressive compared to ANT and may be indicative of a reduced immune response that would favor tumor growth, regardless of cell lineage. Given that sun exposure may lead to CFH secretion by a mechanism which may or may not be linked to IFN-γ, it is impossible to determine given the nature of the tissues samples generated by Mohs surgery without altering the standard of care of these patients.

This work documents both an increase in CFH and FOXP3 in cSCC but does not directly address the relationship between these two findings. Published work suggests a plausible causal link between increased CFH secreted from cSCC and immunoevasion as suggested by increased FOXP3 levels. Expression of CFH by keratinocytes and cSCC cells lines has been well documented (5, 7) and it is expected that the increased expression of this complement regulatory protein would reduce levels of anaphylatoxins within the tumor, shifting the immune response from an effective Th1-mediated to an ineffective regulatory T cell response. However, how this altered CFH might affect the balance between effective and ineffective immune responses is not clear.

Although not immune cells, growing evidence suggests that cancer cells express anaphylatoxin receptors and are able to respond to increased anaphylatoxin levels. Specifically, a wide variety of cancers and cancer cell lines express C3aR and C5aR and respond by increased motility and activation of the ERK1/2 pathway to promote growth (32–37). Most relevant to this work, cultured cSCC respond to both CFH and CFI (5, 6) and the receptor for the more potent C5a can be detected in skin tissue and is expressed in skin cancer lines (11). Indeed, levels of C3aR and C5aR2 mRNA in the GTEx dataset increase with sun exposure while those of C5aR1 do not (**Supplementary Figure 7**). However, particularly as mRNA levels are very low, expression of these receptors must be verified with validated antibodies. Given that increased CFH and CFI would decrease C3a and C5a levels,

increased CFH would not favor tumor progression through canonical complement pathways.

Data presented here helps to solidify the relationship between CFH and tumorigenesis but they also raise many questions about the role of CFH in cancer progression. Specifically, in addition to its role in cSCC, a role for CFH has been described for hepatocellular and clear cell renal cell carcinomas (ccRCC) but not does not appear to promote squamous cell lung carcinoma (6, 38). In addition, CFH may promote ccRCC but does affect tubular cells from which ccRCC arise (6, 39). Thus, the roles for complement proteins are complex and it is difficult to predict how alterations in CFH will ultimately affect tumorigenesis. Indeed, recent data expanding on the link between a CFH allele and the risk for age related macular degeneration has revealed distinct intracellular roles for CFH in metabolism and response to oxidative stress and CFH knock-down may alter NFkB and p53 function (18, 20). Although the complex role of CFH in cancer cells underscores the importance of further investigation of complement in the immune surveillance of cancers. However, the current samples do not allow us to clearly distinguish between intracellular and extracellular roles of CFH and additional studies with different experimental approaches are warranted.

There are many remaining questions regarding the role of CFH in cSCC and clarification of these points may have direct impact on treatment of patients with cSCC. To clarify whether the increase in CFH contributes to or is a result of tumor development, it will be important to establish signaling through anaphylatoxin receptors in cSCC and solidify the evidence of immune modulation. The ability of IFN-γ to increase CFH secretion by keratinocytes documented in cell lines can be replicated in patient samples needs to be investigated. This latter point is of particular importance as a current therapy, imiquimod (used in the treatment actinic keratosis and some cSCC), is associated with enhancing IFN-γ production to mount an effective immune response (40) through altering effector T cell responses (41). However, it should be noted that IFN-γ plays a complex role in immunity in that it both activates effector T cells as well as potentially being involved in induced regulatory T cells (42).

CONCLUSIONS

CFH may be elevated in cSCC tumors excised from patients seen in a routine Mohs microsurgery. This elevation in CFH appears to be independent of sun exposure and may act through derailing an effective immune response. Immune checkpoint therapies targeting anaphylatoxin receptors may be an effective treatment for cSCC in the future.

DATA AVAILABILITY STATEMENT

The datasets presented in this study can be found in online repositories. The names of the repository/repositories and accession number(s) can be found below: The Genotype-Tissue Expression (GTEx) Project portal at https://gtexportal.org/home/.

ETHICS STATEMENT

The studies involving human participants were reviewed and approved by Western IRB (WIRB Protocol #20142461) to Affiliated Laboratories BioRepository. The patients/participants provided their written informed consent to participate in this study. Approval was also obtained from Midwestern University IRB (AZ#807).

AUTHOR CONTRIBUTIONS

EJ, CU, and AP conducted experiments and contributed to data analysis. SE, RA, KL, and EH analysed data and edited the manuscript. KL and EH conceived of the project and coordinated the research endeavours. All authors have approved the manuscript.

FUNDING

This research was funded by MWU Research Facilitation Grants to KL and EH and by graduate student funds to EJ.

ACKNOWLEDGMENTS

We thank Kimbal E. Cooper for critical reading of the manuscript and advice on statistical analysis. In addition, we thank Ariane Buenaventura, Amber Tsang, and Sarah Gallegos for their contributions to preliminary studies and sample collection.

SUPPLEMENTARY MATERIAL

The Supplementary Material for this article can be found online at: https://www.frontiersin.org/articles/10.3389/fonc.2022.819580/full#supplementary-material

Supplementary Figure 1 | IFN-γ With Loading Controls GAPDH and Histone H3. Immunoblot of ANT and cSCC samples probed with anti-IFN-γ, anti-GAPDH, and anti-H3. Bands corresponding to dimer and monomer IFN-γ, and both loading controls, were observed.

Supplementary Figure 2 | FOXP3 and Loading control GAPDH. Immunoblot of ANT and cSCC samples probed with anti-FOXP3 and anti-GAPDH. A longer exposure time was needed to visualize FOXP3 than GAPDH.

Supplementary Figure 3 | CFH in Routine Mohs cSCC Samples by IHC. Additional images at 400x magnification of cSCC removed from routine clinic patients by Mohs surgery (fixed after cryosectioning). Sections were labeled with mouse anti-CFH (OX-24) and an AP-conjugated secondary antibody with permanent red stain. Mayer's Hematoxylin was used as a counterstain (nuclei).

Supplementary Figure 4 | CFH in Advanced cSCC Samples by IHC. Additional images at 400x magnification of advanced cSCC (formalin fixed) array slides. Sections were labeled with mouse anti-CFH (OX-24) and an AP-conjugated secondary antibody with permanent red stain. Mayer's Hematoxylin was used as a counterstain (nuclei).

Supplementary Figure 5 | FOXP3 in Routine Mohs cSCC Samples by IHC. Additional images at 400x magnification of cSCC removed from routine clinic patients by Mohs surgery (fixed after cryosectioning). Sections were labeled with were labeled with a rabbit monoclonal anti-FOXP3 (Cell Marque) and stained with an AP-conjugated secondary antibody and permanent red stain. Mayer's Hematoxylin was used as a counterstain (nuclei).

Supplementary Figure 6 | FOXP3 in Advanced cSCC Samples by IHC. Additional images at 400x magnification of advanced cSCC (formalin fixed) array slides. Sections were labeled with a rabbit monoclonal anti-FOXP3 (Cell Marque) and stained with an HRP-conjugated secondary antibody and DAB stain. Mayer's Hematoxylin was used as a counterstain (nuclei).

Supplementary Figure 7 | Expression of Complement Receptors in GTEx Datasets. Analysis of unpaired GTEx data from sun exposed vs non-sun exposed shows that sun exposed tissue has a significant increase in mRNA expression of C3aR (p=0.0014) and C5aR2 (p=0.0005) compared to non-sun exposed skin. mRNA expression of C5aR1 was not significantly different in this analysis (p=0.4726).

REFERENCES

1. Wells JW, Neters AD. Cutaneous Squamous Cell Carcinoma. In: *Medscape*. (2021). Available at: https://emedicine.medscape.com/article/1965430 (Accessed December 29, 2021).
2. Karia PS, Han J, Schmults CD. Cutaneous Squamous Cell Carcinoma: Estimated Incidence of Disease, Nodal Metastasis, and Deaths From Disease in the United States, 2012. *J Am Acad Dermatol* (2013) 68:957–66. doi: 10.1016/j.jaad.2012.11.037
3. Rogers HW, Weinstock MA, Feldman SR, Coldiron BM. Incidence Estimate of Nonmelanoma Skin Cancer (Keratinocyte Carcinomas) in the U.S. Population, 2012. *JAMA Dermatol* (2015) 151:1081–6. doi: 10.1001/jamadermatol.2015.1187
4. Wang Y, Zhang H, He Y-W. The Complement Receptors C3aR and C5aR Are a New Class of Immune Checkpoint Receptor in Cancer Immunotherapy. *Front Immunol* (2019) 10. doi: 10.3389/fimmu.2019.01574
5. Zhai L, Bell A, Ladomersky E, Lauing KL, Bollu L, Nguyen B, et al. Tumor Cell IDO Enhances Immune Suppression and Decreases Survival Independent of Tryptophan Metabolism in Glioblastoma. *Clin Cancer Res* (2021) 27:6514–28. doi: 10.1158/1078-0432.CCR-21-1392
6. Daugan MV, Revel M, Thouenon R, Dragon-Durey MA, Robe-Rybkine T, Torset C, et al. Intracellular Factor H Drives Tumor Progression Independently of the Complement Cascade. *Cancer Immunol Res* (2021) 9:909–25. doi: 10.1158/2326-6066.CIR-20-0787
7. Riihila PM, Nissinen LM, Ala-aho R, Kallajoki M, Grenman R, Meri S, et al. Complement Factor H: A Biomarker for Progression of Cutaneous Squamous Cell Carcinoma. *J Invest Dermatol* (2014) 134:498–506. doi: 10.1038/jid.2013.346
8. Riihilä P, Nissinen L, Farshchian M, Kivisaari A, Ala-aho R, Kallajoki M, et al. Complement Factor I Promotes Progression of Cutaneous Squamous Cell Carcinoma. *J Invest Dermatol* (2015) 135:579–88. doi: 10.1038/jid.2014.376
9. Timar KK, Pasch MC, van den Bosch NH, Jarva H, Junnikkala S, Meri S, et al. Human Keratinocytes Produce the Complement Inhibitor Factor H: Synthesis Is Regulated by Interferon-Gamma. *Mol Immunol* (2006) 43:317–25. doi: 10.1016/j.molimm.2005.02.009
10. Timár KK, Dallos A, Kiss M, Husz S, Bos JD, Asghar SS. Expression of Terminal Complement Components by Human Keratinocytes. *Mol Immunol* (2007) 44:2578–86. doi: 10.1016/j.molimm.2006.12.014
11. Uhlen M, Zhang C, Lee S, Sjostedt E, Fagerberg L, Bidkhori G, et al. A Pathology Atlas of the Human Cancer Transcriptome. *Science* (2017) 357 (6352):eaan2507. doi: 10.1126/science.aan2507
12. Okroj M, Holmquist E, Nilsson E, Anagnostaki L, Jirstrom K, Blom AM. Local Expression of Complement Factor I in Breast Cancer Cells Correlates With Poor Survival and Recurrence. *Cancer Immunol Immunother: CII* (2015) 64:467–78. doi: 10.1007/s00262-015-1658-8
13. Zhao J, Fan YX, Yang Y, Liu DL, Wu K, Wen FB, et al. Identification of Potential Plasma Biomarkers for Esophageal Squamous Cell Carcinoma by a Proteomic Method. *Int J Clin Exp Pathol* (2015) 8:1535–44.
14. Cui T, Chen Y, Knosel T, Yang L, Zoller K, Galler K, et al. Human Complement Factor H Is a Novel Diagnostic Marker for Lung Adenocarcinoma. *Int J Oncol* (2011) 39:161–8. doi: 10.3892/ijo.2011.1010
15. Campa MJ, Gottlin EB, Bushey RT, Patz EF Jr. Complement Factor H Antibodies From Lung Cancer Patients Induce Complement-Dependent Lysis of Tumor Cells, Suggesting a Novel Immunotherapeutic Strategy. *Cancer Immunol Res* (2015) 3:1325–32. doi: 10.1158/2326-6066.CIR-15-0122
16. Riihilä P, Nissinen L, Farshchian M, Kallajoki M, Kivisaari A, Meri S, et al. Complement Component C3 and Complement Factor B Promote Growth of Cutaneous Squamous Cell Carcinoma. *Am J Pathol* (2017) 187:1186–97. doi: 10.1016/j.ajpath.2017.01.006
17. Riihilä P, Viiklepp K, Nissinen L, Farshchian M, Kallajoki M, Kivisaari A, et al. Tumour-Cell-Derived Complement Components C1r and C1s Promote Growth of Cutaneous Squamous Cell Carcinoma. *Br J Dermatol* (2020) 182:658–70. doi: 10.1111/bjd.18095
18. Armento A, Honisch S, Panagiotakopoulou V, Sonntag I, Jacob A, Bolz S, et al. Loss of Complement Factor H Impairs Antioxidant Capacity and Energy Metabolism of Human RPE Cells. *Sci Rep* (2020) 10:10320. doi: 10.1038/s41598-020-67292-z
19. Roumenina LT, Daugan MV, Petitprez F, Sautès-Fridman C, Fridman WH. Context-Dependent Roles of Complement in Cancer. *Nat Rev Cancer* (2019) 19:698–715. doi: 10.1038/s41568-019-0210-0
20. Borras C, Canonica J, Jorieux S, Abache T, El Sanharawi M, Klein C, et al. CFH Exerts Anti-Oxidant Effects on Retinal Pigment Epithelial Cells Independently From Protecting Against Membrane Attack Complex. *Sci Rep* (2019) 9:13873. doi: 10.1038/s41598-019-50420-9
21. Belden SE, Uppalapati CK, Pascual AS, Montgomery MR, Leyva KJ, Hull EE, et al. Establishment of a Clinic-Based Biorepository. *J Visual Experiments* (2017) (123):55583. doi: 10.3791/55583
22. Crowe AR, Yue W. Semi-Quantitative Determination of Protein Expression Using Immunohistochemistry Staining and Analysis: An Integrated Protocol. *Bio Protoc* (2019) 9(24):e3465. doi: 10.21769/BioProtoc.3465
23. Clark SJ, Ridge LA, Herbert AP, Hakobyan S, Mulloy B, Lennon R, et al. Tissue-Specific Host Recognition by Complement Factor H Is Mediated by Differential Activities of Its Glycosaminoglycan-Binding Regions. *J Immunol* (2013) 190:2049–57. doi: 10.4049/jimmunol.1201751
24. Lilkova E, Petkov P, Ilieva N, Krachmarova E, Nacheva G, Litov L. Molecular Modeling of the Effects of Glycosylation on the Structure and Dynamics of Human Interferon-Gamma. *J Mol Model* (2019) 25:127. doi: 10.1007/s00894-019-4013-8
25. Sareneva T, Pirhonen J, Cantell K, Julkunen I. N-Glycosylation of Human Interferon-Gamma: Glycans at Asn-25 Are Critical for Protease Resistance. *Biochem J* (1995) 308(Pt 1):9–14. doi: 10.1042/bj3080009
26. Kambayashi Y, Fujimura T, Aiba S. Comparison of Immunosuppressive and Immunomodulatory Cells in Keratoacanthoma and Cutaneous Squamous Cell Carcinoma. *Acta Dermato-Venereol* (2013) 93:663–8. doi: 10.2340/00015555-1597
27. Vadasz Z, Toubi E. FoxP3 Expression in Macrophages, Cancer, and B Cells-Is It Real? *Clin Rev Allergy Immunol* (2017) 52:364–72. doi: 10.1007/s12016-016-8572-5
28. Devaud C, Yong CS, John LB, Westwood JA, Duong CP, House CM, et al. Foxp3 Expression in Macrophages Associated With RENCA Tumors in Mice. *PloS One* (2014) 9:e108670. doi: 10.1371/journal.pone.0108670
29. Mauri C, Bosma A. Immune Regulatory Function of B Cells. *Annu Rev Immunol* (2012) 30:221–41. doi: 10.1146/annurev-immunol-020711-074934
30. Rosser EC, Mauri C. Regulatory B Cells: Origin, Phenotype, and Function. *Immunity* (2015) 42:607–12. doi: 10.1016/j.immuni.2015.04.005
31. Fujimura T, Kambayashi Y, Fujisawa Y, Hidaka T, Aiba S. Tumor-Associated Macrophages: Therapeutic Targets for Skin Cancer. *Front Oncol* (2018) 8:3. doi: 10.3389/fonc.2018.00003
32. Nitta H, Wada Y, Kawano Y, Murakami Y, Irie A, Taniguchi K, et al. Enhancement of Human Cancer Cell Motility and Invasiveness by

Anaphylatoxin C5a *via* Aberrantly Expressed C5a Receptor (CD88). *Clin Cancer Res* (2013) 19:2004–13. doi: 10.1158/1078-0432.CCR-12-1204
33. Ding P, Li L, Li L, Lv X, Zhou D, Wang Q, et al. C5aR1 Is a Master Regulator in Colorectal Tumorigenesis *via* Immune Modulation. *Theranostics* (2020) 10:8619–32. doi: 10.7150/thno.45058
34. Kaida T, Nitta H, Kitano Y, Yamamura K, Arima K, Izumi D, et al. C5a Receptor (CD88) Promotes Motility and Invasiveness of Gastric Cancer by Activating RhoA. *Oncotarget* (2016) 7:84798–809. doi: 10.18632/oncotarget.12656
35. Maeda Y, Kawano Y, Wada Y, Yatsuda J, Motoshima T, Murakami Y, et al. C5aR Is Frequently Expressed in Metastatic Renal Cell Carcinoma and Plays a Crucial Role in Cell Invasion *via* the ERK and PI3 Kinase Pathways. *Oncol Rep* (2015) 33:1844–50. doi: 10.3892/or.2015.3800
36. Shu C, Zha H, Long H, Wang X, Yang F, Gao J, et al. C3a-C3aR Signaling Promotes Breast Cancer Lung Metastasis *via* Modulating Carcinoma Associated Fibroblasts. *J Exp Clin Cancer Res* (2020) 39:11. doi: 10.1186/s13046-019-1515-2
37. Chen B, Zhou W, Tang C, Wang G, Yuan P, Zhang Y, et al. Down-Regulation of C3aR/C5aR Inhibits Cell Proliferation and EMT in Hepatocellular Carcinoma. *Technol Cancer Res Treat* (2020) 19:1533033820970668. doi: 10.1177/1533033820970668
38. Mao X, Zhou L, Tey SK, Ma APY, Yeung CLS, Ng TH, et al. Tumour Extracellular Vesicle-Derived Complement Factor H Promotes Tumorigenesis and Metastasis by Inhibiting Complement-Dependent Cytotoxicity of Tumour Cells. *J Extracell Vesicles* (2020) 10:e12031. doi: 10.1002/jev2.12031
39. Mahajan S, Jacob A, Kelkar A, Chang A, McSkimming D, Neelamegham S, et al. Local Complement Factor H Protects Kidney Endothelial Cell Structure and Function. *Kidney Int* (2021) 100:824–36. doi: 10.1016/j.kint.2021.05.033
40. Huang SJ, Hijnen D, Murphy GF, Kupper TS, Calarese AW, Mollet IG, et al. Imiquimod Enhances IFN-Gamma Production and Effector Function of T Cells Infiltrating Human Squamous Cell Carcinomas of the Skin. *J Invest Dermatol* (2009) 129:2676–85. doi: 10.1038/jid.2009.151
41. Yokogawa M, Takaishi M, Nakajima K, Kamijima R, Digiovanni J, Sano S. Imiquimod Attenuates the Growth of UVB-Induced SCC in Mice Through Th1/Th17 Cells. *Mol Carcinogene* (2013) 52:760–9. doi: 10.1002/mc.21901
42. Wood KJ, Sawitzki B. Interferon Gamma: A Crucial Role in the Function of Induced Regulatory T Cells In Vivo. *Trends Immunol* (2006) 27:183–7. doi: 10.1016/j.it.2006.02.008

Conflict of Interest: The authors declare that the research was conducted in the absence of any commercial or financial relationships that could be construed as a potential conflict of interest.

Publisher's Note: All claims expressed in this article are solely those of the authors and do not necessarily represent those of their affiliated organizations, or those of the publisher, the editors and the reviewers. Any product that may be evaluated in this article, or claim that may be made by its manufacturer, is not guaranteed or endorsed by the publisher.

frontiers in Oncology

ORIGINAL RESEARCH
published: 21 February 2022
doi: 10.3389/fonc.2022.818868

Identification of Lactate-Related Gene Signature for Prediction of Progression and Immunotherapeutic Response in Skin Cutaneous Melanoma

Yalin Xie, Jie Zhang, Mengna Li, Yu Zhang, Qian Li, Yue Zheng and Wei Lai**

Department of Dermato-Venereology, The Third Affiliated Hospital of Sun Yat-sen University, Guangzhou, China

OPEN ACCESS

Edited by:
Gagan Chhabra,
University of Wisconsin-Madison, United States

Reviewed by:
Shengqin Su,
Shanghai Hengrui Pharmaceutical Co., Ltd., China
Ruidong Li,
Gilead, United States

****Correspondence:***
Wei Lai
laiwei2@mail.sysu.edu.cn
Yue Zheng
benbenzhu-11@163.com

Specialty section:
This article was submitted to Skin Cancer, a section of the journal Frontiers in Oncology

Received: *20 November 2021*
Accepted: *02 February 2022*
Published: *21 February 2022*

Citation:
Xie Y, Zhang J, Li M, Zhang Y, Li Q, Zheng Y and Lai W (2022) Identification of Lactate-Related Gene Signature for Prediction of Progression and Immunotherapeutic Response in Skin Cutaneous Melanoma. Front. Oncol. 12:818868. doi: 10.3389/fonc.2022.818868

Skin cutaneous melanoma (SKCM) is a skin cancer type characterized by a high degree of immune cell infiltration. The potential function of lactate, a main metabolic product in the tumor microenvironment (TME) of SKCM, remains unclear. In this study, we systemically analyzed the predictive value of lactate-related genes (LRGs) for prognosis and response to immune checkpoint inhibitors (ICIs) in SKCM patients included from The Cancer Genome Atlas (TCGA) database. Cluster 3, by consensus clustering for 61 LRGs, manifested a worse clinical outcome, attributed to the overexpression of malignancy marks. In addition, we created a prognostic prediction model for high- and low-risk patients and verified its performance in a validation cohort, GSE65904. Between TME and the risk model, we found a negative relation of the immunocyte infiltration levels with patients' risk scores. The low-risk cases had higher ICI expression and could benefit better from ICIs relative to the high-risk cases. Thus, the lactate-related prognosis risk signature may comprehensively provide a basis for future investigations on immunotherapeutic treatment for SKCM.

Keywords: skin cutaneous melanoma, prognostic signature, lactate, immunotherapy, TCGA, GEO

INTRODUCTION

Skin cutaneous melanoma (SKCM) is more aggressive than other skin cancer types owing to its rapid progression, poor prognosis, and high mortality (1). Although the cases invasive melanoma account for ~5% of all skin malignant tumors, it causes >75% of skin cancer-related deaths. The five-year survival rates in localized or regional melanoma are 98% and 64%, respectively, however, these rates reduce to 23% in the advanced stages (2), thereby illustrating that early intervention to prevent the disease from metastasizing is essential for improving the clinical prognoses. In the early stages, surgery is the most effective curative strategy, while for the metastatic cases, systemic treatment plays a significant role in inhibiting further disease progression (3).

In recent years, immunotherapy has emerged as the most promising treatment modality against several tumor types. Immunotherapy comprises therapeutic strategies that target various

components and signal pathways of the immune system (4). The specific mechanism of action is based on disrupting the tolerogenic nature of human cancer and rebooting the antitumor effects exerted on the tumor microenvironment (TME), resulting in the activation of autologous immune responses (5). Recently, immune checkpoint inhibitors (ICIs), including monoclonal antibodies targeting CTLA-4 and PD-1, have proved to be the greatest breakthrough in the field of tumor therapy. Although collectively ICIs have a response rate of 30–40% (6), a majority of patients lack satisfactory clinical efficacies owing to the complex mechanisms underlying tumor immunity (7). Furthermore, several reported genomic and immune biomarkers indicate that the therapeutic effects are not targeted and there is an inevitable bias whilst evaluating the treatment efficacies (8). Thus, it is challenging but necessary to identify a better predictor to evaluate the clinical outcomes accurately before prescribing ICI treatment.

TME consists of various cell types and an extracellular matrix, thereby supporting tumor behaviors, including their growth and metastases through the provision of energy and nutrients (9). Usually, the blood vessel network in TME is poorly developed or malformed, and thus, exchanging of nutrients and metabolic wastes is relatively impaired. This causes a breakdown of the metabolic balance in the tumor tissues, characterized by nutrition shortage and metabolite accumulation (10). Consequently, the above-mentioned transfer of metabolic mode in TME is a natural immune suppressor, along with the inactivation of immune cells and a decrease in protective inflammatory reactions (11). Additionally, accumulating evidence shows that targeting the metabolic mode in TME is a promising strategy to potentiate the effects of immunotherapy and is therefore worth further investigation.

Excessive production of lactate is the result of elevated aerobic glycolysis in the TME (12). Lactate is responsible for sustaining the acidic environment by decreasing the pH, thereby inhibiting the immune responses partly by inactivating the T cells as also through negative regulation of the T-regulatory cells in the anticancer immunity (13). Meanwhile, a recent study demonstrates that neutralization of the low pH environment in malignant melanoma aids better clinical efficacy of the anti-PD-1 immune strategy (14). In addition, lactate dehydrogenase is being used in clinical settings for the independent prediction of survival of melanoma patients; it is also recommended in the AJCC guidelines (15). Collectively, this indicates that the identification of lactate-related genes (LRGs) for predicting the prognoses in SKCM patients may aid appropriate guidance for therapeutic regimens.

In this study, we analyzed the complete gene expression profiles related to LRGs in 471 patients from The Cancer Genome Atlas (TCGA) database. Six genes were significantly correlated to lactate metabolism as per the Cox regression model. Next, we used the reconstructed model to assess clinical outcomes and responses to immunotherapy among the SKCM patients, and the results showed that this potential strategy may be useful for survival prediction and could be utilized as a novel immune-targeted therapy.

MATERIALS AND METHODS

Data Collection

The transcriptomic profiles of 472 individuals were obtained from TCGA database (https://portal.gdc.cancer.gov), which consisted of data for one healthy skin and 471 SKCM tissues. We then extracted the data for 556 normal skin tissue samples from the Genotype-Tissue Expression Project (GTEx, https://gtexportal.org/home/) web portal to account for the small number of the controls from TCGA database. The gene expression data from TCGA and GTEx were merged and normalized using the "limma" package in R to control for batch effects (16). The abundances of genes were normalized using their fragments per kilobase million (FPKM) values. Furthermore, the GSE54467 (n=79) dataset (17) was extracted from the Gene Expression Omnibus database (GEO, http://www.ncbi.nlm.nih.gov/geo/) and used as an external confirmation cohort to validate the robustness of the gene signature. Patients with entire clinical data as well as those with a survival duration longer than 0 days were included in current research.

Differential Expression and Functional Enrichment Analyses for LRGs

A total of 184 LRGs were obtained from the Molecular Signatures Database (INCREASED SERUM LACTATE, M35671, http://www.gsea-msigdb.org/gsea/index.jsp) (18). The "limma" package was used to identify the differentially expressed LRGs between SKCM and healthy skin samples with thresholds of $|\log2 \text{ fold change (FC)}| \geq 1$ and standard false discovery rate (FDR) < 0.05. The protein-protein interaction (PPI) network of differentially expressed LRGs was predicted using the STRING webtool (https://string-db.org/) (19). The hub sub-modules in the PPI network were selected using the MCODE plug-in in Cytoscape (20). The Gene Ontology (GO) and the Kyoto Encyclopedia of Genes and Genomes (KEGG) enrichment analyses were performed using the "cluster Profiler" package in R (21).

Consensus Clustering

According to the expression profiles of differentially expressed LRGs in SKCM tissues, consensus clustering was performed using the "ConsensusClusterPlus" package in R by setting the number of groups to 9, the sample resampling to 80%, and the number of iterations to 1000 (22). The optimal cluster number was calculated using the consensus matrix and cumulative distribution function (CDF). The differences in the overall survival (OS) between different clusters were estimated using the Kaplan-Meier method. Comparisons of the distribution of categorical data among the clusters were done using the chi-squared test.

Construction and Validation of Prognostic LRG Signature

Univariate Cox analysis was employed to identify the differentially expressed LRGs having significant ($P < 0.05$) prognostic prediction value. The selected factors were integrated into the least absolute shrinkage and selection operator (LASSO) Cox regression algorithm and the risk of

overfitting was minimized. Lastly, a multivariate Cox regression model was generated for selecting the genes and an LRG-based prognostic model was subsequently established. The risk score for each patient was calculated using the following formula: Risk Score = $\sum_{i=1}^{n} Coef(i) \times x(i)$, where *Coef(i)* and *x(i)* were the regression coefficients in the multivariate Cox regression model and expression of each gene, respectively. The patients were classified either into the high-risk (≥ median number) or the low-risk (< median number) groups according to the median risk score. The survival curve, receiver operating characteristic (ROC) curve, risk score distribution, and heatmap were analyzed and the predictive effectiveness of the clinical signature was thus evaluated. External data from GSE54467 were used to assess the performance of the model in determining clinical outcomes.

For the analysis of the correlation of risk score value based on the signature with clinical parameters in TCGA-SKCM cohort, the chi-square tests were performed. The independence of both the clinical features and the LRG signature was assessed through univariate and multivariate Cox regression analyses. To evaluate the applicability of this signature, stratified Cox survival analysis was performed for subgroups having differential clinical characteristics.

Development of a Nomogram

Nomograms have been widely adopted as auxiliary tools to predict the individual probability of a clinical event in medical fields (23). Nomogram was built by including all independent prognostic factors (24). In this study, the independent prognostic factors were used to construct the nomogram for assessing the 1-, 3-, and 5-year OS in SKCM. Calibration, ROC, and decision curves were used to verify the ability of the nomogram for predicting the prognoses.

Functional Biological Analysis of DEGs in the LRG Signature

The differentially expressed genes (DEGs) between the low- and high-risk groups in TCGA-SKCM were analyzed using the "limma" package in R. Genes with $|log2FC| \geq 1$ and FDR < 0.05 were identified as significant DEGs and included in the subsequent analysis. GO annotation and KEGG analyses of these DEGs between the two subgroups were performed. Additionally, a gene set enrichment analysis (GSEA) was performed to elucidate the significant functional phenotypes that were significantly different between the risk groups. The GSEA function in Java software was executed and the Hallmark gene set "h.all.v7.4.symbols.gmt" was used (18). The phenotypes with nominal $P < 0.05$ and FDR value < 0.25 were considered statistically significant.

Immune Infiltration Analysis

To uncover the relationship between the risk score and tumor-infiltrating immune cells, seven algorithms including TIMER (25), CIBERSORT (26), CIBERSORT-ABS, quanTIseq (27), MCP-counter (28), xCELL (29), and EPIC (30) were executed to calculate the immune infiltration values among the samples in TCGA-SKCM cohort. We used a heatmap to show the tumor immune cell infiltration computed using different algorithms for each patient. The Spearman correlation analysis was performed, and the correlation coefficients were presented on a lollipop plot.

Subsequently, single sample GSEA (ssGSEA) was used to quantitate the differences in the infiltration levels of immunocytes between the low- and high-risk subgroups using the "GSVA" package in R (31). The differences among the 16 immune cell types and 13 immune-related pathways were compared between the two subgroups. ESTIMATE was the algorithm that predicted the tumor purity, and the tumor microenvironment scores (including immune score, stromal score, and ESTIMATE score) for each SKCM sample from the gene expression data using the "ESTIMATE" package in R (32). Violin plots were plotted to demonstrate the differences in scores between the two groups.

Expression of Immune Checkpoint Inhibitors and Immunotherapeutic Responses

To investigate the underlying effects of this signature on the responses to immunotherapy, 47 ICIs were retrieved from published literature, and the expressions of these ICIs between the two groups were analyzed (33). The correlation of the prognostic signature with the expression of two ICIs, including programmed cell death protein 1 (PD-1) and cytotoxic T lymphocyte-associated antigen 4 (CTLA4), was also determined. The immunophenoscore (IPS) algorithms were leveraged to evaluate immunotherapeutic responses as described previously (34).

Tissue Samples

A total of 15 SKCM tissues and 15 normal skin tissues were obtained from patients received surgery at the Third Affiliated Hospital of Sun Yat-Sen University (Guangzhou, China). None of these patients had received pre-surgery chemotherapy or other treatment. All collected samples were stored in a −80°C refrigerator until further quantitative real-time PCR (qRT-PCR) analysis. The written informed consent was acquired from all subjects, and the present research was approved by the hospital ethical committee.

Quantitative Real-Time Polymerase Chain Reaction (qRT-PCR)

Total RNA was extracted using the TRIzol reagent (Invitrogen, Grand Island, NY, USA) and reverse transcribed into cDNA using the PrimeScript RT reagent Kit (TaKaRa, Japan) following the manufacturer's protocols. qRT-PCR was performed with SYBR Green I Master Kit (Roche) on the LightCycler® 480 System (Roche). The relative mRNA levels were normalized against that of GAPDH using the $2^{-\Delta\Delta Ct}$ method. The sequences of the primers used in qRT-PCR are listed in **Table S1**.

Statistical Analysis

All statistical analyses were performed on R unless indicated otherwise, following the methods described above. $P < 0.05$ was considered statistically significant.

RESULTS

Identification of Differentially Expressed LRGs and Functional Enrichment Analysis

The flow chart of the study design is shown in **Figure 1**. First, we analyzed the DEGs between 471 tumor and 557 normal tissues from TCGA and GTEx databases. A total of 7507 DEGs were selected according to the criteria of |log2FC| > 1 and FDR < 0.05. Among them, 3789 DEGs were significantly upregulated in SKCM tissues as compared to the normal skin tissues, while the remaining 3718 were markedly downregulated (**Figure 2A**). In addition, 184 LRGs were obtained from the Molecular Signatures Database. We then acquired 61 differentially expressed LRGs by taking the intersection of DEGs and LRGs sets, which may be involved in the progress of increased serum lactate (**Figure 2B**). A PPI network was constructed for these 61 differentially expressed LRGs (**Figure 2C**). The most significant module was then identified using the MCODE algorithm (**Supplementary Figure 1**). The functions of these 61 differentially expressed LRGs were predicted, and the results of the GO annotation indicated these were markedly augmented in energy metabolism-related processes, including the

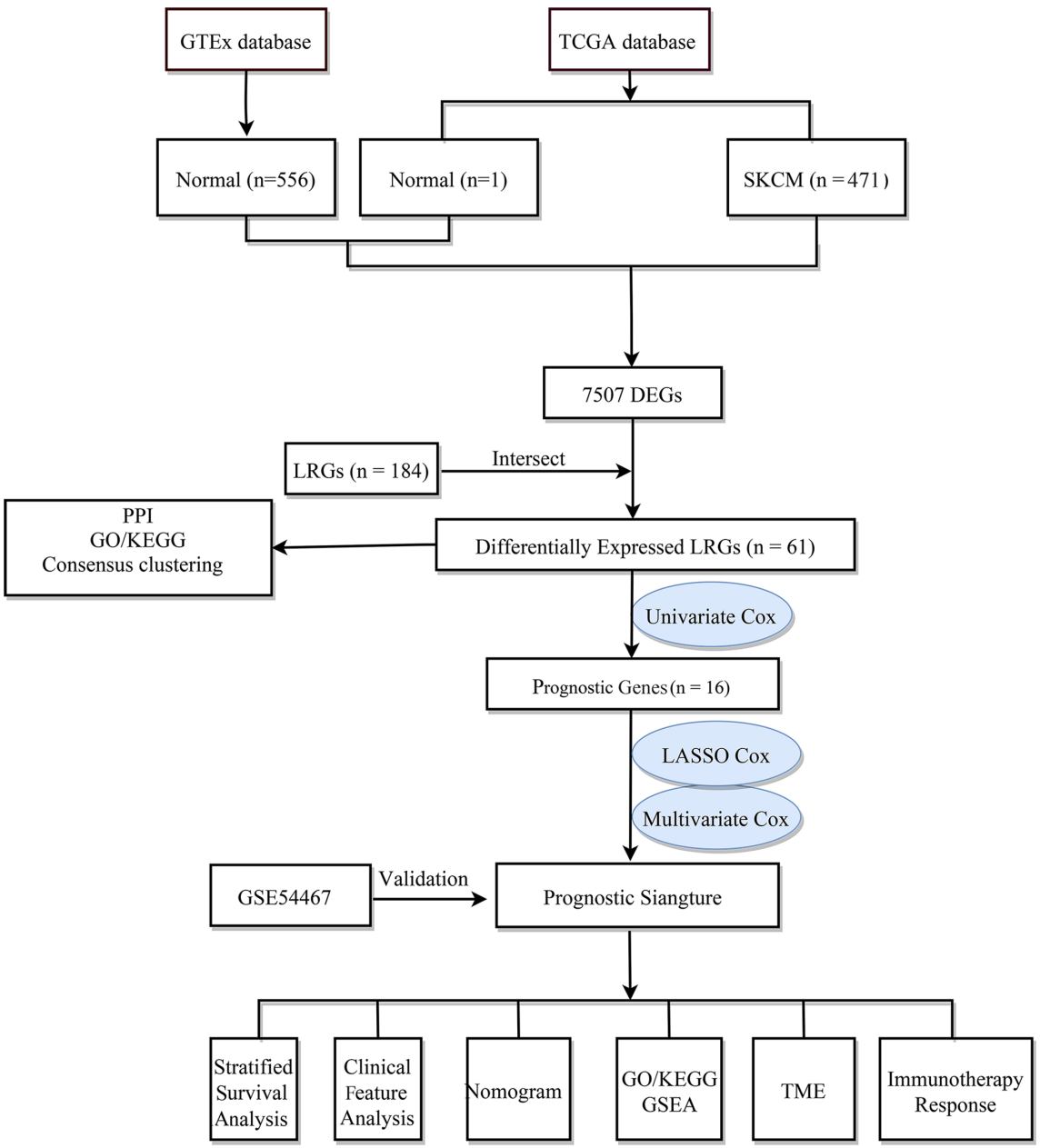

FIGURE 1 | The flow chart of the study design.

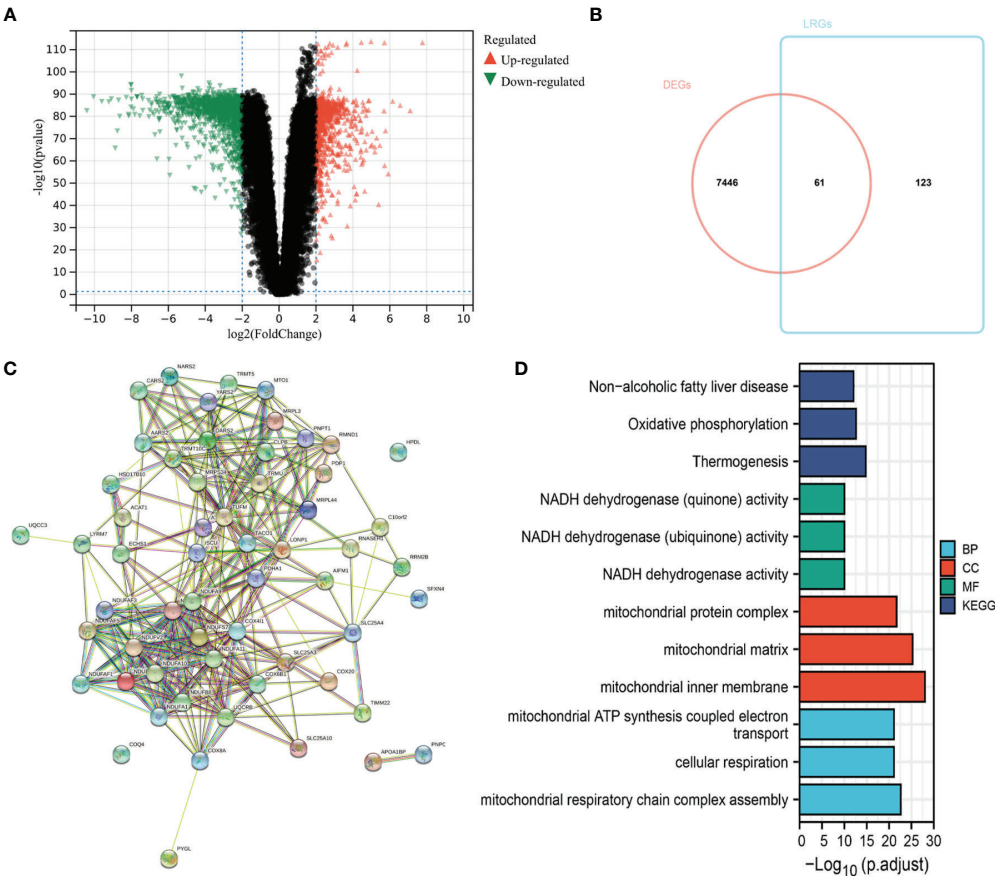

FIGURE 2 | Identification of differentially expressed LRGs in TCGA cohort and functional enrichment analysis. **(A)** Volcano plot showing the DEGs between 471 SKCM and 557 non-tumor healthy samples. **(B)** Venn diagram showing the intersection of DEGs and LRGs. **(C)** The PPI network of differentially expressed LRGs. **(D)** GO and KEGG analyses of differentially expressed LRGs.

mitochondrial respiratory chain complex assembly. The differential genes were mostly correlated with pathways of thermogenesis, oxidative phosphorylation, and non-alcoholic fatty liver disease, as evidenced by the KEGG enrichment analysis (**Figure 2D**).

Determination of SKCM Clusters Using Consensus Clustering

To understand the integral role of lactate in SKCM, the SKCM samples were divided into diverse clusters (K = 2 to 9) according to the differential expressions of the 184 LRGs through an unsupervised consensus clustering method. The optimal division (K = 3) was the optimal number of clusters according to the consensus matrix (**Figure 3A**), consensus CDF curves (**Figure 3B**), and relative change in the area under the CDF curves (**Figure 3C**). The boundary of the consensus matrix was kept relatively strict, and the sample distribution reached maximal stability at K =3. A significant difference was observed in the prognoses\ of the SKCM patients, wherein those belonging to cluster 2 suffered poorer outcomes relative to clusters 1 and 3 (**Figure 3D**). In addition, PCA showed that it was feasible to divide the samples into discrete distribution patterns (**Figure 3E**). The chi-square analysis demonstrated statistically significant differences in the T stage ($P = 0.048$) and Ulceration Status ($P = 0.030$) between the SKCM patients and normal controls (**Figure 3F**).

Construction and Evaluation of the LRG Signature for SKCM

Univariate Cox regression analysis showed that 16 out of the 61 differentially expressed LRGs were significantly associated with OS ($P < 0.05$) in TCGA-SKCM cohort (**Figure 4A**). To narrow down the range of candidate genes and eliminate the risk of overfitting, a LASSO Cox regression was performed, and the penalty parameter was selected based on the minimum criterion. A total of 10 genes were retained for further analysis (**Figure 4B, C**) and six target genes (ISCU, MTO1, SLC25A3, HPDL, NDUFA13, and NARS2) were eventually used to construct the LRG prognostic signature based on the multivariate Cox proportional hazards model. The forest map indicated that ISCU and MTO1 were the protective factors with the hazard ratio (HR) < 1, while SLC25A3, HPDL, NDUFA13, and NARS2 were risk factors having a hazard ratio (HR) > 1 (**Figure 4D**). To better understand the role of these six LRGs, we obtained their expressions from the GEPIA database and found markedly low levels of ISCU and MTO1 in SKCM

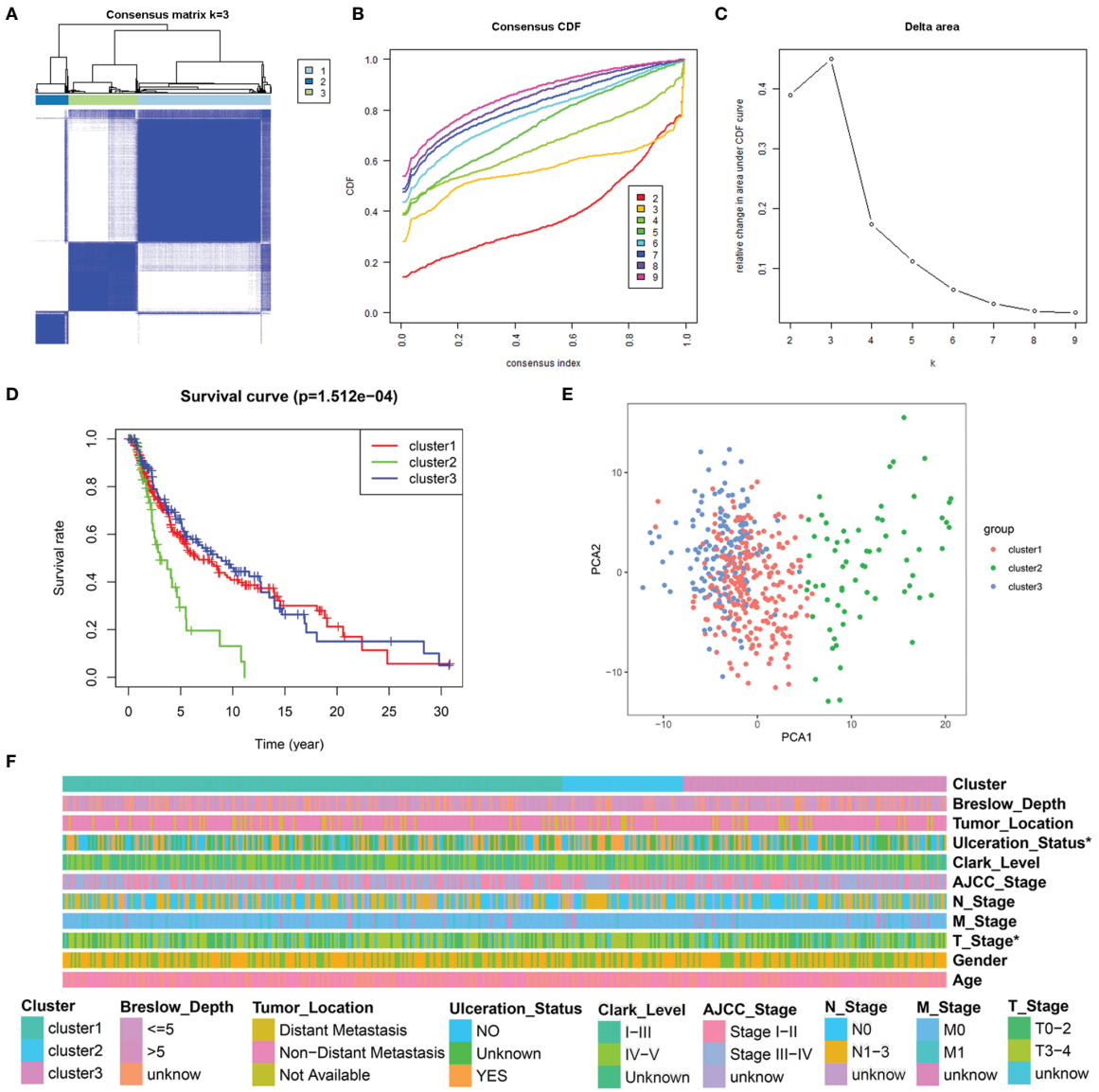

FIGURE 3 | Consensus clustering analysis of 184 LRGs. **(A)** Consensus clustering matrix at K = 3. **(B)** The CDF curves for clusters at k = 2 to 9. **(C)** The relative change in area under CDF curves for different clusters from k = 2 to 9. **(D)** Survival analysis for SKCM samples is stratified to the three clusters. **(E)** PCA plot for the three clusters. **(F)** Heatmap and the clinical parameters of the three clusters. * $P < 0.05$.

compared with normal samples, while those of SLC25A3, HPDL, NDUFA13, and NARS2 were substantially high (**Supplementary Figure 2**). The results were confirmed by qRT-PCR detection for ISCU, SLC25A3, HPDL, and NARS2, whereas no significant differences were present in the expression of MTO1 and NDUFA13 (**Figure 4E**). The Kaplan Meier survival analysis confirmed the enhanced expression of SLC25A3, HPDL, NDUFA13, and NARS2 which could contribute to the poor outcome of SKCM patients; moreover, high levels of ISCU and MTO1 were significantly associated with better survival in patients (**Figure 4F**), consistent with our previous analysis. For both TCGA and GSE54467 cohorts, the risk score for the LRG signature was calculated as follows: Risk Score = (-0.406 * $ISCU_{expression}$) + (-0.415 * $MTO1_{expression}$) + (0.397 * $SLC25A3_{expression}$) + (0.113 * $HPDL_{expression}$) + (0.198 * $NDUFA13_{expression}$) + (0.129 * $NARS2_{expression}$).

SKCM cases were divided into low- and high-risk subgroups based on the median risk score. The Kaplan-Meier survival analysis demonstrated that the high-risk subgroup had a shorter OS than that of the low-risk group in TCGA-SCKM (**Figure 5A**) and GSE54467 cohorts (**Figure 5D**). ROC curves were employed to assess the predictive performance of the LRG signature, and the area under the curve (AUC) for TCGA-SKCM was 0.702 (**Figure 5B**). Similarly, the AUC was 0.621 for the GSE54467 cohort (**Figure 5E**). The distribution of the risk score and survival status in TCGA-SKCM are shown in **Figure 5C**.

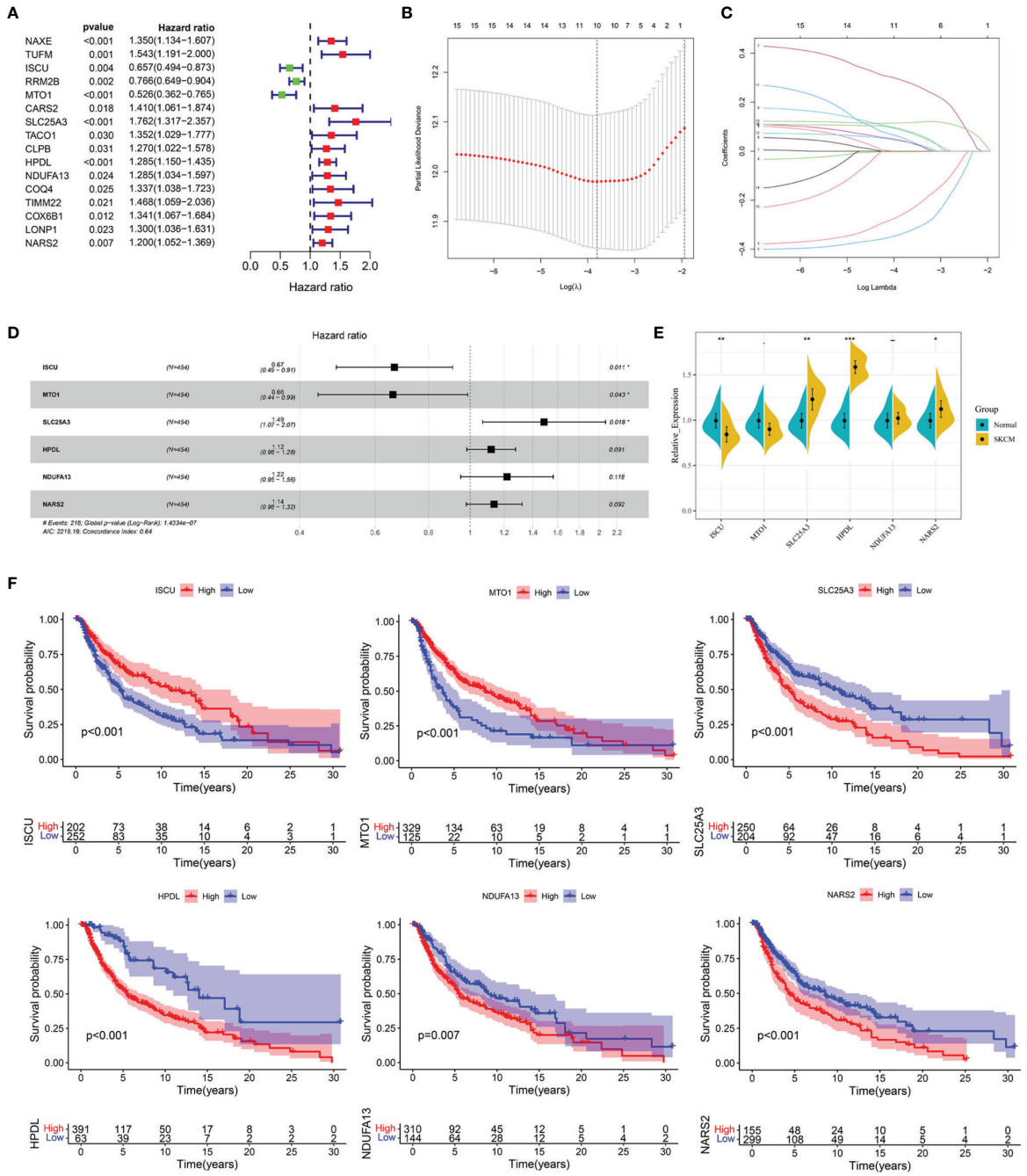

FIGURE 4 | Construction of the LRG prognostic signature in TCGA cohort. **(A)** Identification of the prognosis-related differentially expressed LRGs by univariate Cox regression analysis. **(B, C)** LASSO Cox regression analysis of 16 prognosis-related differentially expressed LRGs. **(D)** Forest plot of the six target genes that compose the LRG signature. **(E)** The expression levels of six target genes by qRT-PCR. **(F)** The Kaplan Meier analysis of the six target genes *P < 0.05; **P < 0.01; ***P < 0.001.

The high-risk group was associated with higher mortality as compared to the low-risk group. Moreover, SLC25A3, HPDL, NDUFA13, and NARS2 were markedly upregulated, while ISCU and MTO1 were substantially downregulated (**Figure 5C**). The results in the GSE54467 cohort were in line with the above-described findings (**Figure 5F**).

Relationship Between the Risk Score and Clinical Features

In addition, the correlation of the signature with the clinical features (age, gender, T stage, M stage, N stage, AJCC stage, Breslow depth, Clark level, ulceration status, and tumor location) was tested in TCGA cohort. It was found that the risk scores for

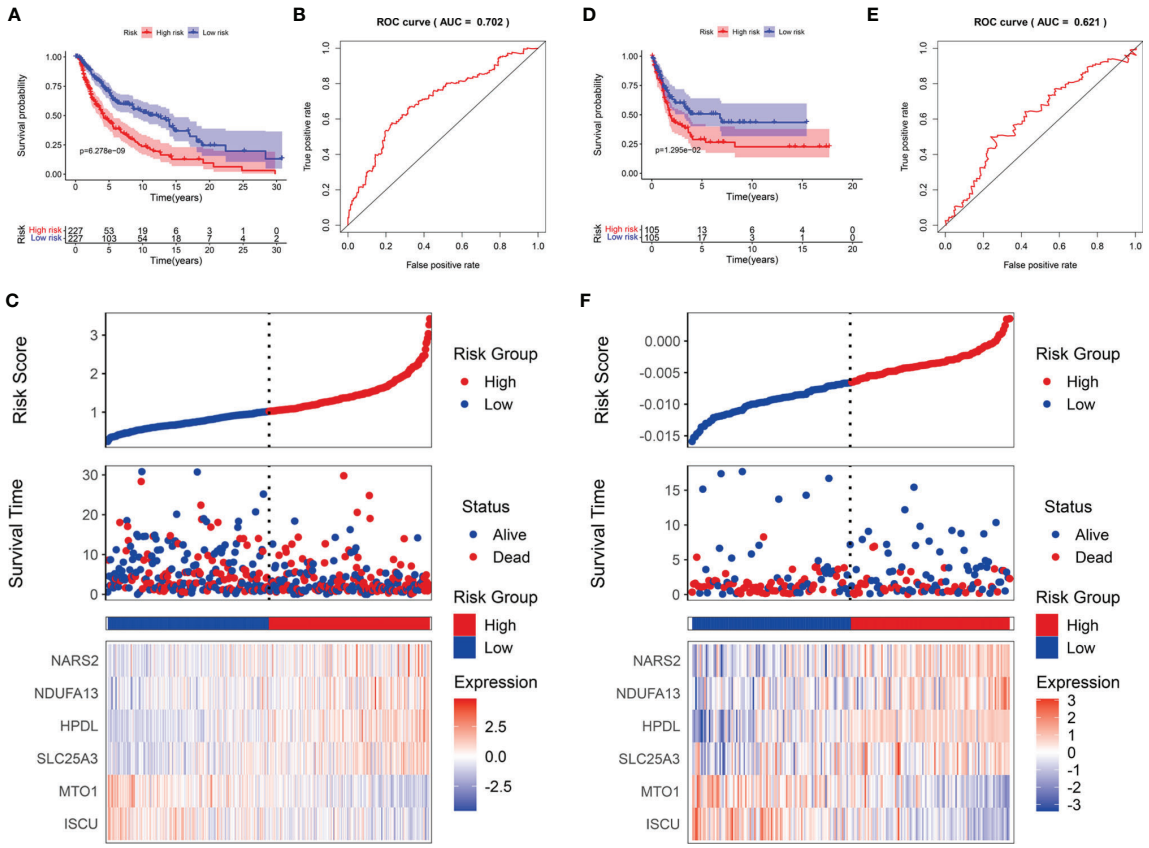

FIGURE 5 | The prognostic value of the LRG signature for SKCM patients. The survival analysis in TCGA cohort **(A)** and GSE54467 cohort **(D)**. ROC curves indicated the predictive efficiency of the prognostic signature in TCGA cohort **(B)** and GSE54467 cohort **(E)**. The risk score distribution, survival status, and heatmap for the expressions of the six genes in TCGA cohort **(C)** and GSE54467 cohort **(F)**.

the low-risk and the high-risk groups were significantly different for the T stage (**Figure 6A**), Breslow depth (**Figure 6B**), Clark level (**Figure 6C**), ulceration status (**Figure 6D**), and tumor location (**Figure 6E**). We also observed that the SKCM patients in the high-risk group had higher risk factors for disease progression, including advanced T stage, >5mm Breslow depth, IV-V Clark level, with ulceration, and distant metastases. In addition, the signature-based risk score was positively correlated with tumor progression. We then compared the differences in risk scores among the different clusters and found that cluster 2 presented a higher risk score than other clusters, which further verified our results (**Supplementary Figure 3A**). However, there were no significant differences in age, gender, M stage, N stage, and AJCC stage (**Supplementary Figures 3B–F**).

We reasonably speculated that the prognostic signature could serve as an independent prognostic factor for patients with SKCM. Therefore, univariate and multivariate Cox regression analyses were performed to confirm this hypothesis. The signature-based risk score was found to be significantly related to OS in univariate Cox analysis (HR = 2.017, $P < 0.001$) (**Figure 6F**). Moreover, multivariate Cox analysis showed that the risk score remained an independent factor (HR = 2.048, $P < 0.001$) (**Figure 6G**). Likewise, the T stage, N stage, and AJCC stage were also independent prognostic factors. Hence, the signature was an independent risk factor that influenced the survival of patients with SKCM.

Further, for validating the stability and applicability of the LRG signature, we performed a stratified survival analysis for the subgroups. In all the subgroups except for the breslow depth > 5 subgroup, the Kaplan-Meier survival curve showed that samples from the high-risk group had poorer clinical outcomes as compared to those belonging to the low-risk group (**Supplementary Figure 4**).

Construction of the Clinical Nomogram

Furthermore, we employed four independent prognostic features of OS, including the signature-based risk score, T stage, N stage, and AJCC stage to construct the nomogram to quantitatively estimate the 1-, 3-, and 5- year survival probabilities of SKCM patients in TCGA cohort (**Figure 7A**). In the nomogram score system, each variable was allocated a point, and then the sum of the points was calculated as the total score, and the predicted risk corresponding to the total score was the probability of survival (35). The accuracy and sensitivity of the predictions were confirmed using the calibration plot for the nomogram. To intuitively illustrate the performance of the nomogram, calibration curves were plotted which showed that the predicted results were consistent with the reality, thereby

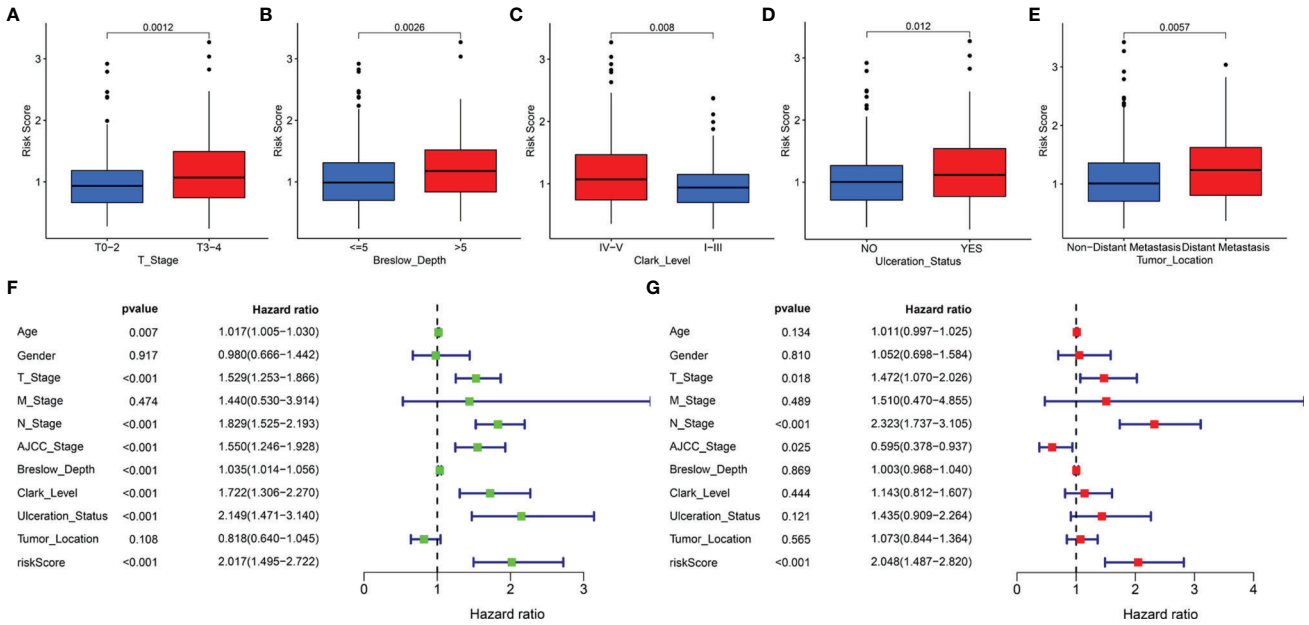

FIGURE 6 | The clinical utility of the LRG signature. The associations between the signature-based risk score and different clinical features, including **(A)** T stage, **(B)** Breslow depth, **(C)** Clark level, **(D)** Ulceration Status, and **(E)** Tumor Location. Univariate **(F)** and multivariate **(G)** Cox analyses for the signature-based risk score and other clinical features in TCGA cohort.

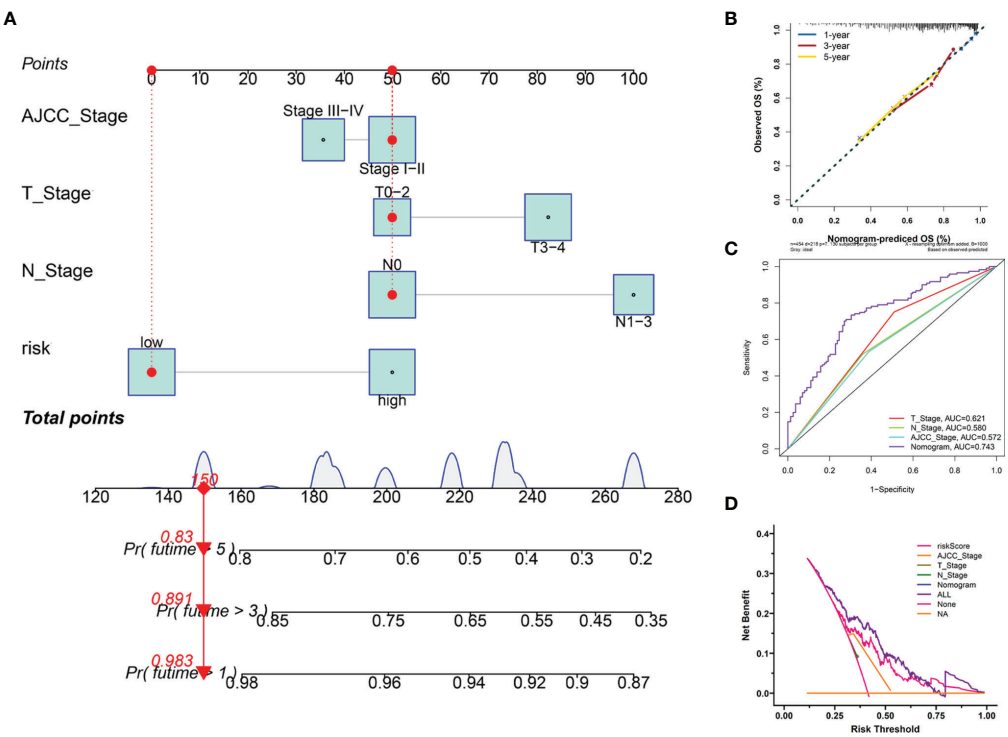

FIGURE 7 | Construction and evaluation of the novel nomogram. **(A)** The nomogram for predicting the survival probability of SKCM patients has four independent prognostic features. **(B)** The calibration plots of the nomogram for predicting OS probability for 1-, 3-, and 5-years. **(C)** ROC analysis of the nomogram. **(D)** DCA of the nomogram.

suggesting a highly accurate and sensitive prediction for SKCM (**Figure 7B**). The ROC curve analysis showed that the nomogram provided adequate discrimination for the two risk groups with an AUC of 0.743, thereby outperforming other independent clinical prognostic features (T stage, AUC =0.621; N stage, AUC = 0.580; AJCC stage, AUC = 0.572) (**Figure 7C**). The decision curves suggested that the nomogram had the highest overall net benefit within the threshold probabilities relative to any other clinical feature (**Figure 7D**).

Identification of the Prognostic Signature-Related Biological Processes and Pathways

To further detect the biological behaviors that were influenced by the prognostic LRG signature, we identified the DEGs between the low- and high-risk groups to perform the functional enrichment analyses. In total, 252 DEGs were screened for the subsequent analysis based on the criteria of $|\log2FC| > 1$ and FDR < 0.05. The results suggested that the top three enriched GO terms for biological processes (BP) were humoral immune response mediated by circulating immunoglobulin, complement activation-classical pathway, and complement activation (**Figure 8A**). The cellular components (CC) significantly associated with these DEGs included the immunoglobulin complex, immunoglobulin complex-circulation, and lateral side of cytomembrane (**Figure 8B**). The molecular function (MF) analysis showed that the DEGs were related substantially with antigen binding, immunoglobulin receptor binding, and peptide antigen binding (**Figure 8C**). Collectively, the GO annotation suggested that the enrichment of the DEGs was mostly related to the immune-associated processes, which was validated by the KEGG analysis (**Figure 8D**). Besides, we also performed GSEA to compare the different hallmark pathways between the low- and high-risk groups. Most enriched hallmark pathways in the low-risk group were involved in immune regulation, including the complement activation, inflammatory responses, IL2-STAT5 signaling, TNFA signaling *via* NFKB, IL6-JAK-STAT3 signaling, and TGF-beta signaling pathways (**Figure 8E**). These findings suggested that the LRG-based prognostic signature was closely related to immunity and the low-risk group had enhanced immune response phenotypes.

Immune Infiltration Characteristics of TME

Following the aforementioned results, we postulated that the impact of LRG signature on the outcomes for a patient with SKCM may be associated with the immune microenvironment. Therefore, we assessed the differences in the immune cell components in SKCM tissues between low- and high-risk groups. The heatmap for various immunocyte components based on TIMER, CIBERSORT, CIBERSORT-ABS, quanTIseq, MCP-counter, xCELL and EPIC algorithms, is shown in **Supplementary Figure 5A**. In addition, Spearman correlation analysis was performed, and the correlation coefficients were visualized using a lollipop plot (**Supplementary Figure 5B**). In total, 93 microenvironment components that were examined were found to be diverse between the two groups. Among these, 79 components were negatively correlated with the signature-based risk score, while the remaining 14 were positively correlated. The detailed correlation between the risk score and six immune cell types was computed based on the TIMER database. With an increase in the risk score, there was a marked decrease in the proportion of immunocytes (B cells, CD4+ and CD8+ T cells, dendritic cells, macrophages, and neutrophils) in SKCM patients (**Figures 9A–F**).

Subsequently, we estimated the tumor purity and the tumor microenvironment scores using the ESTIMATE algorithm, and the results are shown as a heatmap (**Figure 10A**). The enrichment scores of various immune cell types and immune-related pathways between the two groups were compared. We observed that the abundances of the immune cells except for the iDCs and mast cells (**Figure 10B**), as well as all the immune-related pathways (**Figure 10C**), were markedly elevated in the low-risk group. These results suggested that the two subgroups exhibited distinct immune infiltration profiles. The distributions were then estimated using the ESTIMATE algorithm between the low- and high-risk groups. The immune, stromal, and ESTIMATE scores of the low-risk group were found to be significantly higher relative to the high-risk group (**Figures 10D–F**), while the levels of the tumor purity showed a reverse trend (**Figure 10G**). Survival analysis showed that the patients having a higher immune score, higher ESTIMATE score, and lower tumor purity exhibited better prognoses. However, the differences in the stromal scores were not statistically significant (**Supplementary Figure 6**). The above results demonstrated that there was a significant correlation of the signature-based risk score with the tumor immune microenvironment. In addition, the differences in the different immune cell types could account for the observed immune-associated biological phenotypes and pathways related to the LRG signature.

Differential Expression of ICIs and Assessment of Immunotherapy Response

The responses to ICI tumor immunotherapy have made important progress in recent years for several cancer types, including SKCM. To further investigate whether the LRG signature was associated with the ICI-related biomarkers, we compared the levels of expression of 47 genes between the two groups and found that 43 ICI-related genes were significantly differentially expressed and all of them were upregulated in the low-risk group relative to the high-risk group, except for CD276 and TNFRSF14 (**Figure 11A**). PD-1 and CTLA-4 are widely studied ICIs. As expected, the levels of expression of these two genes were negatively correlated with the risk score (**Figure 11B, C**). The IPS scoring scheme was used to simulate the potential immunotherapeutic responses in patients of the low- and high-risk groups. The relative probabilities of responding to $CTLA4_{positive}/PD\text{-}1_{negtive}$, $CTLA4_{negtive}/PD\text{-}1_{positive}$, and $CTLA4_{positive}/PD\text{-}1_{positive}$ treatment in the low-risk group were found to be markedly higher relative to the high-risk group (**Figure 11D**). The differences between the two groups for $CTLA4_{negtive}/PD\text{-}1_{negtive}$ treatment were not statistically significant. Herein, these data demonstrated that the patients with low-risk scores may respond better to the immunotherapy, thereby achieving more satisfactory clinical outcomes.

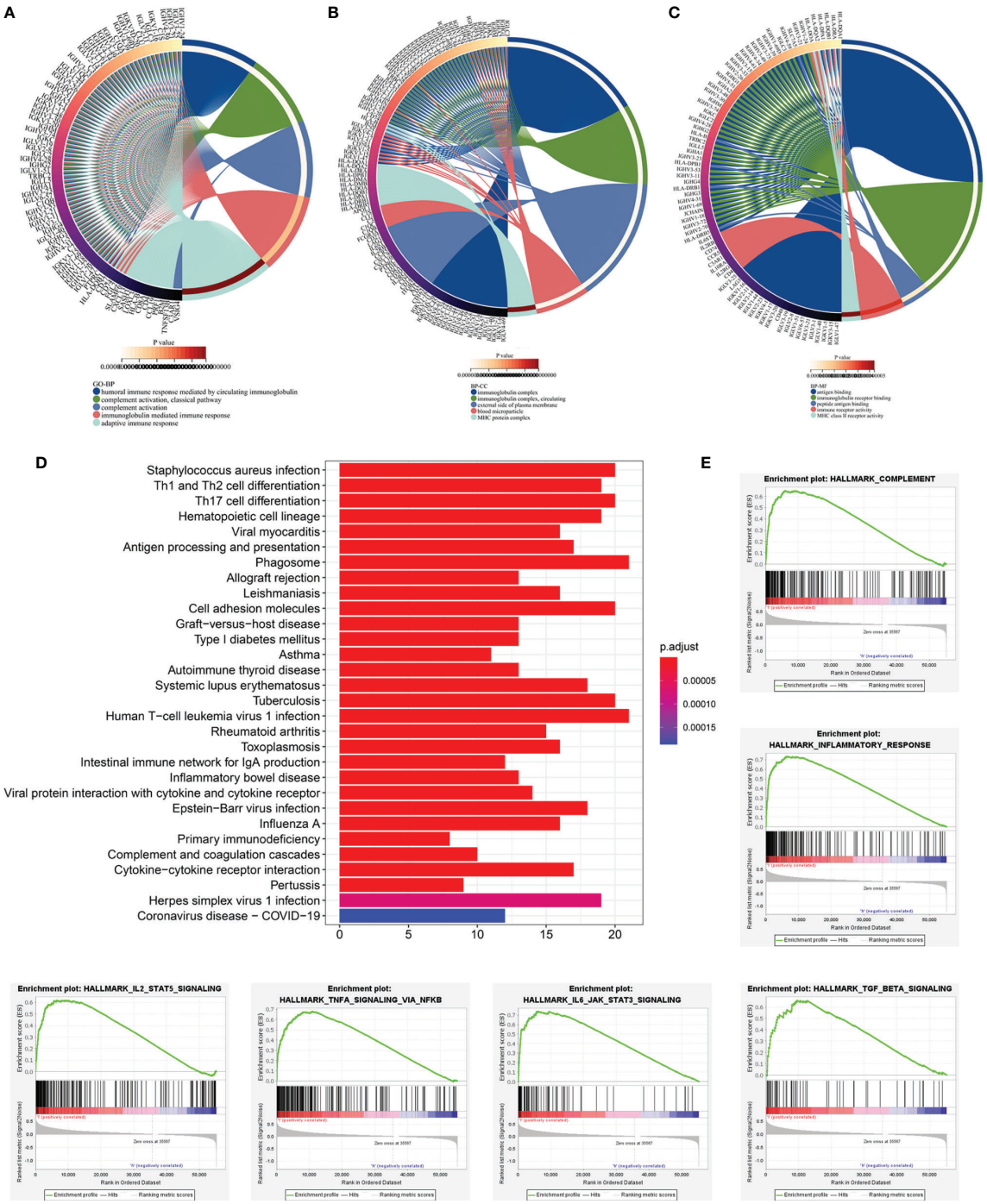

FIGURE 8 | Functional enrichment analyses of DEGs between low-and high-risk subgroups based on LRG signature. Go annotation terms of DEGs between low- and high-risk subgroups for biological process **(A)**, cellular components **(B)**, and molecular functions **(C)**. **(D)** KEGG enrichment analysis for DEGs between low-and high-risk subgroups. **(E)** GSEA findings.

DISCUSSION

In our study, we aimed to identify an expression pattern of LRGs, their prognostic value, their impact on the TME, and immunotherapeutic responses in SKCM. First, we identified 61 differentially expressed LRGs by comparing the gene expressions between the SCKM and normal tissues. GO and KEGG enrichment analyses were performed based on these

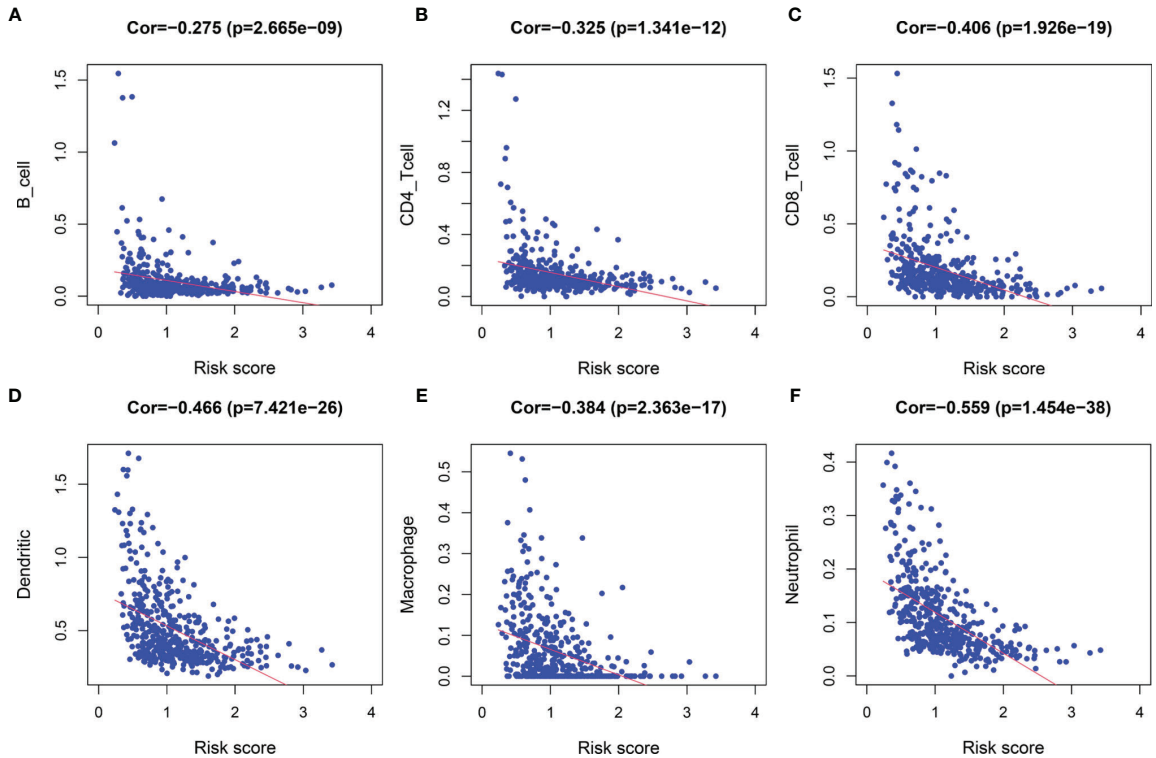

FIGURE 9 | The correlation between the signature and infiltration abundances of six immune cell types. **(A)** B cells, **(B)** CD4+ T cells, **(C)** CD8+ T cells, **(D)** Dendritic cells, **(E)** Macrophages, and **(F)** Neutrophils.

differentially expressed LRGs and the results showed that they were mainly involved in the processes related to energy metabolism. A previous study validates this typical characteristic of tumors, the abnormal energy metabolism, which is substantially different from normal tissues (36). Most tumor cells are highly dependent on aerobic glycolysis, and the remodeling of cellular energy metabolism pathways provides cancer cells with important metabolites, thereby potentiating large-scale biosynthesis, abnormal proliferation, and supporting tumorigenesis. Thus, the inhibition of this metabolic network may serve as a promising therapeutic strategy to selectively kill tumor cells (37).

To further elucidate the relationship between the aforementioned LRGs and survival of patients with SKCM, we determined three subtypes of SKCM, cluster 1, cluster 2, and cluster3, by a consensus clustering method based on the expression profiles of 184 LRGs. The diverse subtypes significantly affected the OS and showed significant differences in clinicopathological features. Specifically, the cases in cluster 2 had poorer prognoses, higher T stage, and with ulceration relative to clusters 1 and 3. Herein, we speculated that lactate metabolism was implicated in the disease progression and clinical outcomes of patients with SKCM.

Next, to evaluate the predictive effect of the LRGs, we constructed a six-LRG prognostic signature by combining Cox regression and Lasso Cox regression analyses. Among the six LRGs, SLC25A3, HPDL, NDUFA13, and NARS2 were risk-associated genes with poorer clinical outcomes, while ISCU and MTO1 were protective factors associated with longer survival duration. Further, we divided the cases into high- and low-risk groups based on the median risk score. As expected, the results of survival analysis were consistent, and the high-risk group presented a significantly worse OS than the low-risk group. Similar results were obtained for the stratified survival analyses among various subgroups. We also observed that SKCM patients belonging to the high-risk group were associated with certain risk factors, for disease progression, including advanced T stage, >5mm Breslow depth, IV-V Clark level, with ulceration, and distant metastases. Univariate and multivariate Cox regression analyses indicated that the signature was an independent risk factor for survival in SKCM.

Some of these six genes comprising the LRG signature have been reported concerning oncogenesis and tumor development. SLC25A3 is a mitochondrial phosphate carrier protein that plays a pivotal role in the aerobic synthesis of the adenosine triphosphate (ATP) (38). Accumulating evidence indicates that homozygous mutations in SLC25A3 are correlated with generalized disorders in mitochondrial-energy metabolism and multisystemic clinical presentation; its high expression is associated negatively with the survival of patients with osteosarcoma (39, 40). 4-hydroxyphenylpyruvate dioxygenase-like protein, HPDL, is a mitochondrial intermembrane space-

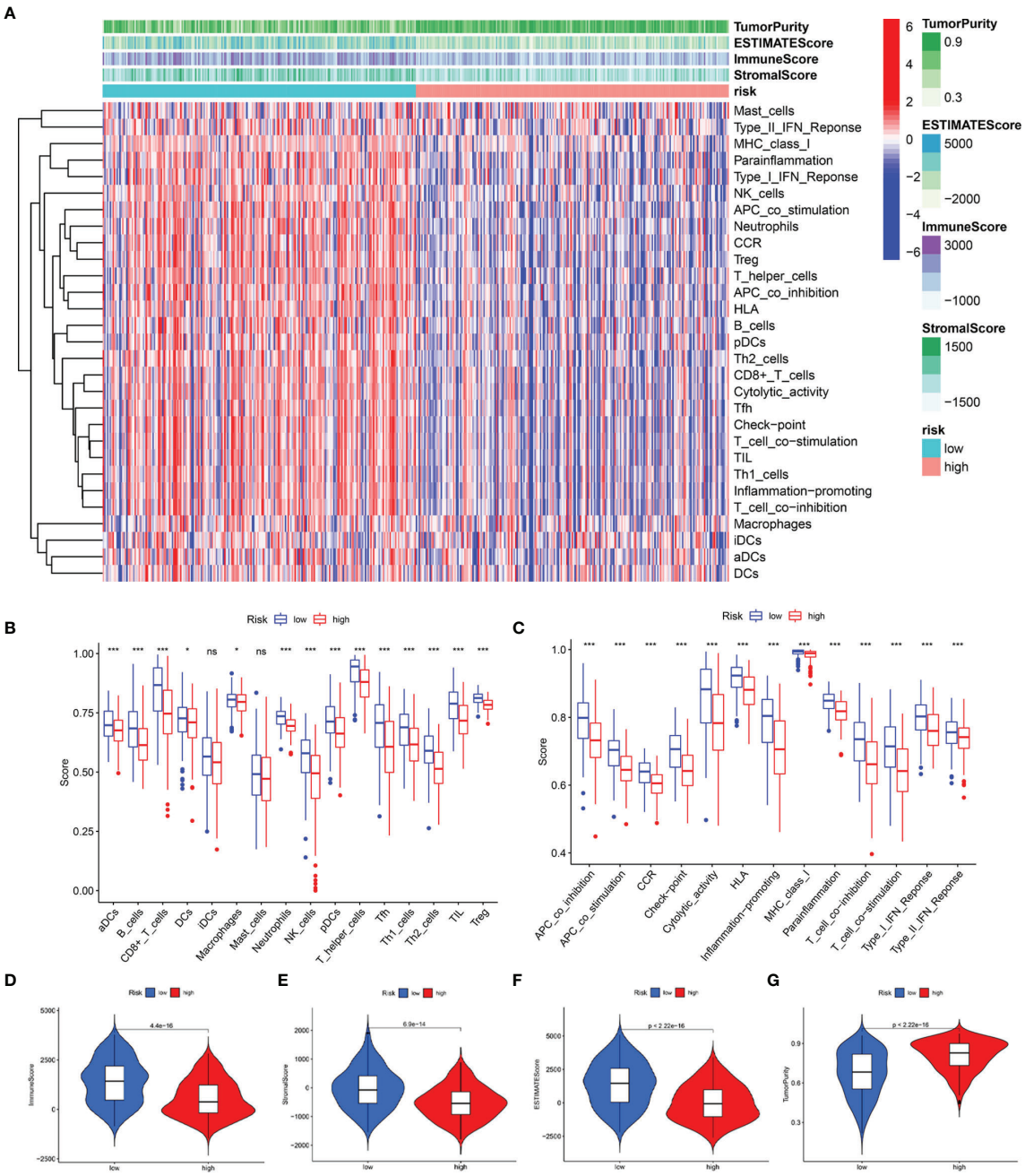

FIGURE 10 | Predicted evaluation of immune microenvironment characteristics. **(A)** Heatmap indicates the scores for tumor purity and the tumor microenvironment between the low- and high-risk groups. **(B)** The differences in the proportions of 16 immune cells between the low- and high-risk groups. **(C)** The differences in the proportions of 13 immune-related pathways between the low- and high-risk groups. The distributions of the immune score **(D)**, stromal score **(E)**, ESTIMATE score **(F)**, and tumor purity **(G)** between the low-and high-risk groups *P < 0.05; ***P < 0.001; ns, no significance.

localized protein that functions as 4-hydroxyphenylpyruvate dioxygenase. It positively regulates mitochondrial bioenergetic processes and ATP generation (41). Meanwhile, HPDL supports tumorigenesis in pancreatic ductal adenocarcinoma in a glutamine metabolism-dependent manner (42). NDUFA13 is a newly identified accessory subunit of mitochondria complex I with a unique molecular structure and a localization that is very close to the subunits of complex I responsible for low electrochemical potential (43). Additionally, it is related to cellular apoptosis in breast cancer (44), the recurrence of prostate cancer (45), and development of squamous cell carcinoma (46). NARS2 is a mitochondrial aminoacyl-tRNA

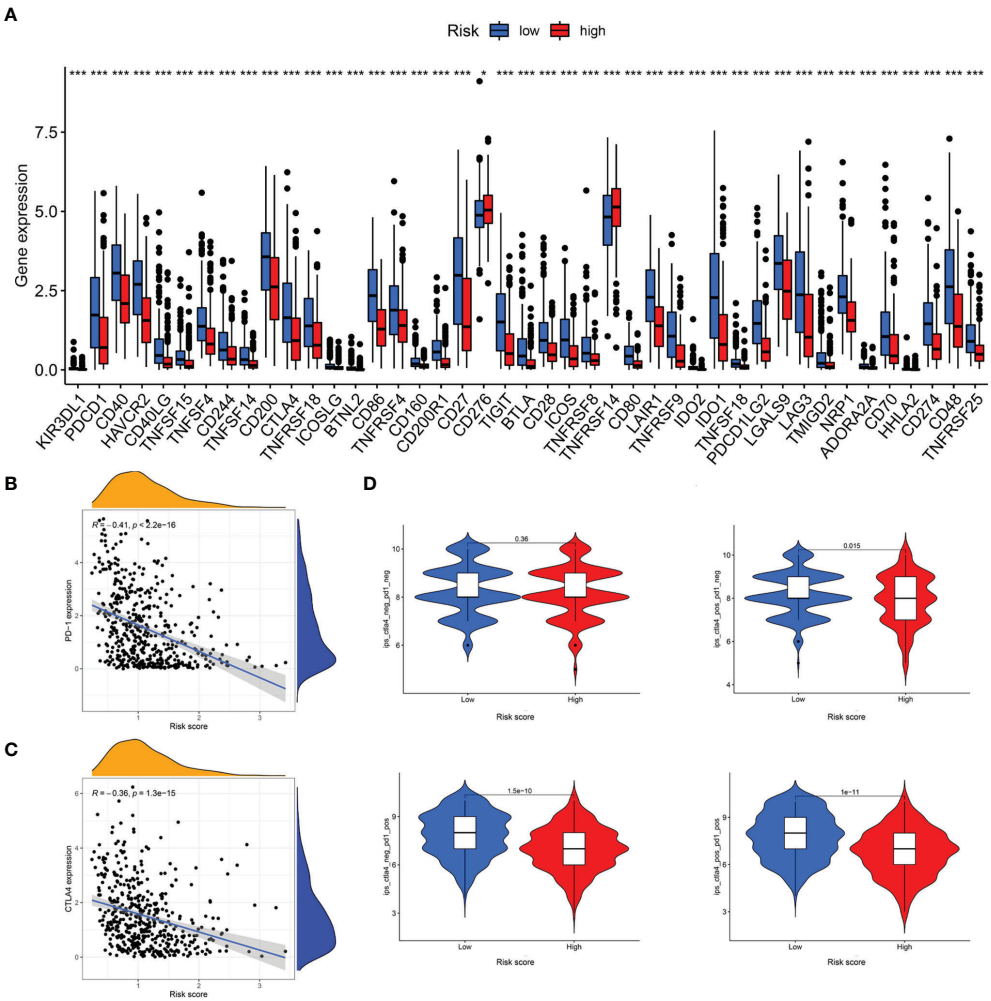

FIGURE 11 | Analysis of immunotherapeutic responses between different risk groups. **(A)** Expression of ICIs in different risk groups. **(B)** The correlation between risk score and PD-1 expression. **(C)** The correlation between risk score and CTLA4 expression. **(D)** IPS scoring scheme estimates the potential responses to immunotherapy in different risk groups *P < 0.05; ***P < 0.001.

synthetase gene, which encodes a member of the class II family of aminoacyl-tRNA synthetases (47). Mutations in this gene are reported to cause genetic disorders related to neurodegeneration, presenting various clinical features, including refractory seizures, rapid brain atrophy (48), Leigh syndrome, or/and Alpers' syndrome (49). Its conjoined expression with GAB2 is a risk factor of non- Hodgkin B-cell lymphoma (50). The iron-sulfur cluster assembly protein, ISCU, is engaged in the transportation of iron-sulfur clusters in mitochondrial complex I enzymes, and also functions in mitochondrial respiration for the energy generation (51). Downregulation of ISCU ultimately disrupts mitochondrial energy metabolism, increases the production of mitochondrial reactive oxygen species (ROS), and enhances cell death through the inhibition of complex I. Chen et al. demonstrate that highly upregulated miR-210 can attenuate mitochondrial respiration, thereby resulting in the production of ROS and lactate generation by targeting ISCU, ultimately facilitating the survival of colon cancer cells under a hypoxic microenvironment (52). MTO1 is a mitochondrial tRNA-modifying enzyme that is reported to be a pathogenic factor for mitochondrial disorders (53). However, its expression profile and regulatory mechanisms in cancer have not yet been reported.

Furthermore, we developed the nomogram to quantitatively estimate the 1-, 3-, and 5- year survival probabilities for patients with SKCM by integrating four independent prognostic features, including the risk score. We verified the biological functions related to the prognostic LRG signature through the functional enrichment analysis of 252 DRGs. The results of GO and KEGG enrichment analyses showed that the biological functions were mostly implicated in immune-relevant processes and pathways. Based on the enrichment analysis of the hallmark pathways in diverse risk groups by GSEA, we found that most immune-related signaling pathways were markedly upregulated in the low-risk group, in line with our expectations. Therefore, we

speculated that lactate metabolism was closely associated with immune-related processes and signaling pathways, thereby indicating its importance in the progression of SKCM.

As metastatic melanoma is characterized by lymphoid infiltration, it is typically regarded as an immunogenic tumor (54). Therefore, immunotherapy is a prospective therapeutic strategy for metastatic melanoma in addition to surgery, chemotherapy, and target therapy. However, a successful mechanism of action underlying responses to immunological strategy involves several factors, both intrinsic and extrinsic to the cancer cells (55). One of the crucial factors is certainly the TME. Accumulating evidence demonstrates that the biologically significant interaction between tumor tissues and the surrounding microenvironment extensively influences all the phases of the tumorigenic processes (56). Specifically, TME comprises stromal cells, immunocytes, and malignant cells, that collectively interplay with tumor cells and impose many challenges for the initiation, progression, and sensitivity/resistance against the immunotherapy (57). Additionally, a recent study shows that TME supporting tumor growth partly relies on its antitumor immune surveillance and this effect is in part sustained by the abnormal metabolism of tumor cells and cancer-associated fibroblasts in the microenvironment (58, 59).

Given these reasons, the activity of intracellular metabolic pathways of immune cells in TME has drawn widespread attention from researchers. Owing to their special metabolic mode, cancer cells tend to utilize glucose and produce excessive lactate even in an environment with a sufficient oxygen supply and release a large amount of lactate into the extracellular microenvironment, thereby causing acidosis, angiogenesis, and immunosuppression simultaneously (58). Consequently, this kind of metabolism modulation breaks the balance of the immune state in the tumor, resulting in an enhanced immunosuppressive effect by promoting the CD4+ CD25+ regulatory T (Treg) cell metabolic profiles and maintaining the acidity of the TME (60). However, excessive lactate attenuates the proliferation of immunocytes, including CD8+ T, natural killer (NK), and dendritic cells (61–63). Moreover, lactate potentiates the anti-inflammatory effects based on activation of the transformation of macrophages, thereby promoting angiogenesis, tissue remodeling, and finally accelerating tumor growth and invasion (63). Taken together, these results demonstrate that lactate in TME plays a key role in the disease progression and mediating the immunotherapeutic responses.

To date, immunotherapeutic strategies have concentrated on using monoclonal antibodies to activate cell-mediated immunity, also called ICIs (64). Although antibodies against CTLA4 and PD-1, used alone or in combination, both can exert a certain curative effect on the unresectable or metastatic melanoma, the clinical benefits remain unsatisfactory owing to the relatively low ORRs and the phenomenon of drug-resistance (65). Thus, the factors that influence clinical effects and drug resistance of immune strategies should be identified. A previous study demonstrates that the PD-L1 status in the tumor is a biomarker that reflects the response or resistance to ICIs, which was consistent with our conclusion (66). Furthermore, some comprehensive studies have revealed a mechanistically meaningful role of targeting TME, evidenced by the positive association of the 'T-cell-inflamed tumor microenvironment' with the effectiveness of diverse immune treatment (67–69).

In our study, we observed that the patients at low-risk tended to present better outcomes and immunotherapeutic responses due to their immune status owing to the TME as compared to the high-risk cases, therefore, in line with the same conclusion as the aforementioned scientific findings. Nevertheless, the main limitation to this study was the lack of experimental data to evaluate the specific mechanism underlying the biological behaviors. Additionally, large-scale multicenter trials are essential to validate the above findings for further clinical application.

In conclusion, we assessed the prognostic significance, effects on the TME, and response to ICIs of LGRs in SKCM. Three subgroups (clusters 1/2/3) identified by consensus clustering based on the expression patterns of LRGs, exhibited dissimilar clinical features. Risk stratification based on the lactate-related prognostic signature was negatively related to clinical prognoses and levels of infiltrating immunocytes in patients. Additionally, the model showed that the low-risk-score patients were likely to benefit more from ICI treatment. Collectively, our findings may be helpful to elucidate the lactate's role in the TME of SKCM. To sum up, the reconstructed prognostic signature may be applied clinically to survival improvement as well as offer a creative target for curing SKCM patients in the future.

DATA AVAILABILITY STATEMENT

Publicly available datasets were analyzed in this study. This data can be found here: https://portal.gdc.cancer.gov/, https://gtexportal.org/home/, and https://www.ncbi.nlm.nih.gov/.

ETHICS STATEMENT

The studies involving human participants were reviewed and approved by Third Affiliated Hospital of Sun Yat-Sen University. The patients/participants provided their written informed consent to participate in this study.

AUTHOR CONTRIBUTIONS

YX conceived, designed, and wrote the manuscript. JZ and ML assisted in specimen collection and performed experimental work. YZhang and QL were responsible for the data analysis and figures plotted. WL and YZheng helped with manuscript and data review. All authors contributed to the article and approved the submitted version.

SUPPLEMENTARY MATERIAL

The Supplementary Material for this article can be found online at: https://www.frontiersin.org/articles/10.3389/fonc.2022.818868/full#supplementary-material

REFERENCES

1. Rodriguez-Hernandez I, Maiques O, Kohlhammer L, Cantelli G, Perdrix-Rosell A, Monger J, et al. WNT11-FZD7-DAAM1 Signalling Supports Tumour Initiating Abilities and Melanoma Amoeboid Invasion. *Nat Commun* (2020) 11(1):5315. doi: 10.1038/s41467-020-18951-2
2. Rebecca VW, Somasundaram R, Herlyn M. Pre-Clinical Modeling of Cutaneous Melanoma. *Nat Commun* (2020) 11(1):2858. doi: 10.1038/s41467-020-15546-9
3. Lee JH, Han SH, Kim YM, Kim SH, Yoo ES, Woo JS, et al. Shikonin Inhibits Proliferation of Melanoma Cells by MAPK Pathway-Mediated Induction of Apoptosis. *Biosci Rep* (2021) 41(1). doi: 10.1042/bsr20203834
4. Vilgelm AE, Saleh N, Shattuck-Brandt R, Riemenschneider K, Slesur L, Chen SC, et al. MDM2 Antagonists Overcome Intrinsic Resistance to CDK4/6 Inhibition by Inducing P21. *Sci Trans Med* (2019) 11(505). doi: 10.1126/scitranslmed.aav7171
5. Huang RZ, Mao M, Zheng J, Liang HQ, Liu FL, Zhou GY, et al. Development of an Immune-Related Gene Pairs Index for the Prognosis Analysis of Metastatic Melanoma. *Sci Rep* (2021) 11(1):1253. doi: 10.1038/s41598-020-80858-1
6. Hamid O, Robert C, Daud A, Hodi FS, Hwu WJ, Kefford R, et al. Five-Year Survival Outcomes for Patients With Advanced Melanoma Treated With Pembrolizumab in KEYNOTE-001. *Ann Oncol: Off J Eur Soc Med Oncol* (2019) 30(4):582–8. doi: 10.1093/annonc/mdz011
7. Saad F, Shore N, Zhang T, Sharma S, Cho HK, Jacobs IA. Emerging Therapeutic Targets for Patients With Advanced Prostate Cancer. *Cancer Treat Rev* (2019) 76:1–9. doi: 10.1016/j.ctrv.2019.03.002
8. Hu-Lieskovan S, Bhaumik S, Dhodapkar K, Grivel JJB, Gupta S, Hanks BA, et al. SITC Cancer Immunotherapy Resource Document: A Compass in the Land of Biomarker Discovery. *J Immunother Cancer* (2020) 8(2). doi: 10.1136/jitc-2020-000705
9. Di Donato M, Zamagni A, Galasso G, Di Zazzo E, Giovannelli P, Barone MV, et al. The Androgen Receptor/Filamin A Complex as a Target in Prostate Cancer Microenvironment. *Cell Death Dis* (2021) 12(1):127. doi: 10.1038/s41419-021-03402-7
10. Clément-Colmou K, Potiron V, Pietri M, Guillonneau M, Jouglar E, Chiavassa S, et al. Influence of Radiotherapy Fractionation Schedule on the Tumor Vascular Microenvironment in Prostate and Lung Cancer Models. *Cancers* (2020) 12(1). doi: 10.3390/cancers12010121
11. Vinay DS, Ryan EP, Pawelec G, Talib WH, Stagg J, Elkord E, et al. Immune Evasion in Cancer: Mechanistic Basis and Therapeutic Strategies. *Semin Cancer Biol* (2015) 35 Suppl:S185–s98. doi: 10.1016/j.semcancer.2015.03.004
12. Yu Q, Wang Y, Dong L, He Y, Liu R, Yang Q, et al. Regulations of Glycolytic Activities on Macrophages Functions in Tumor and Infectious Inflammation. *Front Cell Infect Microbiol* (2020) 10:287. doi: 10.3389/fcimb.2020.00287
13. Angelin A, Gil-de-Gómez L, Dahiya S, Jiao J, Guo L, Levine MH, et al. Foxp3 Reprograms T Cell Metabolism to Function in Low-Glucose, High-Lactate Environments. *Cell Metab* (2017) 25(6):1282–93.e7. doi: 10.1016/j.cmet.2016.12.018
14. Koltai T. Cancer: Fundamentals Behind pH Targeting and the Double-Edged Approach. *OncoTargets Ther* (2016) 9:6343–60. doi: 10.2147/ott.s115438
15. Nakamura Y. Biomarkers for Immune Checkpoint Inhibitor-Mediated Tumor Response and Adverse Events. *Front Med* (2019) 6:119. doi: 10.3389/fmed.2019.00119
16. Ritchie ME, Phipson B, Wu D, Hu Y, Law CW, Shi W, et al. Limma Powers Differential Expression Analyses for RNA-Sequencing and Microarray Studies. *Nucleic Acids Res* (2015) 43(7):e47. doi: 10.1093/nar/gkv007
17. Jayawardana K, Schramm SJ, Haydu L, Thompson JF, Scolyer RA, Mann GJ, et al. Determination of Prognosis in Metastatic Melanoma Through Integration of Clinico-Pathologic, Mutation, mRNA, microRNA, and Protein Information. *Int J Cancer* (2015) 136(4):863–74. doi: 10.1002/ijc.29047
18. Subramanian A, Tamayo P, Mootha VK, Mukherjee S, Ebert BL, Gillette MA, et al. Gene Set Enrichment Analysis: A Knowledge-Based Approach for Interpreting Genome-Wide Expression Profiles. *Proc Natl Acad Sci USA* (2005) 102(43):15545–50. doi: 10.1073/pnas.0506580102
19. Szklarczyk D, Gable AL, Nastou KC, Lyon D, Kirsch R, Pyysalo S, et al. The STRING Database in 2021: Customizable Protein-Protein Networks, and Functional Characterization of User-Uploaded Gene/Measurement Sets. *Nucleic Acids Res* (2021) 49(D1):D605–d12. doi: 10.1093/nar/gkaa1074
20. Doncheva NT, Morris JH, Gorodkin J, Jensen LJ. Cytoscape StringApp: Network Analysis and Visualization of Proteomics Data. *J Proteome Res* (2019) 18(2):623–32. doi: 10.1021/acs.jproteome.8b00702
21. Yu G, Wang LG, Han Y, He QY. Clusterprofiler: An R Package for Comparing Biological Themes Among Gene Clusters. *Omics: J Integr Biol* (2012) 16 (5):284–7. doi: 10.1089/omi.2011.0118
22. Wilkerson MD, Hayes DN. ConsensusClusterPlus: A Class Discovery Tool With Confidence Assessments and Item Tracking. *Bioinf (Oxf Engl)* (2010) 26 (12):1572–3. doi: 10.1093/bioinformatics/btq170
23. Dong Y, Cheng Y, Tian W, Zhang H, Wang Z, Li X, et al. An Externally Validated Nomogram for Predicting Lymph Node Metastasis of Presumed Stage I and II Endometrial Cancer. *Front Oncol* (2019) 9:1218. doi: 10.3389/fonc.2019.01218
24. Iasonos A, Schrag D, Raj GV, Panageas KS. How to Build and Interpret a Nomogram for Cancer Prognosis. *J Clin Oncol: Off J Am Soc Clin Oncol* (2008) 26(8):1364–70. doi: 10.1200/jco.2007.12.9791
25. Li T, Fu J, Zeng Z, Cohen D, Li J, Chen Q, et al. TIMER2.0 for Analysis of Tumor-Infiltrating Immune Cells. *Nucleic Acids Res* (2020) 48(W1):W509–w14. doi: 10.1093/nar/gkaa407
26. Newman AM, Liu CL, Green MR, Gentles AJ, Feng W, Xu Y, et al. Robust Enumeration of Cell Subsets From Tissue Expression Profiles. *Nat Methods* (2015) 12(5):453–7. doi: 10.1038/nmeth.3337
27. Finotello F, Mayer C, Plattner C, Laschober G, Rieder D, Hackl H, et al. Molecular and Pharmacological Modulators of the Tumor Immune Contexture Revealed by Deconvolution of RNA-Seq Data. *Genome Med* (2019) 11(1):34. doi: 10.1186/s13073-019-0638-6
28. Becht E, Giraldo NA, Lacroix L, Buttard B, Elarouci N, Petitprez F, et al. Estimating the Population Abundance of Tissue-Infiltrating Immune and Stromal Cell Populations Using Gene Expression. *Genome Biol* (2016) 17 (1):218. doi: 10.1186/s13059-016-1070-5
29. Aran D, Hu Z, Butte AJ. Xcell: Digitally Portraying the Tissue Cellular Heterogeneity Landscape. *Genome Biol* (2017) 18(1):220. doi: 10.1186/s13059-017-1349-1
30. Racle J, Gfeller D. EPIC: A Tool to Estimate the Proportions of Different Cell Types From Bulk Gene Expression Data. *Methods Mol Biol (Clifton NJ)* (2020) 2120:233–48. doi: 10.1007/978-1-0716-0327-7_17
31. Hänzelmann S, Castelo R, Guinney J. GSVA: Gene Set Variation Analysis for Microarray and RNA-Seq Data. *BMC Bioinf* (2013) 14:7. doi: 10.1186/1471-2105-14-7
32. Yoshihara K, Shahmoradgoli M, Martínez E, Vegesna R, Kim H, Torres-Garcia W, et al. Inferring Tumour Purity and Stromal and Immune Cell Admixture From Expression Data. *Nat Commun* (2013) 4:2612. doi: 10.1038/ncomms3612
33. Xu L, Yu W, Xiao H, Lin K. BIRC5 Is a Prognostic Biomarker Associated With Tumor Immune Cell Infiltration. *Sci Rep* (2021) 11(1):390–. doi: 10.1038/s41598-020-79736-7
34. Charoentong P, Finotello F, Angelova M, Mayer C, Efremova M, Rieder D, et al. Pan-Cancer Immunogenomic Analyses Reveal Genotype-Immunophenotype Relationships and Predictors of Response to Checkpoint Blockade. *Cell Rep* (2017) 18(1):248–62. doi: 10.1016/j.celrep.2016.12.019
35. Xiang G, Dong X, Xu T, Feng Y, He Z, Ke C, et al. A Nomogram for Prediction of Postoperative Pneumonia Risk in Elderly Hip Fracture Patients. *Risk Manage Healthcare Policy* (2020) 13:1603–11. doi: 10.2147/rmhp.s270326
36. Fan T, Sun G, Sun X, Zhao L, Zhong R, Peng Y. Tumor Energy Metabolism and Potential of 3-Bromopyruvate as an Inhibitor of Aerobic Glycolysis: Implications in Tumor Treatment. *Cancers* (2019) 11(3). doi: 10.3390/cancers11030317
37. Phan LM, Yeung SC, Lee MH. Cancer Metabolic Reprogramming: Importance, Main Features, and Potentials for Precise Targeted Anti-Cancer Therapies. *Cancer Biol Med* (2014) 11(1):1–19. doi: 10.7497/j.issn.2095-3941.2014.01.001
38. Mayr JA, Merkel O, Kohlwein SD, Gebhardt BR, Böhles H, Fötschl U, et al. Mitochondrial Phosphate-Carrier Deficiency: A Novel Disorder of Oxidative Phosphorylation. *Am J Hum Genet* (2007) 80(3):478–84. doi: 10.1086/511788
39. Seifert EL, Gál A, Acoba MG, Li Q, Anderson-Pullinger L, Golenár T, et al. Natural and Induced Mitochondrial Phosphate Carrier Loss: DIFFERENTIAL

DEPENDENCE OF MITOCHONDRIAL METABOLISM AND DYNAMICS AND CELL SURVIVAL ON THE EXTENT OF DEPLETION. *J Biol Chem* (2016) 291(50):26126–37. doi: 10.1074/jbc.M116.744714
40. Mayr JA, Zimmermann FA, Horváth R, Schneider HC, Schoser B, Holinski-Feder E, et al. Deficiency of the Mitochondrial Phosphate Carrier Presenting as Myopathy and Cardiomyopathy in a Family With Three Affected Children. *Neuromuscular Disord: NMD* (2011) 21(11):803–8. doi: 10.1016/j.nmd.2011.06.005
41. Husain RA, Grimmel M, Wagner M, Hennings JC, Marx C, Feichtinger RG, et al. Bi-Allelic HPDL Variants Cause a Neurodegenerative Disease Ranging From Neonatal Encephalopathy to Adolescent-Onset Spastic Paraplegia. *Am J Hum Genet* (2020) 107(2):364–73. doi: 10.1016/j.ajhg.2020.06.015
42. Ye X, Wei X, Liao J, Chen P, Li X, Chen Y, et al. 4-Hydroxyphenylpyruvate Dioxygenase-Like Protein Promotes Pancreatic Cancer Cell Progression and Is Associated With Glutamine-Mediated Redox Balance. *Front Oncol* (2020) 10:617190. doi: 10.3389/fonc.2020.617190
43. Hu H, Nan J, Sun Y, Zhu D, Xiao C, Wang Y, et al. Electron Leak From NDUFA13 Within Mitochondrial Complex I Attenuates Ischemia-Reperfusion Injury *via* Dimerized STAT3. *Proc Natl Acad Sci USA* (2017) 114(45):11908–13. doi: 10.1073/pnas.1704723114
44. Angell JE, Lindner DJ, Shapiro PS, Hofmann ER, Kalvakolanu DV. Identification of GRIM-19, a Novel Cell Death-Regulatory Gene Induced by the Interferon-Beta and Retinoic Acid Combination, Using a Genetic Approach. *J Biol Chem* (2000) 275(43):33416–26. doi: 10.1074/jbc.M003929200
45. Rui X, Shao S, Wang L, Leng J. Identification of Recurrence Marker Associated With Immune Infiltration in Prostate Cancer With Radical Resection and Build Prognostic Nomogram. *BMC Cancer* (2019) 19(1):1179. doi: 10.1186/s12885-019-6391-9
46. Kalakonda S, Nallar SC, Jaber S, Keay SK, Rorke E, Munivenkatappa R, et al. Monoallelic Loss of Tumor Suppressor GRIM-19 Promotes Tumorigenesis in Mice. *Proc Natl Acad Sci USA* (2013) 110(45):E4213–22. doi: 10.1073/pnas.1303760110
47. Seaver LH, DeRoos S, Andersen NJ, Betz B, Prokop J, Lannen N, et al. Lethal NARS2-Related Disorder Associated With Rapidly Progressive Intractable Epilepsy and Global Brain Atrophy. *Pediatr Neurol* (2018) 89:26–30. doi: 10.1016/j.pediatrneurol.2018.07.014
48. Mizuguchi T, Nakashima M, Kato M, Yamada K, Okanishi T, Ekhilevitch N, et al. PARS2 and NARS2 Mutations in Infantile-Onset Neurodegenerative Disorder. *J Hum Genet* (2017) 62(5):525–9. doi: 10.1038/jhg.2016.163
49. Lee JS, Yoo T, Lee M, Lee Y, Jeon E, Kim SY, et al. Genetic Heterogeneity in Leigh Syndrome: Highlighting Treatable and Novel Genetic Causes. *Clin Genet* (2020) 97(4):586–94. doi: 10.1111/cge.13713
50. Vasta V, Merritt JL2nd, Saneto RP, Hahn SH. Next-Generation Sequencing for Mitochondrial Diseases: A Wide Diagnostic Spectrum. *Pediatr Int: Off J Jpn Pediatr Soc* (2012) 54(5):585–601. doi: 10.1111/j.1442-200X.2012.03644.x
51. Ma Q, Dasgupta C, Li Y, Huang L, Zhang L. MicroRNA-210 Downregulates ISCU and Induces Mitochondrial Dysfunction and Neuronal Death in Neonatal Hypoxic-Ischemic Brain Injury. *Mol Neurobiol* (2019) 56(8):5608–25. doi: 10.1007/s12035-019-1491-8
52. Chen Z, Li Y, Zhang H, Huang P, Luthra R. Hypoxia-Regulated microRNA-210 Modulates Mitochondrial Function and Decreases ISCU and COX10 Expression. *Oncogene* (2010) 29(30):4362–8. doi: 10.1038/onc.2010.193
53. Kim TW, Kim B, Kim JH, Kang S, Park SB, Jeong G, et al. Nuclear-Encoded Mitochondrial MTO1 and MRPL41 Are Regulated in an Opposite Epigenetic Mode Based on Estrogen Receptor Status in Breast Cancer. *BMC Cancer* (2013) 13:502. doi: 10.1186/1471-2407-13-502
54. Failla CM, Carbone ML, Fortes C, Pagnanelli G, D'Atri S. Melanoma and Vitiligo: In Good Company. *Int J Mol Sci* (2019) 20(22). doi: 10.3390/ijms20225731
55. Lai C, Duan S, Ye F, Hou X, Li X, Zhao J, et al. The Enhanced Antitumor-Specific Immune Response With Mannose- and CpG-ODN-Coated Liposomes Delivering TRP2 Peptide. *Theranostics* (2018) 8(6):1723–39. doi: 10.7150/thno.22056
56. Landi L, D'Incà F, Gelibter A, Chiari R, Grossi F, Delmonte A, et al. Bone Metastases and Immunotherapy in Patients With Advanced Non-Small-Cell Lung Cancer. *J Immunother Cancer* (2019) 7(1):316. doi: 10.1186/s40425-019-0793-8
57. Bian C, Wang Y, Lu Z, An Y, Wang H, Kong L, et al. ImmunoAIzer: A Deep Learning-Based Computational Framework to Characterize Cell Distribution and Gene Mutation in Tumor Microenvironment. *Cancers* (2021) 13(7). doi: 10.3390/cancers13071659
58. Ho YJ, Chu SW, Liao EC, Fan CH, Chan HL, Wei KC, et al. Normalization of Tumor Vasculature by Oxygen Microbubbles With Ultrasound. *Theranostics* (2019) 9(24):7370–83. doi: 10.7150/thno.37750
59. Morén A, Bellomo C, Tsubakihara Y, Kardassis D, Mikulits W, Heldin CH, et al. Lxrα Limits Tgfβ-Dependent Hepatocellular Carcinoma Associated Fibroblast Differentiation. *Oncogenesis* (2019) 8(6):36. doi: 10.1038/s41389-019-0140-4
60. Dastmalchi F, Deleyrolle LP, Karachi A, Mitchell DA, Rahman M. Metabolomics Monitoring of Treatment Response to Brain Tumor Immunotherapy. *Front Oncol* (2021) 11:691246. doi: 10.3389/fonc.2021.691246
61. Haas R, Smith J, Rocher-Ros V, Nadkarni S, Montero-Melendez T, D'Acquisto F, et al. Lactate Regulates Metabolic and Pro-Inflammatory Circuits in Control of T Cell Migration and Effector Functions. *PloS Biol* (2015) 13(7):e1002202. doi: 10.1371/journal.pbio.1002202
62. Grote S, Ureña-Bailén G, Chan KC, Baden C, Mezger M, Handgretinger R, et al. *In Vitro* Evaluation of CD276-CAR NK-92 Functionality, Migration and Invasion Potential in the Presence of Immune Inhibitory Factors of the Tumor Microenvironment. *Cells* (2021) 10(5). doi: 10.3390/cells10051020
63. Certo M, Tsai CH, Pucino V, Ho PC, Mauro C. Lactate Modulation of Immune Responses in Inflammatory Versus Tumour Microenvironments. *Nat Rev Immunol* (2021) 21(3):151–61. doi: 10.1038/s41577-020-0406-2
64. Merino M, Lozano T, Casares N, Lana H, Troconiz IF, Ten Hagen TLM, et al. Dual Activity of PD-L1 Targeted Doxorubicin Immunoliposomes Promoted an Enhanced Efficacy of the Antitumor Immune Response in Melanoma Murine Model. *J Nanobiotechnol* (2021) 19(1):102. doi: 10.1186/s12951-021-00846-z
65. Wang Z, Wu X. Study and Analysis of Antitumor Resistance Mechanism of PD1/PD-L1 Immune Checkpoint Blocker. *Cancer Med* (2020) 9(21):8086–121. doi: 10.1002/cam4.3410
66. Izumi M, Sawa K, Oyanagi J, Noura I, Fukui M, Ogawa K, et al. Tumor Microenvironment Disparity in Multiple Primary Lung Cancers: Impact of Non-Intrinsic Factors, Histological Subtypes, and Genetic Aberrations. *Trans Oncol* (2021) 14(7):101102. doi: 10.1016/j.tranon.2021.101102
67. Koelzer VH, Sokol L, Zahnd S, Christe L, Dawson H, Berger MD, et al. Digital Analysis and Epigenetic Regulation of the Signature of Rejection in Colorectal Cancer. *Oncoimmunology* (2017) 6(4):e1288330. doi: 10.1080/2162402x.2017.1288330
68. Xie XH, Wang LQ, Qin YY, Lin XQ, Xie ZH, Liu M, et al. Clinical Features, Treatment, and Survival Outcome of Primary Pulmonary NUT Midline Carcinoma. *Orphanet J Rare Dis* (2020) 15(1):183. doi: 10.1186/s13023-020-01449-x
69. Danaher P, Warren S, Lu R, Samayoa J, Sullivan A, Pekker I, et al. Pan-Cancer Adaptive Immune Resistance as Defined by the Tumor Inflammation Signature (TIS): Results From The Cancer Genome Atlas (TCGA). *J Immunother Cancer* (2018) 6(1):63. doi: 10.1186/s40425-018-0367-1

Conflict of Interest: The authors declare that the research was conducted in the absence of any commercial or financial relationships that could be construed as a potential conflict of interest.

frontiers in Oncology

ORIGINAL RESEARCH
published: 08 March 2022
doi: 10.3389/fonc.2022.844666

Identification of Novel Molecular Therapeutic Targets and Their Potential Prognostic Biomarkers Based on Cytolytic Activity in Skin Cutaneous Melanoma

Haoxue Zhang[1,2,3†], *Yuyao Liu*[4†], *Delin Hu*[4*] and *Shengxiu Liu*[1,2,3*]

[1] Department of Dermatovenerology, The First Affiliated Hospital of Anhui Medical University, Hefei, China, [2] Key Laboratory of Dermatology, Ministry of Education, Hefei, China, [3] Inflammation and Immune Mediated Diseases Laboratory of Anhui Province, Anhui Medical University, Hefei, China, [4] Department of Burns, The First Affiliated Hospital of Anhui Medical University, Hefei, China

Skin cutaneous melanoma (SKCM) attracts attention worldwide for its extremely high malignancy. A novel term cytolytic activity (CYT) has been introduced as a potential immunotherapy biomarker associated with counter-regulatory immune responses and enhanced prognosis in tumors. In this study, we extracted all datasets of SKCM patients, namely, RNA sequencing data and clinical information from The Cancer Genome Atlas (TCGA) database and the Gene Expression Omnibus (GEO) database, conducted differential expression analysis to yield 864 differentially expressed genes (DEGs) characteristic of CYT and used non-negative matrix factorization (NMF) method to classify molecular subtypes of SKCM patients. Among all genes, 14 hub genes closely related to prognosis for SKCM were finally screen out. Based on these genes, we constructed a 14-gene prognostic risk model and its robustness and strong predictive performance were further validated. Subsequently, the underlying mechanisms in tumor pathogenesis and prognosis have been defined from a number of perspectives, namely, tumor mutation burden (TMB), copy number variation (CNV), tumor microenvironment (TME), infiltrating immune cells, gene set enrichment analysis (GSEA) and immune checkpoint inhibitors (ICIs). Furthermore, combined with GTEx database and HPA database, the expression of genes in the model was verified at the transcriptional level and protein level, and the relative importance of genes in the model was described by random forest algorithm. In addition, the model was used to predict the difference in sensitivity of SKCM patients to chemotherapy and immunotherapy. Finally, a nomogram was constructed to better aid clinical diagnosis.

Keywords: skin cutaneous melanoma, cytolytic activity, genes, prognosis, therapies, clinical guidelines

OPEN ACCESS

Edited by:
Gagan Chhabra, University of Wisconsin-Madison, United States

Reviewed by:
Shengqin Su, Shanghai Hengrui Pharmaceutical Co., Ltd., China
Carolina Constantin, Victor Babes National Institute of Pathology (INCDVB), Romania

***Correspondence:**
Delin Hu
hdl0522@163.com
Shengxiu Liu
liushengxiu@ahmu.edu.cn

†*These authors have contributed equally to this work and share first authorship*

Specialty section:
This article was submitted to Skin Cancer, a section of the journal Frontiers in Oncology

Received: *28 December 2021*
Accepted: *09 February 2022*
Published: *08 March 2022*

Citation:
Zhang H, Liu Y, Hu D and Liu S (2022) Identification of Novel Molecular Therapeutic Targets and Their Potential Prognostic Biomarkers Based on Cytolytic Activity in Skin Cutaneous Melanoma. Front. Oncol. 12:844666. doi: 10.3389/fonc.2022.844666

INTRODUCTION

Skin cutaneous melanoma (SKCM) is one of the most lethiferous malignancies. Though SKCM only constitutes ~5% of all skin cancers, it accounts for >75% of skin cancer deaths (1). Currently, most melanomas are removed *via* the standard surgical technique that excises both the tumor and a margin of normal appearing skin (2). Unfortunately, surgical resection offers so little in the management of individuals with regional or distant metastases (3). Adjuvant therapies, such as radiotherapy, immunotherapy, biochemotherapy, can possibly benefit postoperative patients (4). But the conventional treatments have not improved the outcomes of SKCM, which may be due to the hypo-responsiveness and inherent resistance of melanoma cells (5). Immunotherapy has promised an optimizing future for SKCM in recent years (6–8), managing to enhance the prognosis of SKCM patients. Though it has shown great clinical effect, only a small percentage of patients profit by long-range treatment (9). Many factors like the tumor types (10), and age (11) have potential influence on the efficacy. Therefore, establishment of an efficient prognosis model is essential, and it can direct clinical treatment of SKCM patients.

Immune checkpoints refer to a plethora of inhibitory pathways hardwired into the immune system that are crucial for maintaining self-tolerance and regulating the strength of the peripheric immune system to minimize collateral tissue damage, realizing immune evasion in tumors (12). Therefore, immune checkpoint inhibitors (ICIs) are emerging as a promising antitumor immunotherapy. ICIs are able to unleash anti-tumor immunity and mediate durable cancer regressions (13) *via* inhibition of pathways like the cytotoxic T-lymphocyte-associated protein 4 (CTLA-4), programmed cell death-1 (PD-1), and programmed cell death ligand-1 (PD-L1). Elevated evidences have substantiated the use of ICIs in SKCM (14), starting with the earliest approval of an anti-CTLA-4 drug called ipilimumab for advanced-stage melanoma in 2011 (15). Currently, pembrolizumab and nivolumab, both inhibitors of PD-1, also are popularly used in clinical. Combination ICI therapy has shown unprecedented, long-lasting survival benefits in the treatment of metastatic melanoma (16). However, despite the impressive effects, a large proportion of patients do not respond to these drugs. A key challenge is to understand the variability of immune responses to ICIs. Granule exocytosis (perforin and granzymes) is considered as one of main pathways involved in cytotoxic lymphocyte-mediated tumor cell death, and it plays a crucial role in killing cancer cells during cancer immunosurveillance and immunotherapy (17). Michael et al. innovatively designed the cytolytic activity (CYT) score based on expression levels of granzyme A (GZMA) and perforin (PRF1) that relates with immune responses to ICIs immunotherapies and predicts prognosis (18). Zaravinos et al. once investigated that the CYT-high subgroup in colorectal cancer can be benefited to a higher percentage from ICIs immunotherapies (19). So, it is potentially valuable to explore genes related to CYT and define its ultimate effect.

Thus, on the whole, in this article, we probed the RNA sequence data from 446 SKCM specimens to find that CYT was a valuable prognostic biomarker for patients with SKCM. We also discovered that CYT may regulate tumor mechanism in many ways, which provides new ideas for the immunotherapy on SKCM.

Abbreviations: SKCM, skin cutaneous melanoma; CYT, cytolytic activity; TCGA, The Cancer Genome Atlas; GEO, Gene Expression Omnibus; DEG, differentially expressed genes; NMF, non-negative matrix factorization; TMB, tumor mutation burden; CNV, copy number variation; TME, tumor microenvironment; GSEA, gene set enrichment analysis; ICIs, immune checkpoint inhibitors; CTLA-4, cytotoxic T-lymphocyte-associated protein 4; PD-1, programmed cell death-1; PD-L1, programmed cell death ligand-1; GZMA, granzyme A; PRF1, perforin; OS, overall survival; DSS, disease specific survival; PFS. progression-free-survival; CYTRG, CYT-related gene; GSVA, gene set variation analysis; ESTIMATE, estimation of stromal and immune cells in malignant tumor tissues using expression data; MCP-counter, microenvironment cell populations-counter; TNM, tumor-node-metastasis; ROC, receiver operator characteristic curve; CCM, calibration curve method; PCA, principal component analysis; DCA, decision curve analysis; C-index, concordance index; RMS, restricted mean survival; IC50, half maximal inhibitory concentration; GDSC, genomics of drug sensitivity in cancer; IPS, immunophenoscore; TCIA, the cancer immunome database; HPA, human protein atlas; MAF, mutation annotation format; HRs, hazard ratios; CIs, confidence intervals; AUC, area under curve; IHC, immunohistochemical; NMI, N-Myc interactor; GBP, guanine-binding protein; IFN-γ, interferon- γ; TYRP1, tyrosinase related protein 1; IFITM, interferon-induced transmembrane; CAMs, cell adhesion molecules; DCs, dendritic cells.

MATERIALS AND METHODS

Collection of SKCM Samples and Datasets

As conducting this research, several datasets from public databases were used. We downloaded the HTSeq-FPKM gene expression data and corresponding clinical information of all SKCM patients from the official website of the TCGA database (https://www.cancer.gov). We collected 472 samples in total (namely, one normal tissue sample and 471 SKCM tissue samples). Cases with incomplete clinical data were excluded. Finally, a total of 446 patients with full follow-up information were enrolled. In the process of further validation, we employed GSE65904 and GSE54467 matrices from the public repository of the Gene Expression Omnibu (GEO) (https://www.ncbi.nlm.nih.gov/geo/).

Evaluation of the Prognostic Value of CYT

In order to clearly define the prognostic value of CYT in SKCM, we performed KM survival analysis (an event dependent analyzing form to provide more accurate measurement of survival rates at different intervals (20)) and univariate Cox regression analysis on the overall survival (OS), disease specific survival (DSS), and progression-free-survival (PFS) of patients in the TCGA-SKCM dataset. We also combined results derived from the univariate Cox regression analysis of GSE65904 and GSE54467 to conduct a meta-analysis.

Identification of CYT-Related Genes (CYTRG) and Prognosis-Related CYTRG

Patients in the TCGA-SKCM dataset were grouped into a high-CYT and a low-CYT group by median split, and then we used differential analysis on both groups in order to identify genes that could characterize CYT that 'CYTRG'. Prognosis-correlated

CYTRG for SKCM patients were then recognized using univariate Cox regression analysis on CYTRG and corresponding clinical data.

Identification of Subgroups and Evaluation of Subgroups

Then non-negative matrix factorization (NMF) clustering was applied on the CYTRG to classify new subgroups (clusters 1 and 2) of SKCM patients using the NMF R package. NMF is widely used in bioinformatics and with its ability to extract meaningful information from high-dimensional data (21), the use value of identified CYTRG was accordingly confirmed. We conducted KM survival analysis, compared number of somatic mutations and performed Gene Set Variation Analysis (GSVA) to determine the discrimination between C1 and C2 groups. The Estimation of Stromal and Immune cells in Malignant Tumor tissues using Expression data (ESTIMATE) algorithm was used to calculate stromal score, immune score, and ESTIMATE score of the different subgroups. The abundance of tumor-infiltrating immune cells in the different subpopulations was then assessed using the Microenvironment Cell Populations-counter (MCP-counter) method, which was introduced by Becht et al. (22) that allows the robust quantification of the absolute abundance of eight immune and two stromal cell populations in heterogeneous tissues from transcriptomic data.

Establishment of the CYT–Related Prognostic Model

A total of 446 representative patients were extracted from the TCGA repository. They possessed complete survival information and all relevant clinical features, such as age, sex, tumor stage and tumor-node-metastasis (TNM) stage. We employed lasso-cox regression analysis to screen out crucial CYTRG that have close relation with DSS. Certain CYT-related coefficients (βi) were calculated with the multivariate Cox regression model. The risk score formula (Expi) that was composed of βi and expression levels of CYTRG was set up. The equation 'Risk score = $\sum(\beta_i * Exp_i)$' was used to calculate each risk score for every patient. The samples were classified into either a high-risk or a low-risk cohort according to the cut-of (based on the median risk score). Using R software (version 4.04), KM survival analysis and log-rank test were performed to compare DSS in either high-risk or low-risk group.

Evaluation of This Prognostic Model

Then, a receiver operating characteristic (ROC) curve was generated by the R package survival ROC (23) and was used to understand the diagnostic value of this model (24). Also, we adopted the calibration curve method (CCM), principal component analysis (PCA), decision curve analysis (DCA) to further estimate the accuracy of this prognostic model. We evaluated the prognostic significance of the risk scores and also clinical variables, like age, sex, TNM staging, *via* univariate and multivariate Cox regression analyses. Moreover, according to the results from multivariate Cox regression analysis combined with tumor mutation burden (TMB), a nomogram was then built and concurrently could be used to predict DSS for the 1-year, 3-year, and 5-year of each SKCM patient. Briefly speaking, TMB refers to the number of mutations that exist within a tumor, and high TMB values are observed in melanoma and have been thought to be associated with responses to ICIs (25). The prognostic value of the novel model and the characteristic nomogram was further compared with the tumor staging system, TMB, age, tumor purity and gender in terms of the DCA plots, concordance index (Cindex), and restricted mean survival (RMS) curves.

Drug Sensitivity Analysis

Since chemotherapy is commonly applied to treat SKCM, we utilized R package "pRRophetic" to assess the chemotherapeutic response determined by the half maximal inhibitory concentration (IC50) of each SKCM patient on the Genomics of Drug Sensitivity in Cancer (GDSC) website. Besides, to elucidate the effects of CYT-related genes on drug sensitivity and tolerance in this model, we acquired transcriptome data from the CellMiner database (https://discover.nci.nih.gov/cellminer/) and FDA-certified drug sensitivity-related data. Then we utilized a Pearson correlation test to analyze the relationship between gene expression and drug sensitivity. The programmed cell death 1 (PDCD-1, also known as PD-1) and cytotoxic T-lymphocyte associated protein 4 (CTLA-4) pathways have been implicated in tumor immune evasion. So immune checkpoint inhibitors targeting PD-1 and CTLA-4 may thereby improve antitumor immunity. The immunophenoscore (IPS) was used to predict clinical responses to immune checkpoint inhibitors (26). The data of the IPS in SKCM patients were download from the Cancer Immunome Database (TCIA) (https://tcia.at/home). These results are able to better guide doctors in choosing different drug treatment on patients.

Expression and Modulation of Genes in the Signature

We conducted differential analysis on expression levels of genes in the signature between normal samples and tumor samples. We then searched for differential expression of genes between the high-risk and low-risk groups. The Human Protein Atlas (HPA) database (http://www.proteinatlas.org) was generated by Uhlén et al. (27), and contains an invaluable resource of human protein-coding genes, enlightening researchers on gaining insights of human proteins. Thus we explored the expression of CYTRGs represented in this signature in normal skins and SKCM tissues using the HPA database. The expression of one certain gene was investigated in normal and cancer tissues using the same antibody. Then we conducted spearman correlation analysis to demonstrate the relationship between CYT and genes in our model, which helped to confirm the rationality of CYTRG identified *via* the differential analysis.

Mutation Analysis and Tumor Mutation Burden (TMB) Calculation

Mutation analysis was conducted based on all available somatic mutation data of patients from the TCGA cohort. Then we visualized the somatic mutation data in the Mutation Annotation Format (MAF) using the "maftoools" R package, which is

efficient and comprehensive and provides various functions for cancer genomic analyses (28). Subsequently, tumor mutation burden (TMB) differential analysis was performed between wild and mutation types based on defined genes in the model. We also conducted differential analysis on TMB between the high-risk and low-risk groups, and combined with TMB, we conducted survival analysis between the two groups.

Tumor Microenvironment (TME) Analysis

The newly described algorithm, ESTIMATE (Estimation of Stromal and Immune cells in Malignant Tumor tissues using Expression data) method, applied for assessment of the presence of stromal cells and the infiltration of immune cells in tumor samples using gene expression data (29), was used to calculate interstitial score, immune score, ESTIMATE score, and tumor purity for different molecular subpopulations.

Immune Cell Infiltration, Immune Checkpoint Gene and CYT Analyses

To better clarify the relationship between the tumor immune cell infiltration status and calculated risk scores, 7 software programs, namely, XCELL, TIMER, QUANTISEQ, MCP-counter, EPIC, CIBERSORT-ABS, and CIBERSORT were used to analyze the immune cell infiltration landscape. The lollipop diagram was displayed to show the correlation between risk score and immune infiltrated cells *via* Spearman correlation method. The differences of immune cell content in high-risk and low-risk groups were shown as boxplots using Wilcoxon signed-rank test. Besides, we conducted differential analysis on the mRNA expression of immune checkpoint genes and CYT elements (GZMA and PRF1). We also performed Spearman correlation analysis on PD-1, PD-L1, CTLA-4, CYT, GZMA, PRF1 and calculated risk scores. Furthermore, we ran a correlation analysis between CYT expression and immune cell contents. All results further substantiated the utility value of our signature.

Gene Set Enrichment Analysis

A Gene Set Enrichment Analysis (GSEA) on risk genes was performed to obtain the GO and KEGG pathways of this model. The gene set enrichment study was conducted to that are expressed between the high and low-risk classes of the MsigDB (c2.cp.kegg.v7.4.symbols.gmt;c5.go.v7.4.symbols.gmt). The gene set permutations were tested 1,000 times to demonstrate its ability to function consistently. The phenotype label was used to forecast adverse events.

Prediction of the Possibility That SKCM Patients are Grouped as High Risk

After determining which clinical trait has significant difference, a nomogram was drawn to predict whether a patient with SKCM belongs to the high-risk group. Pathological stage and tumor-bearing state are needed to help doctors better utilize this prognostic model.

Statistical Analysis

All statistical analysis was accomplished by R version 4.0.4 (Institute for Statistics and Mathematics, Vienna, Austria; https://www.r-project.org). The correlation was determined by Spearman correlation analysis. Wilcoxon test and t-test were utilized to compare clinical variables. Survival status was assessed by the Cox regression analysis. OS, DSS and PFS were generated by the Kaplan–Meier method and evaluated by the log- rank test. Two- tailed $p < 0.05$ was considered statistically significant. The sensitivity and specificity of the model were evaluated using ROC curves. Additionally, we verified the confidence of the model using test datasets and entire datasets. Reasonably, hazard ratios (HRs) and 95% confidence intervals (CIs) were used to describe the relative risk.

RESULTS

Patients With High CYT Have Better Prognosis

The study design flowchart is shown in **Figure 1**. In total, 471 SKCM tissues and 1 para-cancer tissue were obtained from the TCGA database. After initial screening, 446 samples with full clinical information were included in our study. Detailed clinical features of the samples are shown in **Table 1**. According to the median value of CYT, we separated all SKCM patients into a high-CYT and a low-CYT group, in which we conducted KM survival analysis, and the results indicated that the high-CYT group had better prognosis. Univariate Cox regression analysis told us that CYT was a protective factor validated in 3 independent datasets, and consequently the conclusion came that the higher CYT, the better prognosis for SKCM patients (**Figure 2A**). However, meta-analysis showed that significant heterogeneity remained when CYT was used to predict the prognosis for SKCM patients (**Figure 2B**). Therefore, to enhance prognosis judgment for SKCM, we performed differential analysis respectively on the high-CYT and low-CYT groups, and finally 864 genes that could manifest features of CYT (CYTRG) were identified (**Figure 2C**), which adequately indicated the exploring value of CYT.

Demonstrating the Value in the Identified CYT-Related Genes (CYTRG)

To verify the high value of CYT-related genes (CYTRG) for research, we applied non-negative matrix factorization (NMF) clustering method based on the 864 identified genes, and an elementary classification of patient subgroups was set through the NMF consensus clustering, eventually with two subgroups (C1 group, C2 group) sorted out (**Figure 2D**). As shown in **Figure 3A**, the DSS time of each patient in clusters 1 and 2 were visualized and the number of patients at risk was also categorized in two lines. The results showed that patients in C1 group have better prognosis than those in C2 group. Additionally, the somatic mutation count in C1 group was also higher than that in C2 group (**Figure 3B**). The GSVA pathways in C1 group and C2 group showed significant difference too (**Figure 3C**). As shown in **Figure 3D**, the SKCM tissues in cluster 1 showed higher stromal score, immune score, and ESTIMATE score than cluster 2. Also, as shown in **Figure 3E**, the Microenvironment

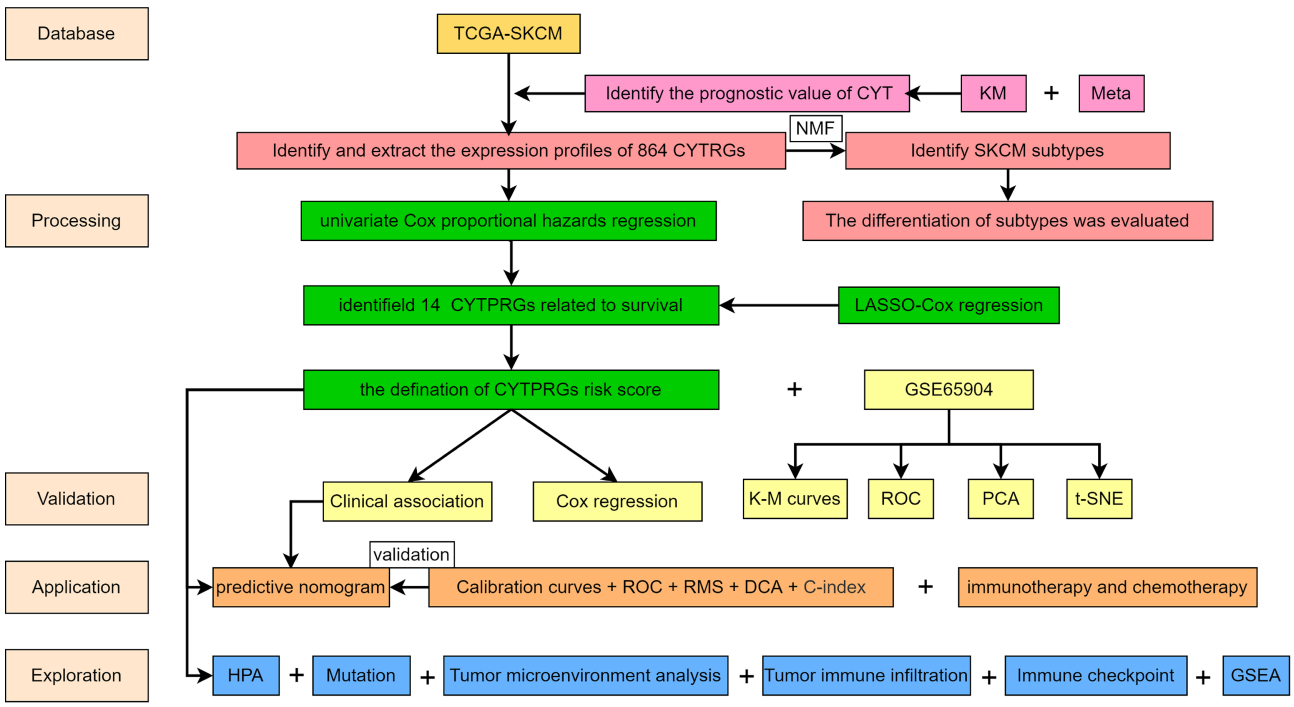

FIGURE 1 | Flow chart of this study.

TABLE 1 | Baseline data of SKCM patients from TCGA cohort.

Covariates	Type	Total	High-risk group	Low-risk group
Age	≤50	139	61	78
	>50	307	162	145
Sex	male	274	146	128
	female	172	77	95
Stage	Stage I	74	26	48
	Stage II	139	91	48
	Stage III	166	76	90
	Stage IV	22	11	11
	unknown	45	19	26
T	T0	23	3	20
	T1	40	14	36
	T2	75	33	42
	T3	87	43	44
	T4	150	99	51
	unknown	71	31	40
M	M0	397	198	199
	M1	23	12	11
	unknown	26	13	13
N	N0	220	115	105
	N1	71	34	37
	N2	49	22	27
	N3	53	25	28
	unknown	53	27	26

Cell Populations-counter (MCP-counter) algorithm was applied to calculate the abundance of immune cells in SKCM tissues, namely, B cells, T cells, NK cells, Neutrophils, Myeloid dendritic cells, Monocytic lineage, Fibroblasts, Endothelial cells, Cytotoxic lymphocytes, $CD8^+$ T cells, with statistically higher abundance of 9 kinds among them in c1 (Neutrophils excluded).

Establishment and Evaluation of CYT-Based Prognostic Model

In the training sets, univariate Cox regression was used on CYTRG to ascertain 553 prognosis-related CYTRG. Then LASSO-Cox regression analysis was conducted and 14 key CYTRG were screened out (**Figures 4A, B**). β_i was calculated using the formula below to establish the risk score model:

$$\text{Risk score} = \Sigma(\beta_i * \text{Exp}_i).$$

This formula was visualized in **Figure 4C**. We set the median score of risk scores as the critical value, and divided 446 patients into the high-risk and low-risk group.

Kaplan–Meier curve showed the DSS of the low-risk group was much better than that of the high-risk group ($p < 0.001$) (**Figure 4D**). ROC had satisfactory sensitivity and specificity (**Figure 4E**). PCA (**Figure 4F**) and t-SNE (**Figure 4G**) indicated high discriminatory power of our model. We obtained similar results using the same methods on the testing sets (**Figures 4H–K**).

Univariate Cox regression analysis (**Figure 5A**) illustrated that indexes CYT, tumor purity, risk score, age and tumor stage were closely associated with DSS. We further performed multivariate Cox analysis (**Figure 5B**), and found that the 14-gene signature could be served as an independent prognostic

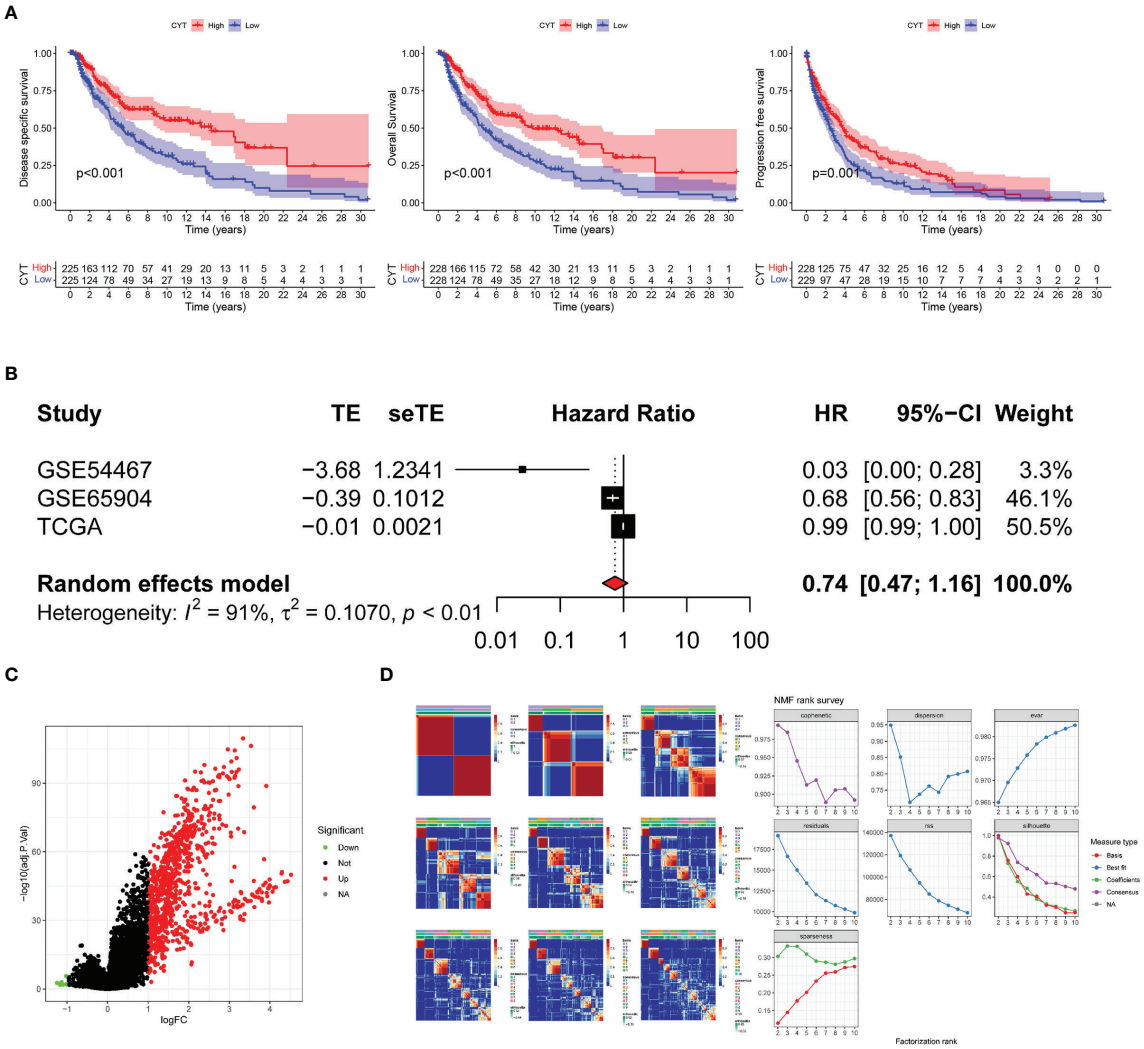

FIGURE 2 | Survival analysis and Meta-analysis. **(A)** Based on values of disease specific survival (DSS), overall survival (OS) and progression-free-survival (PFS), the survival analysis was conducted and the results showed that patients with high-CYT had better prognosis. **(B)** The univariate Cox regression analysis of GSE65904, GSE54467 and the TCGA-SKCM datasets were used to conduct a meta-analysis, which showed that CYT can be a protective factor for SKCM patients with a high heterogeneity, so CYT cannot be used to predict prognosis for SKCM patients directly. The volcano plot displays 864 differentially expressed genes (DEGs) between the high-CYT and low-CYT groups in the TCGA-SKCM cohort **(C)**. Nonnegative matrix factorization (NMF) clustering was conducted and two subgroups were identified the optimal value for consensus clustering **(D)**.

factor for SKCM (p <0.001), which meant that this signature can be useful to well complement traditional forms of tumor staging. Then we drew a nomogram for model visualization and clinical application, namely, age, tumor stage, TMB and risk score (**Figure 6A**). The area under the curve (AUC) values for the 1-, 3-, and 5-year DSS were "0.794", "0.754" and "0.737", predicted by this model (**Figure 6B**). The calibration curve of this predictive model suggested that the model had excellent predictive property and could definitely benefit patients because it exhibited an applicable prediction between the ideal prediction and actual observations (**Figure 6C**). Finally, we used DCA curves, C-index, RMS curves to confirm that this model and the newly-composite nomogram were admissible. The DCA curves showed the comparisons between the clinical net benefit of our model and the nomogram and that of other clinical traits (Staging, TMB, age, tumor putiry, gender) for SKCM patients (**Figure 6D**). Larger net benefits indicated that the model had the excellent clinical effectiveness for bringing benefits for SKCM patients. The C-index of the model and the nomogram was compared with that of other clinical traits, as shown in **Figure 6E**, and the concrete numbers were nearby 0.7, which meant the model was of very moderate to quite important magnitude. RMS curves were recommended by Eng et al. (30) as a flexible and interpretable descriptive technique to represent prognostic biomarkers. As shown in **Figure 6F**, the RMS represents the life expectancy at 20 years (240 months) for SKCM patients with different risk scores. The curve of the model achieved the highest leading position (HR: 5.338;

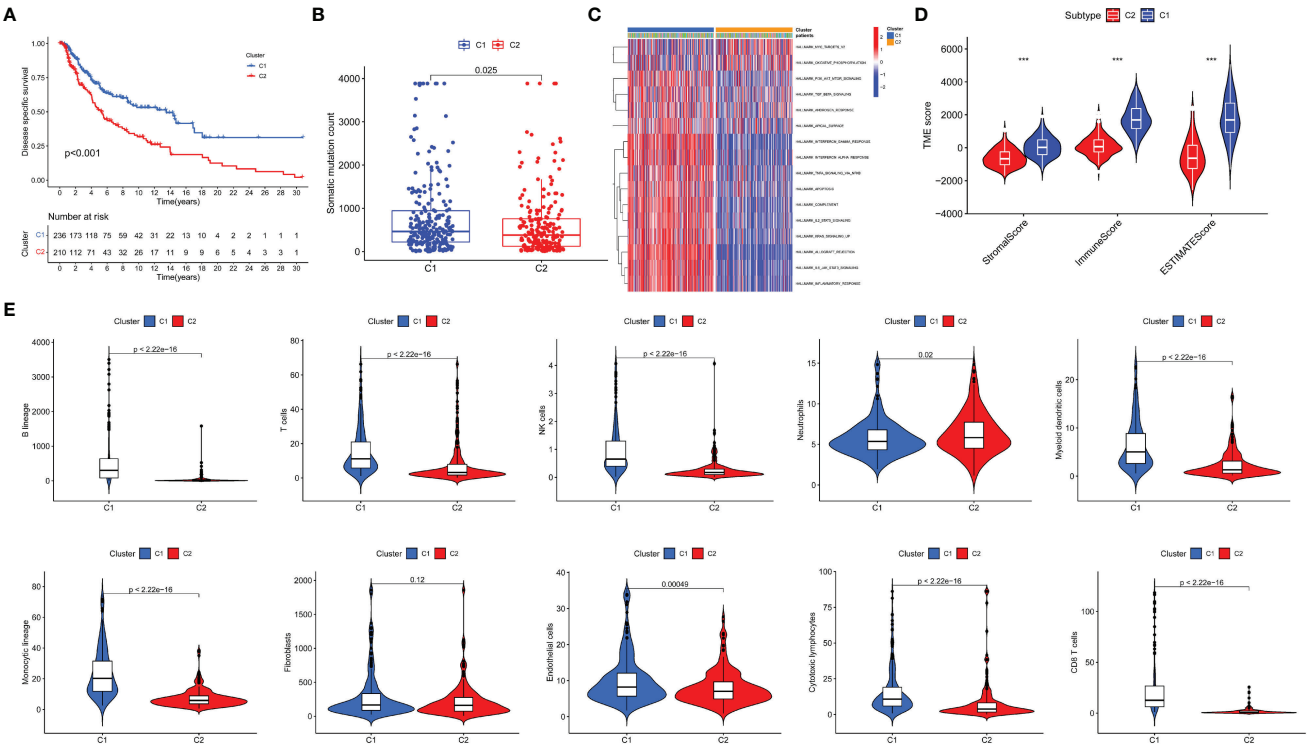

FIGURE 3 | Evaluation of the two newly identified subgroups in terms of their differentiation. Survival analysis **(A)**, Mutation analysis of somatic cells **(B)** and GSEA pathway differential analysis **(C)** on two subgroups. TME analysis of two identified subgroups was conducted **(D)**. The abundance of tumor-infiltrating immune cells was evaluated by MCP-counter and the differential analysis was then conducted **(E)**. *P < 0.05; ***P < 0.001.

P <0.001), indicating the high precision of our 14-gene signature. On the whole, our results validated the accuracy and feasibility of the signature.

Immunotherapeutic and Chemotherapeutic Responses of High- and Low-Risk Patients With SKCM

Immunotherapy has become a pillar of cancer therapy (31). By far the most widely used immunotherapeutic agents are blocking antibodies targeted to immune inhibitory receptors such as CTLA-4, PD-1, and PD-L1 (15). Unfortunately, not all types of cancer respond to it and not all patients can benefit from it. A lot of research show that strategies that combine traditional chemotherapy and burgeoning immunotherapy synergistically improve the outcome of cancer treatment (32). Expression levels of genes identified in this signature were significantly correlated with the sensitivity of various kinds of drugs by analyzing drug responses in the CellMiner database (**Supplementary Figure S1**). Thus, we further estimated the clinical response to immune checkpoint blockade (targeting CTLA-4 and PD-1 in high- and low-risk patients with SKCM). Then we used R package "pRRophetic" on Genomics of Drug Sensitivity in Cancer (GDSC) (https://www.cancerrxgene.org/) to estimate the half maximum inhibitory concentration (IC50) of chemotherapy response in each SKCM patient (**Figures 7A–L**). Results showed that in high-risk group, more promise in response to sorafenib and imatinib were presented, while gefitinib behaved better in low-risk group. We also investigated the response to chemotherapy in high-risk and low-risk patients with SKCM, and found that 9 chemotherapeutic drugs demonstrated obvious differences in estimated IC50 between high-risk and low-risk groups. Among them, 6 categories (gemcitabine, ZM.447439, NVP.BEZ235, roscovitine, NVP.TAE684 and vinblastine) showed increased sensitivity in low-risk group and the rest 3 categories (vinorelbine, docetaxel and doxorubicin) were more susceptive in high-risk group. In addition, IPS grade analysis showed that the IPS grade among low-risk patients was higher, which meant a better immunotherapy effect (**Figures 7M–P**). These results can better guide drug selection of patients and bring benefit for them.

Verification the Expression of Genes in the Signature

In the boxplot (**Figure 8A**), different expression levels of CYTRG in the signature between normal samples and tumor samples are shown. The heatmap shows the same comparisons between high-risk and low-risk groups (**Figure 8B**). Moreover, based on the HPA database, we intended to make a further validation of CYTRGs in this signature, and stepped forward to potentially confirm the value of these CYTRGs. These 9 recognized characteristic genes (*IFITM1*, *UBA7*, *SEMA4D*, *NMI*, *GBP2*, *ERAP2*, *KRT17*, *BCHE*, and *TYRP1*) (**Figure 8C**) from our model were present in the HPA database, whose differential expression levels between normal skin samples and SKCM

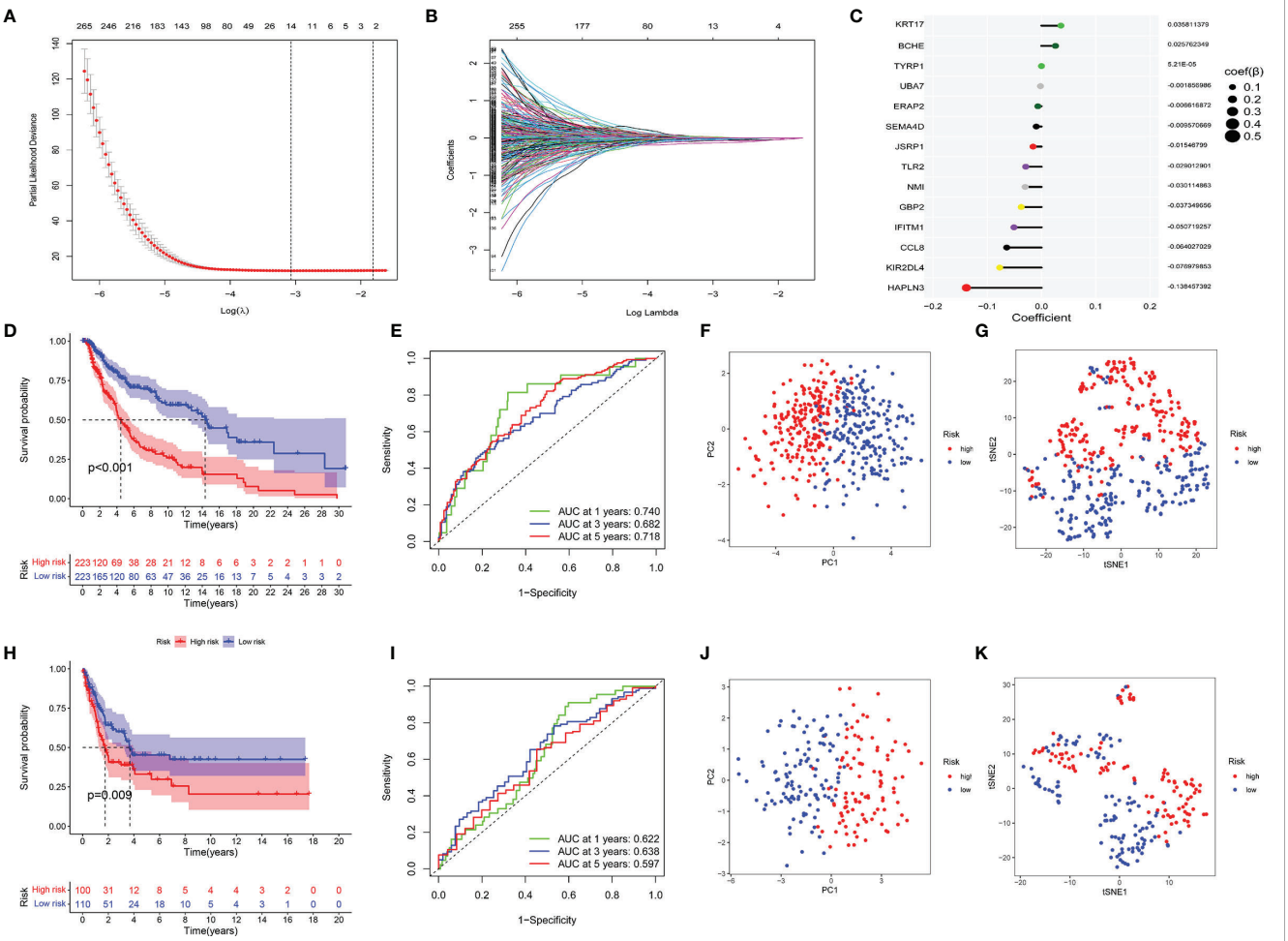

FIGURE 4 | Construction of the CYT-related risk model by Lasso–Cox regression analysis. **(A)** Partial likelihood deviance of variables revealed by the Lasso regression model. The red dots represented the partial likelihood of deviance values, the gray lines represented the standard error (SE), the two vertical dotted lines on the left and right represented optimal values by minimum criteria and 1–SE criteria, respectively. **(B)** Coefficient profiles of the 553 prognosis related CYT-related genes *via* Lasso–Cox regression analysis. **(C)** The coefficient values of 14 key CYT-related genes which were used to build the risk model were listed. Then validating the model. **(D)** Survival analysis, **(E)** ROC analysis, **(F)** Principal component analysis, **(G)** t-SNE analysis of two risk groups of the 14-gene signature in training cohorts, and **(H–K)** in testing cohorts.

samples were consistent with its transcriptional levels in both cohorts, which convincingly supported our findings herein. All immunohistochemical (IHC) images were downloaded from the HPA database. Furthermore, we identified genes with a relative importance >0.4 as the final filtration to highlight the most critical genes. **Figure 8D** shows the relationship between the error rate and the number of classification trees, and it also shows the top five important genes (*IFITM1*, *UBA7*, *CCL8*, *HAPLN3*, and *SEMA4D*). The value of genes in our model was confirmed again from the perspective of gene expression. Promisingly, these results can possibly inspire the scientists to explore CYT-related genes in preventing and curing the disease. The expression levels of CYT were strongly correlated with *KIR2DL4*, *GBP2*, *SEMA4D*, *CCL8*, *UBA7*, *NMI*, *HAPLN3*, *JSRP1*, *TLR2*, and *IFITM1* (cor >0.5), moderately correlated with the expression levels of *ERAP2* (cor >0.3), and weakly correlated with the expression levels of *BCHE*, *KRT17*, and *TYRP1*, which further verified the rationality of differential analysis to identify CYTRG (**Supplementary Figure S2**).

Calculation of Mutations of Somatic Cells in SKCM Patients

The landscape of mutations of 14 hub genes in the signature was shown in the waterfall map (**Supplementary Figure S3A**). The *KIR2DL4* gene nourished the highest frequency of nonsynonymous mutation in SKCM patients. The bulk mutation type of 13 genes is missense mutation, only *ERAP2* gene has the most frequent mutation type as nonsense mutation. The boxplot displays the TMB difference of each gene in TCGA-cohort (**Supplementary Figure S3B**). We used the red color to represent the mutation types, and the blue color to represent the wild types. The diagram shows that the mutation type for each gene owns higher TMB. The result of differential analysis of TMB between the high-risk and

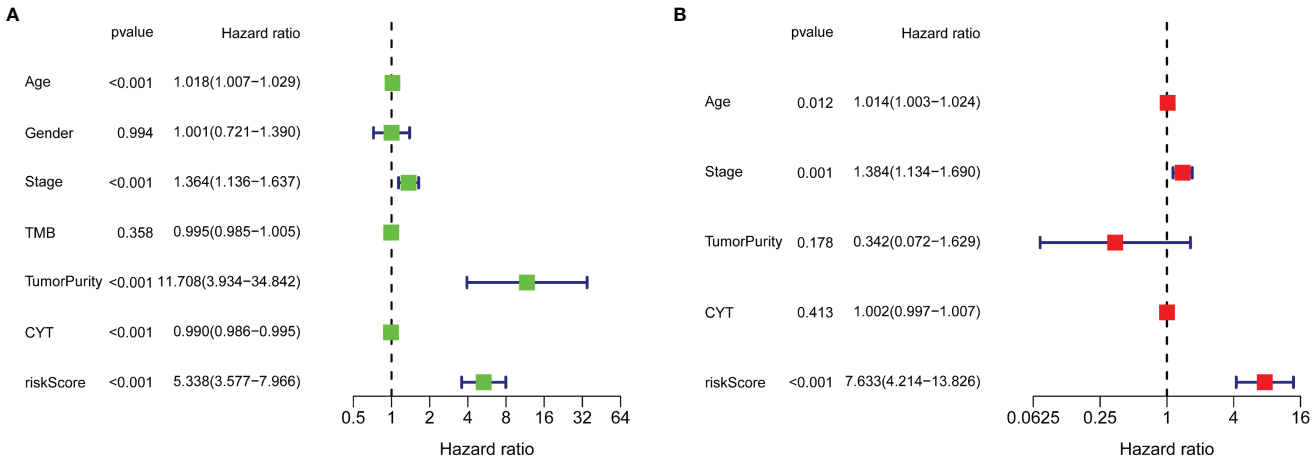

FIGURE 5 | Univariate Cox regression analysis **(A)** and multivariate Cox regression analysis **(B)** illustrated that the 14-gene signature could be used as an independent prognostic factor for SKCM patients.

low-risk group is shown in **Supplementary Figure S3C**. TMB in low-risk group is significantly higher than that in the high-risk group. As shown in **Supplementary Figure S3D**, the survival probability in the high-TMB group is higher than the low-TMB group. On the side, analyzing the survival probability jointly with TMB index, patients in the "high-TMB and low-risk" group have best prognosis (**Supplementary Figure S3E**). All these results bear out that high-TMB truly could be reckoned as a protective factor in SKCM patients. We observed extensive copy number variations (CNV) on fourteen key genes consisting of the groundwork for the signature through the CNV analysis. Among these genes, *HAPLN3*, *ERAP2*, *IFITM1*, *BCHE*, and *NMI* showed high CNV amplification frequency. In contrast, *KIR2DL4*, *CCL8*, *TLR2*, *JSRP1*, *TYRP1*, *GBP2*, *UBA7*, *KRT17*, and *SEMA4D* had significantly high CNV deletion frequency (**Supplementary Figure S3F**). The positions of CNV of the 14 hub genes on human chromosomes are shown in **Supplementary Figure S2G**.

Tumor Microenvironment (TME) in SKCM Patients

We used the ESTIMATE algorithm to calculate estimate score, immune score, stromal score, and tumor purity. Compared with the low-risk group, the immune score, stromal score and estimate score (**Figures 9A–C**) were higher in the high-risk group ($p < 0.001$). Tumor purity (**Figure 9D**) was lower in the low-risk group. Moreover, a correlation analysis suggested risk score had a significant negative relationship with immune score, stromal score and estimate score (**Figures 9E–G**), and it had a significant postitive relationship with tumor purity (**Figure 9H**).

Patients in the Low-Risk Group had Better Immune Function, With Higher Immune Cell Content, Expression of CYT and Immune Checkpoint Genes

To better understand the correlation between risk score and immune cell content, the Spearman correlation analysis and Wilcoxon rank-sum test were run *via* 7 different software programs. The results are shown in **Figure 10A**. The correlation coefficient varied significantly among different types of immune cells, namely, B cells, T cells, macrophages, NK cells, neutrophils, myeloid dendritic cells, etc. Moreover, bulk differential analyzes on the amount of immune cells between the high-risk and low-risk group were also conducted *via* 7 different software programs, and the results are concordant among different software programs and reveal that the content of many immune cells differ vastly between the high-risk and low-risk group (**Figure 10B**). These results manifest that this signature has close correlation with immune, which elucidates that the signature may be an important immune marker. Furthermore, the mRNA expression landscape between the high-risk and low-risk group of a large number of immune checkpoint genes was shown in **Supplementary Figure S4A**. The differential analysis on the expression level of PD-1, PD-L1, and CTLA-4 between the high-risk and low-risk groups was performed. To underline the most widely used immune checkpoint genes, we also performed Spearman correlation analysis on PD-1, PD-L1, CTLA-4 and calculated risk scores. The expression level of the three genes is negatively correlated with the risk scores (**Supplementary Figures S4B–D**). The results showed that their expression level was higher in the low-risk group than that in the high-risk group (**Supplementary Figures S4E–G**). In addition, expression of CYT, GZMA, and PRF1 were higher in the low-risk group than high-risk group (**Supplementary Figures S5A–C**). And they were negatively correlated with risk score for SKCM patients (**Supplementary Figures S5D–F**). In **Supplementary Figures S5G–I**, we could see that CYT, GZMA and PRF1 had significant correlation with many immune cells, especially with $CD8^+$ T cells (correlation coefficient >0.5, $p < 0.001$). Results above may imply that our signature is a good reflection of CYT.

Gene Set Enrichment Analysis

To further verify the observation based on this risk score model, Gene Set Enrichment Analysis (GSEA) was utilized to seek out

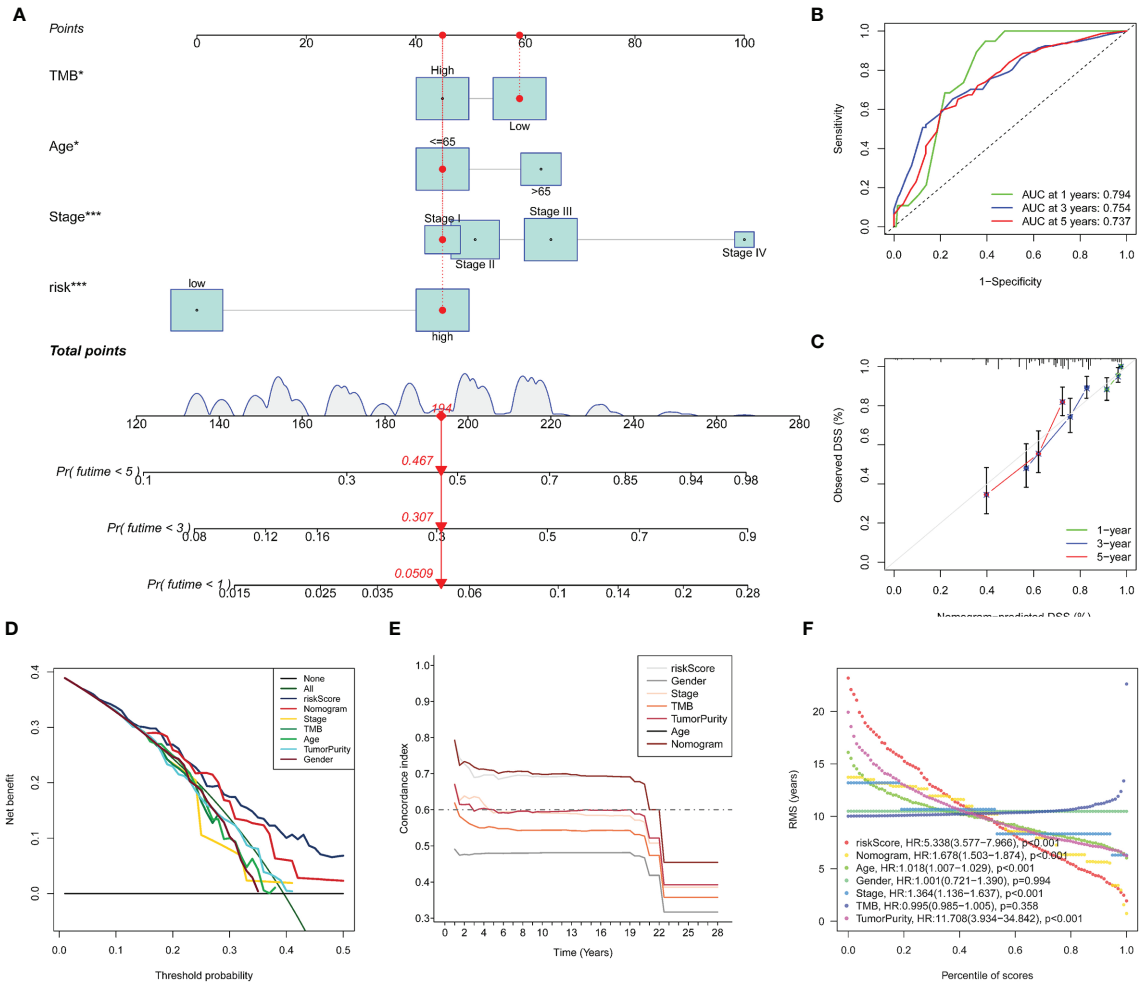

FIGURE 6 | Construction and evaluation of Nomogram. A nomogram constructed by TMB and multi-Cox regression analysis on risk, TNM stage, and age to apply the 14-gene signature in clinical practice **(A)**. ROC curves **(B)** and calibration curves **(C)** indicate that the nomogram is accurate and specific. Further validation of the prognositic value in our signature **(D–F)**. DCA curves for the signature, the nomogram and other clinical traits in terms of their net benefits for SKCM patients **(D)**. Time dependent C-index curves of the model, the nomogram and other clinical traits **(E)**. RMS curves for the signature, the nomogram and other clinical traits and the model has the best potency in predicting prognosis of SKCM patients **(F)**.

enriched pathways in the KEGG and GO databases. We screened out eligible gene sets from KEGG and databases, and selected the most specific pathways. As shown in **Supplementary Figure S6A**, some gene sets were significantly upregulated in the high-risk subgroup, such as nitrogen metabolism, olfactory transduction, oxidative phosphorylation, parkinsons disease and ribosome. Some gene sets were significantly enriched in the low-risk subgroup, such as antigen processing and presentation, cell adhesion molecules cams, chemokine signaling pathway, cytokine–cytokine receptor interaction, hematopoietic cell lineage (**Supplementary Figure S6B**). In GO database, some gene sets were significantly upregulated in the high-risk subgroup, such as cornification, epidermal cell differentiation, epidermis development, keratinization, keratinocyte differentiation (**Supplementary Figure S6C**). Some gene sets were significantly enriched in the low-risk subgroup, such as activation of immune response, adaptive immune response based on somatic recombination of immune receptors built, alpha beta t cell activation, antigen processing and presentation, antigen receptor mediated signaling pathway (**Supplementary Figure S6D**). The abundant results may particularly inspire us to conduct further studies on the pathogenesis of SKCM tumor progression.

Risk Probabilities of SKCM Patients Can be Predicted by This Signature Based on Clinical Traits

For the purpose of letting the signature better serve clinical needs, we conducted a series of analyzes on the relationship between the 14-gene signature and clinical characteristics.

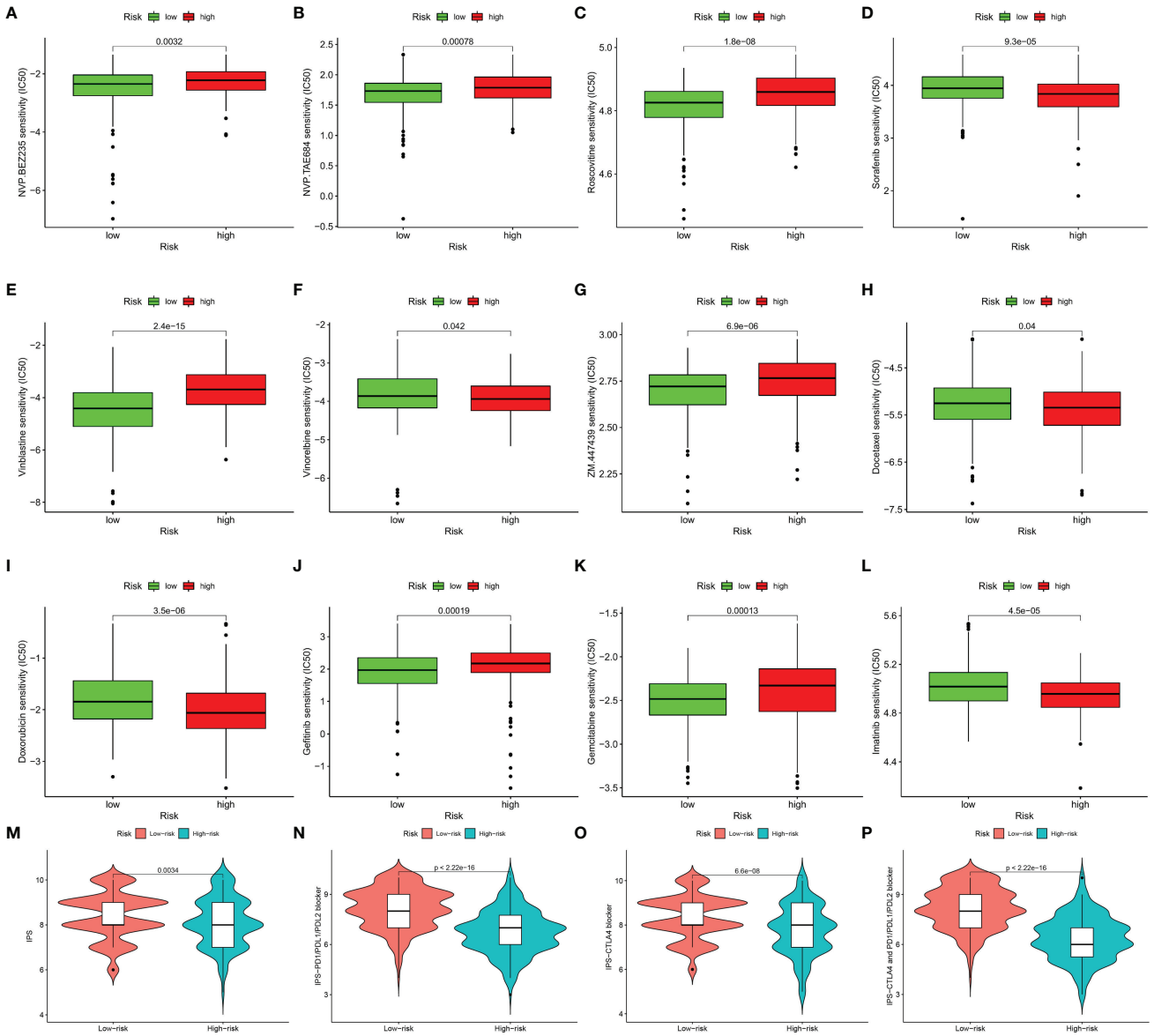

FIGURE 7 | Immunotherapeutic and chemotherapeutic responses high- and low-risk patients with SKCM were shown. Lower IC50 of NVP.BEZ235 **(A)**, NVP.TAE684 **(B)**, roscovitine **(C)**, vinblastine **(E)**, ZM.447439 **(G)**, gefitinib **(J)**, gemcitabine **(K)** were associated with a lower risk score. Lower IC50 of sorafenib **(D)**, vinorelbine **(F)**, docetaxel **(H)**, doxorubicin **(I)**, and imatinib **(L)** were associated with a higher risk score. Distribution of immunophenoscore (IPS) in high-risk *versus* low-risk SKCM subtypes. Violinplot representation of IPS in the high-risk *versus* low-risk groups in CTLA4 negative and PD1 negative group **(M)**, CTLA4 positive and PD1 negative group **(N)**, CTLA4 negative and PD1 positve group **(O)**, and CTLA4 positive and PD1 positive group **(P)**.

Differential analysis on the risk scores of subgroups with various T stage was performed. The diagram shows that along with the progression of the disease, the risk score accordingly elevates (**Supplementary Figure S7A**). Additionally, we introduced a nomogram as a measure of risk scores for SKCM patients (**Supplementary Figure S7B**). Cablibration curves (**Supplementary Figure S7C**), ROC curves (**Supplementary Figure S7D**) and DCA curves (**Supplementary Figure S7E**) were drawn to indicate the predictive accuracy of the signature.

DISCUSSION

The incidence of skin cutaneous melanoma (SKCM) continues to rise globally (33). SKCM is the deadliest type of skin cancer because of its early spread *via* the lymphatic vessels into lymph nodes and distant organs (34), leading to a remarkably poor prognosis and high recurrence rate. Traditional therapies have their limitations in improving the prognosis of SKCM patients. It is gratifying that the treatment landscape has shifted dramatically

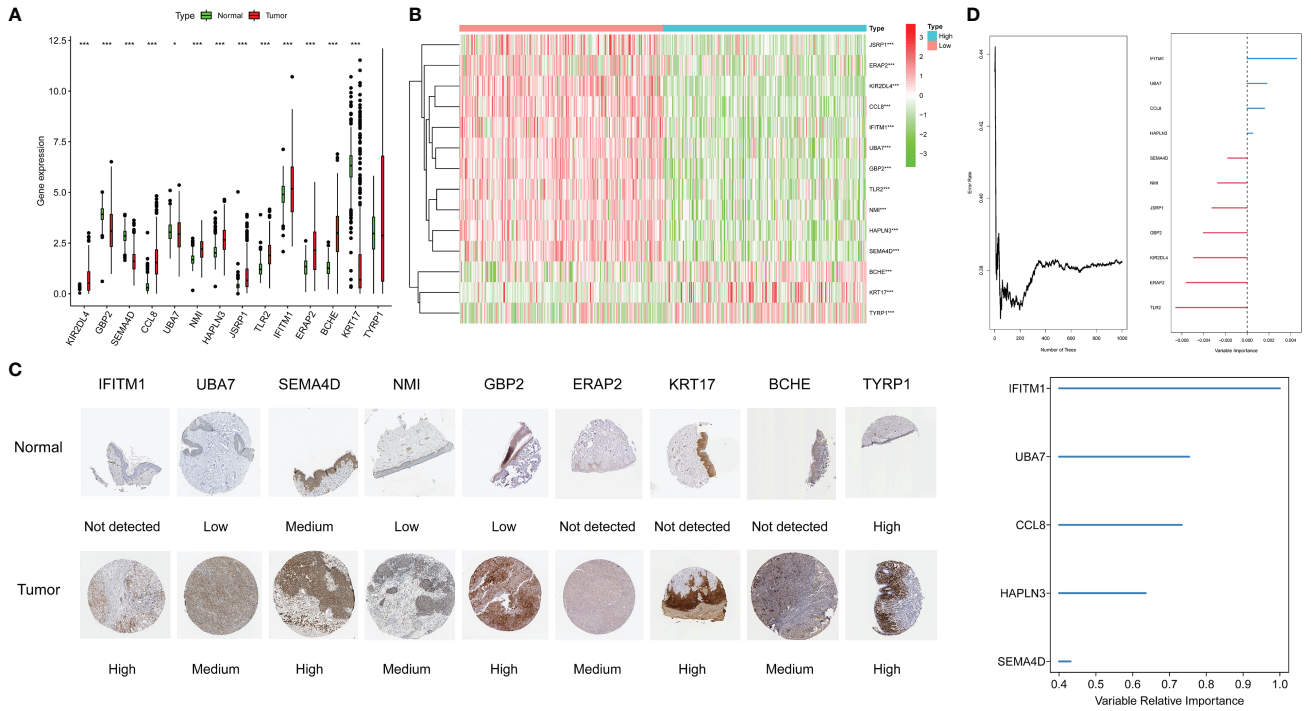

FIGURE 8 | The expression of genes in the signature, the boxplot shows the comparisons between normal types and tumor types **(A)**, the heatmap shows the comparisons between the high-risk and low-risk groups **(B)**, and the immunohistochemical stainings shows 9 gene expression on protein level **(C)**. Error rate for the data as a function of the classification tree, out-of-bag importance values for the predictors **(D)**.

over a short period of time (6). Immunotherapy is reckoned as the most promising one of emerging treatments, but not all patients can benefit from it. Due to ubiquity of the immune system, immune-related adverse effects affect patients and even may lead to potentially life-threating conditions (35). Therefore, the identification of biomarkers that can predict immune responses of patients toward the specific treatment strategy so that doctors can choose the most suitable patients who will benefit from it is a prime objective of tumor study.

We noticed that in 2015, Rooney et al. elucidated the CYT value as the potential landmark that could be used to predict prognosis in cancers and had associations with counter-regulatory immune responses, which may contribute to reveal mechanisms of tumor development (18). Thus, genes associated with the CYT level are needed in order to help us better understand immune changes in human body during immunotherapy treating. It is noteworthy that in colorectal cancer, patients with higher CYT-values showed a more sensitivity to ICIs than those with lower CYT-values (19). Based on this, we identified CYT-related genes (CYTRG), established a CYT-related prognostic model, validated novel therapeutic treating targets for immunotherapies, enriched the thoughts for the treatment on SKCM in this study. For the first time, we surprisingly built a bond between SKCM and CYT score.

The CYT was calculated as the geometric mean of the GZMA and PRF1 expression in TPM. GZMA from NK cells and cytotoxic T lymphocytes (CTLs) activates gasdermin B (GSDMB) to trigger pyrotosis in target cells, which has been thought as a factor enhancing antitumor immunity (36). PRF1 also plays an important role in keeping the ability of NK cells and CTLs to strike down target cells, protecting the organism from immunosuppression and mainting immune regulation (37). Hence, through the primary analysis, we found that CYT was a protective factor for the prognosis of SKCM patients, which was within our expectations. Then, samples from TCGA database were divided into the high- and low-CYT group based on the median value of CYT scores.

Subsequently, 864 CYTRG were screened out, which further confirmed that CYT may possess abundant value in predicting prognosis for SKCM. This assumption was proved then. Fourteen CYTRG with relevant prognostic and predictive implications were identified and were used to construct the risk score model. Among them, eleven (*KIR2DL4*, *GBP2*, *SEMA4D*, *CCL8*, *UBA7*, *NMI*, *HAPLN3*, *JSRP1*, *TLR2*, *IFITM1*, and *ERAP2*) were favorable prognostic factors, whereas the other three (*BCHE*, *KRT17*, and *TYRP1*) were hazardous. Interestingly, some of them have already been verified to play an important part in SKCM. Zhou et al. (38) demonstrated that the low expression of *KIR2DL4* is significantly associated with poor prognosis in SKCM. Moreover, *KIR2DL4* as a receptor on HLA-G, has been thought as one of potential targets for immunotherapy to treat cancer (39). Fillmore et al. established stable clones constitutively expressing *NMI* (N-Myc interactor)

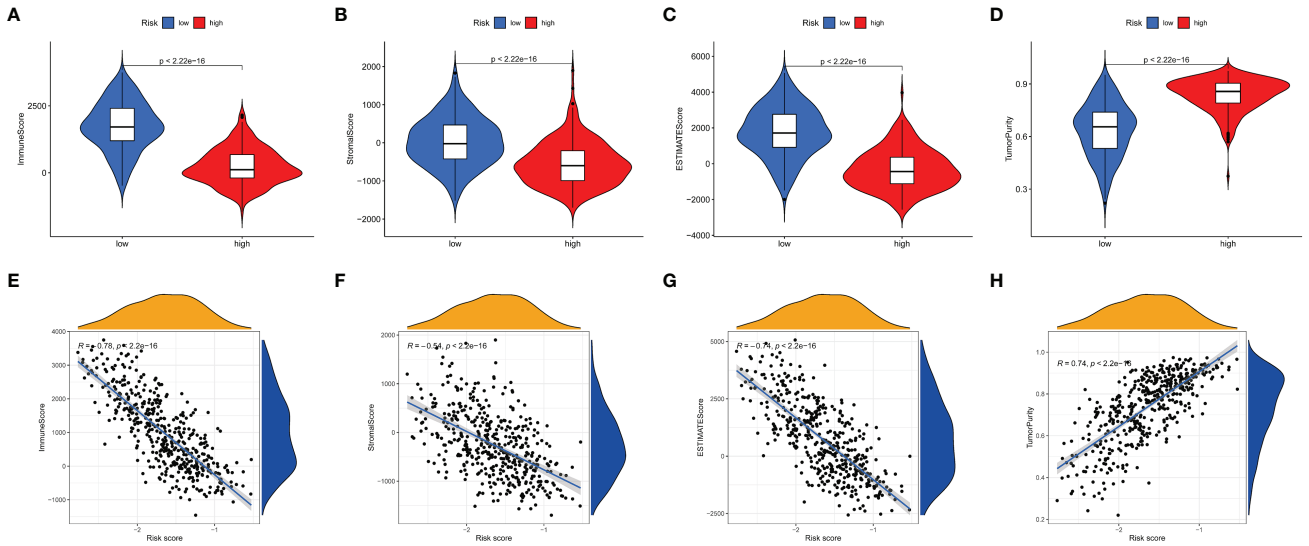

FIGURE 9 | Tumor microenvironment analyses. Comparisons between high-risk group and low-risk group in terms of immune score, stromal score, ESTIMATE score **(A–C)** and tumor purity **(D)**. The relationship between the risks core and immune score, stromal score, ESTIMATE score **(E–G)** and tumor purity **(H)** in tumor tissues.

in both breast and melanoma cell lines and eventually proved that *NMI* retards tumor growth (40). Also, Compagnone et al. (41) once gave evidence that *ERAP2* may promote immune responses mediated by T cells and NK cells to certain cancers, with low expression related to poor prognosis. In consequence, the established signature can provide novel biomarkers for further studies. It could offer ideas for us to assess prognosis of SKCM patients and we found that in the low-risk group, DSS for SKCM patients was indeed longer than that in the high-risk group.

Whereafter, the close relationship between the DSS and CYT and other clinical features was also determined. Moreover, we verified the independence of this 14-gene signature as a prognosis predictor. Besides, a nomogram was built to visualize our model. Nomograms are widely used for cancer prognosis (42). Through multiple analyses, the signature was believed to own a fulfilling distinctness, sensibility and authenticity.

To illustrate that the model is pragmatic in nature on guiding clinical drug use, firstly we found that the expression levels of gene in this signature were expressively correlated with the sensitivity of various kinds of drug in the CellMiner database, which integrates the NCI-60 cell line database and drugs approved by the U.S. Food and Drug Administration, thought as an efficient tool to easily identify drugs that are effective against different types of cancer (43). Next we calculated IC50 to determine chemotherapeutic responses for each SKCM patient. Sorafenib and imatinib elicited a better potency in the high-risk group, while gefitinib did considerably better in the low-risk group. Sorafenib was experimented to prolong OS in mice by inhibiting migration and invasion of melanoma cells and the authors speculated it to be of potential use for treating SKCM (44). As a monotherapy or in combination with chemotherapy, sorafenib is of limited use, hence it is vital to explore biomarkers to choose the suitable patients that are more likely to respond to sorafenib (45). Likewise, as tyrosine kinase inhibitor, imatinib can regulate tumor immunity by depleting effector regulatory T cells (46), and it is gradually studied too (47–49). Gefitinib has also been explored (50, 51). Thus, this possibly could be used as reference for patients with different estimated prognosis *via* our model to choose suitable drugs. Moreover, we investigated various chemotherapeutic drugs. Gemcitabine, ZM.447439 (Aurora kinase inhibitor), NVP.BEZ235 (PI3K inhibitor), Roscovitine, NVP.TAE684 and vinblastine were more sensitive to patients in the low-risk group, while vinorelbine, docetaxel, doxorubicin were more sensitive to patients in the high-risk group. Chemotherapy always has a major role to play among all traditional therapies (5), therefore the findings in our study can be applied for guiding clinical chemotherapy in patients with SKCM.

Through a series of rigorous screening, our model identified that mRNA expression levels of 14 hub genes had differences between the normal/tumor group, and between the high-/low-risk groups. Besides, nine hub genes had differences at the protein expression levels between the normal/tumor tissues. In the further analysis of the 14 hub genes, *IFITM1*, *UBA7*, *CCL8*, *HAPLN3* and *SEMA4D* emerged as the most important ones for the prognosis in SKCM patients. Among all listed genes, *GBP2*, *TYRP1* and *IFITM*1 are of intense interest to further discussion. Guanylate binding protein 2 (*GBP2*) belongs to the vast guanine-binding protein (GBP) family that is consumingly induced by interferon- γ (IFN-γ). Its role in tumorigenesis has received increasing attention in recent years. Notably, Ji et al. (52) demonstrated that *GBP2* reinforces anti-tumor functions by intercepting the Wnt/β-catenin pathway in SKCM and

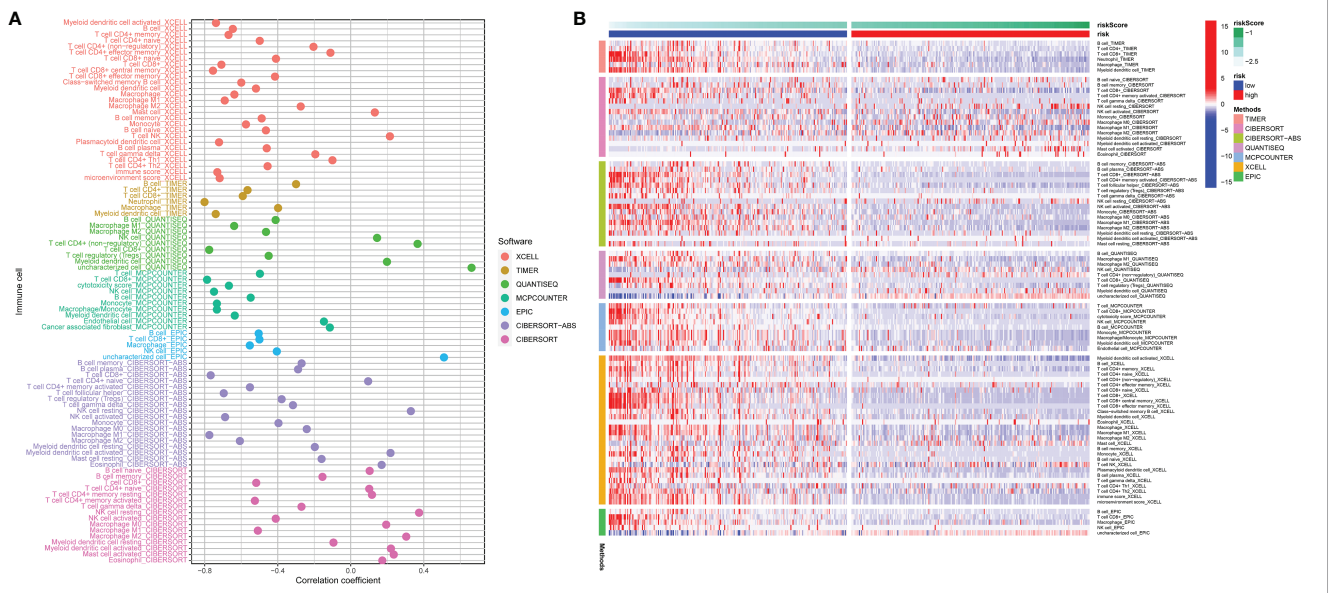

FIGURE 10 | The risk score correlated with the presence of many kinds of immune cells, which was analyzed *via* XCELL, TIMER, QUANTISEQ, MCPCOUNTER, EPIC, CIBERSORT-ABS, CIBERSORT **(A)**. The heatmap shows the differential analysis of different numbers of immune cells between the high-risk and low-risk group **(B)**.

enhances prognosis. Yu et al. (53) found that *GBP2* promotes glioblastoma invasion through Stat3/fibronectin pathway. While in breast cancer, *GBP2* can also be stated as a tumor suppressor gene according to experimental evidence of scientists (54, 55). Sadly, there lacks solid studies on functions of GBP2 in SKCM formation for now, which also gives preliminary inspirations. On the contrary, human tyrosinase related protein 1 (*TYRP1*) is a melanosome protein involved in the pigmentary machinery of melanocytes and well-studied for its emerging roles in the malignant melanocyte and melanoma progression (56). Gilot et al. (57) even explored in depth that a reduction in the *TYRP1* mRNA level should restore the tumor-suppressor activity of miR-16 and highlighted miRNA displacement as a promising targeted therapeutic approach for melanoma. The family of interferon-induced transmembrane (IFITM) proteins is interferon induced antiviral proteins, localized in the plasma and endolysosomal membranes. With regard to IFITM1, also known as 9-27 or Leu13, is reported to be overexpressed in a wide range of neoplasms and thought as an independent prognostic biomarker for patients with certain tumor types (58). Its role in SKCM prgression stays relatively obscure. Yang et al. (59) used to speculate that *IFITM1* functions as a tumor suppressor gene and arrived at a preliminary confirmation of its prognostic role for SKCM. These results support that our model is of great value in predicting prognosis for SKCM patients, and hub genes in the model are potentially important from both a fundamental and practical point of view.

Tumor mutation burden (TMB) refers to the number of gene mutations within tumors. Considering its close connections with immune checkpoint inhibitor (ICI) treatments and other immunotherapies, high-TMB has been focused on its useful role as a novel biomarker for planning treatments and selecting ICIs across some cancer types, melanoma included (60–62). High TMB might promote neoantigen generation and T cells can react to neoepitopes generated from mutated genes that bind to MHC molecules, causing effective antitumor immune response (63). Chalmers et al. (64) analyzed 100,000 human cancer genomes and arrived at a conclusion that a substantial part of cancer patients with high TMB may benefit from immunotherapy. High TMB is associated with better prognosis in patients receiving ICI treatment (65). Herein we analyzed the somatic mutation profiles in SKCM samples. A landscape on mutation types of fourteen key genes in our model was shown. A series of results through the mutation analysis told us that high-TMB was connected with lower risk scores in SKCM patients and patients with higher TMB had better survival. Firstly, our results convey the conclusions that high-TMB in SKCM patients may equal to longer lifespan. Secondly, this might give thoughts for guiding ICI treatment for SKCM patients.

Furthermore, we analyzed tumor microenvironment (TME) by using the ESTIMATE algorithm. TME serves as a nutrient sink on which the tumor cells feed and develop (66). Groundbreaking studies in melanoma, ovarian and colorectal cancer have shown that certain features of the TME—in particular, the degree of tumor infiltration by cytotoxic T cells—can predict a clinical outcome of a patient (67). The classical tool—ESTIMATE computational method was used to estimate the ratio of immune-stromal component in TME, viewed in the form of three sorts of scores: immune score, stromal score, and ESTIMATE score. The stromal scores ranged from −1,778.68 to 1,898.41, the immune scores ranged from −1,458.20 to 3,748.11, and the ESTIMATE scores ranged from −2,582.43 to 5,069.01.

Then we found that stromal scores, immune scores and ESTIMATE scores were all lower in the high-risk group than those in the low-risk group, which meant higher TME score contributed to better prognosis for SKCM patients.

Next, we analyzed the infiltration of immune cells in patients with SKCM. Tumor-infiltrating immune cells play a significant role in regulating responses to immunotherapies. Seven common methods were used to evaluate the correlation between tumor infiltrating immune cells and risk scores, namely, XCELL (68), TIMER (69), QUANTISEQ (70), MCPCOUNTER (22), EPIC (71), CIBERSORT-ABS (72), and CIBERSORT (73). We found that significant relation existed between risk scores and different types of immune cells, such as B cells, T cells, macrophages, NK cells, neutrophils, and myeloid dendritic cells. B cells are considered to be the main effector cells of humoral immunity which inhibit neoplastic progression by secreting immunoglobulins, promoting T cell response, and killing cancer cells directly (74). B cells are also discussed as an important prognostic and predictive biomarker in SKCM (75). Selitsky et al. (76) once experimentally confirmed that B cells can modulate the anti-tumor immune response by mediating proliferation and functional polarization of T cells, and they also found that a potential law in patients receiving CTLA-4 inhibitors where a lack of B cell response is possibly a sign of poor response to ICIs. Moreover, $CD8^+$ and $CD4^+$ T cells have been generally recognized as important anti-tumor immune cell subgroups with their cancer-cell killing efficacy, working as a crucial autoimmune gateway against cancer intrusion of an organism. We also found that in the low-risk group, immune checkpoint genes were higher and so as to Treg cells, which in our view was according to the better immune function compared to the high-risk group. Previous studies have shown that the upregulation of PD-L1 and its connection to antigen-specific $CD8^+$ T cells can explain the confined host immunity in cancers (known as adaptive immune resistance), yet the high expression of PD-1, PD-L1 and other immunosuppressive molecules could be attributed to not only the mutations of tumor cells, but also the induction of tumor-infiltrating cells (12, 77). In TME, higher expression of immunosuppressive molecules can represent stronger immune attack, which can benefit the patients. Low levels of immunosuppressive molecules usually mean that the tumor cells are not recognized by the immune system or the immune system is already in ruins, which to some extent explains why immune checkpoint genes universally express more in the low-risk group. Moreover, we noticed patients in the low-risk group had higher TMB value and prolonged survival than the high-risk group. This also indicated that in the low-risk group, they had better immune functions, because tumor cells should withstand the anti-tumor immunity of the body with continuous mutations and produce more immunosuppressive molecules (termed as immune escape) (78). On the contrary, low TMB may signify a rather powerful invasion of tumor cells or an extremely damaged immune system, by which tumor cells do not need mutations to tolerate tumor immunity. These speculations are consistent with the higher levels of immune infiltrating cells in the low-risk group for SKCM. In further studies, we found that CYT, GZMA and PRF1 were highly expressed in the low-risk group, significantly negatively correlated with risk scores, and expressively positively related with $CD8^+$ T cell content. Thus we hypothesized that high CYT in SKCM could mediate tumor immunity through $CD8^+$ T cell and lead to better outcomes. And there was a moderate positive correlation between CYT and Macrophages 1 (M1), and a moderate negative correlation between CYT and Macrophages 2 (M2). M1 is mainly involved in inflammatory responses and anti-tumor processes, while M2 shows tumor-promoting activity (79). Thus we could better assume that SKCM with higher CYT would have better clinical prognosis because of stronger mmunogenicity and a more favorable TME. Furthermore, GZMA was a potent adjuvant that induced antigen-specific cytotoxic CTLs to play a prominent part in antitumor activity in mice when co-administered with antigen (80). Inoue et al. indicated that more expression levels of PD-1 ligands, GZMA and HLA-A in melanoma tissues may be conductive to respond preferentially to nivolumab treatment by expanding oligoclonal tumor-infiltrating lymphocytes (81). PRF1 was also confirmed to have close relation with better OS by modulating tumor immunity in cancers like head and neck squamous cell carcinoma, ovarian cancer and basal-like breast tumors, and liver cancer (82–84). In summary, our findings show that the patients in the low-risk group had better survival, and provide a theoretical basis for studying pathogeniss and treatment methods of SKCM. CYT, as a protective factor in SKCM, was again confirmed.

Through the GSEA of biological pathways for different risk subgroups in different databases, we found that a diverse array of immune-related signaling pathways showed significant differences, which lies within our expectations. Interestingly, the pathways like activation of immune response, antigen processing and presentation, cell adhesion molecules (CAMs) were significantly downregulated among high-risk group. Antigen processing and presentation is a classic adaptive immune-response course in which dendritic cells (DCs) are considered to play a central role potently and professionally (85). In many tumors, an immunosuppressive microenvironment can be attributed to the dysfunction of DCs to recognize, process, and present tumor antigens to T cells (86). The loss of CAMs in the early stage of melanoma allows the tumor cells to proliferate and intrude the dermis with the reduction of anchorage on the basement membrane and between the ambient keratinocytes (87), which allows distant metastasis in the follow-up mutations. These results illustrate that CYT regulates tumor pathogenesis by modulating various immune responses. Remarkably, our GSEA also offers some new insights into tumor mechanism governing, many of them certainly seem like an untapped area to explore. Parkinsons disease was enriched in the high-risk group. Forés-Martos et al. (88) demonstrated that significant genetic correlations exist between Parkinson's disease, prostate cancer, and melanoma.

As is mentioned above, within this study, we found that PD-1, CTLA4 and PD-L1 genes were expressed more in the low-risk group. PD-1, CTLA4, PD-L1 inhibitors currently are among the hottest ICIs, contribute much to treat cancers, including SKCM. It may roughly possess accurate predictive capacity to identify patients who could respond well to immunotherapies. The

underlying mechanism for this may be ascribed to that the higher TMB in the low-risk group contributes to more neoantigens generated by tumor mutations and more T lymphocytes infiltrated by tumors, which makes the tumor more immunogenic along with a stronger anti-tumor immune response [15]. In fact, this is consistent with the result that SKCM patients with higher TMB expression have better outcomes. However, it is cautionary to note that our results suggest that immune checkpoints are generally upregulated in SKCM patients, noting that they are more prone to immune escape during immunotherapy. These conclusions offer practice guidance, and shed a new light on the immunotherapy for SKCM.

Nevertheless, there were limitations in this study. This was a retrospective study with datasets from the TCGA database, lacking specific clinical information such as treatment and recurrence records. And our conclusions need to be validated *in vivo* or *in vitro* experiments to further examine the function of CYTRGs in SKCM progression and to understand mechanisms of neoplasia better. Still, prospective clinical studies are welcome to verify phenomena reflected in this research.

In summary, our analyses of gene expression matrix and corresponding clinical characteristics identified 14 prognosis-related CYTRGs in skin cutaneous melanoma. Based on the clinical characteristics of CYT, we constructed a novel risk scoring model, which can effectively evaluate the prognosis for SKCM patients and forecast the benefit of SKCM immunotherapy. Our study illustrated that CYT may positively influence the development and outcome of tumors by modulating tumor microenvironment. Thus, poor prognosis of high-risk patients with SKCM may be attributed to the lower immune functions of immune cells. And different sensitivity to therapeutic drugs between the high- and low-risk groups could also be due to differential expressions of immune checkpoints and cytokines. Significantly, our study showed that low-risk patients with SKCM benefit more from immunotherapies and the model can be employed as a key tool to facilitate rational drug use and guide clinical treatment.

CONCLUSION

Our study is the first to establish a 14 CYT-related-gene prognostic model. Abundant analyzes verify that this signature can be used as a promising predictive biomarker and therapeutic target for SKCM patients.

DATA AVAILABILITY STATEMENT

The datasets presented in this study can be found in online repositories. The names of the repository/repositories and accession number(s) can be found in the article/**Supplementary Material**.

AUTHOR CONTRIBUTIONS

HZ is responsible for writing and submitting the papers. YL is responsible for data collection and analysis and the production of pictures. DH and SL are responsible for the ideas and guidance. All authors listed have made a substantial, direct, and intellectual contribution to the work and approved it for publication.

ACKNOWLEDGMENTS

The authors thank the anonymous reviewers for their valuable remarks.

SUPPLEMENTARY MATERIAL

The Supplementary Material for this article can be found online at: https://www.frontiersin.org/articles/10.3389/fonc.2022.844666/full#supplementary-material

Supplementary Figure 1 | Using CellMiner method to conduct correlation analysis between drugs and targeted genes.

Supplementary Figure 2 | The levels of gene in the signature correlate with CYT in SKCM patients.

Supplementary Figure 3 | The landscape of mutations of somatic cells in SKCM patients. **(A)** Waterfall map shows the mutational conditions of 14 genes involved in building the signature. **(B)** Boxplot displays the TMB difference of SKCM patients in TCGA-cohort. The red represents the mutation types, and the blue represents the wild types. *P < 0.05; **P < 0.01; ***P < 0.001. **(C)** Differential analysis of TMB between the high-risk and low-risk group. **(D)** Survival analysis between the high-TMB and low-TMB group. **(E)** Survival anlaysis on the 14-gene signature with the combination of TMB. The copy number variation (CNV) frequency percentage of the fourteen hub genes in SKCM. The red dot represents the CNV amplification, and the green dot represents the CNV deletion **(F)**. The location of CNV of 14 hub genes on human chromosomes **(G)**.

Supplementary Figure 4 | Correlation analysis and differential analysis of immune checkpoint genes. The overview of differential expression of immune checkpoint genes **(A)**. Correlation analysis and differential analysis of PDCD1 **(B, E)**, CTLA4 **(C, F)**, and CD274 **(D, G)**.

Supplementary Figure 5 | Correlation analysis and differential analysis of CYT, GZMA and PRF1. Comparations between high-risk group and low-risk group in terms of CYT, GZMA, PRF1 expression **(A–C)**. The relationship between the risks core and CYT, GZMA, PRF1 expression **(D–F)** and their correlation coefficients **(G–I)**.

Supplementary Figure 6 | Gene set enrichment analysis. Representative enrichment plots generated in the KEGG database, the pathways enriched in the high-risk group **(A)** and low-risk group **(B)** are displayed. Representative enrichment plots generated in the GO database, the pathways enriched in the high-risk group **(C)** and low-risk group **(D)** are displayed.

Supplementary Figure 7 | Correlation analysis on the relationship between the 14-gene signature and clinical characteristics. Differential analysis on risk scores of subgroups with various T stage **(A)**. The nomogram based on OS/follow-up time, tumor status/T stage to evaluate risk scores **(B)**. Cablibration curves **(C)**, ROC curves **(D)**, DCA curves **(E)** indicate the accuracy of the signature.

REFERENCES

1. Rebecca VW, Somasundaram R, Herlyn M. Pre-Clinical Modeling of Cutaneous Melanoma. *Nat Commun* (2020) 11(1):2858. doi: 10.1038/s41467-020-15546-9
2. Ellison PM, Zitelli JA, Brodland DG. Mohs Micrographic Surgery for Melanoma: A Prospective Multicenter Study. *J Am Acad Dermatol* (2019) 81(3):767–74. doi: 10.1016/j.jaad.2019.05.057
3. Raigani S, Cohen S, Boland GM. The Role of Surgery for Melanoma in an Era of Effective Systemic Therapy. *Curr Oncol Rep* (2017) 19(3):17. doi: 10.1007/s11912-017-0575-8
4. Wada-Ohno M, Ito T, Furue M. Adjuvant Therapy for Melanoma. *Curr Treat Options Oncol* (2019) 20(8):63. doi: 10.1007/s11864-019-0666-x
5. Mishra H, Mishra PK, Ekielski A, Jaggi M, Iqbal Z, Talegaonkar S. Melanoma Treatment: From Conventional to Nanotechnology. *J Cancer Res Clin Oncol* (2018) 144(12):2283–302. doi: 10.1007/s00432-018-2726-1
6. Luke JJ, Flaherty KT, Ribas A, Long GV. Targeted Agents and Immunotherapies: Optimizing Outcomes in Melanoma. *Nat Rev Clin Oncol* (2017) 14(8):463–82. doi: 10.1038/nrclinonc.2017.43
7. Franklin C, Livingstone E, Roesch A, Schilling B, Schadendorf D. Immunotherapy in Melanoma: Recent Advances and Future Directions. *Eur J Surg Oncol* (2017) 43(3):604–11. doi: 10.1016/j.ejso.2016.07.145
8. Ralli M, Botticelli A, Visconti IC, Angeletti D, Fiore M, Marchetti P, et al. Immunotherapy in the Treatment of Metastatic Melanoma: Current Knowledge and Future Directions. *J Immunol Res* (2020) 2020:9235638. doi: 10.1155/2020/9235638
9. Rotte A, Bhandaru M, Zhou Y, McElwee KJ. Immunotherapy of Melanoma: Present Options and Future Promises. *Cancer Metastasis Rev* (2015) 34 (1):115–28. doi: 10.1007/s10555-014-9542-0
10. Rossi E, Schinzari G, Maiorano BA, Indellicati G, Di Stefani A, Pagliara MM, et al. Efficacy of Immune Checkpoint Inhibitors in Different Types of Melanoma. *Hum Vaccin Immunother* (2021) 17(1):4–13. doi: 10.1080/21645515.2020.1771986
11. Jain V, Hwang WT, Venigalla S, Nead KT, Lukens JN, Mitchell TC, et al. Association of Age With Efficacy of Immunotherapy in Metastatic Melanoma. *Oncologist* (2020) 25(2):e381–5. doi: 10.1634/theoncologist.2019-0377
12. Pardoll DM. The Blockade of Immune Checkpoints in Cancer Immunotherapy. *Nat Rev Cancer* (2012) 12(4):252–64. doi: 10.1038/nrc3239
13. Topalian SL, Drake CG, Pardoll DM. Immune Checkpoint Blockade: A Common Denominator Approach to Cancer Therapy. *Cancer Cell* (2015) 27(4):450–61. doi: 10.1016/j.ccell.2015.03.001
14. Barrios DM, Do MH, Phillips GS, Postow MA, Akaike T, Nghiem P, et al. Immune Checkpoint Inhibitors to Treat Cutaneous Malignancies. *J Am Acad Dermatol* (2020) 83(5):1239–53. doi: 10.1016/j.jaad.2020.03.131
15. Bagchi S, Yuan R, Engleman EG. Immune Checkpoint Inhibitors for the Treatment of Cancer: Clinical Impact and Mechanisms of Response and Resistance. *Annu Rev Pathol* (2021) 16:223–49. doi: 10.1146/annurev-pathol-042020-042741
16. Himmel ME, Saibil SD, Saltman AP. Immune Checkpoint Inhibitors in Cancer Immunotherapy. *CMAJ* (2020) 192(24):E651. doi: 10.1503/cmaj.191231
17. Martínez-Lostao L, Anel A, Pardo J. How Do Cytotoxic Lymphocytes Kill Cancer Cells? *Clin Cancer Res* (2015) 21(22):5047–56. doi: 10.1158/1078-0432.CCR-15-0685
18. Rooney MS, Shukla SA, Wu CJ, Getz G, Hacohen N. Molecular and Genetic Properties of Tumors Associated With Local Immune Cytolytic Activity. *Cell* (2015) 160(1-2):48–61. doi: 10.1016/j.cell.2014.12.033
19. Zaravinos A, Roufas C, Nagara M, Moreno B, Oblovatskaya M, Efstathiades C, et al. Cytolytic Activity Correlates With the Mutational Burden and Deregulated Expression of Immune Checkpoints in Colorectal Cancer. *J Exp Clin Cancer Res* (2019) 38(1):364. doi: 10.1186/s13046-019-1372-z
20. Barakat A, Mittal A, Ricketts D, Rogers BA. Understanding Survival Analysis: Actuarial Life Tables and the Kaplan-Meier Plot. *Br J Hosp Med (Lond)* (2019) 80(11):642–6. doi: 10.12968/hmed.2019.80.11.642
21. Gaujoux R, Seoighe C. A Flexible R Package for Nonnegative Matrix Factorization. *BMC Bioinf* (2010) 11:367. doi: 10.1186/1471-2105-11-367
22. Becht E, Giraldo NA, Lacroix L, Buttard B, Elarouci N, Petitprez F, et al. Estimating the Population Abundance of Tissue-Infiltrating Immune and Stromal Cell Populations Using Gene Expression [Published Correction Appears in Genome Biol. 2016 Dec 1;17 (1):249]. *Genome Biol* (2016) 17 (1):218. doi: 10.1186/s13059-016-1070-5
23. Blanche P, Dartigues JF, Jacqmin-Gadda H. Estimating and Comparing Time-Dependent Areas Under Receiver Operating Characteristic Curves for Censored Event Times With Competing Risks. *Stat Med* (2013) 32 (30):5381–97. doi: 10.1002/sim.5958
24. Hoo ZH, Candlish J, Teare D. What Is an ROC Curve? *Emerg Med J* (2017) 34 (6):357–9. doi: 10.1136/emermed-2017-206735
25. Ritterhouse LL. Tumor Mutational Burden. *Cancer Cytopathol* (2019) 127 (12):735–6. doi: 10.1002/cncy.22174
26. Charoentong P, Finotello F, Angelova M, Mayer C, Efremova M, Rieder D, et al. Pan-Cancer Immunogenomic Analyses Reveal Genotype-Immunophenotype Relationships and Predictors of Response to Checkpoint Blockade. *Cell Rep* (2017) 18(1):248–62. doi: 10.1016/j.celrep.2016.12.019
27. Uhlén M, Fagerberg L, Hallström BM, Lindskog C, Oksvold P, Mardinoglu A, et al. Proteomics. Tissue-Based Map of the Human Proteome. *Science* (2015) 347(6220):1260419. doi: 10.1126/science.1260419
28. Mayakonda A, Lin DC, Assenov Y, Plass C, Koeffler HP. Maftools: Efficient and Comprehensive Analysis of Somatic Variants in Cancer. *Genome Res* (2018) 28(11):1747–56. doi: 10.1101/gr.239244.118
29. Yoshihara K, Shahmoradgoli M, Martínez E, Vegesna R, Kim H, Torres-Garcia W, et al. Inferring Tumour Purity and Stromal and Immune Cell Admixture From Expression Data. *Nat Commun* (2013) 4:2612. doi: 10.1038/ncomms3612
30. Eng KH, Schiller E, Morrell K. On Representing the Prognostic Value of Continuous Gene Expression Biomarkers With the Restricted Mean Survival Curve. *Oncotarget* (2015) 6(34):36308–18. doi: 10.18632/oncotarget.6121
31. Abbott M, Ustoyev Y. Cancer and the Immune System: The History and Background of Immunotherapy. *Semin Oncol Nurs* (2019) 35(5):150923. doi: 10.1016/j.soncn.2019.08.002
32. Yu WD, Sun G, Li J, Xu J, Wang X. Mechanisms and Therapeutic Potentials of Cancer Immunotherapy in Combination With Radiotherapy and/or Chemotherapy. *Cancer Lett* (2019) 452:66–70. doi: 10.1016/j.canlet.2019.02.048
33. Burns D, George J, Aucoin D, Bower J, Burrell S, Gilbert R, et al. The Pathogenesis and Clinical Management of Cutaneous Melanoma: An Evidence-Based Review. *J Med Imaging Radiat Sci* (2019) 50(3):460–469.e1. doi: 10.1016/j.jmir.2019.05.001
34. Karaman S, Alitalo K. Midkine and Melanoma Metastasis: A Malevolent Mix. *Dev Cell* (2017) 42(3):205–7. doi: 10.1016/j.devcel.2017.07.015
35. Onitilo AA, Wittig JA. Principles of Immunotherapy in Melanoma. *Surg Clin North Am* (2020) 100(1):161–73. doi: 10.1016/j.suc.2019.09.009
36. Zhou Z, He H, Wang K, Shi X, Wang Y, Su Y, et al. Granzyme A From Cytotoxic Lymphocytes Cleaves GSDMB to Trigger Pyroptosis in Target Cells. *Science* (2020) 368(6494):eaaz7548. doi: 10.1126/science.aaz7548
37. Trapani JA, Thia KY, Andrews M, Davis ID, Gedye C, Parente P, et al. Human Perforin Mutations and Susceptibility to Multiple Primary Cancers. *Oncoimmunology* (2013) 2(4):e24185. doi: 10.4161/onci.24185
38. Zhou S, Sun Y, Chen T, Wang J, He J, Lyu J, et al. The Landscape of the Tumor Microenvironment in Skin Cutaneous Melanoma Reveals a Prognostic and Immunotherapeutically Relevant Gene Signature. *Front Cell Dev Biol* (2021) 9:739594. doi: 10.3389/fcell.2021.739594
39. Attia JVD, Dessens CE, van de Water R, Houvast RD, Kuppen PJK, Krijgsman D. The Molecular and Functional Characteristics of HLA-G and the Interaction With Its Receptors: Where to Intervene for Cancer Immunotherapy? *Int J Mol Sci* (2020) 21(22):8678. doi: 10.3390/ijms21228678
40. Fillmore RA, Mitra A, Xi Y, Ju J, Scammell J, Shevde LA, et al. Nmi (N-Myc Interactor) Inhibits Wnt/beta-Catenin Signaling and Retards Tumor Growth. *Int J Cancer* (2009) 125(3):556–64. doi: 10.1002/ijc.24276
41. Compagnone M, Cifaldi L, Fruci D. Regulation of ERAP1 and ERAP2 Genes and Their Disfunction in Human Cancer. *Hum Immunol* (2019) 80(5):318–24. doi: 10.1016/j.humimm.2019.02.014
42. Balachandran VP, Gonen M, Smith JJ, DeMatteo RP. Nomograms in Oncology: More Than Meets the Eye. *Lancet Oncol* (2015) 16(4):e173–80. doi: 10.1016/S1470-2045(14)71116-7
43. Reinhold WC, Sunshine M, Liu H, Varma S, Kohn KW, Morris J, et al. CellMiner: A Web-Based Suite of Genomic and Pharmacologic Tools to

Explore Transcript and Drug Patterns in the NCI-60 Cell Line Set. *Cancer Res* (2012) 72(14):3499–511. doi: 10.1158/0008-5472.CAN-12-1370
44. Takeda T, Tsubaki M, Kato N, Genno S, Ichimura E, Enomoto A, et al. Sorafenib Treatment of Metastatic Melanoma With C-Kit Aberration Reduces Tumor Growth and Promotes Survival. *Oncol Lett* (2021) 22(6):827. doi: 10.3892/ol.2021.13089
45. Mangana J, Levesque MP, Karpova MB, Dummer R. Sorafenib in Melanoma. *Expert Opin Investig Drugs* (2012) 21(4):557–68. doi: 10.1517/13543784.2012.665872
46. Tanaka A, Nishikawa H, Noguchi S, Sugiyama D, Morikawa H, Takeuchi Y, et al. Tyrosine Kinase Inhibitor Imatinib Augments Tumor Immunity by Depleting Effector Regulatory T Cells. *J Exp Med* (2020) 217(2):e20191009. doi: 10.1084/jem.20191009
47. Li C, Han X. Melanoma Cancer Immunotherapy Using PD-L1 siRNA and Imatinib Promotes Cancer-Immunity Cycle. *Pharm Res* (2020) 37(6):109. doi: 10.1007/s11095-020-02838-4
48. Flaherty KT, Hamilton BK, Rosen MA, Amaravadi RK, Schuchter LM, Gallagher M, et al. Phase I/II Trial of Imatinib and Bevacizumab in Patients With Advanced Melanoma and Other Advanced Cancers. *Oncologist* (2015) 20(8):952–9. doi: 10.1634/theoncologist.2015-0108
49. Guo J, Si L, Kong Y, Flaherty KT, Xu X, Zhu Y. Open-Label, Single-Arm Trial of Imatinib Mesylate in Patients With Metastatic Melanoma Harboring C-Kit Mutation or Amplification. *J Clin Oncol* (2011) 29(21):2904–9. doi: 10.1200/JCO.2010.33.9275
50. Wan X, Zhu Y, Zhang L, Hou W. Gefitinib Inhibits Malignant Melanoma Cells Through the VEGF/AKT Signaling Pathway. *Mol Med Rep* (2018) 17(5):7351–5. doi: 10.3892/mmr.2018.8728
51. Patel SP, Kim KB, Papadopoulos NE, Hwu WJ, Hwu P, Prieto VG, et al. A Phase II Study of Gefitinib in Patients With Metastatic Melanoma. *Melanoma Res* (2011) 21(4):357–63. doi: 10.1097/CMR.0b013e3283471073
52. Ji G, Luo B, Chen L, Shen G, Tian T. GBP2 Is a Favorable Prognostic Marker of Skin Cutaneous Melanoma and Affects Its Progression *via* the Wnt/β-Catenin Pathway. *Ann Clin Lab Sci* (2021) 51(6):772–82.
53. Yu S, Yu X, Sun L, Zheng Y, Chen L, Xu H, et al. GBP2 Enhances Glioblastoma Invasion Through Stat3/fibronectin Pathway. *Oncogene* (2020) 39(27):5042–55. doi: 10.1038/s41388-020-1348-7
54. Godoy P, Cadenas C, Hellwig B, Marchan R, Stewart J, Reif R, et al. Interferon-Inducible Guanylate Binding Protein (GBP2) is Associated With Better Prognosis in Breast Cancer and Indicates an Efficient T Cell Response. *Breast Cancer* (2014) 21(4):491–9. doi: 10.1007/s12282-012-0404-8
55. Rahvar F, Salimi M, Mozdarani H. Plasma GBP2 Promoter Methylation is Associated With Advanced Stages in Breast Cancer. *Genet Mol Biol* (2020) 43(4):e20190230. doi: 10.1590/1678-4685-GMB-2019-0230
56. Ghanem G, Fabrice J. Tyrosinase Related Protein 1 (TYRP1/gp75) in Human Cutaneous Melanoma. *Mol Oncol* (2011) 5(2):150–5. doi: 10.1016/j.molonc.2011.01.006
57. Gilot D, Migault M, Bachelot L, Journé F, Rogiers A, Donnou-Fournet E, et al. A non-Coding Function of TYRP1 mRNA Promotes Melanoma Growth. *Nat Cell Biol* (2017) 19(11):1348–57. doi: 10.1038/ncb3623
58. Liang R, Li X, Zhu X. Deciphering the Roles of IFITM1 in Tumors. *Mol Diagn Ther* (2020) 24(4):433–41. doi: 10.1007/s40291-020-00469-4
59. Yang Y, Li Y, Qi R, Zhang L. Development and Validation of a Combined Glycolysis and Immune Prognostic Model for Melanoma. *Front Immunol* (2021) 12:711145. doi: 10.3389/fimmu.2021.711145
60. Chan TA, Yarchoan M, Jaffee E, Swanton C, Quezada SA, Stenzinger A, et al. Development of Tumor Mutation Burden as an Immunotherapy Biomarker: Utility for the Oncology Clinic. *Ann Oncol* (2019) 30(1):44–56. doi: 10.1093/annonc/mdy495
61. Goodman AM, Kato S, Bazhenova L, Patel SP, Frampton GM, Miller V, et al. Tumor Mutational Burden as an Independent Predictor of Response to Immunotherapy in Diverse Cancers. *Mol Cancer Ther* (2017) 16(11):2598–608. doi: 10.1158/1535-7163.MCT-17-0386
62. McNamara MG, Jacobs T, Lamarca A, Hubner RA, Valle JW, Amir E. Impact of High Tumor Mutational Burden in Solid Tumors and Challenges for Biomarker Application. *Cancer Treat Rev* (2020) 89:102084. doi: 10.1016/j.ctrv.2020.102084
63. Arora S, Velichinskii R, Lesh RW, Ali U, Kubiak M, Ennis P, et al. Existing and Emerging Biomarkers for Immune Checkpoint Immunotherapy in Solid Tumors. *Adv Ther* (2019) 36(10):2638–78. doi: 10.1007/s12325-019-01051-z
64. Chalmers ZR, Connelly CF, Fabrizio D, Gay L, Ali SM, Ennis R, et al. Analysis of 100,000 Human Cancer Genomes Reveals the Landscape of Tumor Mutational Burden. *Genome Med* (2017) 9(1):34. doi: 10.1186/s13073-017-0424-2
65. Samstein RM, Lee CH, Shoushtari AN, Hellmann MD, Shen R, Janjigian YY, et al. Tumor Mutational Load Predicts Survival After Immunotherapy Across Multiple Cancer Types. *Nat Genet* (2019) 51(2):202–6. doi: 10.1038/s41588-018-0312-8
66. Binnewies M, Roberts EW, Kersten K, Chan V, Fearon DF, Merad M, et al. Understanding the Tumor Immune Microenvironment (TIME) for Effective Therapy. *Nat Med* (2018) 24(5):541–50. doi: 10.1038/s41591-018-0014-x
67. Giraldo NA, Sanchez-Salas R, Peske JD, Vano Y, Becht E, Petitprez F, et al. The Clinical Role of the TME in Solid Cancer. *Br J Cancer* (2019) 120(1):45–53. doi: 10.1038/s41416-018-0327-z
68. Aran D, Hu Z, Butte AJ. Xcell: Digitally Portraying the Tissue Cellular Heterogeneity Landscape. *Genome Biol* (2017) 18(1):220. doi: 10.1186/s13059-017-1349-1
69. Li T, Fan J, Wang B, Traugh N, Chen Q, Liu JS, et al. TIMER: A Web Server for Comprehensive Analysis of Tumor-Infiltrating Immune Cells. *Cancer Res* (2017) 77(21):e108–10. doi: 10.1158/0008-5472.CAN-17-0307
70. Finotello F, Mayer C, Plattner C, Laschober G, Rieder D, Hackl H, et al. Molecular and Pharmacological Modulators of the Tumor Immune Contexture Revealed by Deconvolution of RNA-Seq Data [Published Correction Appears in Genome Med. *2019 Jul 29;11(1):50] Genome Med* (2019) 11(1):34. doi: 10.1186/s13073-019-0638-6
71. van Veldhoven CM, Khan AE, Teucher B, Rohrmann S, Raaschou-Nielsen O, Tjønneland A, et al. Physical Activity and Lymphoid Neoplasms in the European Prospective Investigation Into Cancer and Nutrition (EPIC). *Eur J Cancer* (2011) 47(5):748–60. doi: 10.1016/j.ejca.2010.11.010
72. Tamminga M, Hiltermann TJN, Schuuring E, Timens W, Fehrmann RS, Groen HJ. Immune Microenvironment Composition in Non-Small Cell Lung Cancer and its Association With Survival. *Clin Transl Immunol* (2020) 9(6):e1142. doi: 10.1002/cti2.1142
73. Newman AM, Liu CL, Green MR, Gentles AJ, Feng W, Xu Y, et al. Robust Enumeration of Cell Subsets From Tissue Expression Profiles. *Nat Methods* (2015) 12(5):453–7. doi: 10.1038/nmeth.3337
74. Tokunaga R, Naseem M, Lo JH, Battaglin F, Soni S, Puccini A, et al. B Cell and B Cell-Related Pathways for Novel Cancer Treatments. *Cancer Treat Rev* (2019) 73:10–9. doi: 10.1016/j.ctrv.2018.12.001
75. Da Gama Duarte J, Peyper JM, Blackburn JM. B Cells and Antibody Production in Melanoma. *Mamm Genome* (2018) 29(11-12):790–805. doi: 10.1007/s00335-018-9778-z
76. Selitsky SR, Mose LE, Smith CC, Chai S, Hoadley KA, Dittmer DP, et al. Prognostic Value of B Cells in Cutaneous Melanoma. *Genome Med* (2019) 11(1):36. doi: 10.1186/s13073-019-0647-5
77. Spranger S, Spaapen RM, Zha Y, Williams J, Meng Y, Ha TT, et al. Up-Regulation of PD-L1, IDO, and T(regs) in the Melanoma Tumor Microenvironment Is Driven by CD8(+) T Cells. *Sci Transl Med* (2013) 5(200):200ra116. doi: 10.1126/scitranslmed.3006504
78. Saleh R, Elkord E. Acquired Resistance to Cancer Immunotherapy: Role of Tumor-Mediated Immunosuppression. *Semin Cancer Biol* (2020) 65:13–27. doi: 10.1016/j.semcancer.2019.07.017
79. Almatroodi SA, McDonald CF, Darby IA, Pouniotis DS. Characterization of M1/M2 Tumour-Associated Macrophages (TAMs) and Th1/Th2 Cytokine Profiles in Patients With NSCLC. *Cancer Microenviron* (2016) 9(1):1–11. doi: 10.1007/s12307-015-0174-x
80. Shimizu K, Yamasaki S, Sakurai M, Yumoto N, Ikeda M, Mishima-Tsumagari C, et al. Granzyme A Stimulates pDCs to Promote Adaptive Immunity *via* Induction of Type I IFN. *Front Immunol* (2019) 10:1450. doi: 10.3389/fimmu.2019.01450
81. Inoue H, Park JH, Kiyotani K, Zewde M, Miyashita A, Jinnin M, et al. Intratumoral Expression Levels of PD-L1, GZMA, and HLA-A Along With Oligoclonal T Cell Expansion Associate With Response to Nivolumab in Metastatic Melanoma. *Oncoimmunology* (2016) 5(9):e1204507. doi: 10.1080/2162402X.2016.1204507
82. Fan C, Hu H, Shen Y, Wang Q, Mao Y, Ye B, et al. PRF1 is a Prognostic Marker and Correlated With Immune Infiltration in Head and Neck

Squamous Cell Carcinoma. *Transl Oncol* (2021) 14(4):101042. doi: 10.1016/j.tranon.2021.101042
83. Alcaraz-Sanabria A, Baliu-Piqué M, Saiz-Ladera C, Rojas K, Manzano A, Marquina G, et al. Genomic Signatures of Immune Activation Predict Outcome in Advanced Stages of Ovarian Cancer and Basal-Like Breast Tumors. *Front Oncol* (2020) 9:1486. doi: 10.3389/fonc.2019.01486
84. Ju M, Jiang L, Wei Q, Yu L, Chen L, Wang Y, et al. A Immune-Related Signature Associated With TME Can Serve as a Potential Biomarker for Survival and Sorafenib Resistance in Liver Cancer. *Onco Targets Ther* (2021) 14:5065–83. doi: 10.2147/OTT.S326784
85. Kotsias F, Cebrian I, Alloatti A. Antigen Processing and Presentation. *Int Rev Cell Mol Biol* (2019) 348:69–121. doi: 10.1016/bs.ircmb.2019.07.005
86. Bandola-Simon J, Roche PA. Dysfunction of Antigen Processing and Presentation by Dendritic Cells in Cancer. *Mol Immunol* (2019) 113:31–7. doi: 10.1016/j.molimm.2018.03.025
87. D'Arcy C, Kiel C. Cell Adhesion Molecules in Normal Skin and Melanoma. *Biomolecules* (2021) 11(8):1213. doi: 10.3390/biom11081213
88. Forés-Martos J, Boullosa C, Rodrigo-Domínguez D, Sánchez-Valle J, Suay-García B, Climent J, et al. Transcriptomic and Genetic Associations Between Alzheimer's Disease, Parkinson's Disease, and Cancer. *Cancers (Basel)* (2021) 13(12):2990. doi: 10.3390/cancers13122990

Conflict of Interest: The authors declare that the research was conducted in the absence of any commercial or financial relationships that could be construed as a potential conflict of interest.

Publisher's Note: All claims expressed in this article are solely those of the authors and do not necessarily represent those of their affiliated organizations, or those of the publisher, the editors and the reviewers. Any product that may be evaluated in this article, or claim that may be made by its manufacturer, is not guaranteed or endorsed by the publisher.

frontiers | Frontiers in Oncology

ORIGINAL RESEARCH
published: 18 May 2022
doi: 10.3389/fonc.2022.816070

Downstream Regulatory Network of MYBL2 Mediating Its Oncogenic Role in Melanoma

Feiliang Zhong[1,2], *Jia Liu*[1,2], *Chang Gao*[3], *Tingting Chen*[4*] and *Bo Li*[1,2,3*]

[1] Frontiers Science Center for Synthetic Biology and Key Laboratory of Systems Bioengineering (Ministry of Education), School of Chemical Engineering and Technology, Tianjin University, Tianjin, China, [2] Collaborative Innovation Center of Chemical Science and Engineering (Tianjin), Tianjin University, Tianjin, China, [3] Life Science Institute, Jinzhou Medical University, Jinzhou, China, [4] School of Basic Medicine, Guangdong Medical University, Dongguan, China

OPEN ACCESS

Edited by:
Gagan Chhabra,
University of Wisconsin-Madison,
United States

Reviewed by:
Tupa Basuroy,
Massachusetts General Hospital and Harvard Medical School, United States
Suzie Chen,
Rutgers, The State University of New Jersey, United States

***Correspondence:**
Tingting Chen
jkf_ctt@163.com
Bo Li
lib028@tju.edu.cn

Specialty section:
This article was submitted to Skin Cancer, a section of the journal Frontiers in Oncology

Received: 16 November 2021
Accepted: 14 April 2022
Published: 18 May 2022

Citation:
Zhong F, Liu J, Gao C, Chen T and Li B (2022) Downstream Regulatory Network of MYBL2 Mediating Its Oncogenic Role in Melanoma. Front. Oncol. 12:816070. doi: 10.3389/fonc.2022.816070

The transcription factor MYBL2 is widely expressed in proliferating cells. Aberrant expression of MYBL2 contributes to tumor malignancy and is associated with poor patient prognosis. However, the downstream transcriptional network that mediates its oncogenic properties remains elusive. In the present study, we observed that MYBL2 was overexpressed in malignant and metastatic melanoma patient samples and that the high expression level of MYBL2 was significantly associated with poor prognosis. A loss-of-function study demonstrated that MYBL2 depletion significantly decreased cell proliferation and migration and prevented cell cycle progression. We also determined that MYBL2 promoted the formation of melanoma stem-like cell populations, indicating its potential as a therapeutic target for treating resistant melanoma. Mechanistically, we constructed an MYBL2 regulatory network in melanoma by integrating RNA-seq and ChIP-seq data. EPPK1, PDE3A, and FCGR2A were identified as three core target genes of MYBL2. Importantly, multivariate Cox regression and survival curve analysis revealed that PDE3A and EPPK1 were negatively correlated with melanoma patient survival; however, FCGR2A was positively correlated with patient survival. Overall, our findings elucidate an MYBL2 regulatory network related to cell proliferation and cancer development in melanoma, suggesting that MYBL2 may be potentially targeted for melanoma diagnosis and treatment.

Keywords: melanoma, MYBL2, ChIP-seq, regulatory network, prognosis

INTRODUCTION

MYB proto-oncogene like 2 (MYBL2, B-MYB), a member of the MYB transcription factor (TF) family, is widely expressed in most proliferating cells and has a wide range of functions (1). It participates in cell cycle regulation, DNA replication, and maintenance of genome integrity (2–4), suggesting that MYBL2 may be a potential key biomarker. In the cell cycle, the transcription level of MYBL2 can be regulated in

an E2F-dependent manner (5). The DREAM complex structure (DP, RB-like, E2F, and MuvB) inhibits cell cycle-related gene expression during the quiescent phase. As cells enter the cell cycle, the MuvB core component of the DREAM complex and FOXM1 cooperate with MYBL2 to co-regulate the expression of G2/M genes (6). MYBL2 is upregulated disproportionately in *p53* gene-mutated tumors, and it can even overcome DNA damage-induced G2 arrest in *p53*-mutated cells (7). The downregulation of MYBL2 leads to cell cycle arrest in the G2/M phase through the p53-p21-DREAM-CDE/CHR pathway (8). MYBL2 participates in different aspects of cell apoptosis and survival by regulating downstream gene and protein interactions. Grassilli et al. demonstrated that MYBL2 regulates anti-apoptotic *Bcl-2* gene upregulation in mouse IL-2-dependent T cells, thus antagonizing doxorubicin-induced apoptosis (9). Moreover, Seong et al. showed that MYBL2 directly interacts with serine–threonine kinase receptor-associated protein (STRAP), so that more tumor suppressor protein TP53 can be translocated to promote cell apoptosis (10). MYBL2 is upregulated in many cancers, such as breast cancer, hepatocellular carcinoma, lung cancer, and colorectal cancer, and upregulated expression of MYBL2 is associated with poor prognosis in patients with cancer. However, additional agents involved in the MYBL2 downstream transcriptional network mediating its cancer-promoting properties remain unclear; furthermore, it is unknown which additional cancer entities are also affected by MYBL2 deregulation (1).

Malignant melanoma (MM) is one of the most aggressive skin tumors originating from melanocytes (11). Although it accounts for only a small number of skin cancers, it is more prone to spread and metastasis; hence, it is the most lethal type of skin cancer (12). Approximately 1.7% of new global cases and 0.6% of new cancer deaths worldwide in 2020 were due to MM (13). In recent years, the discovery of MAPKs and other key signaling pathways, BRAF and other drug targets, and progress in immunotherapy have greatly improved the prognosis of melanoma patients (14). However, due to the strong heterogeneity of melanoma in terms of genetic and epigenetic characteristics, signal transduction pathway activation, and biological behavior, these treatments are still ineffective or suboptimal in a considerable proportion of patients. Cancer stem cells are another major issue for melanoma metastasis and relapse—a small subset of cancer cells can survive and colonize new environments. Therefore, it is essential to develop new and effective approaches targeting cancer stem cells to overcome metastasis and drug resistance in patients with advanced melanoma.

In the present study, we aimed to determine the oncogenic role of MYBL2 and characterize MYBL2-mediated regulatory networks/direct targets in melanoma. Our results indicated that MYBL2 was highly expressed in melanoma samples, revealing a poor prognosis in patients with melanoma. Moreover, we determined that MYBL2 promoted the growth of melanoma cells and melanoma stem-like cell proliferation in a mouse model and in melanoma cells, indicating that MYBL2 may be used as a biomarker or therapeutic target. Next, 11 core target genes of MYBL2 were identified by integrating RNA-seq and ChIP-seq data, suggesting that MYBL2 promoted melanoma growth. Importantly, we identified three key genes (*FCGR2A, PDE3A*, and *EPPK1*) that were correlated with the survival of melanoma patients. These results revealed a MYBL2 regulatory network related to cell proliferation and cancer development pathways in melanoma. MYBL2 may be a potential target for the diagnosis and treatment of melanoma.

MATERIALS AND METHODS

Cell Lines and Cell Culture

Human epidermal melanocyte HEMn-LP, embryonic kidney cell line 293T, and human malignant melanoma cell lines A375 and SK-MEL-28 were purchased from the Cell Resource Center of Peking Union Medical College (IBMS, CAMS/PUMC). The human metastatic melanoma cell line A2058 was kindly provided by Dr. Fang from the Beijing Institute of Genomics. HEMn-LP cells were cultured in 254 medium (Gibco, Thermo Fisher Scientific, Inc.), containing Human Melanocyte Growth Supplement (HMGS, Gibco, Thermo Fisher Scientific, Inc.), 100 μg/ml penicillin, and 100 μg/ml streptomycin. 293T, A375, SK-MEL-28, and A2058 cell lines were cultured in Dulbecco's modified Eagle's medium (DMEM) supplemented with 10% fetal bovine serum (FBS) (Gibco, Thermo Fisher Scientific, Inc.), 100 μg/ml penicillin, and 100 μg/ml streptomycin. The cultures were maintained in a humidified incubator with 5% CO_2 at 37°C under standard cell culture conditions and routinely passaged when 80%–90% confluent.

Data Collection and Bioinformatic Analysis

Melanoma transcriptome data were obtained from The Cancer Genome Atlas (TCGA) database (https://portal.gdc.cancer.gov). Normal skin samples were obtained from the GTEx database. mRNA expression data involving 461 tumors and 558 normal patient samples were collected. For Kaplan–Meier curves, *p*-values and hazard ratios (HRs) with 95% confidence intervals (CIs) were generated by log-rank tests and univariate Cox proportional hazard regression. All analytical methods indicated above and R packages were performed using R software v.4.0.3 (15). $p < 0.05$ was considered to be statistically significant.

Tissue Microarrays and Immunohistochemistry

Skin cancer tissue microarray (TMA) (K063Me01) was purchased from Xi'an Biotech Co., Ltd. (Xi'an, China). Protein expression was detected by immunohistochemistry (IHC) and analyzed according to standard methods and microarray instructions. IHC staining was performed with a specific antibody (MYBL2, Thermo Fisher Scientific, PA5-79713) and then TMAs were examined and independently scored by two pathologists. Tumor stages of the specimens on the TMA were categorized according to the tumor–node–metastasis (TNM) system of the American Joint Committee on Cancer (AJCC) (16). Negative control (NC) groups were examined using conventional hematoxylin and eosin (H&E) staining. H&E

staining was performed according to standard methods. IHC experimental evaluation criteria: After locating the staining results on the chip point by point, the color intensity of the cells was judged as follows: no staining = negative (-), light brown = weakly positive (+), brown = positive (++), and Tan = strongly positive (+++). According to the number of positive cells, subdivision into (-) means that the number of positive cells = <10%, (+) means that the number of positive cells = 10%–25%, (++) means that the number of positive cells is between 26% and 49%, and (+++) means that the number of positive cells = >50%. Finally, a qualitative and semi-quantitative color intensity result was obtained based on a comprehensive evaluation of the two results. At least 5–10 HPFs (high-power fields) were randomly observed, and average values were calculated.

MYBL2 Silencing and Overexpression

Pairs of complementary oligonucleotides encoding shRNAs were cloned into the lentiviral mammalian expression vector pLL3.7 (Addgene, Watertown, USA) according to the manufacturer's instructions. The target sequences of the shRNA were as follows: sh1, 5′-GCTAACAACAAAGTTCCACTT-3′, and sh2, 5′-GCTTGGTGTGACCTGAGTAAA-3′. A non-silencing shRNA sequence without the *MYBL2* shRNA component was used as an NC. For infection, 5×10^5 293T cells were plated in 6-cm plates and transfected 24 h later with 1 μg of DNA from lentiviral backbone vector and packaging plasmids according to the Lipofectamine 3000 transfection kit (Invitrogen, Thermo Fisher Scientific, Inc.) protocol. The medium was replaced with DMEM 24 h post-transfection. Cells were infected for 24 h at 37°C with 2 ml of lentivirus and 8 μg/ml polybrene (Sigma-Aldrich).

Full-length cDNA encoding human MYBL2 was synthesized and inserted into the pCDH-CMV-GFP-T2A-Puro vector (Addgene) to obtain the MYBL2-overexpressing plasmid pCDH-MYBL2. The recombinant lentiviral vector pCDH-MYBL2 was then transfected into melanoma A375 and A2058 cells. The transfection reagent Lipofectamine 3000 (Invitrogen) was mixed with Opti-MEM (Gibco, Thermo Fisher Scientific). Cells were infected for 24 h at 37°C with 2 ml of lentivirus and 8 μg/ml polybrene (Sigma-Aldrich). Cells were selected 48 h later using 1 μg/ml puromycin (Sigma-Aldrich). Knockdown and overexpression efficiency were determined by qPCR of *MYBL2* mRNA and Western blot assays for MYBL2 protein.

Quantitative Real-Time Polymerase Chain Reaction

Total RNA was extracted from cultured cells using TRIzol reagent (Invitrogen, Thermo Fisher Scientific, Inc.) and cDNA was reverse-transcribed using the GeneCopoeia™ First Strand cDNA Synthesis Kit (Genecopoeia, USA). RT-qPCR analysis was performed using the SYBR PCR mix kit (TransGen, Beijing, China) according to the manufacturer's instructions. The samples were run in triplicate in three independent experiments. *GAPDH* RNA was used as a reference housekeeping gene. All primer sequences were designed using Primer v.5.0 software (Premier Biosoft International, Palo Alto, CA, USA) as follows:

homo *MYBL2* forward, 5′-GTCCCCTGTCACTGAGAATAG-3′;
homo *MYBL2* reverse, 5′-GCTCCAATGTGTCCTGTTTG-3′;
homo *GAPDH* forward, 5′-AGCCACATCGCTCAGACAC-3′;
homo *GAPDH* reverse, 5′-TTAAAAGCAGCCCTGGTGAC-3′.

Transcript levels were calculated using the comparative threshold cycle (Ct) method normalized to *GAPDH* abundance.

Western Blotting

Western blot analysis was performed according to standard protocols. PVDF membranes (Bio-Rad, Hercules, CA, USA) were probed with specific antibodies, and immunoreactive proteins were detected using an enhanced chemiluminescence (ECL) kit (Thermo Fisher Scientific). GAPDH served as an internal control and was imaged and analyzed using a C-Digit Blotting Scanner (Azure Biosystems, Inc.). Human anti-MYBL2 antibody was obtained from Thermo Fisher Scientific (PA5-79713).

Cell Proliferation Assay

Inhibition of cell proliferation was quantified by Cell Counting Kit-8 (CCK-8; TransGen, Beijing, China) following the manufacturer's instructions. Ten microliters of CCK-8 kit solution was added to the medium after a total of 3×10^3 cells were seeded into each well of 96-well plates. The optical density (OD) was measured at 450 nm using a microplate reader (Thermo Fisher Scientific, Inc.). Each measurement was repeated three times.

Flow Cytometric Analysis

Flow cytometric analysis was performed to determine the effect of MYBL2 on cell cycle distribution. Briefly, 3×10^5 cells grown in 6-well plates were treated with shRNA for 48 h. The cells were then harvested and fixed in 75% ethanol solution. After centrifugation, cells were washed (PI) for 30 min in the dark. Cell cycle distribution was analyzed by flow cytometry (NovoCyte 2040R; ACEA Bioscience, Inc.; Agilent Technologies).

Wound Healing and Transwell Migration Assays

Cell migration ability was assessed by wound healing and transwell migration assays. In the wound healing assay, in brief, 5×10^5 cells were cultured in 6-well plates in DMEM supplemented with 10% FBS to 80%–90% confluence in 24 h. The plate was scratched using a sterile 10-μl pipette tip to generate a uniform wound in the cell monolayer. The plate was washed with PBS to remove cell debris. After continuous incubation for 24 h, wound closure was monitored using an inverted fluorescent microscope. The width of the wound gap was analyzed using ImageJ software. The wound closure area was calculated as follows: migration area (%) = $(A_0 - An)/A_0 \times 100$, where A_0 represents the area of the initial wound area, and An represents the remaining area of the wound at the metering point.

In the transwell migration assay, cells were collected and seeded into the upper chamber (8 μm) at a density of 1×10^5 cells/well (Corning Inc., Corning, NY, USA). The lower chamber was filled with 800 μl of DMEM supplemented with 10% FBS, and the cells were incubated for 24 h at 37°C. The lower cells were fixed with 4% (w/v) formaldehyde and stained with 0.1%

(w/v) crystal violet for 30 min. The number of migrated cells was counted under a microscope.

Stemness Indices Calculation

From the TCGA database, we downloaded RNA-seq (FPKM, Fragments Per Kilobase per Million) of melanoma cases from the Genomic Data Commons (GDC). Next, we converted the PFKM data to TPM and normalized the data log2 (TPM+1) while keeping samples with clinical information recorded. We then calculated mRNA stemness indices using the OCLR algorithm constructed by Malta et al. (17). Based on the characteristics of mRNA expression, the gene expression profile contained 11,774 genes. We used the same Spearman correlation (RNA expression data) and then subtracted the minimum value and divided the difference by the linear transformation of the maximum value to map the dryness index to the range [0,1]. These analysis methods and R package were implemented by R Foundation for Statistical Computing (15) v.4.0.3.

Colony Formation Assay

For tumorsphere formation, single-cell suspensions were harvested and seeded into 6-well ultra-low adherent cell culture plates at a density of 1,000 cells/ml in serum-free DMEM/F12 medium supplemented with 1% L-glutamine, 1% penicillin/streptomycin, 2% B27 (Invitrogen), 20 ng/ml epidermal growth factor (EGF, Sigma, St. Louis, MO, USA), and 20 ng/ml basic fibroblast growth factor (bFGF, Invitrogen). Seven days after seeding, tumorspheres with diameters > 30 μm were counted using Olympus cellSens Standard software. The total numbers of tumorspheres in 6 random fields under 10× objective lens were determined for each well. The experiments were repeated at least 3 times.

In Vivo Tumorigenicity

Six- to eight-week-old male BALB/c-nu/nu mice were purchased from Biotechnology Co., Ltd. (Beijing, China). Cells (1×10^7) in 100 μl of PBS were injected subcutaneously into the right flank of the mice. Body weight was monitored twice per week. Tumor dimensions were measured using calipers, and tumor volume size was calculated using the equation (length × width^2/2). At the end of the experiment, the mice were euthanized, and the tumors were weighed and processed for further analysis. All animal experiments were performed in accordance with protocols approved by the Animal Ethics and Welfare Committee (AEWC) (approval no. IRM-DWLL-2019102).

Histology and Morphometric Analysis

Tumors were collected and fixed in 10% neutral-buffered formalin. Tissues were sectioned and stained with H&E. Images were acquired using an optical microscope (BX51, Olympus, Tokyo, Japan) to evaluate pathological morphology.

Whole-Transcriptome Sequencing

Total RNA was extracted and lysed in 500 μl of TRIzol reagent (MRC, Carrollton, OH, USA) and sent to China's Shenzhen BGI (Shenzhen, China) for further analysis. An RNA-Seq library was created using the Illumina TruSeq RNA Sample Preparation Kit v.2 using a standard protocol. Genes with a *p*-adjusted value (false discovery rate) < 0.05 were selected for Gene Ontology (GO) analysis and heatmap construction. Pathway analysis was performed using the Kyoto Encyclopedia of Genes and Genomes (KEGG) database.

Chromatin Immunoprecipitation Followed by Gene Sequencing assay

ChIP assays were performed using the SimpleChip Plus Sonication Chromatin IP Kit (Cell Signaling Technology, China) following the manufacturer's instructions. Briefly, A2058 cells were cross-linked with 1% formaldehyde solution for 10 min at room temperature and lysed in ChIP lysis buffer with freshly added 1× protease inhibitor cocktail (Roche Applied Science). Cross-linked DNA was then sheared to ~200- to 700-bp fragments *via* sonication with the following pulse mode settings: 10 s with 50 s cooling, amplitude 30%, and 8 cycles. Chromatin was then immunoprecipitated with pMYBL2 antibody (Abcam, ab76009) and DNA was recovered after phenol/chloroform extraction and ethanol precipitation. High-throughput sequencing using an Illumina HiSeq 3000 Sequencer was performed by the Chinese Shenzhen-based BGI (Shenzhen, China).

Statistics

Statistical analyses were performed using Prism 8 software (GraphPad, La Jolla, CA, USA). For comparisons between two groups, two-tailed Student's *t*-test was used. Kaplan–Meier survival analysis was performed to compare survival curves. The statistical significance of protein associations in the TMA dataset was evaluated using Pearson's chi-squared test. Statistically significant levels were defined as ns (not significant, $p > 0.05$), * $p < 0.05$, ** $p < 0.01$, *** $p < 0.001$. All data are presented as means ± SD.

RESULTS

MYBL2 Is Upregulated in Patients With Melanoma

To determine the role of MYBL2 in human melanoma, paraffin sections of skin cancer TMAs (K063Me01) were stained by IHC. The results showed that MYBL2 protein was highly expressed in tumor cells, and a brown granular distribution was observed in the cells and cytoplasm. In the control group, the expression level of MYBL2 was low; in the malignant melanoma group, the degree of MYBL2 IHC staining was significantly increased, and most samples exhibited moderate positivity. In the metastatic melanoma group, the degree was the deepest, and most samples showed strong positivity (**Figures 1A, B**). Detailed clinical and pathological information are shown in **Table 1**. These results coincided with publicly available datasets of melanoma patients recorded from TCGA using the GEPIA interactive web server (18), which demonstrated that MYBL2 is significantly upregulated in malignant melanoma tissues compared with normal tissues (**Figure 1D**). The expression of MYBL2 was also detected in human melanocytes (HEMn-LP), human malignant melanoma cell lines (A375 and SK-MEL-28), and metastatic melanoma cell

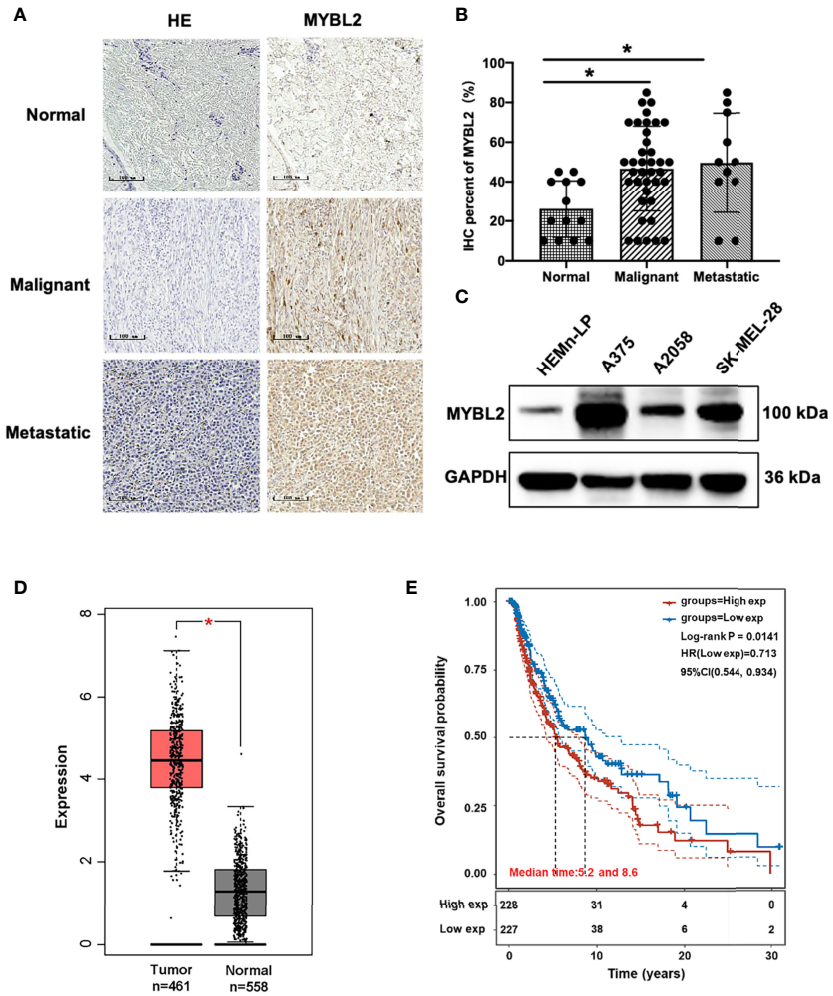

FIGURE 1 | MYBL2 is upregulated in patients with melanoma. **(A)** IHC was performed to detect the expression of MYBL2 in normal skin tissue, malignant melanoma, and metastatic malignant melanoma samples (×200). **(B)** Analysis of IHC showing MYBL2 expression. **(C)** Western blot analysis of MYBL2 in three distinct cell lines: normal stage (HEMn-LP), onset of malignant melanoma (A375 and SK-MEL-28), and metastatic stage (A2058). **(D)** MYBL2 expression in 558 normal human and 461 melanoma patients. Analysis of *MYBL2* mRNA expression across various types of samples based on the melanoma dataset from The Cancer Genome Atlas Genomic Commons (TCGA-GDC) Data Portal using GEPIA interactive web server. Normal skin sample data were obtained from the GTEx database. **(E)** High MYBL2 expression level correlated with poor survival of melanoma patients. Kaplan–Meier curve analysis based on the TCGA Skin Cutaneous Melanoma (SKCM) dataset showing melanoma patient overall survival grouped by high *MYBL2* mRNA expression level (upper quartile, n = 120) versus those with low *MYBL2* expression level (lower quartile, n = 120). *$p < 0.05$.

lines (A2058) by Western blotting. MYBL2 was expressed in all the tested cell lines, and higher expression level was observed in melanoma cell lines (A375, SK-MEL-28, and A2058) than in melanocytes (HEMn-LP) (**Figure 1C**).

Kaplan–Meier analysis based on TCGA data revealed that high MYBL2 expression level was positively correlated with poorer progression-free survival of melanoma patients in the cohort of cutaneous melanoma ($p = 0.0141$, **Figure 1E**). According to MYBL2 expression levels, 455 melanoma patient samples were allocated into low- and high-MYBL2-expressing groups. The Kaplan–Meier survival plot was grouped by the median MYBL2 expression level in melanoma samples. In conclusion, these results illustrated a strong association between MYBL2 expression level and reduced survival in melanoma patients, and suggested that MYBL2 may be a useful biomarker for patient diagnosis and prognosis in melanoma cases.

MYBL2 Is Essential for Melanoma Cell Proliferation and Migration

To study the effects of MYBL2 on the biological behavior of melanoma cells and its role in tumor formation and growth rate, shRNA was used for gene silencing. The effect of *MYBL2* knockdown (KD) was confirmed by qPCR and Western blotting (**Figures 2A–D**). Silencing of *MYBL2* obviously

TABLE 1 | Clinical–pathological information and TNM staging of human melanoma specimens (n = 63) used in this study.

Subject	Location	Type	Subject	Location	Type
A1	Skin	Malignant	B1	Skin	Malignant
A2	Skin	Malignant	B2	Skin	Malignant
A3	Skin	Malignant	B3	Skin	Malignant
A4	Skin	Malignant	B4	Skin	Malignant
A5	Skin	Malignant	B5	Skin	Malignant
A6	Skin	Malignant	B6	Skin	Malignant
A7	Skin	Malignant	B7	Skin	Malignant
A8	Skin	Malignant	B8	Skin	Malignant
C1	Skin	Malignant	D1	Skin	Malignant
C2	Skin	Malignant	D2	Skin	Malignant
C3	Skin	Malignant	D3	Skin	Malignant
C4	Skin	Malignant	D4	Skin	Malignant
C5	Skin	Malignant	D5	Skin	Malignant
C6	Skin	Malignant	D6	Skin	Malignant
C7	Skin	Malignant	D7	Esophagus	Malignant
C8	Skin	Malignant	D8	Urethra	Malignant
E1	Cavidade nasal	Malignant	F1	Lymph node	Metastasis
E2	Cavidade nasal	Malignant	F2	Lymph node	Metastasis
E3	Mediastinum	Malignant	F3	Lymph node	Metastasis
E4	Skin	Malignant	F4	Lymph node	Metastasis
E5	Skin	Malignant	F5	Small intestine	Metastasis
E6	Eye	Malignant	F6	Lymph node	Metastasis
E7	Lymph node	Metastasis	F7	Liver	Metastasis
E8	Lymph node	Metastasis	F8	Lymph node	Metastasis
G1	Skin	Control	H1	Oral cavity	Control
G2	Skin	Control	H2	Esophagus	Control
G3	Skin	Control	H3	Esophagus	Control
G4	Skin	Control	H4	Small intestine	Control
G5	Skin	Control	H5	Small intestine	Control
G6	Skin	Control	H6	Lymph node	Control
G7	Skin	Control	H7	Lymph node	Control
G8	Oral cavity	Control			

inhibited the proliferation of melanoma cells compared to the control (**Figures 2E, F**).

The effects of MYBL2 on cell cycle progression were analyzed using flow cytometry. As shown in **Figures 2G, H**, the proportion of cells in the G2/M cell cycle phase was significantly increased, while the proportion of cells in the G1 phase was markedly decreased in A375 and A2058 cells. These data showed that *MYBL2* KD induced G2/M phase arrest.

To detect the relationship between MYBL2 expression and the migration of melanoma cells, wound healing and transwell migration assays were performed. shMYBL2 plasmids, which were transfected into A375 and A2058 cells, inhibited the migratory ability of these cells (**Supplementary Figure 1** and **Figure 2I**). Wound healing and migration rates of sh1 and sh2 cells were significantly lower than those in the control groups. These studies indicated that MYBL2 promoted the proliferation and migration of melanoma cells.

MYBL2 Promotes Tumor Growth *In Vivo*

We further explored whether MYBL2 affects melanoma growth *in vivo*. A2058 cells stably transfected with the *MYBL2* shRNA vector were inoculated into male nude mice to observe the effects of *MYBL2* KD on tumor growth and progression. As shown in **Figure 3A**, KD of *MYBL2* in tumor cells strongly inhibited tumor cell growth compared to that in the control group. Consistently, *MYBL2* KD tumors had reduced cell proliferation, and the levels of MYBL2 were significantly decreased in MYBL2 KD tumors compared with the control group (**Figure 3B** and **Supplementary Figure 2**). These findings indicated that MYBL2 can affect melanoma cell growth *in vivo*.

MYBL2 Promotes the Growth of Melanoma Stem-Like Cell Populations

The colony-forming assay is related to stem cell features (19–21). To evaluate the stemness of MYBL2-expressing melanoma cells, we downloaded and converted melanoma RNA-Seq (FPKM) data to TPM and normalized the data log2 (TPM+1), while keeping samples with clinical information recorded. We then calculated the stemness indices (mRNAsi) of high MYBL2 (top 50% and 25%) and low MYBL2 (top 50% and 25%) groups using a one-class logistic regression machine-learning algorithm (OCLR) (**Figure 4A**).

Next, we analyzed the effect of *MYBL2* KD on colony formation in A375 and A2058 cells. As shown in **Figure 4B**, *MYBL2* KD significantly inhibited colony-forming ability compared to the

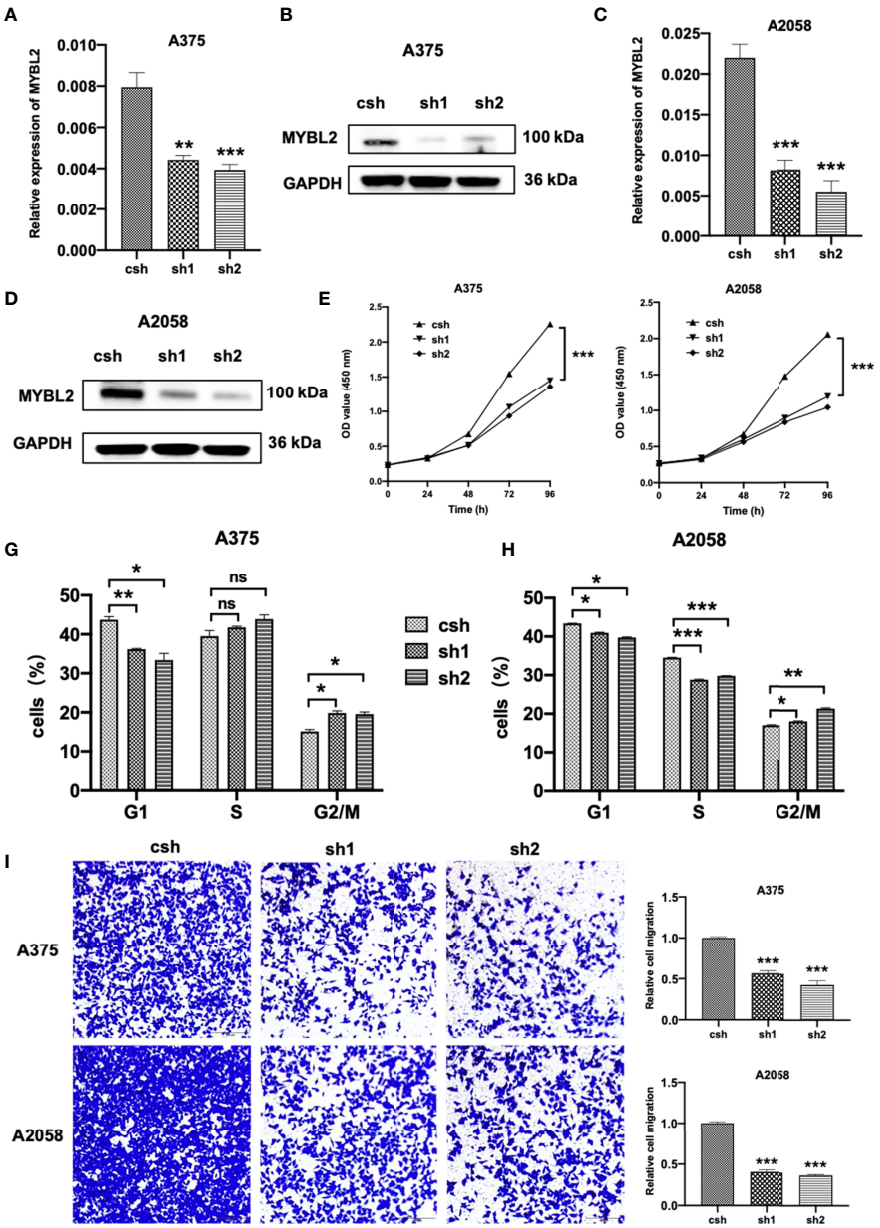

FIGURE 2 | MYBL2 is essential to cell survival in melanoma cells. **(A–D)** qPCR and Western blot analyses of MYBL2 in melanoma cell lines A375 and A2058 using pLL3.7 lentivirus-expressing control shRNA (csh) and 2 different *MYBL2* shRNAs (sh1 and sh2). **(E, F)** Proliferation of cells with csh, sh1, and sh2 targeting *MYBL2* at 0, 24, 48, and 96 h was detected. **(G, H)** Flow cytometric analysis was performed to assess cell cycle phase status after staining with propidium iodide (PI). **(I)** Images and quantitative cell migration of melanoma cells after transfection with *MYBL2*-shRNAs lentiviruses. These experiments were repeated at least 3 times. $^{*}p < 0.05$, $^{**}p < 0.01$, $^{***}p < 0.001$. $^{ns}P > 0.05$, no significant difference.

control cells. These results indicated that MYBL2 may play a major role in stem cell homeostasis in MSLCs.

MYBL2 Resulted In Distinct Genetic Profiling

The introduction of *MYBL2* into A2058 cells was confirmed by qPCR and Western blotting (**Figure 5A**). To explore the molecular mechanism of MYBL2 expression in melanoma, whole transcriptome sequencing of MYBL2-overexpressing A2058 cells was performed. Gene expression analysis using volcano plots showed 1,874 differentially expressed genes, including 810 downregulated genes and 1,064 upregulated genes [genes with a fold change ≥ 2 and a *p*-value (Student's *t*-test) < 0.05] (**Figure 5B**). Moreover, the heatmaps of two replicates of the control and MYBL2-treated samples exhibited highly consistent transcriptional changes (**Figure 5C**).

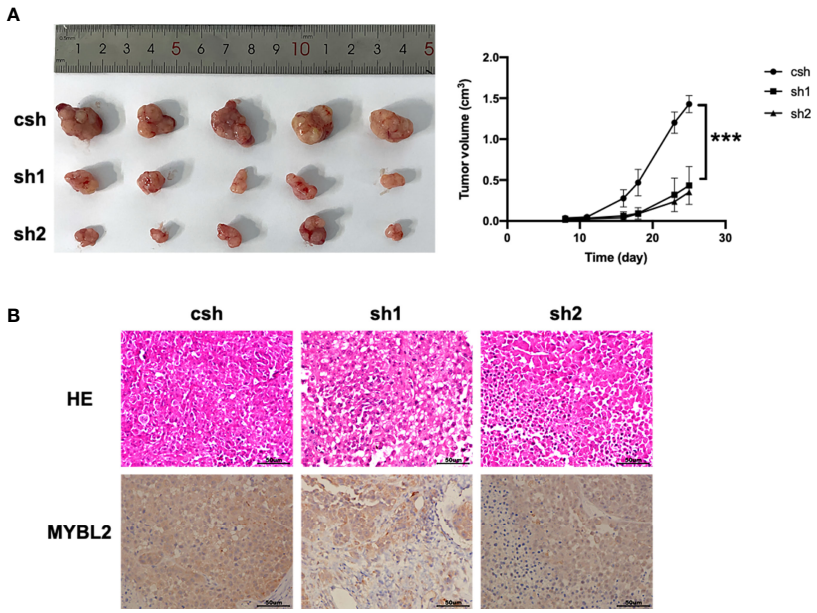

FIGURE 3 | MYBL2 promotes tumor growth and progression in xenograft mice. Twenty-five days after subcutaneous inoculation of melanoma cells, tumors were removed, and diameters were measured (n = 5/group) ± standard deviation (SD). **(A)** Subcutaneous tumors generated in BALB/c-nu/nu mice, with *MYBL2* KD-transduced A2058 cells. **(B)** Histological analysis of 25-day-old subcutaneous tumors after H&E and IHC staining for MYBL2. Magnification × 200. ***$p < 0.001$.

KEGG pathway analysis was performed to detect *MYBL2* gene expression in melanoma cells. The top five pathways following MYBL2 treatment included pathways in cancer, small cell lung cancer, PI3K-Akt signaling pathway, bladder cancer, and inflammatory bowel disease (IBD) (**Figure 5D**).

Identification of MYBL2 Targets in Melanoma Cells

To detect the specific transcription factor binding sites (TFBSs) of MYBL2 in A2058 cells, we performed ChIP-Seq to examine the genome-wide distribution of MYBL2 binding sites. The genomic locations of enriched peaks, annotated to the most proximal transcription start site (TSS), exhibited a wide distribution pattern (**Figure 6A**). In total, 85.7% of MYBL2 binding sites were in distal intergenic regions and 1.53% sites were located near gene promoters, while 2.02% and 10.04% mapped to exons and introns, respectively. Binding regions were identified from +100 kb to −100 kb. We detected only a few peaks close to the ± 3 kb TSS, and several peaks were located in intergenic regions >3 kb from the TSS (**Figure 6B**).

Binding site enrichment is a powerful tool for identifying relationships between characterized TFs of genes determined from genome-scale profiling experiments. We used Logos to display the top-scoring predicted motifs sorted based on *p*-values. The enrichment results identified a series of motifs of TFs with signal transducer and activator of transcription (STAT5, STAT6, and STAT4), SRY-box TF (SOX9, SOX10, and SOX21), E74-like ETS TF (ELF3 and ELF5), Smad TFs (Smad2 and Smad3), NFAT, and ERG (**Figure 6C**). Most of the top enriched TFs are involved in cell proliferation and cancer development (22–26), which could lead to abnormal cell proliferation, cell cycle progression, and apoptosis inhibition in many cancers, thereby enhancing the development of tumors (22); SOX family members are widely involved in the development of human malignant tumors (23). We determined that MYBL2 participates in developmental processes, signaling, and multicellular organismal processes by enriching MYBL2 binding target genes (**Figure 6D**).

MYBL2 target genes revealed the role of MYBL2 in cell proliferation and development. As RNA-Seq and ChIP-Seq are complementary approaches for elucidating gene regulatory mechanisms, we employed a combination of ChIP-Seq and RNA-Seq analysis on a genome-wide level. Integrated ChIP-Seq and RNA-Seq data analysis revealed that there were 11 overlapping genes, including 5 downregulated genes (*SULF2, TPTE, ZNF92, FCGR2A*, and *FAM20C*) and six upregulated genes (*TMEM242, C1QTNF3, PDE3A, NRARP, SOX8*, and *EPPK1*) (**Figures 7A, B**). In univariate Cox proportional hazard regression analysis, 3 of 11 genes (*FCGR2A, PDE3A*, and *EPPK1*) were significantly related to the prognosis of patients with melanoma (**Figure 7C**). To further investigate the prognostic analysis of three genes (*FCGR2A, PDE3A*, and *EPPK1*) in the prognostic model, Kaplan–Meier analysis indicated that three genes were associated with patient survival rate**;** *PDE3A* and *EPPK1* were negatively correlated with survival of melanoma patients; however, *FCGR2A* was positively correlated with melanoma patient survival (**Figure 7D** and

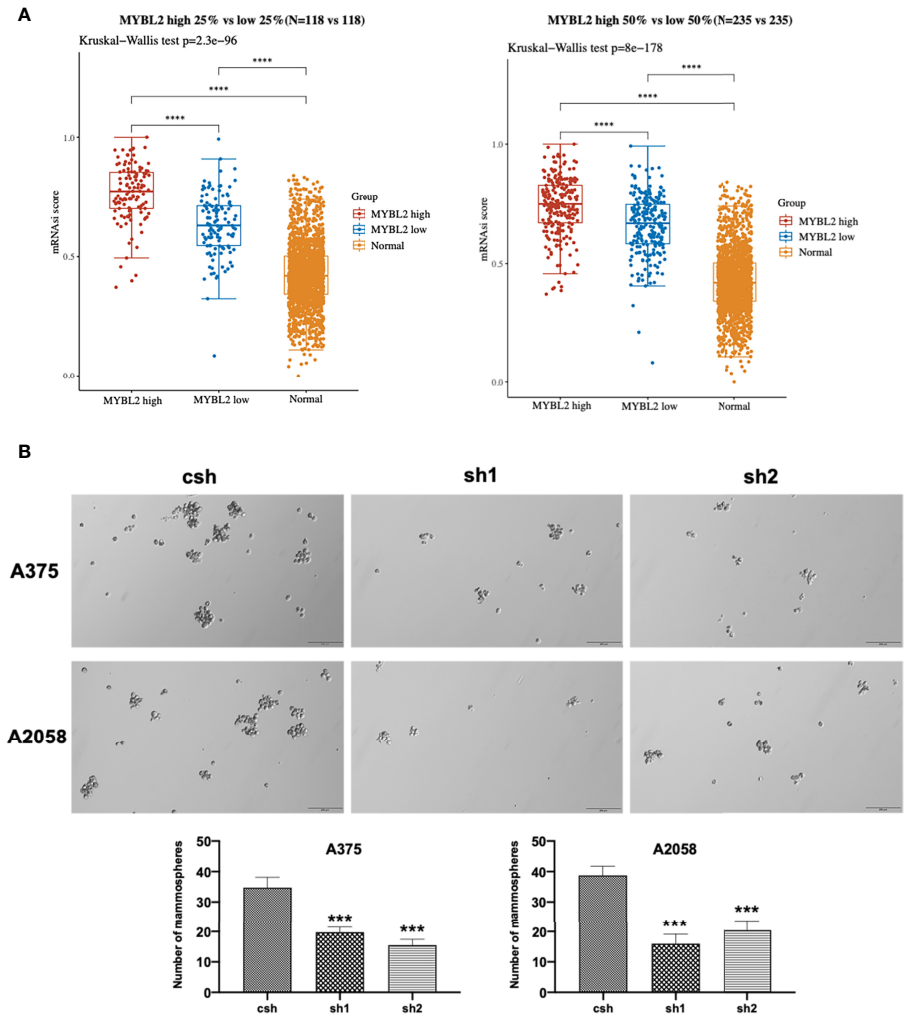

FIGURE 4 | MYBL2 promotes the growth of MSLC populations. **(A)** The distribution of OCLR scores in different groups, where the horizontal axis represents samples of different groups, and the vertical axis represents the distribution of OCLR scores, where different colors represent different groups. The upper left corner represents the significance *p*-value test method. **(B)** Tumorsphere formation in A375 and A2058 expressing csh or *MYBL2* shRNAs (sh1 and sh2). Seven days after seeding, tumorspheres with diameters > 30 μm were counted using Olympus cellSens Standard software. The total numbers of tumorspheres in 6 random fields under 10× objective lens were determined for each well. The experiments were repeated at least 3 times. ****$p < 0.0001$.

Supplementary Figure 3). To determine pairwise correlations involving MYBL2 expression and three genes (*FCGR2A, PDE3A*, and *EPPK1*), we reanalyzed the transcriptome data of melanoma cases from TCGA. We determined that MYBL2 expression was positively or negatively correlated with *PDE3A* (**Supplementary Figure 2B**, $R = 0.1$, $p = 0.03$) and *FCGR2A* (**Supplementary Figure 2C**, $R = -0.15$, $p = 1.23e\text{-}03$) expression. Next, the levels of *EPPK1, PDE3A*, and *FCGR2A* were determined in A375 and A2058 cells infected with *MYBL2*-shRNA lentiviruses by qPCR (**Figure 7E**). We observed that the levels of *EPPK1* and *PDE3A* diminished, while FCGR2A was upregulated in the *MYBL2*-shRNA group compared with the scrambled shRNA group. In summary, these results revealed that three key genes (*FCGR2A, PDE3A*, and *EPPK1*) may be potential prognostic factors in patients with melanoma.

DISCUSSION

Melanoma is a malignant invasive tumor, and its global incidence rate is increasing. In the past decade, great progress has been made in elucidating the mechanisms of melanoma occurrence and progression. The treatment of melanoma patients has improved—local melanoma resection and local lymph node dissection, radiotherapy, chemotherapy or natural chemical combination therapy, gene therapy, and immunotherapy can be used to inhibit the metastasis of melanoma *in vitro* and *in vivo*. However, the long-term prognosis of patients with metastatic melanoma remains unsatisfactory, and the underlying mechanism of the pathogenesis and progression of melanoma remains to be elucidated. Therefore, it is important to identify effective molecular markers to explore new therapeutic targets.

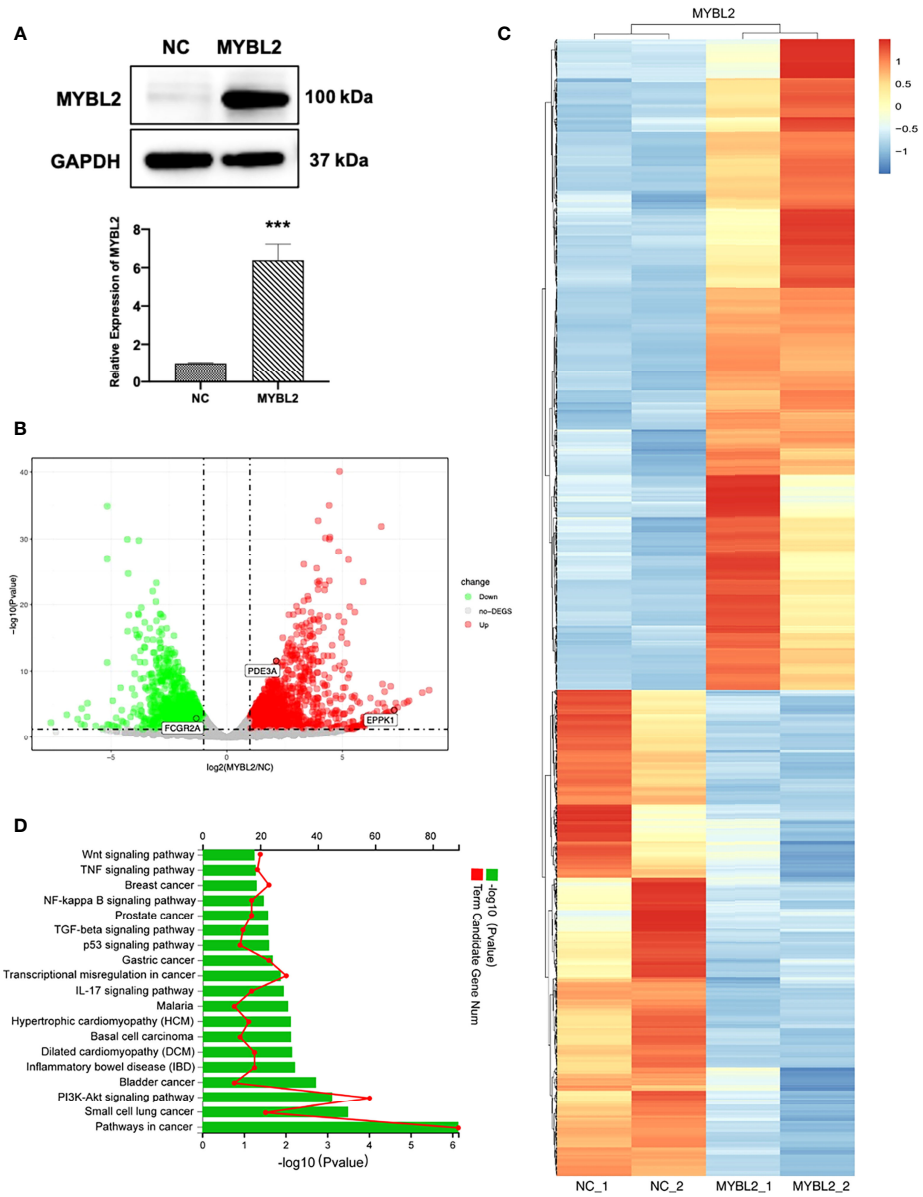

FIGURE 5 | Distinct genetic profiling of MYBL2. **(A)** Western blot of MYBL2 in A2058 cells with control or MYBL2 overexpression. **(B)** Volcano plot showing differential gene expression (1,874 genes, FDR-corrected *p*-value < 0.05) in A2058 cells after overexpression of MYBL2. With ≥2-fold change cutoff, 810 genes were relatively downregulated and 1,064 genes were upregulated. **(C)** Heatmap of A2058 cells with stable MYBL2 overexpression. **(D)** KEGG pathway enrichment analysis (representative pathways) of genes in A2058 cells with stable MYBL2 overexpression. ***$p < 0.001$.

MYBL2 is an important TF that mediates the occurrence and development of many types of tumors. It promotes the malignant transformation of tumors by regulating the biological processes of tumor cell proliferation (27), apoptosis (28), migration (29), and invasion (30). It has typical oncogenic characteristics. The difference in mRNA expression levels between cancer tissues and normal tissues is helpful in determining whether gene expression is related to the occurrence of cancer. In this study, the expression and function of MYBL2 in melanoma were studied in clinical cases and *in vivo* and *in vitro*. We observed that the expression level of MYBL2 in melanoma was higher than that in normal skin tissue and was associated with the progression and poor prognosis of melanoma patients. The results of this study are consistent with those of previous reports. Overexpression of MYBL2 is observed in a variety of tumors and is related to poor prognosis. Previous studies have also indicated that *MYBL2* mRNA is overexpressed in cervical cancer using gene expression profiling and TaqMan PCR (31). Ren et al. also confirmed that the expression of MYBL2 is related to the prognosis of colorectal cancer patients. Through Cox

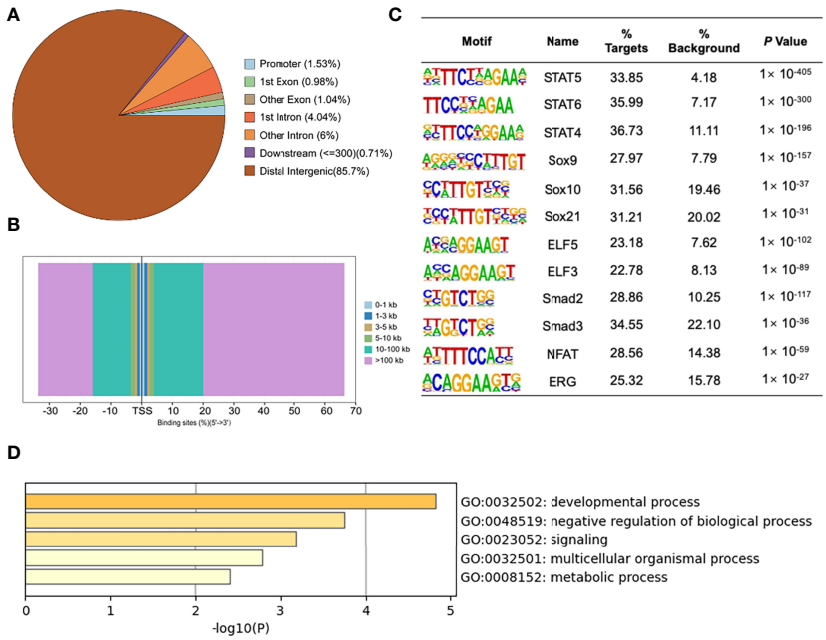

FIGURE 6 | ChIP-Seq profiles of MYBL2 in melanoma cells. **(A)** Pie chart of the percentage of MYBL2-binding sites across different human genomic regions. **(B)** Distribution of MYBL2 binding sites from ±100 kb to the transcriptional start site (TSS) across the human genome (*x*-axis, number of peaks in the genome; *y*-axis, distance relative to the TSS from −100 kb to +100 kb). **(C)** Logos of significantly enriched motifs detected. **(D)** GO enrichment analysis of MYBL2-binding target genes.

multivariate regression analysis of the prognosis of colorectal cancer patients, MYBL2 protein expression and tumor stage were seen to be independent prognostic factors (32). Guan et al. selected cases of primary hepatocellular carcinoma from the TCGA database. Bioinformatic analysis revealed that the expression levels of *MYBL2* mRNA and exon were significantly higher in the death group, and overall patient survival was poorer in the high-expression group of *MYBL2* mRNA and exon. Univariate and multivariate regression analyses confirmed that high expression level of *MYBL2* mRNA was an independent prognostic factor in patients with hepatocellular carcinoma (33).

Further study surrounding the mechanisms involving MYBL2 in melanoma by cytological functional testing is helpful to explain the expression of *MYBL2* in tissues. In a subsequent *in vitro* mechanism study, we determined that shRNA lentivirus-mediated *MYBL2* reduction could inhibit the proliferation, metastasis, and cycle arrest of melanoma cells. MYBL2 can promote cancer progression by promoting tumor cell proliferation and inducing treatment resistance and metastatic diffusion. Ren used siRNA to interfere with the expression of MYBL2 in colon cancer, and the proliferation of tumor cells was decreased (32). Jin et al. also showed that overexpression of MYBL2 can promote the proliferation of non-small cell lung carcinoma (NSCLC) cells, and that the ERK and Akt signaling pathways are involved in the regulation of MYBL2 in NSCLC (34). Other studies have also supported the relationship between MYBL2 and cell proliferation. Cell proliferation is related to the cell cycle; DNA-damaged cells do not progress through the G2/M phase, which leads to an increase in the number of cells arrested in the G2/M phase (35). In our study, we determined that *MYBL2* KD decreased the proportion of cells in the G1 phase and induced G2 phase arrest in human melanoma A375 and A2058 cell lines. These results are consistent with those of previous studies (36–38); however, the underlying mechanisms need to be further explored.

The results of the present study showed that MYBL2 promoted cell proliferation. However, we need to further explore how MYBL2 affects the proliferation of melanoma cells. The integration of ChIP-Seq and RNA-Seq results showed that five genes were downregulated and six genes were upregulated. Moreover, the results of GO analysis showed that MYBL2 influenced a variety of biological processes, particularly cell proliferation and cancer development. When combined with the results of univariate Cox proportional hazard regression analysis, 3 of 11 genes (*FCGR2A, PDE3A*, and *EPPK1*) were related to the prognosis of patients with melanoma. PDE3A plays an important role in oocyte maturation and vascular smooth muscle cell proliferation (39). Moreover, high PDE3A expression level is associated with many types of tumors (40). EPPK1 is part of the epidermal growth factor (EGF) signaling pathway and promotes cell growth in cervical cancer *via* the p38 signaling pathway (41). At present, there are few studies regarding the *FCGR2A* gene, and its function in cancer is still uncertain. Therefore, our results indicate that *FCGR2A, PDE3A*, and *EPPK1* are the main target genes for MYBL2 and may function as novel cancer biomarkers.

In conclusion, by analyzing the expression and prognostic value of MYBL2 in melanoma through multi-platform data

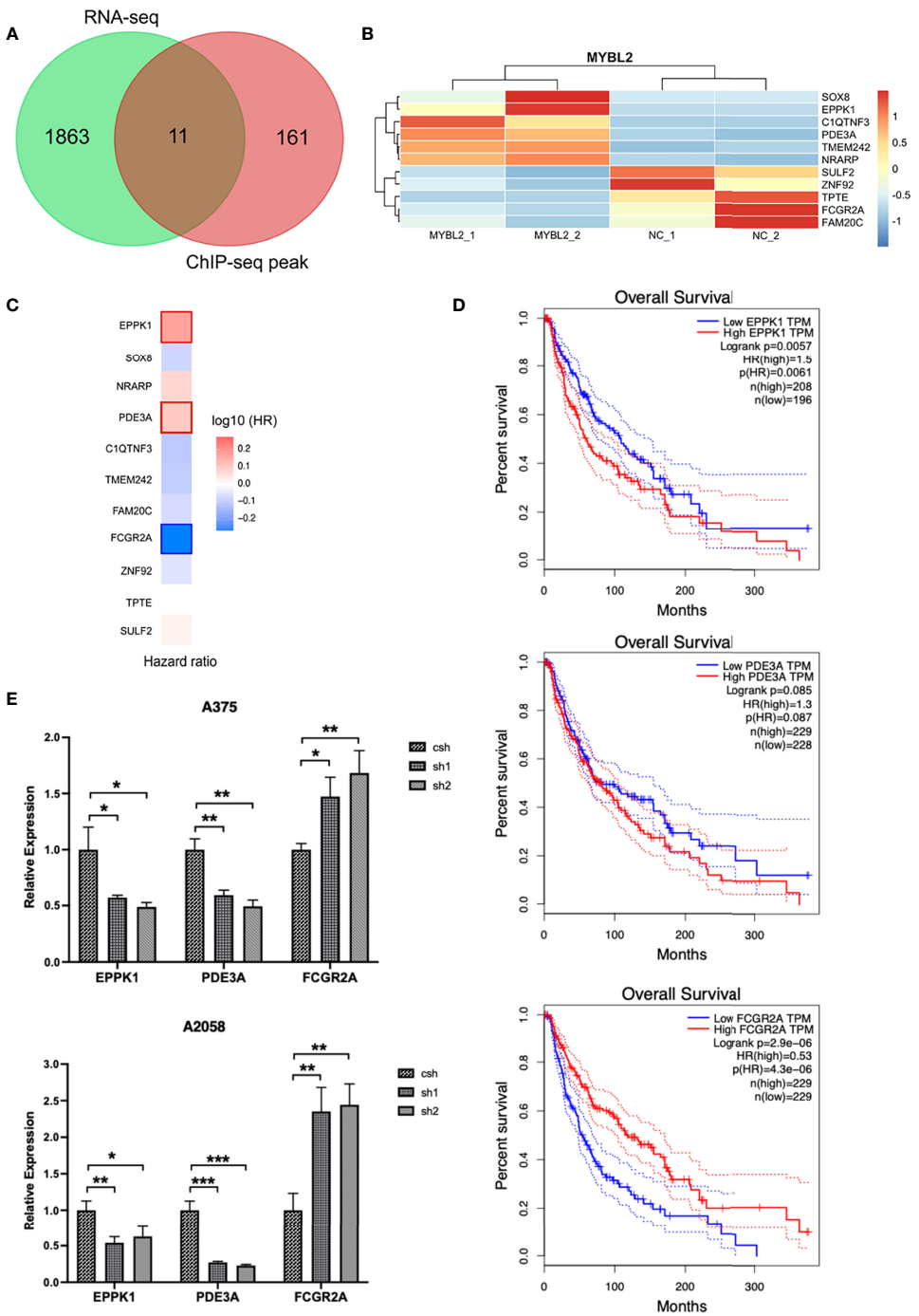

FIGURE 7 | Combined transcriptome profiling and ChIP-Seq analysis identifies 3 highly plausible direct targets of MYBL2. **(A)** Venn diagram showing the overlap of genes among RNA-Seq differentially expressed genes (DEGs) and ChIP-Seq peak. **(B)** Heatmap of 11 significantly DEGs. The data form the transcription profiling of A2058 with overexpressed MYBL2. **(C)** Multivariate Cox regression analysis of 3 significant genes (*EPPK1, PDE3A*, and *FCGR2A*). **(D)** Survival curve of 3 significant differential genes (*EPPK1, PDE3A*, and *FCGR2A*) using Kaplan–Meier curve analysis in melanoma patients. **(E)** Relative expression levels of MYBL2 target genes (*EPPK1, PDE3A*, and *FCGR2A*) in A375 and A2058 cells infected with *MYBL2*-shRNAs lentiviruses compared with scrambled shRNA lentiviruses. $^{*}p < 0.05$, $^{**}p < 0.01$, $^{***}p < 0.001$.

integration, we determined that melanoma has the characteristics of typical MYBL2-dependent tumors. Patients with high MYBL2 expression level suffer a higher risk of recurrence, metastasis, and poorer prognosis. These results suggested that MYBL2 plays important roles in the malignant transformation in melanoma. Moreover, MYBL2 and its downstream transcriptional network can provide effective targets for tumor therapy, and it may be used as a biomarker for the diagnosis and prognosis of melanoma. These findings will provide a reference for the clinical management of melanoma and may lead to further research on the molecular mechanism of melanoma and drug development.

DATA AVAILABILITY STATEMENT

The datasets presented in this study can be found in online repositories. The names of the repository/repositories and accession number(s) can be found at: NCBI with BioProject PRJNA803358 (https://www.ncbi.nlm.nih.gov/bioproject/PRJNA803358).

ETHICS STATEMENT

The studies involving human participants were reviewed and approved by the Ethics Review Committee of Institute of Tongxu First Hospital (Henan, China). Written informed consent to participate in this study was provided by the participants' legal guardian/next of kin. The animal study was reviewed and approved by the Ethics Review Committee of Institute of Radiation Medicine, Chinese Academy of Medical Science and Peking Union Medical College (Tianjin, China).

AUTHOR CONTRIBUTIONS

BL and TC conceived and supervised the study. BL and FZ designed experiments. FZ and JL performed experiments. BL, FZ, TC, and CG analyzed data. BL, TC, and FZ wrote the manuscript. All authors contributed to the article and approved the submitted version.

FUNDING

This work was supported by the Natural Science Foundation of Tianjin city (Grant No. 18JCQNJC13300) and the National Natural Science Foundation of China (Grant Nos. 31861143017 and 81700153).

SUPPLEMENTARY MATERIAL

The Supplementary Material for this article can be found online at: https://www.frontiersin.org/articles/10.3389/fonc.2022.816070/full#supplementary-material

REFERENCES

1. Musa J, Aynaud MM, Mirabeau O, Delattre O, Grunewald TG. MYBL2 (B-Myb): A Central Regulator of Cell Proliferation, Cell Survival and Differentiation Involved in Tumorigenesis. *Cell Death Dis* (2017) 8(6): e2895. doi: 10.1038/cddis.2017.244
2. Iness AN, Felthousen J, Ananthapadmanabhan V, Sesay F, Saini S, Guiley KZ, et al. The Cell Cycle Regulatory DREAM Complex Is Disrupted by High Expression of Oncogenic B-Myb. *Oncogene* (2019) 38(7):1080–92. doi: 10.1038/s41388-018-0490-y
3. Blakemore D, Vilaplana-Lopera N, Almaghrabi R, Gonzalez E, Moya M, Ward C, et al. MYBL2 and ATM Suppress Replication Stress in Pluripotent Stem Cells. *EMBO Rep* (2021) 22:e51120. doi: 10.15252/embr.202051120
4. Clarke M, Dumon S, Ward C, Jager R, Freeman S, Dawood B, et al. MYBL2 Haploinsufficiency Increases Susceptibility to Age-Related Haematopoietic Neoplasia. *Leukemia* (2013) 27(3):661–70. doi: 10.1038/leu.2012.241
5. Wei T, Weiler SME, Toth M, Sticht C, Lutz T, Thomann S, et al. YAP-Dependent Induction of UHMK1 Supports Nuclear Enrichment of the Oncogene MYBL2 and Proliferation in Liver Cancer Cells. *Oncogene* (2019) 38(27):5541–50. doi: 10.1038/s41388-019-0801-y
6. Sadasivam S, DeCaprio JA. The DREAM Complex: Master Coordinator of Cell Cycle-Dependent Gene Expression. *Nat Rev Cancer* (2013) 13(8):585–95. doi: 10.1038/nrc3556
7. Parikh N, Hilsenbeck S, Creighton CJ, Dayaram T, Shuck R, Shinbrot E, et al. Effects of TP53 Mutational Status on Gene Expression Patterns Across 10 Human Cancer Types. *J Pathol* (2014) 232(5):522–33. doi: 10.1002/path.4321
8. Fischer M, Quaas M, Steiner L, Engeland K. The P53-P21-DREAM-CDE/CHR Pathway Regulates G2/M Cell Cycle Genes. *Nucleic Acids Res* (2016) 44 (1):164–74. doi: 10.1093/nar/gkv927
9. Grassilli E, Salomoni P, Perrotti D, Franceschi C, Calabretta B. Resistance to Apoptosis in CTLL-2 Cells Overexpressing B-Myb Is Associated With B-Myb-Dependent Bcl-2 Induction. *Cancer Res* (1999) 59(10):2451–6.
10. Seong HA, Manoharan R, Ha H. B-MYB Positively Regulates Serine-Threonine Kinase Receptor-Associated Protein (STRAP) Activity Through Direct Interaction. *J Biol Chem* (2011) 286(9):7439–56. doi: 10.1074/jbc.M110.184382
11. Sobiepanek A, Milner-Krawczyk M, Lekka M, Kobiela T. AFM and QCM-D as Tools for the Distinction of Melanoma Cells With a Different Metastatic Potential. *Biosens Bioelec* (2017) 93:274–81. doi: 10.1016/j.bios.2016.08.088
12. Zheng W, Li Y, Su Z, Zhang J, Shi F, Liang W, et al. EIF3H Knockdown Inhibits Malignant Melanoma Through Regulating Cell Proliferation, Apoptosis and Cell Cycle. *Exp Cell Res* (2021) 402(1):112488. doi: 10.1016/j.yexcr.2021.112488
13. Sung H, Ferlay J, Siegel RL, Laversanne M, Soerjomataram I, Jemal A, et al. Global Cancer Statistics 2020: GLOBOCAN Estimates of Incidence and Mortality Worldwide for 36 Cancers in 185 Countries. *CA Cancer J Clin* (2021) 71(3):209–49. doi: 10.3322/caac.21660
14. Ribas A, Lawrence D, Atkinson V, Agarwal S, Miller WH Jr, Carlino MS, et al. Combined BRAF and MEK Inhibition With PD-1 Blockade Immunotherapy in BRAF-mutant Melanoma. *Nat Med* (2019) 25(6):936–40. doi: 10.1038/s41591-019-0476-5
15. R Core Team. *R: A Language and Environment for Statistical Computing. R Foundation for Statistical Computing website*. Available at: http://www.R-project.org/ (Accessed 2020).
16. Keung EZ, Gershenwald JE. The Eighth Edition American Joint Committee on Cancer (AJCC) Melanoma Staging System: Implications for Melanoma Treatment and Care. *Expert Rev Anticancer Ther* (2018) 18(8):775–84. doi: 10.1080/14737140.2018.1489246
17. Malta TM, Sokolov A, Gentles AJ, Burzykowski T, Poisson L, Weinstein JN, et al. Machine Learning Identifies Stemness Features Associated With Oncogenic Dedifferentiation. *Cell* (2018) 173(2):338–54.e15. doi: 10.1016/j.cell.2018.03.034

18. Tang Z, Li C, Kang B, Gao G, Li C, Zhang Z. GEPIA: A Web Server for Cancer and Normal Gene Expression Profiling and Interactive Analyses. *Nucleic Acids Res* (2017) 45(W1):W98–102. doi: 10.1093/nar/gkx247
19. Gou S, Liu T, Wang C, Yin T, Li K, Yang M, et al. Establishment of Clonal Colony-Forming Assay for Propagation of Pancreatic Cancer Cells With Stem Cell Properties. *Pancreas* (2007) 34(4):429–35. doi: 10.1097/MPA.0b013e318033f9f4
20. Louis SA, Rietze RL, Deleyrolle L, Wagey RE, Thomas TE, Eaves AC, et al. Enumeration of Neural Stem and Progenitor Cells in the Neural Colony-Forming Cell Assay. *Stem Cells* (2008) 26(4):988–96. doi: 10.1634/stemcells.2007-0867
21. Till JE, McCulloch EA, Siminovitch L. A Stochastic Model of Stem Cell Proliferation, Based on the Growth of Spleen Colony-Forming Cells. *Proc Natl Acad Sci USA* (1964) 51(1):29. doi: 10.1073/pnas.51.1.29
22. Quesnelle KM, Boehm AL, Grandis JR. STAT-Mediated EGFR Signaling in Cancer. *J Cell Biochem* (2007) 102(2):311–9. doi: 10.1002/jcb.21475
23. Castillo SD, Sanchez-Cespedes M. The SOX Family of Genes in Cancer Development: Biological Relevance and Opportunities for Therapy. *Expert Opin Ther Targets* (2012) 16(9):903–19. doi: 10.1517/14728222.2012.709239
24. Wiercinska E, Naber HP, Pardali E, van der Pluijm G, van Dam H, Ten Dijke P. The TGF-β/Smad Pathway Induces Breast Cancer Cell Invasion Through the Up-Regulation of Matrix Metalloproteinase 2 and 9 in a Spheroid Invasion Model System. *Breast Cancer Res Treat* (2011) 128(3):657–66. doi: 10.1007/s10549-010-1147-x
25. Furusato B, Tan S, Young D, Dobi A, Sun C, Mohamed A, et al. ERG Oncoprotein Expression in Prostate Cancer: Clonal Progression of ERG-positive Tumor Cells and Potential for ERG-based Stratification. *Prostate Cancer Prostat Dis* (2010) 13(3):228–37. doi: 10.1038/pcan.2010.23
26. Mancini M, Toker A. NFAT Proteins: Emerging Roles in Cancer Progression. *Nat Rev Cancer* (2009) 9(11):810–20. doi: 10.1038/nrc2735
27. Sun YM, Wang WT, Zeng ZC, Chen TQ, Han C, Pan Q, et al. circMYBL2, a circRNA From MYBL2, Regulates FLT3 Translation by Recruiting PTBP1 to Promote FLT3-ITD AML Progression. *Blood* (2019) 134(18):1533–46. doi: 10.1182/blood.2019000802
28. Bayley R, Blakemore D, Cancian L, Dumon S, Volpe G, Ward C, et al. Mybl2 Supports Dna Double Strand Break Repair in Hematopoietic Stem Cells. *Cancer Res* (2018) 78(20):5767–79. doi: 10.1158/0008-5472.CAN-18-0273
29. Fan X, Wang Y, Jiang T, Cai W, Jin Y, Niu Y, et al. B-Myb Mediates Proliferation and Migration of Non-Small-Cell Lung Cancer Via Suppressing Igfbp3. *Int J Mol Sci* (2018) 19(5):1479. doi: 10.3390/ijms19051479
30. Zhang X, Lv QL, Huang YT, Zhang LH, Zhou HH. Akt/FoxM1 Signaling Pathway-Mediated Upregulation of MYBL2 Promotes Progression of Human Glioma. *J Exp Clin Cancer Res* (2017) 36(1):105. doi: 10.1186/s13046-017-0573-6
31. Astbury K, McEvoy L, Brian H, Spillane C, Sheils O, Martin C, et al. MYBL2 (B-MYB) in Cervical Cancer: Putative Biomarker. *Int J Gynecol Cancer* (2011) 21(2):206–12. doi: 10.1097/IGC.0b013e318205759f
32. Ren F, Wang L, Shen X, Xiao X, Liu Z, Wei P, et al. MYBL2 is an Independent Prognostic Marker That has Tumor-Promoting Functions in Colorectal Cancer. *Am J Cancer Res* (2015) 5(4):1542–52.
33. Guan Z, Cheng W, Huang D, Wei A. High MYBL2 Expression and Transcription Regulatory Activity Is Associated With Poor Overall Survival in Patients With Hepatocellular Carcinoma. *Curr Res Transl Med* (2018) 66 (1):27–32. doi: 10.1016/j.retram.2017.11.002
34. Jin Y, Zhu H, Cai W, Fan X, Wang Y, Niu Y, et al. B-Myb Is Up-Regulated and Promotes Cell Growth and Motility in Non-Small Cell Lung Cancer. *Int J Mol Sci* (2017) 18(6):860. doi: 10.3390/ijms18060860
35. Ouyang G, Yao L, Ruan K, Song G, Mao Y, Bao S. Genistein Induces G2/M Cell Cycle Arrest and Apoptosis of Human Ovarian Cancer Cells Via Activation of DNA Damage Checkpoint Pathways. *Cell Biol Int* (2009) 33 (12):1237–44. doi: 10.1016/j.cellbi.2009.08.011
36. Liu G, Chu H. Andrographolide Inhibits Proliferation and Induces Cell Cycle Arrest and Apoptosis in Human Melanoma Cells. *Oncol Lett* (2018) 15 (4):5301–5. doi: 10.3892/ol.2018.7941
37. Pan Z, Qu C, Chen Y, Chen X, Liu X, Hao W, et al. Bufotalin Induces Cell Cycle Arrest and Cell Apoptosis in Human Malignant Melanoma A375 Cells. *Oncol Rep* (2019) 41(4):2409–17. doi: 10.3892/or.2019.7032
38. Tseng H-W, Li S-C, Tsai K-W. Metformin Treatment Suppresses Melanoma Cell Growth and Motility Through Modulation of microRNA Expression. *Cancers* (2019) 11(2):209. doi: 10.3390/cancers11020209
39. Ai Y, He H, Chen P, Yan B, Zhang W, Ding Z, et al. An Alkaloid Initiates Phosphodiesterase 3A-Schlafen 12 Dependent Apoptosis Without Affecting the Phosphodiesterase Activity. *Nat Commun* (2020) 11(1):3236. doi: 10.1038/s41467-020-17052-4
40. Tian FM, Zhong CY, Wang XN, Meng Y. PDE3A Is Hypermethylated In Cisplatin Resistant Non-Small Cell Lung Cancer Cells and Is a Modulator of Chemotherapy Response. *Eur Rev Med Pharmacol Sci* (2017) 21(11):2635–41.
41. Ma D, Pan Z, Chang Q, Zhang J-j, Liu X, Hua N, et al. KLF5-Mediated Eppk1 Expression Promotes Cell Proliferation in Cervical Cancer Via the p38 Signaling Pathway. *BMC Cancer* (2021) 21(1):1–10. doi: 10.1186/s12885-021-08040-y

Conflict of Interest: The authors declare that the research was conducted in the absence of any commercial or financial relationships that could be construed as a potential conflict of interest.

Publisher's Note: All claims expressed in this article are solely those of the authors and do not necessarily represent those of their affiliated organizations, or those of the publisher, the editors and the reviewers. Any product that may be evaluated in this article, or claim that may be made by its manufacturer, is not guaranteed or endorsed by the publisher.

frontiers | Frontiers in Oncology

ORIGINAL RESEARCH
published: 30 May 2022
doi: 10.3389/fonc.2022.887768

The Genetics of Early-Stage Melanoma in a Veteran Population

*Kevin Cheung[1], Aaron D. Bossler[2], Sarah L. Mott[3], Megan Zeisler[3], Julie McKillip[1], Yousef Zakharia[3], Brian L. Swick[1] and Jennifer G. Powers[1]**

[1] Department of Dermatology, University of Iowa, Iowa City, IA, United States, [2] Department of Pathology, H. Lee Moffitt Cancer Center, Tampa, FL, United States, [3] Holden Comprehensive Cancer Center, University of Iowa, Iowa City, IA, United States

To improve understanding of the genetic signature of early-stage melanomas in Veterans, hotspot mutation profiling using next-generation sequencing (NGS) was performed on melanoma tissue samples from patients at the Iowa City Veterans Affairs Medical Center (VAMC). Genetic analysis identified BRAF (36.3%), TP53 (25.9%), NRAS (19.3%), CDKN2A (11.1%), KIT (8.1%), and BAP1 (7.4%) mutations with the highest prevalence. Although common variants in BRAF were detected at lower rates than what is reported for the general population, 55.6% of cases showed activating mutations in the RAS/RAF pathways. Variants in TP53 and KIT were detected at higher rates than in the general population. Veterans with prior history of melanoma were at significantly higher odds of having TP53 mutation (OR = 2.67, p = 0.04). This suggests that TP53 may be a marker for recurrent melanoma and possibly alternative exposures in the military population. This study provides new information regarding the genetics of melanoma in a Veteran population and early-stage melanomas, highlighting risk factors unique to this population and contributing to the conversation about preventing melanoma deaths in US Military personnel.

Keywords: melanoma, military personnel, veterans, genetic predisposition, risk factors, proto-oncogene, BRAF, TP53

OPEN ACCESS

Edited by:
Gagan Chhabra, University of Wisconsin-Madison, United States

Reviewed by:
Alessio Giubellino, University of Minnesota Twin Cities, United States
Hanggoro Tri Rinonce, Gadjah Mada University, Indonesia

***Correspondence:**
Jennifer G. Powers
jennifer-g-powers@uiowa.edu

Specialty section:
This article was submitted to Skin Cancer, a section of the journal Frontiers in Oncology

Received: *02 March 2022*
Accepted: *26 April 2022*
Published: *30 May 2022*

Citation:
Cheung K, Bossler AD, Mott SL, Zeisler M, McKillip J, Zakharia Y, Swick BL and Powers JG (2022) The Genetics of Early-Stage Melanoma in a Veteran Population. Front. Oncol. 12:887768. doi: 10.3389/fonc.2022.887768

INTRODUCTION

Melanoma incidence has increased significantly over the past three decades. It is currently the fifth most common cause of cancer in men and women in the United States, and in 2021, it accounted for an estimated 4,600 deaths in men and 2,580 in women (1, 2). These findings are especially concerning for the military population as studies have shown that military personnel are at increased risk for melanoma compared to the general population (3–5). With a higher proportion of Caucasian males, military personnel are often at increased sun exposure from operating at more equatorial latitudes compared to the general public, and lack of effective sun protection behaviors (5–9). Additionally, other non-ultraviolet (UV) exposures have been identified to contribute to melanoma risk, including industrial chemicals, polyvinyl chloride, ionizing radiation, and high altitude, especially dependent on the specific duties and occupational environment (10). For instance, while radiation and high altitudes have been studied to increase melanoma risk in airline pilots, air force pilots may be assumed to incur similar exposures.

The genetics and pathophysiology of melanoma have not been well-studied in the Veteran population. Establishing relationships between melanoma genetic mutations and military service and exposures is significant because it may create opportunities to improve prevention and screening as well as optimize treatment for Veterans.

In general, the relationship between UV exposure and the somatic genetic mutations in melanoma has yet to be completely elucidated, and the majority of research on melanoma has thus far been on advanced-stage tumors. Several pathways have been described, including germline mutations in *CDKN2A*, somatic mutations in *BRAF*, and *KIT* tyrosine kinase mutations. *BRAF*, a serine/threonine kinase in the MAPK signaling pathway, was first reported in 46-66% of melanomas (11, 12). *BRAF* mutations are believed to arise from UV damage, though they appear to be more common in skin intermittently exposed to the sun rather than chronically exposed and may also be more common in melanomas in younger patients, lending credence to the Intermittent Exposure Hypothesis (13–17). One thought is that intense intermittent sun exposure causes genetic damage while also triggering immunosuppression, while chronic exposure allows for photo-adaption (18). In contrast, melanomas from chronically sun-damaged skin or from sites not routinely exposed such as acral or mucosal sites do not typically carry *BRAF* mutations and would be more associated with *NRAS* and *KIT* mutations respectively (13, 19). Notably, *NRAS* mutations are associated with nodular subtypes of melanoma and with poorer outcomes (20). Given the equatorial locations of military deployment as well as the nature of military work, military personnel may be more likely to experience chronic occupational sun exposure. Intermittent sun exposure is more sporadic in nature and would be more characteristic of an office employee who only receives intense sun exposure on vacations, for example. Accordingly, melanomas in the military population would be less likely to originate from the *BRAF* pathway when compared to the general population, which was our hypothesis, though this has not been established prior to this study.

While in principal, understanding these distinct genetic pathways is critical in personalizing the different treatment options, such as vemurafenib for *BRAF*, imatinib for *KIT*, or binimetinib for *BRAF* and *NRAS*, this theory has not yet materialized in standard clinical practice aside from using BRAF and MEK inhibitor for BRAF mutation (21). Additionally, earlier stage tumors may provide clearer understanding of the initial drivers of malignant transformation. The purpose of this study is to characterize the genetic signature of early-stage melanomas from Veterans who were successfully screened and timely diagnosed, which may therefore shed light on pathogenesis of melanomas in this population and in turn influence clinical approach to prevention, screening, diagnosis, and treatment.

MATERIALS AND METHODS

Study Population

Tissue samples of confirmed melanoma cases in a 7-year period, between January 1, 2010 to January 1, 2017 were obtained from the Iowa City VAMC. Inclusion criteria included age at least 18 years old, stage at diagnosis 0 to 2. Exclusion criteria included concurrent internal malignant disease, incomplete medical records, and unavailable or inadequate tissue sample. Demographic and clinical data such as gender, race, age, military branch, previous history of melanoma or non-melanoma skin cancer, family history of skin cancer, diagnosis date, tumor stage, primary tumor location, tumor subtype, histopathology, and treatment were obtained by chart review. All human studies were approved by the authors' Institutional Review Board.

Next-Generation Sequencing

Mutational analysis was performed using a custom AmpliSeq™ (Ion Torrent, Thermo Fisher Scientific, Waltham, MA) hotspot or targeted next-generation sequencing (NGS) panel of 25 genes having been reported mutated in melanoma including *BRAF*, *NRAS* and *TP53*. DNA was extracted from unstained sections from formalin-fixed paraffin embedded tissue blocks containing melanoma tumor cells, and 20ng of DNA was used for NGS library preparation. The libraries were bar-coded, clonally amplified, and sequenced on an Ion S5XL. The data were analyzed using the Torrent Suite Software followed by a laboratory-developed pipeline. The assay has an analytic sensitivity of 2.5% for single nucleotide variants (SNV) and small insertions and deletions. Adequate coverage was considered to be at least 250X, indeterminate coverage was considered to be 100-250X, and inadequate coverage was considered to be below 100X.

Statistical Analysis

Firth-penalized logistic regression models were used to assess the association between patient and clinicopathologic characteristics on presence of *BRAF*, *NRAS*, and *TP53* mutations. Estimated effects of predictors are reported as odds ratios (OR) along with 95% confidence intervals. All statistical testing was two-sided and assessed for significance at the 5% level using SAS v9.4 (SAS Institute, Cary, NC).

RESULTS

Of 185 Veterans diagnosed with melanoma from January 1, 2010 to January 1, 2017 at the VAMC, there were 135 Veterans who met our cohort criteria. The demographics of this cohort is outlined in **Table 1** and shows a gender distribution of 96.3% male and 3.7% female. All 125 Veterans with reported race identified as Caucasian (100%) with 10 patients listed as having unknown race. Unknown values may be due to Veteran declining to answer or not being assessed for it. Mean age is 68.5 years. Military branch distribution was skewed towards the Army at 63.0% with 14.1% in the Navy, 11.9% in the Marines, and 11.1% in the Air Force.

Histopathologic features could be found in pathology reports of 110 Veterans of the 135 total Veterans included in this study. Twenty-five Veterans had pathology reports that did not include these features. Of the 110 samples, ulceration was noted for 7

TABLE 1 | Demographics of cohort.

	Stage of Disease			
	0	1	2	All
	N (%)			
All	16	100	19	135
Gender				
Male	15 (93.8)	96 (96.0)	19 (100)	130 (96.3)
Female	1 (6.3)	4 (4.0)	0 (0)	5 (3.7)
Age Range				
18 – 29	1 (6.3)	2 (2.0)	0 (0)	3 (2.2)
30 – 49	1 (6.3)	10 (10.0)	1 (5.3)	12 (8.9)
50 – 64	1 (6.3)	21 (21.0)	3 (15.8)	25 (18.5)
65 – 79	8 (50)	53 (53.0)	12 (63.2)	73 (54.1)
80+	5 (31.3)	14 (14.0)	3 (15.8)	22 (16.3)
Mean Age (SD)	72.3 (16.1)	67.6 (13.2)	70.0 (11.8)	68.5 (13.3)
Race				
Caucasian	14 (100)	93 (100)	18 (100)	125 (100)
Unknown*	2	7	1	10
Ethnicity				
Hispanic	1 (6.7)	0 (0)	0 (0)	1 (0.8)
Non-Hispanic	14 (93.3)	97 (100)	19 (100)	130 (99.2)
Unknown*	1	3	0	4
VA branch				
Army	10 (62.5)	59 (59.0)	16 (84.2)	85 (63.0)
Navy	2 (12.5)	14 (14.0)	3 (15.8)	19 (14.1)
Marines	2 (12.5)	14 (14.0)	0 (0)	16 (11.9)
Air force	2 (12.5)	13 (13.0)	0 (0)	15 (11.1)
VA service yrs				
<2 years	2 (12.5)	6 (6.0)	2 (10.5)	10 (7.4)
2 years service	6 (37.5)	44 (44.0)	9 (47.4)	59 (43.7)
3 years service	3 (18.8)	18 (18.0)	5 (26.3)	26 (19.3)
4 years service	3 (18.8)	18 (18.0)	1 (5.3)	22 (16.3)
>4 years	2 (12.5)	14 (14.0)	2 (10.5)	18 (13.3)
Service-connected disability				
Yes	7 (43.8)	42 (42.0)	10 (52.6)	59 (43.7)
No	9 (56.2)	58 (58.0)	9 (47.4)	76 (56.3)
Service-connected disability for dermatologic condition				
Yes	2 (12.5)	7 (7.0)	2 (10.5)	11 (8.1)
No	14 (87.5)	93 (93.0)	17 (89.5)	124 (91.9)
Smoking status				
Former	5 (38.5)	47 (48.0)	5 (27.8)	57 (44.2)
Current	3 (23.1)	26 (26.5)	4 (22.2)	33 (25.6)
Never	5 (38.5)	25 (25.5)	9 (50.0)	39 (30.2)
Unknown*	3	2	1	6

VA, Veterans Affairs.

**As demographic data is obtained from medical records, there were some unknown values. This may represent either Veterans declining to answer demographic questions or never having been assessed for it.*

(6.4%), mitoses were noted for 25 (22.7%), perineural invasion was noted for 2 (1.8%), regression was noted for 16 (14.5%), and desmoplasia was noted for 4 (3.6%). Tumor-infiltrating lymphocytes and microsatellitosis were assessed but not found in any of the 110 samples. For samples that were noted to have mitoses, the most common number of mitoses per mm^2 noted was 1 (N=13), the greatest number of mitoses per mm^2 noted in a single sample was 8, and the average number of mitoses per mm^2 for the 25 samples that had them was 2.3. These results are summarized in **Table 2**. Immunohistochemistry was only performed on a small subset of these samples and as a result not evaluated. Univariate analysis of histopathologic features with regards to melanoma mutations did not show any with statistical significance.

We analyzed each of the 135 cases of melanoma with next-generation sequencing targeting 25 hotspot mutations to profile the underlying genetic mutations in our cohort. Results of next generation sequencing is summarized in **Table 3** and shows 49 (36.3%) all-type *BRAF* mutations, 35 (25.9%) *TP53* mutations, 26 (19.3%) *NRAS* mutations, 15 (11.1%) *CDKN2A* mutations, 11 (8.1%) *KIT* mutations, and 10 (7.4%) *BAP1* mutations with the highest prevalence. Of the 49 *BRAF* mutations, 46.9% (23) were V600E mutations and 44.9% (22) were V600K. The remaining 8.2% (4) of BRAF mutations were V600N, S594N, N581I, and S607F. Of the 26 NRAS mutations, 38.5% (10) were Q61R mutations, 19.2% (5) were Q61K mutations, 19.2% (5) were Q61L mutations, 7.7% (2) were Q61H mutations, 3.8% (1) was a Q61P mutation, 11.5% (3) were G13R mutations, and 7.7% (2)

TABLE 2 | Histopathologic features in melanomas of 110 patients.

Feature	N	Percent
Ulceration	7	6.4
Mitoses	25	22.7
Perineural invasion	2	1.8
Regression	16	14.5
Tumor-infiltrating lymphocytes	0	0
Microsatellitosis	0	0
Desmoplasia	4	3.6

Histopathologic features could be found in pathology reports of 110 Veterans of the 135 total Veterans included in this study. Twenty-five Veterans had pathology reports that did not include these features. The table shows how many of each feature were noted and the percentage representation out of 110. In 25 samples with mitoses identified, the most common number of mitoses per mm^2 noted was 1 (N=13), the max was 8, and the average was 2.3.

TABLE 3 | Mutations found in melanomas of 135 patients by next-generation sequencing.

Gene	N	Percent
AKT1	1	0.7
BAP1	**10**	**7.4**
BRAF	**49**	**36.3**
***BRAF* V600E**	**23**	**17.0**
***BRAF* V600K**	**22**	**16.3**
***BRAF* V600N**	**1**	**0.7**
***BRAF* S594N**	**1**	**0.7**
***BRAF* N581I**	**1**	**0.7**
***BRAF* S607F**	**1**	**0.7**
CDKN2A	**15**	**11.1**
CTNNB1	1	0.7
EIF1AX	1	0.7
ERBB4	5	3.7
FGFR1	2	1.5
FGFR2	3	2.2
FGFR3	6	4.4
GNA11	2	1.5
GNAQ	2	1.5
HRAS	3	2.2
KIT	**11**	**8.1**
***KIT* L576P**	**3**	**2.2**
***KIT* D579N**	**2**	**0.7**
MET	4	3.0
NRAS	**26**	**19.3**
***NRAS* Codon 61**	**22**	**16.3**
***NRAS* G13R**	**3**	**2.2**
***NRAS* G12D**	**1**	**0.7**
PDGFRA	2	1.5
PIK3CA	3	2.2
PTEN	7	5.2
RAF1	1	0.7
RB1	3	2.2
SF3B1	2	1.5
STK19	4	3.0
TP53	**35**	**25.9**
***TP53* R282W**	**3**	**2.2**
***TP53* S241F**	**3**	**2.2**
***TP53* E286K**	**2**	**1.5**
***TP53* P278S**	**2**	**1.5**
TRRAP	0	0

Breakdown of specific mutations are shown for BRAF, NRAS, KIT, and TP53. Note that NRAS mutations involving codon 61, which typically codes for glutamine, had more variable substitutions and were thus grouped together. Likewise, KIT and TP53 had variable mutations and the full breakdown of mutations is not included in the table.

were G12D mutations. Collectively, 84.6% (22) of NRAS mutations were in codon 61. Activating mutations in the RAS/RAF pathways, including *BRAF* V600E and V600K, *HRAS*, *NRAS*, and *RAF1* mutations, collectively comprised 75 (55.6%) of the cohort. Twenty-three patients (17.0%) had tumor biopsies that were negative for any of the gene mutations targeted, and 54 (40.0%) had biopsies positive for more than one mutation.

To understand the possible associations of demographic and clinical characteristics with the three most common mutations, we performed univariate analysis of the clinicopathologic data for *BRAF*, *NRAS*, and *TP53* mutations. Results for *BRAF* mutations are detailed in **Table 4**. Veterans who had melanoma primary tumor in the head/neck (OR = 0.30, 95% CI 0.12, 0.74) and the extremities (OR = 0.21, 95% CI 0.09, 0.52) were at decreased odds for *BRAF* mutation than those in the trunk ($p < 0.01$) as is seen in other studies (16, 17). Increasing age was associated with decreased odds for having *BRAF* mutation (OR = 0.97, 95% CI 0.94–0.99, $p = 0.01$).

Univariate analysis of clinicopathologic data with *NRAS* mutations are summarized in **Table 5**. Veterans who had melanoma primary tumor in the extremities were at increased odds of *NRAS* mutation than those in the trunk (OR = 2.03, 95% CI 0.79–5.20) while those with head/neck melanoma were at decreased odds (OR = 0.28, 95% CI 0.06–1.25) compared to those with trunk melanoma ($p = 0.02$) as seen in other studies (22–24). Compared to superficial spreading subtypes of melanoma, lesions that were lentigo maligna melanoma (OR = 0.16, 95% CI 0.04–0.67) were at decreased odds of having an *NRAS* mutation ($p = 0.02$). In addition, personal history of non-cutaneous cancer increased odds of *NRAS* (OR = 3.05, 95% CI 1.22–7.59, $p = 0.02$). Moreover, **Figure 1** shows which Veterans had melanomas with isolated or concurrent *BRAF*, *NRAS*, and *TP53* mutations. While some melanomas had either *BRAF* or *NRAS* with *TP53* mutations, *BRAF* and *NRAS* mutations were mutually exclusive.

Results of univariate analysis of *TP53* mutations are summarized in **Table 6**. We observed that Veterans with prior history of melanoma were at increased odds of having a *TP53* mutation (OR = 2.67, 95% CI 1.05–6.80 $p = 0.04$). Unlike what we observed in our data for *BRAF* and *NRAS*, we did not find any association of *TP53* mutations with any anatomic location of melanoma or melanoma subtype. Unexpectedly, our results appear to indicate that neither smoking status nor military branch were associated with *BRAF*, *NRAS*, or *TP53* mutations.

DISCUSSION

The pathogenesis of melanoma development, including relationships to genetic mutations, continues to be elucidated. However, there is currently a dearth of research on melanoma in military personnel. In this study, we have been able to profile tumor hotspot mutations in early-stage melanomas in a veteran population.

Evaluation of the 110 samples with reported histopathologic features in patient medical records show that relatively few of the samples had these notable features. These features, including ulceration, mitoses, and perineural invasion, generally suggest more invasive tumors and have been correlated with poorer prognosis. It is

TABLE 4 | Univariate analysis between demographic and clinical factors and *BRAF* mutations.

Variable		Odds of *BRAF* Mutation			
	Group	N	Odds Ratio	95% CI	P-value
Smoker	Former	57	1.03	0.43 2.48	0.13
	Current	33	2.33	0.89 6.10	
	Never	39	Ref	– –	
VA Branch	Air Force	15	1.85	0.43 7.93	0.31
	Army	85	0.98	0.31 3.08	
	Navy	19	2.31	0.58 9.20	
	Marines	16	Ref	– –	
Age at diagnosis	Units=1	135	0.97	0.94 0.99	**0.01**
Stage at diagnosis	1 or 2	119	1.23	0.41 3.74	0.71
	0	16	Ref	– –	
Anatomic	Extremity	47	0.21	0.09 0.52	**<0.01**
	Head/Neck	39	0.30	0.12 0.74	
	Trunk	49	Ref	– –	
Subtype	In situ	18	0.63	0.20 1.99	0.84
	Lentigo	39	1.09	0.48 2.49	
	Nodular	13	1.00	0.29 3.44	
	Superficial	59	Ref	– –	
Personal history of melanoma	Yes	23	0.46	0.16 1.30	0.14
	No	112	Ref	– –	
Personal history of NMSC	Yes	56	0.74	0.36 1.52	0.41
	No	79	Ref	– –	
Family history of melanoma	Yes	8	1.81	0.43 7.60	0.42
	No	127	Ref	– –	
Family history of NMSC	Yes	11	1.53	0.44 5.30	0.50
	No	127	Ref	– –	

VA, Veterans Affairs; NMSC, Non-melanoma skin cancer.

Univariate analysis was performed on various clinical variables listed in the table to determine the odds of BRAF mutation. For each clinical variable, one group was assigned as a reference for which to compare the odds of other groups, hence the odds ratio of the chosen reference group is 1. Odds ratio for other groups listed within a clinical variable will be in comparison to the reference group odds of BRAF mutation.

unclear why twenty-five samples did not include evaluation of these features, which may limit interpretation. However, the data is consistent with having lower-staged melanomas, which were purposefully selected for this study with intention of identifying earlier features and mutations in pathogenesis. Univariate analysis was performed on histopathologic features and odds of melanoma mutations, but statistical significance was not found. Given the low feature count, we believe that this analysis lacked statistical power to identify significance if any were present.

Of 135 Veterans whose melanoma was analyzed by next-generation sequencing, 49 (36.3%) had *BRAF* mutations, 26 (19.3%) had *NRAS* mutations, and 35 (25.9%) had *TP53* mutations, which were the three most common mutations. *BRAF* was initially found to be in 44-66% of melanomas in the general population, and that has since been corroborated with other reports in that range (11, 12). Our cohort had a lower prevalence of *BRAF* compared to what has been reported in the general population, which supports the idea that Veterans incur chronic sun exposure rather than intermittent sun exposure, though our population was also older. This is in line with the equatorial locations that many Veterans are frequently stationed at globally and domestically as well as previous work that has reported sun protection education and practice gaps in the military (5–9). Moreover, nearly half (44.9%) of the *BRAF* mutations were V600K mutations, which is greater than the 10–30% that has been reported in other studies (25, 26). *BRAF* V600K mutations have been more associated with chronic sun exposure compared to V600E mutations as well as older age and higher risk of metastasis, which suggests a different pathology than the more common V600E mutation (27, 28). In our cohort, *BRAF* was associated with younger age and tumor location in the trunk in this cohort, which are similar findings to what have been reported in the general population (16, 17, 29, 30). While the mean age of diagnosis of melanoma in the general population is 63, the mean age of our cohort approaches 69 years old, which corroborates the lower *BRAF* prevalence and greater percentage of V600K mutations (31).

NRAS mutation prevalence in this cohort was found to be within a comparable range of what has been reported for the general population (19% vs. 20%) (22). This is surprising considering that NRAS is associated with chronic sun damage and would therefore be expected to be at higher prevalence in this population given chronic occupational sun exposure, though that is not the case here. One possibility is that the pathogenesis involving greater cumulative sun exposure in this veteran population favors *BRAF* V600K over *NRAS* mutations. As shown in other studies, *NRAS* and *BRAF* mutations were mutually exclusive, showing distinct pathogenesis (11, 30, 32). Our study showed NRAS to be more common on the extremities, which again supports the connection with chronically sun-damaged skin. Nodular melanoma subtype and extremity anatomic location were also found to be at higher odds for

TABLE 5 | Univariate analysis between demographic and clinical factors and *NRAS* mutations.

Variable		Odds of *NRAS* Mutation			
	Group	N	Odds Ratio	95% CI	P-value
Smoker	Former	57	1.12	0.42 3.00	0.73
	Current	33	0.72	0.21 2.38	
	Never	39	Ref	– –	
VA Branch	Air Force	15	1.62	0.26 10.30	0.73
	Army	85	1.70	0.39 7.42	
	Navy	19	0.83	0.12 5.76	
	Marines	16	Ref	– –	
Age at diagnosis	Units=1	135	0.99	0.96 1.03	0.66
Stage at diagnosis	1 or 2	119	2.79	0.47 16.58	0.26
	0	16	Ref	– –	
Anatomic	Extremity	47	2.03	0.79 5.20	**0.02**
	Head/Neck	39	0.28	0.06 1.25	
	Trunk	49	Ref	– –	
Subtype	In situ	18	0.21	0.03 1.26	**0.02**
	Lentigo	39	0.16	0.04 0.67	
	Nodular	13	1.57	0.45 5.47	
	Superficial	59	Ref	– –	
Personal history of melanoma	Yes	23	0.93	0.30 2.92	0.90
	No	112	Ref	– –	
Personal history of NMSC	Yes	56	1.53	0.65 3.58	0.33
	No	79	Ref	– –	
Family history of melanoma	Yes	8	1.62	0.33 8.12	0.55
	No	127	Ref	– –	
Family history of NMSC	Yes	11	1.08	0.24 4.94	0.92
	No	124	Ref	– –	

VA, Veterans Affairs NMSC, Non-melanoma skin cancer.
Univariate analysis was performed on various clinical variables listed in the table to determine the odds of NRAS mutation. For each clinical variable, one group was assigned as a reference for which to compare the odds of other groups, hence the odds ratio of the chosen reference group is 1. Odds ratio for other groups listed within a clinical variable will be in comparison to the reference group odds of NRAS mutation.

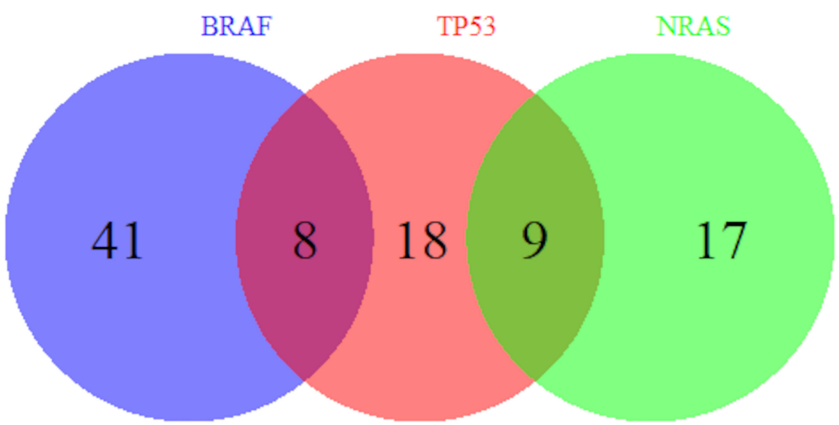

FIGURE 1 | Overlap of *BRAF*, *TP53*, and *NRAS* Mutations. Number of Veterans with melanoma harboring *BRAF*, *TP53*, and *NRAS* mutations out of our cohort of 135 Veterans are shown. A subset of melanomas has both *BRAF* and *TP53* mutations and another subset has both *NRAS* and *TP53* mutations. However, *BRAF* and *NRAS* mutations are mutually exclusive.

NRAS, which agrees with what has been reported in the general population (22–24). Moreover, the breakdown of mutations in *NRAS*, with general predominance of codon 61 mutations, and more specifically Q61R, has been noted in other studies (33, 34). This may suggest that Veterans undergo similar pathogenesis as the general population in *NRAS* mutations, though exact statistical comparison is challenging given the low number of mutations observed. These findings raise the question of how much the genetic profile described in this veteran population results from chronic sun exposure as opposed to other risk factors that have so far not been well-examined, including chemical exposures and ionizing radiation.

TABLE 6 | Univariate analysis between demographic and clinical factors and *TP53* mutations.

Variable	Odds of *TP53* Mutation					
	Group	N	Odds Ratio	CI 95%		P-value
Smoker	Former	57	0.83	0.33	2.07	0.91
	Current	33	0.96	0.34	2.69	
	Never	39	Ref	–	–	
VA Branch	Air Force	15	0.71	0.11	4.53	0.66
	Army	85	1.63	0.44	5.95	
	Navy	19	1.46	0.30	7.07	
	Marines	16	Ref	–	–	
Age at diagnosis	Units=1	135	1.00	0.97	1.03	0.97
Stage at diagnosis	1 or 2	119	0.53	0.18	1.57	0.25
	0	16	Ref	–	–	
Anatomic	Extremity	47	1.19	0.45	3.09	0.25
	Head/Neck	39	2.14	0.83	5.52	
	Trunk	49	Ref	–	–	
Subtype	In situ	18	2.25	0.73	6.92	0.55
	Lentigo	39	1.07	0.41	2.80	
	Nodular	13	1.15	0.28	4.64	
	Superficial	59	Ref	–	–	
Personal history of melanoma	Yes	23	2.67	1.05	6.80	**0.04**
	No	112	Ref	–	–	
Personal history of NMSC	Yes	56	1.47	0.68	3.19	0.33
	No	79	Ref	–	–	
Family history of melanoma	Yes	8	0.54	0.08	3.63	0.53
	No	127	Ref	–	–	
Family history of NMSC	Yes	11	0.37	0.06	2.34	0.29
	No	127	Ref	–	–	

VA, Veterans Affairs; NMSC, Non-melanoma skin cancer.

Univariate analysis was performed on various clinical variables listed in the table to determine the odds of TP53 mutation. For each clinical variable, one group was assigned as a reference for which to compare the odds of other groups, hence the odds ratio of the chosen reference group is 1. Odds ratio for other groups listed within a clinical variable will be in comparison to the reference group odds of TP53 mutation.

TP53 mutation prevalence in this cohort was also higher than what has been reported for the general population (26% vs. 15-20%) (35, 36). Interestingly, having a previous history of melanoma before the current diagnosis for this study was associated with increased odds of having *TP53* mutations. This suggests that *TP53* mutations may be associated with increased risk for recurrence of melanoma. In one study, wild-type p53 enzyme was correlated with a longer relapse-free period in melanoma patients (37). That would suggest that p53 plays an important suppressive role in preventing melanoma tumorigenesis, and that *TP53* mutations may disinhibit melanoma development, leading to recurrence of melanoma. Understanding *TP53* subtypes could therefore be key to stratifying risk in the general population or even specifically within the military, which is especially critical given its higher prevalence in this population.

It is worth noting that *KIT* mutations, which are generally uncommon and have a reported 1-5% prevalence, was found to be 8% in our cohort (38, 39). *KIT* mutations are typically found in melanomas on mucosal and acral areas, which points toward non-UV exposures. Higher *KIT* mutations in Veterans therefore further suggests greater significance of other non-UV related risk factors in the military population. These may also explain melanomas in more varied Fitzpatrick skin types, though our study was limited by access to only types I-III. Unfortunately, the sample size of *KIT* mutations was not large enough to draw statistically meaningful relationships to demographic and clinical data.

These findings help shed light on melanoma in the Veteran population. Few studies have been conducted on trying to understand the pathogenesis of melanoma in military populations, and none have investigated the genetic profile of their melanomas. Additionally, because the study was conducted on earlier staged disease, it is more likely to show the initial drivers of carcinogenesis rather than cumulative mutations over time. This will help better elucidate the pathways that lead to melanoma development in this population. In combination with demographic information and clinic history, associations to exposures and risks can made. For instance, stronger relationships to cumulative sun exposure as well as non-UV exposures have been hinted by the lower prevalence of *BRAF* and increased *KIT* compared to what studies have found in the general population.

However, more work needs to be done to fully understand the exact exposures and mechanism of pathogenesis. This study primarily covered hotspots known to be commonly found in tumors, but other mutations may be missed. Additionally, the cohort consisted of only patients seen at the Iowa City VAMC and with a skew towards Army branch, which may not be completely representative of the military or Veteran population as a whole. Validation at other sites may be important in this regard. Lastly, this study did not have a matched control for direct comparison. While many studies have outlined the general

rates and prevalence of mutations in melanoma in the general population, having a matched control would improve validity and increase the sensitivity of detecting significant deviations from a controlled sample.

In conclusion, we were able to profile 25 hotspot gene mutations in early-stage melanoma in Veterans, which showed lower prevalence of *BRAF*, higher *KIT* and *TP53*, and comparable *NRAS* mutations compared to what has been reported for the general population. In doing so, we were able to shed light on the unique genetic signatures that may be seen in this population. The lower prevalence of *BRAF* mutations and higher percentage being *BRAF* V600K points toward cumulative sun damage as a larger risk factor for Veterans, which in combination with previous studies showing poor sun protection education and practices in the military, strongly advocates for improvement in this regard. The higher *KIT* prevalence suggests increased non-UV risk factors, which will need to be further explored to identify and understand these exposures in order to improve prevention practices. *TP53* mutations was more likely in individuals with previous history of melanoma, which identifies a subpopulation of Veterans who may need closer evaluation of melanoma recurrence. While this study provides new information regarding both genetics of melanoma in a Veteran population and early-stage tumors, more work will need to be done in order to better understand the exact role that these mutations play in pathogenesis. Future studies may include comparative studies with matched controls, validation at other VA medical centers, larger studies to increase statistical power, and expansion of the gene mutation panel to identify other drivers of malignancy. A follow-up study for this cohort may also be considered, though it is unclear how many of these Veterans will continue to receive routine care at the Iowa City VAMC. Ultimately, these findings should influence how we educate, screen, and treat melanoma in Veterans and active military personnel, and pave the way for continued research in this higher risk population.

DATA AVAILABILITY STATEMENT

The datasets presented in this study can be found in online repositories. The names of the repository/repositories and accession number(s) can be found below: http://dx.doi.org/10.17632/sk7g7wncms.1.

ETHICS STATEMENT

The studies involving human participants were reviewed and approved by University of Iowa, Human Subjects Office/IRB. Written informed consent for participation was not required for this study in accordance with the national legislation and the institutional requirements.

AUTHOR CONTRIBUTIONS

JP conceived the original idea, acquired funding, supervised the research study, and helped design the methodology. KC wrote the original draft, helped design the methodology, and assisted in investigation and data curation. AB assisted in investigation, provided resources and methodology for genetic analysis, and helped review and edit the manuscript. SM led statistical analysis, supported data curation and methodology, and reviewed the manuscript. MZ supported statistical analysis and data curation and reviewed the manuscript. JM assisted with project administration and data curation. YZ helped review and edit the manuscript. BS provided access to Veteran Affairs samples and helped review and edit the manuscript. All authors have reviewed the author contributions and agree that the role designations are correct.

FUNDING

This research was funded and supported by the University of Iowa Department of Dermatology.

ACKNOWLEDGMENTS

The authors thank the University of Iowa Department of Dermatology for their support and funding.

REFERENCES

1. Siegel RL, et al. Cancer Statistics, 2021. *CA Cancer J Clin* (2021) 71(1):7–33. doi: 10.3322/caac.21654
2. Miller KD, et al. Cancer Treatment and Survivorship Statistics, 2019. *CA Cancer J Clin* (2019) 69(5):363–85. doi: 10.3322/caac.21565
3. Ramani ML, Bennett RG. High Prevalence of Skin Cancer in World War II Servicemen Stationed in the Pacific Theater. *J Am Acad Dermatol* (1993) 28(5 Pt 1):733–7. doi: 10.1016/0190-9622(93)70102-Y
4. Lea CS, et al. Melanoma Incidence Rates in Active Duty Military Personnel Compared With a Population-Based Registry in the United States, 2000-2007. *Mil Med* (2014) 179(3):247–53. doi: 10.7205/MILMED-D-13-00356
5. Riemenschneider K, Liu J, Powers JG. Skin Cancer in the Military: A Systematic Review of Melanoma and Nonmelanoma Skin Cancer Incidence, Prevention, and Screening Among Active Duty and Veteran Personnel. *J Am Acad Dermatol* (2018) 78(6):1185–92. doi: 10.1016/j.jaad.2017.11.062
6. Erdei E, Torres SM. A New Understanding in the Epidemiology of Melanoma. *Expert Rev Anticancer Ther* (2010) 10(11):1811–23. doi: 10.1586/era.10.170
7. Brown J, et al. Malignant Melanoma in World War II Veterans. *Int J Dermatol* (1984) 23(10):661–3. doi: 10.1111/j.1365-4362.1984.tb01228.x
8. Parker G, Williams B, Driggers P. Sun Exposure Knowledge and Practices Survey of Maintenance Squadrons at Travis AFB. *Mil Med* (2015) 180(1):26–31. doi: 10.7205/MILMED-D-14-00091
9. Powers JG, et al. Skin Cancer Risk Factors and Preventative Behaviors Among United States Military Veterans Deployed to Iraq and Afghanistan. *J Invest Dermatol* (2015) 135(11):2871–3. doi: 10.1038/jid.2015.238
10. Fortes C, de Vries E. Nonsolar Occupational Risk Factors for Cutaneous Melanoma. *Int J Dermatol* (2008) 47(4):319–28. doi: 10.1111/j.1365-4632.2008.03653.x

11. Davies H, et al. Mutations of the BRAF Gene in Human Cancer. *Nature* (2002) 417(6892):949–54. doi: 10.1038/nature00766
12. Hall RD, Kudchadkar RR. BRAF Mutations: Signaling, Epidemiology, and Clinical Experience in Multiple Malignancies. *Cancer Control* (2014) 21 (3):221–30. doi: 10.1177/107327481402100307
13. Curtin JA, et al. Distinct Sets of Genetic Alterations in Melanoma. *N Engl J Med* (2005) 353(20):2135–47. doi: 10.1056/NEJMoa050092
14. Curtin JA, et al. Somatic Activation of KIT in Distinct Subtypes of Melanoma. *J Clin Oncol* (2006) 24(26):4340–6. doi: 10.1200/JCO.2006.06.2984
15. Gilchrest BA, et al. The Pathogenesis of Melanoma Induced by Ultraviolet Radiation. *N Engl J Med* (1999) 340(17):1341–8. doi: 10.1056/NEJM199904293401707
16. Maldonado JL, et al. Determinants of BRAF Mutations in Primary Melanomas. *J Natl Cancer Inst* (2003) 95(24):1878–90. doi: 10.1093/jnci/djg123
17. Bauer J, et al. BRAF Mutations in Cutaneous Melanoma are Independently Associated With Age, Anatomic Site of the Primary Tumor, and the Degree of Solar Elastosis at the Primary Tumor Site. *Pigment Cell Melanoma Res* (2011) 24(2):345–51. doi: 10.1111/j.1755-148X.2011.00837.x
18. Candido S, et al. Analysis of the B-RafV600E Mutation in Cutaneous Melanoma Patients With Occupational Sun Exposure. *Oncol Rep* (2014) 31 (3):1079–82. doi: 10.3892/or.2014.2977
19. Schlaak M, et al. Assessment of Clinical Parameters Associated With Mutational Status in Metastatic Malignant Melanoma: A Single-Centre Investigation of 141 Patients. *Br J Dermatol* (2013) 168(4):708–16. doi: 10.1111/bjd.12140
20. Heppt MV, et al. Prognostic Significance of BRAF and NRAS Mutations in Melanoma: A German Study From Routine Care. *BMC Cancer* (2017) 17 (1):536. doi: 10.1186/s12885-017-3529-5
21. Delyon J, Lebbe C, Dumaz N. Targeted Therapies in Melanoma Beyond BRAF: Targeting NRAS-Mutated and KIT-Mutated Melanoma. *Curr Opin Oncol* (2020) 32(2):79–84. doi: 10.1097/CCO.0000000000000606
22. Ellerhorst JA, et al. Clinical Correlates of NRAS and BRAF Mutations in Primary Human Melanoma. *Clin Cancer Res* (2011) 17(2):229–35. doi: 10.1158/1078-0432.CCR-10-2276
23. Devitt B, et al. Clinical Outcome and Pathological Features Associated With NRAS Mutation in Cutaneous Melanoma. *Pigment Cell Melanoma Res* (2011) 24(4):666–72. doi: 10.1111/j.1755-148X.2011.00873.x
24. Akslen LA, et al. BRAF and NRAS Mutations are Frequent in Nodular Melanoma But are Not Associated With Tumor Cell Proliferation or Patient Survival. *J Invest Dermatol* (2005) 125(2):312–7. doi: 10.1111/j.0022-202X.2005.23788.x
25. Rubinstein JC, et al. Incidence of the V600K Mutation Among Melanoma Patients With BRAF Mutations, and Potential Therapeutic Response to the Specific BRAF Inhibitor PLX4032. *J Transl Med* (2010) 8:67. doi: 10.1186/1479-5876-8-67
26. Li Y, Umbach DM, Li L. Putative Genomic Characteristics of BRAF V600K Versus V600E Cutaneous Melanoma. *Melanoma Res* (2017) 27(6):527–35. doi: 10.1097/CMR.0000000000000388
27. Menzies AM, et al. Distinguishing Clinicopathologic Features of Patients With V600E and V600K BRAF-Mutant Metastatic Melanoma. *Clin Cancer Res* (2012) 18(12):3242–9. doi: 10.1158/1078-0432.CCR-12-0052
28. Adler NR, et al. Tumour Mutation Status and Sites of Metastasis in Patients With Cutaneous Melanoma. *Br J Cancer* (2017) 117(7):1026–35. doi: 10.1038/bjc.2017.254
29. Thomas NE, et al. Number of Nevi and Early-Life Ambient UV Exposure are Associated With BRAF-Mutant Melanoma. *Cancer Epidemiol Biomarkers Prev* (2007) 16(5):991–7. doi: 10.1158/1055-9965.EPI-06-1038
30. Thomas NE, et al. Association Between NRAS and BRAF Mutational Status and Melanoma-Specific Survival Among Patients With Higher-Risk Primary Melanoma. *JAMA Oncol* (2015) 1(3):359–68. doi: 10.1001/jamaoncol.2015.0493
31. Howlader N NA, Krapcho M, et al. *SEER Cancer Statistics Review, 1975-2013*. Bethesda, MD: National Cancer Institute (2015).
32. Omholt K, et al. NRAS and BRAF Mutations Arise Early During Melanoma Pathogenesis and are Preserved Throughout Tumor Progression. *Clin Cancer Res* (2003) 9(17):6483–8.
33. Grill C, Larue L. NRAS, NRAS, Which Mutation Is Fairest of Them All? *J Invest Dermatol* (2016) 136(10):1936–8. doi: 10.1016/j.jid.2016.06.011
34. Helias-Rodzewicz Z, et al. Variation of Mutant Allele Frequency in NRAS Q61 Mutated Melanomas. *BMC Dermatol* (2017) 17(1):9. doi: 10.1186/s12895-017-0061-x
35. Zhang T, et al. The Genomic Landscape of Cutaneous Melanoma. *Pigment Cell Melanoma Res* (2016) 29(3):266–83. doi: 10.1111/pcmr.12459
36. Kim DW, et al. Clinicopathological Features and Clinical Outcomes Associated With TP53 and BRAF(N)(on-)(V)(600) Mutations in Cutaneous Melanoma Patients. *Cancer* (2017) 123(8):1372–81. doi: 10.1002/cncr.30463
37. Florenes VA, et al. TP53 Allele Loss, Mutations and Expression in Malignant Melanoma. *Br J Cancer* (1994) 69(2):253–9. doi: 10.1038/bjc.1994.48
38. Pracht M, et al. Prognostic and Predictive Values of Oncogenic BRAF, NRAS, C-KIT and MITF in Cutaneous and Mucous Melanoma. *J Eur Acad Dermatol Venereol* (2015) 29(8):1530–8. doi: 10.1111/jdv.12910
39. Leichsenring J, et al. Genetic Profiling of Melanoma in Routine Diagnostics: Assay Performance and Molecular Characteristics in a Consecutive Series of 274 Cases. *Pathology* (2018) 50(7):703–10. doi: 10.1016/j.pathol.2018.08.004

Conflict of Interest: The authors declare that the research was conducted in the absence of any commercial or financial relationships that could be construed as a potential conflict of interest.

frontiers | Frontiers in Oncology

ORIGINAL RESEARCH
published: 30 May 2022
doi: 10.3389/fonc.2022.848346

eIF6 as a Promising Diagnostic and Prognostic Biomarker for Poorer Survival of Cutaneous Melanoma

Fangyingnan Zhang[1,2], *Saquib Waheed*[2], *Ubaldo Armato*[2], *Jun Wu*[1,2], *Chao Zhang*[1*] and *Zhibin Li*[2*]

[1] School of Biomedical Engineering, Sun Yat-sen University, Guangzhou, China, [2] Department of Burn and Plastic Surgery, Shenzhen Institute of Translational Medicine, The First Affiliated Hospital of Shenzhen University, Shenzhen Second People's Hospital, Shenzhen, China

OPEN ACCESS

Edited by:
Gagan Chhabra,
University of Wisconsin-Madison,
United States

Reviewed by:
Limin Jiang,
Tianjin University, China
Zhe Li,
The University of Sydney, Australia

***Correspondence:**
Zhibin Li
lzbszu@163.com
Chao Zhang
zhchao9@mail.sysu.edu.cn

Specialty section:
This article was submitted to Skin Cancer, a section of the journal Frontiers in Oncology

Received: 04 January 2022
Accepted: 25 April 2022
Published: 30 May 2022

Citation:
Zhang F, Waheed S, Armato U, Wu J, Zhang C and Li Z (2022) eIF6 as a Promising Diagnostic and Prognostic Biomarker for Poorer Survival of Cutaneous Melanoma. Front. Oncol. 12:848346. doi: 10.3389/fonc.2022.848346

Background: Skin cutaneous melanoma (SKCM) is the deadliest skin cancer and has the most rapidly increasing incidences among all cancer types. Previous research elucidated that melanoma can only be successfully treated with surgical abscission in the early stage. Therefore, reliable and specific biomarkers are crucial to melanoma diagnosis since it often looks like nevi in the clinical manifestations. Moreover, identifying key genes contributing to melanoma progression is also highly regarded as a potential strategy for melanoma therapy. In this respect, translation initiator eIF6 has been proved as a pro-tumor factor in several cancers. However, the role of eIF6 in the skin cutaneous melanoma progression and its potential as a prognostic marker is still unexplored.

Methods: The immunochemical analysis of clinical specimens were served to assess eIF6 expression levels. Gene Expression Profiling Interactive Analysis (GEPIA) database consultations allowed us to find the survival rates of the eIF6-overexpressed patients. eIF6 cellular effects were evaluated in an eIF6-overexpressed A375 cell line constructed with a lentivirus. The analysis of down-stream effectors or pathways was conducted using C-Bioportal and STRING databases.

Results: Our results revealed that eIF6 was highly over-expressed in melanomas compared to normal skin specimens, and thus the abnormally high level of eIF6 can be a diagnostic marker for melanoma. The in silica analysis indicated that patients with eIF6 over-expression had lower survival rates than that low-expression in SKCM. Meanwhile, similar results also could be found in the other four types of cancers. *In vitro*, over-expression of eIF6 increased the proliferation and migration of melanoma cells. Correspondingly, pan-cancer clustering analysis indicated the expression level of intermediate filament proteins was correlated with that of eIF6 expression. In our study, all over-expressed keratin proteins, in accordance with over-expressed eIF6, had a negative correlation with melanoma prognosis. Moreover, the decreased methylation level of keratin genes suggested a new potential regulation mode of eIF6.

Conclusions: The up-regulated eIF6 could be a potential diagnostic and prognostic biomarker of melanoma. This study also provides insights into the potential role of eIF6 in pan-cancer epigenetic regulation.

Keywords: eIF6, melanoma, diagnostic and prognostic, biomarker, tumor therapy

INTRODUCTION

Melanoma, also called malignant melanoma, is a type of skin cancer that arises from pigment-producing cells called melanocytes. It accounts for 10% of newly diagnosed cases of overall skin cancers and further increases in its prevalence and mortality worldwide. To date, the skin melanoma incidence rate has increased five-fold since the mid-1980s (1, 2). Nowadays, melanoma has become the most lethal type of skin cancer, with a mortality rate second behind lung cancer (3). The ideal treatment of melanoma is through surgical resection at the early stage. Otherwise, the survival rate of patients may be decreased significantly when the metastatic dissemination is occurred (4). Therefore, a precise early diagnosis is pivotal to the good prognosis of melanoma. Especially, the clinical manifestations of melanoma are not obvious in the early stage, mostly present as nevi-like skin lesions, which may or may not be associated with ulceration or bleeding. Thus, the clinical diagnoses are frequently unreliable (5, 6). In recent years, newly produced monoclonal antibodies specifically target tumor-associated antigens enable researchers to detect the onset and recurrence of malignant melanomas and make a specific histopathological diagnosis. Actually, monoclonal antibodies (McAbs) are developed for the histopathological diagnosis and classification of the cancers, such as the HMSA1 and HMSA2 McAbs that targeted melanosome-associated antigens. Nevertheless, the specificity of these McAbs were far from satisfaction. Some more specific McAbs, including NK1C3, S-100 and HMB-45, have been developed recently (7–9) to address this shortcoming. However, melanoma shows significant heterogeneity. In clinical cancer diagnosis, the cases with Melan-A negative or even with S100 negative have been often reported (10, 11). Therefore, the researchers hope to seek more specific diagnostic biomarkers to avoid misdiagnosis cases. Meanwhile, drug and immune therapy are the main choices for metastatic melanoma patients. Target therapy with BRAF/MEK inhibitors in metastatic melanoma has shown a high response rate. However, the cases that have resistance to this treatment still frequently occur due to the unsatisfactory selectivity of chemotherapeutic agents. Hence, there is an urgency to seek more promising diagnostic and prognostic biomarkers for melanoma therapy.

Previous reports showed that the continuous proliferating melanoma cells demand a high level of protein synthesis, and the dysregulation of mRNA translation is generally regarded as a typical tumorigenesis feature of melanoma (12, 13). In this process, protein synthesis includes four steps: initiation, elongation, termination, and ribosome recycling. The initiation is the most important step of protein translation because it is both highly regulated and rate-limited. In this respect, a set of proteins named eukaryotic Initiation Factors (eIFs) control the onset of translation in eukaryotic cells (14). Dozens of researches have identified the cancerous function in different eIFs. For example, recent studies have proved that eIF4B contributes to the cellular adaptation of asparagine in BRAF-mutated A375 melanoma. Meanwhile, in prostate cancer cells, eIF5B can activate the PD-1 checkpoint of the T cells by interacting with Wig1, causing T cell exhaustion and promoting tumor development and metastasis (15, 16). Among eIFs, eIF6 has attracted enormous interest because it not only regulates the ribosomal 60S subunit genesis inside the nucleus but also mediates ribosomal assembly in the cytoplasm (17). In 2008, Biffo et al. have firstly proved eIF6 as a rate-limiting factor in cell-cycle and tumorigenesis. Nowadays, the tumor-promoting pathways associated with eIF6 have been found in various types of cancer cells (18). For instance, in the myc-induced lymphomas mice model, eIF6 impairment can significantly reduce the tumor growth and prolong the tumor-free survival time through an mTORC-independent mechanism (19). In contrast, previous research found over-expression of eIF6 in ovarian cells and melanoma cell lines can effectively increase cell mobility and proliferation *via* CDC42 up-regulation (20). Furthermore, the increased eIF6 level has been reported to play a major role in association with poor prognostication of colorectal cancer, non-small cell lung carcinoma and malignant pleural mesothelioma (21–24). Thus, eIF6 is a promising diagnostic and prognostic candidate in melanoma.

In this work, we investigated the eIF6 expression features and its role in melanoma progression using clinical specimens and the TCGA database. We examined the prognostic value of eIF6 according to its expression and analyzed the patients' survival data to infer its potential melanoma-promoting mechanisms. Our results revealed that the high eIF6 expression accompanied more dynamic cell skeleton gene expression and led to accelerated cellular proliferation. These findings elucidated the underlying regulation mechanisms of eIF6 in melanoma, and our pan-cancer analysis also provided clues of an epigenetic function of eIF6 in other types of cancers.

Abbreviations: eIF6, Eukaryotic Initiation Factor 6; GEPIA, Gene Expression Profiling Interactive Analysis; IFs, Intermediate Filaments; KICH, Kidney Chromophobe; LAML, Acute Myeloid Leukemia; PCPG, Pheochromocytoma and Paraganglioma; LGG, Low-Grade Glioma; LIHC, Liver Hepatocellular Carcinoma; LUAD, Lung Adenocarcinoma; PAAD, Pancreatic Adenocarcinoma; GEPIA, Gene Expression Profiling Interactive Analysis; STRING, Search Tool for Recurring Instances of Neighboring Genes; SKCM, Skin Cutaneous Melanoma

METHODS

Gene Expression Profiling Interactive Analysis (GEPIA)

The analysis of patients' survival rates was conducted using GEPIA, a web tool based on TCGA and GTEx databases. Based

on the RNA-sequencing results, GEPIA supplies the expression levels of specific genes in various cancer types compared to those of adjacent normal tissues. GEPIA divides the cancer clinical data into two groups and compares the prognosis based upon the expression levels of the gene of interest. GEPIA is available at http://gepia.cancer-pku.cn/ (25).

c-BioPortal Analysis

The c-Bio Cancer Genomics Portal (http://cbioportal.org) is an open-source online platform supplying a multidimensional view of cancer genomics data. By now, it holds the data from 225 cancer studies. We classified the SKCM samples into an eIF6 overexpressing (i.e., an "altered") group and an "unaltered" group. We compared the two groups' RNA-sequencing data to assess the differences in expressed genes and DNA methylation data. We analyzed the altered group samples in the "TCGA Firehouse Legacy" dataset, which holds data from 479 skin melanoma samples. The search parameters of the altered group were "mRNA expression Z-scores relative to diploid samples". The Z-score threshold was 2, which descripted the variation level of a certain number in samples identification. Since these samples accounted for 14% in all the SKCM patients, the 14% top of eIF6 expressed samples were defined as the "altered" group in SKCM patients (26).

Database for Annotation, Visualization, and Integration Discovery (DAVID) Analysis

We used DAVID to make the annotation and KEGG analysis. Resources in DAVID aim to interpret gene function from an extensive list. DAVID is also capable for KEGG pathway enrichment analysis. We got the list of differentially expressed genes (DEGs) from the c-BioPortal and gave functional annotations using DAVID. The DAVID is available at http://david.niaid.nih.gov (27).

Protein-Protein Interaction Analysis

The Search Tool for Recurring Instances of Neighboring Genes (STRING) database can visualize protein-protein interactions by presenting genes as colored nodes and linking the interacting genes with lines. In the interaction map of STRING, the genes which function or bind closely occupy neighboring places and have thick lines linking each other. STRING is also capable for gene annotation enrichment analysis, classifying the genes by the Gene Ontology terms. The STRING database is available at https://string-db.org/ (28).

Clinical Specimens and Immunochemistry

The First Affiliated Hospital of Shenzhen University provided us with melanoma samples. Immunochemistry experiments were conducted as described in the previous research (29). The antibodies used were purchased from Cell Signaling Technology, Inc. (eIF6, 3263S; HMB45, 38815S; S100, 90393) and Boster Biological Technology Co., Ltd. (Melan-A, M02033).

Cell Lines and Vectors

The A375 cell line was obtained from the American Type Culture Collection (ATCC). The cells were cultured in Dulbecco's Modified Eagle Medium (Bibico, 11965084) containing 10% fetal bovine serum (Gibico, 10099) and 1% Penicillin-Streptomycin (Gibico, 15140122). The eIF6 over-expression cell line was established by infecting A375 cells with lentivirus, and the counterpart GFP-expression A375 cells as the control group. The target genes were carried by pGWLV01 plasmids (bought from GENEWIZ Cooperation). The plasmids were transfected into 293T cells with the help of polyethylenimine to produce virus. The virus was harvested at 48 and 72 h post-transfection and A375 cells were infected in the presence of 10 μg/mL of polybrene and 10 mM HEPES. The infected cells were screened by treatment with puromycin (50 μg/mL) for two days.

Wound Healing Assay

The wound-healing assay was used to test the ability of the cells migration as previously reported (30). Briefly, 2×10^6 cells were plated onto a 100-mm dish to create a confluent monolayer. The cells were scratched and resulting in a straight wound. The wound width was measured after incubation for 24 and 48 h.

Statistical Analysis

The significance test of change was evaluated with *P* value. *P* value < 0.05 was labeled as "*". *P*-value < 0.01 was labeled as "**". *P*-value < 0.001 was labeled as "***".

RESULTS

eIF6 Is Up-Regulated in Skin Melanomas and Is Related to Poor Prognosis

To identify the impact of eIF6 on tumor progression. We first compared the survival rate of 33 common types of cancers during the up-regulation of eIF6. Among them, about 50% of the cancers' survival rates were lower in the eIF6 higher expression group. The patients with low-eIF6 expression survived longer than that of eIF6 over-expression in seven types of cancers. In eIF6 over-expression specimens, the survival rates of brain lower-grade glioma (LGG), liver hepatocellular carcinoma (LIHC), lung adenocarcinoma (LUAD), pancreatic adenocarcinoma (PAAD), and skin cutaneous melanoma (SKCM) were all significantly reduced (**Figure 1A**).

Among these five types of cancers, the eIF6's impact on LGG, LIHC and LUAD progression had been reported previously, while that on melanoma was still unclear. Thus we focused our interests on the melanoma study. We compared the survival curves of melanoma patients with high or low eIF6 expression levels and grouped them according to gradient inclusion criteria. For instance, we compared the top 10% of high-eIF6 expression patients with the bottom 10% of low-eIF6 expression patients. Then, the top 20% of patients were compared with the bottom 20%. In all of the survival curves, melanoma patients with high eIF6 expression had worse prognoses (**Figure 1B**).

Immunochemistry was used to determine the level of eIF6 protein in the melanoma specimens. Hematoxylin and eosin (HE) staining and immunochemistry analysis of HMB-45, S-100, and Melan-A were used to identify melanoma cells. The

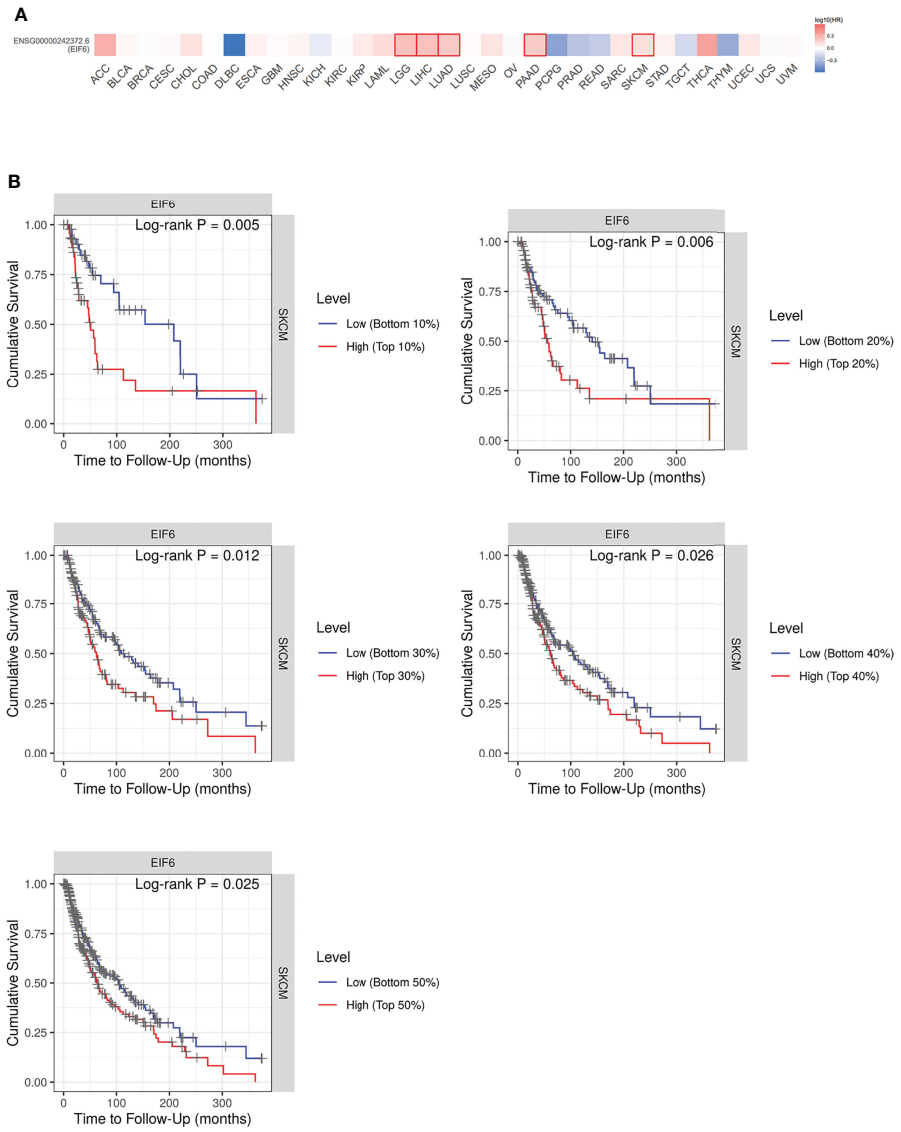

FIGURE 1 | Analysis of the correlation between cancer survival rates and eIF6 expression level. **(A)** Survival analysis of eIF6 in 33 types of cancers: The survival rates of 33 types of cancers were analyzed. The cancer types whose eIF6-high expressed patients showed significantly poorer prognoses were labeled with red frame. The cancer types whose survival rates were improved by high eIF6 levels were labeled with blue. **(B)** Melanoma patients were grouped according to their eIF6 expression levels, and their respective survival rates were compared.

results indicated that melanoma cells had higher levels of eIF6 expression when compared to adjacent normal tissues (**Figure 2**). The eIF6 expression through all the stages of melanoma development was further investigated by GEPIA analysis, the results showed that compared with the stage 0, eIF6 level was up-regulated from stage I to stage IV. Especially in stage I and stage II, eIF6 level was even higher than that in the later stages (**Figure S2**). Additionally, the up-regulated eIF6 expression was further confirmed by Timer analysis, which suggest the potential effectiveness of eIF6 in early stage melanoma diagnosis (**Figure S3**).

eIF6 Promotes the Proliferation and Migration of Melanoma Cell Lines

The poor survival rate of the eIF6 high expression group suggested that eIF6 profoundly impacted the tumor cells. As a translation initiation factor, eIF6 expression is intimately linked to ribosome biogenesis and thus affects protein synthesis. It is possible that eIF6 acts as a rate-limiting factor in cell proliferation. The cellular function of eIF6 was investigated using the melanoma cell line A375. eIF6 was over-expressed with lentivirus, and the over-expressed GFP cells were used as control.

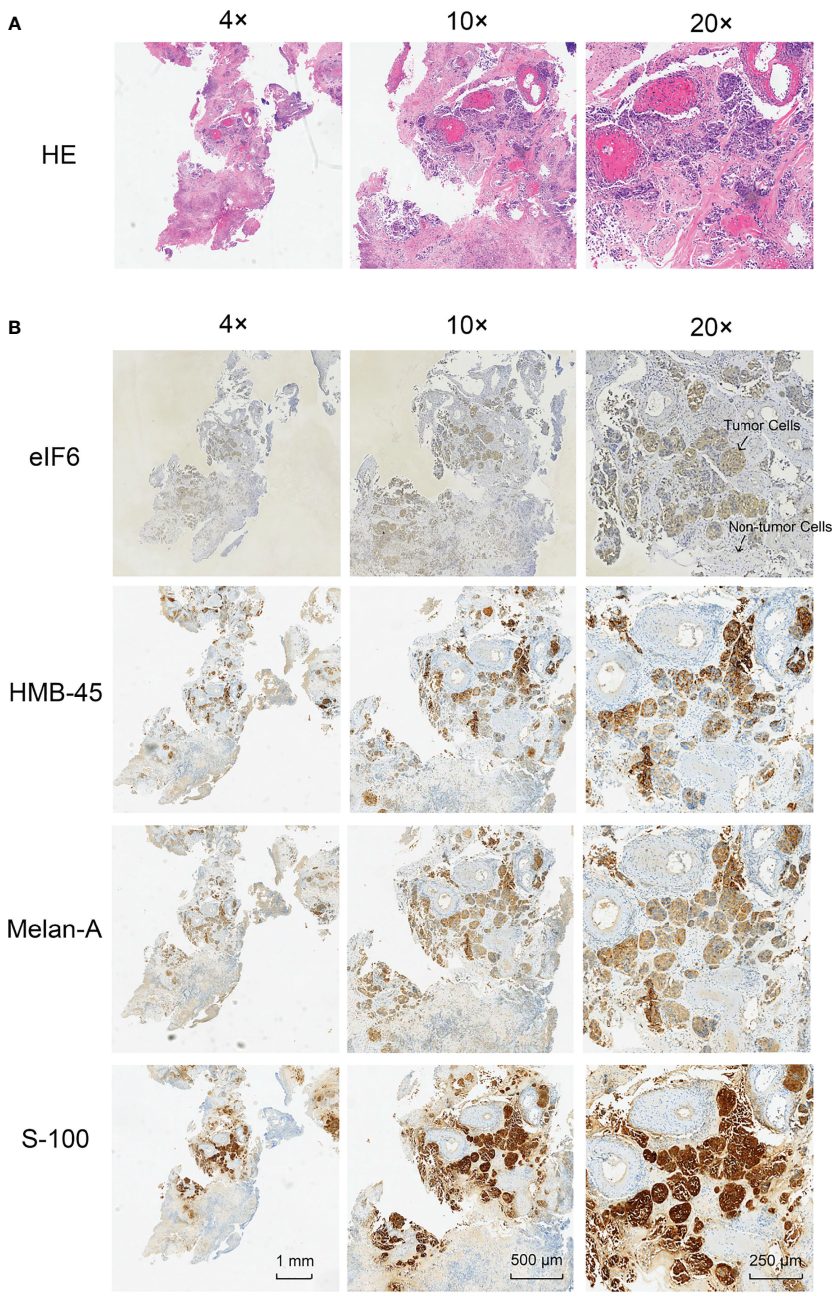

FIGURE 2 | Histological examination of the tumor specimens (Area size: 0.5 cm^2). **(A)** Hematoxylin-eosin staining (H&E) shows the histology of melanoma tumor. **(B)** Immunohistochemical staining of eIF6, HMB-45, Melan-A, and S-100 in melanoma tumor slices, respectively.

While eIF6 was over-expressed, the growth curves of cells showed a significant shifted on day three and four (**Figure 3A**). We examined the cell-cycle markers PCNA and Cyclin D1 to validate the accelerated growth rates of cells. As shown in **Figures 3B, C**, all of these proliferation markers showed a drastic up-regulation accompanied accelerated cell growth phenotypes when eIF6 was over-expressed.

At both 24 and 48 hours, cells migration ability was assessed during the wound healing. We used Image J software to measure the average width of the scratches. As shown in **Figure 4**, after 24-hours incubation, the eIF6 over-expressed group was 10% narrower than the control group. It reached 25% at 48-hours, indicating over-expression of eIF6 could accelerate the migration of malignant melanoma cells *in vitro*.

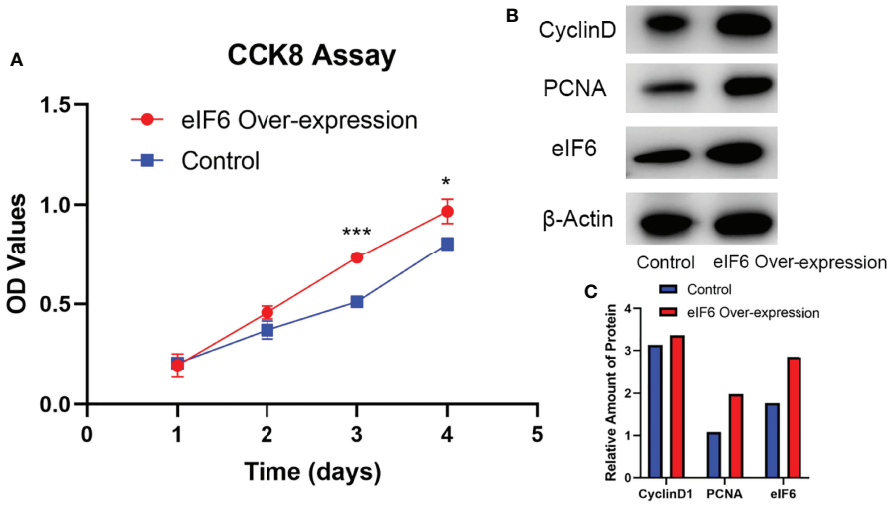

FIGURE 3 | Evaluation of the cellular functions of high-expressed eIF6 in A375 melanoma cells. **(A)** Growth curves comparison between eIF6-overexpressing and wild type (control) A375 cells. The growth rate of eIF6 overexpressing cells was significantly higher than controls. **(B)** Western blot analysis confirms the correlation of up-regulated eIF6 with the cell proliferation marker CyclinD1 and PCNA. **(C)** Quantification of the Western blot results by Image J. The grey density of the bands was measured by Image J, and the target gene expression level was normalized with the grey density of β-actin. The significance test of change was evaluated with P value. P value < 0.05 was labeled as "*". P-value < 0.01 was labeled as "**". P-value < 0.001 was labeled as "***".

Upregulation of Ribosomal Proteins and Intermediate Filaments Is Linked to High eIF6 Expression

Several theories have been proposed to explain how eIF6 contributes to cell proliferation and migration, but none has been accepted as the most plausible. Using high-throughput sequencing data, we investigated the potential downstream effectors of eIF6. The results demonstrated that eIF6 expression significantly affected the survival rates of SKCM, LGG, LIHC, PAAD, and LUAD cells. In addition, we clustered the differentially expressed genes between the eIF6 high expression and low expression groups in these five types of cancers (the list of differential genes is in **Supplementary Table 1**). We found that the ribosomal genes showed an increased mRNA level in the eIF6 high expression group due to the co-expression of ribosomal genes.

In this study, the genes with similar functions were converged together in the protein-protein interaction analysis map (**Figure 5**).

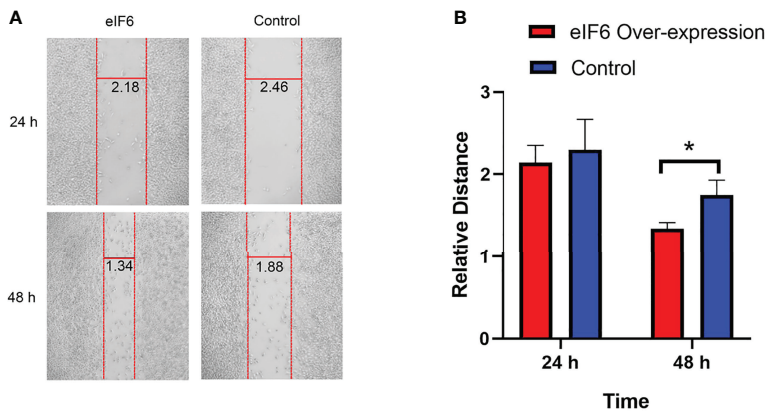

FIGURE 4 | Wound healing assay measures the migration of melanoma cells with over-expression of eIF6. **(A)** The vertical red lines show the wound edges at 24 h and 48 h after scratching, and the horizontal lines show the relative distances between red stripes at the same observation times. The eIF6 over-expression cells migrated more quickly than the control group. **(B)** The spaces between wound edges were measured, and the values were significantly lesser than the eIF6 over-expression group after incubation for 48 h. The significance test of change was evaluated with P value. P value < 0.05 was labeled as "*". P-value < 0.01 was labeled as "**". P-value < 0.001 was labeled as "***".

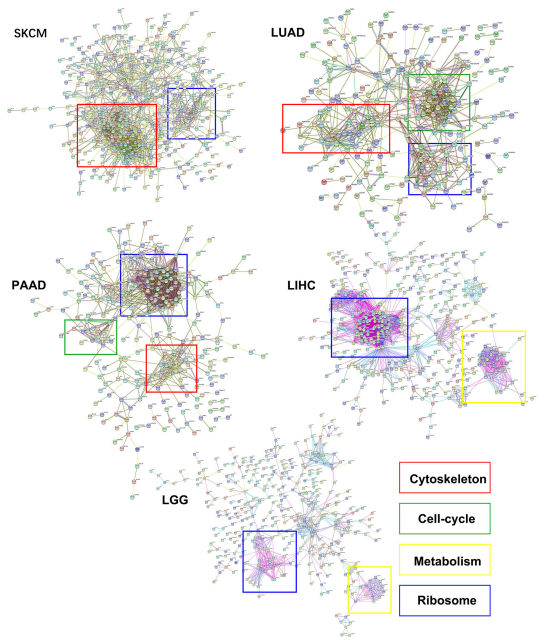

FIGURE 5 | The protein-protein interaction clustering of differentially expressed genes while eIF6 was up-regulated in cancers. The significantly up-regulated genes in the eIF6 altered group were clustered according to protein interactions. The ribosomal proteins formed clusters in all five cancers. The cytoskeletal proteins were clustered in SKCM, LUAD, and PAAD, while the cell-cycle and metabolism proteins were clustered in PAAD and LUAD and LIHC cancers, respectively.

Interestingly, the clustering results showed enrichment of keratin proteins in SKCM, LUAD, and PAAD, but not in LIHC and LGG. It is reasonable to assume that many types of cancers have a specific and well-coordinated genes modulation. This indicated that a more dynamic synthesis of intermediate filaments (IFs) occurred with tissue-specific regulation. Typically, the high intermediate filament protein levels were linked to cell proliferation and migration, requiring active cytoskeleton assembly and disassembly. For example, keratin17 was identified as a significantly up-regulated gene in eIF6-high melanoma, and this gene has been reported for its proliferation-promoting function in multiple cancers (31, 32). In fact, when we studied the up-regulated keratin protein effects on cancer progression, all the keratins we found were linked to lower survival rates in cancers, including melanoma (**Figure S4**). The all genes hazard ratio was above 1, with a $p < 0.05$ except KRTCAP2 (**Table 1**). This finding agreed with the fact that an up-regulated eIF6 could aggravate melanoma progression. Besides, we also identified the eIF6 co-expressed genes associated with RNA processing, metabolism and proliferation in the SKCM, which suggested the complexity of the eIF6 signal regulation network (**Figure S5**).

High eIF6 Expression Is Linked to the Global DNA Demethylation

We further investigated the TCGA Firehouse Legacy sequencing data set. As previously stated, the specimens were grouped according to the level of eIF6 expression. The higher eIF6 expressed groups showed global genome demethylation in SKCM, LIHC, LGG, LUAD, and PAAD (**Figure 6A**). The methylation levels of the SKCM, LIHC, and LGG specimens were showed a significant difference between the eIF6-high and eIF6-low groups. In melanoma, there were 10305 genes had higher methylation levels in the eIF6-low group, while 5395 genes in the eIF6-high group had higher methylation tendencies. In the eIF6-high group, 420 genes were demethylated, and 35 genes were hypermethylated, which was significant larger than that in the eIF6-low group (**Table S2**).

We also clustered the demethylated genes in the five types of cancer, in which WNT and NOTCH family genes were found to be demethylated. These two gene clusters involved cell proliferation, differentiation, and cell fate (33). The methylation level of intermediate filament keratins was also investigated. The methylation levels of multiple keratin genes of the five cancers were decreased. In addition, KRT17 and KRT15 were up-regulated and demethylated in the eIF6-high expressed melanoma, suggesting that DNA demethylation was a potential transcription regulation mechanism of eIF6 (**Figure 6B**).

DISCUSSION

eIF6 has been reported as an essential regulator in liver hepatocellular carcinoma, colorectal carcinoma, and non-small cell lung carcinoma, respectively (21, 23, 24). Our study showed that the eIF6 up-regulation also occurs during melanoma tumorigenesis, which relates to a poorer prognosis. Furthermore, pan-cancer analysis revealed that the up-regulation of eIF6 is associated with demethylation and higher expression levels of intermediate filament keratins, which may account for the increased proliferation and migration rates in multiple types of cancer cells. This study offered a better understanding of the functional role of eIF6 in cancer progression and provided new insights into the potential role of eIF6 as a melanoma predictive biomarker.

Additionally, previous reports showed that both eIF4E and eIF2α are also closely associated with melanoma (34, 35). In this study, the skin melanoma samples exhibited significantly increased eIF6 expression levels than the normal skin samples, corresponding to the up-regulated melanoma cells division rates (**Figure 1**). Earlier studies have suggested that eIF6 is up-regulation in hepatocellular carcinoma, lung adenocarcinoma, and colorectal cancer (21, 23, 24). Similarly, the increased eIF6 expression levels also could be observed in LGG and PAAD using the GEPIA database analysis. Conversely, eIF6 was only significantly down-regulated in LAML (**Figure S1**). These findings revealed that eIF6 up-regulation is a common feature in different cancer groups, implying eIF6 was regulated by an cancer-or proliferation-related upstream regulators. The eIF6 promoter contains a GA-rich sequence, in which a GA binding protein (GABP) complex has been identified as an eIF6 expression modulator (36). In tumorigenesis, GABP is a well-studied transcription

TABLE 1 | Up-regulated keratin genes of the high-eIF6 expression group in SKCM, LUAD, PAAD, LGG, and LIHC.

	Differentially expressed genes between eIF6 altered and unaltered group					Survival analysis	
	Gene symbol	Cytoband	Log (fold change)	p-value	q-value	Hazard ratio	p(HR)
SKCM							
	KRT17	17q21.2	2.67	2.52E-04	6.33E-04	1.5	0.0018
	KRT6B	12q13.13	2.4	2.57E-03	5.40E-03	1.3	0.046
	KRT14	17q21.2	2.35	5.84E-03	0.0115	1.4	0.019
	KRT6A	12q13.13	2.3	7.22E-03	0.0139	1.5	0.0038
	KRT16	17q21.2	2.24	8.45E-03	0.0161	1.3	0.043
	KRT6C	12q13.13	2.12	8.84E-03	0.0167	1.4	0.017
	KRT5	12q13.13	1.98	0.0153	0.0275	1.3	0.036
	KRT1	12q13.13	1.82	0.0202	0.0355	1.3	0.05
	KRTAP19-1	21q22.11	1.7	6.29E-05	1.76E-04	1.7	0.00016
	KRTDAP	19q13.12	1.69	0.0123	0.0227	1.7	0.00015
	KRT15	17q21.2	1.6	2.34E-03	4.96E-03	1.3	0.045
	KRT75	12q13.13	1.54	3.73E-03	7.60E-03	/	/
	KRT19	17q21.2	1.45	7.63E-04	1.76E-03	1.3	0.082
LUAD							
	KRT6A	12q13.13	1.68	3.38E-05	1.99E-04	1.6	0.0033
	KRT16	17q21.2	1.51	2.67E-07	3.04E-06	1.6	0.0022
	KRT6B	12q13.13	1.28	2.09E-04	9.52E-04	1.7	0.00075
	KRT6C	12q13.13	1.27	7.19E-05	3.79E-04	1.8	0.00012
	KRT81	12q13.13	1.19	2.27E-05	1.42E-04	1.7	0.00037
	KRT17	17q21.2	1.08	6.47E-05	3.46E-04	1.6	0.0033
	KRT14	17q21.2	1.01	8.92E-04	3.34E-03	1.1	0.47
PAAD							
	KRT19	17q21.2	1.44	3.25E-08	1.43E-05	1.8	0.0045
	KRT15	17q21.2	1.34	1.69E-03	9.67E-03	1.4	0.091
	KRT18	12q13.13	1.09	2.04E-11	5.08E-08	1.7	0.011
	KRT7	12q13.13	1.07	6.05E-03	0.0239	2	0.001
	KRTCAP2	1q22	1.06	6.86E-05	1.32E-03	1.1	0.59
	KRT8	12q13.13	1.01	1.24E-06	1.38E-04	1.7	0.015
LGG							
	KRT18	12q13.13	1.15	9.89E-03	0.0215	2	0.00034
	KRT7	12q13.13	1.11	4.70E-03	0.0112	2	0.00023
	KRTCAP2	1q22	1.05	2.07E-08	3.48E-07	1.6	0.0075
LIHC							
	KRTCAP2	1q22	1.27	6.75E-11	2.92E-09	1.6	0.0086

This is the list of the keratin genes up-regulated over 2-fold (log fold change > 1) and changed with statistical significance (p-value < 0.05). The hazard ratio analysis allowed us to evaluate the role of these genes in the survival of patients with various cancers. All the listed genes hazard ratios were above 1-fold, which showed that their high expression were correlated with a worse prognosis.

factor involved in regulating proliferation, ribosomes, and metabolism (37). Moreover, other tumor-related transcription factors, such as c-myb, can enhance the activation effect when combined with GABP complex (38). The increased expression of eIF6 in melanoma could be attributed to increased transcription factor binding caused by tumorigenesis. Therefore, the abnormal up-regulation of eIF6 in melanoma is a sign of cancer cell proliferation.

Additionally, the eIF6 level is also predictive of melanoma prognosis. GEPIA analysis revealed a landscape of thirty-three different types of cancers influenced by eIF6 (**Figure 2A**). Among the different types of cancer, high-eIF6 expressed patients had significantly lower survival rates than low-eIF6 expressed patients in SKCM, LGG, LIHC, LUAD, and PAAD. Subsequently, we intensively studied the survival rate of melanoma under different cut-off values (**Figure 2B**). Typically, the prognosis of the high-eIF6 expressed group was significantly poorer than that of the low-eIF6 expressed group. This was because cancer cells proliferate at a high rate, the protein translation requests were also upregulated. However, because eIF6 is a rate-limiting translation regulator, we hypothesized that elevated eIF6 levels aided cancer progression and thus resulted in a worse prognosis by limitation the protein synthesis. The *in vitro* experiments proved that eIF6 over-expressed A375 melanoma cells had a faster proliferation and migration rate (**Figures 3**, **4**). Indeed, a similar phenomenon has been previously observed in another melanoma cell line of WM793 (20). Therefore, it is reasonable to conclude that eIF6 is a critical regulator of tumor growth. Additionally, this hypothesis has also been proven because eIF6 knock-down could efficiently inhibit the progression of hepatocellular carcinoma and non-small cell lung carcinoma (21, 24). Since it has been reported that eIF6 is essential for immune system homeostasis in both mice and humans, we also investigated the tumor immunology of eIF6. Unexpectedly, all the results showed that no significant evidence suggested eIF6 could promote immune infiltration *via* immune modulation (**Figure S6–S10**) (39).

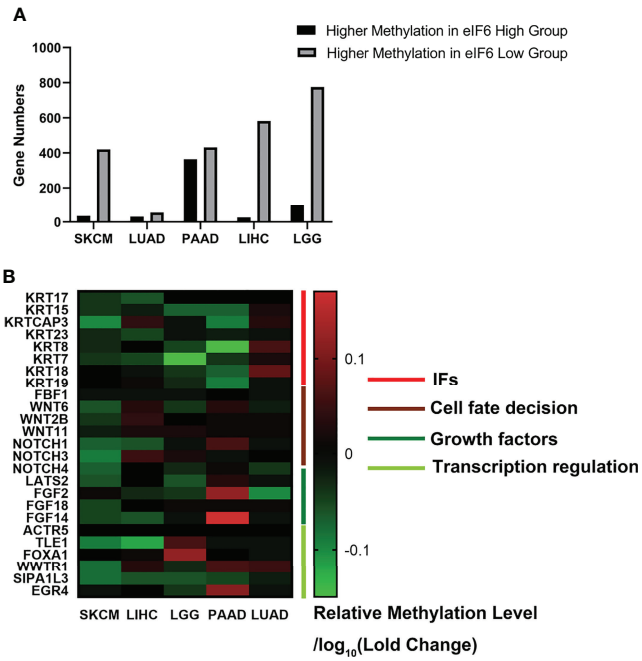

FIGURE 6 | Genome methylation analysis in pan-cancer. **(A)** Comparison of the differentially methylated genes between high-eIF6 and low-eIF6 groups. In all the five cancers analyzed, the low-eIF6 groups had more genes with higher methylation levels than the high-eIF6 groups. **(B)** Heat map of differential methylated genes. The heat map was drawn according to the genes relative methylation level of the eIF6-high group compared to the eIF6-low groups. The demethylated genes were labeled with green. Upregulated keratins were identified as demethylated genes, including KRT17, KRT15, KRT23, and KRT7. Genes functioned in cell fate decisions, and cell growth was also found demethylated.

Besides acting as a nucleolus ribosomal genesis regulator, eIF6 can also regulate specific gene expression (40). We clustered the differential expression genes between high-eIF6 and low-eIF6 patients and found a co-expressive relationship between eIF6 and ribosomal proteins in SKCM, LIHC, LUAD, LGG, and PAAD (**Figure 5**). Since an abrogation of eIF6 hindered ribosomal 60S subunit biogenesis, the ribosomal proteins up-regulation also suggested that there may be a feedback loop involved in the regulation. In cancer cells, the higher ribosomal proteins expression and their corresponding protein translation may account for the lower survival rate of patients. In SKCM, LUAD, and PAAD clustering analysis, we found an up-regulation of keratin proteins in the high-eIF6 expression group (**Figure 5**). All the up-regulated keratins were correlated with the poor survival rate of patients (Hazard Ratio > 1; **Table 1**), which was consistent with the result of eIF6. In general, intermediate filaments (IFs), microtubes and microfilaments make up the cytoskeleton system of animal cells, in which, Keratin proteins are among the main components of IFs. There have been strong evidence indicating that the down-regulation or over-expression of IFs proteins can regulate various cellular behaviors, such as division, migration, growth, and apoptosis (41, 42). In this respect, eIF6 can selectively bind to IFs in mammalian cells, although the biological function of such complexes is not yet been determined, there is some evidence that the complexes formed by eIF6 and IFs are highly regulated during the oogenesis of Xenopus, suggesting they are probably contributing to the early development of embryo, which cells possessed the common feature of continuous mitosis with cancer cells (43). In order to understand this regulation mechanism better, a more detailed analysis is required in further studies. Nevertheless, as shown in **Table 1**, the high expression level of keratins show a dynamic assembly of IFs, contributing to cancer progression and metastasis, eventually leading to a lower patient survival rate.

Despite the detailed mechanisms of eIF6 that regulate keratins transcription remains unclear, eIF6 is commonly regarded as a vital translation regulator. It was reported that eIF6 could bind with chromosome DNA in the mitosis metaphase, which suggested that there may exist an unidentified mechanism that eIF6 directly regulates transcription (44). Herein we proposed a new concept that eIF6 may also regulate DNA methylation. We compared the number of genes whose methylation levels differed between the high-eIF6 and low-eIF6 groups (**Figure 6**). More higher-methylated genes were observed in the low-eIF6 group than that high-eIF6 group in all five types of cancers, suggesting eIF6 is an effective de-methylation regulator. With the up-regulated eIF6 levels, the lesser methylated whole genomes were well-matched with a more active genome transcription and more dynamic cellular activities, proliferation, and migration. In our

TABLE 2 | The list of lesser methylated keratin proteins.

	Gene symble	Cytoband	p-Value	q-Value
SKCM				
	KRTAP19-1	21q22.11	0.0184	0.17
	KRT17	17q21.2	0.0212	0.18
	KRT15	17q21.2	0.0921	0.355
	KRT6B	12q13.13	0.138	0.431
LUAD				
	KRT16	17q21.2	0.0232	0.55
	KRT6B	12q13.13	0.244	0.823
PAAD				
	KRT8	12q13.13	1.93E-04	0.0181
	KRT18	12q13.13	1.40E-03	0.0408
	KRT19	17q21.2	3.01E-03	0.056
	KRT15	17q21.2	5.14E-03	0.0706
LGG				
	KRT7	12q13.13	9.98E-03	0.101

*The methylation levels of the differentially expressed genes listed in **Table 1** were analyzed. A set of keratin genes was lesser methylated in the high-eIF6 group. The lower methylation level of keratins corresponded to their higher expression level in the high-eIF6 group.*

study, the keratin genes up-regulated in high-eIF6 patients had a decreased methylation level (**Table 2**). We conclude that the IFs keratins are the downstream effectors of IF6, and the up-regulation of eIF6 causes a poor melanoma survival rate of patients by de-methylating and activating of keratin genes.

CONCLUSIONS

In summary, the up-regulated eIF6 could be a potential diagnostic and prognostic biomarker indicating poor survival of melanoma. We investigated the survival rate of 33 common types of cancers and found that the up-regulation of eIF6 was generally accompanied lower-survival rate. It is possible that eIF6 acts as a rate-limiting factor that induces higher dynamic cell skeleton gene expression and promotes the proliferation and migration of melanoma, which relates to a poorer prognosis. Herein we proposed that eIF6 is a promising biomarker to improve the assessment of clinical melanoma since the early clinical manifestations of melanoma often look like nevi. Considering the tremendous clinical value of eIF6, we believe that future medical applications will benefit patients.

DATA AVAILABILITY STATEMENT

The datasets presented in this study can be found in online repositories. The names of the repository/repositories and accession number(s) can be found in the article/**Supplementary Material**.

ETHICS STATEMENT

The studies involving human participants were reviewed and approved by the Ethical Committee of the First Affiliated Hospital of Shenzhen University on 20210618. The ethical code is 20210615008. Written informed consent for participation was not required for this study in accordance with the national legislation and the institutional requirements.

AUTHOR CONTRIBUTIONS

FZ executed the experiments and analyzed the data. FZ and JW conceived the project design. FZ, SW, UA, and ZL co-wrote the manuscript. CZ, ZL, and JW supervised the work. All authors contributed to the discussion of results and commented on the final manuscript.

FUNDING

This research was supported by National Natural Science Foundation of China (82172214), Guangdong Basic and Applied Basic Research Foundation (2020A1515010613, 2021A1515220176), The Key Basic Research Project of Shenzhen Science and Technology Program (JCYJ20200109115635440), Retired Expert Program of Guangdong Province (202020031911500002). Shenzhen-Hong Kong-Macau Technology Research Programme (Type C: SGDX2020110309300301).

SUPPLEMENTARY MATERIAL

The Supplementary Material for this article can be found online at: https://www.frontiersin.org/articles/10.3389/fonc.2022.848346/full#supplementary-material

REFERENCES

1. Cockerell CJ. The Pathology of Melanoma. *Dermatol Clin* (2012) 30(3):445–68. doi: 10.1016/j.det.2012.04.007
2. Ahmed B, Qadir MI, Ghafoor S. Malignant Melanoma: Skin Cancer-Diagnosis, Prevention, and Treatment. *Crit Rev Eukaryot Gene Expr* (2020) 30(4):291–97. doi: 10.1615/CritRevEukaryotGeneExpr.2020028454
3. Slominski A, Wortsman J, Carlson AJ, Matsuoka LY, Balch CM, Mihm MC. Malignant Melanoma. *Arch Pathol Lab Med* (2001) 125(10):1295–306 doi: 10.5858/2001-125-1295-MM
4. Davis LE, Shalin SC, Tackett AJ. Current State of Melanoma Diagnosis and Treatment. *Cancer Biol Ther* (2019) 20(11):1366–79. doi: 10.1080/15384047.2019.1640032
5. Muthusamy V, Premi S, Soper C, Platt J, Bosenberg M. The Hematopoietic Stem Cell Regulatory Gene Latexin has Tumor-Suppressive Properties in Malignant Melanoma. *J Invest Dermatol* (2013) 133(7):1827–33. doi: 10.1038/jid.2013.48
6. Divito SJ, Ferris LK. Advances and Short Comings in the Early Diagnosis of Melanoma. *Melanoma Res* (2010) 20(6):450–8. doi: 10.1097/CMR.0b013e32833faf7e
7. Seigler HF. Investigative Studies in the Diagnosis and Treatment of Melanoma. *Invest Radiol* (1986) 21(7):596–600. doi: 10.1097/00004424-198607000-00017
8. Maeda K, Jimbow K. Development of MoAb HMSA-2 for Melanosomes of Human Melanoma and its Application to Immunohistopathologic Diagnosis of Neoplastic Melanocytes. *Cancer* (1987) 59(3):415–23. doi: 10.1002/1097-0142(19870201)59:3<415::aid-cncr2820590311>3.0.co;2-k
9. MacKie RM. Diagnosis, Detection, and Staging of Cutaneous Malignant Melanoma. *Curr Opin Oncol* (1990) 2(2):394–6. doi: 10.1097/00001622-199004000-00024
10. Kooper-Johnson S, Mahalingam M, Loo DS. SOX-10 and S100 Negative Desmoplastic Melanoma: Apropos a Diagnostically Challenging Case. *Am J Dermatopathol* (2020) 42(9):697–99. doi: 10.1097/DAD.0000000000001626
11. Lim E, Browning J, MacGregor D, Davis ID, Cebon JS. Desmoplastic Melanoma: Comparison of Expression of Differentiation Antigens and Cancer Testis Antigens. *Melanoma Res* (2006) 16(4):347–55. doi: 10.1097/01.cmr.0000222588.22493.3f
12. Topisirovic I, Sonenberg N. Translation and Cancer. *Biochim Biophys Acta* (2015) 1849(7):751–2. doi: 10.1016/j.bbagrm.2015.05.004
13. Smith RCL, Kanellos G, Vlahov N, Alexandrou C, Willis AE, Knight JRP, et al. Translation Initiation in Cancer at a Glance. *J Cell Sci* (2021) 134(1):jcs248476. doi: 10.1242/jcs.248476
14. Bhat M, Robichaud N, Hulea L, Sonenberg N, Pelletier J, Topisirovic I. Targeting the Translation Machinery in Cancer. *Nat Rev Drug Discovery* (2015) 14(4):261–78. doi: 10.1038/nrd4505
15. Li Q, Xiao M, Shi Y, Hu J, Bi T, Wang C, et al. Eif5b Regulates the Expression of PD-L1 in Prostate Cancer Cells by Interacting With Wig1. *BMC Cancer* (2021) 21(1):1022. doi: 10.1186/s12885-021-08749-w
16. Iwao Y, Okamoto Y, Shirahama H, Tsukahara S, Tomida A. Eif4b Enhances ATF4 Expression and Contributes to Cellular Adaptation to Asparagine Limitation in BRAF-Mutated A375 Melanoma. *Biochem Biophys Res Commun* (2021) 573:93–9. doi: 10.1016/j.bbrc.2021.08.022
17. Chendrimada TP, Finn KJ, Ji X, Baillat D, Gregory RI, Liebhaber SA, et al. MicroRNA Silencing Through RISC Recruitment of Eif6. *Nature* (2007) 447(7146):823–8. doi: 10.1038/nature05841
18. Gandin V, Miluzio A, Barbieri AM, Beugnet A, Kiyokawa H, Marchisio PC, et al. Eukaryotic Initiation Factor 6 is Rate-Limiting in Translation, Growth and Transformation. *Nature* (2008) 455(7213):684–8. doi: 10.1038/nature07267
19. Miluzio A, Beugnet A, Grosso S, Brina D, Mancino M, Campaner S, et al. Impairment of Cytoplasmic Eif6 Activity Restricts Lymphomagenesis and Tumor Progression Without Affecting Normal Growth. *Cancer Cell* (2011) 19(6):765–75. doi: 10.1016/j.ccr.2011.04.018
20. Pinzaglia M, Montaldo C, Polinari D, Simone M, La Teana A, Tripodi M, et al. EIF6 Over-Expression Increases the Motility and Invasiveness of Cancer Cells by Modulating the Expression of a Critical Subset of Membrane-Bound Proteins. *BMC Cancer* (2015) 15:131. doi: 10.1186/s12885-015-1106-3
21. Sun L, Liu S, Wang X, Zheng X, Chen Y, Shen H. Eif6 Promotes the Malignant Progression of Human Hepatocellular Carcinoma via the mTOR Signaling Pathway. *J Transl Med* (2021) 19(1):216. doi: 10.1186/s12967-021-02877-4
22. Miluzio A, Oliveto S, Pesce E, Mutti L, Murer B, Grosso S, et al. Expression and Activity of Eif6 Trigger Malignant Pleural Mesothelioma Growth In Vivo. *Oncotarget* (2015) 6(35):37471–85. doi: 10.18632/oncotarget.5462
23. Lin J, Yu X, Xie L, Wang P, Li T, Xiao Y, et al. Eif6 Promotes Colorectal Cancer Proliferation and Invasion by Regulating AKT-Related Signaling Pathways. *J BioMed Nanotechnol* (2019) 15(7):1556–67. doi: 10.1166/jbn.2019.2792
24. Gantenbein N, Bernhart E, Anders I, Golob-Schwarzl N, Krassnig S, Wodlej C, et al. Influence of Eukaryotic Translation Initiation Factor 6 on non-Small Cell Lung Cancer Development and Progression. *Eur J Cancer* (2018) 101:165–80. doi: 10.1016/j.ejca.2018.07.001
25. Tang Z, Li C, Kang B, Gao G, Li C, Zhang Z. GEPIA: A Web Server for Cancer and Normal Gene Expression Profiling and Interactive Analyses. *Nucleic Acids Res* (2017) 45(W1):W98–W102. doi: 10.1093/nar/gkx247
26. Cerami E, Gao J, Dogrusoz U, Gross BE, Sumer SO, Aksoy BA, et al. The Cbio Cancer GenomicsPortal:AnOpenPlatformforExploringMultidimensionalCancerGenomics Data. *Cancer Discovery* (2012) 2(5):401–4. doi: 10.1158/2159-8290.CD-12-0095
27. Jiao X, Sherman BT, Huang da W, Stephens R, Baseler MW, Lane HC, et al. DAVID-WS: A Stateful Web Service to Facilitate Gene/Protein List Analysis. *Bioinformatics* (2012) 28(13):1805–6. doi: 10.1093/bioinformatics/bts251
28. Szklarczyk D, Gable AL, Nastou KC, Lyon D, Kirsch R, Pyysalo S, et al. The STRING Database in 2021: Customizable Protein-Protein Networks, and Functional Characterization of User-Uploaded Gene/Measurement Sets. *Nucleic Acids Res* (2021) 49(D1):D605–D612. doi: 10.1093/nar/gkaa1074
29. Zuo H, Song G, Shi W, Jia J, Zhang Y. Observation of Viable Alloskin vs Xenoskin Grafted Onto Subcutaneous Tissue Wounds After Tangential Excision in Massive Burns. *Burns Trauma* (2016) 4:23. doi: 10.1186/s41038-016-0045-9
30. Rodriguez LG, Wu X, Guan JL. Wound-Healing Assay. *Methods Mol Biol* (2005) 294:23–9. doi: 10.1385/1-59259-860-9:023
31. Hu H, Xu DH, Huang XX, Zhu CC, Xu J, Zhang ZZ, et al. Keratin17 Promotes Tumor Growth and is Associated With Poor Prognosis in Gastric Cancer. *J Cancer* (2018) 9(2):346–57. doi: 10.7150/jca.19838
32. Li D, Ni XF, Tang H, Zhang J, Zheng C, Lin J, et al. KRT17 Functions as a Tumor Promoter and Regulates Proliferation, Migration and Invasion in Pancreatic Cancer *via* mTOR/S6k1 Pathway. *Cancer Manag Res* (2020) 12:2087–95. doi: 10.2147/CMAR.S243129
33. Ehebauer M, Hayward P, Arias AM. Notch, a Universal Arbiter of Cell Fate Decisions. *Science* (2006) 314(5804):1414–5. doi: 10.1126/science.1134042
34. Rosenwald IB, Wang S, Savas L, Woda B, Pullman J. Expression of Translation Initiation Factor eIF-2alpha is Increased in Benign and Malignant Melanocytic and Colonic Epithelial Neoplasms. *Cancer* (2003) 98(5):1080–8. doi: 10.1002/cncr.11619
35. Prabhu SA, Moussa O, Miller WHJr, Del Rincón SV. The MNK1/2-Eif4e Axis as a Potential Therapeutic Target in Melanoma. *Int J Mol Sci* (2020) 21(11):4055. doi: 10.3390/ijms21114055
36. Donadini A, Giacopelli F, Ravazzolo R, Gandin V, Marchisio PC, Biffo S. GABP Complex Regulates Transcription of Eif6 (P27bbp), an Essential Trans-Acting Factor in Ribosome Biogenesis. *FEBS Lett* (2006) 580(8):1983–7. doi: 10.1016/j.febslet.2006.02.068
37. Rosmarin AG, Resendes KK, Yang Z, McMillan JN, Fleming SL. GA-Binding Protein Transcription Factor: A Review of GABP as an Integrator of Intracellular Signaling and Protein-Protein Interactions. *Blood Cells Mol Dis* (2004) 32(1):143–54. doi: 10.1016/j.bcmd.2003.09.005
38. Nuchprayoon I, Simkevich CP, Luo M, Friedman AD, Rosmarin AG. GABP Cooperates With C-Myb and C/EBP to Activate the Neutrophil Elastase Promoter. *Blood* (1997) 89(12):4546–54. doi: 10.1182/blood.V89.12.4546
39. Manfrini N, Ricciardi S, Miluzio A, Fedeli M, Scagliola A, Gallo S, et al. High Levels of Eukaryotic Initiation Factor 6 (Eif6) are Required for Immune System Homeostasis and for Steering the Glycolytic Flux of TCR-Stimulated CD4+ T Cells in Both Mice and Humans. *Dev Comp Immunol* (2017) 77:69–76. doi: 10.1016/j.dci.2017.07.022
40. Brina D, Miluzio A, Ricciardi S, Clarke K, Davidsen PK, Viero G, et al. Eif6 Coordinates Insulin Sensitivity and Lipid Metabolism by Coupling Translation to Transcription. *Nat Commun* (2015) 6:8261. doi: 10.1038/ncomms9261
41. Etienne-Manneville S. Cytoplasmic Intermediate Filaments in Cell Biology. *Annu Rev Cell Dev Biol* (2018) 34:1–28. doi: 10.1146/annurev-cellbio-100617-062534

42. Seetharaman S, Etienne-Manneville S. Cytoskeletal Crosstalk in Cell Migration. *Trends Cell Biol* (2020) 30(9):720–35. doi: 10.1016/j.tcb.2020.06.004
43. Carotenuto R, De Marco N, Biffo S, Wilding M, Vaccaro MC, Marchisio PC, et al. Phosphorylation of P27(BBP)/eIF6 and its Association With the Cytoskeleton are Developmentally Regulated in Xenopus Oogenesis. *Cell Mol Life Sci* (2005) 62(14):1641–52. doi: 10.1007/s00018-005-5153-9
44. Scagliola A, Miluzio A, Ventura G, Oliveto S, Cordiglieri C, Manfrini N, et al. Targeting of Eif6-Driven Translation Induces a Metabolic Rewiring That Reduces NAFLD and the Consequent Evolution to Hepatocellular Carcinoma. *Nat Commun* (2021) 12(1):4878. doi: 10.1038/s41467-021-25195-1

Conflict of Interest: The authors declare that the research was conducted in the absence of any commercial or financial relationships that could be construed as a potential conflict of interest.

frontiers | Frontiers in Oncology

TYPE Original Research
PUBLISHED 02 August 2022
DOI 10.3389/fonc.2022.919118

OPEN ACCESS

EDITED BY
Gagan Chhabra,
University of Wisconsin-Madison,
United States

REVIEWED BY
Takamichi Ito,
Kyushu University, Japan
Shengqin Su,
Shanghai Hengrui Pharmaceutical Co., Ltd., China

*CORRESPONDENCE
Bruce Ashford
bruceash@uow.edu.au

SPECIALTY SECTION
This article was submitted to Skin Cancer, a section of the journal Frontiers in Oncology

RECEIVED 13 April 2022
ACCEPTED 27 June 2022
PUBLISHED 02 August 2022

CITATION
Thind AS, Ashford B, Strbenac D, Mitchell J, Lee J, Mueller SA, Minaei E, Perry JR, Ch'ng S, Iyer NG, Clark JR, Gupta R and Ranson M (2022) Whole genome analysis reveals the genomic complexity in metastatic cutaneous squamous cell carcinoma. *Front. Oncol.* 12:919118. doi: 10.3389/fonc.2022.919118

Whole genome analysis reveals the genomic complexity in metastatic cutaneous squamous cell carcinoma

Amarinder Singh Thind[1,2], Bruce Ashford[1,2,3]*, Dario Strbenac[4], Jenny Mitchell[3], Jenny Lee[5,6], Simon A. Mueller[5,7], Elahe Minaei[2,8], Jay R. Perry[2,8], Sydney Ch'ng[4,5], N. Gopalakrishna Iyer[9,10], Jonathan R. Clark[4,5,11], Ruta Gupta[12] and Marie Ranson[2,8]

[1]School of Medicine, University of Wollongong, Wollongong, NSW, Australia, [2]Illawarra Health and Medical Research Institute, Wollongong, NSW, Australia, [3]Illawarra Shoalhaven Local Health District, Wollongong, NSW, Australia, [4]Sydney Medical School, Faculty of Medicine and Health, The University of Sydney, NSW, Australia, [5]Sydney Head and Neck Cancer Institute, Chris O'Brien Lifehouse, Sydney, NSW, Australia, [6]Department of Clinical Medicine, Macquarie University, Sydney, NSW, Australia, [7]Department of Otorhinolaryngology, Head and Neck Surgery, Zurich University Hospital and University of Zurich, Zurich, Switzerland, [8]School of Chemistry and Molecular Bioscience, University of Wollongong, Wollongong, NSW, Australia, [9]Department of Head and Neck Surgery, National Cancer Center, Singapore, Singapore, [10]Duke-NUS Medical School, Singapore, Singapore, [11]Royal Prince Alfred Institute of Academic Surgery, Sydney Local Health District, Sydney, NSW, Australia, [12]Anatomical Pathology, Royal Prince Alfred Hospital, Sydney, NSW, Australia

Metastatic cutaneous squamous cell carcinoma (CSCC) is a highly morbid disease requiring radical surgery and adjuvant therapy, which is associated with a poor prognosis. Yet, compared to other advanced malignancies, relatively little is known of the genomic landscape of metastatic CSCC. We have previously reported the mutational signatures and mutational patterns of CCCTC-binding factor (CTCF) regions in metastatic CSCC. However, many other genomic components (indel signatures, non-coding drivers, and structural variants) of metastatic CSCC have not been reported. To this end, we performed whole genome sequencing on lymph node metastases and blood DNA from 25 CSCC patients with regional metastases of the head and neck. We designed a multifaceted computational analysis at the whole genome level to provide a more comprehensive perspective of the genomic landscape of metastatic CSCC. In the non-coding genome, 3′ untranslated region (3′UTR) regions of *EVC* (48% of specimens), *PPP1R1A* (48% of specimens), and *ABCA4* (20% of specimens) along with the tumor-suppressing long non-coding RNA (lncRNA) LINC01003 (64% of specimens) were significantly functionally altered (Q-value < 0.05) and represent potential non-coding biomarkers of CSCC. Recurrent copy number loss in the tumor suppressor gene *PTPRD* was observed. Gene amplification was much less frequent, and few genes were

recurrently amplified. Single nucleotide variants driver analyses from three tools confirmed *TP53* and *CDKN2A* as recurrently mutated genes but also identified *C9* as a potential novel driver in this disease. Furthermore, indel signature analysis highlighted the dominance of ID signature 13 (ID13) followed by ID8 and ID9. ID9 has previously been shown to have no association with skin melanoma, unlike ID13 and ID8, suggesting a novel pattern of indel variation in metastatic CSCC. The enrichment analysis of various genetically altered candidates shows enrichment of "TGF-beta regulation of extracellular matrix" and "cell cycle G1 to S check points." These enriched terms are associated with genetic instability, cell proliferation, and migration as mechanisms of genomic drivers of metastatic CSCC.

KEYWORDS

CSCC, cutaneous, squamous cell carcinoma, metastases, UTR - Untranslated regions, noncoding, mutations, whole genome sequencing

Introduction

Cutaneous squamous cell carcinoma (CSCC) is the second most common malignancy, after basal cell carcinoma (BCC), affecting up to 1,000,000 people in the United States annually (1). In time, and as a result of the aging population and changing ratios of BCC/CSCC, the mortality rate of CSCC is likely to exceed that of melanoma (2). Although primary CSCC is common, metastasis only occurs in 2%–5% of CSCC (3–5). CSCCs arising in the head and neck generally show a predictable pattern of spread, predominantly metastasizing to the intraparotid, level II (upper jugular), and perifacial lymph nodes (4). CSCCs that have metastasized to regional lymph nodes are associated with a worse prognosis (6), with modest progress made in the management of regionally advanced disease over the last 15 years. Most patients with regional metastases from CSCC of the head and neck are managed with a multimodality approach, which usually involves surgery (parotidectomy and neck dissection) and adjuvant external beam radiotherapy depending on the site and stage at the time of diagnosis (7–9). More recently immunotherapy has attracted great interest as a potential alternative for unresectable or distant metastatic disease (10, 11).

Despite the very high incidence, relatively little is known regarding the genomic landscape of metastatic CSCC. We have previously described the genomic mutational burden, mutational signatures, and mutations in CCCTC-binding factor regions using whole genome sequencing (WGS) data from 15 CSCC metastases (12) and associated cell lines (13). However, the majority of studies to date has reported on somatic variation in primary CSCC (14–17) and/or CSCC metastases (17–21), using whole exome sequencing (WES) and/or targeted next generation sequencing, which by definition focuses on the coding genome. Thus, the extent of analysis of non-coding (including regulatory) regions of the genome is limited and varies across studies. Pickering et al. (21), the only study employing WES and incorporating 32 primary and only seven metastatic samples, did not include regulatory or non-exome regions analysis. Both Li et al. (19) [29 lymph node metastatic formalin fixed paraffin embedded (FFPE) samples] and Zehir et al. (18) (MSK-IMPACT) (28 primary and 27 metastatic FFPE samples) used targeted next-generation sequencing (NGS), with limited non-coding analysis. Zehir et al. (18) specifically included the *TERT* promoter in their targeted panels but otherwise included no regulatory elements. Li et al. (19) similarly did not include regulatory or non-coding variant analysis. Yilmaz et al. (17) performed WES and/or targeted NGS on 18 metastatic and 10 primary FFPE CSCC samples and reported coding gene drivers based purely on mutational frequencies, without adjusting for gene length or covariates. Additional functional driver predictions analysis would be required to confidently call genes as drivers (22). Furthermore, FFPE processing has well-known impacts on the quality of DNA for sequencing analyses (23), and it is important to note that for most of the metastatic studies, FFPE samples were collected. Furthermore, none of these studies addressed variation in either 5′ or 3′ untranslated regions (UTRs) or other non-coding elements such as promoters (other than *TERT* promoter) or long non-coding RNAs (lncRNAs). Sequence variants occurring within these functional non-coding elements are important, as they have the potential to alter gene expression. For example, lncRNAs are thought to influence the expression of proteins by pre- and post-translational influences on DNA/RNA and proteins, chromatin function, miRNA activity, and signaling pathways by an array of mechanisms (24, 25). 3′UTRs regulate

crucial aspects of post-transcriptional gene regulation (26). Mutations in these regions can deregulate gene expression by disrupting miRNA–mRNA interactions, in which both tumor suppressor genes and oncogenes can drive cancer progression (27, 28). This variation in the so-called *cis-elements* can also impact gene expression by altering translation initiation in cancer (29).

Given the shortcomings associated with WES and NGS analyses of complex genomes, in the current report we have performed WGS on 25 metastatic CSCC samples and applied a detailed, multifaceted computational analysis at the whole genome level to provide a comprehensive understanding of the genomic landscape of metastatic CSCC. This included processing of WGS data for somatic variations in both coding and non-coding regions and indel signatures, apart from structural variants and copy number alterations analyses. For non-coding genomic regions, we have focused on UTRs, lncRNA, and promoter regions, as these represent non-coding regions that are most accessible to interrogation in high mutational burden tumors using currently available tools.

Materials and methods

Study population, sample collection, and processing

This study was undertaken with Institutional Human Research Ethics approval (UOW/ISLHD HREC14/397). Thirty-two patients with resectable metastatic CSCC were identified by the treating surgeons preoperatively. Clinicopathological data including age, sex, extent of nodal metastases, histology, and immunosuppression status were collected. In addition to whole blood (for germline DNA), sections of fresh tumor from nodal metastases were collected during surgery and immediately snap frozen. These sections were used for DNA extraction (Qiagen AllPrep, Qiagen, Hilden, Germany) and for cellularity estimates. Only samples with >30% tumor (range, 35%–95%) proceeded to DNA quality control (QC). QC comprised spectrophotometry (Nanodrop 2000 Thermo Fisher Scientific Inc.), gel electrophoresis, and single nucleotide polymorphism (SNP) array. Of the 32 samples sequenced, 25 passed QC (96% from men) (Table 1). The remaining seven samples had insufficient clonal tumor content [median variant reads ≤ 5 or median variant allele frequency (VAF) < 0.1] or had an extreme GC bias as determined by PURity and PLoidy Estimator (PURPLE) (30). Briefly, if more than 220 copy number segments were unsupported by a corresponding structural variants at either end, the sample was flagged as fail-segment. The mean sequencing coverage of the 25 samples was 94.56× (range, 64–143) for tumor and 41.08× (range, 30–56) for blood.

Variant calling and functional significance of SNVs and indels

FASTQ reads were aligned to reference genome GRChr38 using BWA-kit version 0.7.17 (BWA-MEM read aligner) (for details, refer to https://github.com/Sydney-Informatics-Hub/Fastq-to-BAM). The Genome Analysis Tool Kit (GATK) 4.1.2.0 and its BaseRecalibrator tool was used to refine the read alignment. SNPs and insertion–deletion (indel) variants were called by implementing GATK's Best Practices Workflow. These pipelines use HaplotypeCaller for germline short variant discovery and Mutech2 caller for somatic short variant discovery for SNVs and indels (for details, refer to https://github.com/Sydney-Informatics-Hub/Somatic-ShortV). Furthermore, variants effect prediction and annotations were completed using OpenCravat platform (31). Mutation Annotation Format (MAF) files were generated based on variant effect predictor annotations. Three different methods for driver discovery were then used; OncodriveFML (32), MutSigCV (22), and dNdScv (33).

OncodriveFML predicts the functional significance of both coding and non-coding variants, as it is one of the few tools designed for non-coding genomic analysis (32). It first determines the functional impact of the observed somatic mutations using Combined Annotation Dependent Depletion (CADD) for specified genomic elements (UTR, promotor, and coding regions) across the cohort. Later, for the statistical significance, it compares the average functional impact score of the observed mutations in the element with the average functional impact scores of a similar number of the random mutational set. The CADD score provides a priority for identifying mutations with functional, deleterious, and pathogenic impacts. These scores are calculated by combining the information from multiple annotations into a single metric.

MutSigCV identifies genes that are mutated more often than expected by chance and reduces the number of false positives in the generated list of significant genes, which is especially useful for tumors, such as metastatic CSCC, with high mutation rates (22). This is achieved by incorporating various types of information such as patient-specific mutation frequencies and mutation spectra, gene-specific mutation rates, expression levels, and replication times.

dNdScv is designed to test for positive and negative selection in cancer genomes (33). As UV-induced cancer genomes such as CSCC can affect the accuracy of the dNdScv model, we carefully monitored the annotation of CC>TT changes (sometimes reported as C>T changes). Results report significance for missense and truncating mutations and indels as global p-values. Genes that were falsely flagged as significant with negative selection were not considered for this analysis.

For downstream analysis, genes that were predicted to be driver genes by at least two of these tools were considered. First,

10.3389/fonc.2022.919118

TABLE 1 Clinicopathological data of the cohort of 25 patients with CSCC lymph node metastases.

Sample	Age (years)	Sex	Primary location	Metastasis location	Nodal stage[1]	Lymph node ratio[2]	Extracapsular spread	Grade[3]	Immuno-suppressive treatment
CSCC_0001	30	male	left lip	left neck	N3b	3/27	yes	1	no
CSCC_0002	78	male	right ear	right parotid	N3b	2/52	yes	3	no
CSCC_0003	74	male	unknown	right parotid	N3b	2/42	yes	3	no
CSCC_0004	64	male	bilateral lip	bilateral neck	N2c	3/55	no	2	no
CSCC_0005	78	male	left forehead	left parotid	N2a	4/4	Not stated	3	no
CSCC_0006	69	male	left cheek	left neck	N3b	2/42	yes	3	azathioprine
CSCC_0007	87	male	unknown	left neck	N2b	1/16	no	3	no
CSCC_0009	66	male	bilateral forehead	right neck	N3b	3/109	yes	2	cyclosporine A, tacrolimus
CSCC_0010	64	male	left scalp	left neck	N3b	2/11	yes	3	no
CSCC_0011	69	male	unknown	right parotid	N3b	3/108	yes	3	no
CSCC_0012	77	male	right nose	right neck	N3b	4/64	yes	2	no
CSCC_0013	77	male	right pinna	right parotid	N3b	1/1	yes	2	no
CSCC_0014	79	female	left cheek	left perifacial	N3b	1/1	yes	3	no
CSCC_0022	66	male	scalp	left neck	N3b	3/24	yes	3	no
CSCC_0024	54	male	lip	right neck	N3b	3/32	yes	2	no
CSCC_0025	82	male	parotid	Parotid	N1	1/15	no	3	no
CSCC_0066	56	male	Unknown	Parotid	N1	1/1	no	3	no
CSCC_0124	80	male	Parotid	Parotid	N3b	1/6	yes	Not stated	no
CSCC_0125	43	male	parotid	parotid	N3b	1/20	not stated	not stated	no
CSCC_0126	66	male	left temple	left neck	N3b	3/8	yes	3	no
CSCC_0130	70	male	unknown	left parotid	N3b	1/6	yes	3	no
CSCC_0132	76	male	right ear	parotid/neck	N2b	23/43	no	3	no
CSCC_0133	75	male	unknown	parotid	N3b	1/4	yes	not stated	no
CSCC_0134	71	male	unknown	right neck	N3b	9/17	yes	not stated	no
CSCC_0135	82	male	unknown	right neck	3b	1/48	yes	3	no

[1]Staging according to AJCC 8th edition.
[2]Lymph node ratio (Number of positive nodes/total nodes harvested).
[3]Grade 1: well differentiated; Grade 2: moderately differentiated; Grade 3: poorly differentiated.

genes with significant p-values <0.005 were filtered from each of the three tools, and shared genes were determined using a Venn diagram. We then compared the functional impact of SNVs in these selected driver genes to previously reported primary and metastatic CSCC data (18, 19, 21, 34) available on cBioportal (35). This included 92 samples of metastatic CSCC (WES= 10, targeted NGS = 82) and 88 samples of primary CSCC (WES=32, targeted NGS=56).

Copy number variation

Copy number alterations in the 25 metastatic genomes were derived using PURPLE (30), which estimates copy number and purity of tumor sample by using read depth ratio from COBALT and tumor B-allele frequency (BAF) from AMBER. The pipeline is available at github of HMF Tools (https://github.com/hartwigmedical/hmftools). Driver genes with significant amplifications and deletions were then identified using PURPLE driver copy number outputs. For driver genes, PURPLE searches for genes with high level amplification (minimum exonic copy number > 3 * sample ploidy) and deletion (minimum exonic copy number < 0.5) and then uses iteration to establish the most significant focal peaks.

GRIDSS2 and its companion interpreter tool LINX were employed for somatic structural variant analysis and gene fusion (36). COSMIC3-based SNVs and indels signatures from the whole genome were built using MutationalPatterns (37) software.

The driver gene candidates obtained from various genetic alteration analyses such as copy number variation drivers, somatic variant drivers, and other non-coding drivers were combined for enrichment analysis. In the case of copy number

gain/loss, we selected only those genes affected in >20% of the samples in our cohort. Using the Enrichr web application (38), we determined the involvement of the candidate driver genes in various cellular components of the cells, biological pathways, and predicted miRNA and drug targets.

Results

Patient characteristics and clinicopathological data

Twenty-five metastatic CSCC samples from lymph nodes in the head and neck region were collected between 2015 and 2019 that passed WGS QC criteria for analysis (Table 1). The median age of patients was 69 (range, 30–87), and 24/25 (96%) were male. While this sex disparity is a limitation of our study in that potential sex differences may have been missed, it is in keeping with the disease burden seen in our practice in NSW, Australia, particularly for advanced and metastatic CSCC (39). This is in keeping with findings that age, male sex, and immunosuppression are among the risk factors for metastasis (40). Two patients were immunocompromised; one patient was on long-term azathioprine for rheumatoid arthritis, and the other was on a combination of cyclophosphamide and tacrolimus following solid organ transplantation.

The location of the index primary lesion was known in 11 patients (Table 1). Nodal metastases were isolated from the neck in 13 patients and in the parotid in 12 patients. The majority of patients had either moderately differentiated (n = 8) or poorly differentiated (n = 12) CSCC, with evidence of extranodal extension found in 20/25 (80%) nodal samples.

Tumor mutational burden

Based on whole genome level calculations, the average tumor mutational burden (TMB) for SNVs and indels across the 25 cases was 238.7 mutations per megabase (median, 166.99 mutations/Mb; range, 32.52–995.66 mutations/Mb) and 2.25 indel/megabase (range, 0.63–5.9 mutations/Mb), respectively (Figures 1A, B; Supplementary Table S1) with the majority of somatic variants occurring in the non-coding regions as expected (12). The only female tumor in this cohort had the second highest TMB at 499 mutations/Mb. There was no correlation between age, differentiation, nodal stage, or extracapsular spread of the metastasis and TMB.

Mutational signatures

We performed mutational signature analyses of the 25 genomes based on COSMIC V.3.2 (https://cancer.sanger.ac.uk/signatures/). Signatures are designated as single base substitution (SBS) or small insertion and deletion (ID) signatures. SBS signatures 7a and 7b were the most prevalent (Figure 1C; Supplementary Table S2) in keeping with a UV association in metastatic CSCC as we previously reported in a smaller cohort using COSMIC V2 (12). Substantial representation of SBS7c was also seen. SBS32 and SBS7d were observed in one sample. Indel signature analysis showed that ID8, 9, and 13 dominated over others (Figure 1D; Supplementary Table S2).

Short variants

Coding short variants

The overwhelming majority of coding SNVs were missense mutations, followed by nonsense mutation, which represented <5% of variants (Figure 2A). Figure 2B shows various DNA sequence alterations, including single, double, and triple nucleotide variants and insertion and deletion (Supplementary Data 1). Over 80% of SNVs were C>T (Figures 2C, D). This is consistent with the dominant effect of UV radiation on pyrimidine bases and the UV signature referred to above and is independent of the degree of differentiation or any other clinicopathological feature. Genes predicted to be driver genes *via* OncoDriveFML include *TP53*, *CDKN2A*, and *ZNF730* having Q-values <0.1 (Figure 2E). MutSigCV and dNdScv analyses also found *TP53* and *CDKN2A* as the most significant mutated driver genes in our cohort (Supplementary Table S3). Genes that were predicted to be driver genes (p-value < 0.005) by at least two tools were considered for downstream analyses (Figure 2F). This resulted in 12 genes: *TP53*, *CDKN2A*, *C9*, *C9orf131*, *SLC22A6*, *KHDRBS2*, *COLEC12*, *LINGO2*, *CDHR5*, *ZNF442*, *PRLR*, and *DHRS4*. Of this list, *TP53*, *CDKN2A*, and *C9* were shared as significant by all three tools. Interrogation of the cBioPortal dataset for CSCC (metastatic = 92 and primary=88 cases) (18, 19, 21) with short variant analysis (Supplementary Figure S1) revealed recurrent mutations not only in *TP53* and *CDKN2A* but also in *C9*, *COLEC12*, and *SLC22A6*. Not all genes identified as high impact and recurrent variants in our cohort were included in these targeted studies, which underscores the deficiencies of panel-based analyses in discovery projects.

The only sample with no mutation in *TP53* was CSCC_0009 (Figure 2G). The TMB of this sample was 122/Mb or 51% of the average across the cohort. Five samples without *CDKN2A* mutations averaged a TMB of 470/Mb or 201% of the average for the cohort.

Variation in non-coding regulatory regions

The 3′UTRs that potentially play an important role in metastatic CSCC were discovered using OncodriveFML. SNVs within the 3′UTR region of *EVC*, *PPP1R1A*, *ABCA4*, and *LUM* showed significantly higher observed functional impact than the

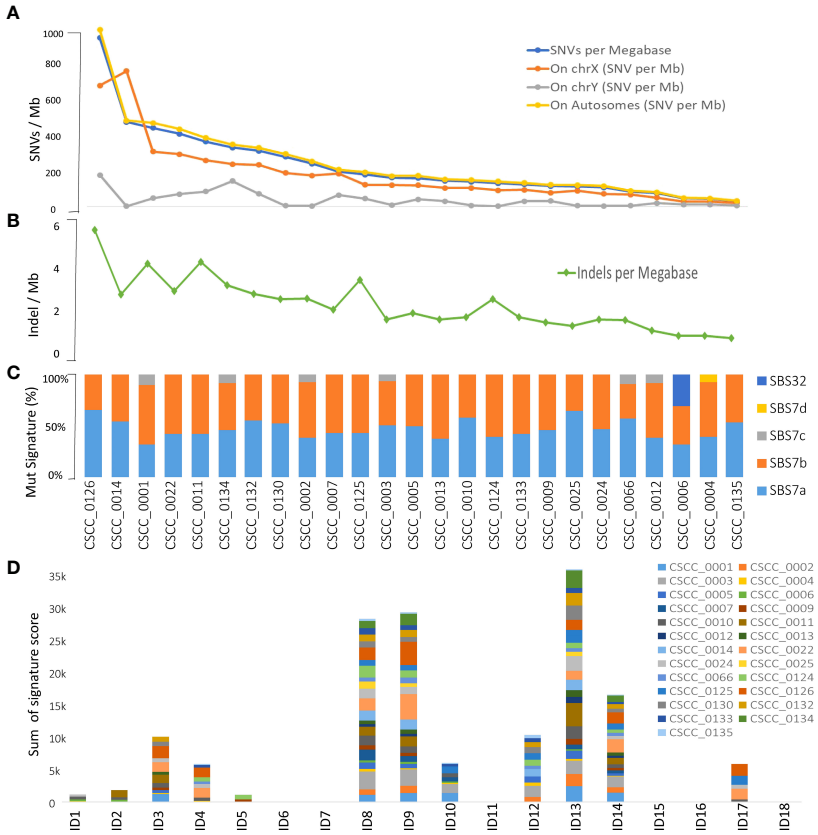

FIGURE 1
Overview of tumor mutational burden and signatures (whole genome-based). Panels **(A, B)** illustrate the indel and SNV mutational burden in each sample, respectively. Panels **(C, D)** show indel (ID) and SNV mutational signatures for each sample, respectively, obtained using COSMIC V3.2 database. Full details are available in Supplementary Table S2.

expected functional impact (Q-value <0.03) (Figure 3A; Supplementary Table S3). We observed variation within the 3′ UTR of both *EVC* and *PPP1R1A* in 48% of samples with a Q-value of 0.011 and 0.022, respectively (Figure 3B; Supplementary Table S4). The unique *PPP1R1A* variant with cDNA change of c.*491C>T [Chr12:54579896 (G to A)] was found in five samples (Supplementary Figure S2).

There are many reported limitations in the analysis and interpretation of 5′UTRs and promoters for high mutational burden tumors (41–43), a finding that we also observed (Supplementary Figure 3). Currently, no robust methodology exists to analyze these regions with confidence in CSCC; thus, analyses of 5′UTRs and promoter regions were not investigated further.

lncRNAs likely to have a potential impact on tumorigenesis were also predicted using OncodriveFML. Four lncRNAs were significantly ($q < 0.05$) biased towards high-impact mutations i.e., *LINC01474* and *LINC01003*, *RP4-597N16.4*, and *RP11-61J19.4* (Figure 3C; Supplementary Table S3). Among these, *LINC01474* and *LINC01003* showed a high statistical significance Q-value of 0.0158. lncRNA *LINC01003* was altered in 64% of the cohort. Another recurrently mutated lncRNA in our cohort was *RP11-61J19.4* (48% of samples) (Figure 3D; Supplementary Table S4).

Structural and copy number variation

The extent of chromosomal copy number gain and loss was averaged across the genome for all 25 tumor samples (Figure 4A; Supplementary Table S5). Chr5p and 8q were the most frequently amplified regions, with 18q being the region with the most recurrent deletion. At sample level (Figure 4B), there were chromosome arm gains in chromosome 7 and 5p in the majority of the samples and losses in 8p, 18q, and 21q. Recurrent gain of 7, 8q, and 5p and loss of 8p, 18, and 21 were also previously reported by Pickering et al. (21). Figure 4B also shows a Circos plot obtained from the PURPLE pipeline for CSCC_0004 as a representative example that summarizes various information at the sample level.

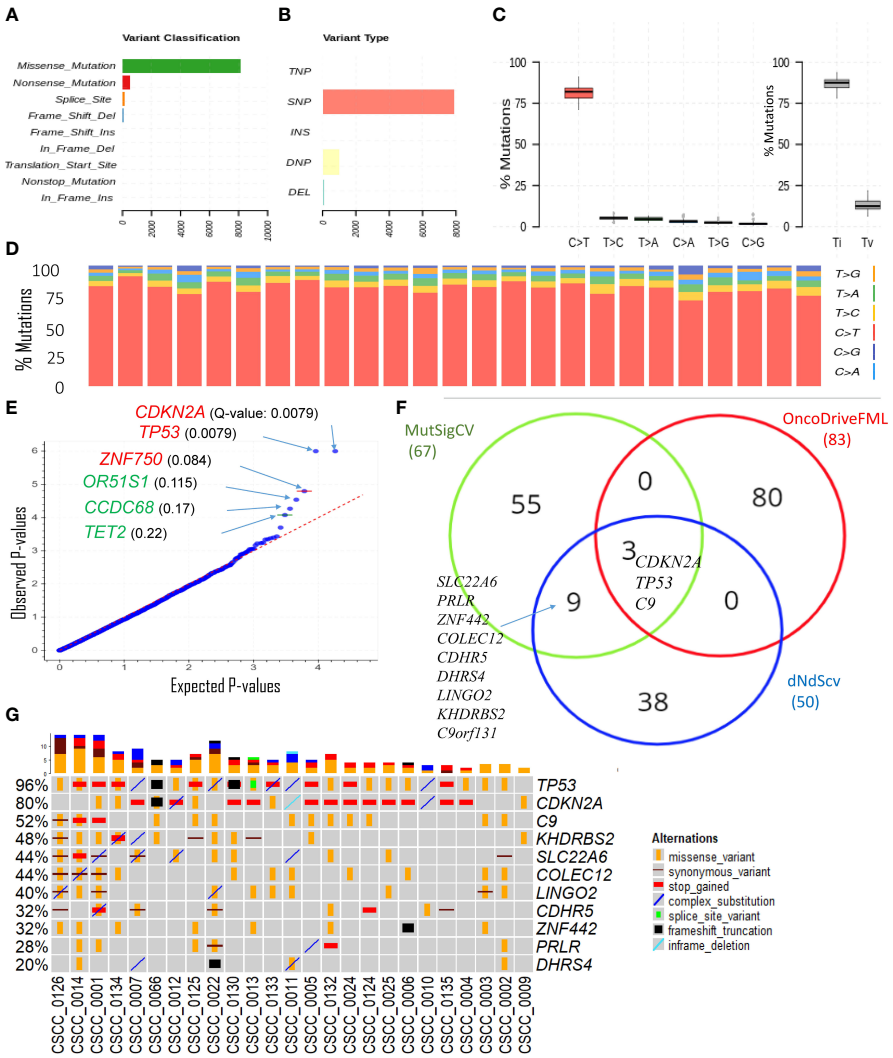

FIGURE 2
Overview of key coding mutations. **(A)** Variants classification, **(B)** variant types, where SNP, DNP, TNP, INS, and DEL are single nucleotide polymorphisms, double nucleotide polymorphisms, triple nucleotide polymorphisms, insertion, and deletion, respectively (**C**, left panel) % of various transitions, (**C**, right panel) Ti (transition) and Tv (transversion) in all 25 samples, and **(D)** % transitions for each sample. **(E)** Driver coding genes prediction results from OncodriveFML tool. The plot shows the most significantly altered genes (in the plots above the red line, Q-values are below 0.1). Q-values are corrected p-values using the Benjamini/Hochberg correction. **(F)** Venn diagram showing the overlap of genes predicted to be driver genes (p-value < 0.005) by three different driver detection tools, i.e., OncoDriveFML, MutSigCV, and dNdScv. (For details, refer to Supplementary Table S3). For further analysis, genes predicted to be driver genes by at least two tools were considered. **(G)** Detailed sample-level information of the SNVs and types of variants in the top altered genes (mentioned in Figure 2).

Structural variation analysis revealed that CSCC metastases are characterized by various complex, deleted, and unbalanced translocation events. Table 2 provides the summary of various structural events observed. Deletion and complex structural variants are common in CSCC; however, unbalanced translocation and other structural events were also observed (Table 2). The detailed effects of these structural events for putative oncogenes and tumor suppressor genes (TSGs) are described in Table 3. Amplification events are linked to complex structural variants. Potential oncogene/TSG driver amplification and deletion were predicted by the PURPLE-GRIDSS-LINX pipeline, as reported in Table 3. Recurrent gene deletions were more common than gene amplifications. The most frequently deleted gene was *PTPRD* (Chr9p, 24% of

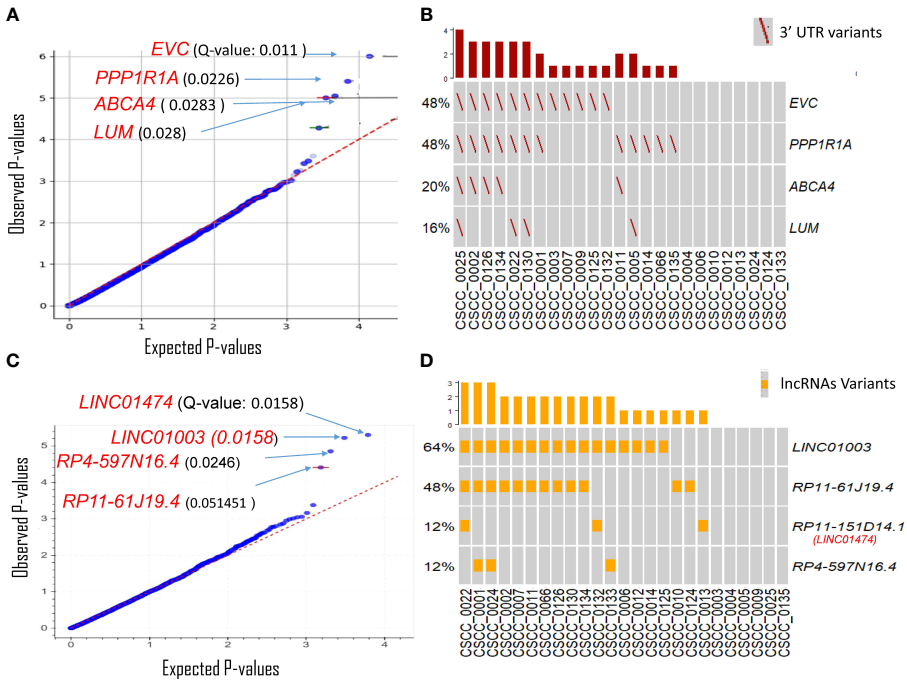

FIGURE 3
Driver genes prediction in non-coding genomic regions. Plots show the result of OncodrivFML (2.2.0) tool and mutations in the most significantly altered non-coding genes or regions in the cohort of 25 patient samples. **(A)** Potential 3′UTR regions associated driver candidates. **(B)** Variants with significantly altered 3′UTR regions. **(C)** Potential lncRNA driver candidates. **(D)** Variants with significantly altered lncRNAs. Plots in panels **(A)** and **(C)** show the frequency of observed mutations with respect to the expected frequency of the mutations in the corresponding regions. Q-values are corrected p-values using the Benjamini/Hochberg correction. The plots in panels **(B, D)** show frequencies of 3′UTR and lncRNAs variants among the cohorts, respectively.

TABLE 2 Summary of various event categories of structural variants.

Sample	SGL	DEL	DUP	Complex	UNBAL_trans	Pair.other	INF
CSCC_0001	*SMAD4*	*SMAD4*					
CSCC_0002		*CDKN2A*					
CSCC_0005			*MYC*	*MYC*			
CSCC_0007				*CRLF2*			
CSCC_0009		*PTPRD*					
CSCC_0011		*PTPRD*		*CALR*	*HEBP2- NTRK2*		
CSCC_0012		*PTPRD*		*EGFR*		*PTPRD*	
CSCC_0013		*APC*					
CSCC_0014		*CREBBP*					*CREBBP*
CSCC_0025		*CDKN2C*			*PARD6G*		
CSCC_0066		*PTPN13*					
CSCC_0124		*NEGR1*				*NEGR1*	
CSCC_0132		*PTPRD*		*RAF1-FGF3-CCND1*			
CSCC_0133	*PTPRD*	*PTPRD*		CALR-chr1-chr3-chr6-chr8-chr22			
CSCC_0134				*MCL1, CCND1-FGF3*-Chr17			
CSCC_0135		*PTPRD*					

For more details, refer to Supplementary Figures S4 and S5. Association can be noted between gain (Table 3) and complex SV events. The gene list was derived using LINX output. Only samples with events are shown in the table.
NBAL_TRANS, unbalanced translocation; INF, inferred breakend; DEL, deletion; DUP, duplication; SGL, single breakend SV support

10.3389/fonc.2022.919118

TABLE 3 List of reportable drivers (likelihood type onco/TSG) genes.

Sample	DEL	GAIN	LOH_CHR	LOH_ARM	LOH	LOH_SV_TELO	LOH_SV_CENTRO
CSCC_0001	*SMAD4*					*SMAD4*	
CSCC_0002	*CDKN2A*						
CSCC_0003	*KDM6A*		*KDM6A*				
CSCC_0005		*MYC*					
CSCC_0007		*CRLF2*					
CSCC_0009	*PTPRD*			*PTPRD*			
CSCC_0011	*PTPRD*	*CALR*		*PTPRD*			
CSCC_0012	*PTPRD*	*EGFR*	*PPP2R3B, PUDP, STS,WWC3*		*PTPRD*		
CSCC_0013	*APC*			*APC*			
CSCC_0014	*CREBBP*					*CREBBP*	
CSCC_0025	*CDKN2C, PARD6G*		*PARD6G*	*CDKN2C*			
CSCC_0066	*PTPN13*		*PTPN13*				
CSCC_0124	*NEGR1*				*NEGR1*		
CSCC_0132	*PTPRD*	*RAF1,CCND1,FGF3*		*PTPRD*			
CSCC_0133	*PTPRD*	*CALR*					*PTPRD*
CSCC_0134		*MCL1,CCND1,FGF3*					
CSCC_0135	*PTPRD*			*PTPRD*			

The types of drivers are as follows: GAIN, amplification by SV; DEL, homozygous deletion; LOH, focal LOH; LOH_ARM, chromosome arm level LOH; LOH_CHR, chromosome level LOH; LOH_SV_TELO, LOH from SV to telomere; LOH_SV_CENTRO, LOH from SV to centromere. Only samples with events are shown in the table.

samples). *PTPRD* deletion is already reported in primary and metastatic CSCC (44, 45). Deletion of *PTPRD* (n=6) and *CDKN2A* (Chr9p) (n=1) did not co-occur in our cohort (Table 3), although *PTPRD* loss and significant mutation of *CDKN2A* co-occurred in six samples (CSCC_9, 11, 12, 133, 132, and 134) (Table 3; Figure 2G). Deep deletion of *CDKN2A* was reported in only 2/92 cases available on cBioPortal (Supplementary Figure S1).

Loss of heterozygosity (LOH) was found at the focal, arm, chromosome, telomere, and centromere levels. The most common LOH events were that at the chromosome and arm level with these events concentrated to *PTPRD* locus (Table 3). No recurrent events for other genes were observed (Table 3). Various examples of *PTPRD* structural events are reported in Supplementary Figure S4. A few other examples of the unbalanced translocation and complex structural variants are shown in Supplementary Figure S5.

The most frequently amplified genes (2/25, 8%) were *CALR*, *CCND1*, and *FGF3* (Table 3). Interestingly, *EGFR* was amplified in only one sample. Amplification of *CCDN1* and *FGF3* co-occurred in two samples (CSCC_0134 and CSCC_0132). *CCDN1* and *FGF3* are next to each other on the chromosome. These two cases had extensive nodal involvement (>50% of lymph nodes harboring tumor).

Despite this widespread genomic instability, only two coding–coding gene fusions were observed in our cohort. The first was between *STRN* and *DLG2* in sample CSCC_0009 (*STRN*: exon 1 ENST00000263918; *DLG2*: exon 7 ENST00000376104). *STRN* encodes a calcium-dependent calmodulin-binding protein (46). *DLG2* plays a role in pain signaling, and deletion is seen in both human and canine osteosarcoma (47). We noted above that CSCC_0009 is the only sample without *TP53* mutations. CSCC_0009 came from a patient who had undergone liver transplantation and was on immunosuppressive therapy. The primary tumor that gave rise to this metastasis showed perineural involvement, which was also present in the metastatic deposit. The second gene fusion was between *NTRK2* and *HEBP2* in CSCC_0011. This seems to be caused by an unbalanced translocation event (Supplementary Figure S5B).

Enrichment analysis

Gene enrichment analysis was performed using the 21 genetically altered candidates identified above as significant/candidate driver genes, i.e., *TP53*, *CDKN2A*, *C9*, *KHDRBS2*, *SLC22A6*, *COLEC12*, *LINGO2*, *CDHR5*, *ZNF442*, *C9orf131*, *PRLR*, *DHRS4*, *PPP1R1A*, *EVC*, *LUM*, *ABCA4*, *LINC01003*, *LINC01474 (RP11-151D14.1)*, *RP4-597N16.4*, *RP11-61J19.4*, and *PTPRD*. The top significant pathway enrichment terms [Bio Planet 2019 (48)] are shown in Figure 5A. Most of the significant BioPlanet-enriched terms come from *TP53* and *CDKN2A*, such as TP53 network, tumor suppressor ARF, CTCF pathway, and cell cycle (G1/S checkpoint). However, *CDKN2A*, *LUM*, *CDHR5*, and *COLEC12* contribute to important cancer-related enrichment pathways, such as "TGF-

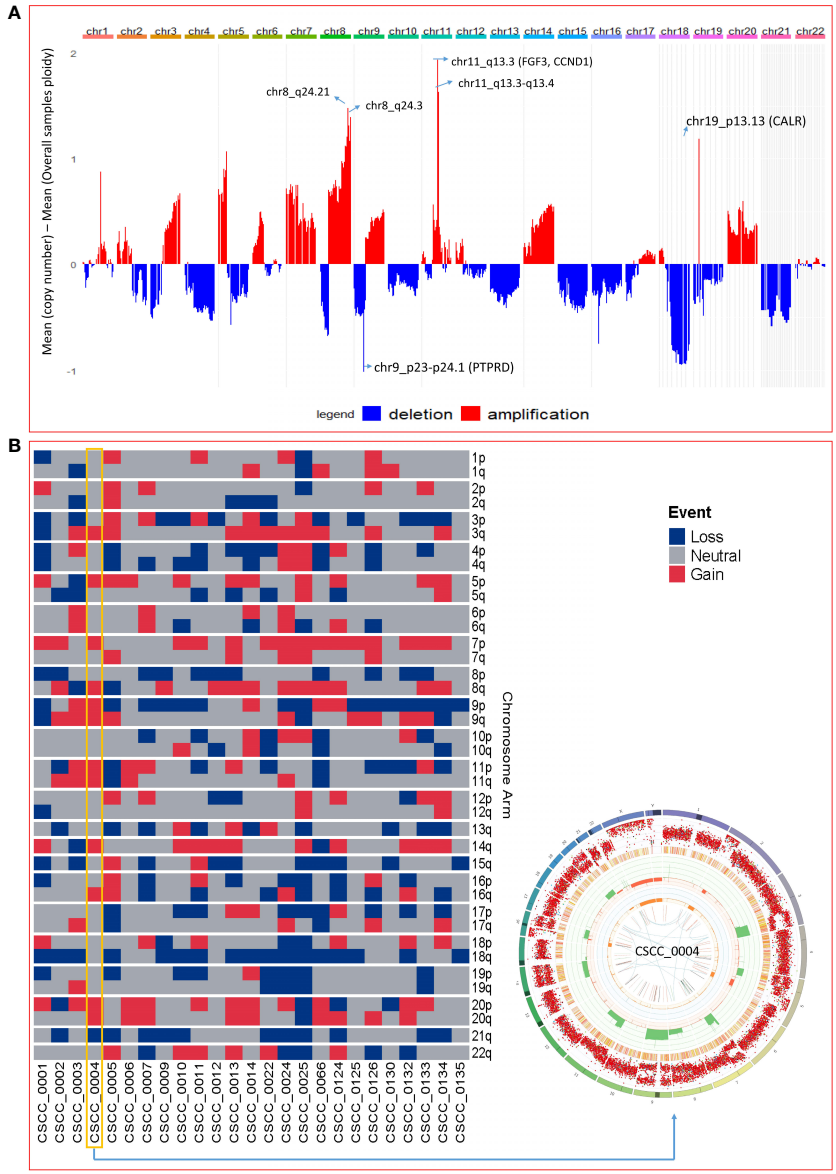

FIGURE 4
Chromosomal and recurrent genetic copy number variation. (**A**) Combined chromosomal CNV across 25 metastatic CSCC samples at the chromosomal level. The X-axis represents the differences of mean minimum copy number (bands) and means of overall samples ploidy (after adjustment for purity). Refer to Supplementary Table S5. **(B)** Chromosomes arm loss and gain at the sample level (red denotes a gain, and blue denotes a loss). Both arms of chromosomes 7 and 5p show gains. 8p, 18q, and 21q show loss. (A chromosome arm is defined to be deleted if at least half of its bases are one or more copies less than the sample ploidy. A chromosome arm is defined to be amplified if at least half of its bases are one or more copies more than the sample ploidy.). Also shown is a Circos plot obtained from the PURPLE pipeline for CSCC_0004 as a representative example that summarizes various information at the sample level. (More details of interpretation at https://github.com/hartwigmedical/hmftools/blob/master/purple/README.md#circos).

beta regulation of extracellular matrix." Full details of these enrichment analyses are available in Supplementary Table S6.

The Jensen diseases enrichment tool identified skin cancer with highest significance (Figure 5B), with Jensen compartment-based enrichment analysis showing that most of these genes belong to the extracellular compartment (Figure 5C). Other ontology enrichment analysis (MGI mammalian phenotype level 4 2021; Supplementary Table S6) showed enrichment of increased fibroblast proliferation MP:0011703 where *CDKN2A*, *TP53*, and *LUM* alterations are the main contributors.

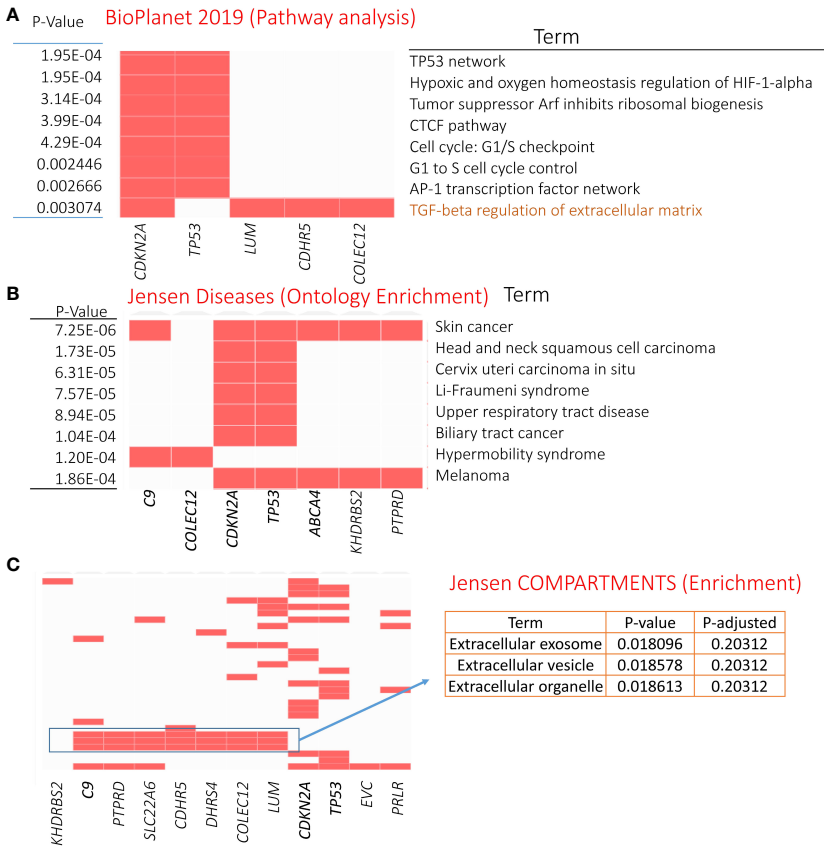

Term	P-value	P-adjusted
Extracellular exosome	0.018096	0.20312
Extracellular vesicle	0.018578	0.20312
Extracellular organelle	0.018613	0.20312

FIGURE 5
Enrichment analysis results of genetically mutated genes (21 candidates). **(A)** GO-Cellular Component terms showing eight significantly enriched terms (obtained from BioPlanet 2019). Panels **(B, C)** showing most significant Jensen diseases and Jensen compartments enriched terms, respectively. For details, refer to Supplementary Table S6.

We also performed enrichment analyses to predict drugs and miRNA targets for these driver candidates. Figure 6A shows the top 10 significant hits against drug annotations, which suggests that many of these driver genes are known therapeutic targets (dSig; Supplementary Table S6). With respect to miRNA targets, *hsa-miR-331-5p* was predicted to interact with six driver gene candidates, including *TP53* and *C9* (Figure 6B). For this prediction, the enricher platform uses TargetScan miRNA database (50). At the same time, *hsa-miR-1181* was one of the most significantly enriched miRNAs for these driver candidates, but can target only two driver genes.

Discussion

This is the largest study to employ WGS to assess the mutational landscape of metastatic CSCC and demonstrates the breadth of somatic variation across non-coding and coding regions. Furthermore, we updated and expanded the understanding of UV-mutational signature patterns in metastatic CSCC (12), including the identification of novel indel (ID) signature patterns. This highlights for the first time the nature and depth of variation within regulatory regions, with special attention devoted to UTR and lncRNA. Additionally, we reported various structural events at whole genome scale for this diseases and also compared driver genes and SNVs to previous WES/targeted NGS studies on metastasis CSCC.

At 238 mutations/Mb (median of 166.99 mutations/Mb) within metastatic CSCC at the whole genome scale, the rate of TMB is substantially higher than that of other cancers known to have a high mutational burden, including melanoma, which is 49 mutations/Mb (51). Pickering et al. (21) found a median of 61.2 mutations/Mb from their WES of high-risk primary (n= 32) and metastatic (n =7) CSCC. Their finding shows lower TMB than our study because they analyzed only coding DNA, which has much lower TMB than non-coding DNA in CSCC (12). The high TMB was associated with substantial structural variation, without recurrent gene fusions.

Alexandrov et al. (52) detailed patterns of mutational signatures in 23,829 tumor samples (1,965 WGS) from the

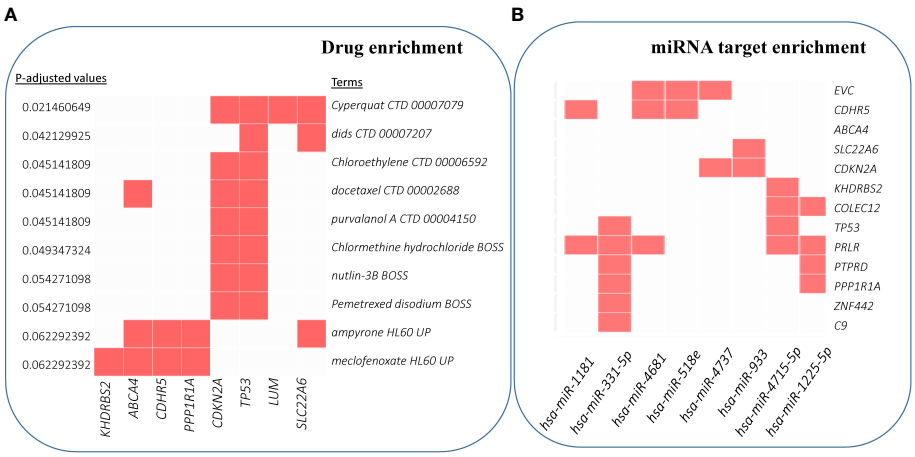

FIGURE 6
Enrichment analysis results for drug and miRNA targets. **(A)** Over-enrichment analysis of 20 driver candidates (deleted *PTPRD* excluded) against DSigDB (Drug SIGnatures DataBase) (49) annotation showing top 10 significantly enriched Drug/Compound. **(B)** Computationally predicted targets of miRNAs (TargetScan miRNA 2017). The x-axis represents the significance of the term (decreasing from left to right). (For details, refer to Supplementary Table S6).

Pan Cancer Analysis of Whole Genomes (PCAWG) datasets including 17 small ID signatures, expanded to 18 in COSMIC version 3.2 (https://cancer.sanger.ac.uk) (53). However, no cutaneous SCCs (primary or metastatic) are included in this dataset. We identified the predominance of ID signatures 8, 9, and 13 (100% of samples effected) in our 25 metastatic CSCC samples. ID8 is thought to be both related to double-strand DNA break repair dysfunction and to age-related changes. Melanoma is the only other cancer type reported to have a predominant ID 13 signature (52). Our data also provide evidence of concomitance of ID13 with SBS 7a and 7b (Figures 1C, D; Supplementary Table S2) in keeping with a UV-mediated mechanism for this signature. While we found ID9 to be a dominant indel signature in CSCC, it is rare in melanoma (2/104) but predominant in soft tissue sarcoma (52). The mechanism of ID9 is unclear, but this departure from what is found in melanoma clearly shows some point of difference in these UV-induced skin cancers. When comparing the TMB associated with ID9 signature among different cancers, the dominance in CSCC is clearly visible (Figure 7). One case of SBS32 is due to azathioprine exposure.

We identified substantial somatic variation within the 3′ UTR region of *EVC*, *LUM*, and *PPP1R1A*. *EVC* affects ciliary Hedgehog (Hh) regulation. Aberrant overexpression of *EVC* (and upregulation of Hh) has been reported in adult T-cell leukemia as a result of epigenetic modulation (54). The expression of *EVC* is reduced in nodal deposits of metastatic breast cancer compared with primary breast cancer, suggesting a role in the metastatic process (55). *LUM* is a major keratan sulfate proteoglycan that plays a role in collagen fibril organization, circumferential growth, epithelial cell migration, and tissue repair, among many other functions (56). *PPP1R1A* encodes a protein phosphatase inhibitor, which appears to have a variable but significant role in the metastatic process. For example, it is overexpressed in Ewing sarcoma and has been proposed as a driver of metastasis (57). Conversely, levels of *PPP1R1A* were reduced in breast cancer when compared to adjacent non-diseased breast tissue (58). Within our cohort, we observed a unique recurrent missense mutation in the 3′UTR of *PPP1R1A* in five samples.

LINC01003 was the most mutated lncRNA in our cohort (64% of samples). In multiple myeloma, *LINC01003* behaves as a tumor suppressor genomic element. Upregulation suppresses multiple myeloma by repressing cell viability and adhesion and promoting apoptosis. This effect is *via* its sponge effect on miR-33a-5p and its target *PIM1* (59).

As has been frequently reported for CSCC (5) (Supplementary Figure S1), *TP53* and *CDKN2A* were also the most recurrently altered genes in our cohort. Loss of function mutations within *TP53* and *CDKN2A* are well known to adversely impact cell cycle pathway control and DNA repair mechanisms, thus increasing TMB. Furthermore, *TP53* and *CDKN2A* mutations in other squamous cell carcinomas such as NSCLC (60) and HNSCC (61) correlates with response to immune checkpoint inhibitors. With *TP53* and *CDKN2A* as driver genes in our study, the generally high response rates to immune checkpoint inhibitors in advanced and metastatic CSCC is not surprising. Kilnakis et al. (62) describe a pattern of *TP53* mutation that differed between primary and metastatic disease in head and neck (mucosal) SCC. They found an overall

lower rate of mutations in metastatic tumors but a higher concentration of missense mutations in the DNA binding regions of the gene. However, Yilmaz et al. (17) reported a significantly higher *TP53* mutation frequency in metastatic (85%) compared to primary CSCC (corrected p-value <0.002). Our cBioPortal dataset analysis indicated no difference in variant frequency for *TP53* between primary and metastatic CSCC (refer to Supplementary Figure S1), suggesting retention in metastatic tumors.

Of note in our study was the absence of significant or recurrent SNVs affecting *NOTCH1/2*. Inman et al. (15) compared well-differentiated to moderately and poorly differentiated primary CSCC and identified *NOTCH1*, *NOTCH2*, *TP53*, and *CDKN2A* as the most commonly mutated genes, with *ATP1A1*, *HERC6*, *MAPK1P1L*, *GRHL2*, *TRAPPC9*, *FLNB*, and *MAP3K9* identified as common early events in primary CSCC. Within this group, *GRHL2* was associated with less well-differentiated tumors including those with a worse prognosis. In our cohort, only a single splice variant in *GRHL2* was identified, suggesting that its role in metastatic disease is limited.

C9 (encodes complement component 9) was also identified as a potential driver gene by three driver identification tools, with SNVs identified in 52% of the samples in our cohort. C9 is part of the membrane attack complex (MAC) and has been shown to modulate cellular behavior in the tumor microenvironment (TME) (63). Since the TME plays a crucial role in tumorigenesis, progression, metastasis, and recurrence, C9 might have significant potential in CSCC progression to metastasis. Various other components of the complement system have been linked to CSCC progression and immunosuppression and implicated as potential therapeutic targets (64–66). With respect to *C9* specifically, it appears to be recurrently mutated in CSCC specimens (31% in primary and 10% in metastatic CSCC) as identified in the cBioPortal database (Supplementary Figure S1). and high expression levels have been proposed as a potential biomarker for the detection of gastric cancers (67) (68). Furthermore, the restrained expression of *C9* in tumor-associated macrophages promotes non-small cell lung cancer progression (69).

Apart from *TP53*, *CDKN2A*, and *C9*, we identified nine other potential driver genes with the most recurrently mutated gene being *KHDRBS2* (48% of cohort) with various impacts, including stop gained, complex, and synonymous types apart from missense variant across the cohort. In the cBioPortal database, this gene is mutated in 20% of metastatic CSCC specimens (Supplementary Figure S1), suggesting that it is a reasonably recurrently mutated gene in this disease.

A comparison of mutational frequency of primary and metastatic CSCC on the cBioPortal data suggests the potential of *COLEC12* (primary=25%; metastatic=60%) and *SLC22A6* (primary=16%; metastatic=30%) as drivers in metastatic CSCC (Supplementary Figure S1). Both *COLEC12* and *SLC33A6* are mutated in 44% of the samples in our cohort, and many of them are high-impact SNVs. *COLEC12* is involved in leukocyte recruitment and cancer metastasis (70) and regulates the apoptosis of osteosarcoma (70). Moreover, *COLEC12* is a potential biomarker of anaplastic thyroid cancer (ATC) (71).

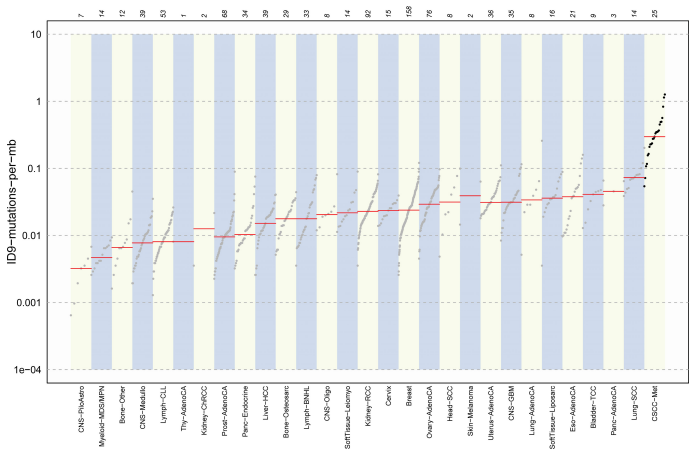

FIGURE 7
Comparison plot of ID9 mutations for various cancers. CSCC shows the highest ID9 mutations per Mb. The bottom x-axis represents the cancer types, and the upper x-axis shows the number of samples measured for specific cancer types. y-Axis indicates the number of mutations per Mb. Data for other cancers was obtained from ID9 signature details from COSMIC V3.2 and compared with CSCC data. CSCC data is calculated as ID9 signature score/3100 (coverage for hg38 genome).

In one study of cancerous gastric stromal cells (GSCs), the role of *COLEC12* is found in mediating the crosstalk between GSCs and dendritic cells (DCs) (72). On the other hand, *SLC22A6* is known as an organic anion transporter 1 (*OAT1*). Expression and function alterations of *OAT1* play an essential role in therapeutic efficacy and the toxicity of many drugs, such as for anti-cancer drugs methotrexate, bleomycin, and cisplatin-related toxicity (73–75). *OAT1* variation associated with cardiotoxicity in pediatric acute lymphoblastic leukemia and osteosarcoma (76). Furthermore, the role of *OAT1* in breast cancer metastasis has been reported (77). Important cancer-related roles of the other potential CSCC drivers are reported in Supplementary Table S7.

Loss of *PTPRD* was the most prominent copy number alteration in our 25 samples. *PTPRD* encodes protein tyrosine phosphatase receptor D, which belongs to a family of receptors whose action opposes that of the tyrosine kinases, which are central to cell growth and differentiation and oncogenic transformation. Large-scale genomic events impacting *CDKN2A* can also affect *PTPRD* due to their proximity on chr9 (78). In head and neck SCC, *PTPRD* inactivation significantly increases *STAT3* hyperactivation, which was associated with decreased survival and resistance to epidermal growth factor receptor (EGFR)-targeted therapy (79). *PTPRD* has been implicated as a tumor suppressor in several cancers with inactivating somatic variants found in >50% of GBM and between 10% and 20% of head and neck mucosal SCC (HNSCC) (80). Lambert et al. (45) described deletions of *PTPRD* in 37% of metastatic primary CSCC and metastases. In addition, some of their cases also displayed a variant in the minor allele concordant with the deletion leading to a LOH event. It is thus possible that *PTPRD* plays a tumor suppressor role in preventing metastatic CSCC.

There were no recurrently amplified genes except for *CALR*, *CCND1*, and *FGF3*, which were each only amplified in 2/25 samples (Table 3). *CALR* encodes a ubiquitous endoplasmic-reticulum-bound calcium receptor (81). Cellular stress can move *CALR* fragments to the plasma membrane from the ER and influence immune recognition of cancer cells. Recent analysis of *CALR* fragments in myeloproliferative disease suggests an immunosuppressive influence of extracellular *CALR* (82). Cyclin D1 (*CCND1*) amplification is associated with nodal metastasis and worse survival in oral SCC (83). In a review of *CCND1* copy number variation in metastatic non-cutaneous melanoma, amplification was prominent in those patients whose disease did not respond to immune checkpoint inhibition (84). *FGF3* amplification is more common in metastatic breast cancer than primary tumors (85). Targetable *FGF3* amplification was associated with a poorer prognosis and lung metastasis in hepatocellular carcinoma (86). This amplification was seen in only 2% of total HCC but was most common in those cancers showing rapid response to sorafenib.

With respect to enrichment of driver gene alterations observed in our samples, dysregulation of the cell cycle pathway appears to be the central genomic theme of metastatic CSCC supported mainly by *TP53* and *CDKN2A*. *CDKN2A* encodes the CDK inhibitor $p16^{INK4a}$. This inhibitor is an important controller of the activity of CDKs and progression from G1 to mitosis in the cell cycle. Inactivating mutations in *CDKN2A* with effects on $p16^{INK4a}$ regulatory functions uncouple cell cycle control to promote cell survival and tumorigenesis (87). CDK4/6 inhibitors such as palbociclib, which has demonstrated response in metastatic breast cancer, may likewise be a potential therapeutic strategy for metastatic CSCC. Interaction between *CDKN2A* and *TP53* through *MDM2* and its regulation by ARF (also encoded by *CDKN2A*) further disable cell cycle and apoptotic pathways (GO: molecular function enrichment shows MDM2/MDM4 family protein binding). The pro-tumorigenic functions of the p53-MDM2-ARF network is gaining traction as a target for novel therapeutic strategies (88), which could also be applied to CSCC.

The cellular process defined by the term "TGF beta regulation of extra cellular matrix" was also significantly enriched showing a role for *LUM*, *CDHR5*, *COLEC12*, and *CDKN2A* in this process (Figure 5A). Compartment enrichment analysis found that these genetically altered genes are part of the extracellular compartment. Our previous differential expression study confirmed that TGFβ and the extracellular matrix component have an important role in metastatic CSCC (89). Inactivation of cell cycle control (through *CDKN2A* alterations for example) would allow tumor cells to escape from TGFβ-mediated suppressive effects. As loss of this growth-inhibitory response occurs at a level downstream of the core TGFβ signaling pathway, TGFβ then switches to a tumor-progression factor promoting epithelial-to-mesenchymal transition while inhibiting proliferation, differentiation, and the antitumor activity of multiple immune cells (90). As TGFβ receptor inhibition in combination with gemcitabine or immunotherapy is showing promise in other cancers (91, 92), this approach may also be applicable to metastatic CSCC.

Finally, *miR-331-5p* shows promise as a potentiator of CSCC drivers. *miR-331-5p* downregulation contributes to chemotherapy resistance/relapse in leukemia (93), and it inhibits proliferation by targeting PI3K/Akt and ERK1/2 pathways in colorectal cancer (94).

Conclusion

WGS provides insight into the unparalleled burden of mutation within metastatic CSCC, and our study has provided a deeper understanding of the genomic complexity of this disease. The functional impact of the varied and complex

genetic alterations observed in metastatic CSCC should be validated in the future in confirmatory studies comparing whole genomes of non-metastatic primary tumors to metastatic tumors. This knowledge would significantly contribute to the identification of biomarkers in primary CSCC for predicting metastasis.

Data availability statement

The original contributions presented in the study are included in the article/supplementary materials. The variant call format files have been deposited at the European Genome-Phenome Archive, which is hosted by the EMBL-European Bioinformatics Institute and the Center for Genomic Regulation, under accession number EGAS00001006378.

Ethics statement

This study was undertaken with Institutional Human Research Ethics approval (UOW/ISLHD HREC14/397). The patients/participants provided their written informed consent to participate in this study.

Author contributions

AT and DS performed the bioinformatics analyses. BA and NGI conceived the idea and assisted in bioinformatics analyses. BA, AT, and MR drafted manuscript versions. BA, MR, RG, and JC obtained funding for the project. BA, JC, JM, SM, SC, and RG collated samples and/or clinical data. JP and EM completed tissue processing. All authors reviewed and edited the manuscript. All authors contributed to the article and approved the submitted version.

Funding

This work was funded by the Illawarra Cancer Carers, The Head and Neck Research Fund, Royal Prince Alfred Institute of Academic Surgery, The Cancer Institute NSW translational program grant, Chris O'Brien Lifehouse, National Health and Medical Research Council Project Grant APP1181179, and Tour de Cure. The authors would like to acknowledge A/Prof Carsten Palme and Dr. Kerwin Shannon for suggestions and National Computational Infrastructure (NCI-GADI) and Sydney Informatics Hub for computational services.

Conflict of interest

The authors declare that the research was conducted in the absence of any commercial or financial relationships that could be construed as a potential conflict of interest.

Publisher's note

All claims expressed in this article are solely those of the authors and do not necessarily represent those of their affiliated organizations, or those of the publisher, the editors and the reviewers. Any product that may be evaluated in this article, or claim that may be made by its manufacturer, is not guaranteed or endorsed by the publisher.

Supplementary material

The Supplementary Material for this article can be found online at: https://www.frontiersin.org/articles/10.3389/fonc.2022.919118/full#supplementary-material

References

1. Rogers HW, Weinstock MA, Feldman SR, Coldiron BM. Incidence estimate of nonmelanoma skin cancer (Keratinocyte carcinomas) in the US population, 2012. *JAMA Dermatol* (2015) 151(10):1081–6. doi: 10.1001/jamadermatol.2015.1187

2. Waldman A, Schmults C. Cutaneous squamous cell carcinoma. *Hematol Oncol Clin North Am* (2019) 33(1):1–12. doi: 10.1016/j.hoc.2018.08.001

3. Venables ZC, Autier P, Nijsten T, Wong KF, Langan SM, Rous B, et al. Nationwide incidence of metastatic cutaneous squamous cell carcinoma in England. *JAMA Dermatol* (2019) 155(3):298–306. doi: 10.1001/jamadermatol.2018.4219

4. Forest VI, Clark JJ, Veness MJ, Milross C. N1S3: A revised staging system for head and neck cutaneous squamous cell carcinoma with lymph node metastases: Results of 2 Australian cancer centers. *Cancer: Interdiscip Int J Am Cancer Soc* (2010) 116(5):1298–304. doi: 10.1002/cncr.24855

5. Ashford BG, Clark J, Gupta R, Iyer NG, Yu B, Ranson M. Reviewing the genetic alterations in high-risk cutaneous squamous cell carcinoma: A search for prognostic markers and therapeutic targets. *Head Neck* (2017) 39(7):1462–9. doi: 10.1002/hed.24765

6. Mooney CP, Clark JR, Shannon K, Palme CE, Ebrahimi A, Gao K, et al. The significance of regional metastasis location in head and neck cutaneous squamous cell carcinoma. *Head Neck* (2021) 43(9):2705–11. doi: 10.1002/hed.26744

7. Veness MJ. Treatment recommendations in patients diagnosed with high-risk cutaneous squamous cell carcinoma. *Australas Radiol* (2005) 49(5):365–76. doi: 10.1111/j.1440-1673.2005.01496.x

8. Garcia-Foncillas J, Tejera-Vaquerizo A, Sanmartin O, Rojo F, Mestre J, Martin S, et al. Update on management recommendations for advanced cutaneous squamous cell carcinoma. *Cancers (Basel)* (2022) 14(3):629. doi: 10.3390/cancers14030629

9. Stanganelli I, Spagnolo F, Argenziano G, Ascierto PA, Bassetto F, Bossi P, et al. The multidisciplinary management of cutaneous squamous cell carcinoma: A comprehensive review and clinical recommendations by a panel of experts. *Cancers (Basel)* (2022) 14(2):377. doi: 10.3390/cancers14020377

10. Migden MR, Rischin D, Schmults CD, Guminski A, Hauschild A, Lewis KD, et al. PD-1 blockade with cemiplimab in advanced cutaneous squamous-cell carcinoma. *N Engl J Med* (2018) 379(4):341–51. doi: 10.1056/NEJMoa1805131

11. Aboul-Fettouh N, Morse D, Patel J, Migden MR. Immunotherapy and systemic treatment of cutaneous squamous cell carcinoma. *Dermatol Pract Concept* (2021) 11(Suppl 2):e2021169S. doi: 10.5826/dpc.11S2a169S

12. Mueller SA, Gauthier MA, Ashford B, Gupta R, Gayevskiy V, Ch'ng S, et al. Mutational patterns in metastatic cutaneous squamous cell carcinoma. *J Invest Dermatol* (2019) 139(7):1449–1458 e1. doi: 10.1016/j.jid.2019.01.008

13. Perry J, Ashford B, Thind AS, Gauthier M-E, Minaei E, Major G, et al. Comprehensive mutational and phenotypic characterization of new metastatic cutaneous squamous cell carcinoma cell lines reveal novel drug susceptibilities. *Int J Mol Sci* (2020) 21(24):9536. doi: 10.3390/ijms21249536

14. Zilberg C, Lee MW, Yu B, Ashford B, Kraitsek S, Ranson M, et al. Analysis of clinically relevant somatic mutations in high-risk head and neck cutaneous squamous cell carcinoma. *Modern Pathol* (2018) 31(2):275–87. doi: 10.1038/modpathol.2017.128

15. Inman GJ, Wang J, Nagano A, Alexandrov LB, Purdie KJ, Taylor RGc, et al. The genomic landscape of cutaneous SCC reveals drivers and a novel azathioprine associated mutational signature. *Nat Commun* (2018) 9(1):3667. doi: 10.1038/s41467-018-06027-1

16. Al-Rohil RN, Tarasen AJ, Carlson JA, Wang K, Johnson A, Yelensky R, et al. Evaluation of 122 advanced-stage cutaneous squamous cell carcinomas by comprehensive genomic profiling opens the door for new routes to targeted therapies. *Cancer* (2016) 122(2):249–57. doi: 10.1002/cncr.29738

17. Yilmaz AS, Ozer HG, Gillespie JL, Allain DC, Bernhardt MN, Furlan KC, et al. Differential mutation frequencies in metastatic cutaneous squamous cell carcinomas versus primary tumors. *Cancer* (2017) 123(7):1184–93. doi: 10.1002/cncr.30459

18. Zehir A, Benayed R, Shah RH, Syed A, Middha S, Kim HR, et al. Mutational landscape of metastatic cancer revealed from prospective clinical sequencing of 10,000 patients. *Nat Med* (2017) 23(6):703–13. doi: 10.1038/nm.4333

19. Li YY, Hanna GJ, Laga AC, Haddad RI, Lorch JH, Hammerman PS. Genomic analysis of metastatic cutaneous squamous cell carcinoma. *Clin Cancer Res* (2015) 21(6):1447–56. doi: 10.1158/1078-0432.CCR-14-1773

20. Chang D, Shain AH. The landscape of driver mutations in cutaneous squamous cell carcinoma. *NPJ Genom Med* (2021) 6(1):61. doi: 10.1038/s41525-021-00226-4

21. Pickering CR, Zhou JH, Lee JJ, Drummond JA, Peng SA, Saade RE, et al. Mutational landscape of aggressive cutaneous squamous cell carcinoma. *Clin Cancer Res* (2014) 20(24):6582–92. doi: 10.1158/1078-0432.CCR-14-1768

22. Lawrence MS, Stojanov P, Polak P, Kryukov GV, Cibulskis K, Sivachenko A, et al. Mutational heterogeneity in cancer and the search for new cancer-associated genes. *Nature* (2013) 499(7457):214–8. doi: 10.1038/nature12213

23. Hedegaard J, Thorsen K, Lund MK, Hein AM, Hamilton-Dutoit SJ, Vang S, et al. Next-generation sequencing of RNA and DNA isolated from paired fresh-frozen and formalin-fixed paraffin-embedded samples of human cancer and normal tissue. *PloS One* (2014) 9(5):e98187. doi: 10.1371/journal.pone.0098187

24. Statello L, Guo CJ, Chen LL, Huarte M. Author correction: Gene regulation by long non-coding RNAs and its biological functions. *Nat Rev Mol Cell Biol* (2021) 22(2):159. doi: 10.1038/s41580-021-00330-4

25. Cesana M, Cacchiarelli D, Legnini I, Santini T, Sthandier O, Chinappi M, et al. A long noncoding RNA controls muscle differentiation by functioning as a competing endogenous RNA. *Cell* (2011) 147(2):358–69. doi: 10.1016/j.cell.2011.09.028

26. Barrett LW, Fletcher S, Wilton SD. Regulation of eukaryotic gene expression by the untranslated gene regions and other non-coding elements. *Cell Mol Life Sci* (2012) 69(21):3613–34. doi: 10.1007/s00018-012-0990-9

27. Liu W, Wang X. Prediction of functional microRNA targets by integrative modeling of microRNA binding and target expression data. *Genome Biol* (2019) 20 (1):18. doi: 10.1186/s13059-019-1629-z

28. Schuster SL, Hsieh AC. The untranslated regions of mRNAs in cancer. *Trends Cancer* (2019) 5(4):245–62. doi: 10.1016/j.trecan.2019.02.011

29. Kobayashi H, Tomari Y. RISC assembly: Coordination between small RNAs and argonaute proteins. *Biochim Biophys Acta (BBA)-Gene Regul Mech* (2016) 1859 (1):71–81. doi: 10.1016/j.bbagrm.2015.08.007

30. Priestley P, Baber J, Lolkema MP, Steeghs N, de Bruijn E, Shale C, et al. Pan-cancer whole-genome analyses of metastatic solid tumours. *Nature* (2019) 575 (7781):210–6. doi: 10.1038/s41586-019-1689-y

31. Pagel KA, Kim R, Moad K, Busby B, Zheng L, Tokheim C, et al. Integrated informatics analysis of cancer-related variants. *JCO Clin Cancer Inform* (2020) 4:310–7. doi: 10.1200/CCI.19.00132

32. Mularoni L, Sabarinathan R, Deu-Pons J, Gonzalez-Perez A, López-Bigas N. OncodriveFML: A general framework to identify coding and non-coding regions with cancer driver mutations. *Genome Biol* (2016) 17(1):128. doi: 10.1186/s13059-016-0994-0

33. Martincorena I, Raine KM, Gerstung M, Dawson KJ, Haase K, Van Loo P, et al. Universal patterns of selection in cancer and somatic tissues. *Cell* (2017) 171 (5):1029–1041.e21. doi: 10.1016/j.cell.2017.09.042

34. Gao J, Aksoy BA, Dogrusoz U, Dresdner G, Gross B, Sumer SO, et al. Integrative analysis of complex cancer genomics and clinical profiles using the cbioportal. *Sci Signal* (2013) 6(269):pl1. doi: 10.1126/scisignal.2004088

35. Cerami E, Gao J, Dogrusoz U, Gross BE, Sumer SO, Aksoy BA, et al. The cbio cancer genomics portal: An open platform for exploring multidimensional cancer genomics data. *Cancer Discovery* (2012) 2(5):401–4. doi: 10.1158/2159-8290.CD-12-0095

36. Cameron DL, Baber J, Shale C, Valle-Inclan JE, Besselink N, van Hoeck A, et al. GRIDSS2: Comprehensive characterisation of somatic structural variation using single breakend variants and structural variant phasing. *Genome Biol* (2021) 22(1):202. doi: 10.1186/s13059-021-02423-x

37. Blokzijl F, et al. MutationalPatterns: Comprehensive genome-wide analysis of mutational processes. *Genome Med* (2018) 10(1):1–11. doi: 10.1186/s13073-018-0539-0

38. Kuleshov MV, Jones MR, Rouillard AD, Fernandez NF, Duan Q, Wang Z, et al. Enrichr: A comprehensive gene set enrichment analysis web server 2016 update. *Nucleic Acids Res* (2016) 44(W1):W90–7. doi: 10.1093/nar/gkw377

39. Wilson A GD, Nankervis J, Clark J, Gupta R, Ashford B. Defining the incidence of cutaneous squamous cell carcinoma in coastal NSW Australia. *Aust J Derm* (2022) 63(2):213–6. doi: 10.1111/ajd.13830

40. Tokez S, Wakkee M, Kan W, Venables ZC, Mooyaart AL, Louwman M, et al. Cumulative incidence and disease-specific survival of metastatic cutaneous squamous cell carcinoma: A nationwide cancer registry study. *J Am Acad Dermatol* (2021) 86(2):331–8. doi: 10.1016/j.jaad.2021.09.067

41. Mao P, Brown AJ, Esaki S, Lockwood S, Poon GMK, Smerdon MJ, et al. ETS transcription factors induce a unique UV damage signature that drives recurrent mutagenesis in melanoma. *Nat Commun* (2018) 9(1):2626. doi: 10.1038/s41467-018-05064-0

42. Perera D, Poulos RC, Shah A, Beck D, Pimanda JE, Wong JW. Differential DNA repair underlies mutation hotspots at active promoters in cancer genomes. *Nature* (2016) 532(7598):259–63. doi: 10.1038/nature17437

43. Sabarinathan R, Mularoni L, Deu-Pons J, Gonzalez-Perez A, López-Bigas N. Nucleotide excision repair is impaired by binding of transcription factors to DNA. *Nature* (2016) 532(7598):264–7. doi: 10.1038/nature17661

44. Purdie KJ, Harwood CA, Gulati A, Chaplin T, Lambert SR, Cerio R, et al. Single nucleotide polymorphism array analysis defines a specific genetic fingerprint for well-differentiated cutaneous SCCs. *J Invest Dermatol* (2009) 129(6):1562–8. doi: 10.1038/jid.2008.408

45. Lambert SR, Harwood CA, Purdie KJ, Gulati A, Matin RN, Romanowska M, et al. Metastatic cutaneous squamous cell carcinoma shows frequent deletion in the protein tyrosine phosphatase receptor type d gene. *Int J Cancer* (2012) 131(3): E216–26. doi: 10.1002/ijc.27333

46. Du QY, Yao JH, Zhou YC, Xu LJ, Zhao FY, Yang Y. High STRN expression promotes HCC invasion and migration but not cell proliferation or apoptosis through facilitating epithelial-mesenchymal transition. *BioMed Res Int 2020* (2020), 6152925. doi: 10.1155/2020/6152925

47. Shao YW, Wood GA, Lu J, Tang QL, Liu J, Molyneux S, et al. Cross-species genomics identifies DLG2 as a tumor suppressor in osteosarcoma. *Oncogene* (2019) 38(2):291–8. doi: 10.1038/s41388-018-0444-4

48. Huang R, Grishagin I, Wang Y, Zhao T, Greene J, Obenauer JC, et al. The NCATS BioPlanet – an integrated platform for exploring the universe of cellular signaling pathways for toxicology, systems biology, and chemical genomics. *Front Pharmacol* (2019) 10. doi: 10.3389/fphar.2019.00445

49. Yoo M, Shin J, Kim J, Ryall KA, Lee K, Lee S, et al. DSigDB: Drug signatures database for gene set analysis. *Bioinformatics* (2015) 31(18):3069–71. doi: 10.1093/bioinformatics/btv313

50. Agarwal V, Bell GW, Nam JW, Bartel DP. Predicting effective microRNA target sites in mammalian mRNAs. *Elife* (2015) 4:e05005. doi: 10.7554/eLife.05005

51. Hayward NK, Wilmott JS, Waddell N, Johansson PA, Field MA, Nones K, et al. Whole-genome landscapes of major melanoma subtypes. *Nature* (2017) 545 (7653):175–80. doi: 10.1038/nature22071

52. Alexandrov LB, Kim J, Haradhvala NJ, Huang MN, Tian Ng AW, Wu Y, et al. The repertoire of mutational signatures in human cancer. *Nature* (2020) 578 (7793):94–101. doi: 10.1038/s41586-020-1943-3

53. Tate JG, Bamford S, Jubb HC, Sondka Z, Beare DM, Bindal N, et al. COSMIC: The catalogue of somatic mutations in cancer. *Nucleic Acids Res* (2019) 47(D1):D941–d947. doi: 10.1093/nar/gky1015

54. Takahashi R, Yamagishi M, Nakano K, Yamochi T, Yamochi T, Fujikawa D, et al. Epigenetic deregulation of Ellis van creveld confers robust hedgehog

signaling in adult T-cell leukemia. *Cancer Sci* (2014) 105(9):1160–9. doi: 10.1111/cas.12480

55. Mamoor S. *EVC is differentially expressed in lymph node metastasis in human breast cancer*. OSF Preprints (2021). doi: 10.31219/osf.io/twb9n

56. Chakravarti S. Functions of lumican and fibromodulin: Lessons from knockout mice. *Glycoconjugate J* (2002) 19(4):287–93. doi: 10.1023/A:1025348417078

57. Luo W, Xu C, Ayello J, Dela Cruz F, Rosenblum JM, Lessnick SL, et al. Protein phosphatase 1 regulatory subunit 1A in Ewing sarcoma tumorigenesis and metastasis. *Oncogene* (2018) 37(6):798–809. doi: 10.1038/onc.2017.378

58. Yuan CL, Jiang XM, Yi Y, E JF, Zhang ND, Luo X, et al. Identification of differentially expressed lncRNAs and mRNAs in luminal-b breast cancer by RNA-sequencing. *BMC Cancer* (2019) 19(1):1171. doi: 10.1186/s12885-019-6395-5

59. Wu L, Xia L, Chen X, Ruan M, Li L, Xia R. Long non-coding RNA LINC01003 suppresses the development of multiple myeloma by targeting miR-33a-5p/PIM1 axis. *Leuk Res* (2021) 106:106565. doi: 10.1016/j.leukres.2021.106565

60. Assoun S, Theou-Anton N, Nguenang M, Cazes A, Danel C, Abbar B, et al. Association of TP53 mutations with response and longer survival under immune checkpoint inhibitors in advanced non-Small-Cell lung cancer. *Lung Cancer* (2019) 132:65–71. doi: 10.1016/j.lungcan.2019.04.005

61. Deneka AY, Baca Y, Serebriiskii IG, Nicolas E, Parker MI, Nguyen TT, et al. Association of T P53 and CDKN2A mutation profile with tumor mutation burden in head and neck cancer. *Clin Cancer Res* (2022) 28(9):1925–37. doi: 10.1158/1078-0432.CCR-21-4316

62. Klinakis A, Rampias T. TP53 mutational landscape of metastatic head and neck cancer reveals patterns of mutation selection. *EBioMedicine* (2020) 58:102905. doi: 10.1016/j.ebiom.2020.102905

63. Zhang R, Liu Q, Li T, Liao Q, Zhao Y. Role of the complement system in the tumor microenvironment. *Cancer Cell Int* (2019) 19:300. doi: 10.1186/s12935-019-1027-3

64. Rahmati Nezhad P, Riihila P, Knuutila JS, Viiklepp K, Peltonen S, Kallajoki M, et al. Complement factor d is a novel biomarker and putative therapeutic target in cutaneous squamous cell carcinoma. *Cancers (Basel)* (2022) 14(2):305. doi: 10.3390/cancers14020305

65. Johnson EM, Uppalapati CK, Pascual AS, Estrada SI, Averitte RL, Leyva KJ, et al. Complement factor h in cSCC: Evidence of a link between sun exposure and immunosuppression in skin cancer progression. *Front Oncol* (2022) 12:819580. doi: 10.3389/fonc.2022.819580

66. Riihila P, Nissinen L, Knuutila J, Rahmati Nezhad P, Viiklepp K, Kahari VM, et al. Complement system in cutaneous squamous cell carcinoma. *Int J Mol Sci* (2019) 20(14):3550. doi: 10.3390/ijms20143550

67. Chong PK, Lee H, Loh MC, Choong LY, Lin Q, So JB, et al. Upregulation of plasma C9 protein in gastric cancer patients. *Proteomics* (2010) 10(18):3210–21. doi: 10.1002/pmic.201000127

68. Joshi V, Shah A, Brown I, Winterford C, Hill M. Complement component C9 as a new biomarker for esophageal adenocarcinoma. *J Clin Oncol* (2017) 35(4_suppl):19–9. doi: 10.1200/JCO.2017.35.4_suppl.19

69. Li L, Yang H, Li Y, Li XD, Zeng TT, Lin SX, et al. Hypoxia restrains the expression of complement component 9 in tumor-associated macrophages promoting non-small cell lung cancer progression. *Cell Death Discov* (2018) 4:63. doi: 10.1038/s41420-018-0064-3

70. Li GZ, Deng JF, Qi YZ, Liu R, Liu ZX. COLEC12 regulates apoptosis of osteosarcoma through toll-like receptor 4-activated inflammation. *J Clin Lab Anal* (2020) 34(11):e23469. doi: 10.1002/jcla.23469

71. Espinal-Enríquez J, Muñoz-Montero S, Imaz-Rosshandler I, Huerta-Verde A, Mejía C. Genome-wide expression analysis suggests a crucial role of dysregulation of matrix metalloproteinases pathway in undifferentiated thyroid carcinoma. *BMC Genomics* (2015) 16(1):207. doi: 10.1186/s12864-015-1372-0

72. Chang LL, Hsu WH, Kao MC, Chou CC, Lin CC, Liu CJ, et al. Stromal c-type lectin receptor COLEC12 integrates h. pylori, PGE2-EP2/4 axis and innate immunity in gastric diseases. *Sci Rep* (2018) 8(1):3821. doi: 10.1038/s41598-018-20957-2

73. Li Q, Shu Y. Role of solute carriers in response to anticancer drugs. *Mol Cell Ther* (2014) 2:15. doi: 10.1186/2052-8426-2-15

74. Sweet DH. Organic anion transporter (Slc22a) family members as mediators of toxicity. *Toxicol Appl Pharmacol* (2005) 204(3):198–215. doi: 10.1016/j.taap.2004.10.016

75. Hu S, Leblanc AF, Gibson AA, Hong KW, Kim JY, Janke LJ, et al. Identification of OAT1/OAT3 as contributors to cisplatin toxicity. *Clin Transl Sci* (2017) 10(5):412–20. doi: 10.1111/cts.12480

76. Sági JC, Egyed B, Kelemen A, Kutszegi N, Hegyi M, Gézsi A, et al. Possible roles of genetic variations in chemotherapy related cardiotoxicity in pediatric acute lymphoblastic leukemia and osteosarcoma. *BMC Cancer* (2018) 18(1):704. doi: 10.1186/s12885-018-4629-6

77. Sutherland R, Meeson A, Lowes S. Solute transporters and malignancy: Establishing the role of uptake transporters in breast cancer and breast cancer metastasis. *Cancer Metastasis Rev* (2020) 39(3):919–32. doi: 10.1007/s10555-020-09879-6

78. Ortiz B, White JR, Wu WH, Chan TA. Deletion of ptprd and Cdkn2a cooperate to accelerate tumorigenesis. *Oncotarget* (2014) 5(16):6976–82. doi: 10.18632/oncotarget.2106

79. Veeriah S, Brennan C, Meng S, Singh B, Fagin JA, Solit DB, et al. The tyrosine phosphatase PTPRD is a tumor suppressor that is frequently inactivated and mutated in glioblastoma and other human cancers. *Proc Natl Acad Sci USA* (2009) 106(23):9435–40. doi: 10.1073/pnas.0900571106

80. Peyser ND, Du Y, Li H, Lui V, Xiao X, Chan TA, et al. Loss-Of-Function PTPRD mutations lead to increased STAT3 activation and sensitivity to STAT3 inhibition in head and neck cancer. *PloS One* (2015) 10(8):e0135750. doi: 10.1371/journal.pone.0135750

81. Holmström MO, Martinenaite E, Ahmad SM, Met Ö, Friese C, Kjær L, et al. The calreticulin (CALR) exon 9 mutations are promising targets for cancer immune therapy. *Leukemia* (2018) 32(2):429–37. doi: 10.1038/leu.2017.214

82. Liu P, Zhao L, Loos F, Marty C, Xie W, Martins I, et al. Immunosuppression by mutated calreticulin released from malignant cells. *Mol Cell* (2020) 77(4):748–760.e9. doi: 10.1016/j.molcel.2019.11.004

83. Miyamoto R, Uzawa N, Nagaoka S, Hirata Y, Amagasa T. Prognostic significance of cyclin D1 amplification and overexpression in oral squamous cell carcinomas. *Oral Oncol* (2003) 39(6):610–8. doi: 10.1016/S1368-8375(03)00048-4

84. Yu J, Yan J, Guo Q, Chi Z, Tang B, Zheng B, et al. Genetic aberrations in the CDK4 pathway are associated with innate resistance to PD-1 blockade in Chinese patients with non-cutaneous melanoma. *Clin Cancer Res* (2019) 25(21):6511–23. doi: 10.1158/1078-0432.CCR-19-0475

85. Rinaldi J, Sokol ES, Hartmaier RJ, Trabucco SE, Frampton GM, Goldberg ME, et al. The genomic landscape of metastatic breast cancer: Insights from 11,000 tumors. *PloS One* (2020) 15(5):e0231999. doi: 10.1371/journal.pone.0231999

86. Arao T, Ueshima K, Matsumoto K, Nagai T, Kimura H, Hagiwara S, et al. FGF3/FGF4 amplification and multiple lung metastases in responders to sorafenib in hepatocellular carcinoma. *Hepatology* (2013) 57(4):1407–15. doi: 10.1002/hep.25956

87. Zhao R, Choi BY, Lee MH, Bode AM, Dong Z. Implications of genetic and epigenetic alterations of CDKN2A (P16(INK4a)) in cancer. *EBioMedicine* (2016) 8:30–9. doi: 10.1016/j.ebiom.2016.04.017

88. Kung C-P, Weber JD. It's getting complicated–a fresh look at P53-MDM2-ARF triangle in tumorigenesis and cancer therapy. *Front Cell Dev Biol* (2022) 10:818744.

89. Minaei E, et al. Cancer progression gene expression profiling identifies the urokinase plasminogen activator receptor as a biomarker of metastasis in cutaneous squamous cell carcinoma. *Front Oncol* (2022) 12:835929. doi: 10.3389/fonc.2022.835929

90. Siegel PM, Massagué J. Cytostatic and apoptotic actions of TGF-β in homeostasis and cancer. *Nat Rev Cancer* (2003) 3(11):807–20. doi: 10.1038/nrc1208

91. Melisi D, Garcia-Carbonero R, Macarulla T, Pezet D, Deplanque G, Fuchs M, et al. Galunisertib plus gemcitabine vs. gemcitabine for first-line treatment of patients with unresectable pancreatic cancer. *Br J Cancer* (2018) 119(10):1208–14. doi: 10.1038/s41416-018-0246-z

92. Kim YJ, Hwang JS, Hong YB, Bae I, Seong Y-S. Transforming growth factor beta receptor I inhibitor sensitizes drug-resistant pancreatic cancer cells to gemcitabine. *Anticancer Res* (2012) 32(3):799–806.

93. Feng DD, Zhang H, Zhang P, Zheng YS, Zhang XJ, Han BW, et al. Down-regulated miR-331-5p and miR-27a are associated with chemotherapy resistance and relapse in leukaemia. *J Cell Mol Med* (2011) 15(10):2164–75. doi: 10.1111/j.1582-4934.2010.01213.x

94. Zhao D, Sui Y, Zheng X. MiR-331-3p inhibits proliferation and promotes apoptosis by targeting HER2 through the PI3K/Akt and ERK1/2 pathways in colorectal cancer. *Oncol Rep* (2016) 35(2):1075–82. doi: 10.3892/or.2015.4450

frontiers | Frontiers in Oncology

TYPE Systematic Review
PUBLISHED 23 September 2022
DOI 10.3389/fonc.2022.819051

OPEN ACCESS

EDITED BY
Colette Pameijer,
College of Medicine, The Pennsylvania State University, United States

REVIEWED BY
Alessio Giubellino,
University of Minnesota Twin Cities, United States
Ondřej Kodet,
Charles University, Czechia

*CORRESPONDENCE
Ningzheng Tai
nz_tai1970@hotmail.com

†These authors have contributed equally to this work and share first authorship

SPECIALTY SECTION
This article was submitted to Skin Cancer, a section of the journal Frontiers in Oncology

RECEIVED 20 November 2021
ACCEPTED 01 September 2022
PUBLISHED 23 September 2022

CITATION
Lei X, Zhang Y, Mao L, Jiang P, Huang Y, Gu J and Tai N (2022) Prognostic value of receptor tyrosine kinases in malignant melanoma patients: A systematic review and meta-analysis of immunohistochemistry. *Front. Oncol.* 12:819051. doi: 10.3389/fonc.2022.819051

Prognostic value of receptor tyrosine kinases in malignant melanoma patients: A systematic review and meta-analysis of immunohistochemistry

Xuan Lei[1†], Yiming Zhang[2†], Lianghao Mao[2†], Pan Jiang[2], Yumeng Huang[1], Jia Gu[1] and Ningzheng Tai[1*]

[1]Department of Burns and Plastic Surgery, Affiliated Hospital of Jiangsu University, Zhenjiang, China, [2]Department of Orthopedics, Affiliated Hospital of Jiangsu University, Zhenjiang, China

Background: Substantial evidence suggests that receptor tyrosine kinases (RTKs) are overexpressed in tumors; however, few studies have focused on the prognostic value of RTKs in melanoma.

Objectives: The objective of this study is to evaluate the association between overexpression of RTKs and survival in melanoma patients based on immunohistochemistry (IHC) analysis.

Methods: Our review is registered on PROSPERO (http://www.crd.york.ac.uk/PROSPERO), registration number CRD42021261460. Seven databases were searched, and data were extracted. We used IHC to measure the association between overexpression of RTKs and overall survival (OS), disease-free survival (DFS), progression-free survival (PFS), and clinicopathology in melanoma patients. Pooled analysis was conducted to assess the differences between Hazard Ratios along with 95% confidence intervals.

Results: Of 5,508 publications examined following the database search, 23 publications were included in this study, which included data from a total of 2,072 patients. Vascular endothelial growth factor receptor 2 (VEGF-R2) overexpression was associated with worse OS and DFS in melanoma. Furthermore, there was an association between OS and the expression of several RTKs, including epidermal growth factor receptor (EGFR), mesenchymal-epithelial transition factor (MET), vascular endothelial growth factor receptor 1 (VEGF-R1), and insulin-like growth factor 1 receptor (IGF-1R). There were no significant correlations between EGFR overexpression and worse DFS or PFS. EGFR overexpression was associated with worse OS cutaneous and nasal melanoma, but not uveal melanoma. However, MET overexpression was related to worse OS in both cutaneous and uveal melanoma. Furthermore, EGFR overexpression was associated with a worse

OS in Europe compared to other geographic areas. Moreover, EGFR and MET overexpression showed significant prognostic value in patients with the cut-off "≥10% staining".

Conclusions: Our findings build concrete evidence that overexpression of RTKs is associated with poor prognosis and clinicopathology in melanoma, highlighting RTK expression has the potential to inform individualized combination therapies and accurate prognostic evaluation.

KEYWORDS

receptor tyrosine kinases, malignant melanoma, prognostic value, survival analysis, clinicopathological features

Introduction

Malignant melanoma is a type of skin tumor with a high mortality rate. If not detected early, melanoma will deteriorate and metastasize. Malignant melanoma most frequently occurs in males aged 50–70 years, although the incidence of malignant melanoma in young people, especially females, has increased in recent years (1). The advent of immunotherapy and targeted therapy for melanoma, such as anti-programmed death ligand 1 (PD-L1) and cytotoxic T-lymphocyte associated protein 4 (CTLA-4), has improved the survival rate of melanoma patients. Despite these therapeutic advances, patients with advanced malignant melanoma often develop drug resistance. Once distant metastasis occurs, the sustained response rate to drug therapy is only about 30% (2). Therefore, it is essential to further study melanoma pathogenesis as well as identify new biomarkers and combination treatment options to effectively treat this disease.

Receptor tyrosine kinases (RTKs) are single transmembrane receptors that participate in the development and progression of a variety of tumors. In solid tumors, overexpression or mutations of RTKs promotes the malignant biological behavior of tumor cells. Additionally, RTK overexpression is closely related to the maintenance of tumor stemness, drug resistance, recurrence, and high-metastasis rate (3–6). Some RTKs, such as epidermal growth factor receptor (EGFR) and vascular endothelial growth factor receptor (VEGFR), may represent potential biomarkers that can assist in the prognostic evaluation and inform treatment options. Faião-Flores et al. demonstrated receptor tyrosine kinase-like orphan receptor 1/2 (ROR1/2) and insulin-like growth factor 1 receptor (IGF-1R) signaling were critical pathways that participated in the escape of advanced uveal melanoma from MEK inhibition (7). Some small molecule tyrosine kinase inhibitors (TKIs) targeting carcinogenic-related RTKs have been put into clinical trials (8–10). However, it is still necessary to explore the value of RTKs as a prognostic tool, which can lead to accurate diagnosis and inform individualized treatment regimens. In some cancers, a number of RTKs, including EGFR or VEGFR, have been demonstrated as prognostic markers and there are targeting drugs for individualized therapy. However, it is still unclear which RTKs may represent prognostic biomarkers in melanoma as there is minimal evidence from comprehensive analysis to prove it. The exploration of carcinogenic RTKs has become a trendy field in cancer research. Deciphering the prognostic value of RTKs from a comprehensive analysis can provide substantial evidence for clinical survival estimation and inform the use of individualized, combined therapies especially for patients with advanced melanoma.

Because substantial evidence suggests that RTKs are overexpressed in tumors; however, few studies have focused on the prognostic value of RTKs in melanoma. To determine the prognostic value of RTKs, we systematically evaluate the association between overexpression of RTKs and clinicopathological features in patients with malignant melanoma.

Materials and methods

This systematic review and meta-analysis followed the Preferred Reporting Items for Systematic Reviews and Meta-Analyses (PRISMA) guidelines and checklist. This study was preregistered on PROSPERO (https://www.crd.york.ac.uk/PROSPERO/) under number CRD42021261460.

Search strategy

Three independent reviewers (XL, YZ, LM) searched seven databases: PubMed, Cochrane, EBSCOhost, Embase, Ovid,

ScienceDirect, and Web of Science without language restriction on 1st August 2021. Our search keywords were: "Melanoma" AND ["Receptor Tyrosine Kinases" OR "EGFR (Epidermal Growth Factor Receptor)" OR "IGFR (Insulin-Like Growth Factor Receptor)" OR "PDGFR (Platelet-Derived Growth Factor Receptor)" OR "VEGFR (Vascular Endothelial Growth Factor Receptor)" OR "FGFR (Fibroblast Growth Factor Receptor)" OR "NGFR (Nerve Growth Factor Receptor)" OR "HGFR (Hepatocyte Growth Factor Receptor)" OR "EPHR (EPH Receptor)" OR "AXLR (AXL Receptor)" OR "CCKR (CCK Receptor)" OR "TIER (TIE Receptor)" OR "RYKR (RYK Receptor)" OR "DDR (Discoidin Domain Receptor)" OR "RETR (RET Receptor)" OR "ROSR (ROS Receptor)" OR "LTKR (Leukocyte Receptor)" OR "ROR (Receptor Tyrosine Kinase Like Orphan Receptor)" OR "MUSKR (Muscle Associated Receptor)" OR "LMR(Lemur Receptor)"].

Inclusion and exclusion criteria

Studies were included in our meta-analysis and systematic review if they met the following criteria: (i) clinical study of RTK expression in melanoma; (ii) patients were diagnosed with melanoma by pathological or histological examination; (iii) immunohistochemical staining (IHC) was used to detect expression of RTKs in melanoma tissue; (iv) studies provided sufficient survival information for extraction or calculation of the individual Hazard Ratios (HR) and 95% Confidential Intervals (CI). We excluded studies if they met the following exclusion criteria: (i) melanoma was diagnosed without pathological or histological examination; (ii) basic research using cell line or animal model experiment; (iii) duplicate articles; (iv) review, conference abstracts, case reports, and letters. Two trained investigators independently screened study titles, abstracts, and full-text manuscripts for eligibility and disagreements were resolved by consensus of a third investigator.

Data extraction

Two independent reviewers (PJ and YH) extracted the following data from each selected manuscript: author name, year of publication, country, median patient age, study type, tissue type, RTKs and their expression, antibody used, cut-off value, clinicopathological features, follow-up time, outcome of study (time to event variables), HRs with 95% CIs for survival data, and Kaplan–Meier curves. Survival data were obtained from Kaplan–Meier curves. For studies without HR and 95% CI, we used the methodology previously proposed by Tierney and colleagues (11). Then, a third investigator (JG) verified the accuracy of the synthesized data, and disagreements were resolved by consensus.

Quality assessment

Quality assessment was performed by two investigators (XL and JG) independently using the 20-item Reporting Recommendations for Tumor Marker Prognostic Studies (REMARK) checklist (12, 13). The detailed explanation of 20 items used the checklist of McShane LM (14). According to the 20 items, each study was characterized as fully satisfied, partially satisfied, not satisfied, unclear, and not applicable. Discrepancies were resolved by a third investigator (LM).

Statistical analysis

The primary outcomes were Overall Survival (OS), Disease-Free Survival (DFS), and Progression-Free Survival (PFS). HR measuring the association between RTKs and its prognostic data were directly extracted from studies or estimated from the Kaplan–Meier survival curves with their 95% CI. Review Manager 5.3 was used for meta-analysis. Estimates of OS, DFS, or PFS were reported using HR and 95% CI. I^2 value was used to describe heterogeneity among studies and $P<0.05$ indicated statistical significance. Subgroup analyses were used to study the prognostic value of RTKs by clinicopathological features, including disease type, geographic area, and the cut-off for each RTK marker.

Results

A total of 5,508 citations were identified from seven electronic databases (886 from PubMed, 74 from Cochrane, 285 from EBSCOhost, 2,234 from Embase, 421 from Ovid, 294 from ScienceDirect, and 1,314 from Web of Science). We excluded 5,478 studies after removing duplicates and screening titles and abstracts based on the exclusion criteria. Subsequently, 30 studies were assessed for eligibility by full-text reviewing. Among these studies, four studies were excluded due to the lack of sufficient survival data, two studies were excluded for not defining groups by RTKs expression and one was excluded because the HR or CI was not reported. Finally, 23 studies met the inclusion criteria and were selected for this meta-analysis. Among the included studies, eight studies used the Tierney method to estimate survival data from Kaplan–Meier curves due to the lack of direct survival data. The flow diagram shown in Figure 1 depicts the complete selection process.

Study characteristics

The characteristics of 23 studies are presented in Table 1, which includes a total of 2,072 patients (15–37). Sample sizes

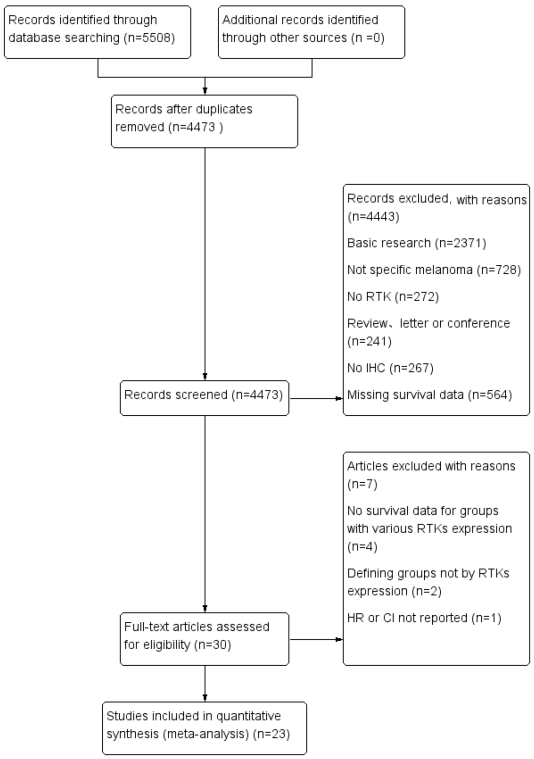

FIGURE 1
PRISMA flow diagram of selection process.

ranged from 10 to 238. A total of 12 different RTKs were evaluated: EGFR, human epidermal growth factor receptor (HER)2, HER3, HER4, IGF-1R, VEGF-R1, VEGF-R2, VEGF-R3, mesenchymal-epithelial transition factor (MET), C-KIT, EphrinA1, and EphA2. RTK relative expression, antibodies used, and cut-off of biomarkers in each study are detailed in Table 2.

Quality of eligible studies

The REMARK checklist is widely used as a guideline to analyze the reporting of tumor markers in prognostic studies. In general, the overall quality of the 23 included studies was relatively high based on the REMARK checklist (Table S1), and the detailed clarification of 20 items followed the McShane LM checklist (Table S2) (14). Most studies failed to provide the rationale for their sample size, investigate assumptions, conduct sensitivity analyses, and conduct internal validation. In addition, due to the lack of standard prognostic markers recognized by the public, none of the studies showed a comparison of RTK expression with such indicators. Several studies did not clearly define all endpoints and missed estimated effects in multivariable analyses (15, 17, 19, 22, 25, 28, 29). However, because most included studies were retrospective and fulfilled the majority of our criteria, they have provided sufficient and convincing data for a comprehensive analysis.

Association between RTKs and OS

All included studies reported on the correlation between RTKs and OS (15–37). From these studies, we found that there was an association between overexpression of RTKs and OS. Worse survival could be found in patients with overexpression of EGFR (HR = 1.36; 95% CI, 1.07-1.73, P = 0.01, I^2 = 31%), MET (HR = 1.54; 95% CI, 1.18-2.00, P = 0.001, I^2 = 6%), VEGF-R1 (HR = 2.06; 95% CI, 1.03-4.15, P = 0.04), and VEGF-R2 (HR = 2.97; 95% CI, 1.51-5.86, P = 0.002, I^2 = 0%) (Figure 2). However, there was no statistical difference between OS and IGF-1R (HR = 1.31; 95% CI, 0.92-1.87, P = 0.13, I^2 = 88%), VEGF-R3 (HR = 1.76; 95% CI, 0.99-3.14, P = 0.05, I^2 = 69%), C-KIT (HR = 0.65; 95% CI, 0.32-1.34, P = 0.24, I^2 = 48%), EphrinA1 (HR = 1.38; 95% CI, 0.20-9.40, P = 0.74, I^2 = 92%), and EphA2 (HR = 2.95; 95% CI, 0.84-10.30, P = 0.09, I^2 = 85%) (Figure S1). Sensitivity analysis showed that there was a statistical difference between OS and IGF-1R using a fixed effects model (HR = 1.50; 95% CI, 1.31-1.73, P < 0.00001) without heterogeneity after excluding one study by Al-Jamal

TABLE 1 Characteristics of included studies.

Author	Year	Country	Case	Age	Breslow thickness	Metastasis	Disease type	Follow-up	Outcome	Significant findings
Al-Jamal	2011	Finland	167	NG	NG	53 (29.52%)	uveal melanoma	20 years (16-25)	OS	IGF-IR did not independently predict metastasis from primary uveal melanoma.
Boone	2011	Belgium	114	52 years (37–64)	NG	25 (21.9%)	melanoma	33 months (17–50)	OS, DFS	EGFR involves in progression and metastasis of a subset of melanomas.
Chen	2012	China	56	44 ± 2 years (18-78)	NG	5 (8.93%)	uveal melanoma	45.8 ± 3.0 months (6-156)	OS	Overexpression of EphA2 is correlated with prognosis of choroidal melanoma.
Das	2019	Sweden	40	64 years (42–86)	NG	NG	cutaneous melanoma	NG	OS	Higher MET expression had a shorter OS in cutaneous melanoma.
Economou	2005	Sweden	132	63 years (25–85)	NG	55 (41.67%)	uveal melanoma	NG	OS	IGF-1R may play as a prognostic role in uveal melanoma.
Eliopoulos	2002	UK	51	NG	≥10 mm 51 ≤1 mm11	15 (29.41%)	melanoma	NG	OS	HER-2 overexpression has no prognostic significance in thick melanoma.
Ericsson	2002	Sweden	36	61 years (23-87)	NG	18 (50%)	uveal melanoma	138.25 ± 90.99 months (1-245)	OS	High IGF-1R expression is a predictor for the metastasis of uveal melanoma:
Giatromanolaki	2012	Greece	60	NG	≤8 mm 26 (43.33%) >8 mm 34 (56.67%)	NG	uveal melanoma	80 months (1-154)	OS	pVEGFR2/KDR was significantly related with poor prognosis of uveal melanoma.
Hurks	2000	Netherland	22	66 years (38-91)	NG	7 (31.82%)	uveal melanoma	NG	OS	EGFR expression is an important prognostic factor in human uveal melanoma.
Jafari	2018	Switzerland	238	62.3 ± 15.8 years	2.3 ± 2.7 mm	19 (25.3%)	melanoma	5.71 years	OS, DFS	VEGF-C and VEGF-R2 might be new prognostic marker in melanoma.
Katunarić	2014	Croatia	110	52.25 years (31–79)	3.8 mm (0.8–15)	NG	melanoma	NG	OS	EGFR protein overexpression is correlated with shorter OS in melanoma.
Langer	2011	Germany	10	65 years (55–75)	NG	NG	esophageal melanoma	NG	OS	Esophageal melanomas harbor genetic aberrations of c-Kit, KRAS, and BRAF.
Liu	2008	China	56	56.05 ± 11.34 years (27–81)	1.83 ± 1.03 mm (0.3–4.1)	31 (55.36%)	melanoma	NG	OS, DFS	VEGF-C and VEGF-D may be indicators for prognostic evaluation of melanoma.
Mallikarjuna	2007	India	60	45 years (9-74)	NG	6 (10%)	uveal melanoma	28.2± 32.44 months	OS	High c-Met expression is associated with death due to uveal melanoma.
Mo	2020	China	91	NG	NG	NG	melanoma	NG	OS	EphA2-high/ephrinA1-low exhibited poorer outcomes than EphA2-high/ ephrinA1-high in melanoma
Monteiro	2019	Germany	NG	NG	NG	NG	melanoma	NG	OS	High expression of VEGFR-3 is associated with poor OS in melanoma.
Nielsen	2014	Belgium	105	52 years (25–87)	2.3 mm (0.7–45.0)	105 (100%)	melanoma	NG	PFS	HER4 is associated with PFS of malignant melanoma.
Potti	2004	USA	202	57 years (15–101)	2.6 mm (0.4-8)	NG	melanoma	NG	OS	Both c-Kit and VEGF may have significant therapeutic implications in melanoma.

(Continued)

TABLE 1 Continued

Author	Year	Country	Case	Age	Breslow thickness	Metastasis	Disease type	Follow-up	Outcome	Significant findings
Reschke	2008	Germany	130	19-90 years	range 0.4-17 mm	53 (40.77%)	cutaneous melanoma	56 ± 25 months	OS	HER3 is a determinant for poor prognosis in melanoma.
Straume	2002	Norway	176	NG	NG	56 (31.82%)	recurrent melanoma	76 months (13-210)	OS	Ephrin-A1/EphA2 pathway might be important for patient survival of melanoma.
Trocmé	2012	Sweden	128	63 ± 11.9 years	NG	58 (45%)	uveal melanoma	NG	OS	Nuclear HER3 is associated with favorable overall survival in uveal melanoma.
Yoshida	2014	USA	24	60.58 ± 14.89 years	NG	24 (100%)	Metastatic uveal melanoma	NG	OS	IGF-1R expression is correlated with poor prognosis in metastatic uveal melanoma.
Zhu	2018	China	64	62 years (27–85)	NG	NG	mucosal melanoma	NG	OS	Positive HER4 expression is correlated with the prognosis in mucosal melanoma.

NG, not given.

et al. (15). Furthermore, we discovered that there existed a statistical difference of pooled effect with no heterogeneity between VEGF-R3 and OS (HR = 2.46; 95% CI, 1.45-4.19, P = 0.0009) after excluding one study by Monteiro et al. (29) by using a fixed effects model.

Association between RTKs and DFS and PFS

Three studies reported DFS as the outcome, which included a total of 408 patients (17, 26, 33). Two studies (26, 33) found a significant association between increased VEGF-R3 and worse DFS in melanoma patients (HR = 3.07; 95% CI, 1.76-5.36, P < 0.0001, I^2 = 44%) (Figure 3A). In addition, there was a significantly worse DFS in patients with overexpression of VEGF-R1 (HR = 2.50; 95% CI, 1.02-6.09, P = 0.04) and VEGF-R2 (HR = 7.35; 95% CI, 2.24-24.14, P = 0.001) (Figures 3B,C). However, one study by Boone et al. (17) reported that no significant association in patients with EGFR overexpression (HR = 3.03; 95% CI, 0.15-63.30, P = 0.47). One study by Nielsen et al. (30) found that there was no statistically significant association between high HER-4 and worse PFS (HR = 1.21; 95% CI, 0.75-1.95, P = 0.43) (Figure S2).

Association between RTKs and clinicopathological features

Nine studies (17, 21, 23, 24, 27, 30, 32, 35, 37) reported on EGFR and OS. Among them, five (17, 21, 24, 30, 32) reported on cutaneous melanoma, three (23, 27, 35) reported on uveal melanoma, and one (37) reported on nasal melanoma. We performed a subgroup analysis to assess whether the prognostic value of RTKs was related to pathology. By using a fixed effects model, we conducted a pooled analysis from six studies (17, 21, 24, 30, 32, 37), which demonstrated that EGFR overexpression was associated with significantly worse OS in patients with cutaneous melanoma (HR = 1.63; 95% CI, 1.13-2.36, P = 0.009, I^2 = 0%) and nasal melanoma (HR = 3.51; 95% CI, 1.21-10.18, P = 0.02). However, there were no significant association between EGFR overexpression and uveal melanoma (HR = 1.07; 95% CI, 0.77-1.49, P = 0.68, I^2 = 0%) (Figure 4A). Three studies (19, 20, 27) reported on the association between pathology and MET expression. MET overexpression was associated with a worse OS in cutaneous melanoma (HR = 3.23; 95% CI, 1.15-9.08, P = 0.03) and uveal melanoma patients (HR = 1.46; 95% CI, 1.11-1.92, P = 0.007, I^2 = 0%) using a fixed effects model (Figure 4B). To find whether the prognostic value of RTKs is related to geographic research area, we performed a subgroup analysis for various categories: Europe, America, and Asia. Pooled analysis of EGFR expression from seven studies (17, 21, 23, 24, 27, 30, 32, 35, 37) demonstrated that EGFR overexpression was associated with a worse OS in Europe Genesis(HR = 1.41; 95% CI, 0.95-2.10, P = 0.09, I^2 = 28%) and Asia (HR = 1.92; 95% CI, 0.78-4.75, P = 0.16, I^2 = 61%) compared to other geographic areas (Figure 4C). After excluding one study by Trocme et al. (35), a statistically significant association was found in European patients with EGFR overexpression (HR = 1.63; 95% CI, 1.13-2.36, P = 0.009, I^2 = 0). However, we could not study the overall effect of other RTKs due to the lack of sufficient studies and huge heterogeneity within the limited studies.

Association between RTKs and biomarker cut-off

Biomarker cut-offs represented an important source of heterogeneity. Among the eight studies (17, 21, 24, 27, 30, 32,

10.3389/fonc.2022.819051

TABLE 2 Expression of RTKs in studies.

Author	RTK	Antibody used for evaluation	Cut-off	RTK overexpression
Al-Jamal	IGF-1R	N-20; sc-712, Santa Cruz Biotechnology, Calif; dilution 1:500	≥ 15%	88 (68%)
Boone	EGFR	Zymed Laboratories Inc, CA, USA	≥ 10%	13 (11.4%)
Chen	EphA2	Santa Cruz, USA; dilution 1:200	moderate to strong staining	21 (62.5%)
Das	MET ERBB3	ERBB3: Cell Signaling Technologies; dilution 1:250 MET: Cell Signaling Technologies; dilution 1:300	≥ 20%	ERBB3 12 (92%) MET 9 (43%)
Economou	c-Met IGF-1R	IGF-1R: N-20, Santa Cruz Biotechnology, Inc. (Santa Cruz, CA) c-Met: ImmunKemi (Novocastra Ltd., Newcastle-upon-Tyne, UK)	≥ 10%	c-Met:75 (56.82%) IGF-1R:42 (31.82%)
Eliopoulos	HER2	DAKO Ltd, Cambridgeshire, UK	≥ 10%	15 (29.41%)
Ericsson	IGF-1R	Oncogene Science (Manhasset, NY); dilution 1:1000	≥ 50%	15 (41.67%)
Giatromanolaki	VEGFR2	34a; Oxford University, UK	≥50%	14 (23.3%)
Hurks	EGFR	R-1; Santa Cruz Biotechnology, Santa Cruz, CA; dilution 1:20	NG	6 (28.57%)
Jafari	VEGF-R1 VEGF-R2 VEGF-R3	R&D systems	NG	VEGF-R1 22 (52%) VEGF-R2 68 (57.3%) VEGF-R3 34 (52.7%)
Katunarić	EGFR	Membrane EGFR (Dako) nuclear EGFR (Leica Microsystems)	≥ 10%	NEGFR 24 (21.82%) MEGFR 31 (28.18%)
Langer	C-KIT PDGFR-A	C-KIT: A4502; Dako, Glostrup, Denmark PDGFR-A: 3164; Cell Signaling Technologies, Beverly, MA, USA	intensity > 1+	C-KIT 8 (80%) PDGFR-A 0
Liu	VEGFR-3	Santa Cruz Biotechnology, Inc., Santa Cruz, CA; dilution 1:200	≥ 10% of tumor cells ≥ 5% in endothelial cells	34 (60.71%)
Mallikarjuna	EGFR c-met	EGFR (R-1; 200 µl/ml) c-Met (DQ-13; 100 µg/ml) Santa Cruz Biotechnology, CA, USA	> 10%	EGFR 18 (30%) c-met 33 (55%)
Mo	EphrinA1 EphA2	NG	NG	EphA2 26 (28.6%) ephrinA1 28 (30.8%)
Monteiro	VEGFR-3	NG	NG	NG
Nielsen	HER-4	RB-9045-P1; Thermo Scientific; dilution 1:50	NG	NG
Potti	HER-2/neu c-Kit	A4502; IMPATH, Calif., USA	≥2+ or greater Immunostaining	HER-2/neu 2 (0.9%) c-Kit 46 (22.8%)
Reschke	HER3	clone C-17; Santa Cruz; dilution 1:50	German immunohistochemical scoring (GIS) > 6	moderate to high 85 (65%) high in metastases 35 (40%)
Straume	Ephrin-A1 EphA2	Ephrin-A1: pAb SC-911; Santa Cruz EphA2: pAb SC-924; Santa Cruz	staining index = 9	FGFR 17 (11.7%) Ephrin-A1 23 (15.8%) EphA2 23 (15.9%)
Trocmé	HER3	clone C-17; Santa Cruz; dilution 1:50	"2," strong staining intensity	42 (33%)
Yoshida	IGF-1R	Ventana Medical Systems	3+ staining intensities >85% percentages of positive cells	17 (70.83%)
Zhu	HER4	clone: PC100; Vebdor: Thermo Fisher Scientific Co., (Waltham, Massachusetts, USA); dilution 1: 300	positive tumor cells (Range: 0–100%)	45 (70.3%)

NG, not given.

35, 37) that reported on EGFR and OS, four (17, 21, 24, 27) of them used "≥10% of the tumor" as the cut-off, one (35) used "≥2+ staining", one (37) used "0–100% staining", one (32) used "German immunohistochemical scoring (GIS)>6", and one (30) did not provide a clear definition. The study that used a cut-off of "≥10% of the tumor" revealed a significant association between EGFR expression and OS (HR = 1.60; 95% CI, 1.08-2.37, P = 0.02, I^2 = 0%), whereas the rest studies did not show strong power due to the limited study quantity (Figure 5A). Three studies (19, 20, 27) reported the cut-offs for MET expression: two of them (20, 27) used "≥10%" and the other one (19) used "≥20%". A statistically significant association was found in both two cut-off categories

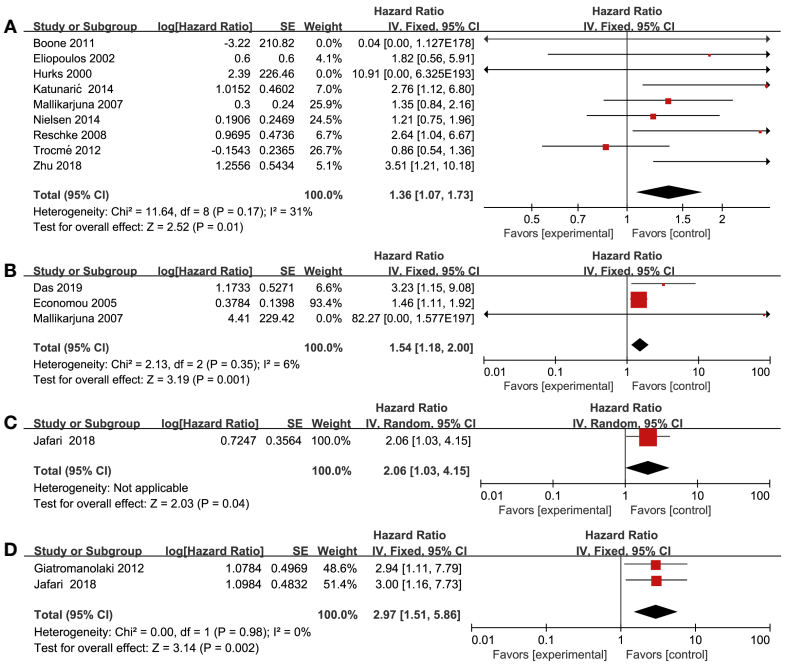

FIGURE 2
Forest plot illustrating the association between various RTKs and OS in melanoma. **(A)** EGFR, **(B)** MET, **(C)** VEGF-R1, **(D)** VEGF-R2.

("≥10%", HR = 1.46; 95% CI, 1.11-1.92, P = 0.007, I^2 = 0%) (Figure 5B). Due to the lack of studies focusing on other RTKs and biomarker cut-offs, we could not measure the pooled effect of these variables.

Discussion

To our knowledge, this is the first and largest meta-analysis that systematically explores the prognostic value of RTKs in malignant melanoma, which included 23 studies with a total of 2,072 patients. Our findings suggest that overexpression of RTKs, based on IHC analysis, is closely associated with poor prognosis in malignant melanoma patients. Furthermore, the prognostic value of the examined RTKs varied according to the clinicopathological characteristics of patients, such as pathological subtype, geographical area, and cut-offs of biomarkers, highlighting the clinical and predictive value of RTK expression.

The pooled prognostic value of RTK overexpression in melanoma has major implications for the field with respect to accurate survival estimation and the selection of individualized combination therapies. By comprehensively gathering and evaluating studies utilizing IHC analysis for resected melanoma, we innovatively investigated the relationship between overexpression of RTKs and survival outcomes. Our results indicated the prognostic value of overexpression of RTKs, including EGFR, MET, VEGF-R1, VEGF-R2, VEGF-R3, and IGF-1R. Numerous studies have reported that aberrant overexpression of RTKs were related with the pathogenesis of melanoma and these RTKs might be used as therapeutic targets. The abnormal expression and activation of EGFR are closely related to the progression and drug resistance of melanoma patients (38, 39). In our study, we also found an association between EGFR overexpression and worse OS in melanoma patients. Additionally, VEGFR has been identified as a potential therapeutic target for the treatment of melanoma, which may inhibit malignant melanoma metastasis and progression. Furthermore, several VEGFR inhibitors have been used in clinical trials to treat melanoma patients (40–42). Roger et al. found VEGFR expression can be used to evaluate chemotherapy efficacy and prognosis of melanoma patients following chemotherapy treatment (43). Our findings are consistent with their conclusions as the pooled HRs of survival data concerning VEGFR overexpression are relatively higher than other RTKs. Hepatocyte growth factor receptor (c-mesenchymal-epithelial transition factor, c-Met) is a transmembrane protein encoded by the Mesenchymal-epithelial transition factor (Met) gene, which is usually abnormally expressed in melanoma due to increased copy number, exon skipping, and gene mutations (19, 44). Several studies also found that c-MET may represent a potential

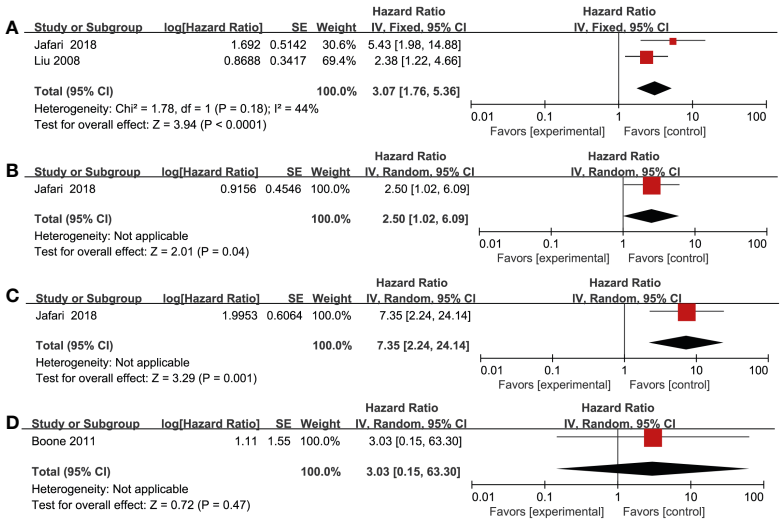

FIGURE 3
Forest plot illustrating the association between various RTKs and DFS in melanoma. **(A)** VEGF-R3, **(B)** VEGF-R1, **(C)** VEGF-R2, **(D)** EGFR.

biomarker and therapeutic target for melanoma, which warrants further exploration (45, 46). We also found that MET overexpression is associated with worse OS in melanoma patients, which could be partly explained by the oncogenic role of the Met pathway in the process of drug resistance and immune response. In addition, Villanueva et al. observed that the increased IGF-1R in post-relapse melanoma is consistent with acquired BRAF inhibitors resistance, which also confirmed the prognostic value of IGF-1R in disease progression (47). With more and more clinical trials targeting RTKs, the prognostic value of RTKs and combined therapies are expected to bring new hope to advanced melanoma patients.

In this meta-analysis, the association between the prognostic value of RTK overexpression and the clinicopathological characteristics of melanoma, including pathological subtype, geographic area, and the cut-offs for IHC analysis, was also explored. RTK expression or mutations depends on the melanoma subtype, such as mucosal melanoma (vs. cutaneous melanoma), acral lentiginous melanoma (vs. other cutaneous melanoma), and amelanotic melanoma (vs. melanotic melanoma). Due to the heterogeneity of melanoma, it is critical to investigate relevant RTKs based on their expression and prognostic value by disease subtype. By utilizing subgroup analysis, we found EGFR overexpression was associated with worse OS in cutaneous melanoma and nasal sinus melanoma, but not uveal melanoma. Moreover, MET overexpression was associated with worse OS in both cutaneous melanoma and uveal melanoma. Topcu-Yilmaz et al. suggested that EGFR overexpression was significantly correlated with clinicopathological parameters, such as mitosis rate, in uveal melanomas (48). We believe that the difference may be related to the different evaluating outcomes given we focused on survival data such as OS, PFS, and DFS. In addition, c-Kit mutations and expression were found in mucosal melanoma, acral lentiginous melanoma, and amelanotic melanoma. However, there was no significant association between OS and c-KIT in our study, which might be attributed to melanoma anatomical heterogeneity.

The incidence and prognosis of melanoma patients from various geographic regions were quite different. For instance, the proportion of acral melanoma in black patients with cutaneous melanoma was 80.0%, whereas it was relatively infrequent in Caucasian patients (49, 50). Furthermore, African descendants had more advanced disease stages and higher melanoma-specific mortality compared to Caucasians who usually had a better prognosis (51–53). In our study, we found a statistically significant association between EGFR expression and patients in Europe compared to other geographic areas. However, due to a lack of enough studies on these markers, we could not conduct a comprehensive analysis on the relationship between other RTKs and geographic factors, which might affect the geographic location-specific clinical application of RTK biomarkers for prognostic prediction.

The major strength of our study was the overall prognostic analysis of RTKs and their connection with clinicopathological characteristics. We strictly evaluated the quality of all included studies using the REMARK guidelines. We found some reports did not clearly define all endpoints and overlooked estimated effects in multivariable analyses, which were excluded from our analysis. Furthermore, we explored heterogeneity due to varying biomarker cut-offs used in different studies, which may directly

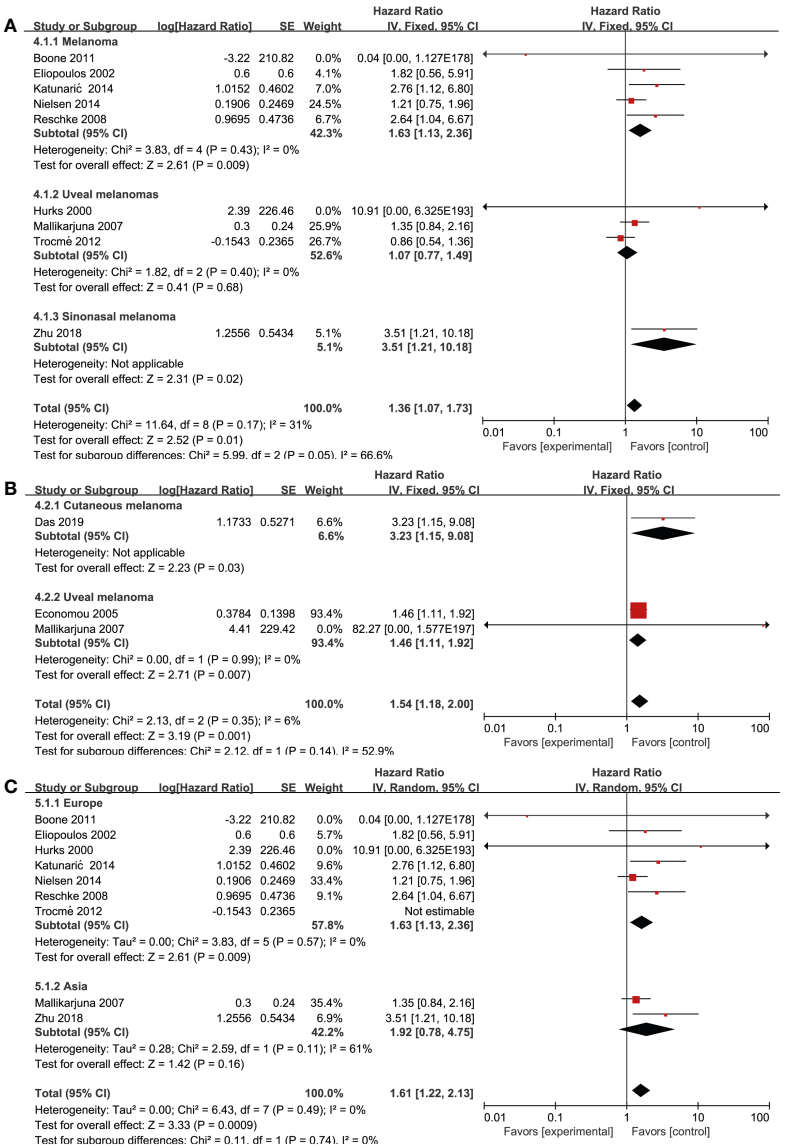

FIGURE 4
Prognosis of various RTK and clinicopathological features. **(A)** EGFR and disease type, **(B)** MET and disease type, **(C)** EGFR and geographical areas.

influence the definition of RTK overexpression. We found that studies with EGFR or MET overexpression showed significant prognostic value in patients when the cut-off "≥10% staining of tumor cells" was applied. However, some included studies did not define the specific cut-off or used different cut-off standards from staining scores or other evaluation scores such as GIS scores. Future studies should unify on the cut-offs of biomarkers to conduct homogeneous research. Besides, single-target therapies are often ineffective and prone to recurrence in cancer treatment (54). Currently, most studies focusing combining targeting RTKs with immunotherapy are confined to basic studies, although several therapies using multi-target TKIs, such as imatinib and ipilimumab, have entered clinical trials (55). Due to the existing diversity in patients' genetic subtypes and pathological characteristics, targeting prognostic RTKs with combination therapies may provide a comprehensive treatment regimen which may produce a long-term therapeutic effect and reduce immune-related adverse events.

This meta-analysis suffers from several limitations. First, due to the lack of sufficient studies reporting clinicopathology issues, such as recurrence, invasion (Breslow thickness), and distant metastasis, we could not conduct a comprehensive analysis on the relationship between these clinicopathologic variables and prognosis or survival. Also, we could not measure the

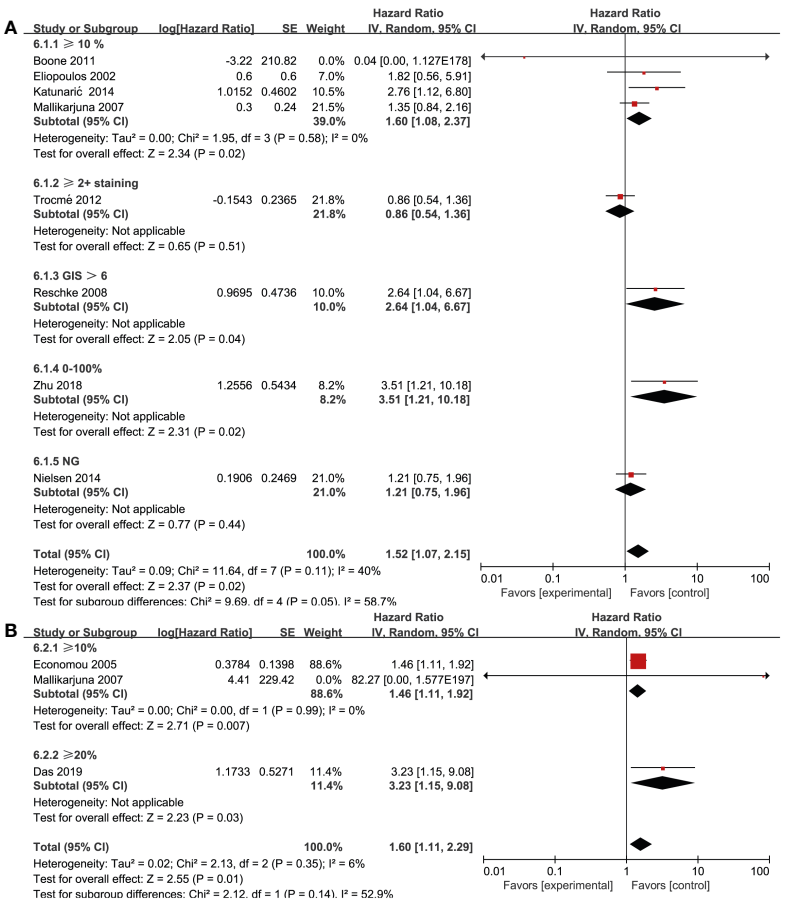

FIGURE 5
Association of various RTKs and cut-off. **(A)** EGFR, **(B)** MET.

publication bias due to the limited number of studies on each outcome. Additionally, some heterogeneity may arise due to the fact that survival data from several studies were estimated from Kaplan–Meier curves, which increased the chances of deviation to some extent. Most cases were retrospective analyses rather than randomized controlled clinical trials or prospective cohort studies, which may lead to publication bias. Finally, some RTKs have been studied extensively, whereas others are disadvantaged by limited studies. Such analysis can serve as preliminary findings on these lesser studied RTKs, although studies with large sample sizes are needed to get much more data to draw reliable conclusions.

In conclusion, our study provides concrete evidence that overexpression of RTKs is associated with poor prognosis and clinicopathology in malignant melanoma, highlighting the value of RTK in individualized combination therapies and accurate prognostic evaluation. The standard evaluating procedures and proper patients based on RTK expression should be further investigated. Randomized controlled trials or prospective cohort studies with large sample sizes are still required to comprehensively improve the prognostic application and combination therapies targeting RTKs in cancer research.

Data availability statement

The original contributions presented in the study are included in the article/Supplementary Material. Further inquiries can be directed to the corresponding author.

Author contributions

XL, YZ and NT contributed to conception and design. XL, LM and PJ contributed to the methodology. XL, YZ and LM searched the literature. PJ, YH and JG extracted the data and conducted the statistical analysis. XL, JG and LM contributed the quality assessment. XL, YZ and LM wrote the manuscript. NT

revised the manuscript. All authors contributed to the article and approved the submitted version.

Funding

This work was supported by the Postgraduate Practice Innovation Program of Jiangsu Province (SJCX20_1434).

Conflict of interest

The authors declare that the research was conducted in the absence of any commercial or financial relationships that could be construed as a potential conflict of interest.

Publisher's note

Supplementary material

The Supplementary Material for this article can be found online at: https://www.frontiersin.org/articles/10.3389/fonc.2022.819051/full#supplementary-material

References

1. Welch HG, Mazer BL, Adamson AS. The rapid rise in cutaneous melanoma diagnoses. *New Engl J Med* (2021) 384:72–9. doi: 10.1056/NEJMsb2019760

2. Versluis JM, Hendriks AM, Weppler AM, Brown LJ, de Joode K, Suijkerbuijk KPM, et al. The role of local therapy in the treatment of solitary melanoma progression on immune checkpoint inhibition: A multicentre retrospective analysis. *Eur J Cancer (Oxford Engl* (2021) 1990):151. doi: 10.1016/j.ejca.2021.04.003

3. Aldonza MBD, Ku J, Hong JY, Kim D, Yu SJ, Lee MS, et al. Prior acquired resistance to paclitaxel relays diverse EGFR-targeted therapy persistence mechanisms. *Sci Adv* (2020) 6:eaav7416. doi: 10.1126/sciadv.aav7416

4. Saraon P, Snider J, Kalaidzidis Y, Wybenga-Groot LE, Weiss K, Rai A, et al. A drug discovery platform to identify compounds that inhibit EGFR triple mutants. *Nat Chem Biol* (2020) 16:577–86. doi: 10.1038/s41589-020-0484-2

5. Zhang Y, Liu S, Zhou S, Yu D, Gu J, Qin Q, et al. Focal adhesion kinase: Insight into its roles and therapeutic potential in oesophageal cancer. *Cancer Lett* (2021) 496:93–103. doi: 10.1016/j.canlet.2020.10.005

6. Pietrobono S, Anichini G, Sala C, Manetti F, Almada LL, Pepe S, et al. ST3GAL1 is a target of the SOX2-GLI1 transcriptional complex and promotes melanoma metastasis through AXL. *Nat Commun* (2020) 11:5865. doi: 10.1038/s41467-020-19575-2

7. Faião-Flores F, Emmons MF, Durante MA, Kinose F, Saha B, Fang B, et al. HDAC inhibition enhances the *In vivo* efficacy of MEK inhibitor therapy in uveal melanoma. *Clin Cancer Res* (2019) 25:5686–701. doi: 10.1158/1078-0432.ccr-18-3382

8. Greenhalgh J, Boland A, Bates V, Vecchio F, Dundar Y, Chaplin M, et al. First-line treatment of advanced epidermal growth factor receptor (EGFR) mutation positive non-squamous non-small cell lung cancer. *Cochrane Database Syst Rev* (2021) 3:Cd010383. doi: 10.1002/14651858.CD010383.pub3

9. Cascone T, Xu L, Lin HY, Liu W, Tran HT, Liu Y, et al. The HGF/c-MET pathway is a driver and biomarker of VEGFR-inhibitor resistance and vascular remodeling in non-small cell lung cancer. *Clin Cancer Res* (2017) 23:5489–501. doi: 10.1158/1078-0432.ccr-16-3216

10. Guo R, Luo J, Chang J, Rekhtman N, Arcila M, Drilon A. MET-dependent solid tumours - molecular diagnosis and targeted therapy. *Nat Rev Clin Oncol* (2020) 17:569–87. doi: 10.1038/s41571-020-0377-z

11. Tierney JF, Stewart LA, Ghersi D, Burdett S, Sydes MR. Practical methods for incorporating summary time-to-event data into meta-analysis. *Trials* (2007) 8:16. doi: 10.1186/1745-6215-8-16

12. McShane LM, Altman DG, Sauerbrei W, Taube SE, Gion M, Clark GM. REporting recommendations for tumor MARKer prognostic studies (REMARK). *Nat Clin Pract Oncol* (2005) 2:416–22. doi: 10.1038/ncponc0252

13. Sauerbrei W, Taube SE, McShane LM, Cavenagh MM, Altman DG. Reporting recommendations for tumor marker prognostic studies (REMARK): An abridged explanation and elaboration. *J Natl Cancer Institute* (2018) 110:803–11. doi: 10.1093/jnci/djy088

14. McShane LM, Altman DG, Sauerbrei W, Taube SE, Gion M, Clark GM. Reporting recommendations for tumor marker prognostic studies (REMARK). *J Natl Cancer Institute* (2005) 97:1180–4. doi: 10.1093/jnci/dji237

15. Al-Jamal RT, Kivelä T. Prognostic associations of insulin-like growth factor-1 receptor in primary uveal melanoma. *Can J Ophthalmol* (2011) 46:471–6. doi: 10.1016/j.jcjo.2011.09.013

16. All-Ericsson C, Girnita L, Seregard S, Bartolazzi A, Jager MJ, Larsson O. Insulin-like growth factor-1 receptor in uveal melanoma: a predictor for metastatic disease and a potential therapeutic target. *Invest Ophthalmol Vis Sci* (2002) 43:1–8.

17. Boone B, Jacobs K, Ferdinande L, Taildeman J, Lambert J, Peeters M, et al. EGFR in melanoma: clinical significance and potential therapeutic target. *J Cutan Pathol* (2011) 38:492–502. doi: 10.1111/j.1600-0560.2011.01673.x

18. Chen LX, Sun BC, Li XR, He YJ, Song GX. [Overexpression of the receptor tyrosine kinase EphA2 in choroidal melanoma: correlation with vesculogenic mimicry and prognosis]. *[Zhonghua yan ke za zhi] Chin J Ophthalmol* (2012) 48:985–90. doi: 10.3760/cma.j.issn.0412-4081.2012.11.007

19. Das I, Wilhelm M, Höiom V, Franco Marquez R, Costa Svedman F, Hansson J, et al. Combining ERBB family and MET inhibitors is an effective therapeutic strategy in cutaneous malignant melanoma independent of BRAF/NRAS mutation status. *Cell Death Dis* (2019) 10:663. doi: 10.1038/s41419-019-1875-8

20. Economou MA, All-Ericsson C, Bykov V, Girnita L, Bartolazzi A, Larsson O, et al. Receptors for the liver synthesized growth factors IGF-1 and HGF/SF in uveal melanoma: intercorrelation and prognostic implications. *Invest Ophthalmol Vis Sci* (2005) 46:4372–5. doi: 10.1167/iovs.05-0322

21. Eliopoulos P, Mohammed MQ, Henry K, Retsas S. Overexpression of HER-2 in thick melanoma. *Melanoma Res* (2002) 12:139–45. doi: 10.1097/00008390-200204000-00006

22. Giatromanolaki A, Sivridis E, Bechrakis NE, Willerding G, St Charitoudis G, Foerster MH, et al. Phosphorylated pVEGFR2/KDR receptor expression in uveal melanomas: relation with HIF2α and survival. *Clin Exp Metastasis* (2012) 29:11–7. doi: 10.1007/s10585-011-9424-6

23. Hurks HMH, Metzelaar-Blok JAW, Barthen ER, Zwinderman AH, De Wolff-Rouendaal D, Keunen JEE, et al. Expression of epidermal growth factor receptor: Risk factor in uveal melanoma. *Invest Ophthalmol Visual Sci* (2000) 41:2023–7.

24. Katunaric M, Jurisic D, Petkovic M, Grahovac M, Grahovac B, Zamolo G. EGFR and cyclin D1 in nodular melanoma: correlation with pathohistological parameters and overall survival. *Melanoma Res* (2014) 24:584–91. doi: 10.1097/cmr.0000000000000123

25. Langer R, Becker K, Feith M, Friess H, Hofler H, Keller G. Genetic aberrations in primary esophageal melanomas: molecular analysis of c-KIT, PDGFR, KRAS, NRAS and BRAF in a series of 10 cases. *Modern Pathol* (2011) 24:495–501. doi: 10.1038/modpathol.2010.220

26. Liu BQ, Ma J, Wai XL, Su F, Li XM, Yang SC, et al. Lymphangiogenesis and its relationship with lymphatic metastasis and prognosis in malignant melanoma. *Anatomical Record-Advances Integr Anat Evolutionary Biol* (2008) 291:1227–35. doi: 10.1002/ar.20736

27. Mallikarjuna K, Pushparaj V, Biswas J, Krishnakumar S. Expression of epidermal growth factor receptor, ezrin, hepatocyte growth factor, and c-met in

uveal melanoma: An immunohistochemical study. *Curr Eye Res* (2007) 32:281–90. doi: 10.1080/02713680601161220

28. Mo J, Zhao X, Dong X, Liu T, Zhao N, Zhang D, et al. Effect of EphA2 knockdown on melanoma metastasis depends on intrinsic ephrinA1 level. *Cell Oncol (Dordrecht)* (2020) 43:655–67. doi: 10.1007/s13402-020-00511-x

29. Monteiro AC, Muenzner JK, Andrade F, Rius FE, Ostalecki C, Geppert CI, et al. Gene expression and promoter methylation of angiogenic and lymphangiogenic factors as prognostic markers in melanoma. *Mol Oncol* (2019) 13:1433–49. doi: 10.1002/1878-0261.12501

30. Nielsen TO, Poulsen SS, Journe F, Ghanem G, Sorensen BS. HER4 and its cytoplasmic isoforms are associated with progression-free survival of malignant melanoma. *Melanoma Res* (2014) 24:88–91. doi: 10.1097/cmr.0000000000000040

31. Potti A, Moazzam N, Langness E, Sholes K, Tendulkar K, Koch M, et al. Immunohistochemical determination of HER-2/neu, c-kit (CD117), and vascular endothelial growth factor (VEGF) overexpression in malignant melanoma. *J Cancer Res Clin Oncol* (2004) 130:80–6. doi: 10.1007/s00432-003-0509-8

32. Reschke M, Mihic-Probst D, van der Horst EH, Knyazev P, Wild PJ, Hutterer M, et al. HER3 is a determinant for poor prognosis in melanoma. *Clin Cancer Res* (2008) 14:5188–97. doi: 10.1158/1078-0432.ccr-08-0186

33. Seyed Jafari SM, Wiedmer C, Cazzaniga S, Frangež Ž., Shafighi M, Beltraminelli H, et al. Correlation of vascular endothelial growth factor subtypes and their receptors with melanoma progression: A next-generation tissue microarray (ngTMA) automated analysis. *PLoS One* (2018) 13:e0207019. doi: 10.1371/journal.pone.0207019

34. Straume O, Akslen LA. Importance of vascular phenotype by basic fibroblast growth factor, and influence of the angiogenic factors basic fibroblast growth factor/fibroblast growth factor receptor-1 and ephrin-A1/EphA2 on melanoma progression. *Am J Pathol* (2002) 160:1009–19. doi: 10.1016/S0002-9440(10)64922-X

35. Trocme E, Mougiakakos D, Johansson CC, All-Eriksson C, Economou MA, Larsson O, et al. Nuclear HER3 is associated with favorable overall survival in uveal melanoma. *Int J Cancer* (2012) 130:1120–7. doi: 10.1002/ijc.26118

36. Yoshida M, Selvan S, McCue PA, DeAngelis T, Baserga R, Fujii A, et al. Expression of insulin-like growth factor-1 receptor in metastatic uveal melanoma and implications for potential autocrine and paracrine tumor cell growth. *Pigment Cell Melanoma Res* (2014) 27:297–308. doi: 10.1111/pcmr.12206

37. Zhu W, Li S, Zou B, Liu H, Wang S. Expressions and clinical significance of HER4 and CD44 in sinonasal mucosal malignant melanoma. *Melanoma Res* (2018) 28:105–10. doi: 10.1097/CMR.0000000000000428

38. Wang J, Huang SK, Marzese DM, Hsu SC, Kawas NP, Chong KK, et al. Epigenetic changes of EGFR have an important role in BRAF inhibitor-resistant cutaneous melanomas. *J Invest Dermatol* (2015) 135:532–41. doi: 10.1038/jid.2014.418

39. Ji Z, Erin Chen Y, Kumar R, Taylor M, Jenny Njauw C-N, Miao B, et al. MITF modulates therapeutic resistance through EGFR signaling. *J Invest Dermatol* (2015) 135:1863–72. doi: 10.1038/jid.2015.105

40. Li J, Qin S, Xu RH, Shen L, Xu J, Bai Y, et al. Effect of fruquintinib vs placebo on overall survival in patients with previously treated metastatic colorectal cancer: The FRESCO randomized clinical trial. *JAMA* (2018) 319:2486–96. doi: 10.1001/jama.2018.7855

41. Albiges L, Barthélémy P, Gross-Goupil M, Negrier S, Needle MN, Escudier B. TiNivo: safety and efficacy of tivozanib-nivolumab combination therapy in patients with metastatic renal cell carcinoma. *Ann Oncol* (2021) 32:97–102. doi: 10.1016/j.annonc.2020.09.021

42. Schöffski P, Mir O, Kasper B, Papai Z, Blay JY, Italiano A, et al. Activity and safety of the multi-target tyrosine kinase inhibitor cabozantinib in patients with metastatic gastrointestinal stromal tumour after treatment with imatinib and sunitinib: European organisation for research and treatment of cancer phase II trial 1317 'CaboGIST'. *Eur J Cancer (Oxford England: 1990)* (2020) 134:62–74. doi: 10.1016/j.ejca.2020.04.021

43. Mouawad R, Spano JP, Comperat E, Capron F, Khayat D. Tumoural expression and circulating level of VEGFR-3 (Flt-4) in metastatic melanoma patients: correlation with clinical parameters and outcome. *Eur J Cancer* (2009) 45:1407–14. doi: 10.1016/j.ejca.2008.12.015

44. Song KY, Desar S, Pengo T, Shanley R, Giubellino A. Correlation of MET and PD-L1 expression in malignant melanoma. *Cancers (Basel)* (2020) 12(7). doi: 10.3390/cancers12071847

45. Barisione G, Fabbi M, Gino A, Queirolo P, Orgiano L, Spano L, et al. Potential role of soluble c-met as a new candidate biomarker of metastatic uveal melanoma. *JAMA Ophthalmol* (2015) 133:1013–21. doi: 10.1001/jamaophthalmol.2015.1766

46. Puri N, Ahmed S, Janamanchi V, Tretiakova M, Zumba O, Krausz T, et al. C-met is a potentially new therapeutic target for treatment of human melanoma. *Clin Cancer Res* (2007) 13:2246–53. doi: 10.1158/1078-0432.ccr-06-0776

47. Villanueva J, Vultur A, Lee JT, Somasundaram R, Fukunaga-Kalabis M, Cipolla AK, et al. Acquired resistance to BRAF inhibitors mediated by a RAF kinase switch in melanoma can be overcome by cotargeting MEK and IGF-1R/PI3K. *Cancer Cell* (2010) 18:683–95. doi: 10.1016/j.ccr.2010.11.023

48. Topcu-Yilmaz P, Kiratli H, Saglam A, Söylemezoglu F, Hascelik G. Correlation of clinicopathological parameters with HGF, c-met, EGFR, and IGF-1R expression in uveal melanoma. *Melanoma Res* (2010) 20:126–32. doi: 10.1097/CMR.0b013e328335a916

49. De Wet J, Tod B, Visser WI, Jordaan HF, Schneider JW. Clinical and pathological features of acral melanoma in a south African population: A retrospective study. *South Afr Med J = Suid-Afrikaanse Tydskrif vir Geneeskunde* (2018) 108:777–81. doi: 10.7196/SAMJ.2018.v108i9.13435

50. Dika E, Veronesi G, Altimari A, Riefolo M, Ravaioli GM, Piraccini BM, et al. BRAF, KIT, and NRAS mutations of acral melanoma in white patients. *Am J Clin Pathol* (2020) 153:664–71. doi: 10.1093/ajcp/aqz209

51. Shaikh WR, Dusza SW, Weinstock MA, Oliveria SA, Geller AC, Halpern AC. Melanoma thickness and survival trends in the united states, 1989 to 2009. *J Natl Cancer Institute* (2016) 108(1). doi: 10.1093/jnci/djv294

52. Anaba EL. Comparative study of cutaneous melanoma and its associated issues between people of African decent and caucasians. *Dermatologic Ther* (2021) 34:e14790. doi: 10.1111/dth.14790

53. Mahendraraj K, Sidhu K, Lau CSM, McRoy GJ, Chamberlain RS, Smith FO. Malignant melanoma in African-americans: A population-based clinical outcomes study involving 1106 African-American patients from the surveillance, epidemiology, and end result (SEER) database (1988-2011). *Med (Baltimore)* (2017) 96:e6258. doi: 10.1097/md.0000000000006258

54. Liguoro D, Fattore L, Mancini R, Ciliberto G. Drug tolerance to target therapy in melanoma revealed at single cell level: What next? *Biochim Biophys Acta Rev Cancer* (2020) 1874:188440. doi: 10.1016/j.bbcan.2020.188440

55. Reilley MJ, Bailey A, Subbiah V, Janku F, Naing A, Falchook G, et al. Phase I clinical trial of combination imatinib and ipilimumab in patients with advanced malignancies. *J Immunother Cancer* (2017) 5:35. doi: 10.1186/s40425-017-0238-1

frontiers | Frontiers in Oncology

TYPE Original Research
PUBLISHED 14 November 2022
DOI 10.3389/fonc.2022.903554

OPEN ACCESS

EDITED BY
Wen-Qing Li,
Beijing Cancer Hospital, Peking University, China

REVIEWED BY
Luca Falzone,
G. Pascale National Cancer Institute Foundation (IRCCS), Italy
Ronald Wong,
Institute of Molecular Biology, Germany

*CORRESPONDENCE
RongYi Chen
rongyichen_smu@smu.edu.cn
Zuhua Wang
wangrui551601@163.com

†These authors have contributed equally to this work

SPECIALTY SECTION
This article was submitted to Skin Cancer, a section of the journal Frontiers in Oncology

RECEIVED 24 March 2022
ACCEPTED 12 October 2022
PUBLISHED 14 November 2022

CITATION
Zhang J, Yang H-Z, Liu S, Islam MO, Zhu Y, Wang Z and Chen R (2022) PCDH9 suppresses melanoma proliferation and cell migration. *Front. Oncol.* 12:903554. doi: 10.3389/fonc.2022.903554

PCDH9 suppresses melanoma proliferation and cell migration

Jiaojiao Zhang[1,2†], Hui-Zhi Yang[3†], Shuang Liu[1†], Md Obaidul Islam[4], Yue Zhu[5,6], Zuhua Wang[5,6*] and RongYi Chen[1*]

[1]Dermatology Department, Dermatology Hospital, Southern Medical University, Guangzhou, Guangdong, China, [2]College of Food and Health, Zhejiang Agriculture and Forestry University, Hangzhou, Zhejiang, China, [3]The Seventh Affiliated Hospital of Southern Medical University, Foshan, Guangdong, China, [4]Department of Surgery, University of Miami, Miami, FL, United States, [5]College of Pharmaceutical Sciences, Guizhou University of Traditional Chinese Medicine, Guiyang, Guizhou, China, [6]Nano-drug Technology Research Center at Guizhou University of Traditional Chinese Medicine, Guiyang, Guizhou, China

Background: Melanoma has dramatically increased during last 30 years with low 5-year survival and prognosis rate.

Methods: Melanoma cells (A375 and G361) were chosen as the *in vitro* model. The immunohistochemical (IHC) analysis and bioinformatics mining exhibited the suppression of PCDH9 on melanoma. The interference and overexpression of PCDH9 were infected by lentivirus. The effects of PCDH9 on melanoma cells were assessed in terms of alteration of PCDH9 such as cell viability, apoptosis, cell cycle, and wound-healing assay. Moreover, expressions of PCDH9 with other genes (MMP2, MMP9, CCND1, and RAC1) were also assessed by PCR.

Results: The alteration of PCDH9 has a negative correlation with MMP2, MMP9, and RAC1 but had a positive correlation with CCND1 (Cyclin D1) and apoptosis. Increase of PCDH9 could suppress melanoma cells and inhibit migration but not exert significant effects on cell cycle. IHC showed lower PCDH9 expression in melanoma tissue with main expression in cytoplasm.

Conclusion: Overexpressed PCDH9 suppressed melanoma cells, and PCDH9 can be considered as an independent prognostic factor for melanoma; even re-expression of PCDH9 can serve as a potential therapeutic strategy for melanoma treatment.

KEYWORDS

PCDH9, RAC1, melanoma cell suppression, MMP2, MMP9, CCND1 (Cyclin D1)

Abbreviations: ALM, acral lentiginous melanoma; CCK-8, Cell Counting Kit-8; HCC, hepatocellular carcinoma; IHC, immunohistochemical; MM, malignant melanoma; MMPs, metalloproteinases; PCDH9, protocadherin-9; RAC1, Ras-related C3 botulinum toxin substrate 1.

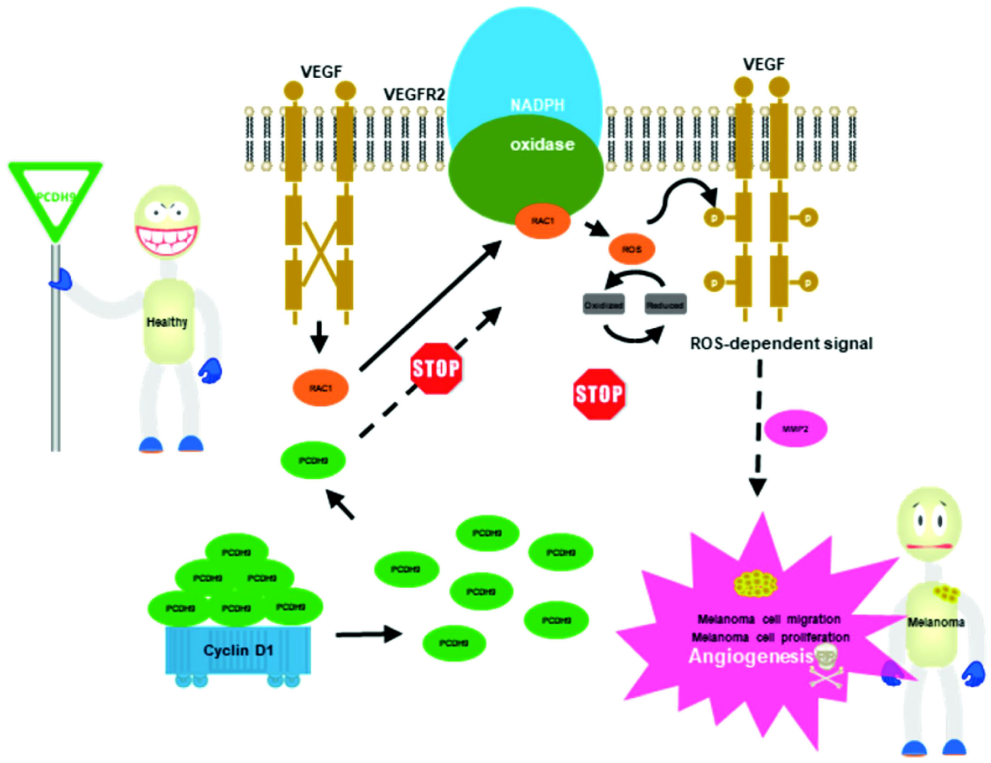

GRAPHICAL ABSTRACT
Proposed model for the role of PCHD9 regulates melanoma. Increase of PCDH9 suppressed NADPH oxidase activity, decreased ROS generation, and ROS-induced angiogenesis. PCDH9 can target complex-bound Rac1 to weaken angiogenesis by regulating NADPH oxidase, ROS production, and DNA damage susceptibility through cyclin D1 trafficking. VEGF binding to VEGFR2 leads to activating and translocating RAC1 into the plasma membrane. Whereas ROS-dependent signaling events may trigger angiogenesis (i.e., cell migration and proliferation) and influence MMP2 that affect growth factor and tumor promoter stimulation as well.

Introduction

Cutaneous melanoma, a type of skin cancer, develops in melanocytes, which takes up to 2% of all cancer deaths globally (1). The incidence rates of cutaneous melanoma are quite different among countries: lower incidence in Asia than in the West due to genetic sensitivity responses among populations. According to WHO's Global Health Estimates, there are 0.43–0.48 new cases per 100,000 people in East and Southeast Asia, whereas 12.6–18.8 new cases per 100,000 people in North America and Europe each year (1). The prognosis of melanoma varies in different diagnostic stages: a 5-year survival rate of 98% for patients with non-metastatic cutaneous melanomas compared with 62% and 16% for patients suffering regional and distant metastatic melanoma, respectively (2). The melanoma characters of Asian and European population are different in subtypes frequencies, risk factors, and mutation patterns (3). Although the incidence rate of cutaneous melanoma is lower in the Asian population, the mortality rate is higher and commonly with poorer prognosis (4). Therefore, the existing studies based on the Caucasian populations are not suitable for melanoma in Asian countries. For the above reason, we conduct the study of melanoma inhibition by resveratrol and found that this natural product can suppress A375 (a melanoma cell line) along with protein expression fluctuation (PCDH9, RAC1, and Cyclin D1) (5). On the basis of this, the Chinese patients' skin biopsy was assessed by immunohistochemistry (IHC) following the work by Dinehart et al. (6), in which the varieties of protocadherin 9 (PCDH9) expressions were found among patients' skin, normal skin, and pigmented nevus tissue.

PCDH9 belongs to protocadherin, which constitutes the largest subfamily of cadherin group (including type I classical cadherins, type II atypical cadherins, desmosomal cadherins, flamingo cadherins, and protocadherin) (7). The protocadherin subfamily is calcium-dependent cell-cell adhesion molecules that revealed six extracellular cadherin repeats with conserved calcium ion–binding domain (8). The focused PCDH9, a member of δ1-subfamily (including PCDH1, PCDH7, PCDH9, and PCDH11), is involved in cell adhesion establishment and

disruption (9). Previous studies have revealed a strong correlation between δ-PCDHs and tumor suppressor, along with the low expressions of δ-PCDH that correlate with poor prognosis. Meanwhile, studies found that δ-PCDH inhibits tumor cell proliferation by regulating cell proliferation (10). In addition, studies found that the overexpression of PCDH9 could suppress different cancers (11, 12) and tumor cells by arresting cell cycle at G0/G1 phase (13, 14). However, scarce data of PCDH9 focus on inhibiting melanoma. Moreover, the role of P-cadherin behaves differently depending on tumor cell context (15). Interestingly, melanoma cells represent unique response to cadherins. Unlike tissues like bladder (16, 17), the effective role of P-cadherin exhibits suppressive behavior on melanoma, whose membranous expression decreased at the metastatic stage (18, 19). RAC1, a GTPase, has been studied profoundly as a conserved member of RHO family and has been recognized as a central signaling hub for oncogene transforming. Meanwhile, some investigations discover its activating mutations in malignancies especially malignant melanoma (20). In addition, RAC1 expression correlates with melanocyte proliferation and can evade immune checkpoint (21). RAC1 also plays important roles in tumor biology by modulating cell processes (22, 23). Hence, RAC1 is a good indicator to reflect the effect of PCDH9 on melanoma. RAC1 functions as a molecule switch between active guanosine triphosphate (GTP)-bound and inactive guanosine diphosphate (GDP)-bound states through conformation changes closed to the nucleotide-binding site (7). RAC1 could affect cellular adhesion, migration, and invasion (24), and it plays important roles in tumor biology by modulating cell processes (22, 23). Furthermore, the activities of RAC1 have been reported to involve different stages of oncogenesis, such as initiation, progression, invasion, and metastasis (25), even it was ranked as the third most frequently occurring mutation in melanoma induced by UV (26, 27). In addition, some reported reactive oxygen species (ROS) involve in tumor cell migration and invasion (28, 29), and a key component of NAPDH-oxidase complex is formed by RAC1, one of the major enzymatic sources of ROS in various tissues (30). However, it is reported that RAC1-dependent nicotinamide adenine dinucleotide phosphate (NADPH) oxidase complex is involved in endothelial migration by mediation of angiotensin-1 (Ang-1) and vascular endothelial growth factor (VEGF) (31, 32). As known, the endothelial migration is essential for tumor cell invasion, where RAC1–NADPH oxidase complex induce expression of matrix metalloproteinases (MMPs) after growth factor and tumor promoter stimulation (33, 34). MMPs are involved in extracellular matrix (ECM) regulation, which is important in the maintenance of microenvironment and homeostasis (35). MMP2 and MMP9 belonging to MMPs are classified as gelatinases. Moreover, several studies demonstrated the important role of MMPs in melanoma (35). MMP2 has high expression levels in primary nodular melanoma that is the predominant subtype in Yogyakarta, Indonesia (1, 36). In addition, MMP2 has been believed to act as a pro-tumorigenic and pro-metastatic factor in different cancers including melanoma (37), whereas MMP9 shares the similar effect on tumor that can reconstruct the ECM to make tumor invasive process easier along with highest presence in tumor development (including melanoma). MMP9 has also been considered as an indicator of invasiveness in malignant melanoma and a marker of treatment by BRAF (B-Raf proto-oncogene, serine/threonine kinase) inhibitors, a common genetic mutation in melanoma (38). Hence, MMP2 and MMP9 were chosen as tumorigenic indicators to exhibit the correlation between PCDH9 and melanoma suppression. CCND1 encodes Cyclin D1 protein that belongs to highly conserved cyclin family that exhibits periodicity abundance throughout cell cycle. Cyclin D1–CDK4 complex regulates cell cycle during G1/S transition. Cyclin D1 is the component of ternary complex (Cyclin D1/CDK4/CDKN18) and is required for the Cyclin D1–CDK4 complex translocation. CCND1 was selected to compare with the cell cycle assay due to our previous investigation of melanoma inhibition by resveratrol (5).

According to previous studies of ours and others, the main objective of this investigation is to clarify the role of PCDH9 in melanoma and to provide evidence and a novel possible treatment of melanoma. Certain assays (cell viability, apoptosis and cell cycle assays, and PCR) were performed to explore the alteration influence of PCDH9 in melanoma cells. Currently, we found that the following: 1) overexpression of PCDH9 could suppress melanoma cells and inhibit migration; 2) the alteration of PCDH9 had a negative correlation with MMP2, MMP9, and RAC1 but positive correlation with CCND1 (Cyclin D1) and apoptosis; 3) although the cell regulator gene, CCND1 (Cyclin D1) altered with PCDH9 but did not exert significant effects on cell cycle; and 4) the IHC results exhibited the lower positive percentage of PCDH9 expression in human melanoma tissue than in normal skin or/and pigmented nevus tissue, and IHC also showed the PCDH9 expression in melanoma tissue and mainly expressed in the cytoplasm. It suggests that Cyclin D1 (CCND1) could affect tumorigenesis by mechanism of nuclear trafficking (39) but not *via* cell regulating. Together, our results reveal that the alteration of PCDH9 expression could suppress melanoma proliferation and cell migration.

Material and methods

Chemical and antibodies

Dulbecco's modified Eagle's medium (DMEM), fetal bovine serum (FBS), phosphate buffer solution (PBS) (pH = 7.2), Diethyl Pyrocarbonate (DEPC)-treated water (Ambion), and

TRIzol reagent (Invitrogen) were purchased from Gibco (Thermo Fisher Scientific, Shanghai, China); ethanol (70%), isopropyl alcohol, and Triton X-100 were bought from Sigma-Aldrich (Shanghai, China); Cell Counting Kit-8 (CCK-8) was bought from Dongren Chemical Technology (Shanghai, China); GV358-PCDH9 lentivirus and GV358-siRNA (short interfering RNA) lentivirus were designed by GeneChem (Shanghai, China); SYBR® Premix Ex Taq™ Ex Taq ™ II and PrimeScript™ RT reagent Kit with gDNA Eraser were bought from Takara Bio Inc. (Beijing, China); water was obtained from EPED-20TF (Nanjing, China).

Cell culture

Both cell lines A375 and G361 (ATCC® CRL-1619™) were bought from the American Type Culture Collection (ATCC) (MD, USA). They were grown in DMEM supplemented with 10% heat-inactivated FBS as well as penicillin (100 IU/ml) and streptomycin (100 μg/ml). Cells were maintained in a CO_2 incubator at 37°C under a humidified atmosphere (95% air, 5% CO_2).

Sample collection and preparation

Tissues [human normal skin tissue (n = 45), human pigmented nevus (n = 30), and primary malignant melanoma tissue (n = 30)] were collected and prepared as paraffin specimens until use. These tissues were ethically acquired from the outpatient clinic of the Affiliated Hospital of Guangdong Medical University with Chinese population (Han people) with personal identifiers redacted. The protocol of biopsy was proceeded according to the Ethical Committee of Guangzhou Medical University (PJ2015055KT).

Immunohistochemical stains

The paraffin specimens were deparaffinizated including two 100% xylene changes (xylene I, 10 min; xylen II, 10 min) followed by rehydration with a graded series of ethanol (anhydrous ethanol I, 5 min; anhydrous ethanol II, 5 min; 95%, 85%, and 75% ethanol, 5 min each) and then rinsed under distilled running water for 3–5 min. Antigen retrieval consisted of a 2-min incubation of slides in citric acid retrieval solution heated to 98°C with a commercial steamer following a cool down step to room temperature (cold water and ice pack were added), slides were transferred into a wet box and were then rinsed three times with PBS. After protein blocking, primary antibodies (1:200) (anti-PCDH9, Sigma-Aldrich; lot #; HPA015581) were incubated at 4°C overnight. After being in room temperature for 30 min, the slides were washed three times with PBS for 3 min each. After removing PBS and protein blocking, secondary antibodies (1:1,000) were added at room temperature for 1 h. The slides were then washed three times with PBS for 3 min each. After removing PBS, one drop of the prepared Diaminobenzidine (DAB) solution (1 ml A:1 drop B:1 drop C) for DAB staining was added, and the slides were observed under a microscope. After being rinsed in running water for 10 min, hematoxylin was added for 1 min, and then, the slides were washed by water for 5 min. The slides were then dehydrated in a series of ethanol (75%, 85%, 95%, and 100%) and 100% xylene changes and mounted with a coverslip with dry neutral resin.

Evaluation of various protein expressions in MM

Various protein expressions in MM were evaluated by semi-quantitative analysis, according to the staining intensity and the percentage of positive cells. The score standards of staining intensity were as follows: no coloration, 0; low intensity (light yellow), 1; medium intensity (light brown), 2; and high intensity (dark brown), 3. Five fields of view were randomly selected under a microscope (×400), and 500 cells were counted as one unit; meanwhile, the percentage of positive cells was calculated. The percentage scores were as follows:<5%, 0; 6%–25%, 1; 26% ~50%, 2; 51%~75%, 3; and >75%, 4. The score standards were the product of staining intensity and percentage of positive cells: 0, negative (−); 1 to 4, positive (+); 5 to 8, moderately positive (++); and 9 to 12, strongly positive (+++).

Survival analysis

Gene Expression Profiling Interactive Analysis (GEPIA) is web server for comprehensive expression analyses (40). This web-based tool is based on The Cancer Genome Atlas (TCGA) (41) and Genotype-Tissue Expression (GTEx) (42). The GEPIA web server provides survival analysis. GEPIA was used to analyze the tumor metastasis indicators of this study, i.e., MMP2.

Transfection

Melanoma cells (A375 and G361) were seeded in six-well plates (1×10^5 cell per well) the day before transfection and were transfected by two types of lentiviruses (siRNA and PCDH9) (S3). Control groups were transfected with the empty vector. Blank groups were treated with transfection reagent only. Transfection was performed using GeneChem Transfection

Reagent (Shanghai, China), according to the manufacturer's instructions. Seventy-two hours after transfection, cells were observed by a fluorescent inverted microscope as screened by puromycin. The efficiency of PCDH9 alteration in melanoma cells was detected by real-time PCR.

Cell viability by Cell Counting Kit-8

Cells were seeded into 96-well plates at a density of 2×10^5 cells per well and treated by non-transfected plasmid, transfected with empty plasmid, and transfected with PCDH9-overexpressed plasmid as explained above. After incubation at 24, 48, 72, and 96 h, 10 µl of CCK-8 was added to each well, and cells were incubated for another 4 h at 37°C. The level of colored formazan derivative was analyzed on Thermo Scientific Multiskan FC (Vantaa, Finland) at a wavelength of 450 nm. The viable cells were directly proportional to the formazan production, and the percentage of viable ones was calculated. Equations 1 and 2 were utilized to determine the viability rate and inhibition rate, respectively

$$V\,\% = \frac{As - Ab}{Ac - Ab} \times 100\,\% \qquad \text{(Equation 1)}$$

$$I\,\% = \frac{Ac - As}{Ac - Ab} \times 100\,\% \qquad \text{(Equation 2)}$$

V%: the viability rate;

A_s: the absorbing values of experimental wells (cells with medium, CCK-8, and PCDH9-overexpressed plasmid);

A_b: the absorbing values of blank wells (medium, CCK-8, and empty plasmid);

A_c: the absorbing values of control wells (cells with medium and CCK-8);

I%: the inhibition rate.

Apoptosis detection by flow cytometer

Apoptosis was analyzed by cytometric analysis, using FITC Annexin V Apoptosis Detection Kit (BD, USA). Cells were seeded in six-well plate at a density of 1×10^6 cells per well. Briefly, cells were treated with Camptothecin stock solution (10 mg of lyophilized powders were dissolved in 2.87 ml of Dimethyl Sulfoxide (DMSO) to make 10 mM stock solution; 1 µl was used) and incubated for 5 h at 37°C. After that, the cells were centrifuged (1,000 rpm for 10 min), washed twice with cold PBS, and resuspended in 1× binding; 5 µl of FITC Annexin V and 5 µl of PI (Bio-Rad) were added to cell suspension, incubated, and protected from light for 15 min at room temperature. Finally, samples were analyzed using the BD FACS Canto II flow cytometer.

Cell cycle assay

Cell cycle was analyzed using the flow cytometry. Briefly, cells were seeded in six-well plates at a density of 1×10^6 cells per well. Cells were then detached, centrifuged at (1,000 rpm for 10 min), and then vortexed with 5 ml of cold 75% ethanol. Cells were incubated at −20°C for 2 h and washed twice with PBS to remove ethanol. Cells were resuspended in 0.5 ml of PI/RNase staining buffer (Bio-Rad) for 15 min at room temperature; samples were analyzed using the BD FACS Canto II flow cytometer.

Wound-healing assay

Cells were seeded into six-well plates at a density of 1.5×10^5 cells per well until confluency of 80%–100% is reached and then scratched by a sterile 10-µl pipette tip. Cells were washed twice with PBS; then, a complete medium was added to allow cells moving into the gap and photographed by using an inverted microscope DMI3000B (Leica, Germany) at 0, 24, and 48 h. ImageJ (MD, USA) was used to measure the wound space. Migration rate was calculated as the proportion of initial scratch distant of each sample and the mean distance between the borderlines of the remaining free cells after migration.

Quantitative real-time PCR analysis

Each frozen pellet of melanoma cells (A375 and G361), treated in different experimental conditions, was homogenized in a lysis buffer. Total RNA was isolated through the TRIzol Reagent Total RNA isolation system (Thermo Fisher Scientific, USA) according to the manufacturer's reference guide. Total RNA was quantified by nanodrop and was reverse-transcribed by a PrimeScript RT reagent kit (TaKaRa) and referred to SYBR Green qPCR assay introduction (SYBR® Premix Ex TaqTM II kit) by MasterCycler Gradient PCR (Thermo Fisher Scientific, USA). The reaction mixture (20 µl) was taken and incubated for 3 min at 95°C. Quantification of genes was performed with the $2^{-\Delta\Delta CT}$ method, as described previously (43): The sample was cycled (95°C, 10 s; 60°C, 20 s) for 40 times by the ABI7500Fast Real-time PCR System Amplifier (Thermo Fisher Scientific, USA). The primers designed for selected genes (PCDH9, CCND1, MMP2, MMP9, and RAC1) and amplicon sizes are shown in Supplementary Table S1.

Statistical analysis

Data are shown as means ± SEM from at least three independent experiments. Two-tailed Student's t-test was used

to compare differences between two groups. One-way ANOVA followed by least significant difference *post hoc* tests was used to compare differences among three or more groups (Originlab 2020, Northampton, MA, USA). A value of $p< 0.05$ was considered statistically significant, whereas a value of $p< 0.01$ was considered highly statistically significant. *$p< 0.05$, **$p< 0.01$, and ***$p< 0.001$.

Results

PCDH9 protein expressed differences in normal skin, pigmented nevus, and melanoma tissue tested by IHC stains

IHC results showed that the positive percentage of PCDH9 expression was lower in human melanoma tissue than in normal skin or/and pigmented nevus tissue; in addition, PCDH9 was mainly expressed in the cytoplasm, whereas a small amount was expressed in the nuclei. A positive percentage of PCDH9 was expressed in normal skin or/and pigmented nevus tissue but only 23.3% (7 of 30) in melanoma tissue, which was lower than that in non-tumor tissue (Table 1, Figure 1A). The IHC results are consistent with the studies of δ-PCDHs that include PCDH9 and are involved in cell adhesion establishment and disruption. Moreover, δ-PCDHs are demonstrated as tumor suppressors by regulating cell proliferation, and the lower expressions of δ-PCDH have poorer prognosis (10). Moreover, the expression of PCDH9 was significantly lower in high-grade and worse histological type of tumors of glioma, gastric, and prostatic cancers (44, 45).

The survival analysis of MMP2

GEPIA was used for survival analysis of MMP2: The cutoff was set as median; the hazards ratio are calculated based on Cox pH model; all datasets were selected (BRAF Hotspot Mutants, NF1 Any Mutants, RAS Hotspot Mutants, Triple WT). The survival rate of highly expressed MMP2 is poorer than that of lowly expressed MMP2, and the HR is 1.5 ($p< 0.05$) (Figure 1B). The result of MMP2 survival analysis revealed the positive correlation between MMP2 and poor prognosis of melanoma, and it is consistent to the previous studies (1, 35) due to pro-tumorigenic and pro-metastatic effects of MMP2 (37).

PCDH9 expression affected selected genes expression

PCDH9 was overexpressed by lentivirus with PCDH9 plasmid (Figure 2A) and interfered by lentivirus with siRNA (Figures 2D, E). The relative expression of selected genes (CCND1, MMP2, and RAC1) varied with PCDH9 expression, but the effectiveness on them was different. PCDH9 and CCND1 (Cyclin D1) exhibited a positive correlation (Figures 2B–E), whereas MMP2, MMP9, and RAC1 exhibited a negative correlation with both melanoma A375 and G361 cells (Figures 2B–E).

Effects of overexpressed PCDH9 on cell viability

The overexpression of PCDH9 reduced the proliferation of melanoma cells. Overexpressed PCDH9 groups showed indeed a lower viability than control groups (Figure 3). As time passed, the viability of melanoma cells tended to stabilize, but PCDH9-overexpressed groups had less viable cells than control groups in different durations, and the differences between PCDH9 and control groups were significant (24, 48, 72, and 96 h) (Figures 3A, B).

Effects of PCDH9 alteration on apoptosis and cell cycle

The apoptosis percentage of PCDH9 overexpression was exhibited by Supplementary Figures S1A (A375) and Supplementary Figures S1B (G361), whereas the apoptosis percentage of PCDH9 interference was exhibited by Supplementary Figures S1C (A375) and Supplementary Figures S1D (G361). The cell cycle percentage of PCDH9 overexpression was exhibited by Supplementary Figures S2A (A375) and Supplementary Figures S1B (G361), whereas the cell cycle percentage of PCDH9 interference was exhibited by Supplementary Figures S2C (A375) and Supplementary Figures S1D (G361).

TABLE 1 The positive percentage of PCDH9 expression in normal skin, pigmented nevus, and melanoma tissues.

Type	Total	PCDH9 (–)	PCDH9 (+)	Positive Percentage
Normal skin	45	0	45	100.0%
Pigmented nevus	30	0	30	100.0%
Melanoma	30	23	7	23.3%

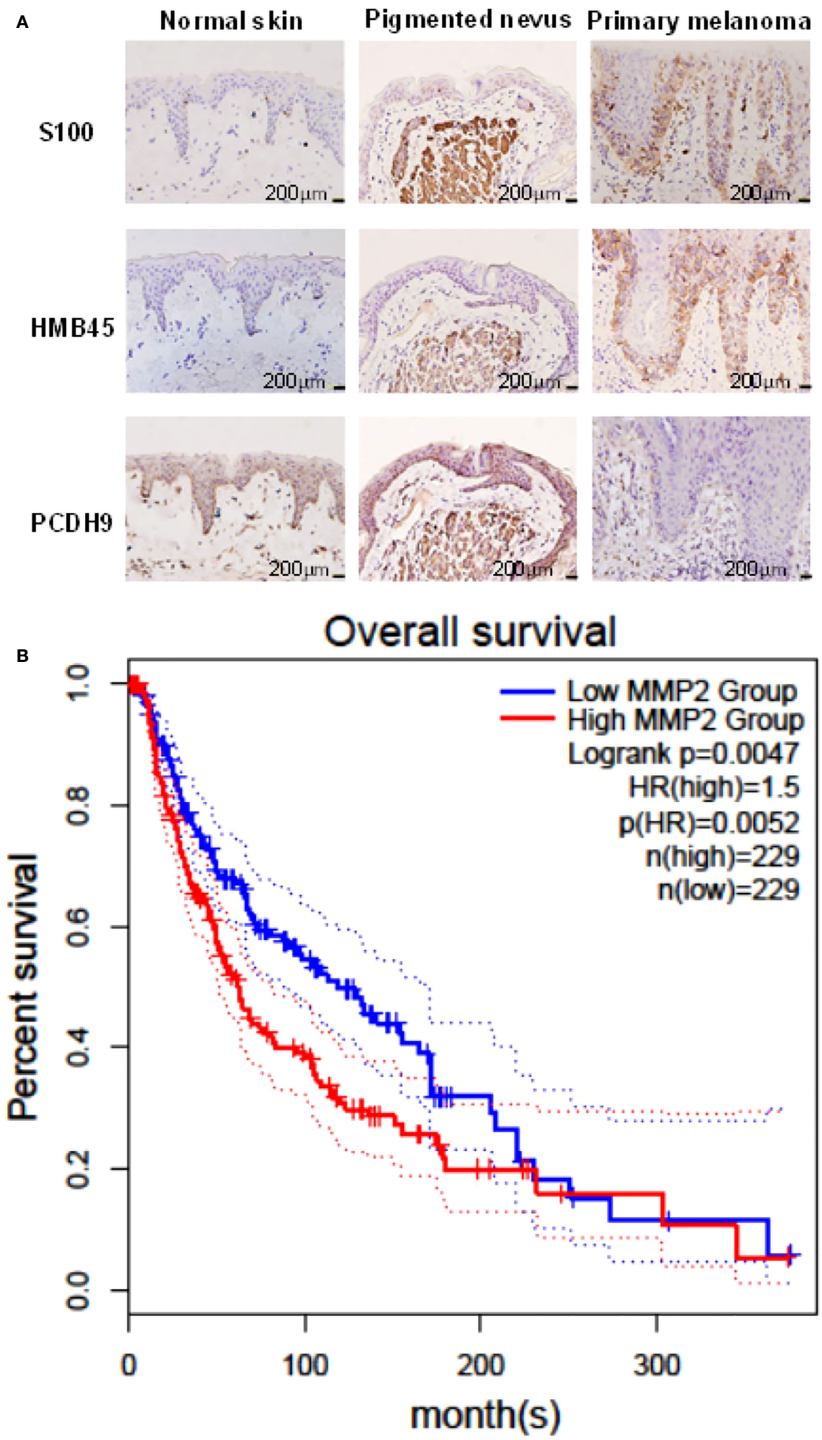

FIGURE 1
(A) Immunohistochemical analyses of PCDH9 expression in normal skin, pigmented nevus, and melanoma tissue. Positive percentage of PCDH9 expression was lower in human melanoma tissue than in normal skin or/and pigmented nevus tissue. PCDH9 was mainly expressed in cytoplasm but a small amount in nuclei. S100 and HMB45 are melanoma markers. The scale bar represents 200 μm. **(B)** Survival curves of MMP2 in normal and skin cutaneous melanoma (SKCM) tissues based on TCGA data in GEPIA. Red line represents the samples with MMP2 highly expressed (n = 229), whereas blue line exhibits lowly expression (n = 229) (log rank, p = 0.0047). HR represents hazard ratio. The p-value of HR is less 0.05 (p = 0.0052).

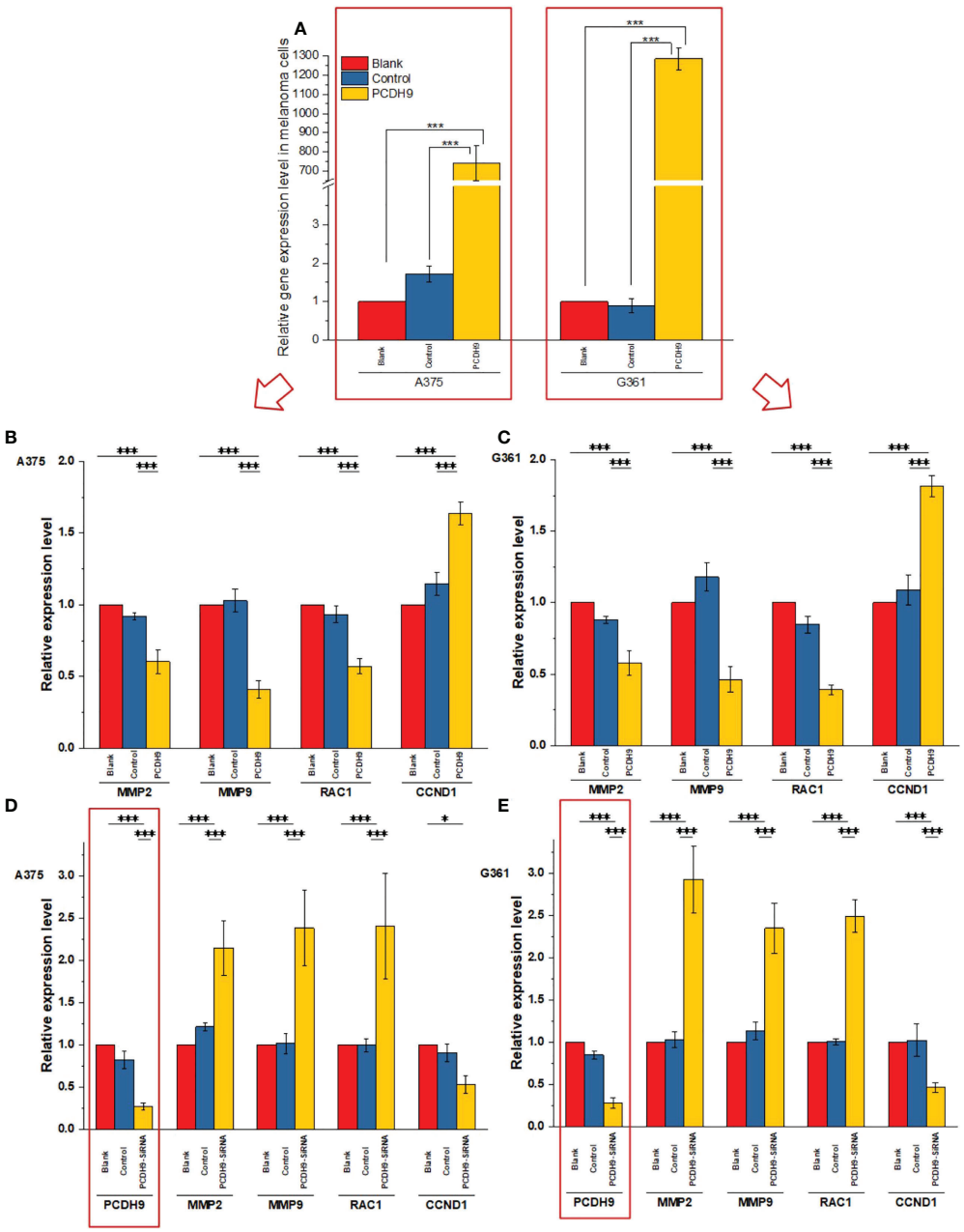

FIGURE 2
Effects of overexpressed and interfered PCDH9 in melanoma cells measured by PCR analysis **(A)**. The expressions of PCDH9 were significantly upregulated by lentivirus infection. Overexpressed PCDH9 significantly upregulated CCND1 and downregulated RAC1 and MMP9 in both cells [A375 **(B)** and G361 **(C)**]. Interfered PCDH9 downregulated CCND1 and upregulated RAC1 and MMP2 in both cells [A375 **(D)** and G361 **(E)**]. *$p < 0.05$, and ***$p < 0.001$ compared in groups by using one-way ANOVA followed by least significant difference *post hoc* tests.

The overexpressionof PCDH9 promoted the apoptosis in both melanoma cells (Figure 4A), whereas the interfered PCDH9 barely influenced the apoptosis in both cell lines (Figure 4B). The alteration of PCDH9 and apoptosis exhibited a positive correlation (Figure 4). Regarding the cell cycle arrest, there was no discrepancy between overexpressed PCDH9 or interfered PCDH9 groups and other groups (blank and control groups) in both cell lines (A375 and G361) (Figures 5A–D). Cyclin D1, encoded by CCND1, is the component of ternary complex (Cyclin D1/CDK4/CDKN18) that can regulate cell cycle during G1/S transition, but the changes of PCDH9 did not affect cell cycle. The results revealed that PCDH9 may affect melanoma cells by different ways.

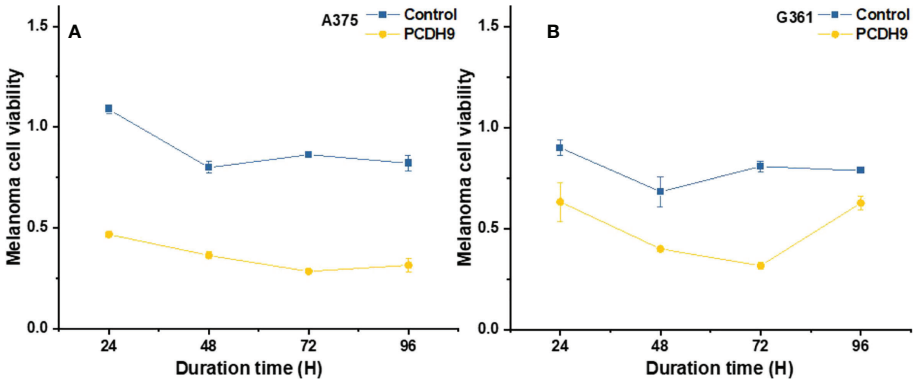

FIGURE 3
The viability of melanoma cells significantly was reduced by overexpressed PCDH9 in A375 **(A)** and G361 **(B)** cells. The alteration of PCDH9 expression significantly affected the apoptosis of melanoma cells by using one-way ANOVA followed by least significant difference *post hoc* tests.

Effects of overexpressed PCDH9 on wound healing

With respect to cell migration, after quantifying the scratched boundary by ImageJ (Figures 6A, C), the results revealed that the relative density decreased with the duration of cell culture in the blank and control groups ($p< 0.001$), whereas the relative wound density did not significantly change in the overexpressed PCDH9 groups ($p > 0.05$) (Figures 6B, D). The relative wound density of scratched boundary was significantly different in the overexpressed PCDH9 groups compared with the blank and control groups after 24 and 48 h ($p< 0.001$) (Figures 6B, D). The wound did not heal so much, when PCHD9 were overexpressed (Figure 6).

Discussion

Specimen investigations of IHC assay exhibited lower PCDH9 expressions in malignant melanoma specimens than in benign nevus tissue or/and normal skin. Moreover, our study revealed that PCDH9 was mainly expressed in the cytoplasm rather than in nuclei. This result is consistent with other cancers like glioma, gastric, and prostatic, in which lower expression of PCDH9 was observed in high-grade and worse histological type of tumors (44, 45). The survival analysis of MMP2 associated the high expression with the lower survival rate and the low expression with the higher survival rate. The HR was 1.5 ($p< 0.05$). Our study agreed with the previous investigations that MMP2 and MMP9 can represent a biomarker of malignant

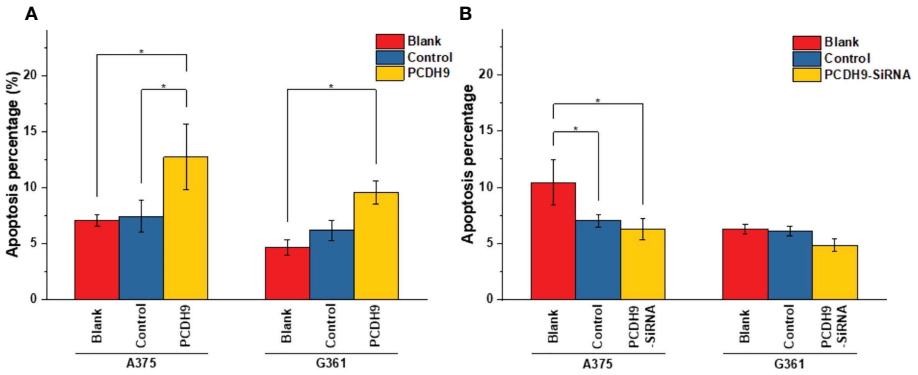

FIGURE 4
The apoptosis percentage of PCDH9 overexpression was exhibited by **(A)** A375 and **(B)** G361. The overexpression of PCDH9 significantly promoted apoptosis in both cell lines. *$p< 0.05$ compared in groups by using one-way ANOVA followed by least significant difference *post hoc* tests. The interference of PCDH9 reduced apoptosis in A375 cell line and in a more modest manner in G361 cell lines. *$p < 0.05$ compared in groups by using one-way ANOVA followed by least significant difference *post hoc* tests.

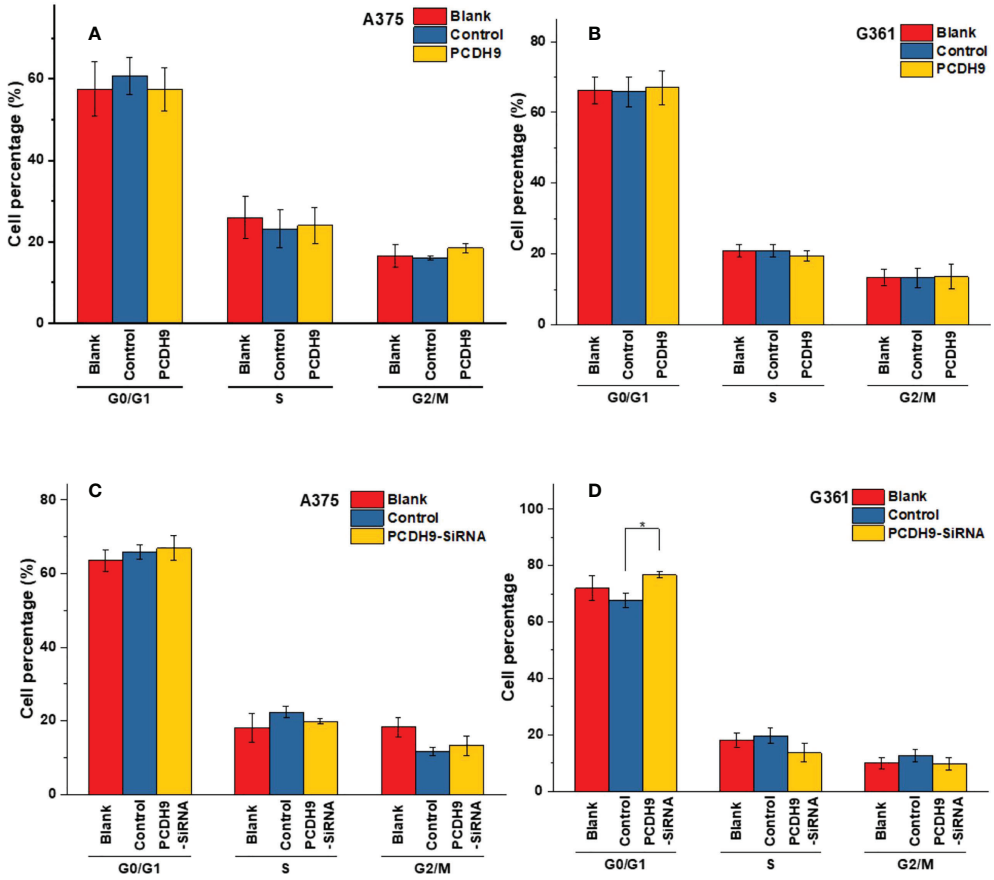

FIGURE 5
The varieties of PCDH9 expression did not significantly affect melanoma cell regulation. The cell percentage of melanoma cells affected by overexpressed PCDH9 in different cell period time in A375 **(A)** and G361 **(B)** cell lines. The cell percentage of melanoma cells affected by PCDH9 interference in different cell period time in A375 **(C)** and G361 **(D)** cell lines. *$p < 0.05$ compared in groups by using one-way ANOVA followed by least significant difference *post hoc* tests.

melanoma (37), and downregulating MMP2 expression would increase prognostic survival. We explored and performed a series of investigations, including cell viability assay, apoptosis assay, and PCR of PCDH9 alteration by lentivirus (GV358-PCDH9 and GV358-SiRNA) in A375 and G361. According to our results, overexpressed PCDH9 upregulated expressions of CCND1, whereas MMP2, MMP9, and RAC1 were downregulated. Interfered PCDH9 induced downregulation of CCND1, whereas MMP2, MMP9, and RAC1 were upregulated. The results agreed with the previous studies that the lower expression of PCDH9 was associated with the worse mean survival rate (44, 45). The alteration of PCDH9 exhibited positive correlation with apoptosis that the apoptosis was promoted with overexpressed PCDH9 but decreased with interfered PCDH9. The overexpression of PCDH9 reduced the viability of melanoma cells. Our results agreed with recent studies that found lower PCDH9 expression in various cancer types (41, 46, 47). The alteration of PCDH9 affected CCND1 (Cyclin D1), the cell regulator protein. The previous investigations of hepatocellular carcinoma (HCC) found that PCDH9 suppresses HCC cells by inducing cell cycle arrest at G0/G1 phase (13). Our results suggested that the effect of PCDH9 on melanoma by RAC1 suppresses RAC1-dependent NADPH oxidase activity to decrease ROS generation and ROS-induced angiogenesis. PCDH9 can target complex-bound RAC1 to weaken angiogenesis by regulating NADPH oxidase, ROS production, and DNA damage susceptibility through cyclin D1 trafficking. VEGF binding to VEGFR2 leads to activating and translocating RAC1 into the plasma membrane, whereas ROS-dependent signaling events may trigger angiogenesis (i.e., cell migration and proliferation) and influence MMP2, which affect growth factor, tumor promoter stimulation, and prognostic survival as well. Moreover, RAC1 could affect cellular adhesion, migration, and invasion as well (24). However, the alteration of PCDH9 expression did not affect melanoma cell regulation in a significant manner ($p > 0.05$). This result suggests

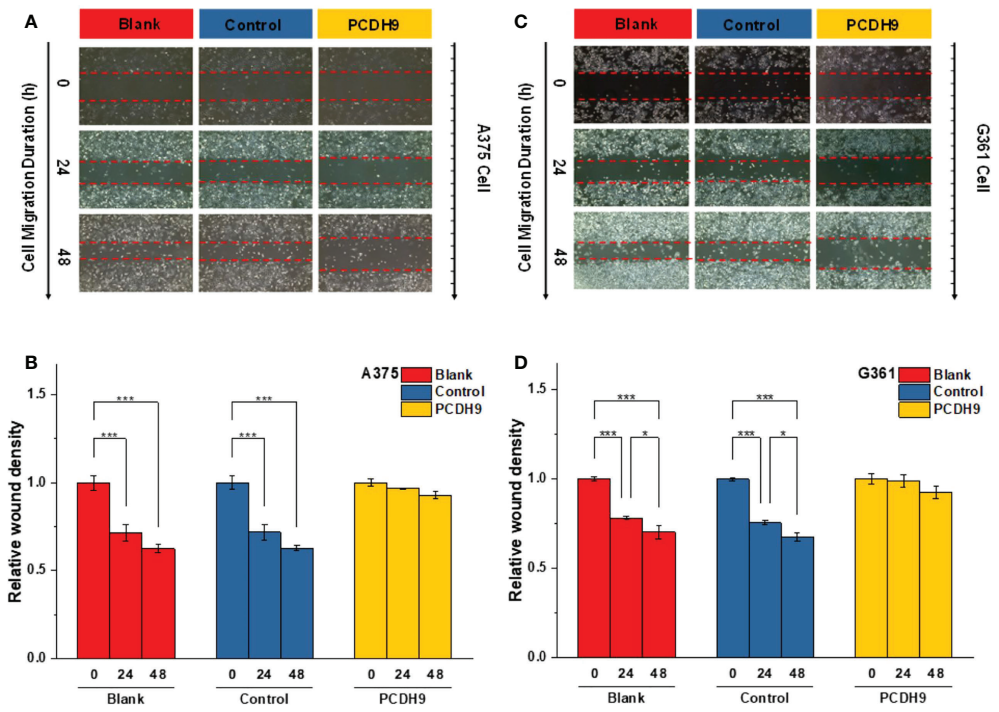

FIGURE 6
The scratched boundary of migrator cells was observed by inverted microscope DMI3000B (Leica, Germany). Representative image of melanoma cells invaded from the scratched boundary in A375 **(A)** and G361 **(C)** cell lines. Relative density of scratched boundary was not altered in overexpressed PCDH9 groups comparing with blank and control groups in A375 **(B)** and G361 **(D)** cell lines. *$p < 0.05$, and ***$p < 0.001$ compared in groups by using one-way ANOVA followed by least significant difference *post hoc* tests.

that PCDH9 and Cyclin D1 (CCND1) could affect melanoma cell by different mechanisms. Cyclin D1 (CCND1) could affect tumorigenesis *via* nuclear trafficking (44), which resulted in PCDH9 mainly expressed in the cytoplasm but not in the nucleus. The results of wound-healing assay revealed that the overexpression of PCDH9 could inhibit the cell migration or the duration, which similar to PCDH9 affecting on HCC (48). Recently, Gross et al. found the role of store-operated Ca^{2+} entry (SOCE) in melanoma metastasis that the suppression of Ca^{2+} signaling worsened the melanoma progression and that the concentration of extracellular Ca^{2+} could play the important role (49). Unlike most tissues, melanocytes grow within the extracellular Ca^{2+}; in contrary, non-native tissues will be tolerated at high concentration of extracellular Ca^{2+} (49). In the context of SOCE role, we speculate that the binding between PCDH9 and calcium ion can increase the adhesion of melanocytes, whereas the adhesion of non-native cells increases in lower expressions of PCDH9 that can enhance the migration of melanoma cells. To conclude, the increase of PCDH9 could suppress melanoma cells by observing the deregulation of MMP2, MMP9, and RAC1. Although the alteration of PCDH9 could influence CCND1 but not the cell cycle, which suggested it may affect melanoma cells by other mechanisms, such as SOCE combined melanoma cell migration, RAC1-dependent NADPH oxidase correlated with GTP-GDP switch. In summary, PCDH9 can be considered as an independent prognostic factor for melanoma, and re-expression of PCDH9 can serve as a potential therapeutic strategy for melanoma treatment.

Data availability statement

The datasets generated during and/or analyzed during the current study are available from the corresponding author upon reasonable request.

Ethics statement

The protocol of biopsy was proceeded according to the Ethical Committee of Guangzhou Medical University (PJ2015055KT). The patients/participants provided their written informed consent to participate in this study. Written

informed consent was obtained from the individual(s) for the publication of any potentially identifiable images or data included in this article.

Author contributions

Conceptualization: JZ, RC, and ZW. Data curation: JZ, YZ, and SL. Formal analysis: JZ, H-ZY, SL, and MI. Project administration: RC and ZW. Resources: RC. Visualization: JZ. Writing original draft: JZ. Review and editing: JZ, RC, and MI. All authors contributed to the article and approved the submitted version.

Funding

This research was supported by the Natural Science Foundation of Guangdong Province of China (2016A030313682 and 2020A1515010281).

Acknowledgments

The authors thank Maurizio Battino and Francesca Giampieri (Department of Clinical Sciences, Faculty of Medicine, Polytechnic University of Marche, Ancona, Italy) and Gianluca Storci (Department of Experimental, Diagnostic, and Specialty Medicine, University of Bologna, Italy) for their insight and helpful discussion. We also thank Dr. Jingquan He (Shanghai Biotree Biotechnology, Ltd., Shanghai, China) for his company and his support in protein complex immunoprecipitation.

Conflict of interest

The authors declare that the research was conducted in the absence of any commercial or financial relationships that could be construed as a potential conflict of interest.

Publisher's note

Supplementary material

The Supplementary Material for this article can be found online at: https://www.frontiersin.org/articles/10.3389/fonc.2022.903554/full#supplementary-material

References

1. Zamolo G, Grahovac M, Žauhar G, Vučinić D, Kovač L, Brajenić N, et al. Matrix metalloproteinases MMP-1, MMP-2, and MMP-13 are overexpressed in primary nodular melanoma. *J Cutan Pathol* (2020) 47(2):139–45. doi: 10.1111/cup.13603

2. Moschos SJ, Trembath D, Collichio FA, Lee CB, Zagar TM, Ewend MG. Chapter 17 - brain metastases from cutaneous melanoma: Biology and its implications for more rational therapeutic approaches. In: Hayat MA, editor. *Brain metastases from primary tumors, Volume 3*. San Diego: Academic Press (2016). p. 237–54.

3. Chang JW, Guo J, Hung CY, Lu S, Shin SJ, Quek R, et al. Sunrise in melanoma management: Time to focus on melanoma burden in Asia. *Asia Pac J Clin Oncol* (2017) 13(6):423–7. doi: 10.1111/ajco.12670

4. Sung H, Ferlay J, Siegel RL, Laversanne M, Soerjomataram I, Jemal A, et al. Global cancer statistics 2020: GLOBOCAN estimates of incidence and mortality worldwide for 36 cancers in 185 countries. *CA Cancer J Clin* (2021) 71(3):209–49. doi: 10.3322/caac.21660

5. Yang HZ, Zhang J, Zeng J, Liu S, Zhou F, Zhang F, et al. Resveratrol inhibits the proliferation of melanoma cells by modulating cell cycle. *Int J Food Sci Nutr* (2020) 71(1):84–93. doi: 10.1080/09637486.2019.1614541

6. Dinehart MS, Dinehart SM, Sukpraprut-Braaten S, High WA. Immunohistochemistry utilization in the diagnosis of melanoma. *J Cutan Pathol* (2020) 47(5):446–50. doi: 10.1111/cup.13648

7. Hodis E, Watson IR, Kryukov GV, Arold ST, Imielinski M, Theurillat JP, et al. A landscape of driver mutations in melanoma. *Cell.* (2012) 150(2):251–63. doi: 10.1016/j.cell.2012.06.024

8. Isacke CM, Horton MA. "Adhesion molecule families," In: *The adhesion molecule FactsBook*. San Diego, CA, USA: Academic Press, (2000). p. 7–32.

9. Peek SL, Mah KM, Weiner JA. Regulation of neural circuit formation by protocadherins. *Cell Mol Life Sci* (2017) 74(22):4133–57. doi: 10.1007/s00018-017-2572-3

10. Emond MR, Biswas S, Morrow ML, Jontes JD. Proximity-dependent proteomics reveals extensive interactions of protocadherin-19 with regulators of rho GTPases and the microtubule cytoskeleton. *Neuroscience.* (2021) 452:26–36. doi: 10.1016/j.neuroscience.2020.09.033

11. Wang C, Yu G, Liu J, Wang J, Zhang Y, Zhang X, et al. Downregulation of PCDH9 predicts prognosis for patients with glioma. *J Clin Neurosci* (2012) 19 (4):541–5. doi: 10.1016/j.jocn.2011.04.047

12. Bidoki SH, Bayatani A, Sarlak M, Rasouli M, Mostafaie P, Saghafi M, et al. Assessing expression of TGF-B2 and PCDH9 genes in breast cancer patients. *Age.* (2018) 7:20.

13. Lv J, Zhu P, Zhang X, Zhang L, Chen X, Lu F, et al. PCDH9 acts as a tumor suppressor inducing tumor cell arrest at G0/G1 phase and is frequently methylated in hepatocellular carcinoma. *Mol Med Rep* (2017) 16(4):4475–82. doi: 10.3892/mmr.2017.7193

14. Wang C, Tao B, Li S, Li B, Wang X, Hu G, et al. Characterizing the role of PCDH9 in the regulation of glioma cell apoptosis and invasion. *J Mol Neurosci* (2014) 52(2):250–60. doi: 10.1007/s12031-013-0133-2

15. Vieira AF, Paredes J. P-cadherin and the journey to cancer metastasis. *Mol Cancer.* (2015) 14:178. doi: 10.1186/s12943-015-0448-4

16. Wang P, Lin SL, Zhang LH, Li Z, Liu Q, Gao JX, et al. The prognostic value of p-cadherin in non-muscle-invasive bladder cancer. *Eur J Surg Oncol* (2014) 40 (3):255–9. doi: 10.1016/j.ejso.2013.12.018

17. Arenas MI, Romo E, Royuela M, Fraile B, Paniagua R–. N- and p-cadherin, and alpha-, beta- and gamma-catenin protein expression in normal, hyperplastic and carcinomatous human prostate. *Histochem J* (2000) 32(11):659–67. doi: 10.1023/A:1004111331752

18. Van Marck V, Stove C, Van Den Bossche K, Stove V, Paredes J, Vander Haeghen Y, et al. P-cadherin promotes cell-cell adhesion and counteracts invasion in human melanoma. *Cancer Res* (2005) 65(19):8774–83. doi: 10.1158/0008-5472.CAN-04-4414

19. Jacobs K, Feys L, Vanhoecke B, Van Marck V, Bracke M. P-cadherin expression reduces melanoma growth, invasion, and responsiveness to growth factors in nude mice. *Eur J Cancer Prev* (2011) 20(3):207–16. doi: 10.1097/CEJ.0b013e3283429e8b

20. Cannon AC, Uribe-Alvarez C, Chernoff J. RAC1 as a therapeutic target in malignant melanoma. *Trends Cancer.* (2020) 6(6):478–88. doi: 10.1016/j.trecan.2020.02.021

21. Araiza-Olivera D, Feng Y, Semenova G, Prudnikova TY, Rhodes J, Chernoff J. Suppression of RAC1-driven malignant melanoma by group a PAK inhibitors. *Oncogene.* (2018) 37(7):944–52. doi: 10.1038/onc.2017.400

22. Aznar S, Fernandez-Valeron P, Espina C, Lacal JC. Rho GTPases: potential candidates for anticancer therapy. *Cancer Lett* (2004) 206(2):181–91. doi: 10.1016/j.canlet.2003.08.035

23. del Pulgar TG, Benitah SA, Valerón PF, Espina C, Lacal JC. Rho GTPase expression in tumourigenesis: evidence for a significant link. *Bioessays.* (2005) 27 (6):602–13. doi: 10.1002/bies.20238

24. Espina C, Cespedes MV, Garcia-Cabezas MA, Gomez del Pulgar MT, Boluda A, Oroz LG, et al. A critical role for Rac1 in tumor progression of human colorectal adenocarcinoma cells. *Am J Pathol* (2008) 172(1):156–66. doi: 10.2353/ajpath.2008.070561

25. Vega FM, Ridley AJ. Rho GTPases in cancer cell biology. *FEBS Lett* (2008) 582(14):2093–101. doi: 10.1016/j.febslet.2008.04.039

26. Davis MJ, Ha BH, Holman EC, Halaban R, Schlessinger J, Boggon TJ. RAC1P29S is a spontaneously activating cancer-associated GTPase. *Proc Natl Acad Sci U S A.* (2013) 110(3):912–7. doi: 10.1073/pnas.1220895110

27. Ellenbroek SI, Collard JG. Rho GTPases: functions and association with cancer. *Clin Exp Metastasis.* (2007) 24(8):657–72. doi: 10.1007/s10585-007-9119-1

28. Bae YS, Oh H, Rhee SG, Yoo YD. Regulation of reactive oxygen species generation in cell signaling. *Mol Cells* (2011) 32(6):491–509. doi: 10.1007/s10059-011-0276-3

29. Wu WS. The signaling mechanism of ROS in tumor progression. *Cancer Metastasis Rev* (2006) 25(4):695–705.

30. Bedard K, Krause KH. The NOX family of ROS-generating NADPH oxidases: physiology and pathophysiology. *Physiol Rev* (2007) 87(1):245–313. doi: 10.1152/physrev.00044.2005

31. Harfouche R, Malak NA, Brandes RP, Karsan A, Irani K, Hussain SN. Roles of reactive oxygen species in angiopoietin-1/tie-2 receptor signaling. *FASEB J* (2005) 19(12):1728–30. doi: 10.1096/fj.04-3621fje

32. Ushio-Fukai M, Alexander RW. Reactive oxygen species as mediators of angiogenesis signaling. role of NAD (P) h oxidase. *Mol Cell Biochem* (2004) 264(1-2):85–97. doi: 10.1023/B:MCBI.0000044378.09409.b5

33. Binker MG, Binker-Cosen AA, Richards D, Oliver B, Cosen-Binker LI. EGF promotes invasion by PANC-1 cells through Rac1/ROS-dependent secretion and activation of MMP-2. *Biochem Biophys Res Commun* (2009) 379(2):445–50. doi: 10.1016/j.bbrc.2008.12.080

34. Steinbrenner H, Ramos MC, Stuhlmann D, Mitic D, Sies H, Brenneisen P. Tumor promoter TPA stimulates MMP-9 secretion from human keratinocytes by activation of superoxide-producing NADPH oxidase. *Free Radic Res* (2005) 39 (3):245–53. doi: 10.1080/10715760500053487

35. Napoli S, Scuderi C, Gattuso G, Di Bella V, Candido S, Basile MS, et al. Functional roles of matrix metalloproteinases and their inhibitors in melanoma. *Cells.* (2020) 9(5):1151. doi: 10.3390/cells9051151

36. Rinonce HT, Aji RPM, Hayati N, Pudjohartono MF, Kameswari B, Irianiwati. Low BRAF V600 mutation prevalence in primary skin nodular melanoma in Indonesia: a real-time PCR detection among Javanese patients. *BMC Proc* (2019) 13(Suppl 11):15. doi: 10.1186/s12919-019-0175-8

37. Marusak C, Bayles I, Ma J, Gooyit M, Gao M, Chang M, et al. The thiirane-based selective MT1-MMP/MMP2 inhibitor ND-322 reduces melanoma tumor growth and delays metastatic dissemination. *Pharmacol Res* (2016) 113(Pt A):515–20. doi: 10.1016/j.phrs.2016.09.033

38. Salemi R, Falzone L, Madonna G, Polesel J, Cinà D, Mallardo D, et al. MMP-9 as a candidate marker of response to BRAF inhibitors in melanoma patients with BRAF(V600E) mutation detected in circulating-free DNA. *Front Pharmacol* (2018) 9:856. doi: 10.3389/fphar.2018.00856

39. Kim JK, Diehl JA. Nuclear cyclin D1: an oncogenic driver in human cancer. *J Cell Physiol* (2009) 220(2):292–6. doi: 10.1002/jcp.21791

40. Tang Z, Li C, Kang B, Gao G, Li C, Zhang Z. GEPIA: A web server for cancer and normal gene expression profiling and interactive analyses. *Nucleic Acids Res* (2017) 45(W1):W98–102. doi: 10.1093/nar/gkx247

41. Chang K, Creighton CJ, Davis C, Donehower L, Drummond J, Wheeler D, et al. The cancer genome atlas pan-cancer analysis project. *Nat Genet* (2013) 45 (10):1113–20. doi: 10.1126/science.abm0829

42. Consortium TG, Ardlie KG, Deluca DS, Segre AV, Sullivan TJ, Young TR, et al. The genotype-tissue expression (GTEx) pilot analysis: Multitissue gene regulation in humans. *Science* (2015) 348(6235):648-60. doi: 10.1126/science.1262110

43. Livak KJ, Schmittgen TD. Analysis of relative gene expression data using real-time quantitative PCR and the 2–DDCT method. *Methods* (2001) 25(4):402–8. doi: 10.1006/meth.2001.1262

44. Ren S, Wei GH, Liu D, Wang L, Hou Y, Zhu S, et al. Whole-genome and transcriptome sequencing of prostate cancer identify new genetic alterations driving disease progression. *Eur Urol.* (2018) 73(3):322–39. doi: 10.1016/j.eururo.2017.08.027

45. Chen Y, Xiang H, Zhang Y, Wang J, Yu G. Loss of PCDH9 is associated with the differentiation of tumor cells and metastasis and predicts poor survival in gastric cancer. *Clin Exp metastasis.* (2015) 32(5):417–28. doi: 10.1007/s10585-015-9712-7

46. Wang C, Chen Q, Li S, Li S, Zhao Z, Gao H, et al. Dual inhibition of PCDH9 expression by miR-215-5p up-regulation in gliomas. *Oncotarget.* (2017) 8 (6):10287–97. doi: 10.18632/oncotarget.14396

47. Xie Z, Zhou F, Yang Y, Li L, Lei Y, Lin X, et al. Lnc-PCDH9-13: 1 is a hypersensitive and specific biomarker for early hepatocellular carcinoma. *EBioMedicine.* (2018) 33:57–67. doi: 10.1016/j.ebiom.2018.06.026

48. Zhu P, Lv J, Yang Z, Guo L, Zhang L, Li M, et al. Protocadherin 9 inhibits epithelial–mesenchymal transition and cell migration through activating GSK-3β in hepatocellular carcinoma. *Biochem Biophys Res Commun* (2014) 452(3):567–74. doi: 10.1016/j.bbrc.2014.08.101

49. Gross S, Hooper R, Tomar D, Armstead AP, Shanas N, Mallu P, et al. Suppression of Ca2+ signaling enhances melanoma progression. *EMBO J* (2022) 41 (19):e110046.

Frontiers in Oncology

Advances knowledge of carcinogenesis and tumor progression for better treatment and management

The third most-cited oncology journal, which highlights research in carcinogenesis and tumor progression, bridging the gap between basic research and applications to imrpove diagnosis, therapeutics and management strategies.

Discover the latest Research Topics

See more →

Frontiers

Avenue du Tribunal-Fédéral 34
1005 Lausanne, Switzerland
frontiersin.org

Contact us

+41 (0)21 510 17 00
frontiersin.org/about/contact